SECTION A

JOURNAL OF RESEARCH

of the NATIONAL BUREAU OF STANDARDS

JNBAAR 78A (2) 95 - 314, Mar.-Apr. 1974

U.S. DEPARTMENT OF COMMERCE / National Bureau of Standards

Physics and Chemistry

Journal of Research

of the

National Bureau of Standards

A. Physics and Chemistry

Mar.–Apr. • 1974

VOLUME • 78A

NUMBER • 2

Editor: C. W. Beckett

Associate Editor: D. D. Wagman

Publication dates:
Feb. 1, Apr. 1, June 1, Aug. 1, Oct. 1, Dec. 1, 1974

J. Res. Nat. Bur. Stand. (U.S.), A

JOURNAL OF RESEARCH

The National Bureau of Standards Journal of Research reports research and development in the fields of activity shown at right. Also included from time to time are survey articles on topics closely related to the Bureau's scientific and technical program.

The Journal is published in two separate sections as follows:

A. Physics and Chemistry

Contains papers of interest primarily to scientists working in these fields. Issued six times a year. Annual subscription: domestic, $17.00; foreign, $21.25. Single copy, varies.

B. Mathematical Sciences

Presents studies and compilations designed mainly for the mathematician and the theoretical physicist. Issued quarterly. Annual subscription: domestic, $9.00; foreign, $11.25. Single copy, $2.25.

The National Bureau of Standards[1] was established by an act of Congress March 3, 1901. The Bureau's overall goal is to strengthen and advance the Nation's science and technology and facilitate their effective application for public benefit. To this end, the Bureau conducts research and provides: (1) a basis for the Nation's physical measurement system, (2) scientific and technological services for industry and government, (3) a technical basis for equity in trade, and (4) technical services to promote public safety. The Bureau consists of the Institute for Basic Standards, the Institute for Materials Research, the Institute for Applied Technology, the Institute for Computer Sciences and Technology, and the Office for Information Programs.

THE INSTITUTE FOR BASIC STANDARDS provides the central basis within the United States of a complete and consistent system of physical measurement; coordinates that system with measurement systems of other nations; and furnishes essential services leading to accurate and uniform physical measurements throughout the Nation's scientific community, industry, and commerce. The Institute consists of a Center for Radiation Research, an Office of Measurement Services and the following divisions:

Applied Mathematics — Electricity — Mechanics — Heat — Optical Physics — Nuclear Sciences[2] — Applied Radiation[2] — Quantum Electronics[3] — Electromagnetics[3] — Time and Frequency[3] — Laboratory Astrophysics[3] — Cryogenics[3].

THE INSTITUTE FOR MATERIALS RESEARCH conducts materials research leading to improved methods of measurement, standards, and data on the properties of well-characterized materials needed by industry, commerce, educational institutions, and Government; provides advisory and research services to other Government agencies; and develops, produces, and distributes standard reference materials. The Institute consists of the Office of Standard Reference Materials and the following divisions:

Analytical Chemistry — Polymers — Metallurgy — Inorganic Materials — Reactor Radiation — Physical Chemistry.

THE INSTITUTE FOR APPLIED TECHNOLOGY provides technical services to promote the use of available technology and to facilitate technological innovation in industry and Government; cooperates with public and private organizations leading to the development of technological standards (including mandatory safety standards), codes and methods of test; and provides technical advice and services to Government agencies upon request. The Institute consists of a Center for Building Technology and the following divisions and offices:

Engineering and Product Standards — Weights and Measures — Invention and Innovation — Product Evaluation Technology — Electronic Technology — Technical Analysis — Measurement Engineering — Structures, Materials, and Life Safety[4] — Building Environment[4] — Technical Evaluation and Application[4] — Fire Technology.

THE INSTITUTE FOR COMPUTER SCIENCES AND TECHNOLOGY conducts research and provides technical services designed to aid Government agencies in improving cost effectiveness in the conduct of their programs through the selection, acquisition, and effective utilization of automatic data processing equipment; and serves as the principal focus within the executive branch for the development of Federal standards for automatic data processing equipment, techniques, and computer languages. The Center consists of the following offices and divisions:

Information Processing Standards — Computer Information — Computer Services — Systems Development — Information Processing Technology.

THE OFFICE FOR INFORMATION PROGRAMS promotes optimum dissemination and accessibility of scientific information generated within NBS and other agencies of the Federal Government; promotes the development of the National Standard Reference Data System and a system of information analysis centers dealing with the broader aspects of the National Measurement System; provides appropriate services to ensure that the NBS staff has optimum accessibility to the scientific information of the world. The Office consists of the following organizational units:

Office of Standard Reference Data — Office of Technical Information and Publications — Library — Office of International Relations.

---

[1] Headquarters and Laboratories at Gaithersburg, Maryland, unless otherwise noted; mailing address Washington, D.C. 20234.
[2] Part of the Center for Radiation Research.
[3] Located at Boulder, Colorado 80302.
[4] Part of the Center for Building Technology.

U.S. DEPARTMENT OF COMMERCE
Frederick B. Dent, Secretary
NATIONAL BUREAU OF STANDARDS
Richard W. Roberts, Director

Order all publications from the Superintendent of Documents
U.S. Government Printing Office, Washington, D.C. 20402

The Secretary of Commerce has determined that the publication of this periodical is necessary in the transaction of the public business required by law of this Department. Use of funds for printing this periodical has been approved by the Director of the Office of Management and Budget through June 30, 1976.

JOURNAL OF RESEARCH of the National Bureau of Standards—A. Physics and Chemistry
Vol. 78A, No. 2, March–April 1974

The Formation of Curved Polymer Crystals: Polyoxymethylene

F. Khoury and J. D. Barnes

Institute for Materials Research, National Bureau of Standards, Washington, D.C. 20234

(November 14, 1973)

An optical and electron microscopical study is presented of the habits exhibited by chain-folded polyoxymethylene crystals grown from hot 0.02 percent solutions of the polymer in orthodichlorobenzene when these solutions are cooled to temperatures (T_c) between 140 and 80 °C inclusive. In contrast with the lamellar crystals formed in the $T_c = 140$ and 120 °C preparations, which crystals were six-sectored and nearly planar, the crystals formed below $T_c = 120$ °C exhibited multisectored dendritic habits and were all the more pronouncedly curved the lower the temperature at which they grew. The most pronouncedly curved crystals which were observed were hollow bowl shaped dendrites having a radius of curvature of $\sim 2\ \mu$m which were formed in the 80 °C preparations. The possible origins of why the lamellar crystals of polyoxymethylene were all the more pronouncedly curved the lower the crystallization temperature are considered in the light of conjectures which have been previously advanced concerning the formation of curved crystals of poly(4-methylpentene-1). Among the features which are discussed is the role played by the bulkiness of the chain folds.

Key words: Chain-folded; curved; crystal; electron microscopy; optical microscopy; polymer; polyoxymethylene; solution grown.

1. Introduction

We report in this paper the outcome of a study of the habits exhibited by lamellar crystals of polyoxymethylene (POM) grown at different supercoolings from hot 0.02 percent solutions of the polymer in orthodichlorobenzene [1].[1] This survey of the effect of supercooling on the growth habits of POM crystals was undertaken with the specific purpose of determining whether increasing the degree of supercooling at which POM is crystallized from solutions having the same concentration of polymer leads to the formation of lamellar crystals which are all the more pronouncedly curved, i.e., have a smaller radius of curvature, the higher the conditions of supercooling (lower crystallization temperatures) which prevail during the growth of the crystals. We first observed the incidence of this latter phenomenon in a previous study of the crystallization of poly(4-methylpentene-1) (P4MP) from solution [2]. Briefly, it was found that the habits of P4MP crystals ranged from very nearly planar chain-folded lamellae which were formed at high crystallization temperatures, to distinctly curved hollow bowl-shaped multilayered lamellar crystals having a radius of curvature of $\sim 2.5\ \mu$m which were formed at much lower temperatures. Our observations on this effect of increasing supercooling on the habits of P4MP crystals have been described and discussed in detail in a previous paper [2]. The objective of the present study was to determine whether an analogous phenomenon manifests itself when POM is crystallized from solution at different supercoolings. This has indeed been found to be the case as will be described in Section 3 of this paper.

We shall not dwell at this stage on the nature of the considerations which originally led us to speculate that there might exist a phenomenological similarity between the effect of supercooling on the character of solution grown crystals of P4MP and POM insofar as the formation of curved lamellar crystals is concerned. This matter is deferred to Section 4 where the observations derived from the present study on the formation and characteristics of curved crystals of POM are discussed in the light of conjectures which we have previously advanced [2] concerning the origins of curvature in P4MP crystals and the causes of the enhancement of this feature the greater the supercooling at which the crystals of that polymer are grown from solution. We shall limit ourselves at this stage to merely pointing out previously reported observations concerning the habits of solution-grown crystals of POM, which observations anteceded for the most part the undertaking of the present study.

POM has been crystallized from solution in the form of hexagonal-shaped chain-folded lamellar crystals which are six-sectored[2] [3–8]. As indicated schemat-

[1] Figures in brackets indicate the literature references at the end of this paper.

[2] The terms sector and fold-domain are used synonymously throughout this paper.

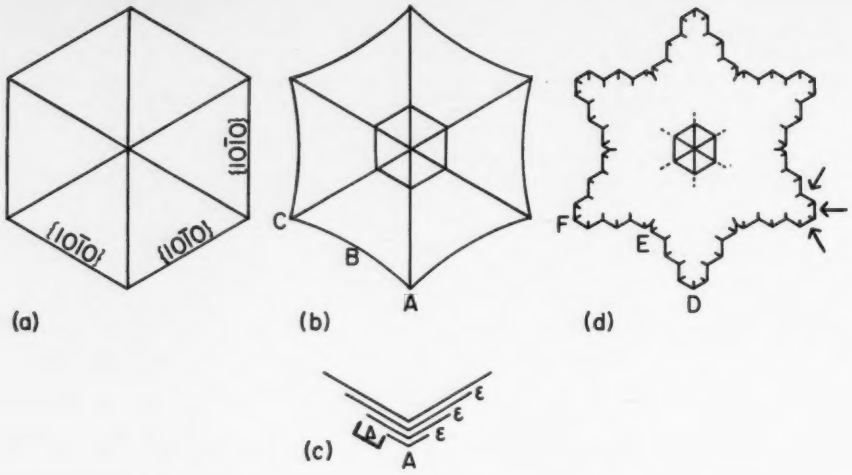

FIGURE 1. *Schematic representation of lateral growth habits exhibited by chain-folded crystals of POM.*

(a) Hexagonal shaped six-sectored lamella bound by {10$\bar{1}$0} growth faces. (b) Star-shaped six-sectored habit, SS, resulting from the preferential initiation of new {10$\bar{1}$0} planes at the leading corners of a hexagonal shaped six-sectored precursor crystal. (c) Larger scale representation of a leading corner of an SS type lamella (e.g., corner A in (b)) depicting the lag Δ between the extremities ε of successive {10$\bar{1}$0} planes originating from the corner. (d) Starlike dendritic multisectored habit, SD, resulting from the generation of new sectored outgrowths at the leading corners of a hexagonal shaped six-sectored precursor crystal; the arrows point to {10$\bar{1}$0} microfacets along which the chain molecules fold.

ically in figure 1a, these crystals are bound laterally by {10$\bar{1}$0} faces at which growth occurs through the accretion of chain molecules which fold along correspondingly parallel {10$\bar{1}$0} planes. Several observations, namely, the diffraction contrast characteristics manifested in both dark-field and bright-field electron micrographs of six-sectored crystals sedimented and dried on a flat substrate [5, 6], the appearance exhibited by the crystals when they are examined as they sediment and dry on a substrate during the evaporation of the liquid in which they were grown [6], the not infrequent incidence of pleats in sedimented crystals [6–8],[3] the slightly 'warped' appearance of, and the shadow density distribution about, some sedimented crystals [4], have been adduced as evidence that six-sectored chain-folded lamellae of POM are not perfectly flat as grown [4–7]. The matter of the as-grown conformation (nonplanar character) of six-sectored chain-folded lamellae of POM will be considered further in Section 3.2 of this paper in the light of both the aforementioned observations as well as some similar and additional ones obtained in the present study which includes an examination of such crystals as viewed under the optical microscope while they are in suspension in liquid. It is appropriate, however, by way of background, to summarize at this juncture the possibilities and conjectures which have been previously advanced concerning the nature and origins of the nonplanar character of six-sectored lamellar crystals of POM.

The possibility was raised in an earlier paper [4] that six-sectored crystals of POM may be hollow pyramidal in character, the implication being that the chain folds in successive {10$\bar{1}$0} fold planes in the constituent fold-domains (sectors) in these crystals might be regularly staggered. This latter possibility remained conjectural (e.g., see review [7]) for lack of definitive evidence. More recently another source of the nonplanar character of six-sectored lamellae has come to light. Briefly, an analysis due to Bassett [5] of {10$\bar{1}$0} dark field Moiré patterns exhibited by bilayered crystals, whose two constituent superimposed chain-folded layers were six-sectored and slightly rotated relative to one another about an axis perpendicular to the layers, indicated that there exists in each constituent sector of the six-sectored layers a fractional difference of $\sim 3.2 \times 10^{-3}$ between the interplanar spacing of the {10$\bar{1}$0} planes which are fold planes and the interplanar spacing of the other two families of {10$\bar{1}$0} planes in each sector which are not fold planes.[4] This distortion of the metrically hexagonal unit cell [9] (or more accurately the subcell) of POM in the constituent sectors of six-sectored lamellae has been attributed by Bassett et al. [5, 6] to an asymmetric bulkiness of the chain folds. Bassett et al. [5, 6] have suggested that the nonplanar character of six-sectored lamellae is a consequence (in part at any rate) of slight buckling caused by internal stresses associated with the distortion of the subcell in its constitutent fold domains. In the absence of a regular staggering of chain-folds such buckling may be envisaged to impart a slight conicalness to the lamella

[3] Some of the monolayered crystals in [6] exhibit pleats, others do not. All the monolayered crystals in figure 1 [7] exhibit pleats. None of the monolayered crystals in figure 3a [8] exhibit pleats.

[4] For the sake of brevity we shall denote the {10$\bar{1}$0} planes along which the chain molecules are folded in POM crystals as {10$\bar{1}$0}$_f$ planes in the rest of this paper. The {10$\bar{1}$0} planes which are not fold planes will be denoted {10$\bar{1}$0}$_{nf}$.

which would have otherwise been flat. The possibility was however advanced by Bassett et al. [6], that the nonplanar character of six-sectored lamellae might be due to a combination of two factors, namely, a regular staggering of chain folds coupled with an additional slight buckling of the resulting hexagonally based hollow pyramidal crystal, which buckling is associated with the distortion of the subcell in its constituent sectors as mentioned above. We shall not pursue the matter of the nature and origins of the as-grown conformation of six-sectored lamellae any further at this stage. As pointed out earlier this aspect will be considered and discussed again in Section 3.2 where observations bearing on the question of whether or not regular fold staggering occurs in six-sectored crystals of POM will be presented.

Having outlined some of the morphological characteristics of six-sectored lamellar crystals of POM and having given an indication of some of the views and conjectures pertaining to the nature and origins of their nonplanar character, we pass on to a summary of previous observations on the nature of POM crystals whose habits differ from but are related to that of the hexagonally shaped six-sectored crystals discussed in the previous two paragraphs. Such crystals, which have been described by Reneker and Geil [4], consisted of a basal (leading) chain-folded lamella upon which additional chain-folded terraces of much smaller lateral extent than that of the basal lamella had developed in spiral-like fashion through the agency of screw dislocations generated intermittently at the periphery of the basal lamella during its outward growth. The basal lamella in these crystals exhibited a distinct six-pointed star-like overall shape; its sides were not smooth but appeared faintly microfaceted. In addition, the terraces which developed upon the basal lamella exhibited incipient star-like lateral profiles. Reneker and Geil [4] have pointed out that such crystals evolve from a hexagonal six-sectored precursor lamella bound laterally by $\{10\bar{1}0\}$ faces growing under conditions (high supercooling, see later) which favor the preferential deposition of chain molecules, and hence the preferential initiation of new $\{10\bar{1}0\}_f$ planes, at the corners of that lamella. Given this latter feature, the precursor may be envisaged to develop into one of two distinguishable types of six-pointed star-shaped lamellae (which are depicted schematically in figure 1b and figure 1d) depending on the relative magnitudes of the rate of initiation R_i of new $\{10\bar{1}0\}_f$ planes at the leading corners of the precursor and the rate R_p at which these planes propagate therefrom along its $\{10\bar{1}0\}$ faces.

A schematic representation of the star-shaped six-sectored type of lamella (see illustration in figure 11, ref. [4]) which would be expected to develop when the ratio $R = R_i/R_p$ is relatively small is depicted in figure 1b. For the sake of brevity and in order to avoid confusion such star-shaped six-sectored lamellae will be referred to as type (SS) lamellae in this paper. The formation of this type of lamella would be expected to occur over a range of values of the ratio R. Within this range the larger the ratio R, the smaller will be the lateral dimensions which the precursor will attain before a change in its lateral shape from hexagonal to star-like (SS) will manifest itself. Furthermore as may be visualized with reference to figure 1b and figure 1c the lag in distance (Δ) between the advancing extremities (ϵ) of successive $\{10\bar{1}0\}_f$ planes originating from the corners (e.g., A) will tend to be smaller and, correspondingly, the fronts (e.g., AB and CB) which delineate the extremities of the succession of parallel $\{10\bar{1}0\}_f$ planes advancing in staggered formation from each corner will tend to be steeper, i.e., more pronouncedly reentrant, in the fully grown lamella. As pointed out by Geil [7] however, this latter trend will ultimately break down in that at larger values of R and hence smaller (Δ) reentrant $\{10\bar{1}0\}$ microfacets along which chain folding occurs will develop, as a consequence of which a star-shaped dendritic lamella will evolve from the hexagonal precursor. A schematic representation of such a lamella is depicted in figure 1d. Lamellae of this type will henceforth be referred to as (SD) lamellae in order to distinguish them from the (SS) lamellae discussed above from which they differ in the following two interrelated respects. First, in contrast with the sides (e.g., ABC, figure 1b) of (SS) lamellae, the sides (e.g. DEF, figure 1d) of (SD) lamellae are microfaceted, the microfacets along which the chain molecules fold are $\{10\bar{1}0\}$ microfacets. Second, in contrast with the (SS) lamellae which are six-sectored, the (SD) lamellae are multisectored. This latter feature is an inherent consequence of their lateral mode of propagation which is characterized by the repeated generation of new sectored outgrowths bound by $\{10\bar{1}0\}$ facets at the leading corners of the developing lamella throughout its growth.[5] A progressive transformation in the character of the developing lamella from hexagonal six-sectored, to (SS), and then to (SD) may be envisaged to occur during its early stages of development, the onset of the (SD) character manifesting itself at a smaller stage in the lateral growth of the lamella the higher the rate of initiation of $\{10\bar{1}0\}_f$ planes at its leading corners relative to the rate at which the planes propagate along the sides of the crystal.

Judging from the microfaceted character of the periphery of the basal lamella as well as some of the terraces which developed therefrom in the star-shaped type of crystal shown by Reneker and Geil (fig. 6, ref. [4]), that crystal may be classified as an incipient (SD) crystal. Although the range of conditions which lead to the formation of this type of crystal rather than hexagonal six-sectored ones were not investigated at the time, the dendritic character of these (SD) crystals indicated in itself that their formation occurs at high supercoolings. Two additional features exhibited in these crystals should be mentioned. First, denoting the bisector of the line joining adjacent leading corners of the basal lamella as a "slow growth line," Reneker and Geil [4] have pointed

[5] The (SS) and (SD) types of lamellae depicted in fig. 1b and fig. 1d have been previously referred to as "star-shaped" crystals and "dendritic" crystals respectively [4, 7].

out that the spiral terraces which developed upon the basal lamella originated from screw dislocations which were usually situated along the slow growth lines, and that in most instances these dislocations occurred in pairs of opposite hand lying along the slow growth lines. Second, and of particular interest in connection with the present study, the incidence of pleats in the interior of such crystals which had been deposited and dried upon a substrate was noted [4]. The occurrence of these pleats provided us at the outset of the present study with an indication that type (SD) crystals were probably not planar as-grown. The as-grown conformation of such crystals remained undetermined however. As will be seen in what ensues the present study sheds further light upon the matter of the as-grown conformations of multisectored dendritic lamellar crystals of POM as well as upon how the conformations of such crystals differ from hexagonal six-sectored and (SS) type crystals.

2. Experimental Details

2.1. Materials and Preparation Methods

The polyoxymethylene used in this study was Delrin (Type 500–NC–10)[6] supplied in the form of pellets ~ 2 mm in length and ~ 2 mm in diameter. In order to facilitate rapid dissolution of the polymer in solvent, the pellets were cut into slices ~ 40 μm in thickness. Distilled orthodichlorobenzene, in which it was initially established the polymer dissolves at 180 °C but not at room temperature, was used as a solvent. Solutions having a polymer concentration of 0.02 percent (expressed as grams of polymer per 100 ml of solvent at room temperature) were prepared in 10 ml quantities by mixing appropriate amounts of the solvent and sliced polymer at room temperature and then immersing the mixture (contained in a covered test tube, internal diameter ~ 2 cm) for half an hour in a bath held at 180 °C.

The objective of the present study was to establish from the outset a procedure under which the polymer crystallizes from the above mentioned solutions at some predetermined temperature in the form of hexagonal shaped six-sectored lamellar crystals (i.e., such as that depicted schematically in fig: 1a), and then to proceed therefrom with a survey of the habits exhibited by crystals grown at higher supercoolings. Accordingly, exploratory experiments were carried out which resulted in the adoption of a procedure which yielded, upon crystallization at 140 °C, hexagonal six-sectored lamellar crystals which were of suitable size for examination by both optical and electron microscopical techniques. This procedure was as follows. After being held at 180 °C for half an hour a 0.02 percent solution of the POM in orthodichlorobenzene was transferred to a bath held at 120 °C and kept in that bath for 1 hour; the solution exhibited a distinctly cloudy appearance indicative of the occurrence of crystallization within the first five minutes. The resulting preparation was then transferred to and kept for 15 minutes in another bath held at 153 °C at which temperature (the 'seeding' temperature, henceforth denoted T_s) the polymer dissolved. In order to ensure uniform heating throughout the preparation after it was transferred from the bath at 120 °C to the bath at $T_s = 153$ °C it was shaken continuously for about 2 minutes; within that period the polymer dissolved and the solution became clear. After 15 minutes at 153 °C had elapsed the resulting solution was transferred to the final crystallization bath held at 140 °C at which temperature the occurrence of crystallization manifested itself (as evidenced by the distinct cloudiness of the preparation) within 15 minutes.

The same preparative procedure as that described above was used in crystallizing the polymer at higher supercoolings. In these experiments the preparations were transferred from the bath at $T_s = 153$ °C to a bath held at one of the following temperatures: 120, 114, 100, and 80 °C. These preparations as well as the 140 °C preparations were kept in the final crystallization bath for several hours. For the sake of brevity in what ensues the temperature of the final crystallization bath will henceforth be denoted T_c.

Table 1 summarizes the crystallization conditions adopted in this study. This crystallization procedure is akin in principle to the self-seeding procedure used by Blundell et al. in the case of polyethylene [10]. All the bath temperatures were controlled to within ± 0.1 °C. For reasons which will not be dwelt on at this stage (they will be mentioned in Section 3) two series of experiments were carried out which differed only in the treatment of the preparations after they had been maintained at T_c for several hours. As indicated in table 1, in one series the preparations were removed after several hours (usually 24 hours) from the T_c bath and allowed to cool to room temperature under ambient conditions, whereas in the other series the mother liquor was exchanged isothermally at T_c with fresh solvent (preheated to T_c, see below) before the preparation was allowed to cool to room temperature under ambient conditions, the purpose of this exchange being to eliminate polymer which may have remained in solution at T_c and thus to prevent any further crys-

TABLE 1. *Summary of crystallization procedure*

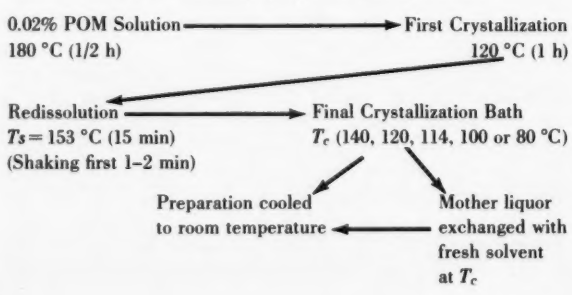

[6] Trade names identified in this paper are given solely for indicating the source and type of materials or instruments used. This in no way implies endorsement or recommendation by the National Bureau of Standards.

tallization during the final cooling of the preparation to room temperature. The exchange of the mother liquor with fresh solvent was carried out as follows using a filtration vessel akin in design to one previously described by Bassett and Keller [11]: Each preparation was rapidly transferred from the bath at T_c and poured into the isothermally controlled filtration vessel maintained at T_c, this was followed by alternate filtration and addition of fresh preheated (to T_c) orthodichlorobenzene to the suspension of crystals, care being taken to ensure that the crystals were continuously immersed in liquid and not allowed to dry and form a mat between successive additions of fresh solvent to the suspension. Three exchanges of the liquid medium were carried out in each instance. After a final addition of fresh solvent to the suspension of crystals, the filtration vessel containing the latter suspension was allowed to cool to room temperature.

2.2. Microscopy

(i) Optical Microscopy

The "uncollapsed" shapes of the crystals were examined by observing them as they tumbled or were induced to tumble slowly while in suspension in liquid at room temperature under a microscope using phase contrast optics. Glass slides having a shallow central well in which droplets containing crystals in suspension were deposited, were used for this purpose. Because of the close match between the refractive indices of orthodichlorobenzene and POM,[7] the crystals were only faintly perceptible in the latter medium. In order to distinctly perceive and examine the conformations of the crystals the orthodichlorobenzene in which they were in suspension was diluted with compatible liquids having appreciably higher or lower refractive indices. These liquids were added to the suspension of crystals in orthodichlorobenzene previously placed in the well of the slide, and the well was then covered with a thin coverglass. Several liquids covering a range of refractive indices were used including ethyl alcohol (refractive index $n_D = 1.3611$ at 20°C [12] and methylene iodide $n_D = 1.7559$ at 10°C [12]). Dilution with the latter liquid was found most convenient for recording and exhibiting the conformational characteristics of the crystals photographically. The optical micrographs shown in Section 3 depict the crystals in suspension in orthodichlorobenzene diluted with methylene iodide.[8]

(ii) Electron Microscopy

For the examination of the crystals in the electron microscope droplets of each preparation containing crystals in suspension in orthodichlorobenzene were deposited on electron microscope grids covered with a thin carbon film. The solvent was allowed to evaporate at room temperature after which the dried crystals were either examined as such in the electron microscope or were first shadowed with a platinum-palladium alloy (80% Pt/20% Pd). The electron microscope used in this study was a JEM 6a[6] which was operated at 80 Kv using the double condenser system.

POM undergoes molecular scission and decomposes into volatile products upon irradiation with an electron beam. Individual unshadowed crystals have been observed to vanish completely within a very short period after exposure to the electron beam at the operating intensities normally used for clear visual observation of the images on the fluorescent screen of the electron microscope [5]. Shadowed crystals undergo similar decomposition, but the disposition of the shadowing metal about each crystal before irradiation remains unchanged however after the polymer has been volatilized and one is left with a direct replica of the lateral profile and topography of the original crystal as deposited on the carbon substrate [4]. Figures 5, 13, 19, 20, 21, 38 in Section 3 are such "replicas". The remaining bright-field or dark-field electron micrographs of shadowed or unshadowed crystals shown in Section 3 were recorded at very low beam intensities. Under these conditions the crystals and their diffraction contrast characteristics were preserved long enough (a few minutes) for their images to be recorded photographically. The bright field images were recorded using an objective aperture which passed the central beam and masked all the $\{hki0\}$ diffraction spots at the back focal plane of the objective lens.

3. Observations on the Morphologies of Polyoxymethylene Crystals

3.1. General

A description is presented in ensuing subsections of the outcome of a combined optical and electron microscopical examination of the habits exhibited by the lamellar crystals of POM grown from the solutions prepared in the manner described in Section 2.1 when these solutions were transferred to baths held at one of the following temperatures, namely $T_c° = 140$, 120, 114, 100, and 80 °C. By way of a brief introduction, which serves to set the body of morphological data derived from the present study in perspective relative to the previous studies summarized in Section 1, it may be pointed out in anticipation of Sections 3.2 to 3.4 that the lateral modes of propagation of the lamellar crystals formed in the various preparations examined in the present study varied as follows: At $T_c = 140$ °C the lamellae were six-sectored and exhibited the familiar hexagonal habit depicted in figure 1a; at $T_c = 120$ °C lamellar crystals exhibiting an SS mode

[7] The refractive index of orthodichlorobenzene is $n_D = 1.5485$ at 20 °C [12]. The following values have been reported by Jaffe and Wunderlich [13] for the refractive indices of light vibrating parallel to and perpendicular to the fiber axis in POM fibers produced by polymerizing trioxane in the solid state: $n_{\parallel} = 1.553$ (highest value observed) and $n_{\perp} = 1.489$; $\bar{n} = (2n_{\perp} + n_{\parallel})/3 = 1.510$. It is not our intention to dwell here on the extensive literature concerning the nature of the orientation of the chain molecules in the fibrous products of the solid state polymerization of trioxane. It may be pointed out that preferential orientation of the chain molecules parallel to the fiber axis in the "extended chain crystal" samples used for the above mentioned refractive index measurements [13] is indicated by the fact that $n_{\parallel} > n_{\perp}$. It should however be noted in this connection that instances of the occurrence of pseudo-twinned and/or twinned regions (differentiated as W "twinned" and T twinned respectively by Colson and Reneker [14]), within which the orientation of the chain molecules deviates from the fiber axis direction in the constituent fibrous products of the solid state polymerization of trioxane, have been observed by means of electron diffraction [7, 14]. An extensive bibliography and discussion of this topic may be found in a recently reported investigation [14].

[8] The methylene iodide used was supplied by the manufacturer with copper metal immersed in the liquid to enhance its stability.

of lateral propagation akin to that illustrated in figure 1b were formed; in the case of the $T_c = 114$°C preparations, SD lamellar crystals exhibiting a dendritic lateral habit akin to that shown in figure 1d were formed, whereas in the case of the $T_c = 100$ and 80 °C preparations dendritic crystals were formed whose lateral growth involved the generation of new sectored outgrowths about the entire periphery of the basal lamella.

3.2. Crystals Formed at $T_c = 140$ °C

(i) Preliminary Comments

At this temperature individual preparations yielded both the familiar monolayered six-sectored lamellar crystals bound laterally by $\{10\bar{1}0\}$ growth faces as well as multilayered crystals whose constituent lamellae were also six-sectored and bound laterally by $\{10\bar{1}0\}$ faces. Apart from some negligible effects associated with the different after-treatment procedures to which the preparations were subjected after crystallization at 140 °C, the populations of monolayered and multilayered crystals formed in different $T_c = 140$ °C preparations were indistinguishable from one another insofar as the habits of the crystals were concerned.

Observations concerning some effects associated with the two after-treatment procedures to which the preparations were subjected after having been maintained at $T_c = 140$ °C for 24 hours will first be presented below. This will be followed by a consideration of observations pertaining to the conformation of monolayered crystals, after which salient characteristics exhibited by multilayered crystals will be described.

(ii) Effects Associated With the Different After-Treatment Procedures to Which the Preparations Were Subjected

In the case of preparations which had been kept at 140 °C for 24 hours and were then removed from the crystallization bath and allowed to cool to room temperature under ambient conditions, an examination of the crystals in the electron microscope revealed that the lamellae were bordered laterally by a very narrow strip which was thinner than the interior of the lamellae indicating that it resulted from further growth which the crystals underwent upon cooling to room temperature due to crystallization of polymer which had remained in solution in the mother liquor at 140 °C. The occurrence of this additional growth upon cooling the $T_c = 140$ °C preparations without filtration is illustrated in figure 2. A view of a hexagonal monolayer crystal formed in such a preparation is shown in figure 2a. A view at higher magnification of the lower right hand corner of the same crystal is shown in figure 2b in which a thinner outer strip bordering the periphery of the crystal may be discerned (see barbed arrow). Evidently the extent of the additional lateral growth represented by this strip is minimal compared to the lateral dimensions attained by the crystal at 140 °C.

In the case of preparations which were subjected, at 140 °C, to the filtration and dilution (washing) procedure described in Section 2.1, the effect was that in addition to eliminating polymer which had remained in solution in the mother liquor at 140 °C, this procedure caused a very mild and interestingly selective etching of the chain-folded lamellae. Although barely perceptible in low magnification electron micrographs such as those of the crystals shown in figure 3 and figure 4 this etching is clearly seen at high magnifications as illustrated in figure 5 in which portions of two contiguous sides of a monolayered crystal and portions of the corresponding adjoining sectors which they subtend are shown. The crystal from which this micrograph was obtained had been shadowed before it was exposed to the electron beam. The barbed arrow in figure 5 points in the direction of shadowing. The micrograph was recorded after the polymer had "vaporized" under the influence of the electron beam leaving behind an exact replica (see Section 2.1) of the original crystal. The occurrence of minute voids (see unbarbed arrows)[9] resulting from the selective etching of polymer in the interior of the lamella during filtration and washing can be readily discerned in figure 5. These voids which are apparently randomly dispersed about the interior of the lamella are characteristically longer than they are wide. The lengths

[9] Note that the elongated features (voids) pointed to by the unbarbed arrows are distinctly lighter (absence of evaporated metal) on the side closest to the origin of shadowing and much darker (accumulation of metal) on the side further away from the origin of shadowing; this clearly indicates that these features are voids and not ridges.

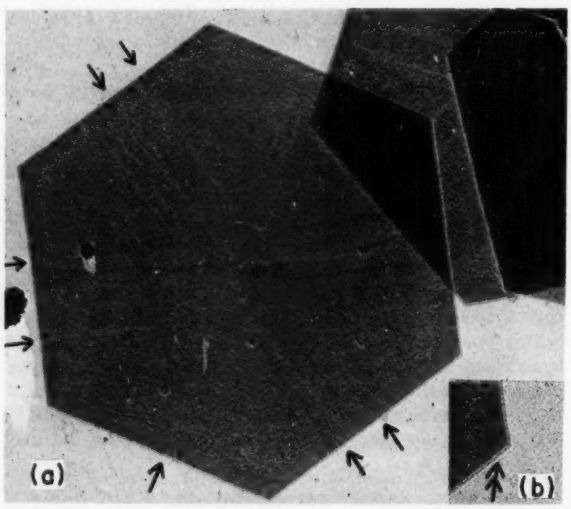

FIGURE 2. *(a) Electron micrograph of a monolayer crystal formed in a $T_c = 140$ °C preparation which had not been subjected to filtration and washing at 140 °C prior to cooling to room temperature.*

Unbarbed arrows point to streaks running at right angles to outer edges of the crystal (see text, section 3.2 (iii)). Pt/Pd shadowed. X3500.

(b) A view at higher magnification of lower right hand corner of the same crystal showing thin outer strip (see barbed arrow) formed upon cooling preparation to room temperature.

Pt/Pd shadowed. X6900.

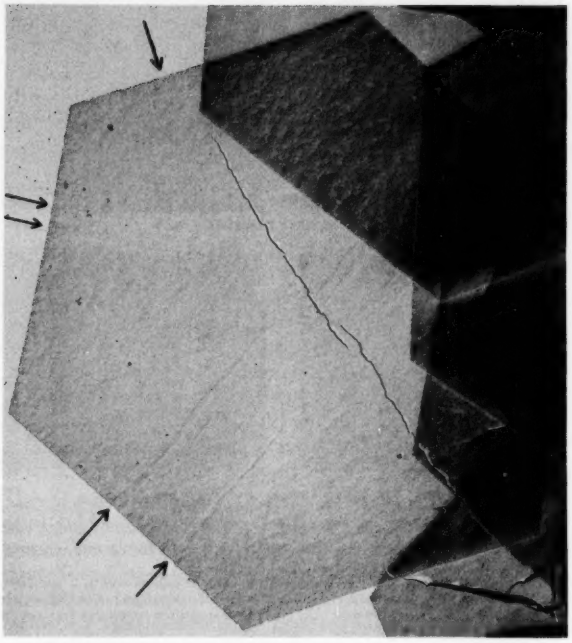

FIGURE 3. *Electron micrograph of a monolayer crystal formed in a $T_c = 140\,°C$ preparation which had been subjected to filtration and washing at 140 °C prior to cooling to room temperature.*

Arrows point to streaks running at right angles to the outer edges of the crystal (see text sec. 3.2 (iii)). Pt/Pd shadowed. X4300.

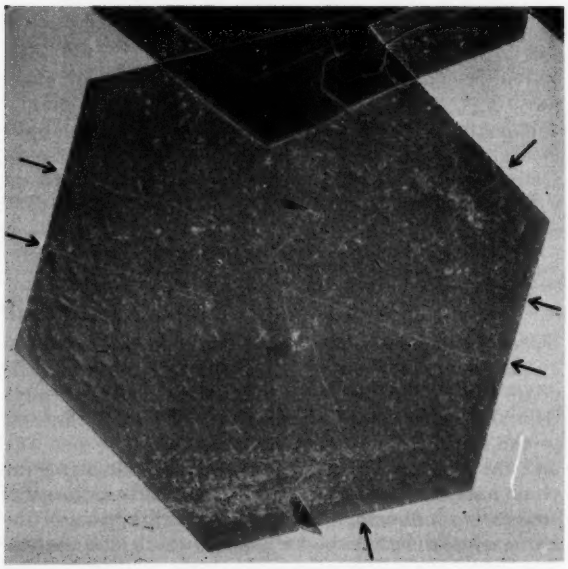

FIGURE 4. *Electron micrograph of a monolayer crystal formed in a $T_c = 140\,°C$ preparation which had been subjected to filtration and washing at 140 °C prior to cooling to room temperature.*

Arrows point to streaks running at right angles to the outer edges of the crystal (see text. sec. 3.2 (iii)). Pt/Pd shadowed. X4000.

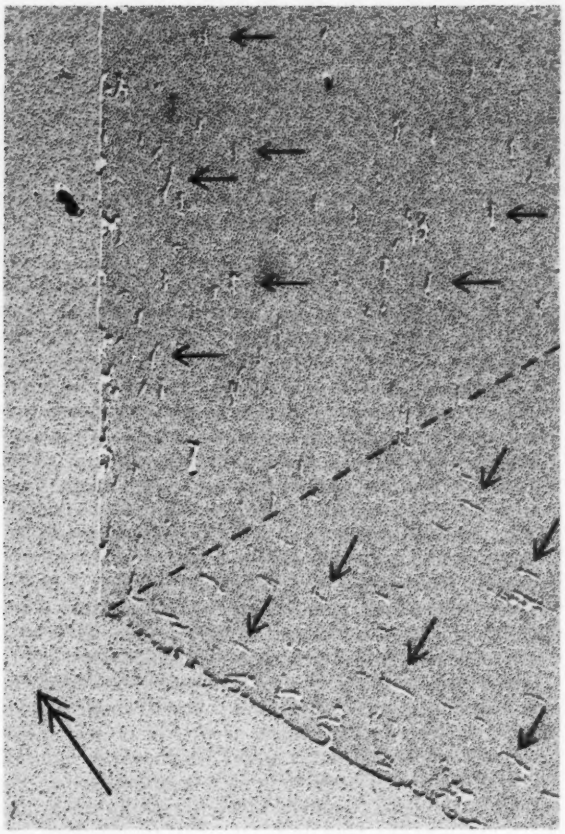

FIGURE 5. *Electron micrograph of a corner and adjoining portions of a six-sectored monolayered crystal formed in a $T_c = 140\,°C$ preparation which had been subjected to filtration and washing at 140 °C prior to cooling to room temperature.*

This image of a shadowed crystal was recorded after the polymer had vaporized under the influence of the electron beam. Dashed line denotes boundary between the adjoining pair of sectors subtended by the two contiguous $\{10\bar{1}0\}$ crystal edges portions of which are visible in the field of view. Barbed arrow denotes direction of shadowing. Unbarbed arrows in the interior of each sector point to some of the numerous elongated voids which are oriented with their longer dimension preferentially parallel to the outer $\{10\bar{1}0\}$ edge which subtends the particular sector in which they are situated. Pt/Pd shadowed. X33700.

of the discernible voids in figure 5 vary in the range 0.03 μm to 0.16 μm and they are approximately 0.016 μm wide. In addition, as may be seen from a consideration of the voids situated on opposite sides of the dotted line (which corresponds to the sector boundary) in figure 5, the voids are characteristically oriented with their longer dimension preferentially parallel to the outer edge ($\{10\bar{1}0\}$ growth face) which subtends the particular sector in which they are situated, thus attesting to the preferential etching of polymer in a direction parallel to the $\{10\bar{1}0\}$ planes along which the chain molecules are folded in each sector. This directionally selective etching in the constituent sectors is certainly consistent with the six-sectored nature of these hexagonal-shaped lamellae of POM, indeed it provides in itself further substantiation that such lamellae consist of six distinguishable fold domains.

The nature of the dispersed sites at which this selective etching occurs preferentially in each sector remains undetermined at present. Finally, as may also be seen in figure 5, the slightly "nibbled" appearance exhibited by the otherwise straight lateral edges of the lamella indicates that some etching also occurred at its periphery during filtration and washing.

(iii) Observations Pertaining to the Conformation of the Hexagonal Shaped Monolayered Crystals

A description will first be presented in this section of the outcome of a direct examination of the conformation of the crystals in suspension in liquid as seen under the optical microscope. The observations derived from this optical microscopical study will then be considered in the light of the various views, summarized in Section 1, which have been previously advanced concerning the possible origins of the nonplanar character of six-sectored lamellae of POM. Some conclusions concerning both the origins and nature of the nonplanar character of the crystals obtained in the present study will be subsequently advanced and discussed in association with various features exhibited by the crystals in the electron microscope. These latter features, which bear on the nonplanar character of the crystals, have been variously observed in different previous studies [4–8].

Four optical phase contrast micrographs representing different views of a monolayered single crystal (same unfiltered preparation as that of crystal shown in fig. 2) in suspension in liquid are shown in figure 6. Figures 6a to 6d were recorded sequentially as the crystal tumbled extremely slowly in the liquid. Figure 6a represents the lamella as viewed edge-on, i.e., with its central axis of six-fold symmetry lying parallel to the field of view, whereas in figure 6d this central axis is oriented at right angles to the field of view. Figures 6b and 6c show the same crystal at successive stages in its change in orientation from that shown in figure 6a to that shown in figure 6d. An edge-on view of a monolayered crystal from a filtered preparation (same preparation as the crystals in figs. 3, 4) is shown in figure 7.

Figures 6a and 7 serve to illustrate a characteristic feature of the hexagonal shaped monolayered crystals formed at $T_c = 140$ °C. namely they exhibit an essentially linear profile when viewed edge-on,[10] thus indicating that any departure from planarity in the shape of these crystals is only slight. The problem is how slight? Previous views which have been advanced concerning the possible origins of the nonplanar character of hexagonal six-sectored lamellae of POM provide a framework of reference which serves as a basis for discussing this problem in comparative terms.

One possible source of nonplanarity which may be envisaged [4–7] is that the folds in successive $\{10\bar{1}0\}_f$ planes in each sector might be regularly staggered in a direction parallel to the c axis. The following considerations may be raised regarding this suggestion. One chain in a 29/16 helical conformation passes through the metrically hexagonal unit cell of POM, the axis of the helix is parallel to the c axis of the unit cell and the repeat distance per monomer unit along the chain axis is 1.93 Å [9]. The oxygen (or carbon) atoms of successive monomer units in the helical chains of the POM crystal lattice lie in planes which are perpendicular to the c-crystallographic axis and are spaced 1.93 Å apart in that direction. This feature restricts the magnitude of the regular stagger (if it did occur) between successive $\{10\bar{1}0\}_f$ planes in the constituent fold domains of six-sectored lamellae to a distance corresponding to the repeat distance of one monomer

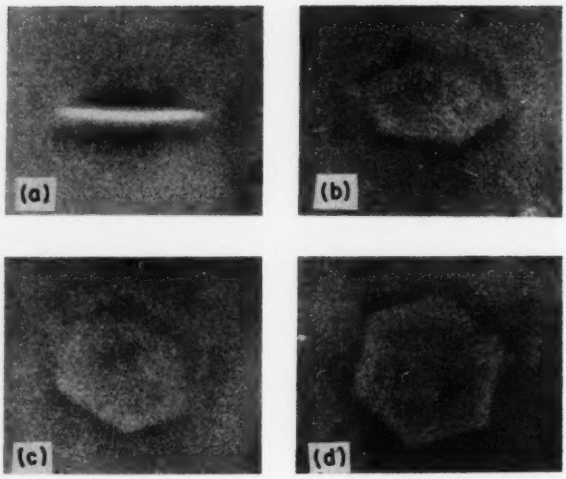

FIGURE 6. *Sequence of optical micrographs of a monolayered lamellar crystal formed in a $T_c = 140$ °C preparation which had not been filtered and washed prior to cooling to room temperature.*

The crystal is depicted as seen consecutively in different perspectives as it was slowly tumbling while in suspension in liquid. (a) and (d) show the crystal as viewed edge-on and flat-on respectively; (b) and (c) depict the crystal at intermediate inclinations between the extremes shown in (a) and (b). Phase Contrast. X1300.

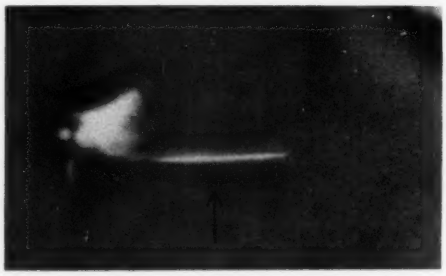

FIGURE 7. *Optical micrograph showing an edge-on view of a monolayered lamellar crystal (arrow) formed in a $T_c = 140$ °C preparation which had been filtered and washed prior to cooling to room temperature.*

The crystal is in suspension in liquid. The structure on the left hand side of the micrograph is a complex multilayered crystal (see sec. 3.2 (iv)) situated at a different level in the liquid. Phase Contrast. X1000.

[10] It is noteworthy that this feature is exhibited by the monolayered crystals from both filtered and unfiltered preparations. In short, the mild etching which occurred in the lamellae formed in the preparations which had been subjected to a final filtration and washing procedure at 140 °C did not apparently affect the conformation of the lamellae.

unit in the c axis direction, i.e., 1.93 Å, or to whole number multiples thereof. It may be readily calculated that if a regular stagger of 1.93 Å between the folds in successive $\{10\bar{1}0\}_f$ planes (whose interplanar spacing is 3.87 Å) in each sector did occur a hexagonal based hollow pyramidal crystal having an angle of elevation of 26.5° (the angle between the base and the line joining the apex of the pyramid to the midpoint of one of its basal edges) would result. The essentially linear profile which the monolayered six-sectored crystals formed in the $T_c = 140$ °C preparations exhibit when viewed edge-on as shown in figures 6–7 argues against the incidence of such regular fold staggering in these crystals.

The other cause of nonplanarity which has been proposed is that six-sectored lamellae buckle slightly under the influence of stresses which result from the accommodation across fold domain boundaries of the asymmetric distortion of the POM unit cell which occurs, as shown by Bassett [5], in each fold domain. The observations and views of Bassett [5] and Bassett et al. [6] concerning this matter have been summarized briefly in Section 1. They bear to be reiterated and considered in somewhat more detail at this juncture. The basic feature of interest in this connection is the following fact derived by Bassett [5] from an analysis of Moiré patterns exhibited by bilayered crystals of POM, namely that the spacing between the $\{10\bar{1}0\}_f$ planes differs by approximately 0.32 percent from the spacing between the $\{10\bar{1}0\}_{nf}$ planes in each fold domain in six-sectored chain folded lamellae of POM. As a result of this distortion of the subcell in each domain, which distortion has been attributed to an asymmetric bulkiness of the chain folds, there results a lattice mismatch across the boundaries between adjacent fold domains in the lamella [5]. It was suggested that stresses resulting from the accommotion of this mismatch at the fold domain boundaries cause the lamella to buckle slightly. The following considerations pertaining to nature and magnitude of such buckling may be advanced.

It is not possible to distinguish between whether $d_{\{10\bar{1}0\}_f} > d_{\{10\bar{1}0\}_{nf}}$ or vice versa from Moiré patterns [5]. All that can be derived from the Moiré patterns is the magnitude of the difference between $d_{\{10\bar{1}0\}_f}$ and $d_{\{10\bar{1}0\}_{nf}}$, one is therefore faced with two possibilities concerning the inequality between these interplanar spacings. Different conformations which it may be envisaged a six-sectoral lamella of POM might adopt as a consequence of this inequality in interplanar spacings depending on which of the spacings, $d_{\{10\bar{1}0\}_f}$ or $d_{\{10\bar{1}0\}_{nf}}$ is the larger in the fold domains are discussed below with reference to figures 8 to 10.

The dotted lines in figure 8a represent the outline of the periphery and the sector boundaries in an imagined planar six-sectored lamella in which $d_{\{10\bar{1}0\}_f} = d_{\{10\bar{1}0\}_{nf}}$ and in which the stems of the folded molecules are at right angles to the surface of the lamella. It may be calculated that if $d_{\{10\bar{1}0\}_f} > d_{\{10\bar{1}0\}_{nf}}$ by about 0.32 percent then each sector will be expanded in a direction

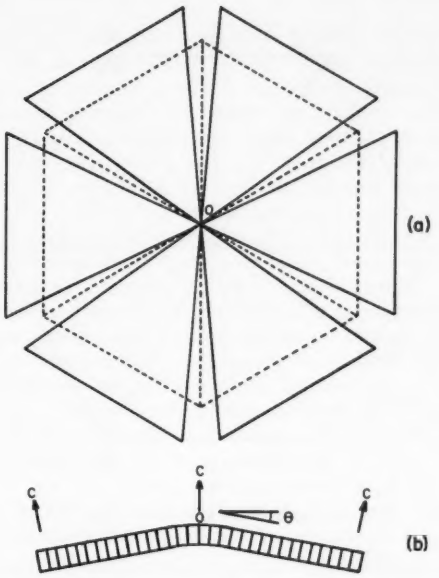

FIGURE 8. *(a) Schematic representation of an idealized six-sectored lamella in which* $d_{\{10\bar{1}0\}_f} = d_{\{10\bar{1}0\}_{nf}}$ *in each sector (– – –), and distorted sectors in which* $d_{\{10\bar{1}0\}_f} > d_{\{10\bar{1}0\}_{nf}}$ (———). *(b) Schematic representation of central cross-sectional view of two opposite sectors in a slightly conical six-sectored lamella.*

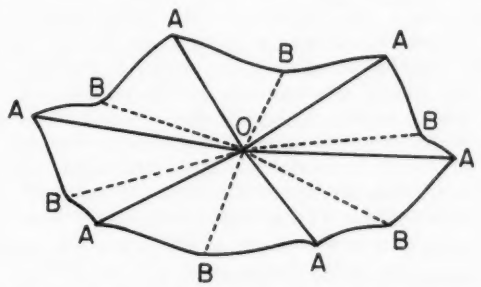

FIGURE 9. *Three dimensional perspective of a possible six-sectored lamella having a six-fold symmetrical wavy conformation resulting from* $d_{\{10\bar{1}0\}_f} < d_{\{10\bar{1}0\}_{nf}}$ *in each sector.*

Lettering corresponds to that in figure 10.

normal to its outer edge and that there will be an angular deficit of 12.6′ between each pair of adjacent sectors as shown in exaggerated fashion by the full lines in figure 8a. A reconstruction of the lamella from the distorted sectors such that there be continuity between sectors at the center (O) as well as across sector boundaries may be accomplished by simultaneously lifting the sectors out of the plane of the diagram at (O) where they are initially in contact. While this operation brings the sectors in lateral contact with one another, there would result in view of the thickness of the sectors, a V-shaped groove along the sector boundaries if the sectors were kept flat. This feature may be overcome by a bending or buckling of the individual sectors so that contact between

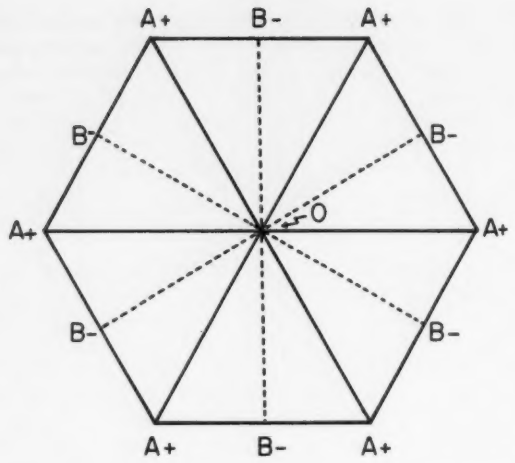

FIGURE 10. *Topographical 'map' of a six-sectored lamella such as that shown in figure 9 as seen along its central axis.*

The center (O) lies in the plane of the diagram whereas the corners (A) and the midpoints (B) lie respectively above (+) and below (−) the plane passing through (O) at right angles to the central axis of the lamella.

adjacent sectors is made throughout their thickness. By the same token continuity between the sectors at the apex (O) would be maintained by a slight bending of the sectors at (O). The gist of these considerations is that if $d_{\{10\bar{1}0\}_f} > d_{\{10\bar{1}0\}_{nf}}$ one might expect the buckled lamella to have an essentially conical shape and be slightly rounded at the apex (O) as shown in figure 8b which represents a cross-sectional view of two opposite sectors in the lamella. It is also envisaged that the stems of the folded molecules are oriented at right angles to the surface of the lamella throughout. Finally, it may be estimated (geometrically) on the basis of the 0.32 percent difference between $d_{\{10\bar{1}0\}_f}$ and $d_{\{10\bar{1}0\}_{nf}}$ that the angle of elevation (θ) of the conical lamella would be about 4.5°.

Turning to the case where $d_{\{10\bar{1}0\}_f} < d_{\{10\bar{1}0\}_{nf}}$ the application of a 0.32 percent difference between these spacings in each sector will result in an excess of 12.6′ from the ideal of 60° in the angle subtended by the outer edge of each sector at the center of the lamella. This angular excess may be accommodated by bending or buckling of the sectors, we can imagine that in this situation the lamella might adopt a six-fold symmetrical wavy conformation such as that illustrated in figure 9, the stems of the folded molecules being normal to the surface of the lamella throughout. A topographical map of such a crystal is depicted in figure 10 which represents a projection of the crystal as seen along its central axis. The lettering in figure 10 corresponds to that in figure 9. The center (O) of the crystal lies in the plane of the diagram. The plus and minus signs in figure 10 which are assigned to the corners (A) of the lamella and the midpoints (B) of the outer edges of the sectors respectively, serve to indicate that points (A) lie above and points (B) lie below the plane of the diagram and hence the center (O). It may be estimated (geometrically) that angle of inclination of the line joining AB in each sector relative to the plane of reference passing through the center of the crystal (O) at right angles to its central axis would be approximately 5° and that the angle of inclination of the line joining O to B relative to the same plane of reference would be about 1.5°.

Simplified as the considerations advanced in the preceding two paragraphs may be, it is fairly evident that departures from planarity resulting solely from buckling due to the incidence of an asymmetric distortion of the unit cell in fold domains would be substantially smaller than would be the case if regular fold staggering occurred, and too small to be established unequivocally and determined quantitatively from an examination of the crystals in suspension in liquid under the optical microscope. (Sinuous shapes of greater complexity than those discussed with reference to figure 8 and figures 9 and 10 may also be envisaged).

In summary the optical microscopical observations described above strongly suggest that regular fold staggering did not occur in the monolayered six-sectored crystals formed in the $T_c = 140$ °C preparations in the present study and that, borrowing in part from Bassett [6], any departure from planarity in the crystals is due to slight buckling associated with the asymmetric distortion of the subcell in the fold domains. The fact that the crystals are indeed not planar in their original as-grown state is reflected by several features which they exhibit when examined in the electron microscope. These features are described below where they are discussed (in conjuction with the 'models' depicted in figures 8, 9, and 10).

Faint streaks of varying lengths which run at right angles to the edges of the crystals may be seen in the bright field electron micrographs of the monolayered crystals shown in figure 2 (crystal from an unfiltered preparation) and figures 3 and 4 (crystals from a filtered preparation) in which it may also be seen that these streaks, which are pointed to by unbarbed arrows, are confined within the borders of the constituent sectors in the crystals, i.e., they do not cross over from one sector to an adjacent one, and that furthermore they exhibit either brighter or darker contrast relative to the surrounding portions of the sector in which they are situated. The occurrence of these streaks is a manifestation of diffraction contrast corresponding to variations in the orientation of the stems of the folded molecules (i.e., the c axis of the POM subcell) within the constituent sectors in these sedimented crystals relative to their surface. This latter feature is also evidenced in $\{10\bar{1}0\}$ dark field images obtained from such crystals, as indicated below.

A dark field electron micrograph obtained from a crystal formed in the same unfiltered preparation as that in figure 2 is shown in figure 11a. A diagram of a six-sectored lamella in which the sectors are identified as s_1 to s_6 to correspond to the sectors in the crystal shown in figure 11a, is depicted in figure 11b as an aid to the description of the features exhibited in figure

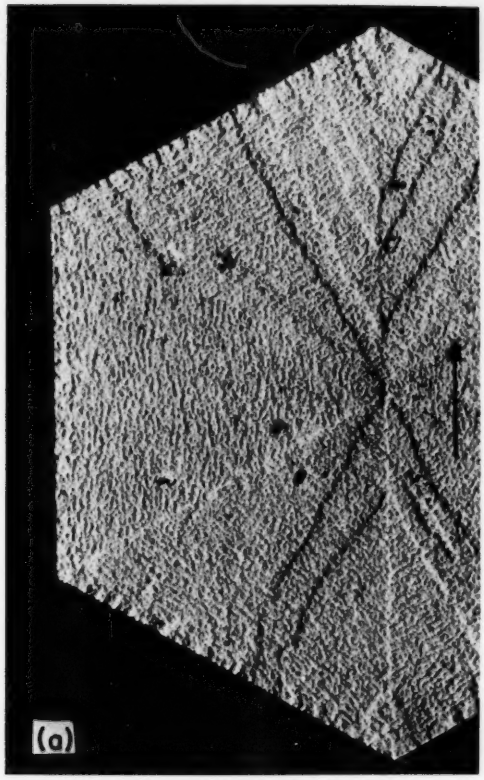

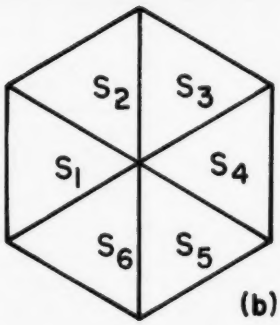

FIGURE 11(a). *{10$\bar{1}$0} dark field electron micrograph of a monolayered crystal formed in a $T_c = 140$ °C preparation which had not been filtered and washed prior to cooling to room temperature.*

This image was formed using the diffraction spot from the {10$\bar{1}$0} planes in the crystal which are parallel to the vertical arrow in the picture; X5300.

(b) Schematic representation of a six-sectored crystal with sectors identified, see text.

11a. The 10$\bar{1}$0 diffraction spot which was used to form the image shown in the latter figure corresponds to the {10$\bar{1}$0} planes in the crystal which run parallel to the vertical arrow shown in figure 11a; these planes are fold planes in sectors s_1 and s_4 but not so in the other four sectors. As may be seen in figure 11a streaks which are either darker or brighter than the overall background intensity exhibited by the crystal and which run at right angles to the crystal edges may be seen in the sectors in which the {10$\bar{1}$0} planes which are imaged are not fold planes (sectors s_2, s_3, s_5, s_6, figure 11b), no such streaks occur however in the two remaining sectors (s_1 and s_4). A similar systematic absence of streaks in the pair of opposite sectors in which the {10$\bar{1}$0} planes which are imaged are the $\{10\bar{1}0\}_f$ planes, which are parallel to the crystal edges which subtend the sectors, has been observed in dark field images by Bassett [5]. On the basis of this systematic absence Bassett [5] and Bassett et al. [6] concluded that the streaks are a consequence of and correspond to the occurrence in each sector of a slight tilting of the crystal lattice relative to the surrounding portions of the sector about an axis normal to the {10$\bar{1}$0} growth face which subtends each sector. The incidence of such localized tilting was considered to occur when the crystals are sedimented and dried on a flat substrate [5, 6] and was adduced as evidence that the crystals are not flat as grown.

It may be noted that apart from the incidence of the aforementioned streaks, short range variations in brightness occur in all the sectors which exhibit as a consequence a somewhat "grainy" appearance as may be seen in figure 11a. It should be borne in mind in this connection that the lamella shown in figure 11a is a crystal from a preparation which had not been filtered and diluted prior to being cooled to room temperature from 140 °C, thus there are no small etched voids in the crystal such as those which occur, as pointed out earlier, in crystals from preparations which had been filtered and diluted at 140 °C. In short, the possibility of artifacts resulting from etching does not arise in connection with above mentioned "granularity" which has also been observed by Garber and Geil [8]. The fact that this feature is also manifested in sector s_1 in which the {10$\bar{1}$0} planes which are imaged are the $\{10\bar{1}0\}_f$ planes which are parallel to the {10$\bar{1}$0} growth face which subtends that sector may be interpreted as indicating that there occur within each sector of the crystal in its sedimented state small short range variations in the orientation of the $\{10\bar{1}0\}_f$ planes relative to the incident beam due to the localized incidence of tilting within each sector about a direction parallel to the corresponding {10$\bar{1}$0} growth face, or at any rate about directions having a component vector parallel to that face. It is not unreasonable to expect that such misorientations would be manifested in a nonplanar crystal when it collapses on a flat substrate. It seems from a close examination of the sectors that the variations in brightness associated with these misorientations do not occur in an entirely random fashion about each sector, rather there is a suggestion that the regions of darker contrast occur as narrow fuzzy lines which traverse each sector along paths (of varying lengths) which meander along a direction parallel to the outer edge of the sector.

In addition to the effects due to diffraction contrast which have been described in the previous three paragraphs, which effects as has been pointed out evidence

in themselves the nonplanar as-grown character of the six-sectored lamellae, this latter feature is further substantiated by the occurrence in some crystals of slight pleats, (such as that which can be seen in the crystal shown in figure 3) resulting from the collapse of the crystals.

In summary we find that whereas the electron microscopical observations indicate that the monolayered six-sectored crystals formed in our $T_c = 140$ °C preparations are not flat as grown, the optical microscopical observations on the crystals (as viewed in suspension in liquid) argue against the incidence of regular fold staggering, and favor the view that the nonplanar character of the crystals is due to slight buckling associated with the asymmetric distortion of the subcell in the fold domains due to the bulkiness of the chain folds. The question as to whether the as-grown shape of the slightly buckled crystals corresponds to or approximates that considered earlier with reference to figure 8 ($d_{\{10\bar{1}0\}_f} > d_{\{10\bar{1}0\}_{nf}}$) or that depicted in figures 9 and 10 ($d_{\{10\bar{1}0\}_f} < d_{\{10\bar{1}0\}_{nf}}$) remains uncertain however. The localized misorientations of the lattice about individual sectors, which misorientations result from tilting either about an axis perpendicular to or an axis parallel to the corresponding $\{10\bar{1}0\}$ growth face (both types of tilt apparently occur), and the incidence of pleating, do not lend themselves to an unequivocal "reconstruction" of the uncollapsed shape of the crystals. The matter of the conformation of these crystals will be referred to again in the general discussion presented in Section 4. It suffices for the present to note that the six-sectored monolayered crystals formed in the $T_c = 140$ °C preparations are not perfectly flat, and that their departure from planarity is apparently only slight and not inconsistent with the possible slightly buckled conformations considered earlier with reference to figures 8–10.

(iv) Multilayered Crystals Formed at $T_c = 140$ °C

As pointed out in Section 3.2 (i) both monolayered crystals such as those described in Section 3.2 (ii) and 3.2 (iii) as well as numerous multilayered crystals whose constituent lamellae are bound laterally by $\{10\bar{1}0\}$ growth faces are formed in individual preparations at $T_c = 140$ °C. The optical and electron micrographs shown in figures 12–15 (filtered preparation) serve to illustrate the diversity in the character of these multilayered crystals which may in essence be divided into two categories, namely, simpler ones whose constituent chain folded lamellae are apparently stacked parallel or essentially parallel to one another, and a variety of more complex ones in which the constituent lamellae are not coplanar. The latter crystals are "axialitic" (see later) in character.

No appreciable splaying is observed between the constituent chain-folded lamellae in the simpler multilayered crystals. When viewed edge-on while in suspension in liquid these crystals exhibit an overall essentially linear profile as may be seen in figure 12. This type of crystal may be identified with crystals (from the same preparation) such as crystal (A) shown in figure 13 which does not exhibit in the sedimented state any pronounced collapse features or deformation, in contrast with crystals (B) and (C) in figure 13 and the crystal shown in figure 14. Crystal (A) in figure 13 is composed of superimposed chain-folded layers which have developed in a spiral-like fashion through the agency of screw dislocations located at or near the center of the basal lamella. It may also be noted that successive layers in the crystal

FIGURE 12. *Optical micrograph showing an edge-on view of a multilayered crystal formed in a* $T_c = 140$ *°C preparation which has been filtered and washed at 140 °C prior to cooling to room temperature.*

The crystal is in suspension in liquid. Phase contrast. X1400.

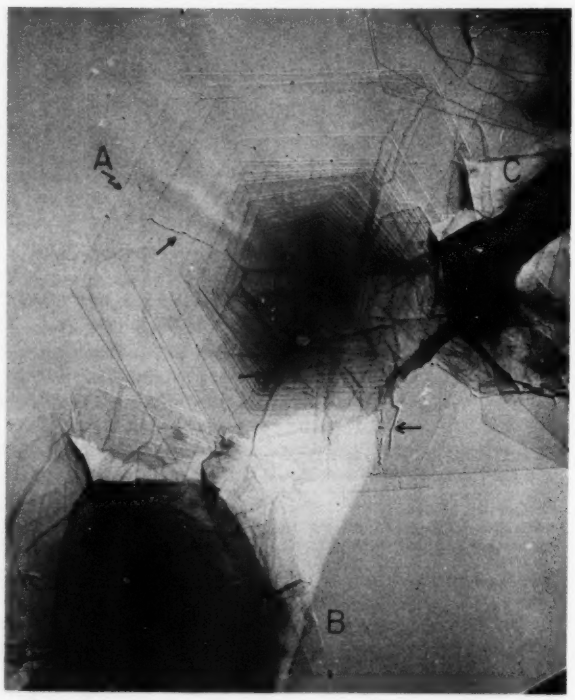

FIGURE 13. *'Replica' of multilayered crystals formed in a* $T_c = 140$ *°C preparation which had been filtered and washed at 140 °C prior to cooling to room temperature.*

Image recorded after prolonged exposure to the electron beam [11], see text. Pt/Pd shadowed, X3200.

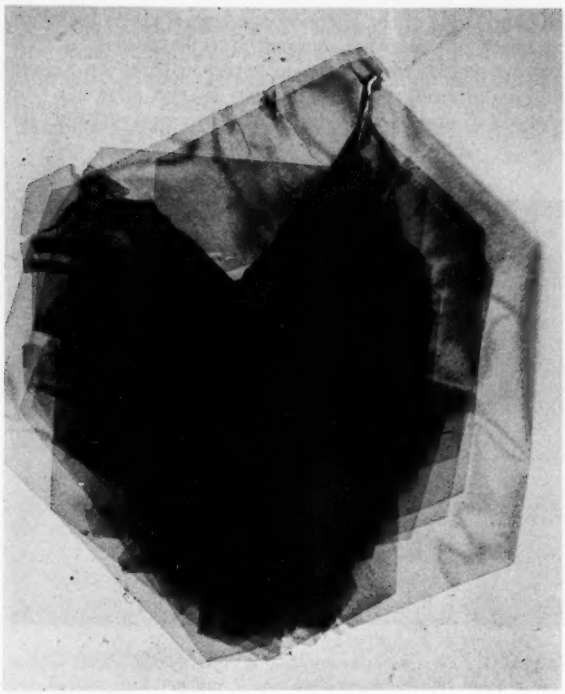

FIGURE 14. *Electron micrograph of a complex multilayered crystal formed in a* $T_c = 140$ *°C preparation which had been filtered and washed prior to cooling at room temperature.*

Pt/Pd shadowed, X4100.

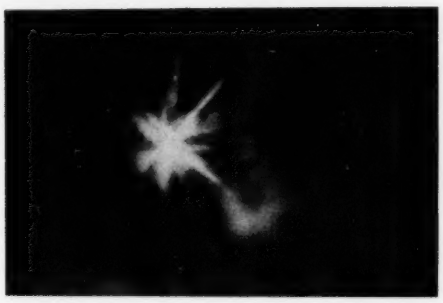

FIGURE 15. *Optical micrograph of complex 'axialitic' multilayered crystal (arrow) formed in a* $T_c = 140$ *°C preparation which had been filtered and washed at 140 °C prior to cooling to room temperature.*

The crystal is in suspension in liquid. Phase contrast, X1000.

are slightly rotated relative to one another about the central axis of the crystal. This feature is not uncommon in multilayered polymer crystals [3, 15]. In addition, slight pleating may be observed (unbarbed arrows) in the interior of crystal (A) which suggests that the crystal was not perfectly planar as grown. In contrast with this latter type of crystal, the central portions of the multilayered crystals (B) and (C) shown in figure 13 and that shown in figure 14 exhibit a highly complex and confused appearance as a consequence of substantial distortions and/or folding which the constituent lamellae (or more accurately some of the lamellae) in these crystals undergo when the crystals collapse upon drying on a flat substrate.[11] These crystals may be identified with the more complex "axialitic" species of crystals which are observed under the optical microscope. Such a crystal in suspension in liquid is shown in figure 15 in which the thin "branches" which extend radially outwards from the center of the object shown therein are lamellae (or stacks of lamellae) which are viewed edge-on or nearly so. Such crystals would be expected to undergo substantial deformations when they collapse upon drying on a substrate.

The nearly planar overall character of the simpler multilayered crystals which exhibit no appreciable splaying between their constituent lamellar layers is consistent with the nearly planar nature of the monolayered crystals (Section 3.2 (iii)) grown in the same preparations. The causes of the wide and variable divergences in orientation (i.e., splaying) among the constituent lamellae in the multilayered "axialitic" crystals we have observed has not been pursued in the present study and remains undetermined. Finally, it should be pointed out that essentially planar as well as "axialitic" multilayered crystals such as those shown above in figures 12–15 were also observed in preparations which had not been subjected to filtration and washing prior to being cooled from $T_c = 140$ °C to room temperature.

3.3 Crystals Formed in Preparations Cooled to $T_c = 120$ °C

The onset of cloudiness and hence crystal growth in these preparations occurred before temperature equilibrium at $T_c = 120$ °C was attained in the solutions following transfer from the T_s bath to the T_c bath. Both six-sectored monolayered crystals as well as multilayered crystals whose constituent terraces were six-sectored were formed in individual preparations. An examination of these crystals in suspension in liquid revealed that, as was the case for $T_c = 140$ °C, the monolayered crystals formed in the $T_c = 120$ °C preparations (both filtered and unfiltered) were essentially planar, i.e., they exhibited an apparently linear profile when viewed edge-on as shown in figure 16. Furthermore, multilayered crystals similar to the different ones (i.e., the nearly planar and the "axialitic" ones) which were observed in the $T_c = 140$ °C preparations were seen under the optical microscope in the $T_c = 120$ °C preparations. The only apparent difference in

[11] The electron micrograph in figure 13 was recorded after prolonged exposure of the crystals to the electron beam. Although the polymer in the outer portions of the crystals had volatilized, and although most of the polymer in the interior of crystal (A) had also volatilized, this was not the case in the central region of crystals (B) and (C) as evidenced by the opacity of the inner portions of these latter crystals which opacity remained indefinitely. Bassett [5] has previously observed that although chain scission resulting in the volatilization of the polymer is the predominant effect of electron irradiation on POM, portions of thicker regions in POM crystals did not volatilize indicating the incidence of cross-linking.

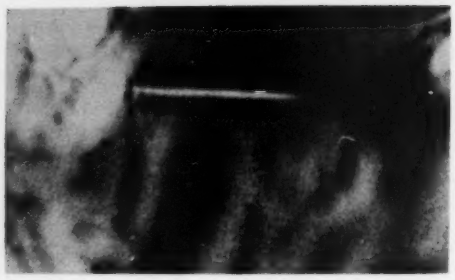

FIGURE 16. *Optical micrograph showing an edge-on view of a monolayered crystal (arrow) formed in a* $T_c = 120$ *°C preparation which had not been filtered and washed prior to cooling to room temperature.*

The crystal is in suspension in liquid. Phase contrast, X1200.

habit between the crystals formed in the $T_c = 120$ °C and those formed in the $T_c = 140$ °C preparations was the fact (which was only detectable in the electron microscope, see below) that the $\{10\bar{1}0\}$ lateral edges of the monolayered crystals as well as the lateral edges of the basal lamella in the multilayered crystals formed in the $T_c = 120$ °C preparations were usually faintly cusped, i.e., slightly concave relative to the interior of the lamellae. This feature which was observed in crystals from both filtered and unfiltered preparations is illustrated and discussed below.

The monolayered crystal shown in figure 17 was formed in a preparation which had not been filtered prior to the final cooling of the preparation to room temperature from 120 °C. The multilayered crystal shown in figure 18 was formed in a preparation which had been subjected to filtration and washing prior to being allowed to cool to room temperature. Although slight, the cusped character of the edges of the lamella shown in figure 17, the edges of the basal layer of the crystal shown in figure 18 and the visible edges shown in figure 19 of lamellae (E) and (F) from a filtered preparation, is nonetheless evident.

One would expect on the basis of the previous studies which were summarized and discussed in Section 1 (with reference to fig. 1) that at a sufficiently high undercooling SS type lamellae such as those shown in figures 16–18 would be formed rather than hexagonal ones. The manifestation of the incipient SS lateral profile illustrated above in lamellae from both the filtered as well as the unfiltered preparations indicates that this feature is a characteristic of the crystals as they grew in the $T_c = 120$ °C bath, and this is confirmed by the ensuing observations. Thus, in addition to eliminating uncrystallized polymer from the preparation, the application of the filtration and washing procedure at 120 °C resulted in a very mild etching of the lamellae, which etching was similar in character to that observed in the lamellae from filtered $T_c = 140$ °C preparations, as illustrated in the "replica" shown in figure 20 in which (G) and (H) are portions of two different partially overlapping lamellae (same preparation as crystals shown in figs. 18 and 19). The portions (JK) and (LM) of the respective edges of these lamellae intersect one another almost at right angles at (N). Narrow voids which are oriented with their longer dimension preferentially parallel to the edge (JK) in crystal (G) and to the edge (LM) in crystal (H) may be

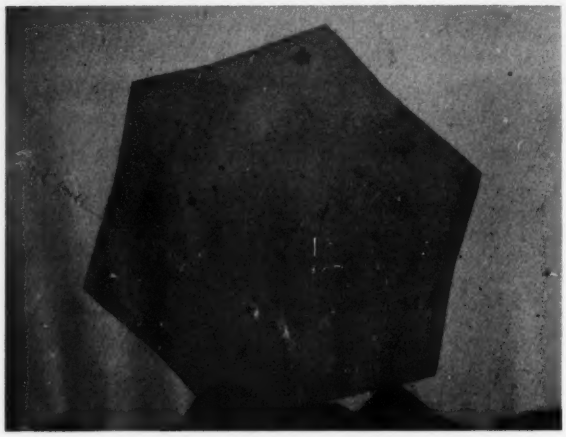

FIGURE 17. *Electron micrograph of a monolayered crystal formed in a* $T_c = 120$ *°C preparation which had not been filtered and washed prior to cooling to room temperature.*

Pt/Pd shadowed, X2800.

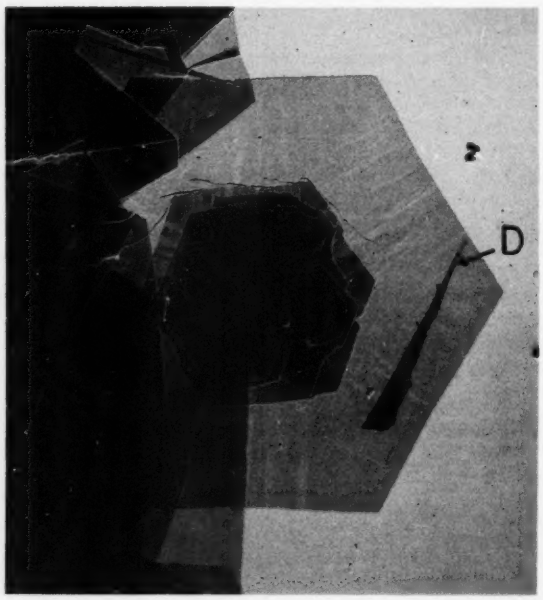

FIGURE 18. *Electron micrograph of a multilayered crystal formed in a* $T_c = 120$ *°C preparation which had been filtered and washed prior to cooling to room temperature.*

(D) is a fragment which had broken off another crystal. Pt/Pd shadowed, X3700.

seen in figure 20 (e.g., see arrows). In addition to this asymmetric etching which follows the orientation of the $\{10\bar{1}0\}_f$ planes along which the chain molecules are folded in the constituent sectors of these six-sectored lamellae, as was the case in the lamellae in the $T_c =$ 140 °C crystals which had been filtered and washed, the nibbled appearance of the edges (JK) and (LM) indicates that some etching has also occurred at the periphery of the lamellae. This latter feature coupled with the incidence of etching in the interior of the lamellae eliminates the possibility that the slightly hexacuspid lateral profile exhibited by the lamellae in the filtered preparation resulted from further growth below 120 °C due to a failure to eliminate uncrystallized polymer prior to cooling to room temperature. It may also be noted that in the case of the unfiltered preparations, a very narrow thinner outer strip was observed bordering the entire periphery of the lamellae. The incidence of this feature, which escapes detection at low magnifications (e.g., fig. 17) in the electron microscope is illustrated in the high magnification "replica" shown in figure 21. While the occurrence of the very narrow thinner outer strip around the entire periphery of the lamellae from the unfiltered preparation clearly indicates that all the polymer had not crystallized even after the preparation had been maintained at 120 °C for 24 hours, it is evident that the width of the strip (which represents the additional growth which the lamellae underwent when the preparation was allowed to cool to room temperature from 120 °C) is minimal, thus further confirming that the hexacuspid character of

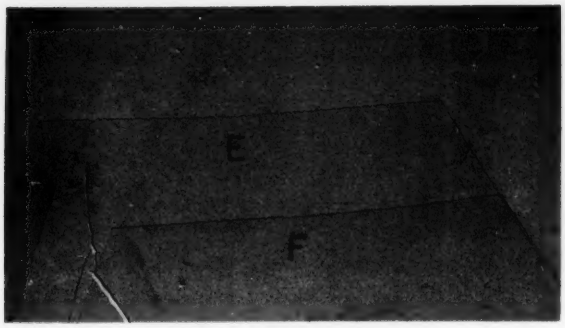

FIGURE 19. *Electron micrograph ('replica') showing edges of two overlapping lamellar crystals (E) and (F) formed in a* $T_c = 120$ *°C preparation which had been filtered and washed at 120 °C prior to cooling to room temperature.*

Pt/Pd shadowed, X5800.

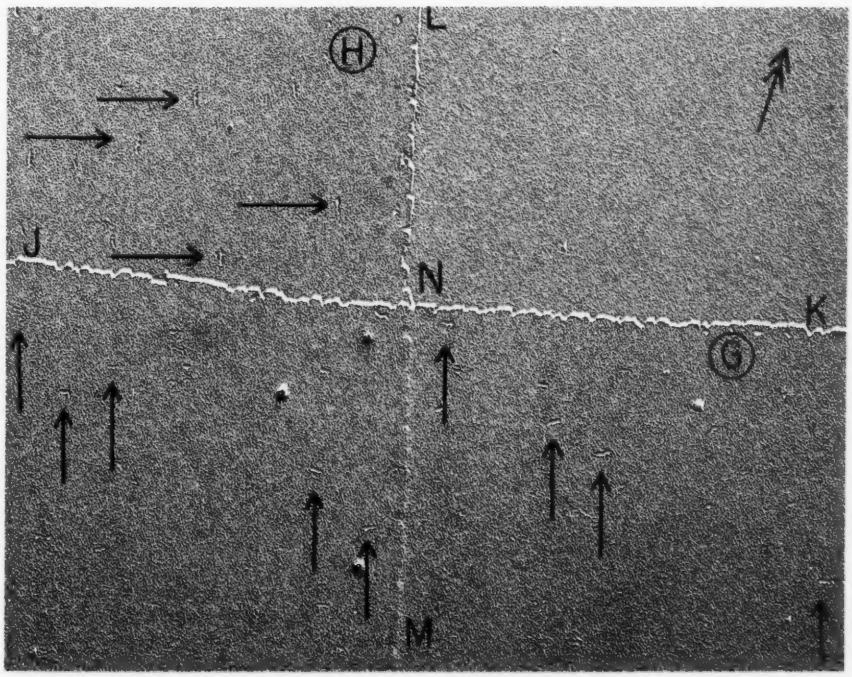

FIGURE 20. *Electron micrograph ('replica') showing portions of two partially overlapping lamellar crystals, (G) and (H) formed in a* $T_c = 120$ *°C preparation which had been filtered and washed at 120 °C prior to cooling to room temperature.*

Lamella (G) lies above lamella (H) in lower left-hand corner of image. Barbed arrow denotes direction of shadowing. Unbarbed arrows point to narrow voids which are oriented with their longer dimension preferentially parallel to side (JK) in lamella (G) and to side (LM) in lamella (H). Pt/Pd shadowed, X29000.

FIGURE 21. *Electron micrograph ('replica') showing a portion of the periphery of a monolayered crystal formed in a* T_c *= 120 °C preparation which had not been filtered and washed at 120 °C prior to cooling to room temperature.*

Arrows point to a thinner narrow strip which borders the periphery of the lamella and which was formed when the preparation cooled from 120 °C to room temperature. Pt/Pd shadowed, X12000.

FIGURE 22. *Electron micrograph of the central portion of a monolayered crystal formed in a* $T_c = 120$ *°C preparation which had not been filtered and washed at 120 °C prior to cooling to room temperature.*

Barbed arrow points to a pleat near the center of the crystal. Unbarbed arrows point in the direction of streaks due to diffraction contrast. Pt/Pd shadowed, X5300.

the lateral profile of the sedimented lamellae, which feature is discernable at low magnifications under the electron microscope (e.g., fig. 17), is not merely a consequence of any additional growth which occurred below 120 °C due to the omission of the filtration procedure.

As was the case for the monolayered crystals formed in the $T_c = 140$ °C preparations, the essentially linear profile exhibited by the incipient SS monolayered crystals formed in the $T_c = 120$ °C preparations when the crystals are viewed edge-on in suspension in liquid argues against the incidence of regular fold staggering in these crystals. These crystals are, however, not perfectly planar, as evidenced by the incidence of pleats in the central region of the lamellae. A view at high magnification of a pleat (barbed arrow) near the center of a monolayered crystal is shown in figure 22, in which the unbarbed arrows point in the direction of faint streaks (due to diffraction contrast) which are of the same kind as those seen in the $T_c = 140$ °C crystals. Such streaks may also be seen (running characteristically at right angles to the edges of the lamellae) in the basal lamella of the multilayered crystal in figure 18. These streaks also attest to the not perfectly planar character of the monolayered SS type lamellae as well as the constituent lamellae in the nonaxialitic multilayered crystals formed in the 120 °C preparations. The departure from planarity in these crystals is however apparently slight as was the case in the monolayered crystals and the nonaxialitic multilayered crystals formed in the $T_c = 140$ °C preparations, and may be attributed to the same causes (i.e., those indicated in Section 3.2 (iii), with reference to figs. 8–10).

3.4. Crystals Formed in Solutions Cooled to $T_c = 114$ °C, $T_c = 100$ °C and $T_c = 80$ °C

(i) General Remarks

As was the case for the $T_c = 120$ °C preparations, the onset of crystallization occurred before temperature equilibrium was attained in the polymer solutions after they were transferred to the baths at $T_c = 114$ °C, $T_c = 100$ °C or $T_c = 80$ °C. It could be readily predicted on the basis of the observations made on the crystals formed in the unfiltered $T_c = 140$ °C and $T_c = 120$ °C preparations that the amount of residual polymer remaining in solution in the $T_c = 114$ °C, 100 °C or 80 °C preparations would be negligible. Crystals formed in preparations which had been subjected to filtration at T_c as well as preparations in which this after-treatment procedure was omitted were examined. In the case of the unfiltered $T_c = 114$ °C preparations further growth upon cooling to room temperature was negligible. No detectable evidence of further growth upon final cooling from T_c to room temperature was observed in crystals formed in the unfiltered $T_c = 100$ °C or the $T_c = 80$ °C preparations. Furthermore, no detectable evidence of any etching was observed in any of the filtered preparations. In short, the characteristics of the habits of the crystals formed in the $T_c = 114$ °C, $T_c = 100$ °C and the $T_c = 80$ °C preparations which are described below are representative of the manner in which the crystals grew in the crystallization baths maintained at T_c.

(ii) Crystals Formed in Solutions Cooled to $T_c = 114$ °C

The crystals formed in the $T_c = 114$ °C preparations exhibited a distinctly dendritic mode of lateral propagation, i.e., their lateral growth habit was akin to the SD habit depicted schematically in figure 1d. An example of the crystals formed in the $T_c = 114$ °C preparations is shown in figure 23 in which the following characteristic features exhibited by these crystals may be noted. The first feature is the overall profile of the basal lamella which is pronouncedly star-like in shape;

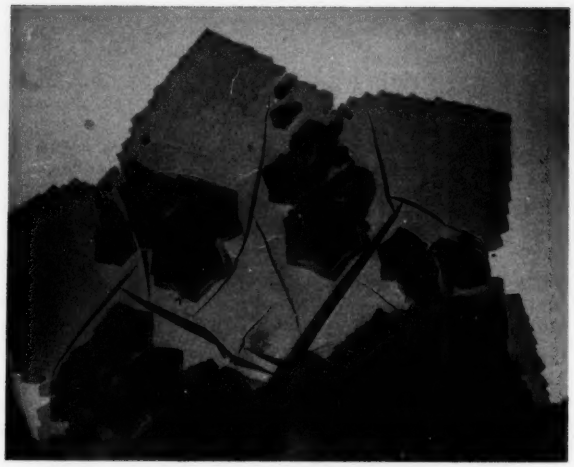

FIGURE 23. *Electron micrograph of a dendritic crystal formed in a* $T_c = 114$ *°C preparation.*

Note the microfaceted character of the edges of the basal lamella, and the pleats in the interior of the crystal. Pt/Pd shadowed, X3100.

this feature contrasts with the hexagonal profile and the incipient hexacuspid profile exhibited by the lamellae we have described in sections 3.2 and 3.3, respectively. The second feature to be noted is the distinctly microfaceted nature of the periphery of the basal lamella. This feature contrasts with the smooth (i.e., no microfaceting observed) lateral edges of the hexagonal and incipiently hexacuspid lamellae formed in the $T_c = 140$ °C and the $T_c = 120$ °C preparations, respectively. The third characteristic is the intermittent incidence of the generation of screw-dislocation-like defects at the periphery of the basal lamella during its outward growth, from which defects additional chain folded terraces develop in spiral-like fashion upon the basal lamella. It may be noted that the generation of these defects, and hence it may be adduced the onset of (SD) lateral growth, occurred after the basal lamella had attained between one third to one half its ultimate maximum outward span. Fourth, numerous pleats which may be readily seen in figure 23 were always observed in the interior of these crystals. The occurrence of these pleats in the crystals as seen lying on a flat substrate suggests in itself that the overall conformation of these cyrstals as-grown is not planar. Indeed, as described below, they exhibit a distinguishably non-planar conformation when viewed in suspension in liquid under the optical microscope.

Two different views of a crystal in suspension in liquid as seen under the optical microscope are shown in figure 24. In figure 24a the crystal is oriented with its central axis of six-fold symmetry slightly inclined with respect to the normal to the field of view. The bright "spots" which may be seen in the interior of the crystal correspond to spiral terraces such as those which may be clearly seen in figure 23. Figure 24b depicts the same crystal as seen edge-on, i.e., with its central axis in the plane of the field of view. The arrow in

FIGURE 24. *Optical micrographs showing two perspectives of a dendritic crystal formed in a* $T_c = 114$ *°C preparation.*

The crystal is in suspension in liquid. (a) Central axis of crystal is slightly inclined with respect to the normal to the field of view. (b) The same crystal oriented as seen edge on, i.e., with its central axis (arrow) in the plane of the field of view. Phase contrast, X500.

figure 24b which points to the pole of the crystal also corresponds in direction to that of the central axis of the crystal. The crystal exhibits an overall appreciably curved profile in this latter perspective suggesting that these crystals possess a dished overall conformation. Their departure from planarity, although still slight in comparison with crystals formed in the $T_c = 100$ °C and $T_c = 80$ °C preparations (see later), is more pronounced than that of the monolayered and non-axialitic multilayered crystals formed in the $T_c = 140$ °C and $T_c = 120$ °C preparations. It may be roughly estimated from their edge-on profile as seen in suspension in liquid that the overall radius of curvature of the crystals such as those shown in figures 23 and 24 is about 20–30 μm.

(iii) Crystals Formed in Solutions Cooled to $T_c = 100$ °C and $T_c = 80$ °C

In addition to the fact that the onset of crystallization occurred well before temperature equilibrium was attained at T_c, the crystallization of the polymer in these preparations was also characterized by the fact that the inception of new crystals occurred over a wide temperature range as the solutions cooled to T_c. The populations of crystals formed in the $T_c = 100$ °C and the $T_c = 80$ °C preparations were very similar to one another in that: (a) they consisted in each case of a mixture of differently curved six-fold symmetrically shaped dendritic chain folded crystals whose lateral dimensions (as measured from pole to periphery) and corresponding conformations (curvatures) varied widely from crystal to crystal over essentially the same range for both $T_c = 100$ °C and $T_c = 80$ °C. and that (b) the lower the temperature at which individual crystals started to grow during the cooling of the solutions to T_c, as evidenced inter alia (see below) by their relatively smaller lateral dimensions, the more pronouncedly curved was their overall conformation.

The phase contrast optical micrographs shown in figures 25 to 27 represent crystals (in suspension in liquid and randomly oriented with respect to the viewing direction) grown in a $T_c = 100$ °C preparation, those shown in figures 28 and 29 represent crystals grown in a $T_c = 80$ °C preparation. Crystal (N) in

530-326 OL - 74 - 2

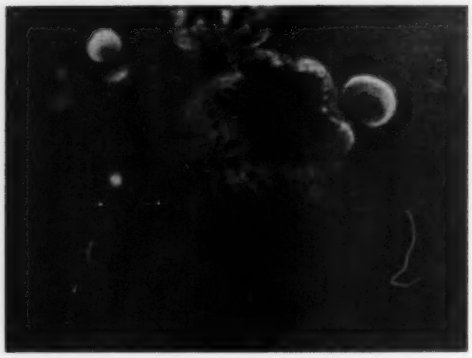

FIGURE 25. *Optical micrograph of crystals formed in a* $T_c = 100$ *°C preparation.*

Crystals are in suspension in liquid. Crystal (N) which is similar to crystal (Q) in figure 28 [12] is representative of the largest and least curved (referring to the overall conformation of the crystal) crystals formed in the $T_c = 100$ °C preparations. Phase contrast, X825.

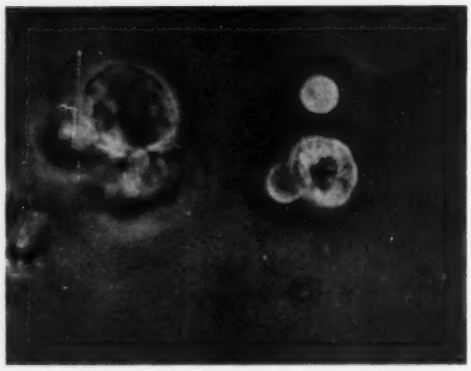

FIGURE 26. *Optical micrograph of crystals formed in a* $T_c = 100$ *°C preparation.*

Crystals are in suspension in liquid, see text. Phase contrast, X825.

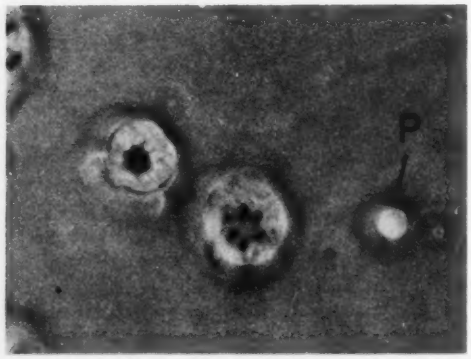

FIGURE 27. *Optical micrograph of crystals formed in a* $T_c = 100$ *°C preparation.*

Crystals are in suspension in liquid, see text. Phase contrast, X825.

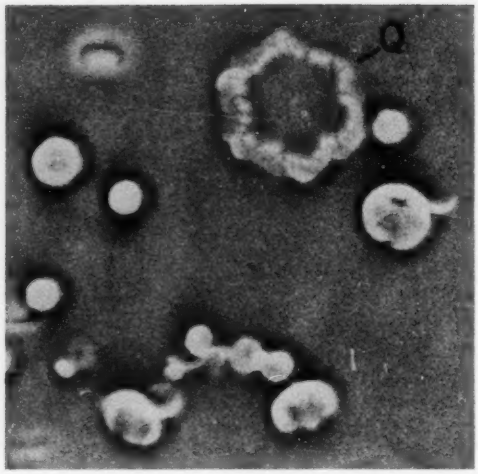

FIGURE 28. *Optical micrograph of crystals formed in a* $T_c = 80$ *°C preparation.*

Crystals are in suspension in liquid. see text. Phase contrast, X825.

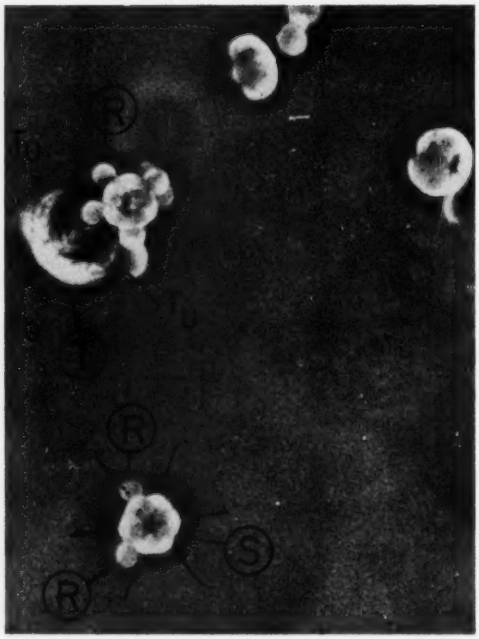

FIGURE 29. *Optical micrograph of crystals formed in a* $T_c = 80$ *°C preparation.*

Crystals are in suspension in liquid. see text. Phase contrast, X825.

figure 25 ($T_c = 100$ °C) and crystal (Q) in figure 28 ($T_c = 80$ °C), which are similar to one another,[12] are representative of the largest and least curved (i.e., their *overall* conformation is least curved) among the

[12] Whereas crystal (Q) in figure 28 is oriented with its central axis very nearly normal to the field of view, the central axis of crystal (N) in figure 25 is distinctly inclined with respect to the viewing direction.

dendritic crystals formed in the $T_c = 100$ °C and the $T_c = 80$ °C preparations respectively, whereas crystal (P) in figure 27 ($T_c = 100$ °C) and crystals (R) in figure 29 ($T_c = 80$ °C) which are hollow bowl-shaped (see below) are representative of the smallest and most pronouncedly curved crystals formed in these preparations. Crystals whose sizes and corresponding overall curvatures fall between the examples identified above of the opposite extremes of the spectrum of differently curved crystals formed in these preparations may also be seen in the fields of view shown in figures 25 to 29.

With the qualified exception of the largest and least curved among the crystals formed in each preparation, i.e., crystals such as (N) in figure 25 and (Q) in figure 28 whose growth spanned the entire temperature range over which crystallization occurred in these preparations and whose overall conformation will be considered later in this section, the remaining more pronouncedly curved crystals formed in the $T_c = 100$ °C and the $T_c = 80$ °C preparations were hollow bowl-like in shape. The diameter of the smallest and most curved among these bowls was 4–5 μm (e.g. crystals R. fig. 29). The overall conformations of these bowls of different sizes were six-fold symmetrical in character as shown schematically in figure 30. Figure 30a represents a bowl as viewed at right angles to its central axis of six-fold symmetry O′O (O is the pole of the crystal), and figure 30b represents the bowl as seen along its central axis in relation to a hexagonal six-sectored precursor (see later). As shown in these diagrams the six-fold symmetrical nature of the overall shape of these hollow bowl-shaped objects, which are in fact variously curved 'six-armed' starlike dendrites, is characterized by six longitudes (OU_{1-6}) along which the growth of the curved lamellar wall has progressed most rapidly, whereas the development of the wall is effectively slower and tapers off symmetrically between the (OU) longitudes. This six-fold symmetrical variation in the development of the constituent curved lamellar wall in those bowls is evidenced under the optical microscope by a corresponding six-fold symmetrical variation in contrast about the outer circular outline of the bowls (with the exception of the smallest and most pronouncedly curved bowls in which this variation in contrast could not be resolved) when they are viewed along their central axis while in suspension in liquid. This feature may be seen most evidently in the appropriately oriented crystal (S) in figure 29 in which the six regions of higher contrast which are pointed to by unbarbed arrows correspond to the hatched regions shown in figure 30b at which regions the projected thickness of the curved lamellar wall in the direction parallel to the central axis of the bowl is effectively greater than elsewhere about its circumference in that projection. As shown schematically in figure 30a the orientation of the surface of the lamellar wall and hence the *c* axis in all these bowls changes through ~ 90° or more on proceeding from the pole (O) to the extremities U_{1-6}. This feature is revealed by examining the crystals at right angles to their central axis as is the case for crystal (T) in figure 29 where the arrows (T_o) and (T_u) are drawn normal to the outer surface of the bowl at its pole and at or very near its rim, respectively. Additional aspects concerning the shapes of the hollow bowl-like crystals of various sizes whose main conformational characteristics have been outlined above, as well as the matter of the conformation of the largest among the crystals formed in these preparations (i.e., crystals such as (N) in fig. 25 and (Q) in fig. 28) which has not been dwelt on so far, will be considered at the end of this section where they will be discussed in connection with the morphological characteristics which the variously curved crystals exhibited in the electron microscope. These latter characteristics which are exemplified in figures 31 to 38 are described below.

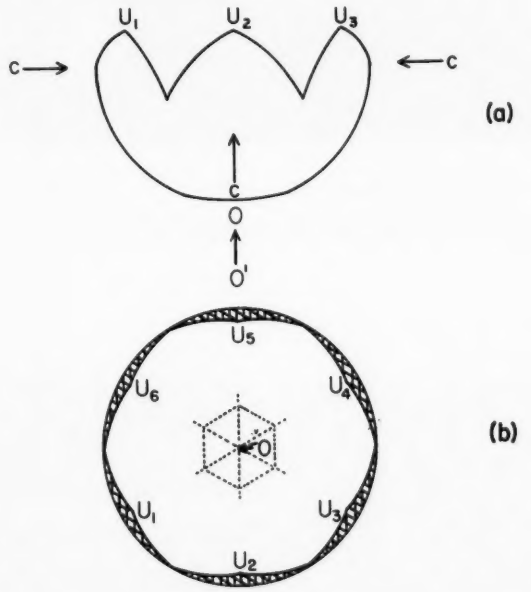

FIGURE 30. *Schematic representation of six-fold symmetrical character of hollow bowl-shaped crystals formed in the* $T_c = 100$ *°C and the* $T_c = 80$ *°C preparations. (a) Side view along a direction normal to the central axis (O′O) of the crystal. (b) A view depicting a bowl as seen along its central axis in relation to a hexagonal six-sectored precursor. The points (U) denote the leading extremities of the bowl in which the orientation of the surface of the crystal and hence the c axis, changes through ~ 90° between the pole (O) and the extremities (U).*

The examples of crystals shown in figures 31 to 37 which have been drawn in part from a $T_c = 100$ °C preparation (figs. 31–34) and in part from a $T_c = 80$ °C preparation (figs. 35–37) are illustrative of the spectrum of crystals of different sizes and curvatures which were formed in both the $T_c = 100$ °C as well as the $T_c = 80$ °C preparations. It may be noted that the crystals from the T_c 100 °C preparation are shown in sequence in figures (31, 32), figure 33, and figure 34 according (broadly speaking) to diminishing actual size, as are in essence the crystals from the 80 °C preparation which

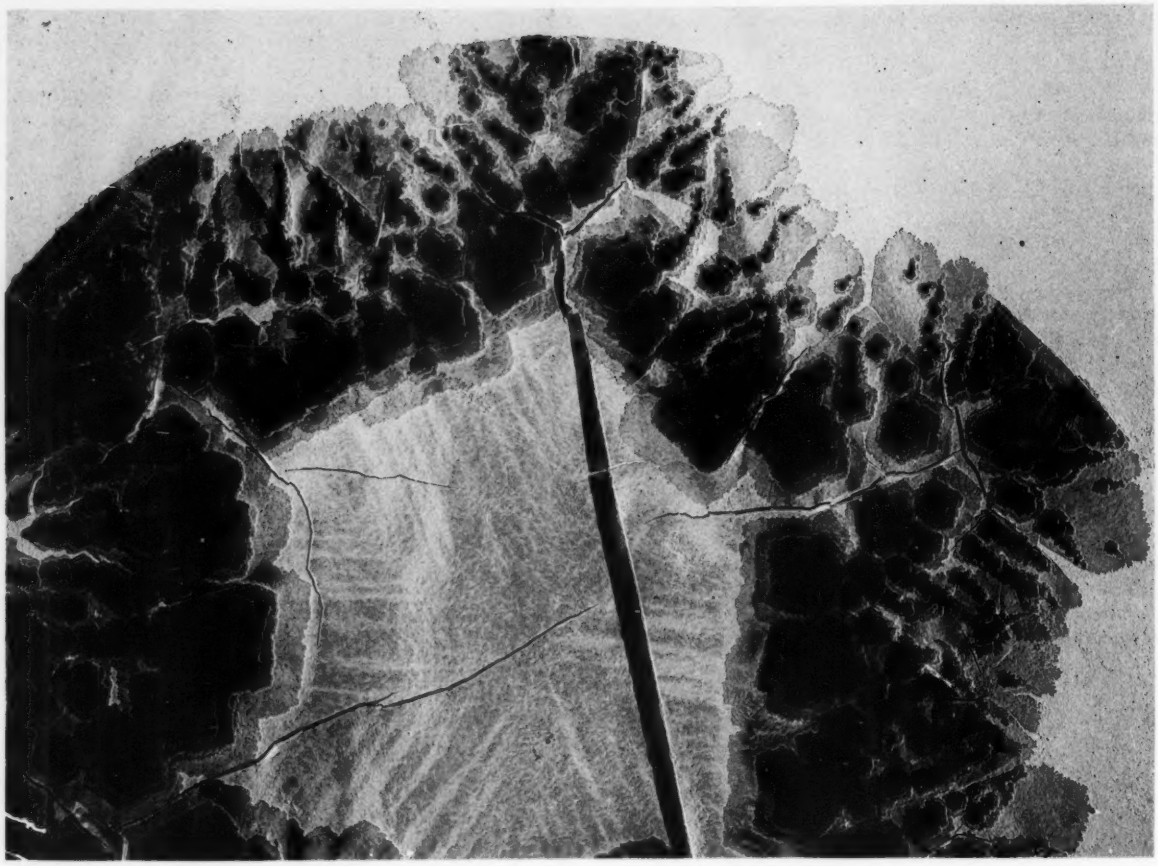

FIGURE 31. *Electron micrograph of a crystal formed in a* $T_c = 100$ *°C preparation; see text.*

Pt/Pd shadowed, X7100.

are shown in figures 35 to 37. The crystals shown in figure 31 and figure 32 are illustrative of the larger species of crystals which were formed in the $T_c = 100$ °C and the $T_c = 80$ °C preparations, i.e., they correspond quite closely to crystals such as crystal (N) in figure 25 ($T_c = 100$ °C) and crystal (Q) in figure 28 ($T_c = 80$ °C). Crystals (X) and (Y) in figure 37 are illustrative of the smaller among the crystals formed in these preparations, i.e., they correspond closely to crystals such as (P) in figure 27 ($T_c = 100$ °C) and (R) in figure 29 ($T_c = 80$ °C). It should be noted that most of the crystals shown in figures 31 to 37 had settled on the carbon film substrate with their central axis normal or preferentially normal to the substrate and subsequently collapsed (were flattened) in that orientation relative to the substrate upon drying, the evident exceptions are: the crystal shown in figure 32, and the two smaller crystals (X) and (Y) in figure 37 all of which settled and were flattened "sideways" upon the substrate, i.e., with their central axis preferentially parallel to the substrate.

It has been pointed out earlier in this paper that dendritic (multisectored) growth in POM chain-folded crystals is characterized (inter alia) by (a) the recurring generation of screw dislocation-like defects at the periphery of the constituent basal (leading) lamella in such crystals and (b) by the formation through the agency of these defects of additional chain-folded terraces which develop in a spiral-like fashion upon the basal lamella. Since these two features, which

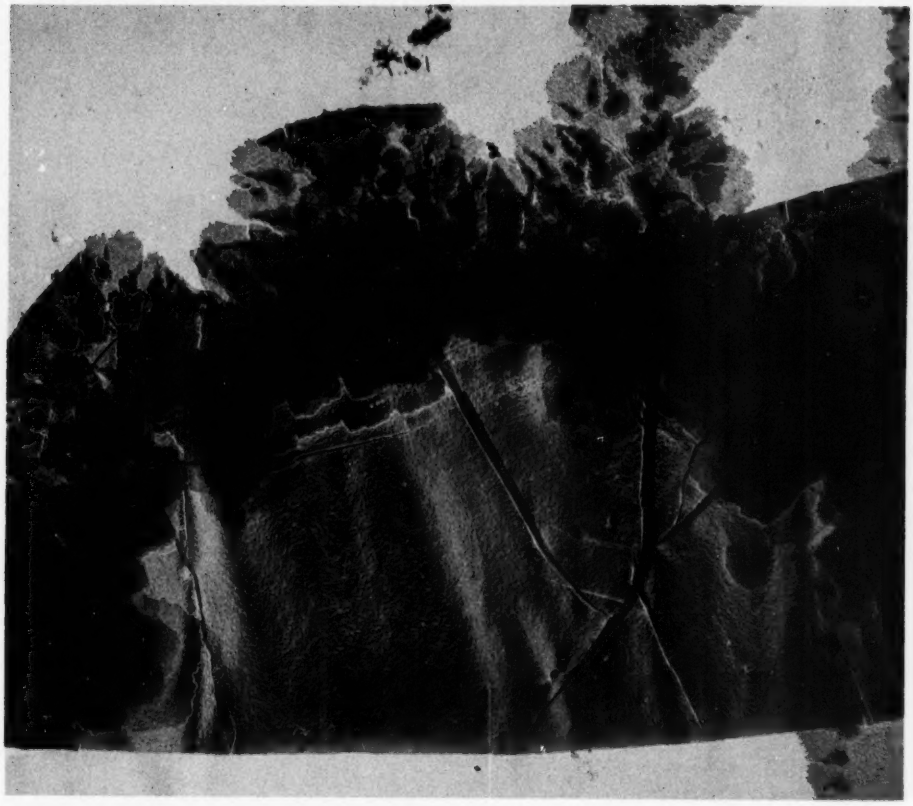

FIGURE 32. *Electron micrograph of a crystal formed in a* $T_c = 100$ *°C preparation.*

This crystal is similar to that shown in figure 31, however, it folded about its diameter when it collapsed upon the substrate; see text. Pt/Pd shadowed. X8300.

occur in association with the incidence of multisectored lateral growth, distinguish the development of dendrites from that of hexagonal six-sectored and SS type lamellae, it is of interest to note, as may be seen from a consideration of the crystals shown in figures 31 and 32, that there is a distinct difference in morphology between the central and outer portions of these examples of the largest among the crystals formed in the $T_c = 100$ °C and the $T_c = 80$ °C preparations. Whereas the inner (central) portion of the basal lamella in these crystals is devoid of spiral terraces, the development of the outer portions of these crystals is characterized by the profuse formation of spiral terraces. The absence of spiral terrace formation in the inner region of these crystals, coupled with the six-fold symmetrical disposition of the streaks due to diffraction contrast which may be readily seen in the central spiral-terrace-free portion of the basal lamella in the crystal shown in figure 31, may be readily adduced as evidence that these largest crystals (see also fig. 32) evolved from an initially formed six-sectored precursor lamella, which continued to grow laterally (during the early stages of the cooling of the solution to T_c) in a six-sectored fashion to an appreciable size (6–7 μm as measured from the origin of the basal lamella to the 'row' of spiral terraces closest to the origin), before it underwent a change in lateral habit to multisectored dendritic growth entailing the generation of screw dislocation-like defects and the evolution of spiral terraces therefrom as the crystal continued to grow at

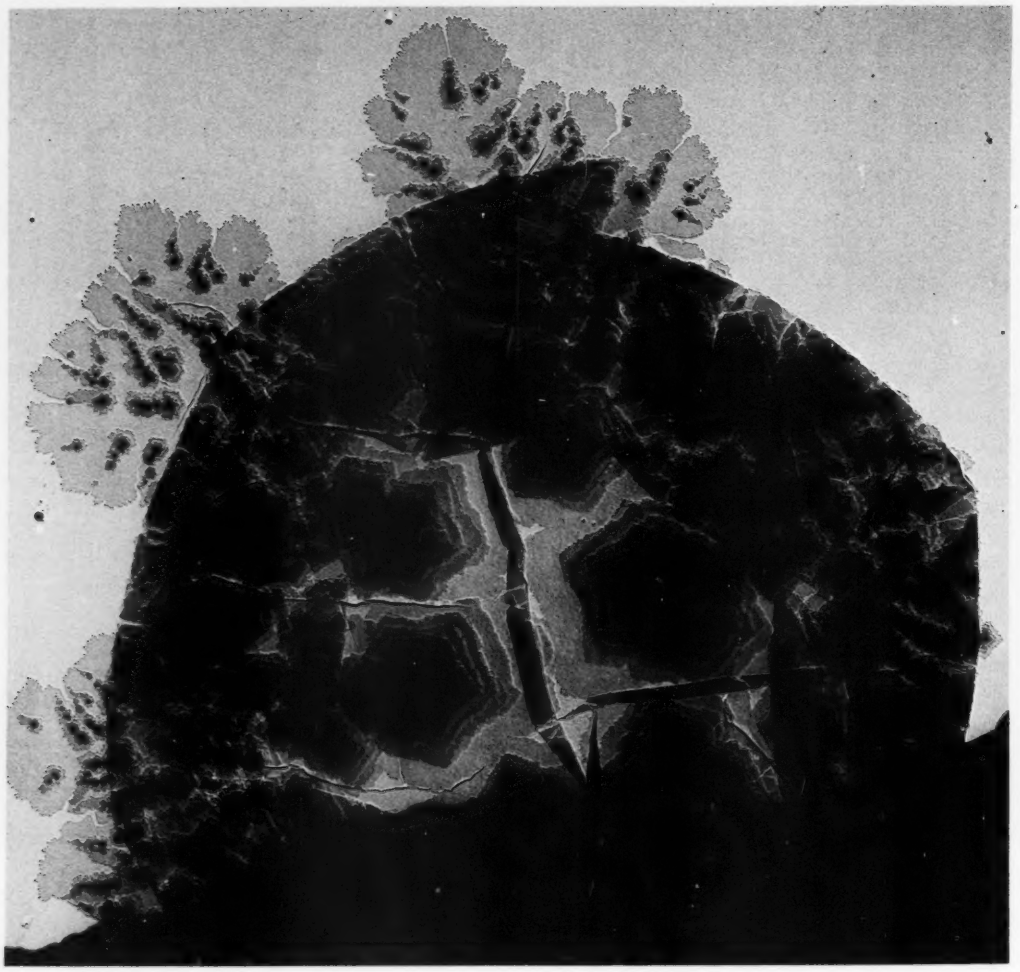

FIGURE 33. *Electron micrograph of a crystal formed in a* $T_c = 100$ *°C preparation; see text.*

Pt/d shadowed. X8500.

lower temperatures. The occurrence of this transformation in lateral habit was not peculiar to these largest crystals whose growth as indicated earlier spanned the entire, or close to the entire temperature range over which crystallization occurred during the cooling of the solutions to T_c. Thus, as may be seen for example from a consideration of the relatively smaller crystals shown in figures 33 to 35, their central or polar portion is also free of active screw-dislocation-like defects. However, as may be judged from the entire series of micrographs shown in figures 31 to 37 the lateral extent of the spiral terrace free polar portion of the basal lamella in the crystals formed in both the $T_c = 100$ °C and the $T_c = 80$ °C preparations varied from crystal to crystal in a manner commensurate with crystal size and curvature and hence with the order in which the crystals

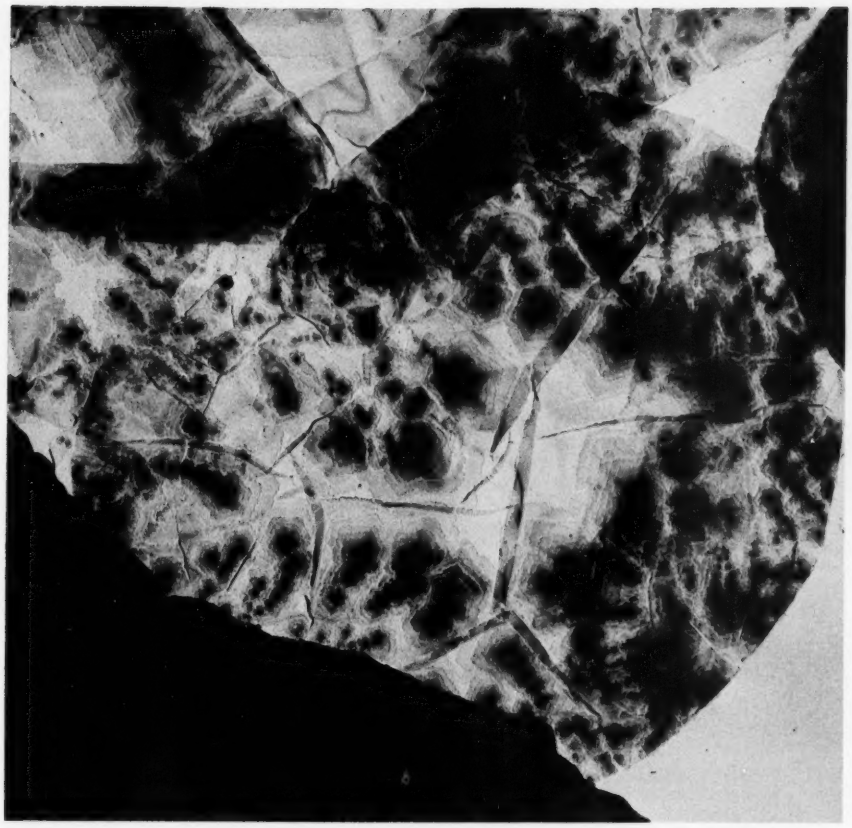

FIGURE 34. *Electron micrograph of a crystal formed in a* $T_c = 100$ *°C preparation; see text.*

Pt/Pd shadowed. X8300.

started to grow during the cooling of the solutions to T_c. Thus, for example, the distance between the center or pole of the basal lamella and the center(s) of the closest set of spiral terraces to it (i.e., the first set of spiral terraces which were initiated at its periphery during growth) is ~ 6–7 μm in the larger among the crystals (figs. 31 and 32) as indicated earlier, as compared to ~ 3 μm in the intermediate sized crystals (figs. 33 and 35), and to ~ 1 μm or less in the smaller and more pronouncedly curved crystals such as (V) and (W) in figure 36 and (X) and (Y) in figure 37. This trend clearly illustrates that, not unexpectedly, the onset of dendritic growth involving multisectoring and the generation of screw dislocation-like defects at the periphery of the basal lamella in the crystals formed in the $T_c = 100$ °C and the $T_c = 80$ °C preparations manifested itself at an earlier stage in the development of the basal lamella during the course of its growth the lower the temperature at which it started to grow during the cooling of the solutions to T_c.

In the light of the lateral habits exhibited by the crystals formed in the $T_c = 120$ °C and the $T_c = 114$ °C preparations it may be reasonably assumed that the *onset* of dendritic SD growth during the cooling of the $T_c = 100$ °C and the $T_c = 80$ °C preparations to T_c occurred most probably at a temperature in the range

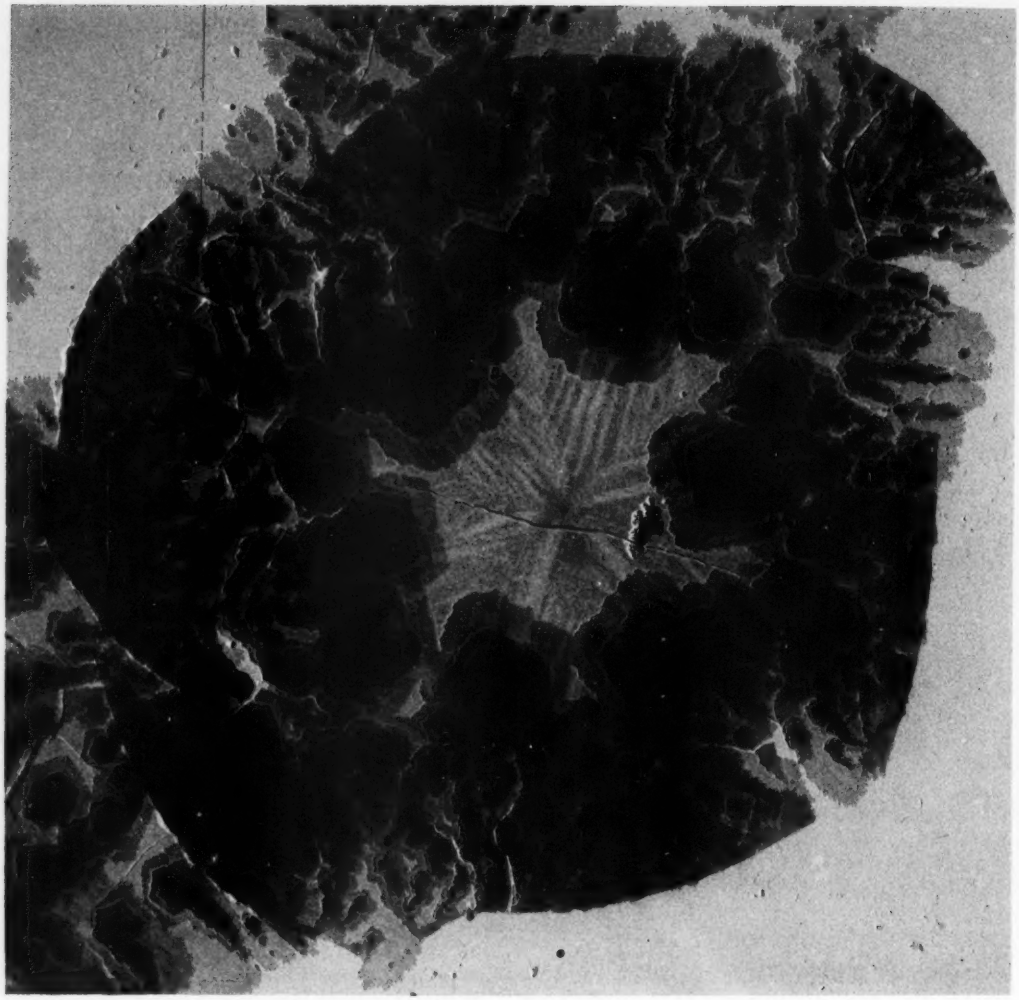

FIGURE 35. *Electron micrograph showing a crystal formed in a* $T_c = 80\,°C$ *preparation; see text.*

Pt/Pd shadowed, X8500.

120 to 114 °C or below. It is evident from a consideration and comparison of the crystals shown in figures 31 to 37 that below that temperature the lateral propagation of the crystals is characterized by the fact that as the solutions continued to cool to T_c the initiation of new families of spiral terraces at the periphery of the crystals tended to increase correspondingly as the temperature decreased.[13]

[13] There is an apparent slight reversal in this trend during the final stages of crystallization near to or at T_c, which reversal may be attributed to the depletion of polymer in the mother liquor.

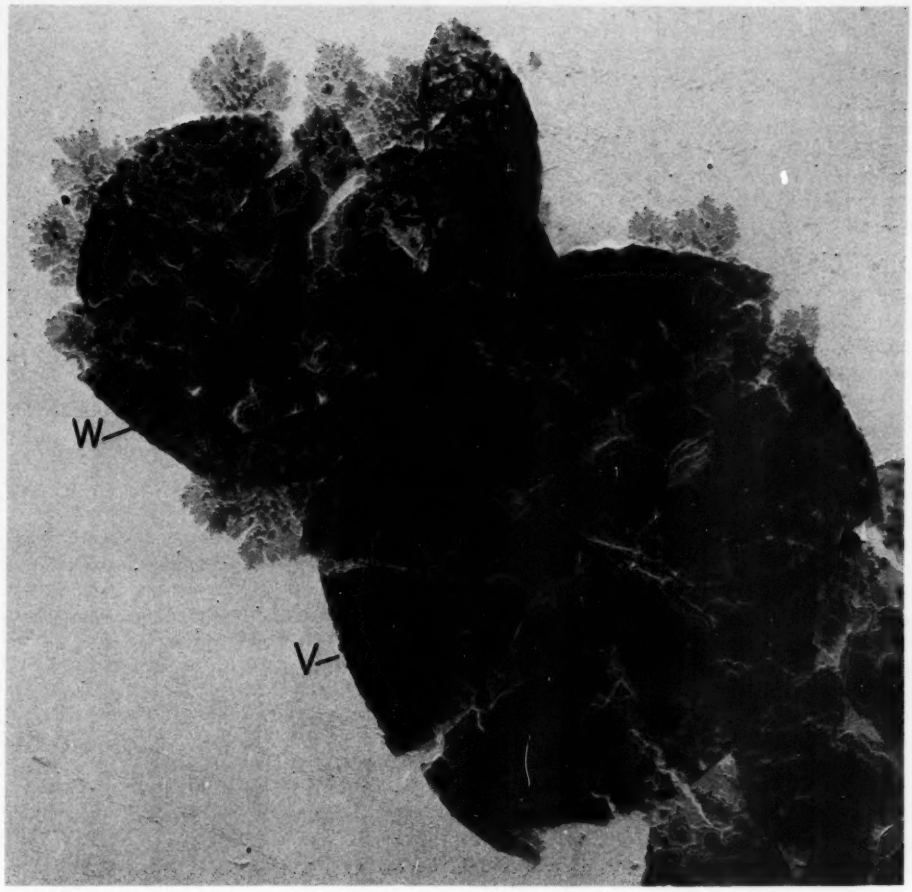

FIGURE 36. *Electron micrograph showing two crystals, (V) and (W), formed in a* $T_c = 80$ *°C preparation; see text.*

Pt/Pd shadowed, X8500.

There is an additional feature concerning the lateral propagation of the crystals below the temperature at which the onset of (SD) growth occurred during the cooling of the solutions to $T_c = 100$ and 80 °C which should also be noted, and that is the fact that the periphery of the leading (basal) lamellar layer in the crystals as well as the periphery of the subsidiary layers (spiral terraces) in these crystals is finely serrated as may be judged from a consideration of several of the crystals shown in figures 31 to 37 and as may be seen in figure 38 in which the arrow points to a portion of the periphery of the leading (basal) chain folded layer in a crystal (formed in a $T_c = 80$ °C preparation) as seen at a high magnification. The contrast between, the finely serrated (pronouncedly microfaceted) profile of the periphery of the leading chain folded layer in the crystals formed in these preparations on the one hand, and the more regular laterally stepped character of the basal lamella in the SD crystals formed in the $T_c = 114$ °C preparations on the

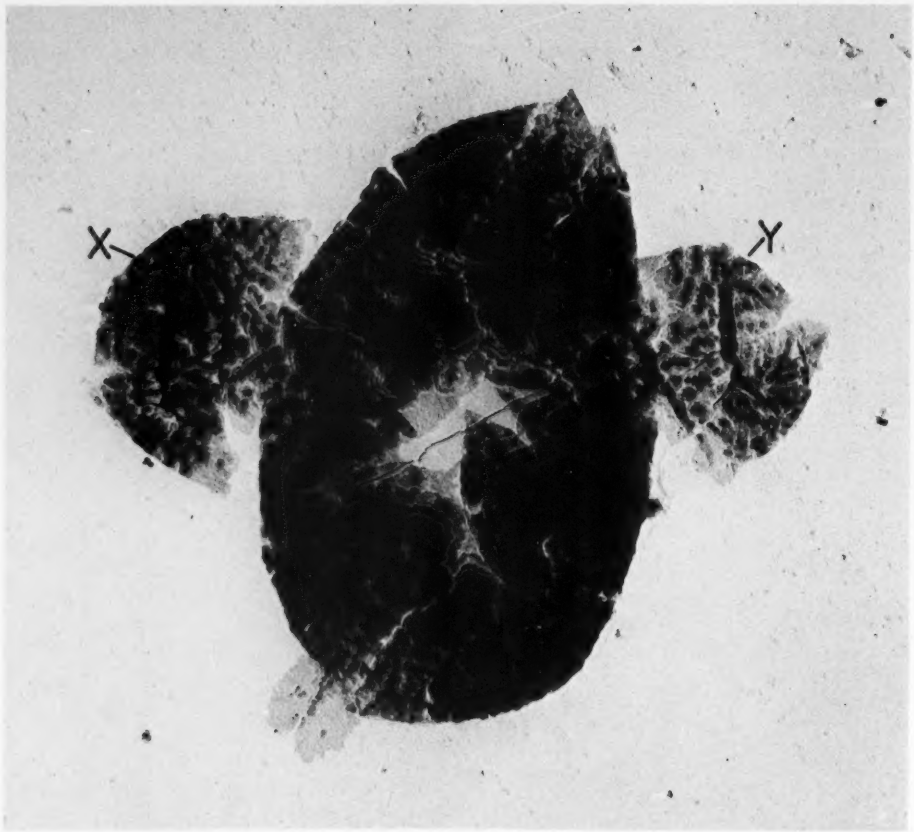

FIGURE 37. *Electron micrograph showing two (X and Y) among the smaller crystals formed in a* $T_c = 80$ *°C preparation; see text.*

Pt/Pd shadowed. X8500.

other hand, is self evident and points to the occurrence of a further transition in lateral growth habit as the temperature of the $T_c = 100$ °C and the $T_c = 80$ °C preparations decreased below the temperature at which the onset of SD growth manifested itself during the cooling of the preparations to T_c. A schematic representation of the likely nature of this transition is shown in figure 39b which it is to be compared with the SD mode of growth shown in figure 39a (see also fig. 1a). The essential difference between the SD habit depicted in figure 39a and that depicted in figure 39b (which will henceforth be referred to as SDD) is that whereas in the former case the initiation of new sectored outgrowths at the periphery of the basal lamella is limited to its six-leading corners (e.g., corner A in fig. 39), in the latter case new-sectored outgrowths are also initiated at subsiduary leading corners in the developing lamella such as for example corners B in figure 39a and subsequently at corners such as C in figure 39b, and so forth, which mode of growth involves more pronounced multisectoring than SD growth.

It is evident from the electron microscopial observations which have been described above that under the essentially similar conditions of supercooling which apparently prevailed during the crystallization of the polymer in the $T_c = 100$ °C and the $T_c = 80$ °C preparations, the history of the lateral development of individual crystals varied from crystal to crystal according to when each started to grow as the preparations cooled to T_c due to the fact that whereas hexagonal six-sectored and/or SS growth prevailed during

FIGURE 38. *Electron micrograph ('replica') showing a portion of the outer region of a crystal formed in a* $T_c = 80$ *°C preparation.*

Arrow points to the finely serrated periphery of the crystal. Pt/Pd shadowed. X28100.

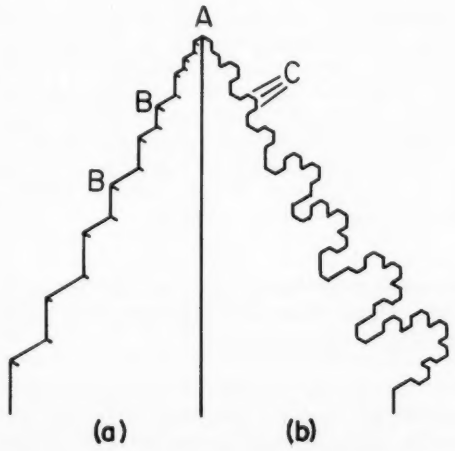

FIGURE 39. *Schematic representation of (a) SD dendritic growth and (b) SDD dendritic growth; see text.*

the early stages of cooling, this was followed by the onset of SD growth, and subsequently SDD growth, as the temperature of the preparations decreased progressively to T_c. Accordingly, the extent of lateral propagation in the hexagonal six-sectored and SS modes was minimal (or tended towards a minimum) in the crystals which were initiated last in the preparations, in which crystals, it may also be surmised, the extent of SD growth relative to the extent of SDD growth was probably also at a minimum. It is, however, not possible to determine from the electron micrographs the stage in development at which the transition from SD to SDD growth occurred during the course of the formation of the variously sized crystals formed in these preparations. Judging from the separation between reentrant microcorners along the finely serrated periphery of the basal lamella in the crystals formed in the preparations (e.g., see fig. 38) the lateral extent of the sectored outgrowths which developed successively at the periphery of the crystals during the final stages of crystallization was approximately 0.04 μm.

Summarizing the electron microscopial observations on the lateral modes of development associated with the formation of the crystals grown in the $T_c = 100$ °C and the $T_c = 80$ °C preparations and the optical microscopial observations described earlier concerning the variations in conformation (curvature) among the crystals formed in each case, there are four main trends which emerge. *First*, the lateral development of the crystals, which broadly speaking involves transitions from hexagonal-six-sectored and/or SS growth, to multisectored (SD) and then (SDD) dendritic growth with decreasing temperature, is characterized by the fact that the extent of lateral growth in the hexagonal six-sectored and/or SS modes during the initial stages of development of the crystals was all the more diminished the lower the temperature at which the crystals were initiated during the cooling of the solutions to T_c. *Second*, the lateral development of the crystals corresponding to the multisectored SD and subsequently SDD stages of growth (which may be considered collectively for the present purpose) during the more advanced stages of the cooling of the preparation is characterized by the fact that the frequency of the formation of successive arrays of new sectored outgrowths at the periphery of the growing crystals increased with decreasing temperature, the end result being that the corresponding portions of the crystals were all the more pronouncedly multisectored (i.e., they were composed of a finer mosaic of fold domains). Judging from the separation between neighboring reentrant corners at the periphery of the leading lamella in the crystals (e.g., see fig. 38) the lateral extent of the sectored outgrowths which developed at the edges of the lamella during the final stages of growth was about 0.04 μm. *Third*, the multisectored SD and SDD stages in the growth of the leading lamella are characterized by the generation of screw dislocation-like defects at the periphery of the lamella. The incidence of these defects (which give rise to the development of spiral terraces) tended to increase the lower the growth temperature following the onset of dendritic growth. *Fourth*, the variations in conforma-

tion among the crystals formed in the $T_c = 100$ °C and the $T_c = 80$ °C preparations are characterized by the fact that the crystals formed in each case were all the more pronouncedly curved the lower temperature at which they started to grow during the cooling of the solutions to T_c. There was considerable overlap between the conformations of the crystals formed in the $T_c = 100$ °C preparations and those formed in the $T_c = 80$ °C preparations. The crystals formed in these preparations ranged from the larger species such as (N) in figure 25 ($T_c = 100$ °C preparation) and (Q) in figure 28 ($T_c = 80$ °C preparation) to small hollow bowl shaped crystals such as (P) (diameter 5–6 μm) in figure 27 in the case of $T_c = 100$ °C and such as (R) in figure 29 (diameter 4–5 μm) for $T_c = 8$ °C.

Finally we turn to some additional comments concerning the conformations of the crystals formed in the $T_c = 100$ °C and $T_c = 80$ °C preparations in the light of the changes in lateral growth regime which it was pointed out above occur with decreasing growth temperature in these preparations, as well as in the light of the conformations and corresponding lateral growth characteristics exhibited by the crystals formed at all higher T_c. It has been pointed out earlier that with the qualified exception of the largest among the crystals formed in the $T_c = 100$ °C and the $T_c = 80$ °C preparations (such as (N) in fig. 25 and Q in fig. 28) the remainder of the crystals formed in these preparations were hollow bowl shaped objects, as depicted schematically in figure 30. Before dwelling on the overall conformation of the former crystals, the following factors pertaining to the variations in curvature among the latter six-fold symmetrical hollow bowl-shaped ones may be noted, these factors also bear on the nature of the conformation of the former larger crystals as will become evident in due course. It is evident from a comparison between, on the one hand the nearly planar six-sectored lamellar crystals formed in the $T_c = 140$ °C and the $T_c = 120$ °C preparations, and on the other hand the perceptibly dished overall character of the dendritic crystals formed in the $T_c = 114$ °C preparations and the hollow bowl shaped dendritic crystals formed in the $T_c = 100$ °C and $T_c = 80$ °C preparations, that the more pronouncedly curved character of the latter dished and hollow bowl-shaped crystals as compared to the crystals formed in the $T_c = 140$ °C and $T_c = 120$ °C preparations occurs in association with the manifestation of multisectored dendritic lateral growth. It is also evident from a comparison between the dished crystals formed in the $T_c = 114$ °C preparations and the hollow bowl shape crystals formed in the $T_c = 100$ °C and $T_c = 80$ °C preparations (as well as from the variations in curvature among the bowl-like crystals formed in the latter preparations) that the lower the temperature at which growth progressed in a dendritic manner below circa 114 °C the more pronouncedly curved were the corresponding portions of the crystals, (which trend occurred in association with a corresponding enhancement in multisectoring as well as an enhancement in the generation of screw dislocation-like defects at the periphery of the leading lamella). This trend is one of the two features which underlies the fact that the *overall* conformation of individual bowl-shaped crystals formed in the $T_c = 100$ °C and the $T_c = 80$ °C preparations was all the more pronouncedly curved the lower the temperature at which the crystals started growing during the cooling of the preparations to T_c. The other feature is that the extent of lateral development in a six-sectored (and hence essentially planar) manner during the early stages of growth of these crystals was all the more diminished the lower the temperature at which they started to grow during the cooling of the solutions to T_c. Conversely in this latter connection, the higher the temperature at which a crystal started to grow the larger the extent of its lateral development in a six-sectored and nearly planar fashion prior to the onset of dendritic growth, and hence the *overall* curvature of the crystal tended to be less pronounced as evidenced by the larger species of crystals, such as (N) in figure 25 and (Q) in figure 28, in which the incidence of pronounced curvature is confined to the outer dendritic portions of the crystals. Although the change in orientation of the surface of the larger crystals between their pole and the six leading corners of the crystals is about 90° (note the "rounded hexagonal" outline of crystal Q in fig. 28), the overall conformation of these crystals is somewhat more complex than is the case of the hollow bowl-shaped crystals which started to grow at lower temperatures. This is due to the extensive separation between the six leading portions of the outer dendritic region in the larger crystals, which portions tend to have a radius of curvature comparable to that of the smallest and most pronouncedly curved crystals (e.g., (P) in fig. 27 and (R) in fig. 29) formed in the preparations. The appearance exhibited by the outer dendritic region of these larger crystals as seen in different perspectives under the optical microscope indicates that each of the six leading portions of these crystals tends to be curled in a quasi bowl-like fashion.

4. Discussion of the Origins of the Dependence of the Curvature of POM Crystals on Crystallization Temperature

The observations described in Section 3 clearly reveal a distinct trend in the effect of growth temperature on the conformation (curvature) of POM crystals. Thus, setting the axialitic among the crystals formed in the $T_c = 140$ °C and the $T_c = 120$ °C preparations as a species apart, it is evident that there is a progressive change in conformation from the nearly planar nature of the six-sectored monolayer and nonaxialitic multilayered crystals formed in the $T_c = 140$ °C and the $T_c = 120$ °C preparations, to the comparatively more pronouncedly curved overall conformation of the perceptibly *dished* dendritic crystals (radius of curvature roughly ~ 20–30 μm) formed in the $T_c = 114$ °C preparations, to the even more pronouncedly curved overall conformations of the hollow bowl-like dendritic

crystals formed in the $T_c = 100$ °C and the $T_c = 80$ °C preparations (radius of curvature of smallest bowls 2–3 μm). Noting, as pointed out in Section 3.4 that the onset of crystallization in the $T_c = 114$ °C, the $T_c = 100$ °C and the $T_c = 80$ °C preparations occurred before thermal equilibrium was reached at these temperatures, the results described in Section 3, looked upon collectively, may be summarized as follows: (a) A transition from nearly planar six-sectored to curved multisectored dendritic lateral growth occurred apparently in the range 120 to 114 °C, and furthermore the lower the temperature at which growth occurred thereafter the more pronouncedly multisectored were the corresponding portions of the crystals, as evidenced by the contrast between the SD profile of the periphery of the dished crystals formed in the $T_c = 114$ °C preparations and the SDD profile of the periphery of the hollow bowl-shaped crystals formed in the $T_c = 100$ °C and the $T_c = 80$ °C preparations. (b) In contrast with the nearly planar character of the hexagonal six-sectored and SS crystals formed in the $T_c = 140$ °C and the $T_c = 120$ °C preparations respectively, the lower the temperature at which growth occurred (dendritically) below $T_c = 120$ °C, the more pronouncedly curved were the corresponding portions of the crystals, and the greater was the tendency for screw dislocation-like defects to be generated at the periphery of the basal lamella, through the agency of which defects spiral terraces evolved.

As will become apparent, the discussion presented in what ensues on why it is that the multisectored dentritic crystals grown in the $T_c = 114$ °C, 100°, and 80° preparations were all the more pronouncedly curved the lower the crystallization temperature which prevailed during the course of their growth, in contrast with the nearly planar nature of the six-sectored monolayered and the non-axialitic multilayered crystals formed in the $T_c = 140$ °C and the $T_c = 120$ °C preparations, is rooted in considerations similar to the ones upon which our previous deliberations on the origins of curvature in P4MP crystals and its variation with crystallization temperature were based [2]. It is therefore appropriate, by way of background and for the purposes of comparison, to summarize briefly pertinent features of our previous observations on the effect of crystallization temperature on P4MP crystals grown from 0.1 percent solutions of the polymer in equivolume mixtures of xylene and amyl acetate at temperatures in the range 90 to 50 °C, which crystals were all the more pronouncedly curved the lower the growth temperature. Accordingly, to indicate the extremes in the dependence of the conformations of P4MP crystals on crystallization temperature, it may be noted that the crystals varied from nearly planar ones (formed at 90 °C) whose constituent square shaped lamellae were four-sectored, bounded laterally by {100} faces, and only slightly buckled, to distinctly curved four-fold symmetrical hollow bowl-shaped crystals (formed in solutions cooled to 50 °C) whose radius of curvature was ~ 2.5 μm. Furthermore, in contrast with the four-sectored character of the lamellae in the essentially planar crystals formed at 90 °C, the constituent lamellae in all the distinctly dished or bowl-like P4MP crystals formed in the temperature range 90 to 50 °C were multisectored, their lateral growth being characterized by the development at their periphery of successive arrays of {100} microfaceted sectored out-growths at a frequency (per unit path length from pole to periphery) which was greater the lower the crystallization temperature. In short, in addition to the fact that the P4MP crystals were all the more pronouncedly curved the lower the growth temperature, their constituent lamellae were correspondingly all the more pronouncedly multisectored. As pointed out earlier, a similar morphological association between enhancement in curvature and increased multisectoring with decreasing growth temperature is exhibited in POM crystals grown at different temperatures. Bearing in mind this phenomenological similarity between the effect of temperature on the growth habits of POM and P4MP crystals it is also of interest to note that, as is the case for the six-sectored monolayered and non-axialitic multilayered POM crystals formed at low supercoolings ($T_c = 140$ °C and the $T_c = 120$ °C preparations), the four-sectored crystals of P4MP formed at 90 °C were not perfectly planar. The slight departure from planarity in these latter crystals has been attributed to buckling under the influence of the bulkiness of the chain folds [2, 5, 6] as is the case for the six-sectored lamellae of POM (see discussion in Section 3.2 (iii) and references [5, 6]), which attributions stem respectively from Bassett's [5] observations that $d_{\{200\}_f}$ differs from $d_{\{200\}_{nf}}$ by ~ 0.1 percent in each of the four constituent fold domains in four-sectored lamellae of P4MP, and that $d_{\{10\bar{1}0\}_f}$ differs from $d_{\{10\bar{1}0\}_{nf}}$ by ~ 0.32 percent in each of the six constituent fold domains in six-sectored lamellae of POM.

The similarities pointed above between the origins (the bulkiness of chain folds) of the slightly buckled character of POM (six-sectored) and P4MP (four-sectored) crystals formed at low supercoolings, coupled with the phenomenological similarities between the effect of increasing supercooling on the curvature and fold domain structure in crystals of these polymers, provide the basis of the ensuing discussion of why it is that the POM crystals grown at high undercoolings were all the more pronouncedly curved the lower the growth temperature in terms of assumptions and conjectures analogous to the ones which were advanced (in the form of a working 'model', see figure 37, reference [2]) and discussed in our previous deliberations on the origins of curvature and its variation in P4MP crystals. To recapitulate briefly in this latter connection the assumptions and conjectures which were advanced and discussed in the case of P4MP were: (i) the sectored outgrowths which develop successively at the periphery of multisectored lamellae of P4MP are possessed of a slight intrinsic conicalness; (ii) this intrinsic conicalness (angle of

elevation of ~ 2°) in sectored outgrowths is a consequence of buckling under the influence of the bulkiness of the chain folds which leads to a difference of ~ 0.1 percent between $d_{\{200\}_f}$ and $d_{\{200\}_{nf}}$ in their constituent fold domains as is the case in four-sectored lamellae; (iii) the overall curvature of multisectored P4MP lamellae is a cumulative consequence of the intrinsic conicalness of the sectored outgrowths which develop in successive arrays at their periphery, and is governed by the frequency (per unit path length from pole to periphery) at which new sectored outgrowths are generated during the growth of the lamellae, the higher that frequency the smaller the radius of curvature of the lamellae. As suggested below a similar rationale may be advanced in the case of POM.

Given, as indicated in Section 3.2 and Section 3.3, that the six-sectored monolayered crystals and the nonaxialitic six-sectored multilayered crystals formed in the $T_c = 140$ °C and the $T_c = 120$ °C preparations are not perfectly flat, and given as discussed in section 3.2(iii) with reference to Bassett et al. [5, 6], that this latter feature may be attributed to slight buckling under the influence of the bulkiness of the chain folds, i.e., that it is a consequence of both stresses which arise at the sector boundaries where the mismatch in spacing between $\{10\bar{1}0\}_f$ planes in one sector and the $\{1010\}_{nf}$ planes in adjoining sectors must be accommodated, as well as stresses at the fold surfaces, then it may be reasonably presumed that by the same token the sectored outgrowths which develop successively at the periphery of the multisectored dendritic lamellae of POM are also intrinsically slightly buckled. This latter premise would not account in itself for the fact that the multisectored dendritic crystals formed in the $T_c = 114$, 100, and 80 °C preparations were collectively more pronouncedly curved than the nearly planar six-sectored crystals formed in the $T_c = 140$ °C and the $T_c = 120$ °C preparations, nor would it account for the fact that the dendritic crystals were all the more pronouncedly curved the lower the temperature at which growth took place below $T_c = 120$ °C during the course of their formation. This latter trend may be hypothetically accounted for on the basis of the following assumptions concerning the intrinsic conformation of sectored outgrowths, which assumptions are similar to those which were considered in our previous discussion of the formation of curved multisectored lamellar crystals of P4MP. The first assumption is that irrespective of the conditions of crystallization $d_{\{10\bar{1}0\}_f} \neq d_{\{10\bar{1}0\}_{nf}}$ in the constituent sectors of chain-folded lamellae of POM due to the bulkiness of of the chain folds. The second assumption is that the magnitude of the difference between $d_{\{10\bar{1}0\}_f}$ and $d_{\{10\bar{1}0\}_{nf}}$ is the same irrespective of the conditions of crystallization, i.e., it is 0.32 percent [5] in both six-sectored lamellae as well as in the constituent sectors in the sectored outgrowths which develop successively at the periphery of the dendritic POM crystals. The third assumption is that $d_{\{10\bar{1}0\}_f} > d_{\{10\bar{1}0\}_{nf}}$. In short, on the basis of these assumptions it is envisaged as discussed in section 3.2(iii) that six-sectored lamellae possess a slight intrinsic conicalness, that they have an angle of inclination (θ) of a few degrees (circa 4°), that they are slightly rounded at the pole, and that the molecular stems are oriented at right angles to the surface of the crystal throughout (see fig. 8b). With these assumptions in mind, which assumptions will be the subject of further discussion in due course, we proceed to consider below the development of a multisectored dendritic lamella from an initially formed six-sectored precursor crystal.

A plan view representing a six-sectored precursor is shown schematically in figure 40a (efghkl) and a side view depicting the cross section of the crystal corresponding to a cut along one of its diagonals (eOh in fig. 40a) is shown in figure 40b in which (O′O) is the normal to the surface of the lamella at its pole (O). (O′O) is normal to the plane of reference (mm) (fig. 40b). The normals to the surface of the lamella at (e) and (h) are (ee′) and (hh′) respectively. In accordance with the visualization indicated above that the six-sectored precursor is slightly conical and rounded at the pole, it is assumed as shown in figure 40b, that on proceeding from its pole (O) to its periphery following radial paths outwards along the surface, e.g., along the diagonal path (Oh), there occurs within a small distance (On), where (On) ≪ (Oh), a gradual inclination of θ° in the lamella relative to the plane (mm), and that beyond (n) the inclination of the lamella remains essentially constant. In other words, it is assumed that the angle between the surface normals and hence the

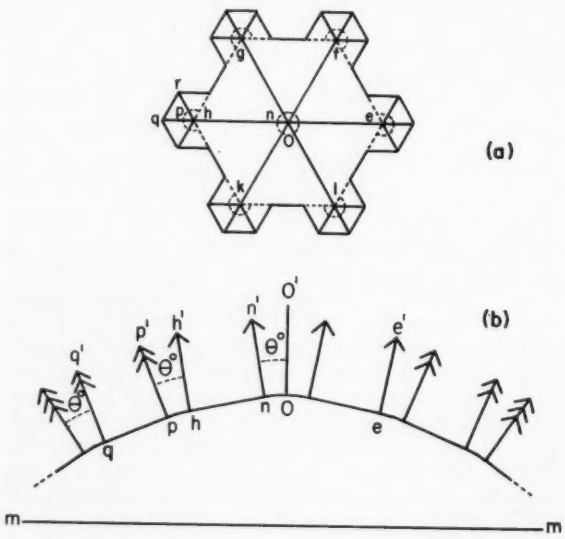

FIGURE 40(a). *Plan view representing sectored outgrowths developing at the periphery of a six-sectored precursor crystal.*

(b) Edge-on view of a diagonal cross-section of the developing multi-sectored dendritic crystal depicted in (a), showing conjectured incremental contribution of sectored outgrowths to the overall curvature of the lamella, see text.

molecular stems at (O) and (n) is equal to the angle of inclination $\theta°$, and that the normals (nń) and (hh́) to the surface, as well as the molecular stems at (n) and (h), are parallel to one another.

With the above features attributed to a six-sectored lamella in mind, the formation is imagined of sectored outgrowths centered about the corners (efghkl) of the precursor lamella as shown in figure 40a. In essence then figure 40a represents an early stage in the evolution of an SD multisectored dendritic lamella of POM. As pointed out earlier it is assumed in what follows that $d_{\{10\bar{1}0\}_f} > d_{\{10\bar{1}0\}_{nf}}$ and that the difference between these interplanar spacings ($\sim 0.32\%$) is independent of the crystallization conditions and is the same in both the fold domains of the six-sectored precursor as well as in the constituent fold domains in the sectored outgrowths which develop therefrom. Accordingly, each sectored outgrowth shown in figure 40a may be considered to have a slight intrinsic "conicalness" akin to that of the central six-sectored precursor. This conicalness is not centered however about the normal to the lamella at the pole (O) but, rather, about the surface normals at (e, f, g, h, k, l) about which the outgrowths develop. As shown cross-sectionally in figure 40b, this conicalness is envisaged to lead to a corresponding increase in the inclination of the peripheral regions of the developing lamella relative to the plane (mm) by an additional increment of $\theta°$ (this increment could be as large as $2\theta°$ as is the case between opposite sectors in the six-sectored precursor). By analogy with the six-sectored precursor, this additional inclination is depicted in figure 40b as occuring close to the center of initiation of each outgrowth e.g., between (h) and (p) where (hp) is much smaller than (hq). Thus, in this view, the total inclination of the developing multisectored lamella relative to the reference plane (mm) on proceeding outwards from (O) to (q) along the surface of the crystal is envisaged to be $2\theta°$ as shown in figure 40b, i.e., an increase of $\theta°$ in the inclination of the growing lamella relative to the plane (mm) over that of the six-sectored precursor has resulted from the development of the inherently nonplanar sectored outgrowth centered about the precursor's periphery at (h). The same argument applies to the other sectored outgrowths shown in figure 40a. By the same token it may be visualized that the development of a new set of sectored outgrowths centered about the leading corners, such as (q), of the sectored outgrowths shown in figure 40a will lead to a further inclination $\theta°$ of the lamella relative to the plane (mm) and hence, cumulatively, to a total inclination of $3\theta°$ of the surface of the lamella (and correspondingly to a change of $3\theta°$ in the orientation of the molecular stems) relative to the plane (mm) on proceeding from the pole O to the periphery of the newest sectored outgrowth, and so forth, the end result being that the resulting multisectored lamella will exhibit an overall curved conformation. Similar considerations apply to the case of SDD growth in which the generation of new sectored outgrowths would not be limited to the leading corners such as (q) in figure 40a but would also occur at their other corners such as (r).

Thus, as was the case in our previous discussion on the formation of variously curved crystals of P4MP [2], the thrust of the hypothetical representation of the development of curved multisectored lamellae of POM given above is that the overall curvature of the lamella is a cumulative consequence of the combined effects of two factors namely, the intrinsic conicalness of $\theta°$ (due to the bulkiness of the chain folds) of the new sectored outgrowths which are generated successively at the periphery of the lamella during growth, and the frequency per unit path length from pole to periphery at which new sectored outgrowths are formed. Conceptually, for a constant conicalness $\theta°$ in sectored outgrowths one would expect that the smaller the lateral dimensions which sectored outgrowths attain before new outgrowths develop therefrom in a developing multisectored lamella the larger will be the number of quasi-discrete inclinations of $\theta°$ per unit path length from pole to periphery, consequently the average radius of curvature of the lamella will be correspondingly smaller.

The observation that the lower the temperature at which growth occurred in the basal (leading) lamella in the dendritic crystals of POM the more pronouncedly multisectored and the more pronouncedly curved were the corresponding regions of the lamella, is qualitatively consistent with the hypothetical explanation given above of the observed variations of the curvature of POM crystals formed at different supercoolings in terms of the inherently nonplanar character of sectored outgrowths and the frequency at which they are generated at the periphery of the growing crystals. However, the assumptions concerning the inherent conformation of six-sectored lamellae as well as that of sectored outgrowths upon which this hypothetical explanation is based, remain open to question. These assumptions are discussed further below.

Accepting that the premise that $d_{\{10\bar{1}0\}_f} > d_{\{10\bar{1}0\}_{nf}}$ in the constituent fold domains of both six-sectored lamellae as well as multisectored lamellae is correct, the possibility cannot be discounted that the disparity between $d_{\{10\bar{1}0\}_f}$ and $d_{\{10\bar{1}0\}_{nf}}$, which was assumed above to be independent of the conditions of crystallization, may actually differ depending on the latter conditions. In short, it may be envisaged that at low crystallization temperatures, which favor the more rapid folding of the chain molecules along the lateral facets of the sectored outgrowths which develop at the periphery of growing dendrites, the folds may tend to be less regular and hence have bulkier conformations thus giving rise to larger differences between $d_{\{10\bar{1}0\}_f}$ and $d_{\{10\bar{1}0\}_{nf}}$ and correspondingly to a more pronounced intrinsic buckling of the sectored outgrowths. In other words, the intrinsic conicalness (angle of inclination $\theta°$ in fig. 40b) of sectored outgrowths could conceivably tend to be larger the lower the crystallization temperature. In terms of the hypothetical "model" depicted in figure

40b this would mean that multisectored lamellae will be more pronouncedly curved the lower the crystallization temperature not only as discussed earlier, because of the larger frequency at which new sectored outgrowths are formed, and corresponding increments in inclination of $\theta°$ occur, per unit path length from pole to periphery, but also because these increments tend to be intrinsically larger the lower the crystallization temperature. To this consideration must be added another possibility namely that even if the bulkiness of the folds and the disparity between $d_{\{10\bar{1}0\}_f}$ and $d_{\{10\bar{1}0\}_{nf}}$ are not dependent on growth temperature, the intrinsic buckling of sectored outgrowths may tend to be enhanced in some degree at lower crystallization temperatures due to the fact that the fold period and hence the thickness of sectored outgrowths become smaller the lower the crystallization temperature [6, 16].

All the considerations advanced above have been based on the premise that sectored outgrowths possess an intrinsic conicalness, which premise derives from the assumption that $d_{\{10\bar{1}0\}_f} > d_{\{10\bar{1}0\}_{nf}}$. We have described in Section 3.2 (iii) and Section 3.3 the various features—such as the streaks due to diffraction contrast, and the incidence of slight pleats—which evidence the fact that six-sectored lamellae are not prefectly planar. We have also pointed out that it is not possible to establish with any certainty from the various "collapse features" exhibited in electron micrographs by six-sectored lamellae whether their as-grown shape, and hence as presumed earlier that of sectored outgrowths in dendritic lamellae, is intrinsically conical ($d_{\{10\bar{1}0\}_f} > d_{\{10\bar{1}0\}_{nf}}$, see fig. 8) as assumed above, or whether they possess, as-grown, an intrinsic convoluted conformation such as that depicted schematically in figure 9 ($d_{\{10\bar{1}0\}_f} < d_{\{10\bar{1}0\}_{nf}}$). Although the matter of the exact intrinsic conformation of the six-sectored lamellae and the sectored outgrowths in the dendritic crystals remains uncertain, the overall dished and hollow bowl shaped nature of the dendritic crystals formed in the $T_c = 114$ °C preparations and in the $T_c = 100$ and 80 °C preparations respectively tend to argue in favor of an effective slight "conicalness" in the sectored outgrowths which develop successively at their periphery.

There is a growth feature associated with the manifestation of multisectoring in the curved dendrites formed in the $T_c = 114$, 100, and 80 °C preparations which we have ignored in our discussion so far, namely the occurrence of the generation of screw dislocation-like defects about the periphery of the basal (leading) multisectored lamella in these crystals during the course of its growth. These defects, whose incidence tends to be all the more frequent the lower the growth temperature, result from a relative displacement of adjoining peripheral portions of the basal lamella in a direction perpendicular to the surface of the lamella through a distance equal to its thickness. Whether these defects which are generated preferentially at reentrant corners at the periphery of the basal lamella—which corners define the outer extremity of the contact boundary between neighboring sectored outgrowths—result from a shearing of the lamella at that boundary due to localized stresses presumably associated with the bulkiness of the chain folds, or whether these defects result from built-in departures in height registry at the boundary between neighboring intrinsically buckled sectored outgrowths remains an open question. Whichever the case may be, the incidence of these screw dislocation like defects entails the occurrance of stresses resulting from their accommodation in the lattice. Whether these stresses tend to act in a manner such as to effectively enhance or diminish the intrinsic bulking of sectored outgrowths which has been proposed above, remains undetermined. It may be noted in this connection that following the occurrence of a screw dislocation-like defect at a reentrant corner the portions of the growing basal layer which were displaced relative to one another frequently heal (i.e., height registry is restored) as a consequence of the generation of a screw dislocation-like defect of opposite hand as has been previously observed [4], which feature is suggestive of a tendency for the localized distortion of the lamella associated with a single such defect to be compensated [4]. The net effect, if any, of the incidence of the screw dislocation-like defects on the conformation of the sectored outgrowths in their immediate vicinity and hence, cumulatively, the influence of these defects on the overall conformation of the curved dendrites remains unknown however, as is the possible contribution of stresses arising from the accomodation of departures in both height and lateral registry [2] between impinging (see fig. 39b) sectored outgrowths, which misregisters may be envisaged to occur (without necessarily leading to screw dislocation-like defects from which new terraces evolve) in the case of (SDD) lateral growth due to the inherently slightly buckled character of the outgrowths.

Given that the overall radius of curvature of the most pronouncedly curved hollow bowl-like crystals such as crystals (R) in figure 29 ($T_c = 80$ °C preparation) is ~ 2 μm, and assuming that the hypothetical model depicted in figure 40 in essentially correct and that the incremental inclination associated with the development of each successive sectored outgrowth at the periphery of the basal lamella is $\theta = 4°$, it may be calculated (assuming sphericity to a first approximation) that the average interval (e.g., hq in fig. 40a) between successive incremental inclinations of $\theta°$ would be about 0.14 μm. In other words the lateral extent to which sectored outgrowths would be expected to develop at the periphery of the constituent basal lamella in these crystals before new sectored outgrowths evolved therefrom would be about 0.14 μm. This calculated estimate is greater, by a factor of three to four times the observed estimate of ~ 0.04 μm (see Sec. 3.4 (iii)) corresponding to the lateral extent of sectored outgrowths which developed during the final stages of the development of the crystals formed in the $T_c = 100$ and 80 °C preparations, which latter

estimate was based on the separation between reentrant microcorners at the periphery of the basal lamella in the crystals. It may be rationalized that the experimental estimate of roughly 0.04 μm corresponds to the development of the bowls at the lowest temperature at which growth occurred in the preparations and that, averaged over the entire course of the development of these most pronouncedly curved bowls, the interval between successive inclinations of $\theta°$ may be reasonably presumed to be larger than 0.04 μm. The complexity of the morphology of the interior of the crystals coupled with the undetermined nature of the role of the various factors discussed in the previous four paragraphs frustrates the pursuit of this matter on a quantitative basis.

In summary, it is evident from a consideration of the conjectures upon which the hypothetical model depicted in figure 40 is based in the light of the various factors discussed in the previous four paragraphs, that these conjectures remain speculative. To recapitulate briefly, these conjectures are: (1) The primary source of the curvature of a multisectored lamella of POM is an intrinsic conicalness (angle of inclination θ circa 4°) in the sectored outgrowths which develop in successive arrays at its periphery; (ii) the intrinsic conicalness in sectored outgrowths is a consequence of buckling under the influence of the bulkiness of the chain folds which leads to a difference of about 0.32 percent between $d_{\{10\bar{1}0\}_f}$ and $d_{\{10\bar{1}0\}_{nf}}$ in their constituent fold domains (the buckling is envisaged to be due to stresses resulting from the accommodation of the mismatch in spacing at the fold domain boundaries between the $\{10\bar{1}0\}_f$ planes in one sector and the $\{10\bar{1}0\}_{nf}$ planes in adjoining ones, as well as due to stresses at the fold surfaces); (iii) the overall curvature of a multisectored lamella is a cumulative consequence of the intrinsic conicalness of the sectored outgrowths which develop in successive arrays at its periphery and is governed by the frequency per unit path length from pole to periphary at which new sectored outgrowths are generated during the growth of the crystal, the higher that frequency the smaller the radius of curvature of the crystal.[14]

In conclusion, the observations derived from the present study of the effect of supercooling on the curvature of POM crystals viewed in the light of our previous study on the formation of curved crystals of P4MP [2], show that there is a phenomenological similarity in the effect of supercooling on the habits of the crystals of these two polymers. In both cases the lamellar crystals tend to be all the more pronouncedly curved the lower the crystallization temperature and the degree of multisectoring in the lamellae tends to be correspondingly all the more pronounced (i.e., the lamellae tend to be constituted of a finer mosaic of fold domains). Although the generation of screw dislocation-like defects at the periphery of the leading multisectored lamella in the crystals formed at higher supercoolings occurs in the case of both polymers, POM exhibits a pronounced propensity for the development of spiral terraces from these defects, in contrast, whereas additional chain folded terraces evolve from these defects in P4MP multisectored lamellae, there seems to be a suppression of continued "spiraling" [2]. Finally, although the observed variations in the curvature of POM and P4MP crystals with crystallization temperature lend themselves to similar hypothetical accountings, these accountings remain speculative in view of the undetermined role of numerous factors in both cases, which factors are for the most part common to both polymers.

[14] It may be noted in connection with these conjectures which are analogous to those we previously advanced in the case of P4MP, that the study of POM reported herein, which as pointed out in Section 1 was undertaken at the outset with the specific purpose of determining whether increasing supercooling leads to the formation of POM crystals which are all the more pronouncedly curved the lower the crystallization temperature, was prompted by the evidence available at the time that (a) both six-sectored lamellae [3–6] and dendritic crystals [4] (see also section 1) of POM were not perfectly planar although their respective conformations remained uncertain, and that (b) the non-planar character of six-sectored lamellae was associated with the incidence of a distortion of the subcell in their constituent sectors due to the bulkiness of the chain folds [5, 6]. These features viewed in the light of the observations and conjectures which we had previously advanced concerning the formation of curved crystals of P4MP [2] led us to speculate that the effect of supercooling on the conformation of POM crystals might be similar to that observed in the case of P4MP.

The authors wish to express their thanks to R. K. Eby and D. H. Reneker for their encouragement and for the benefit of helpful discussions.

5. References

[1] The observations reported in this paper were first presented before the Division of High Polymer Physics of the American Physical Society. Khoury, F., and Barnes, J. D., Bull. Am. Phys. Soc. **12**, 385 (1967), GD2.
[2] Khoury, F., and Barnes, J. D., J. Res. Nat. Bur. Stand. (U.S.), **76A** (Phys. and Chem.), 225 (1972).
[3] Geil, P. H., Symons, N. K. J., and Scott, R. G., J. Appl. Phys. **30**, 1516 (1959).
[4] Reneker, D. H., and Geil., P. H., J. Appl. Phys. **31**, 1916 (1960).
[5] Bassett, D. C., Phil. Mag. **10**, 595 (1964).
[6] Bassett, D. C., Dammont, F. R., and Salovey, R., Polymer (London) **5**, 579 (1964).
[7] Geil, P. H., J. Macromol Sci. (Chem.) **A1**, 325 (1967).
[8] Garber, C. A., and Geil, P. H., Makromoleculare Chem. **113**, 236 (1968).
[9] Carazzolo, G., J. Polymer Sci. **A1**, 1573 (1963).
[10] Blundell, D. J., Keller, A., and Kovacs, A. J., J. Polymer Sci. **B4**, 481 (1966).
[11] Bassett, D. C., and Keller, A., Phil. Mag. **7**, 1553 (1962).
[12] Handbook of Chemistry and Physics, 48th Edition, The Chemical Rubber Co., Cleveland, Ohio (1967–1968).
[13] Jaffe, M., and Wunderlich, B., Kolloid-Z. u. Z. Polymere, **216–217**, 203 (1967).
[14] Colson, J. P., and Reneker, D. H., J. Appl. Phys. **41**, 4296 (1970).
[15] The manifestation of rotations between successive terraces originating from screw dislocations in chain folded polymer crystals has been discussed by Keller with particular reference to crystals of polyethylene, and of polyethylene oxide copolymers. Keller, A., Kolloid Z.u.Z. Polymere **219**, 118 (1967).
[16] Korenaga, T., Hamada, and F., Nakajima, A., Polymer Journal (Japan) **3**, 21 (1972).

(Paper 78A2–805)

530-326 OL - 74 - 3

JOURNAL OF RESEARCH of the National Bureau of Standards—A. Physics and Chemistry
Vol. 78A, No. 2, March–April 1974

Solid-Phase Behavior of Several Long-Chain *n*-Paraffins, Esters, and a Ketone

Peter K. Sullivan*

Institute for Materials Research, National Bureau of Standards, Washington, D.C. 20234

(December 18, 1973)

The long-spacings of the compounds methyl stearate, ethyl stearate, *n*-butyl stearate, 2-nonadecanone, *n*-eicosane, *n*-hexatriacontane and *n*-tetratetracontane have been examined as a function of temperature by means of low-angle x-ray diffraction. The intensity of the long-spacing was also determined versus temperature. The effect of annealing temperature and time was examined by means of the DSC. Dielectric loss was studied in two crystalline phases of *n*-butyl stearate.

Key words: Dielectric loss; *n*-paraffins, phase transitions, x-ray scattering.

1. Introduction

Various aspects of the properties of long-chain compounds have been studied by many workers over the years. For example, the crystal structure, as well as the heats and temperatures of transitions are basic properties which have been established for a number of compounds [1, 2].[1]

In this article some of the thermal properties of several long-chain esters and *n*-paraffins are presented. In particular, the differential scanning calorimeter (DSC) has been used to investigate the dependence of the DSC traces on the temperature and time of annealing.

All of these compounds crystallize in a lamellar form and the thickness of the lamellae depends both on the molecular length and the thermal history of the sample. The dependence of this lamellar thickness on temperature for the paraffins, esters and ketone has been studied by means of low-angle x-ray scattering. In an earlier article [3] we have found that the intensity of the long-spacing may increase with increasing temperature for *n*-paraffins. Similar observations have been made by Fischer et al. [4, 5]. In this article the dependence of the intensity of the long-spacing on temperature was further investigated and in particular samples with and without solid-solid phase transitions were examined. Dielectric loss was studied for *n*-butyl stearate.

2. Experimental Detail

2.1. Apparatus

a. X-Ray Diffraction

X-ray diffraction was observed using nickel-filtered Cu radiation collimated with a Kratky[2] low-angle camera. The detector system was a scintillation counter with pulse height analyzer. The sample holder consisted of an insulated box with beryllium windows; temperature control was achieved with a thermistor system, as described in an earlier article [3]. All temperatures in the x-ray experiments are within ± 0.5 K.

b. Differential Scanning Calorimetry (DSC)

All samples were examined at a heating rate of 2.5 K/min (unless otherwise specified). Samples examined below 320 K involved the use of the liquid nitrogen jacket. The annealed samples were maintained at the desired temperatures in a separate bath and then transferred to the precooled DSC holder.

c. Melting Ranges

The melting ranges (± 0.1 K) of the various samples were determined by means of an optical microscope

*Present address: Celanese Research Co., P.O. Box 1000, Summit, N.Y. 07901.

[1] Figures in brackets indicate the literature references at the end of this paper.

[2] Certain commercial materials and equipment are identified in this paper in order to specify adequately the experimental procedure. In no case does such identification imply recommendation or endorsement by the National Bureau of Standards, nor does it imply that the material or equipment is necessarily the best availaale for the purpose.

and a Mettler FP21 hot stage, at a heating rate of 0.2 K/min. No correction was made on the temperatures for the effect of heating rate.

d. Dielectric Loss

The capacitance and dissipation factor of the sample over the frequency range 2×10^2 Hz to 5×10^4 Hz were determined using a General Radio 1615 transformer ratio arm bridge. Over the frequency range 10 Hz to 2×10^2 Hz, the Scheiber low frequency bridge [6] was employed. A three terminal cell with gold plated electrodes was used and the cell was kept in a constant temperature bath (± 0.5 K). The cell was kept under a positive nitrogen pressure in order to keep the sample dry. A small gap (0.35 mm) was allowed between the top electrode and the sample in order to allow for sample expansion. The dielectric loss $\epsilon''(\nu)$ was determined from the measured values of sample capacitance and dissipation factor, using a correction term to account for the gap capacitance. Because of uncertainties in the sample thickness, the estimated uncertainty in $\epsilon''(\nu)$ is 10 to 20 percent.

2.2. Samples

Since homologous impurities often occur in these compounds, some attempt was made to determine the composition and to improve the purity. Solution crystallization is one means of purification and Brown [7] and Sedgwick [8] et al. have discussed the solubility of the esters in various solvents. All samples were dried under vacuum.

a. Methyl Stearate

Commercial methyl stearate was examined on a gas chromatograph (apiezon packed column, helium carrier gas) and was found to contain at least 3 percent impurities. For this reason the purification techniques of zone refining, vacuum distillation and solution recrystallization were examined on various samples. Based on gas chromatograph analyses, the technique of solution recrystallization from acetone appears to be the quickest and most effective means of removing the impurities involved. The method of solution recrystallization employed was at a concentration of 15 g ester to 1500 ml (reagent grade) acetone. The solution was kept at 268 K until crystallization occurred (a few hours) and the crystals removed by filtration. A total of three recrystallizations were performed; the crystals were then melted and passed through a fine glass frit in order to remove particulate matter.

b. Ethyl Stearate

Similarly, commercial ethyl stearate was examined on the gas chromatograph and was found to contain more than 20 percent impurities. Solution recrystallization from acetone (at 261 K) as above was found to remove the impurities observable by gas chromatography.

c. *n*-Butyl Stearate

Commercial *n*-butyl stearate was recrystallized twice from acetone as above at 257 K. A gas chromatograph analysis of the sample showed that a 1 percent higher molecular weight impurity still remained. Further recrystallization did not remove this impurity.

d. 2-Nonadecanone

Commercial 2-nonadecanone was examined on the gas chromatograph and was found to contain approximately 5 percent impurities. The sample was vacuum distilled and the middle fraction, bp 438 to 440 K, was collected. The sample was then recrystallized from acetone as above at 273 K. This process was found to remove the impurities.

e. n-Eicosane [n-$C_{20}H_{42}$]

Commercial *n*-eicosane (listed as 99%) was examined on the gas chromatograph and no homologous impurities were found. The sample was recrystallized from acetone as above at 283 K.

f. *n*-Hexatriacontane [n-$C_{36}H_{74}$]

Commercial n-$C_{36}H_{74}$ was recrystallized four times from benzene (15 g paraffin to 1500 ml benzene). Crystallization occurred at approximately 311 K.

g. *n*-Tetratetracontane [n-$C_{44}H_{90}$]

A 0.2 g portion of the n-$C_{44}H_{90}$ sample synthesized by Clark [9] was recrystallized from 40 ml of benzene. Crystallization occurred at approximately 313 K.

3. Results

3.1. Methyl Stearate

a. DSC Studies

A typical DSC curve of the purified methyl stearate is shown in figure 1. The heating rate is 2.5 K/min. The purification scheme led to an increase in the melting point. Further purification did not increase the melting point nor decrease the width of the curve. The observed melting range for the solution crystallized samples was 311.0 to 312.6 K (optical microscope); for melt crystallized samples, 310.8 to 311.4 K.

b. X-Ray Scattering

Since it was somewhat more convenient to handle solution recrystallized samples in the x-ray sample holder, a portion of the previously purified methyl stearate was further recrystallized from acetone (15 g/1500 ml) and dried under vacuum. Strips of the dried filter cake were placed in the sample holder and the scattering of x-rays at small-angles was examined as a function of temperature. The first order diffraction maximum is shown in figure 2 and corresponds to a Bragg spacing of 47.4 Å. This is consistent with the

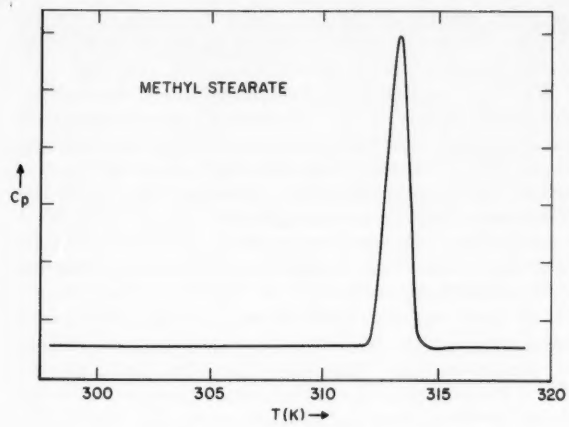

FIGURE 1. *DSC trace of methyl stearate.*

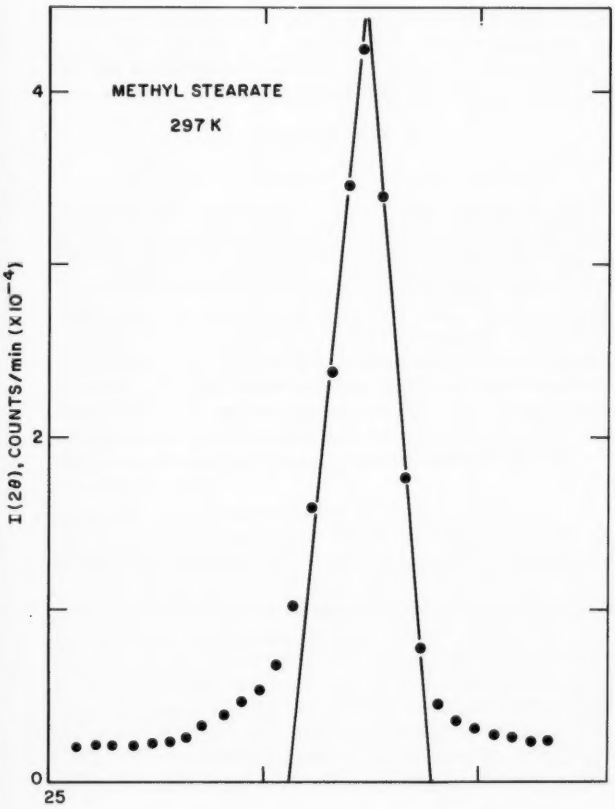

FIGURE 2. *X-ray diffraction from methyl stearate at 297 K.*

(002) diffraction maximum of the monoclinic form of methyl stearate [.0]. In table 1 are shown the values of this diffraction maximum (normalized to the value at 235 K) over the temperature range 235 K $\leq T \leq$ 307 K. The long-spacing was constant within 0.1 Å up to 312.3 K, at which temperature the sample was found to be slowly melting. No decrease in the intensity of this long-spacing occurred up to 312.0 ±0.15 K, so that the melting point of the sample must be above this temperature.

TABLE 1. *X-ray diffraction intensities and long-spacings as a function of temperature for methyl and ethyl stearate*

Methyl stearate			Ethyl stearate		
T(K)	$A(T)$ /A(235K)	l(Å)	T(K)	$A(T)$ /A(235K)	l(Å)
307	1.0	47.3	297	1.0	25.1
297	1.0	47.3	273	1.0	25.0
272	1.0	47.4	250	1.0	25.1
254	1.0	47.4	235	1.0	25.1
235	1.0	47.4			

c. Discussion

The DSC trace (fig. 1) indicates only a single phase transition. However, there is evidence in the literature of more than one crystalline form. For example, Aleby and von Sydow [10] report two different melting points. Also Simonelli [11] found in a dilatometric study that the data was consistent with a solid-solid phase transtion near the melting point. Guy and Smith [12] report a transition at 310.7 K. And Smit [13] reports that the rate of the solid-solid phase transition within 0.5 K of the melting point is extremely slow. Craig [14] has found hysteresis in the volume as a function of temperature for solid methyl stearate, such that the specific volume at any temperature depends on the previous thermal history of the sample. And finally, Markley [1] also indicates two mp's. We note that the mp of 312.3 K observed in this study by means of the decrease in the intensity of the (002) maximum is in agreement with the value observed with the optical microscope (311.9 to 312.6 K) and with that found by Francis [15] and by Aleby [10].

Since the long-spacing of the solution recrystallized form is constant up to the mp and this form exhibits the higher mp, it appears likely that this form does not undergo any solid-solid phase transitions. Based on the literature cited above and on the observation in this article that the melt crystallized form has a lower mp, it is probable that the form which crystallizes from the melt slowly transits to the more stable form. It appears that under the conditions of the experiment, the DSC is unable to resolve the phase transition in melt crystallized methyl stearate, since it occurs too close to the mp and proceeds too slowly.

3.2. Ethyl Stearate

a. DSC Studies

A DSC trace of the purified ethyl stearate (final stage of purification was solution recrystallization) is shown in figure 3a. The corresponding melting range — as deter-

mined on the optical microscope—was 306.9 to 307.3 K. When a sample was crystallized from the melt—but cooled no lower than 298 K—the subsequent DSC trace on heating is as shown in figure 3b. The melting range now observed was 304.6 to 304.8 K (on the optical microscope). The average difference in the mp's of the two forms, based on the DSC scans and the observations on the optical microscope, was 2.4 K. Francis and Piper [15] reported mp's of 304.6 K and 307.1 K for the α and γ forms respectively, i.e., a difference of 2.5 K.

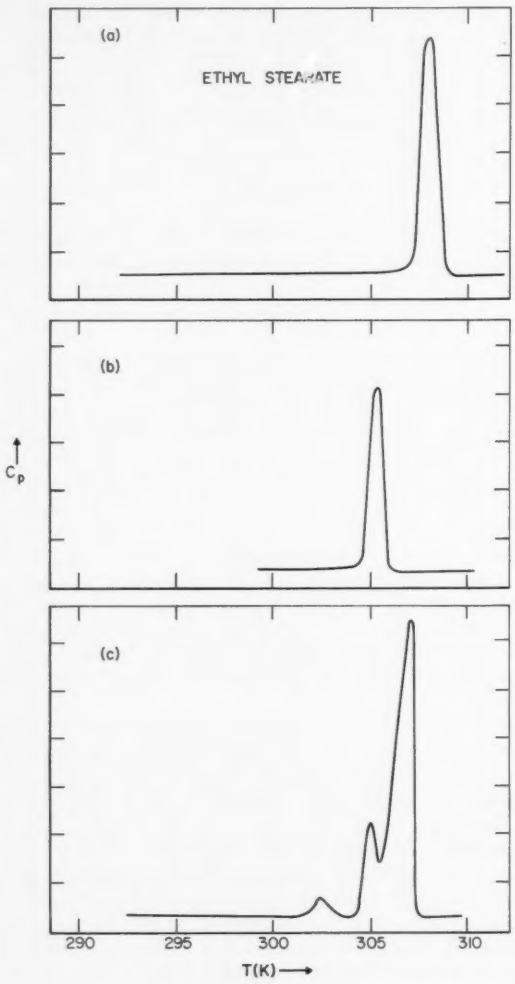

FIGURE 3. *(a) DSC trace of solution-recrystallized or annealed ethyl stearate; (b) DSC trace of melt-crystallized ethyl stearate (sample cooled to 298 K); and (c) DSC trace of melt-crystallized ethyl stearate (sample cooled below 298 K).*

Based on the areas under the melting transitions on the DSC scans—and on the literature value [16] for the heat of fusion of n-$C_{20}H_{42}$ (as a calibration of the DSC), i.e., 16.70 kcal/mol, then the heat of fusion of the form melting at 306.9 to 307.3 K is approximately 15.5 kcal/mol; the heat of fusion of the form melting at 304.6 to 304.8 K is approximately 9.8 kcal/mol.

When a sample was crystallized from the melt—and cooled below 298 K—a solid-solid phase transition was observed in the DSC trace at 296 K (cooling rate 2.5 K/min). This transition was also observed on the optical microscope at 296.6 K (cooling rate 2 K/min). When this sample was subsequently reheated, the DSC trace was as indicated in figure 3c. The transition in figure 3b and the middle transition in figure 3c occurred at the same temperature.

The melt recrystallized form (i.e., fig. 3c) slowly transformed to the higher melting form, which exhibits no solid-solid phase transitions (i.e., fig. 3a). The rate of the transformation of the lower melting form to the higher melting form (i.e., fig. 3c → fig. 3a) was found to be temperature dependent. At 293 K, about 30 days is required; at 273 K, more than 120 days. The lowest temperature transition shown in figure 3c was found to slowly merge with the higher temperature transitions. The time required for this process was observed to be temperature dependent. At 296 K, the time required was 2 hours; at 293 K, 7 hours; at 284 K, 90 hours; at 281 K, 240 hours; at 273 K, 1630 hours.

b. X-Ray Scattering

(i) Temperature Dependence of the Intensity of the Low-Angle Diffraction

Strips of the dried filter cake from the acetone-recrystallized ethyl stearate were placed in the sample holder and the small-angle scattering examined. The first order diffraction maximum corresponds to a spacing of 25.4 Å, which is in agreement with the (002) spacing of the monoclinic form (also solution crystallized) found by Aleby [17]. In table 1 are shown the value of this long spacing and the relative integrated intensity of the diffraction maximum (normalized to the value at 235 K) over the temperature range $235 \leq T \leq 297$ K. The long spacing was found constant within 0.1 Å.

A quenched sample of ethyl stearate was prepared by pouring a portion of the melt into a beaker at the temperature of liquid nitrogen. This sample was ground into a powder and dried for 3 hours under vacuum. A DSC scan of this sample was as indicated in figure 3c. The low-angle scattering was examined periodically over a period of 26 days at room temperature and the long-spacing of 25.4 Å was constant within 0.1 Å. A DSC scan was taken of the (x-rayed) sample after 26 days and corresponded to figure 3a. There was also no significant change in the observed intensity of the (002) diffraction maximum over the 26 day period.

(ii) Solid-Solid Phase Transformation

A sample of ethyl stearate was melted in the x-ray sample holder. The liquid was cooled below its melting point and the freshly crystallized sample was observed to always exhibit a long-spacing of 28.5 Å. The 28.5 Å spacing corresponds to the molecule in an extended (nontilted) form. The long-spacing spontaneously

changed to the 25.4 Å form and the time for the completion of the transformation,

$$l(28.5\text{ Å}) \rightarrow l(25.4\text{ Å})$$

was found to be strongly temperature dependent. In table 2 is shown the amount of time as a function of temperature to complete the transformation $l(28.5\text{ Å}) \rightarrow l(25.4\text{ Å})$. It was also found that this transformation was irreversible, i.e., the reverse reaction, $l(25.4\text{ Å}) \rightarrow l(28.5\text{ Å})$, was not found to occur when either partially transformed or completely transformed samples were

TABLE 2. *Time dependence as a function of temperature for the long-spacing transition l(28.5 Å)→ l(25.4 Å) for ethyl stearate*

Ethyl stearate	
T(K)	$l(28.5\text{ Å}) \rightarrow l(25.4\text{ Å})$ time required (min.)
303.9	2075
303.2	725
302.4	475
301.7	307
300.8	135
299.3	20.5
297.9	4.1

subsequently reheated. The relative amount transformed was approximately linear with time. This is illustrated in figure 4 for the transformation at 299.3 K. The ordinate is the relative amount of the 28.5 Å phase remaining, as determined by $\frac{I(t)-I(\infty)}{I(t_0)-I(\infty)}$ where $I(t)$ is the intensity of the (002) diffraction maximum (either peak height or integrated intensity) as a function of time. There is an induction time for the start of the transformation, as reflected by the t_0 term in the abscissa. At 302.4 K, t_0 is approximately 300 min, at 300.8 K, 40 min.

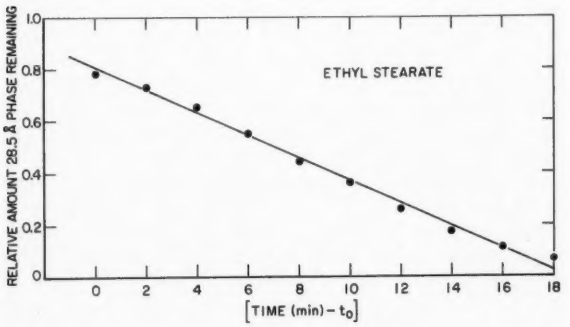

FIGURE 4. *Time dependence for the phase transition l(28.5 Å) → l(25.4 Å) at 299.3 K.*

c. Discussion

The x-ray and DSC data are consistent with at least four crystalline forms. The crystal structure of the stable form (i.e., fig. 3a) has been studied by Aleby [17]. As with methyl stearate, ethyl stearate was also observed to undergo very slow solid-solid phase transformations. The intensity of the long-spacing of the stable form was found to be temperature independent in the range covered. However, one should also notice that the intensity of the long-spacing of the quenched sample—which did undergo solid-solid phase transitions, but no tilt transition during and after the initial x-ray scan—was also independent of temperature. The long-spacing of the quenched sample was constant at 25.4 Å over the period of 26 days at 297 K—during which time the DSC scans went from that corresponding to figure 3c to that of figure 3a. This indicates that none of the DSC transitions of figure 3c are associated with tilt transitions. All of the DSC transitions on heating occur for the 25.4 Å spacing and so involve some kind of rotational reorganization with respect to the lateral packing of the molecules. The solid-solid transition which occurs at 296 K on a DSC cooling curve probably is associated with the tilt transition (see table 2), since the rate of the transition becomes large around this temperature. The observed long-spacings of 28.5 Å and 25.4 Å agrees within 0.1 Å of the values reported by Malkin [18].

3.3. *n*-Butyl Stearate

a. DSC Studies

While the original sample was found to have a broad melting range, the purified sample was found to have a sharp melting point. A typical DSC curve of the purified sample is shown in figure 5a. In addition to the solid-liquid transition at 299.9 to 300.1 K (optical microscope) observed on heating, two solid-solid phase transitions (288.4 and 284.5 K) were found for all samples freshly crystallized from the melt. These solid-solid phase transitions were found to be reversible and occurred without much supercooling. If the samples were allowed to stand at 293 K for one month or longer, a phase transformation occurred so that the heat capacity versus temperature curve was as shown in figure 5b. It can be seen that a new solid-solid phase transition occurred (294 K) and the two transitions (at 288.4 and 284.5 K) were no longer present. The transition at 294 K was found to be irreversible, i.e., if the sample were heated through this transition (without melting the sample) and then cooled, only the transitions at 288.4 and 284.5 K again occurred. If the sample were subsequently reheated, the transition at 294 K was no longer found (i.e., unless the sample was again annealed for one month at 293 K). The rate of the transformation (fig. 5a → fig. 5b) was found to be dependent on temperature. At 293 K, 30 days was required; at 289 K, 15 days; at 284 K, 7 days; at 277 K, 2 days; and at 272 K, 2 days.

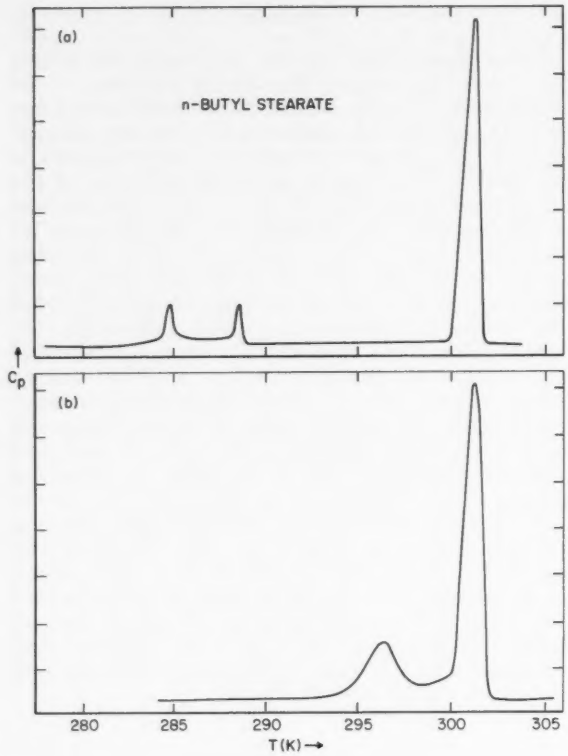

FIGURE 5 (*a*) *DSC trace of unannealed* n-*butyl stearate; and* (*b*) *DSC trace of annealed* n-*butyl stearate.*

b. X-Ray Scattering

Strips of the filter cake from an acetone recrystallization (sample dried under vacuum one hour, using a liquid nitrogen trap) were placed in the (previously cooled) sample holder and the small-angle scattering examined. The first order diffraction maximum is shown in figure 6 and corresponds to a Bragg spacing of 27.6 Å. Malkin [19] has reported a value of 27.2 Å for the β form of *n*-butyl stearate.

A solid-solid phase transition involving a change in the long-spacing was observed at 296.6 K for the solution recrystallized sample. Below 296 K, the stable phase corresponded to $l = 27.6$ Å; above 296.6 K, the observed spacing was 31.0 Å. It was found that while the process $l(27.6\text{ Å}) \rightarrow l(31.0\text{ Å})$ at 296.6 K was rapid (and complete), the reverse process $l(31.0\text{ Å}) \rightarrow l(27.6$ Å) at 296 K was slow (and incomplete). Thus, after five days at 296 K, only about ½ the sample was in the 27.6 Å form. The spacing of 31.0 Å is consistent with the chains in a vertical form, as reported by Malkin [19]. Dryden [20] has reported a value of 31.7 Å.

In order to determine if the DSC transition at 294 K and the transition $l(27.6\text{ Å}) \rightarrow l(31.0\text{ Å})$ at 296.6 K were identical, several samples were prepared with the 31.0 Å spacing. These samples were maintained at 274 K for three days in the x-ray sample holder; the spacing remained constant at 31.0 Å, indicating that the rate of the transformation $l(31.0\text{ Å}) \rightarrow l(27.6\text{ Å})$ may be slow at this temperature or that impurities may be affecting the transition. However, all samples so annealed exhibited the DSC trace of figure 5b, so that the transition at 294 K does not appear to be the tilt transition.

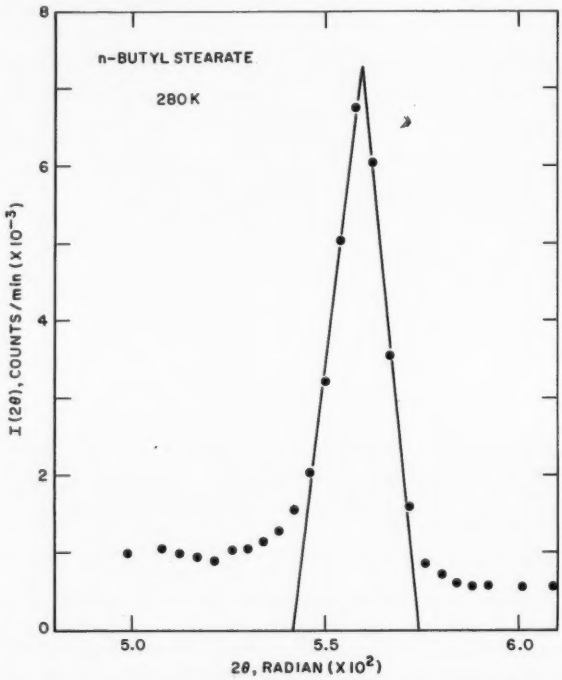

FIGURE 6. *X-ray diffraction from* n-*butyl stearate at 280 K.*

c. Dielectric Loss

The sample was ground to a powder and pressed into a disc of 2.54 cm diameter and 0.2 cm thickness. The sample was kept at 277 K for approximately 4 months, so that its DSC corresponded to figure 5b. The sample was placed in the previously cooled cell (273 K) and the system kept under a positive nitrogen pressure. The dielectric loss was examined below (285.0 K) and above (297.1 K) the solid-solid phase transition in figure 5b, and the data is shown in figure 7. It can be seen that below the phase transition temperature there is no loss peak and $\epsilon''(\nu) < 0.0035$ over the frequency range covered. However, above the phase transition temperature a loss peak occurs. Little change in the loss peak was observed over a period of 30 days at 297 K. The sample was again cooled to 273 K and kept at this temperature for 4 days, so that its DSC curve corresponded to figure 5b. The loss was again examined at 285 K and $\epsilon''(\nu) < 0.0027$ over the frequency range covered.

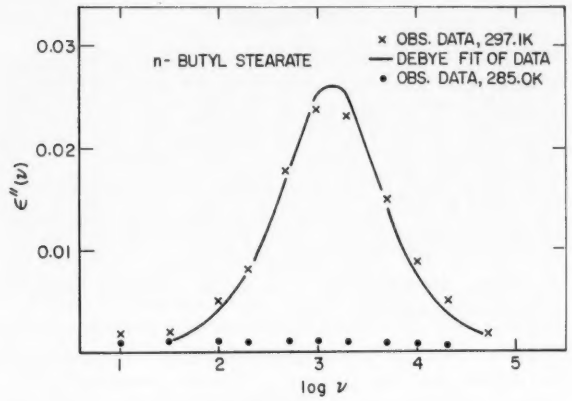

FIGURE 7. *Dielectric loss for* n*-butyl stearate.*

· obs. data at 285.0 K,
X obs. data at 297.1 K,
—— Debye fit of data at 297.1 K

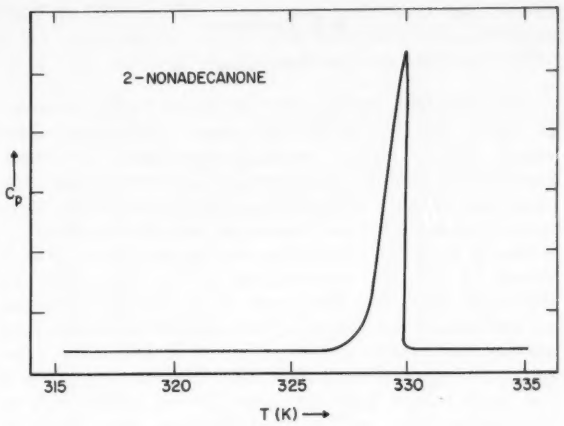

FIGURE 8. *DSC trace of 2-nonadecanone.*

3.4. 2-Nonadecanone

a. DSC Studies

The original sample was found to have a rather broad melting curve. A typical DSC run on the purified sample is shown in figure 8. No solid-solid phase transitions were found in either the solution or melt recrystallized samples. The melting range was found to be 328.3 to 328.5 K, as determined on the optical microscope. Saville and Shearer [21] have reported a mp of 328.7 to 329.4 K.

b. X-Ray Scattering

The observed (002) diffraction maximum for the purified 2-nonadecanone corresponds to a value of 51.8 Å. Saville and Shearer [21] reported a value of 52.9 Å. As can be seen in table 3, the long-spacing was constant within 0.1 Å over the temperature range 236 K $\leq$ T $\leq$ 325 K. The relative integrated intensity of the (002) maximum (normalized to the value of 236 K) was observed to decrease slightly over this temperature range.

c. Discussion

The observed long-spacing of 51.8 Å corresponds to the length of two molecules. As with methyl stearate, it appears likely that the ketone groups in adjacent lamellae are nearest each other in 2-nonadecanone, giving rise to the 51.8 Å repeat distance.

TABLE 3. *X-ray diffraction intensities and long-spacings as a function of temperature for 2-nonadecanone and* n*-eicosane*

2-nonadecanone			n-$C_{20}H_{42}$		
T(K)	$A(T)/A(236K)$	l(Å)	T(K)	$A(T)/A(233K)$	l(Å)
325	0.97	51.8	308	1.1	25.4
			297	1.05	25.4
296	0.96	51.8	275	1.0	25.4
236	1.0	51.8	233	1.0	25.4

d. Discussion

As with methyl and ethyl stearates, *n*-butyl stearate also undergoes slow solid-solid phase transformations. The reversible phase transitions at 288.4 and 284.5 K occur at the temperatures where Dryden [20] has found discontinuities in the frequency of maximum dielectric absorption versus $1/T$ plots. In agreement with the observation of Dryden [20], the long-spacing corresponding to figure 5a is 31.0 Å over the temperature range 280 to 299.9 K. Thus, the reversible phase transitions appear to involve a change in the lateral packing of the molecules.

The choice of *n*-butyl stearate for the dielectric loss experiment was prompted by the DSC studies. While annealed samples of methyl and ethyl stearate showed no solid-solid phase transitions on the DSC, the annealed samples of *n*-butyl stearate always exhibited the transition below the mp (fig. 5b). For this reason the sample could be prepared in the form of a disk suitable for the dielectric cell, then annealed for a long period of time (several months) and its loss examined. Then the sample could be heated through its solid-solid phase transition, while in the dielectric cell. Under these conditions, there is no change in the concentration of chemical impurities in the sample and any loss associated with the volume defects introduced by the solid-solid phase transition might be observed. As it turned out, the system kept at a temperature above the phase transition temperature of figure 5b does show a loss peak, which does not change with time. It appears then that the loss peak is not caused by the volume defects introduced by the phase transitions. It is also possible that the mobility of the impurities is greater in the high temperature phase.[3]

[3] This suggestion was made by Prof. E. R. Fitzgerald (Johns Hopkins Univ.).

3.5. Eicosane

a. DSC Studies

A typical DSC trace of the purified n-$C_{20}H_{42}$ is shown in figure 9a. No solid-solid phase transitions were found when either solution-crystallized or melt-crystallized samples were heated. However, when the melt was cooled, in addition to the liquid-solid transition, a solid-solid phase transition was always observed within 3 K of the crystallization temperature. This is shown in the DSC trace of figure 9b. The solid-solid transition was also observed as an abrupt transition on the optical microscope. This transition as observed on the microscope occurred 5 to 6 K below the crystallization temperature (309.2 K). The melting point of the form which had not been cooled sufficiently to experience the solid-solid transition was 309.3 to 309.5 K. The melting point of the form which had been cooled through the transition was 309.7 to 309.9 K (both observed on the optical microscope). A solid-solid phase transition has been reported by Seyer et al. [22] and by Schaerer et al. [16, 23]. The melting points of the two forms are in agreement with those reported by Schaerer [23]. Based on the areas under the DSC curves for the solid-solid and crystallization transitions, and on the literature value [16] for the heat of fusion of the higher melting form of n-$C_{20}H_{42}$, the heat of the solid-solid transition is approximately 7 kcal/mole.

b. X-ray Scattering

A portion of the recrystallized sample of n-$C_{20}H_{42}$ was examined in the x-ray camera. The first order diffraction maximum at 297 K corresponds to a spacing of 25.4 Å. This is in agreement with the value reported by Crissman et al. [24] for the triclinic form. As can be seen in table 3, the long-spacing of 25.4 Å was constant within 0.1 Å over the temperature range $233 \leq T \leq 308$ K. The integrated intensity of the first order low-angle maximum (normalized to the value of 233 K) increased slightly (about 10%) over this same temperature range.

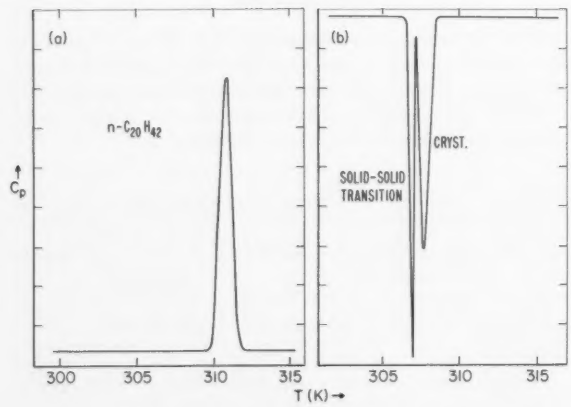

FIGURE 9 (*a*) *DSC trace of* n-$C_{20}H_{42}$ (*heating*); *and* (*b*) *DSC trace of* n-$C_{20}H_{42}$ (*cooling*).

c. Discussion

For the n-paraffins with an even number of carbon atoms from n-$C_{22}H_{46}$ to n-$C_{42}H_{86}$, a reversible phase transition [2] occurs below the mp. The transition is reversible in the sense that it occurs on both heating and cooling the sample. n-$C_{20}H_{42}$ appears to be a borderline case. When the sample is crystallized from the melt, it apparently can crystallize into the rotator state and subsequently into the stable form, as evidenced by the DSC transition shown in figure 9b. However, the transition does not again occur when the sample is heated (fig. 9a).

3.6. *n*-Hexatriacontane

a. DSC Studies

A typical DSC scan of the purified sample is shown in figure 10. In addition to the solid-liquid transition at 348.9 K (determined on the optical microscope), two solid-solid phase transitions were observed, one at 347.0 K (optical microscope and DSC) and the other at 340.7 K (DSC). The lower temperature solid-solid transition (340.7 K) was found to be irreversible, i.e., it did not occur on a subsequent heating scan on a sample crystallized from the melt. The higher temperature solid-solid transition (347.0 K) was found to be reversible. Schaerer [16] et al. report a mp of 349.1 K.

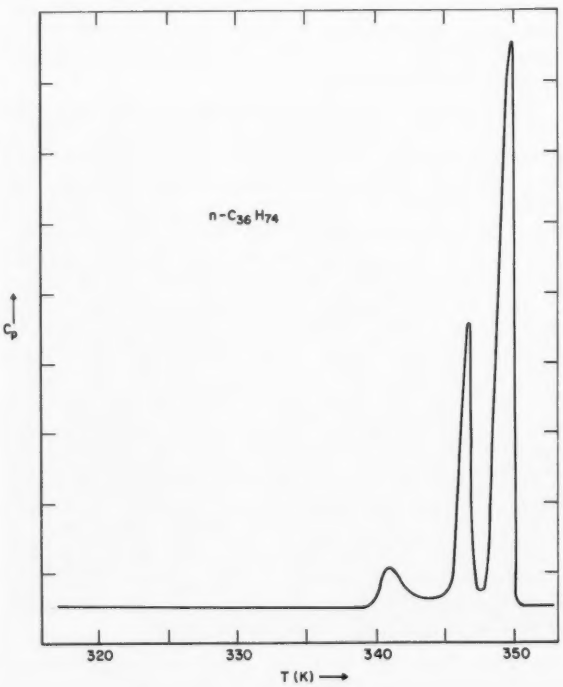

FIGURE 10. *DSC trace of* n-$C_{36}H_{74}$.

b. X-Ray Scattering

A portion of the benzene recrystallized sample was examined in the x-ray camera. The first order diffraction maximum corresponds to a spacing of 42.4 Å, which is consistent with the monoclinic form reported by Shearer and Vand [25]. It can be seen in table 4 that the spacing of 42.4 Å was observed over the temperature range $192.6 \leq T \leq 333.6$ K. The heating path over this range was in this order: 297, 333.6, 297, 229.5, 297, 192.6, and 297 K. The integrated intensities at 297 K were reproducible within ± 5 percent.

When the sample was heated above 340.7 K, the 42.4 Å spacing was no longer observed. The spacing increased approximately 4 Å, as can be seen in table 4. Furthermore, the long-spacing did not return to the 42.4 Å value when the sample was cooled to room temperature. The heating path for the sample after the solid-solid phase transition was (in order): 344.0, 297, 324.6, 337.9, 344.0, 330.7, 319.0, and 297 K. The integrated intensities at 297 K were reproducible within ± 2 percent. The intensity data in table 4 have been normalized to 297 K, so that the values before and after the transition at 297 K are adjusted to be equal. However, the observed values of the intensity before and after the long-spacing transition were approximately equal at room temperature.

From table 4 one can see that the relative intensity change over $192.6 \leq T \leq 333.6$ K, i.e., over a 141 K temperature range, is 19 percent (before the long-spacing transition). However, over the temperature range $297 \leq T \leq 344.0$ K, i.e., over a 47 K temperature range, the relative intensity change is more than 100 percent (after the long-spacing transition). This is shown in figure 11, in which the relative integrated intensity is plotted as a function of temperature.

c. Discussion

The phase transition at 347.0 K is apparently the rotator type transition [2] and involves a change in the lateral packing of the molecules. The phase transition at 340.7 K is a tilt transition (with little change in the lateral packing of the molecules). In a previous article [3] it was found that crystallization from toluene by quenching the sample in a dry-ice acetone bath led to the orthorhombic phase, with a long-spacing of 47.7 Å (at 297 K). When this orthorhombic form was heated to 345 K, the long-spacing decreased to 45.7 Å. Also, when the monoclinic form was heated to 344 K, the long-spacing increased to 46.2 Å (table IV). It appears that these systems are both approaching a phase with long-spacing around 46 Å above 341 K.

3.7. *n*-Tetratetracontane

a. DSC Studies

A typical DSC scan of the solution recrystallized n-$C_{44}H_{90}$ sample is shown in figure 12. In addition to the solid-liquid transition, 359.3 to 359.5 K (optical microscope), a solid-solid transition was observed at 348.2 K (DSC). This solid-solid transition was found to be irreversible, i.e., it did not occur on a cooling curve, nor reoccur on the subsequent heating curve.

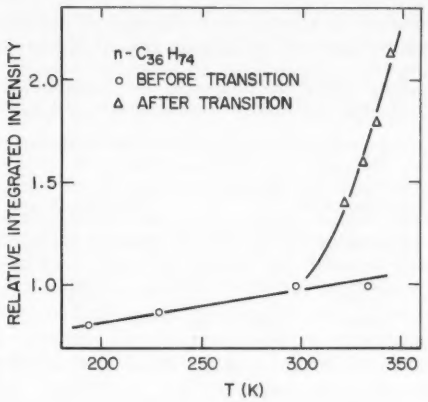

FIGURE 11. *Relative integrated intensity of (002) diffraction maximum of* n-$C_{36}H_{74}$.

0 before phase transition
Δ after phase transition

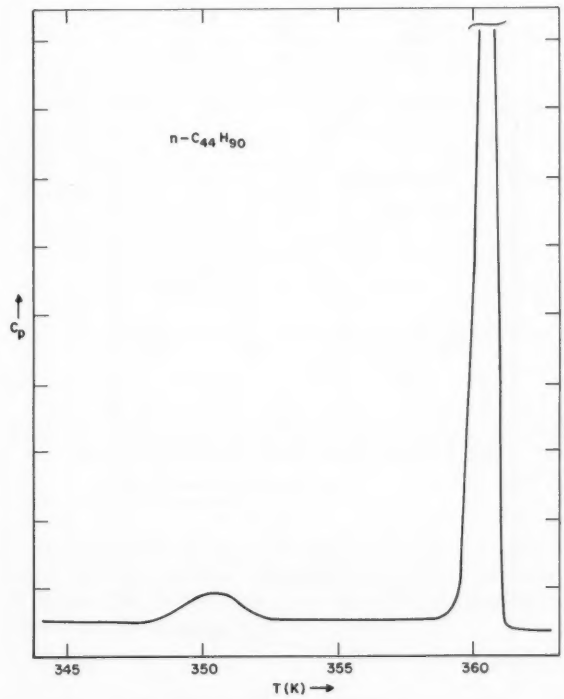

FIGURE 12. *DSC trace of* n-$C_{44}H_{90}$.

b. X-Ray Scattering

A portion of the benzene recrystallized sample was examined in the x-ray camera. The first order diffrac-

tion maximum at 297 K was observed to be 51.2 Å. In table 4 are shown the long-spacing, as well as the relative integrated intensity of the first-order diffraction maximum (normalized to the value at 161.7 K) over the temperature range $161.7 \leq T \leq 354.9$ K. The relative integrated intensities as a function of temperature are shown in figure 13. It can be seen that the relative intensity of the maximum changed continuously over the temperature range $161.7 \leq T \leq 347.2$ K, but above the temperature of the solid-solid transition (348.2 K), the relative intensity increased sharply.

TABLE 4. *X-ray diffraction intensities and long-spacings as a function of temperature for* n-*hexatriacontane and* n-*tetratetracontane*

n-$C_{36}H_{74}$

Before transition			After transition		
T(K)	$A(T)/A$(297 K)	l(Å)	T(K)	$A(T)/A$(297 K)	l(Å)
333.6	1.00	42.4	344.0	2.13	46.2
297	1.00	42.4	337.9	1.80	46.8
229.5	0.87	42.4	330.7	1.61	46.7
192.6	0.81	42.4	324.6	1.41	47.1
			319.0	1.41	46.8
			297	1.00	47.3

n-$C_{44}H_{90}$

T(K)	$A(T)/A$(161.7 K)	l(Å)
354.9	3.15	53.3
350.8	2.35	53.9
347.2	1.16	51.1
297	1.17	51.2
161.7	1.00	51.5

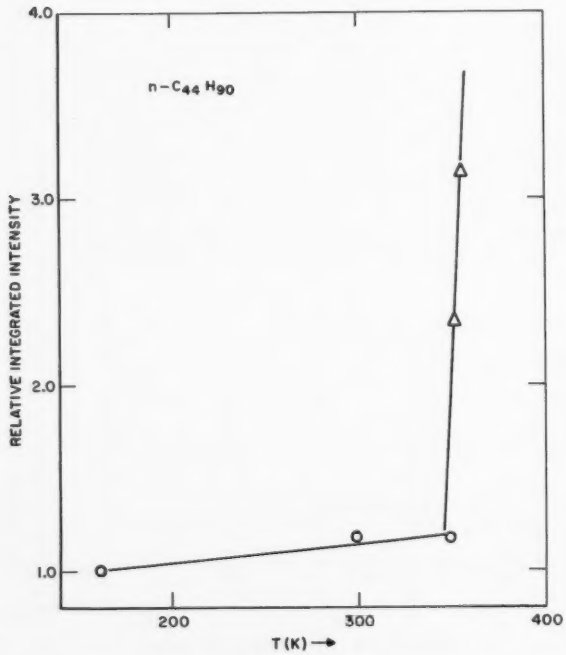

FIGURE 13. *Relative integrated intensity of (002) diffraction maximum of* n-$C_{44}H_{90}$ *as a function of temperature.*

0 before phase transition
Δ after phase transition

c. Discussion

n-$C_{44}H_{90}$, like n-$C_{20}H_{44}$, shows no phase transition to the rotator state when the sample is heated. However, n-$C_{44}H_{90}$ also did not exhibit this transition as the sample was cooled from the melt. The observed long-spacing of 51.2 Å is consistent with a monoclinic form, based [2] on a long-spacing of 57.9 Å for the orthorhombic form. The DSC transition at 348.2 K is a tilt transition, with the long-spacing increasing almost 3 Å.

4. General Discussion

From the above observations, it can be seen that except for 2-nonadecanone, all samples underwent solid-solid phase transitions. Furthermore, in some cases the rates of such transitions can be quite slow. Thus, one must be careful about the thermal history and purity of paraffin systems in order to insure the achievement of a stable form. With respect to crystal spacings and dielectric loss, some discussion is given below for systems in a stable form, and the effect of the phase transitions.

4.1. X-Ray Scattering

All samples in the x-ray sample holder were examined with respect to the height of the sample above the x-ray beam, i.e., in the plane normal to the propagation direction of the primary beam. This allows a determination of the uniformity of the scattering with respect to the height of the sample, which can change as the sample temperature changes. Care was taken to insure the same portion of the sample was examined as the temperature was changed.

a. *n*-Paraffins

For a given crystalline phase, the temperature dependence of the intensity of a diffraction maximum is determined by the temperature dependence of the scattering factor $F(T)$:

$$I(T) = \text{constant}\,|F(T)|^2. \qquad (1)$$

If the scattering units in the system undergo small oscillations, then the Debye-Waller factor can be separated out of $F(T)$. However, at the low angles of scattering of interest in this article, the effect of this factor is small. For n-paraffins, the remaining temperature dependence of $F(T)$ can be related [3] to the interlamellar distance. At temperatures T_1 and T_2, one has:

$$\frac{I(T_2)}{I(T_1)} = \left[\frac{F(T_2)}{F(T_1)}\right]^2 \cong \left[\frac{A(T_2)}{A(T_1)}\right]^2, \qquad (2)$$

where $A(T)$ is the temperature dependent interlamellar distance. Processes that lead to an increase in $A(T)$, i.e., an increase (with increasing temperature) in the concentration of voids on the surfaces of the lamellae, should lead to an increase in the integrated intensity of the maximum relative to some lower temperature.

In the case of n-$C_{20}H_{42}$ over the temperature range 233 K $\leq T \leq$ 308 K (table 3), the long-spacing is constant at 25.4 Å and the relative change in the integrated intensity of the first-order diffraction maximum is 10 percent. For n-$C_{36}H_{74}$ over the temperature range 192.6 $\leq T \leq$ 333.6 K, the relative change in the integrated intensity is 19 percent, with the long-spacing constant at 42.4 Å. And for n-$C_{44}H_{90}$ over 161.7 $\leq T \leq$ 347.2 K, the intensity change is 16 percent and the long-spacing changed slightly.

It appears that for the n-paraffins, when the long-spacing is very nearly constant, the change in the relative integrated intensity of the first order (00l) maximum is 10 to 20 percent (in the temperature range considered). However, after the system has experienced a solid-solid phase transition, the temperature coefficient of the relative integrated intensity appears to increase substantially. This is shown for n-$C_{36}H_{74}$ in figure 11. In this case the solid-solid phase transition occurred at 340.7 K, such that the long-spacing increased approximately 4 Å (table 4). The situation is similar for n-$C_{44}H_{90}$, as is shown in figure 13. The transition occurred at 348.2 K and the long-spacing increased approximately 2.5 Å. The data appears to be consistent with the view that the solid-solid phase transitions—which involve a volume change—are one mechanism to generate substantial amounts of vacancies on the surfaces of the lamellae.

b. Long-Chain Esters and the Ketone

From table 1, one notes that for methyl stearate, there is no observable change in the relative integrated intensity of the (002) diffraction maximum over the temperature range 235 K $\leq T \leq$ 307 K. The long-spacing was constant within 0.1 Å. Similarly, for solution recrystallized ethyl stearate, there is no change in the relative intensity of the first order maximum over 235 K $\leq T \leq$ 297 K. Also, the long-spacing was constant within 0.1 Å. And for 2-nonadecanone, the relative intensity change over 236 K $\leq T \leq$ 325 K was 4 percent and the long-spacing constant at 51.8 Å. It appears that without the vacancy producing mechanism of a tilt transition, the esters and the ketone have a small temperature coefficient for the relative intensity change with temperature of the (00l) maxima.

We note that a tilt transition has been observed for ethyl stearate crystallized from the melt. However, since the sample was crystallized in the x-ray sample holder, only a small drop of liquid was involved. It was then difficult to determine the uniformity of the intensity of scattering from the crystalline sample as the height was changed, even though the location of the maxima could easily be determined. Thus we cannot say from the data if the intensity of the long-spacing maximum for this sample increased due to the tilt transition.

The intensity of the 25.4 Å spacing of the quenched sample of ethyl stearate (sec. 3.2b) was observed to be constant over a period of 26 days at room temperature. However, the sample has undergone solid-solid phase transitions as evidenced by the initial and final DSC scans. It appears that these phase transitions have no measurable effect on the intensity of the low-angle maxima.

However, it is also possible that the (00l) diffraction intensities for these compounds are not as sensitive to surface voids, as is the case for the n-paraffins. One possible reason for this could be that the mechanisms of the phase transitions are different from those of the n-paraffins. In order to compare the relative intensity change with temperature of the n-paraffins, esters and the ketone, an estimate was made of the (002) diffraction intensity as a function of temperature for n-paraffins and branched paraffins, all of the same total number of carbon atoms. The results are shown in figure 14 and the calculation follows.

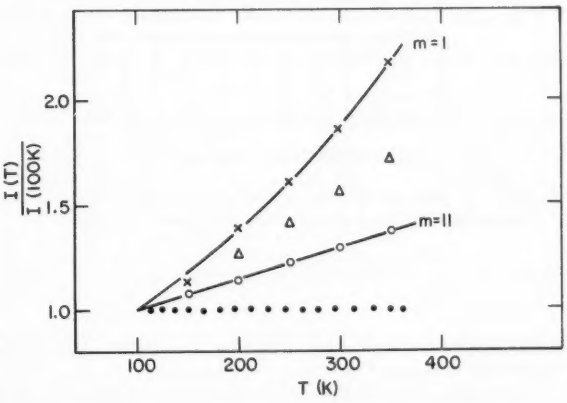

FIGURE 14. *Estimate of the relative integrated intensity as a function of temperature for the (002) diffraction maximum.*

·, 0, X branched paraffins (see text)
Δ linear paraffin

We consider as the scattering unit two lamellae of each system. For the n-paraffin this unit is indicated in figure 15a. In the usual notation [26], the scattering factor for the n-paraffin is:

$$F(\theta) = \sum_{j=0}^{n'} f_j(\theta) e^{ik_0 \cdot r_j}, \qquad (3)$$

where there are $n'+1$ scatterers (i.e., CH_2 groups) in the two lamellae and each $-CH_2-$ group has a scattering factor $f(\theta)$. For the (00l) maxima discussed in this article, one can write eq (3) as:

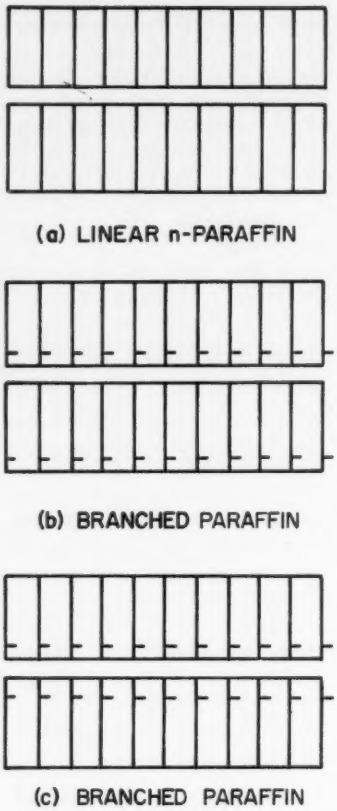

FIGURE 15. *Repeat unit for (a) linear paraffin and (b), (c) branched paraffins, with different arrangement of side group.*

$$F(\theta)=2N\sum_{j=0}^{n} f_j(\theta)e^{i\mathbf{k}\cdot\mathbf{r}_j}, \tag{4}$$

where there are N molecules in a lamella and each molecule has $n+1$ units.

Summing over the scattering for one molecule and assuming $f_{CH_3}(\theta)\simeq f_{CH_2}(\theta)$, one has for the n-paraffin:

$$F(\theta)\cong 2Nf_{CH_2}(\theta)e^{ik(\sin\theta)nx}\,\frac{\sin[k(\sin\theta)(n+1)x]}{\sin[k(\sin\theta)x]}, \tag{5}$$

where nx is the projection of $\mathbf{r}_n$ onto $\mathbf{s}$.

For the branched paraffin, with one $-CH_3$ group in the mth position along the chain, there are two possibilities with respect to how the molecules are arranged in the crystal, indicated in figures 15b and 15c. Ethyl stearate and n-butyl stearate are essentially examples of case (b), while methyl stearate and 2-nonadecanone are examples of case (c) (the scattering factor of oxygen at these low-angles is considered approximately that of a $-CH_2-$ group).

For case (b), eq (3) becomes:

$$F(\theta)\cong 2Nf_{CH_2}(\theta)e^{ik(\sin\theta)nx}\left\{e^{ik(\sin\theta)(2m-n)x}+\frac{\sin[k(\sin\theta)(n+1)x]}{\sin[k(\sin\theta)x]}\right\}. \tag{6}$$

And finally, for case (c), eq (3) becomes:

$$F(\theta)\cong 2iNf_{CH_2}(\theta)e^{ik(\sin\theta)nx}\sin[k(\sin\theta)(2m-n)x]. \tag{7}$$

One can write the temperature dependent scattering factor $F(\theta, T)$ in terms of the temperature dependent molecular length $l(T)$ and interlamellar distance $A(T)$, where $l(T)=(n+1)x+A(T)$. Suppose that the change with temperature of $A(T)$ is the same for the linear paraffin and both cases of the branched paraffin. Assume this change is $\frac{0.2\ \text{Å}}{100\ \text{K}}$ which is about the change in the a axis observed by Cole and Holmes [27] for n-$C_{36}H_{74}$.

Recalling that $I(\theta, T)$ is proportional to $|F(\theta, T|^2$, then from eqs (5), (6), and (7) one can estimate the change with temperature of the relative intensities of the low-angle maxima for the various cases of the linear and branched paraffins, all with the same total number of carbon atoms.

The results of these calculations are shown in figure 14. Case (c), the dotted line in figure 14, is found to be practically temperature independent (1% decrease) over the range of the calculation. The observed data for methyl stearate and 2-nonadecanone (tables 1 and 3), which approximate case (c), are consistent with the calculation. For case (c), there is a negligible temperature effect (for the intensity of the (002) maximum) of the location of the side group on the chain.

For the calculation with the branched paraffin of case (b), the location of the side group on the chain does affect the temperature dependence of the intensity of the (002) maximum. When the side group is near the center of the chain ($m=11$), the intensity increase over the 250 K temperature range is about 37 percent. When the side group is near the end of the chain ($m=1$), the intensity increase is estimated to be 120 percent. All cases with $1\leq m\leq 11$ fall between the two solid lines of figure 14. The n-paraffin case (Δ in fig. 14) falls between $m=1$ and $m=11$. For ethyl stearate ($m=3$), the estimated increase in intensity is 22 percent over $200\leq T\leq 300$ K. There is no observed intensity change (c.f. tab. 1) over this temperature range. In fact, the long-spacings for methyl stearate, ethyl stearate, 2-nonadecanone and n-$C_{20}H_{42}$ are practically constant over the temperature ranges of observation, so that the assumed interlamellar expansion of $\frac{0.2\ \text{Å}}{100\ \text{K}}$ is probably too large. Thus the estimates shown in figure 14 should only be considered as an upper bound.

4.2. Dielectric Relaxation

It appears that the loss peak at 297.1 K for n-butyl stearate is an equilibrium property of the material,

since little change in the peak was observed over a period of 30 days. The solid line in figure 7 is a fit of the data to a Debye curve, using the observed values of $\epsilon'(0)-\epsilon'(\infty)=0.053$ and a relaxation time of $\tau=1.1\times10^{-4}$ s. The loss was calculated [28] from the equation:

$$\epsilon''(\omega)=\frac{[\epsilon'(0)-\epsilon'(\infty)]\omega\tau}{1+\omega^2\tau^2}. \quad (8)$$

It can be seen that the Debye curve is a reasonable approximation to the observed data.

For the sample of *n*-butyl stearate stored at 273 K for 4 days (which is sufficient time for the solid-solid phase transition to complete itself), the loss is quite small at 285 K. Furthermore, a long annealing time, e.g., 4 months at 277 K, does not appreciably change the loss, so that below the solid-solid phase transition shown in figure 5b, the equilibrium value of the loss (over the frequency range 10 Hz to 2×10^4 Hz) is quite small. While the long annealing time should allow the healing out of volume defects, once the phase transition has completed itself, further annealing does not appear to reduce the loss measurably.

Dryden [20] has similarly observed a loss peak in *n*-butyl stearate at 293 K, with τ approximately 1.5×10^{-4} s. Also, Dryden found from a plot of log $\omega_{max.}$ versus 1/T that two discontinuities occurred, one at approximately 287 K, the other at 284 K. These temperatures correspond to the phase transition temperatures observed with the DSC in this article, viz; 288.4 and 284.5 K. However, it should be pointed out that the loss peaks Dryden has observed at 293 K and lower are probably not equilibrium properties, since as discussed in section 3.3(a), the system is slowly undergoing a phase transition to a more stable form.

Dryden and Welsh [29] have also shown that $\epsilon'(0)-\epsilon'(\infty)$, for similar long-chain esters, increases with increasing amounts of added impurity. However, the data shown in figure 7 at 285.0 K and 297.1 K is for the same sample, so that the impurity level is constant. Thus, in addition to chemical impurities as a cause of dielectric loss, the crystalline phase of the substance is also an important factor.

5. Conclusions

For a series of long chain *n*-paraffins, long chain esters and a long chain ketone, the intensity change of the long-spacing (determined by x-ray scattering) was no more than 10 to 20 percent over a temperature range of 100 K, when no tilt transition occurred. However the temperature coefficient of the intensity of the long-spacing was found to increase substantially for *n*-paraffins when a tilt transition occurred. The dielectric loss in an annealed sample of *n*-butyl stearate was found to be quite small. However at 297.1 K, a distinct loss peak was observed, which did not change with time. Both reversible solid-solid phase transitions (n-$C_{36}H_{74}$, *n*-butyl stearate) and irreversible transitions (ethyl stearate, *n*-butyl stearate, n-$C_{20}H_{42}$) were observed with these systems. The rate of the irreversible phase transitions (*n*-butyl stearate and ethyl stearate) were found to be strongly temperature dependent.

The author is pleased to acknowledge the assistance and numerous helpful discussions of Anthony J. Bur and James J. Weeks.

6. References

[1] Markley, K. S., Fatty Acids, (Interscience, 1947).
[2] Broadhurst, M. G., J. Res. Nat. Bur. Stand. (U.S.), **66A** (Phys. and Chem.) No. 2, 241–249 (May–June 1962).
[3] Sullivan, P. K. and Weeks, J. J., J. Res. Nat. Bur. Stand. (U.S.), **74A** (Phys. and Chem.), No. 2, 203–214 (Mar.–Apr. 1970).
[4] Fischer, E. W., J. Pure and Applied Chem. **26,** 385 (1971).
[5] Heitz, W., Wirth, T., Peters, R., Strobl, G., and Fischer, E. W., Die Makromolekulare Chemie **162,** 63 (1972).
[6] Scheiber, D. J., J. Res. Nat. Bur. Stand. (U.S.), **65C** (Eng. and Instr.), 23 (1961).
[7] Brown, J. B., J. Am. Oil Chem. Soc. **32,** 646 (1955).
[8] Sedgwick, R. S., Hoerr, C. W., and Harwood, H. J., J. Org. Chem. **17,** 327, (1952).
[9] Clark, S. G., M. S. Thesis, The Penn State Univ., 1956
[10] Aleby, S., and von Sydow, E., Acta Cryst. **13,** 487 (1960).
[11] Simonelli, A. P., Ph. D. Thesis, Univ. Wisc., 1960.
[12] Guy, J. B., and Smith, J. C., J. Chem. Soc. 615 (1939).
[13] Smit, W M., Anal. Chim. Acta, **17,** 27, (1957).
[14] Craig, B. M., J. Am. Oil Chemists Soc. **34,** 30, (1957).
[15] Francis, F. and Piper, S. H., J. Am. Chem. Soc., **61,** 577, (1939).
[16] Schaerer, A. A., Busso, C. J., Smith, A. E. and Skinner, L. B., J. Am. Chem. Soc. **77,** 2017 (1955).
[17] Aleby, S., Acta Cryst. **15,** 1248 (1962).
[18] Malkin, T., J. Chem. Soc. 2796 (1931).
[19] Malkin, T., Trans. Faraday Soc. **29,** 977 (1933).
[20] Dryden, J. S., J. Chem. Phys. **26,** 604 (1957).
[21] Saville, W. B. and Shearer, G., J. Chem. Soc. 591 (1925).
[22] Seyer, W. F., Patterson, R. F. and Keays, J. L., J. Am. Chem. Soc. **66,** 179 (1944).
[23] Schaerer, A. A., Boyle, G. G., and Mazee, W. M., Rec. Trav. Chim. **75,** 513 (1956).
[24] Crissman, J. M., Passaglia, E., Eby, R. K., and Colson, J. P., J. Appl. Cryst. **3,** 194, (1970).
[25] Shearer, H. M. M., and Vand, V., Acta Cryst. **9,** 379 (1956).
[26] James, R. W., Optical Principles of the Diffraction of X-Rays (Cornell Univ. Press, Ithaca, N.Y., 1965).
[27] Cole, E. A., and Holmes. D. R., J. Polymer Sci. **46,** 245 (1960).
[28] Debye, P., Polar Molecules (Dover Pub. Inc., N.Y., 1929).
[29] Dryden, J. S., and Welsh, H. K., Disc. Faraday Soc. **48,** 211 (1969).

(Paper 78A2–806)

JOURNAL OF RESEARCH of the National Bureau of Standards—A. Physics and Chemistry
Vol. 78A, No. 2, March–April, 1974

Simultaneous Measurements of Heat Capacity, Electrical Resistivity, and Hemispherical Total Emittance by a Pulse Heating Technique: Vanadium, 1500 to 2100 K*

A. Cezairliyan, F. Righini, and J. L. McClure**

Institute for Materials Research, National Bureau of Standards, Washington, D.C. 20234

(November 30, 1973)

Simultaneous measurements of heat capacity, electrical resistivity, and hemispherical total emittance of vanadium in the temperature range 1500 to 2100 K by a subsecond duration, pulse heating technique are described. The results are expressed by the relations:

$$c_p = 56.34 - 3.839 \times 10^{-2} T + 1.563 \times 10^{-5} T^2$$
$$\rho = 8.794 + 6.282 \times 10^{-2} T - 6.804 \times 10^{-6} T^2$$

where c_p is in $J \cdot mol^{-1} \cdot K^{-1}$, ρ is in $10^{-8}\ \Omega \cdot m$, and T is in K. The values for the hemispherical total emittance are: 0.313 at 1900 K and 0.332 at 2000 K. Estimated inaccuracies of the measured properties are: 3 percent for heat capacity, 0.5 percent for electrical resistivity and 5 percent for hemispherical total emittance.

Key words: Electrical resistivity; emittance; heat capacity; high-speed measurements; high temperature; thermodynamics; thermophysics; vanadium.

1. Introduction

In this paper, application of a pulse heating technique to the simultaneous measurements of heat capacity, electrical resistivity, and hemispherical total emittance of vanadium in the temperature range 1500 to 2100 K is described.

The method is based on rapid resistive self-heating of the specimen from room temperature to high temperatures (above 1500 K) in less than one second by the passage of an electrical current pulse through it; and on measuring, with millisecond resolution, such experimental quantities as current through the specimen, potential drop across the specimen, and specimen temperature. Details regarding the construction and operation of the measurement system, the methods of measuring experimental quantities, and other pertinent information, such as the formulation of relations for properties, error analysis, etc. are given in earlier publications [1, 2][1].

In the following sections of this paper a new approach—tabular format—is adopted in presenting information on the specimen, measurements, system characteristics, results, and errors.

The reasons for adopting this format are: (1) to facilitate the preparation of manuscripts, (2) to standardize the contents of the papers on measurements using the present or similar systems in other laboratories, (3) to facilitate information retrieval by the reader, (4) to provide a means for efficient and accurate identification, coding, characterization, and data reduction by scientific and technical information centers, and (5) to ultimately lead to the computerized preparation of papers.

* This work was supported in part by the U.S. Air Force Office of Scientific Research.
** Guest scientist from the Istituto di Metrologia "G. Colonnetti" in Torino, under a fellowship from the Consiglio Nazionale delle Ricerche of Italy.

[1] Figures in brackets indicate the literature references at the end of this paper.

530-326 OL - 74 - 4

2. Measurements

The details regarding the vanadium specimen used in the present measurements are given in table 1. A summary of the measurement technique and the operational characteristics of the system is given in table 2. The polynomial functions (obtained by the least squares method) that represent the experimental results are given in table 3. The final values on properties at 100 degree temperature intervals computed using the functions are given in table 4. The experimental results are presented in the appendix. Each number tabulated in the appendix represents results from over 50 original data points. An estimate of errors in the measured and computed quantities is given in table 5. All values reported in this paper are based on the International Practical Temperature Scale of 1968 [3]. In all computations, the geometrical quantities are based on their room temperature (298 K) dimensions.

TABLE 1. Specimen information

No.	Item	Unit	Explanation
1	Substance		Vanadium (polycrystalline)
2	Source*		Materials Research Corporation
3	Purity		99.9+%
4	Impurities		Listed in table 1a
5	Geometry		Tube made from rod by electro-erosion
6	Dimensions		
	total length	mm	76.26
	effective** length	mm	25.53
	outside diameter	mm	6.3
	wall thickness	mm	0.5
	blackbody hole	mm	0.5 × 1 (rectangular)
7	Weight		
	total weight	g	4.319
	effective** weight	g	1.438
8	Characteristics		
	atomic weight		50.942
	density	$g \cdot cm^{-3}$	6.1
	resistivity at 293 K	$10^{-8}\Omega \cdot m$	21.7
9	Special treatment		Heat treated by pulse heating before the experiments (30 pulses to 1900 K)

*The supplier is identified in this paper in order to adequately characterize the specimen. Such an identification does not imply recommendation or endorsement by the National Bureau of Standards.

**Effective refers to the portion of the specimen between the voltage probes.

TABLE 1a. Impurities in the specimen*

(according to the manufacturer's analysis)

Element	C	Fe	Nb	N	O	P
ppm	120	20	60	10	15	15
Element	Si	Ta	Ti	W	Zr	
ppm	50	70	10	30	15	

*The total amount of all other detected elements is less than 50 ppm, each element being below 10 ppm limit.

TABLE 2. Measurement technique and system characteristics

No.	Item	Unit	Explanation and Data
1	General technique		Pulse heating (subsecond)
2	Voltage measurement		Across tungsten knife-edge probes
3	Current measurement		Across standard resistor (0.001 Ω) in series with the specimen
4	Temperature measurement		High-speed photoelectric pyrometer [4]
5	Specimen environment		Vacuum ~ 1.3×10^{-3} $N \cdot m^{-2}$ (~ 10^{-5} torr)
6	Power source		Battery bank (14series-connected 2V batteries, capacity 1100 A·h each)
7	Recording		Digital data acquisition system
8	Signal resolution		~ 0.01% (at full scale)
9	Time resolution	ms	0.4
10	Data processing		Time-sharing computer
11	Date of measurements		August 1973
12	Number of experiments		4
13	Temperature range	K	1500–2100
14	Temperature subranges	K	I (1480–1710) II (1690–1890) III (1810–2050) IV (2000–2130)
15	Experiment duration	ms	600–620
16	Current pulse length	ms	400–420
17	Imparted power	W	4000–5200
18	Current	A	1300–1600
19	Rate of current change	$A \cdot ms^{-1}$	0.3–0.6
20	Heating rate	$K \cdot ms^{-1}$	3.9–4.5
21	Cooling rate	$K \cdot ms^{-1}$	0.04–0.15
22	Radiative heat loss (% of input power)		1% at 1500 K 4% at 2100 K

TABLE 3. Functional representation of results on vanadium

Heat capacity ($J \cdot mol^{-1} \cdot K^{-1}$)	Resistivity ($10^{-8}\Omega \cdot m$)	Hemispherical total emittance
$c_p = A + BT + CT^2$	$\rho = A + BT + CT^2$	$\epsilon = A + BT$
$A = 56.34$	$A = 8.794$	$A = -5.413 \times 10^{-2}$
$B = -3.839 \times 10^{-2}$	$B = 6.282 \times 10^{-2}$	$B = 1.930 \times 10^{-4}$
$C = 1.563 \times 10^{-5}$	$C = -6.804 \times 10^{-6}$	
$1500\ K < T < 2100\ K$	$1500\ K < T < 2100\ K$	$1880\ K < T < 2050\ K$
$\sigma^* = 1.1\%$	$\sigma^* = 0.06\%$	$\sigma^* = 0.05\%$

*Standard deviation.

TABLE 4. Results on properties of vanadium

T (K)	c_p ($J \cdot mol^{-1} \cdot K^{-1}$)	ρ ($10^{-8}\Omega \cdot m$)	ϵ
1500	33.92	87.72	- - -
1600	34.93	91.89	- - -
1700	36.25	95.92	- - -
1800	37.88	99.83	- - -
1900	39.82	103.59	0.313
2000	42.08	107.22	0.332
2100	44.65	110.71	- - -

TABLE 5. Error analysis (at 2000 K)

Quantity	Imprecision*	Inaccuracy**
Temperature	0.5 K	4 K
Voltage	0.03%	0.1%
Current	0.03%	0.1%
Heat capacity	1%	3%
Electrical resistivity	0.1%	0.5%
Hemispherical total emittance	0.1%	5%

*Imprecision refers to the standard deviation of an individual point as computed from the difference between measured value and that from the smooth function obtained by the least squares method.

**Inaccuracy refers to the estimated total error (random and systematic).

3. Discussion

The heat capacity, electrical resistivity, and hemispherical total emittance of vanadium measured in this work are presented and compared graphically with those reported in the literature in figures 1, 2 and 3, respectively.

The heat capacity results of this work are approximately 6–8 percent lower than those of Jaeger and Veenstra [5] and Fieldhouse and Land [6], and are approximately 8 percent higher than those of Peletskii et al. [7] over the respective overlapping regions. The results reported in the literature were for temperatures below 1900 K. In this work, the measurements are extended to 2100 K, which is approximately 90 K below the melting point of vanadium.

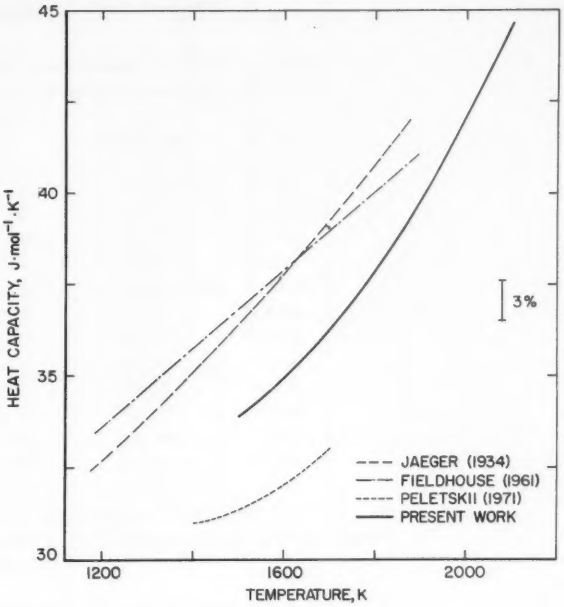

FIGURE 1. *Heat capacity of vanadium reported in the literature.*

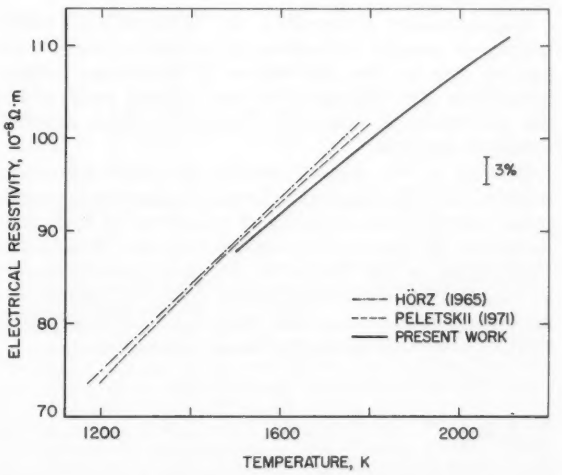

FIGURE 2. *Electrical resistivity of vanadium reported in the literature.*

The electrical resistivity results are in reasonably good agreement (maximum differences about 2%) with those reported by Hörz et al. [8] and Peletskii et al. [7]. At 293 K, the observed electrical resistivity is approximately 3 percent higher than the value ($21.02 \times 10^{-8}\Omega \cdot m$) reported by Peletskii et al. [7]. In the range of the present measurements, vanadium showed a negative departure from linearity in the

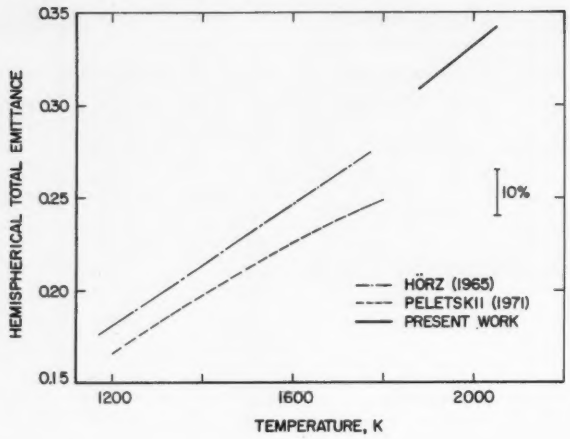

FIGURE 3. *Hemispherical total emittance of vanadium reported in the literature.*

temperature dependence of electrical resistivity. A similar behavior was previously noted for niobium [9] and tantalum [10], which belong to the same group (V) on the periodic table.

Considerable differences in hemispherical total emittance results of various investigators may be expected due to the differences in specimen surface conditions. The difference of the present results from the extrapolated values of Hörz et al. [8] is approximately 6 percent.

Similar to the earlier results on other refractory metals [2, 9, 10, 11] obtained with the present measurement system, heat capacity of vanadium at high temperatures is considerably higher than the Dulong and Petit value of $3R$. Some of this departure is due to $c_p - c_v$ and the electronic terms. However, they do not account for the entire difference. Heat capacity above the Debye temperature may be expressed by

$$c_p = A - \frac{B}{T^2} + CT + \Delta c$$

where the constant term is $3R$ (24.943 J · mol^{-1} · K^{-1}), the term in T^{-2} is the first term in the expansion of the Debye function, the term in T represents $c_p - c_v$ and electronic contributions, and the quantity Δc represents excess in measured heat capacity at high temperatures, which is not accounted for by the first three terms. The coefficients B (1.50×10^5) and C (4.86×10^{-3}) were obtained from heat capacity values at 270 K [12, 13] and at 1000 K. The value at 1000 K was estimated based on the extrapolation of the present work results and the low temperature results reported in the literature [12, 13].

Using the above equation and the heat capacity results of this work, the quantity Δc was computed for temperatures above 1500 K. The results for Δc in J · mol^{-1} · K^{-1} are: 1.8 at 1500 K, 4.2 at 1800 K, and 9.5 at 2100 K.

Although the mechanisms of vacancy generation become important at high temperatures, it was not possible to attribute the high heat capacity values entirely to vacancies. To demonstrate this, a crude estimate of the contribution of vacancies to heat capacity was made using the method described in a previous publication [2]. The results indicate that vacancy contribution would be small, approximately 0.03 J · mol^{-1} · K^{-1} at 1500 K and 0.5 J · mol^{-1} · K^{-1} at 2100 K, and would not account for the high heat capacity values. If the entire difference between measured and computed (using the first three terms in the above equation) heat capacities is attributed to vacancies, values of 1.1 eV for vacancy formation energy and 3.8 percent for vacancy concentration at the melting point are obtained. Both of these values, especially the concentration, seem to be unrealistic for vanadium.

The new format adopted in this paper has demonstrated the feasibility of concise yet complete and systematic documentation of measurements performed with the present system. For reasons enumerated in the Introduction, it is hoped that the approach of a standardized quasi-tabular presentation will find wide acceptance among the experimenters in the same and related fields.

The authors express their gratitude to C. W. Beckett for his encouragement of research in high-speed thermophysical measurements and to M. S. Morse for his help with the electronic instrumentation.

4. Appendix

TABLE A–1. Experimental results on heat capacity and electrical resistivity of vanadium

Temperature (K)	c_p ($J \cdot mol^{-1} \cdot K^{-1}$)	Δc_p* (%)	ρ ($10^{-8}\Omega \cdot m$)	$\Delta\rho$* (%)
1500	33.48	−1.32	87.66	−0.06
1550	34.50	+0.33	89.81	−0.01
1600	35.32	+1.10	91.93	+0.05
1650	35.88	+0.92	94.03	+0.12
1700	35.81	−1.23	95.83	−0.09
1750	37.20	+0.46	97.86	−0.03
1800	38.26	+0.99	99.87	+0.05
1850	38.61	−0.53	101.69	−0.03
1900	39.71	−0.30	103.56	−0.02
1950	40.80	−0.29	105.40	−0.02
2000	41.96	−0.30	107.20	−0.01
2050	42.72	−1.43	109.01	+0.03
2100	45.34	+1.51	110.70	0.00

*The quantities Δc_p and $\Delta\rho$ are percentage deviations of the individual results from the smooth functions represented by the pertinent equations in table 3.

TABLE A–2. Experimental results on hemispherical total emittance of vanadium

Temperature (K)	ϵ	$\Delta\epsilon$* (%)	Temperature (K)	ϵ	$\Delta\epsilon$* (%)
1874.5	0.307	−0.12	2022.6	0.336	−0.06
1878.4	0.308	−0.03	2028.0	0.337	−0.02
1882.4	0.309	+0.03	2033.4	0.338	+0.01
1886.4	0.310	+0.06	2038.9	0.339	+0.02
1890.5	0.311	+0.06	2044.5	0.341	+0.02
1894.7	0.312	+0.03	2050.1	0.342	+0.01

*The quantity $\Delta\epsilon$ is percentage deviation of the individual results from the smooth function represented by the pertinent equation in table 3.

5. References

[1] Cezairliyan, A., Design and operational characteristics of a high-speed (millisecond) system for the measurement of thermophysical properties at high temperatures. J. Res. Nat. Bur. Stand. (U.S.) **75C** (Eng. and Instr.), No. 1, 7–18 (Jan.–Mar. 1971).

[2] Cezairliyan, A., Morse, M. S., Berman, H. A., and Beckett, C. W., High-speed (subsecond) measurement of heat capacity, electrical resistivity, and thermal radiation properties of molybdenum in the range 1900 to 2800 K. J. Res. Nat. Bur. Stand. (U.S.) **74A** (Phys. and Chem.), No. 1, 65–92 (Jan.–Feb. 1970).

[3] International Practical Temperature Scale of 1968. Metrologia **5**, 35 (1969).

[4] Foley, G. M., High-speed optical pyrometer. Rev. Sci. Instr. **41**, 827 (1970).

[5] Jaeger, F. M., and Veenstra, W. A., The exact measurement of the specific heats of solid substances at high temperatures. VI. The specific heats of vanadium, niobium, tantalum and molybdenum. Rec. Trav. Chim. **53**, 677 (1934).

[6] Fieldhouse, I. B., and Lang, J. I., Measurement of thermal properties. Report WADD TR 60–904 (1961).

[7] Peletskii, V. E., Druzhinin, V. P., and Sobel', Ya. G., Thermophysical properties of vanadium at high temperatures. High Temp.–High Press. **3**, 153 (1971).

[8] Hörz, G., Gebhardt, E., and Dürrschnabel, W., Emissionsvermögen und elektrischer widerstand von vanadium, vanadium-stickstoff- und vanadium-sauerstoff-mischkristallen. Z. Metallkunde **56**, 554 (1965).

[9] Cezairliyan, A., High-speed (subsecond) measurement of heat capacity, electrical resistivity, and thermal radiation properties of niobium in the range 1500 to 2700 K. J. Res. Nat. Bur. Stand. (U.S.) **75A** (Phys. and Chem.), No. 6, 565–571 (Nov.–Dec. 1971).

[10] Cezairliyan, A., McClure, J. L., and Beckett, C. W., High-speed (subsecond) measurement of heat capacity, electrical resistivity, and thermal radiation properties of tantalum in the range 1900 to 3200 K, J. Res. Nat. Bur. Stand (U.S.) **75A** (phys. and Chem.), No. 1, 1–13 (Jan.–Feb. 1971).

[11] Cezairliyan, A., and McClure, J. L., "High-speed (subsecond) measurement of heat capacity, electrical resistivity, and thermal radiation properties of tungsten in the range 2000 to 3600 K", J. Res. Nat. Bur. Stand. (U.S.) 75A (Phys. and Chem.), No. 4, 283–290 (July–Aug. 1971).

[12] Bieganski, Z., and Stalinski, B., Heat capacities and thermodynamic functions of vanadium and vanadium hydride within the range 24 to 340 K. The hydrogen contribution to the heat capacity of transition metal hydrides. Bull. Acad. Polon. Sci. Ser. Sci. Chim. **9**, 367 (1961).

[13] Anderson, C. T., The heat capacities of vanadium, vanadium trioxide, vanadium tetroxide and vanadium pentoxide at low temperatures. J. Am. Chem. Soc. **58**, 564 (1936).

(Paper 78A2–807)

JOURNAL OF RESEARCH of the National Bureau of Standards—A. Physics and Chemistry
Vol. 78A, No. 2, March–April, 1974

The Shape of Idealized Grain Boundaries

S. R. Coriell

Institute for Materials Research, National Bureau of Standards, Washington, D.C. 20234

(December 3, 1973)

Mullins has treated a two-dimensional model of grain boundary motion in which each point on the boundary moves toward its center of curvature with a speed proportional to its curvature. For boundaries which preserve shape under uniform magnification, an integral representation of the boundary shape is found. We then obtain several analytic results from approximate evaluations of the integral.

Key words: Boundary shape; curvature; grain boundary.

The motion of an idealized grain boundary in two dimensions has been treated by Mullins [1].[1] In this model, a given point on the grain boundary moves towards its center of curvature with a speed that is proportional to the curvature. Recently Sun and Bauer [2] have extended the Mullins treatment by numerically solving the differential equation for the boundary shape for the case of boundaries which are invariant under magnification. They have used the results to measure grain boundary mobilities [3].

The shape of a boundary which is invariant under magnification is given by

$$r(\theta, t) = R(\theta)\ T(t) \tag{1}$$

where r and θ are polar coordinates and t is the time. $T(t) = [T^2(0) + 2ct]^{1/2}$, where c is a separation constant and $R(\theta)$ satisfies the nonlinear differential equation

$$\{R^2 + 2R_\theta^2 - RR_{\theta\theta}\} / \{R^2\,[R^2 + R_\theta^2]\} = -\,(c/k). \tag{2}$$

Here, the subscript θ denotes differentiation with respect to θ and $k = M\sigma$ where M is a mobility and σ is the boundary free energy.

The purpose of this note is to obtain some analytic results for $R(\theta)$; in particular, the solution of eq (2) can be reduced to a single quadrature. Following standard techniques [4], we find

$$\theta(R) - \theta_0 = \int_{R_0}^{R} d\alpha\, \alpha^{-1} \{C_1\alpha^2 \exp(c\alpha^2/k) - 1\}^{-1/2}, \tag{3}$$

where $\theta(R_0) = \theta_0$ and C_1 is an integration constant. Sun and Bauer consider that a free surface acts as a mirror plane; thus for a free surface along the ray $\theta = \theta_0$ we take as an additional boundary condition $R_\theta = 0$ at R_0. Introducing the change of variable $\eta = (\alpha^2/R_0^2) - 1$, eq (3) becomes

$$\theta(R) - \theta_0 = \tfrac{1}{2} \int_0^{\rho} d\eta (1+\eta)^{-1} \{(1+\eta) \exp(b\eta) - 1\}^{-1/2}, \tag{4}$$

where $\rho = (R^2/R_0^2) - 1$ and $b = (c/k)\ R_0^2$. The boundary shapes for different values of b have been discussed by Mullins. Figure 3 of reference [1] and figure 1 of reference [2] illustrate boundary shapes for various values of b. In reference [1], $R_0 = 3/2$ and $\theta_0 = \pi/2$ and in reference [2], $\theta_0 = 0$ and α and $f(\alpha)$ are equal to our $\theta(\infty) - \theta_0$ and b, respectively. From the equation for $T(t)$, we see that $b > 0$ yields solutions which increase in size with time while $b < 0$ gives solutions which shrink toward the origin $r = 0$. For example, from eq. (2) it is clear that $b = -1$ is a circle of radius R_0; eq (4) is singular in this case since when $R(\theta) = R_0$, $\theta \neq \theta(R)$. The case $b = 0$ corresponds to a straight line. For $b > 0$, Sun and Bauer [2] solved numerically a differential equation, equivalent to eq (2), to obtain the boundary shape. For $b > 0$, R ranges from R_0 to infinity. For $b < 0$, R ranges from R_0 to a value of R at which the quantity $[(1+\rho) \exp(b\rho) - 1]$ becomes negative. It follows that for $-1 < b < 0$, R is greater than R_0 while for $b < -1$, R is less than R_0.

Although it does not appear possible to evaluate the right-hand side of eq (4) analytically, we can obtain some approximate analytic results. For values $|b\rho|$

[1] Figures in brackets indicate the literature references at the end of this paper.

$=|(b/R_0^2)(R^2-R_0^2)|<<1$(and $b \neq -1$), we have $(1+\eta)$ exp $(b\eta)-1 \cong (1+b)\eta\ \{1+(b\eta)\ (1+b/2)/(1+b)\}$ and integration of eq (4) gives

$$\cos\{2(1-b^2/2)^{1/2}\ (\theta-\theta_0)\}$$

$$=\{1-\rho(1-b-b^2)/(1+b)\}/\{1+\rho\}\cdot \qquad (5)$$

When $b>>1$, the only contribution to the integrand occurs for η near zero. We can than approximate the integrand by $\{\exp(b\eta)-1\}^{-1/2}$. Upon integration and rearrangement, we obtain

$$R=R_0\{1-(2/b)\ \ln\cos[b(\theta-\theta_0)]\}^{1/2} \qquad (6)$$

We see that $\theta-\theta_0=\pi/2b$ when R is infinite. Thus, eq (6) gives the shape of a grain boundary which makes a very small angle with a free surface.

Finally, for R infinite, we obtain an approximate analytic formula for $\theta(\infty)-\theta_0$ as a function of b. We rewrite the integrand of eq (4) in the form $[(1+b)\eta]^{-1/2}\ [1+\eta]^{-1}$ exp $[-b\eta/2]\ [1+\{1-b\eta-e^{-b\eta}\}/\{\eta(1+b)\}]^{-1/2}$. Expanding the last factor in powers of $b\eta$, yields

$$[1+\{1-b\eta-e^{-b\eta}\}/\{\eta(1+b)\}]^{-1/2}$$

$$=1+\alpha_1\eta+\alpha_2\eta^2+\ \ldots,$$

where $\alpha_1=b^2/4(1+b)$ and $\alpha_2=\{b^3/96(1+b)\}\{[9b/(1+b)]-8\}$. The resulting integrals can be evaluated in terms of error functions to give

$$\theta(\infty)-\theta_0=\{\pi/2b(1+b)\}^{1/2}\{g+\alpha_1(1-g)$$

$$+\alpha_2\ (g-1+b^{-1})\}, \qquad (7)$$

where $g=(\pi b/2)^{1/2}$ exp $(b/2)$ erfc $[(b/2)^{1/2}]$. The α_2 term is small compared to the leading term. Thus, eq (7) provides an analytic representation of the numerical results for b as a function of $\theta(\infty)-\theta_0$, which are given in figure 2 of reference [2]. It is perhaps surprising that eq (7) is a good approximation for all values of b, since it is based on an expansion in powers of $(b\eta)$. However, when $b\eta$ is not small, the integrand is very small due to the exponential term and makes a negligible contribution to the integral. For $b<<1$, eq (7) yields

$$\theta(\infty)-\theta_0=\frac{\pi}{2}\ [1-(2b/\pi)^{1/2}]$$

and for

$$b\to\infty,\ \theta(\infty)-\theta_0=b^{-1}$$

$$(\pi/2)^{1/2}\ [1+(1/4)+(1/32)]=1.61/b,$$

which is in reasonable agreement with the result $(\pi/2b)$ obtained from eq (6). As an example of an intermediate value of b, we find that for $b=7.1$, $\theta(\infty)-\theta_0=10.0°$ in agreement with Sun and Bauer.

References

[1] Mullins, W. W., J. Appl. Phys. **27**, 900 (1956).
[2] Sun, R. C., and Bauer, C. L., Acta Met. **18**, 635 (1970).
[3] Sun, R. C., and Bauer, C. L., Acta Met. **18**, 639 (1970).
[4] Murphy, G. M., Ordinary Differential Equations and Their Solutions (Van Nostrand, Princeton, N. J. 1960), p. 159–161 and p. 26.

(Paper 78A2–808)

JOURNAL OF RESEARCH of the National Bureau of Standards—A. Physics and Chemistry
Vol. 78A, No. 2, March–April 1974

Reactions of Fluorocarbon Ions in C_2F_6. Implications for the Radiolysis*

L. W. Sieck, R. Gorden, Jr., and P. Ausloos

Institute for Materials Research, National Bureau of Standards, Washington, D.C. 20234

(September 17, 1973)

Reactions of the fragment ions formed in the photoionization of C_2F_6, Xe-C_2F_6, and Kr-C_2F_6 mixtures have been investigated in the NBS photoionization mass spectrometer using both helium (21.2 eV) and neon (16.66–16.84 eV) resonance radiation. Contrary to previously held views, it is shown that CF_3^+ ions having no internal excitation energy undergo the F^- transfer reaction:

$$CF_3^+ + C_2F_6 \rightarrow CF_4 + C_2F_5^+. \qquad \text{(a)}$$

A rate constant of $4 \pm 1 \times 10^{-11}$ cm^3/molecule $-$s is determined for reaction (a) at pressures below 10^{-2} torr. On the basis of the collision rate for these reactants, it can be estimated that, on the average, each CF_3^+ ion undergoes 16 unreactive collisions before undergoing reaction (a). Therefore, from the facts that (1) in pure C_2F_6, all CF_3^+ ions undergo reaction (a) at high pressures, and (2) CF_3^+ ions formed by charge transfer from Xe^+ ions with a maximum of 8.4 kJ/Mol (2 kcal/mol) excess energy undergo reaction (a), one must conclude that reaction (a) is either thermoneutral or exothermic for ground state CF_3^+ ions. Therefore, the earlier estimate for $\Delta H_f(C_2F_5^+)$ of $\sim$33 kJ/mol (8 kcal/mol) must be revised downward: $\Delta H_f(C_2F_5^+) \leq 3.8$ kJ/mol (0.9 kcal/mol).

The $C_2F_5^+$ ion is unreactive towards C_2F_6, but does react with alkanes through the H^- transfer reaction:

$$C_2F_5^+ + RH \rightarrow C_2F_5H + R^+. \qquad \text{(b)}$$

It is suggested that the CF_4 observed in previous gas and liquid phase radiolysis studies of C_2F_6-O_2 mixtures can be entirely ascribed to reaction (a). Small concentrations of impurities or accumulated products will react with the $C_2F_5^+$ ions under normal low dose rate radiolysis conditions.

Key words: Fluorocarbons; heats of formation; ion-molecule reactions; mass spectrometry; photoionization; rate constants.

1. Introduction

The direct and the rare gas-sensitized radiolysis of gaseous and liquid C_2F_6 has been investigated extensively [1].[1] In addition, several mass spectrometric studies have dealt with the reactions of the perfluorinated ions (mainly CF_3^+ and $C_2F_5^+$) formed in C_2F_6 by electron impact [2].

The main reaction channel of the CF_3^+ ion with C_2F_6 is as follows:

$$CF_3^+ + C_2F_6 \rightarrow CF_4 + C_2F_5^+. \qquad (1)$$

From the generally accepted heats of formation of these species [3–4] (for $C_2F_5^+$ only an estimated heat of formation was available), it was calculated that reaction (1) was endothermic by at least 29 kJ/mol (7 kcal/mol) [2]. On this basis, the observation of reaction (1) in the ion source of the mass spectrometer has been explained as the reaction of an internally excited CF_3^+ ion. Since this seemed to indicate that the dissociation of the $C_2F_6^+$ ion resulted in the formation of excited CF_3^+ fragment ions:

$$C_2F_6^+ \rightarrow (CF_3^+)^* + CF_3 \qquad (2)$$

the charge exchange reactions of the CF_3^+ ion formed in reaction (2) were investigated in a tandem mass spectrometer [2b]. In these experiments, CF_3^+ ions having an average kinetic energy of 0.3 eV[2], were

*Work supported in part by the U.S. Atomic Energy Commission.

[1] Figures in brackets indicate the literature references at the end of this paper.

[2] 1 eV = 96.485 kJ · mol^{-1}.

reacted with a variety of compounds having ionization potentials above and below the reported value for CF_3 (9.17 eV) [3]. The results suggested that some fraction of the CF_3^+ ions had as much as 2.9 eV internal energy under the conditions of these experiments, since charge exchange was found to occur with C_2H_4 (I.P. = 10.5 eV), C_3H_8 (I.P. = 11.1 eV), and C_2H_6 (I.P. = 11.5 eV) [5]. However, these same charge transfer reactions were not detected in experiments carried out in an ion cyclotron resonance instrument (icr) [2c], and it was concluded that the internally excited CF_3^+ ions initially produced in reaction (2) had sufficient time to relax during the long time scale of the icr experiment (10^{-3} s between collisions).

The present study was undertaken with the intention of examining the effect of varying internal energy on the reactions of the CF_3^+ ion, and to see if reaction (1) can also occur for ground state CF_3^+ ions. The CF_3^+ ions were produced by photoionization of C_2F_6 using neon (16.66–16.84 eV) and helium (21.2 eV) resonance radiation, and by the charge exchange reaction between C_2F_6 and Xe^+ and Kr^+ ions:

$$Xe^+ (Kr^+) + C_2F_6 \rightarrow Xe(Kr) + CF_3^+ + CF_3. \qquad (3)$$

The reactions of the CF_3^+ ions formed in these ways were examined in the NBS high pressure photoionization mass spectrometer [5], at a temperature of 300 K. Under these conditions, the ions have no excess kinetic energy.

2. Experimental Procedure

All experiments were carried out on the NBS high pressure photoionization mass spectrometer, which has been described in detail previously [5]. The instrument was equipped with the enclosed neon and helium resonance light sources, which deliver photons of 16.66–16.84 eV and 21.2 eV, respectively.

Meaningful experiments could not be carried out at pressures above about 0.5 torr in C_2F_6, because of the appearance of product ions due to reaction with impurities, as well as to a general deterioration of the performance of the quadrupole mass analyzer apparently because of adsorption of C_2F_6 on the detector surface. During the early stages of this study, it was found that the mass spectrum obtained from the photoionization of C_2F_6 at pressures above approximately 0.1 torr exhibited a number of product ions such as CF_2Cl^+ and $C_2F_3Cl^+$, which were obviously produced in reactions of CF_3^+ and $C_2F_5^+$ with chlorinated impurities present in the sample (mainly CF_3Cl). CF_3Cl has also been reported as an impurity in C_2F_6 in several radiolysis investigations [1]. The effects due to this impurity were reduced when the C_2F_6 was subjected to gas chromatographic purification, but remaining traces prevented quantitative results from being obtained at C_2F_6 pressures above about 0.5 torr. However, for all of the experiments reported here, the total contribution from impurity ions never exceeded 2 percent of the composite mass spectrum.

3. Results and Discussion

3.1. Photoionization of Pure C_2F_6

When C_2F_6 was irradiated with 21.2 eV photons, the major primary ions observed at low pressures ($< 10^{-4}$ torr) were CF_3^+ (58.5%) and $C_2F_5^+$ (36.8%). Other ions observed were CF^+, 3.8 percent, and CF_2^+, 0.9 percent. Figure 1 shows the variations in the intensities of the CF_3^+, $C_2F_5^+$, and CF^+ ions as the pressure of C_2F_6 in the reaction chamber of the mass spectrometer was increased. These results show that reaction (1) does occur under these conditions. That is, the intensity of the CF_3^+ ion shows a decrease with increasing C_2F_6 pressure, and the ionic product of the reaction between CF_3^+ and C_2F_6 must be $C_2F_5^+$ since no other ions show an increase in intensity in this pressure range. From the data obtained at low pressures ($< 10^{-2}$ torr), an average rate coefficient of $4 \pm 1 \times 10^{-11}$ cm^3/molecule-second can be estimated for reaction (1). Within experimental error, the same rate coefficient for this reaction is obtained in experiments in which ionization of C_2F_6 is effected by 16.66–16.84 eV photons; (in that case, only CF_3^+, 39% and $C_2F_5^+$, 61%, ions are observed in the system at the "zero" pressure limit). It is important to note that this estimate of the rate coefficient for reaction (1) is based on a slope of a decay curve for CF_3^+ which represents the reaction of only 5 percent of these ions. Nevertheless, this value agrees within the

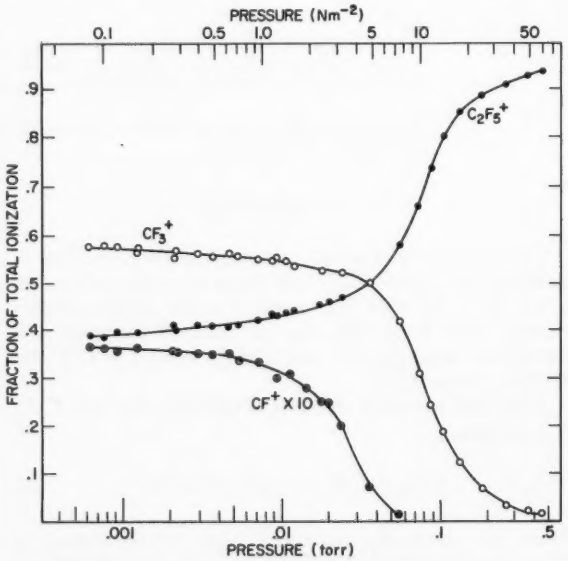

FIGURE 1. *Photoionization of* C_2F_6 *at 58.4 nm (21.2 eV).*

Fractional intensities of CF^+, CF_3^+, and $C_2F_5^+$ as a function of pressure.

experimental limits with the value of 3.4×10^{-11} cm^3/molecule-second reported earlier [2b].

Because the residence time of the ions in the mass spectrometer is not precisely known at pressures above 10^{-2} torr, reliable rate coefficient estimates can not be obtained from the data taken in the higher pressure ranges. These results are, however, of interest, since they show that at pressures around 0.5 torr, essentially all of the CF_3^+ ions have reacted to form $C_2F_5^+$ (the fact that the ion currents shown in the figure do not add up to 100 percent in the high pressure region is to be explained by the impurity effects described in the Experimental Section). This observation is in general agreement with the results obtained by Marcotte and Tiernan [2b] in a time-of-flight mass spectrometer, which showed that at a pressure of ~0.4 torr, about 50 percent of the CF_3^+ ions had reacted with C_2F_6. Since the observed rate constant for reaction (1) is about 4×10^{-11} cm^3/molecule-second, and the rate constant for collisions between such fluorocarbon ions and C_2F_6 is on the order of 7×10^{-10} cm^3/molecule-second [6–7], a CF_3^+ ion undergoes ~16 unreactive collisions with C_2F_6 on the average before reacting. This means that if only CF_3^+ ions having excess internal energy could undergo reaction (1), one would expect to observe a decrease in the rate of reaction (1) as collisional deactivation becomes more important at higher pressures. The fact that all CF_3^+ ions eventually react in our system is inconsistent with this interpretation.

The results given in Figure 1 also confirm the observation made previously [2] that the $C_2F_5^+$ ions produced either as primary fragments or as reaction products do not react further with C_2F_6.

The results obtained in the 21.2 eV photoionization experiments also lead to estimates of the values of the rate coefficients for the reactions of the CF^+ and CF_2^+ ions with C_2F_6 of $1.9 \pm 0.4 \times 10^{-10}$ cm^3/molecule-second and $1.45 \pm 0.30 \times 10^{-9}$ cm^3/molecule-second, respectively.

3.2. Photoionization of C_2F_6—Rare Gas Mixtures

Figures 2 and 3 show the results of experiments in which krypton or xenon was irradiated with 16.66–16.84 eV photons in the presence of small amounts (8.2 %) of added C_2F_6. In such experiments, most of the initial ionization is effected in the rare gas, which, upon collision with C_2F_6 molecules, transfers charge (if charge transfer is exothermic) according to reaction (3). The energies available from the recombination energies of the rare gas ions are 14.0 and 14.7 eV in the case of Kr^+, and 12.13 or 13.44 eV in the case of Xe^+ [5]. Therefore, charge transfer from these ions to C_2F_6 should not result in the formation of $C_2F_5^+$ fragment ions since there is insufficient energy available (the observed appearance potential of $C_2F_5^+$ from C_2F_6 is about 15.4 eV) [7]. Actually, in the case of Kr^+ ions,

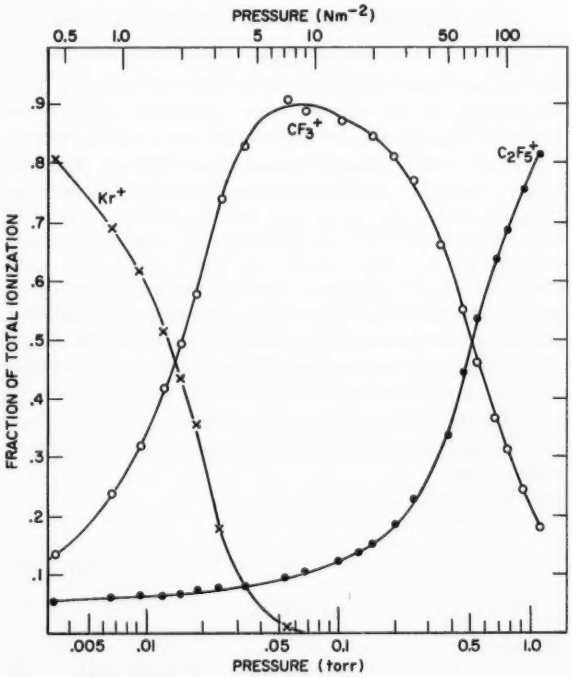

FIGURE 2. *Photoionization of* Kr-C_2F_6 (1:0.08) *mixture at 74.4–73.6 nm (16.67–16.84 eV).*

Fractional intensities of Kr^+, CF_3^+, and $C_2F_5^+$ as a function of pressure.

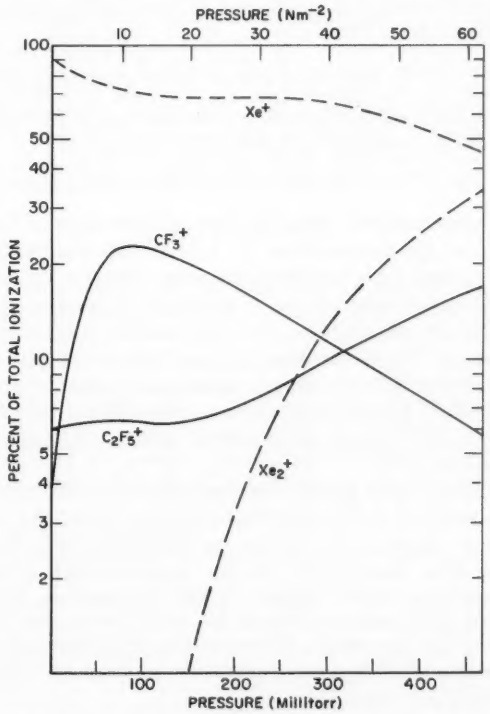

FIGURE 3. *Photoionization of* Xe-C_2F_6 (*1:0.08*) *mixture at 74.4–73.6 nm (16.67–16.84 eV).*

Fractional intensities of Xe^+, Xe_2^+, CF_3^+ and $C_2F_5^+$ as a function of pressure.

reported charge transfer spectra of C_2F_6 confirm that process (3) accounts for 93–98 percent of the Kr^+-C_2F_6 reactive encounters. In the case of xenon ions, only those ions produced in the $^2P_{1/2}$ state (13.44 eV) have sufficient energy to undergo reaction (3), while the ground state $^2P_{3/2}$ Xe^+ ions (12.13 eV) will be unreactive with C_2F_6.

The results presented in figure 2 show that the intensity of the Kr^+ ion diminishes as that of CF_3^+ increases because of the occurrence of reaction (3) as the pressure is increased in the Kr-C_2F_6 mixture. At pressures above 0.05 torr, reaction of the CF_3^+ ion to form $C_2F_5^+$ is observed. At the low pressure limit, where charge exchange does not occur to any appreciable extent, some $C_2F_5^+$ is produced by direct photoionization of C_2F_6.

More interesting conclusions can be derived from the results given in figure 3 which shows the data obtained in the xenon-C_2F_6 mixture irradiated with 16.67–16.84 eV photons in the photoionization mass spectrometer. Here the $Xe^+(^2P_{1/2})$ ions (apparently about 30% of the Xe^+ ions formed under these conditions) undergo reaction (3) to produce CF_3^+ ions in C_2F_6. The interesting point here is that if one accepts a heat of formation of CF_3^+ of 414 kJ/mol (99.1 kcal/mol) [3], then the CF_3^+ ions formed in reaction (3) involving $Xe^+(^2P_{1/2})$ and C_2F_6 can only have a *maximum* of 8.4 kJ/mol (2 kcal/mol) excitation energy. Even so, these CF_3^+ ions undergo reaction (1) to from $C_2F_5^+$ product ions (fig. 3). Since it is to be expected that an endothermic reaction would proceed at a rate which would not be observable under these experimental conditions, we are forced to conclude that if the overall sequence (reaction (3) followed by reaction (1)):

$$Xe^+(^2P_{1/2}) + 2C_2F_6 \rightarrow CF_3 + CF_4 + C_2F_5^+ + Xe \quad (4)$$

is thermoneutral, then the heat of formation of $C_2F_5^+$ can not be greater than 12 kJ/mol (2.9 kcal/mol). If we accept, as is probably the case, that the CF_3^+ ions have no internal energy at the time of reaction (1), a value for $\Delta H_f(C_2F_5^+)$ of 4 kJ/mol (0.9 kcal/mol) is obtained. Thus we must conclude that the value of 34 kJ/mol (8.1 kcal/mol) calculated earlier [1b] for $\Delta H_f(C_2F_5^+)$ is too high, and reaction (1) has therefore erroneously been assumed to be an endothermic reaction.

Figure 3 also shows that there is a slight increase in the yield of $C_2F_5^+$ at pressures below about 0.1 torr, where reaction (1) can not be important. It is likely that this observation is an experimental artifact caused by slight changes in the composition of the xenon-C_2F_6 mixture due to fractionation at the automatic leak assembly. However, the possibility can not be excluded that a reaction occurs between $Xe^+(^2P_{1/2})$ and C_2F_6 to form $C_2F_5^+$:

$$Xe^+(^2P_{1/2}) + C_2F_6 \rightarrow XeF + C_2F_5^+. \quad (5)$$

Accepting an estimate of the Xe-F bond strength of 134 ± 17 kJ/mol (32 ± 4 kcal/mol) [8], one obtains an estimate for $\Delta H_f(XeF)$ of − 54 ± 17 kJ/mol (− 13 ± 4 kcal/mol) and on this basis, reaction (5) may be slightly exothermic. In this connection, it should be pointed out that when Marcotte and Tiernan [2b] impacted Xe^+ ions onto C_2F_6 in a tandem mass spectrometer, they observed $C_2F_5^+$ as the major product ion (79%) even though, as discussed above, charge transfer from Xe^+ ions to yield this fragment is strongly endothermic. This unusual result could perhaps be explained by the occurrence of a reaction such as (5), which might be favored for ions which are translationally heated. On the other hand, it should be mentioned that in experiments carried out in this laboratory in an icr instrument, there was no evidence for the production of $C_2F_5^+$ ions through a reaction of Xe^+ with C_2F_6.

A final point to be mentioned in connection with the results given in figure 3 is the formation of Xe_2^+ as a product ion in a pressure region in which this ion would not be observed in pure xenon. This can be explained by the occurrence of a switching reaction involving the $XeC_2F_6^+$ association ion and xenon atoms:

$$XeC_2F_6^+ + Xe \rightarrow (Xe)_2^+ + C_2F_6 \quad (6)$$

Apparently the $XeC_2F_6^+$ is not detected in our experiments due to the fact that the dissociative lifetime of $XeC_2F_6^+$ is much shorter than the total ion transit time in our instrument.

3.3. Photoionization of C_2F_6-Alkane Mixtures

In view of the fact that the photoionization curves of $C_2F_5^+$ and CF_3^+ indicate that these species probably do contain excess energy when formed by fragmentation of $C_2F_6^+$ [7], and because these species have been reported, under certain conditions [2b] to undergo charge transfer with molecules such as ethane and propane, with which charge transfer involving ground state ions would be endothermic, it was considered worthwhile to add ethane to C_2F_6 irradiated with 16.66–16.84 eV photons. The results of such experiments, in which C_2F_6 containing 5 percent ethane was irradiated at various pressures with 16.66–16.84 eV photons are given in figure 4. It is seen that there is no evidence for charge transfer reactions from CF_3^+ or $C_2F_5^+$ to C_2H_6. However, both these fluorinated ions undergo exothermic hydride transfer reactions with ethane:

$$CF_3^+ + C_2H_6 \rightarrow CF_3H + C_2H_5^+$$

$$- 112 \text{ kJ/mol } (- 26.9 \text{ kcal/mol}) \quad (7)$$

$$C_2F_5^+ + C_2H_6 \rightarrow C_2F_5H + C_2H_5^+$$

$$- 125 \text{ kJ/mol } (- 30 \text{ kcal/mol}). \quad (8)$$

Small amounts of $C_2H_4^+$ and $C_2H_6^+$ are observed, and can be attributed to direct photoionization of the

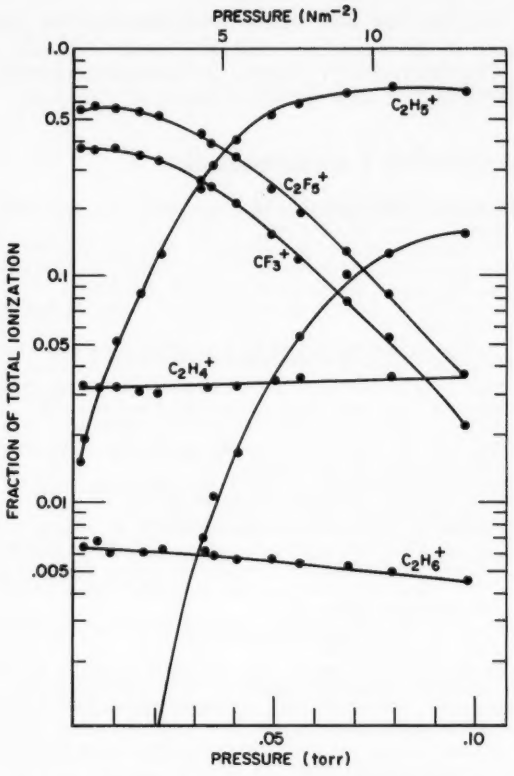

FIGURE 4. *Photoionization of* C_2F_6-C_2H_6 *(1:0.05) mixture at 74.4–73.6 nm (16.67–16.84 eV).*

Fractional intensities of $C_2H_4^+$, $C_2H_5^+$, $C_2H_6^+$, $C_4H_9^+$, CF_3^+, and $C_2F_5^+$ as a function of pressure.

ethane additive. At pressures above about 0.03 torr, the $C_4H_9^+$ product ion is formed through the occurrence of the well-known reaction sequence:

$$C_2H_5^+ + C_2H_6 \rightarrow (C_4H_{11}^+)^* \rightarrow C_4H_9^+ + H_2 \qquad (9)$$

Addition of higher alkanes, C_3H_8 (I.P. 11.1 eV) and *n*-C_4H_{10} (I.P. 10.6 eV) indicates that in these cases H^- transfer to CF_3^+ and $C_2F_5^+$ is also the only reaction mode. It should be noted that because we are dealing here with dilute C_2F_6-alkane mixtures the CF_3^+ and $C_2F_5^+$ ions will probably be collisionally deactivated at the time of reaction with the alkane molecule.

3.4. Implications for Radiolysis

In the 70 eV mass spectrum, CF_3^+ and $C_2F_5^+$ account for 48 percent and 25.5 percent of the cations, respectively. The parent ion is absent, as is the case for many halocarbons. Since the parent ion apparently has a short lifetime, and it may therefore be anticipated that fragmentation will still be important at the pressures encountered in radiolysis experiments. However, the relative abundances of the various fragment ions can not be predicted with certainty, since these will depend on the density of the system. It can, however, be surmised that the major ion in the mass spectrum, CF_3^+, will be present in the gas phase radiolysis of C_2F_6 and possibly even in the liquid phase radiolysis.

In some of the experiments performed during the course of this study in the photoionization mass spectrometer, up to 10 percent oxygen was added to C_2F_6 and no interactions between O_2 and the fluorocarbon ions were observed. Thus, it is of interest that radiolysis experiments carried out on C_2F_6 in the presence of 1 mol percent oxygen, at a pressure of two atmospheres [1a], show the formation of CF_4 as a product with a G value of 1.3 [$M/N_+ = 0.46$ since $W(C_2F_6) = 35.8$ eV. (table 1)] In the same study [1a], the yields of C_3F_8 and C_4F_{10} are reduced to zero when oxygen is added, indicating that the fluorocarbon radicals are effectively scavenged by oxygen. Therefore, reaction of CF_3 can not contribute to the formation of CF_4 in the presence of oxygen. These results indicate that the formation of CF_4 in this experiment can be attributed to reaction (1), and therefore, that ionization of C_2F_6 at a pressure of two atmospheres leads to the formation of CF_3^+ fragment ions with an ion pair yield of approximately 0.46. It may also be mentioned that an alternate channel for formation of CF_4 which has been mentioned, namely the decomposition of excited C_2F_6

$$C_2F_6^* \rightarrow CF_4 + CF_2 \qquad (10)$$

can be excluded since the formation of this product is inhibited by the addition of bromine to the system [1g]. There is no reason to expect that small concentrations of bromine would have any effect on the primary decomposition of an electronically excited molecule.

Similar conclusions can be reached in the radiolysis of C_2F_6 in the liquid phase [1d] (table 1). That is, the addition of 10 percent oxygen inhibits the formation of C_3F_8 and C_4F_{10}, but CF_4 is formed in the presence of

TABLE 1. *Product yields per 100 eV (G) in* C_2F_6 *Radiolysis*

Conditions	$G(CF_4)$	$G(C_3F_8)$	$G(n\text{-}C_4F_{10})$	Other	Reference
Gas, 2 atm (200 kNm^{-2})	2.5	0.45	0.20		[1a].
Gas, 2 atm (200 kNm^{-2}) + 1% O_2	1.3	0.0	0.0		[1a].
Gas, (7–500 kNm^{-2}) + Br_2	undetectable	0.0	0.0	$G(CF_3Br) = 2.70 \pm 0.3$	[1g].
				$G(C_2F_5Br) = 3.00 \pm 0.3$	[1g].
Liquid	1.72	0.87	0.45		[1d].
Liquid + ~ 10% O_2	0.97	0.0	0.0		[1d].

oxygen with a G value of approximately unity. Thus, as in the gas phase, evidence points to the formation of CF_4 through reaction (1). We can tentatively conclude, therefore, that ionic fragmentation to form CF_3^+ does occur in the liquid phase radiolysis of C_2F_6.

As pointed out earlier in the discussion, reaction (1) is a slow reaction. This means that if any other reactive compound is present in the system—as an impurity, an additive, or as an accumulated product—the CF_3^+ ions may be intercepted by the foreign compound before reacting with C_2F_6. Consequently, one would expect the yield of CF_4 to be sensitively affected by the presence of foreign compounds in the system. The reduction of the yield of CF_4 in the radiolysis of C_2F_6 when bromine is added illustrates this point [1g]. The results presented in that study showed that a small concentration of CF_3Cl impurity affected the ion-molecule kinetics of the system strongly, especially with respect to the fate of the unreactive $C_2F_5^+$ ion.

We do not at present have any information concerning the ionic reactions which occur when bromine, chlorine, or HCl are added to C_2F_6, as they were in a recent radiolysis study [1g]. It is of interest, however, that in that study CF_3Cl was found as a product in the radiolysis of C_2F_6-HCl mixtures, while CF_3 radicals are known to react with HCl to give CF_3H, exclusively [9]. As pointed out by the authors of that study, this may be considered as evidence of a contribution from ionic processes.

The authors would like to thank Drs. John Eyler and Sharon Lias for performing several confirmatory experiments in relation to this study using an ion cyclotron resonance instrument. They would also like to thank Dr. Lias for her help in the preparation of the final version of the manuscript and Dr. Eugene Domalski of the Thermochemistry Section for providing essential thermodynamic information pertinent to this study.

4. References

[1a] Kevan, L., and Hamlet, P., J. Chem. Phys. **42**, 2255 (1965).
[b] Kevan, L., Ibid. **44**, 683 (1966).
[c] Fessenden, R. W., and Schuler, R. H., Ibid. **43**, 2704 (1965).
[d] Sokolowska, A., and Kevan, L., J. Phys. Chem. **71**, 2220 (1967).
[e] Sokolowska, A., and Kevan, L., Ibid. **72**, 253 (1968).
[f] Askew, W. C., Reed, T. M., and Mailen, J. C., Radiat. Res. **33**, 282 (1968).
[g] Cooper, R., and Haysom, H. R., J. Chem. Soc. Faraday Trans. II, **69**, 904 (1973).
[2a] King, J., Jr., and Elleman, D. D., J. Chem. Phys. **48**, 412 (1968).
[b] Marcotte, R. E., and Tiernan, T. O., Ibid. **54**, 3385 (1971).
[c] Su, T., and Kevan, L., J. Phys. Chem. **77**, 148 (1973).
[3] Walter, T. A., Lifshitz, C., Chupka, W. A., and Berkowitz, J., J. Chem. Phys. **51**, 3531 (1969).
[4a] JANAF Thermochemical Tables. Nat. Stand. Ref. Data Ser., Nat. Bur. Stand. (U.S.), 37 (June 1971).
[b] Franklin, J. L., Dillard, J. G., Rosenstock, H. M., Herron, J. T., Draxl, K., and Field, F. H., Ionization Potentials, Appearance Potentials, and Heats of Formation of Gaseous Positive Ions. Nat. Stand. Ref. Data Ser., Nat. Bur. Stand. (U.S.), NSRDS–26, 289 pages (1969).
[5a] Sieck, L. W., Searles, S. K., and Ausloos, P., J. Amer. Chem. Soc. **91**, 7627 (1969).
[b] Sieck, L. W., Gorden, R., Jr., Ausloos, P., Lias, S. G., and Field, F., Radiat. Res. (in press).
[6] Kevan, L., and Futrell, J. H., J. Chem. Soc. Faraday Trans. II, No. 5, 2 (1972).
[7] Noutary, C. J., J. Res. Nat. Bur. Stand. (U.S.), 72A (Phys. and Chem.), 479–485 (Sept.–Oct. 1968).
[8] Johnson, G. K., Malm, J. G., and Hubbard, W. N., J. Chem. Thermodynamics **4**, 879 (1972).
[9] Amphlett, J. C., and Whittle, E., Trans. Faraday Soc. **61**, 484 (1965).

(Paper 78A2–809)

JOURNAL OF RESEARCH of the National Bureau of Standards—A. Physics and Chemistry
Vol. 78A, No. 2, March–April 1974

A Simple Technique for the Generation of Dilute Mixtures of Pollutant Gases

W. Tsang

Institute for Materials Research, National Bureau of Standards, Washington, D.C. 20234

(November 30, 1973)

The pyrolysis of compounds whose decomposition produces equal numbers of reactive and stable molecules provides a simple quantitative means of generating dilute mixtures of formaldehyde, acetaldehyde and acrolein. The requirements with respect to the thermal stability of such "parent" compounds are discussed and the possible extentions to other reactive gas systems are considered.

Key words: Acetaldehyde; acrolein; air pollution; calibration; decomposition; formaldehyde; reactive gases.

1. Introduction

The capability of generating accurately known dilute mixtures of reactive gases is important for the quantitative understanding of air pollution chemistry. For example, such mixtures are needed in the calibration of measuring instruments, in toxicity investigations and in physico-chemical studies on the rates and mechanisms of pollutant formation. The reactive nature of some of these gases may make it advisable to use dynamic methods for sample generation. This is exemplified by the use of permeation tubes for SO_2 generation. A general survey on this subject can be found in a recent text [1].[1] The present report deals with the production of dilute mixtures of formaldehyde, acetaldehyde and acrolein using the gas phase pyrolysis of selected "parent" molecules. Although these aldehydes are present in automobile exhausts [2] and may be important intermediates in photochemical smog formation [3], the main aim of this investigation is to demonstrate the feasibility of this technique and to call attention to certain attractive features which make it worthy of further exploitation.

In the past formaldehyde [4], ketene [1], butadiene [1] have been generated in this manner. The prime goal has been preparative, in the sense of obtaining gases in as pure a state as possible. This study may be considered an extention to smaller concentrations of the earlier work, and as before the current application uses gas phase unimolecular reactions. Specific interest will be focused on processes of the type

$$S-R \xrightarrow{k} S+R$$

where R is the reactive species and S a stable compound for which calibration mixtures can be prepared in the ordinary manner. The concentration of S and R at any time is then

$$S=R=(SR)_{initial}\times(1-e^{-kt}) \text{ where } k=A\exp(-E/RT)$$

with A and E (activation energy) constants. Thus the absolute concentration of the two products is dependent on the concentration of the "parent" SR, the reaction time t and the temperature T. However, the stoichiometry requires equal concentrations of S and R, therefore a determination of the concentration of S determines the concentration of R. Note that this will be true regardless of the value of the three operational variables that control the absolute concentration. In other words, gas generation based on this method does not require much experimental skill in preparing the sample or in setting the reaction conditions. Furthermore, changes in concentration can be effected with ease. Here, one has the option of varying the concentration of the parent and/or the reaction temperature. For the latter a wide range of concentrations can be generated by the adjustment of a rheostat. The method also provides a convenient means of storing reactive or possibly toxic gases until needed. For example, acrolein is a very strong lachrymator and may be a hazard if carelessly handled. Finally for the calibration of a whole series of compounds R_1, R_2, etc. having parents AR_1, AR_2, etc. it will be possible to base all the calibrations on the one set of standard samples for stable constituent A.

The aim of this study is to demonstrate that there exist compounds which behave in the desired fashion over a sufficiently wide range of reaction conditions. For this purpose it is possible to draw on the large volume of recent experimental data on molecular

[1] Figures in brackets indicate the literature references at the end of this paper.

decompositions and equally important, the work of Benson and co-workers [5] in rationalizing these results. The processes of interest are those that are truly molecular in character, that is the reaction occurs as written, and which do not have significant side reactions. The avoidance of surface or chain induced decomposition processes is of prime importance. These processes are frequencly irreproducible and thus completely unsuitable for the present purposes. The monograph by Benson and O'Neal [5] suggests a large number of compounds that have the potentialities of fulfilling the requirements. They are characterized by six-centered transition states with A-factors in the 10^{12}/s range and activation energies of between 40–50 kcal/mol.[2] The latter is about 30 kcal/mol lower than that for most C–C bond breaking reactions and provides a degree of assurance that radicals will not be present in the system. The specific reactions which are the subject of this investigation are:

(a) for formaldehyde, $H_2C = C(CH_3)CH_2CH_2OH$ (3-methyl-3-butene-1-ol)$\rightarrow i\text{-}C_4H_8 + HCHO$

(b) for acetaldehyde, $H_2C = CHCH_2CHOHCH_3$ (3-pentene-2-ol)$\rightarrow C_3H_6 + CH_3CHO$

(c) for acrolein, (oxacyclohexene-2)

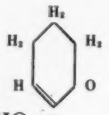

$\rightarrow C_2H_4 + C_2H_3CHO$

It should be emphasized that the "parent" compounds have been selected purely on the basis of availability, relative purity and other such non-critical reasons. They should not be regarded as the optimum for any particular application.

[2] 1 kcal/mol = 4.184 kJ/mol.

2. Experimental Procedure

The experimental set-up is shown schematically in figure 1. Although gas chromatographic detection is used, any other system with the necessary sensitivity is equally satisfactory. The key component is the reactor assembly and can be visualized as simply a plug-in module between the inlet and the detection system. The pyrolyzer is from Chemical Data System [6] and consists of a heated gold coil $\frac{1}{8}$" diameter and with an internal volume of about 6 cm³. With the gas chromatographic flow rates of 20–50 cm³/min heating times are of the order of seconds. The range of temperatures is from 40 to 700 °C. The use of a flow reactor is necessary because of the need for delivering the desired gas mixture to the detector as rapidly as possible. Gold is employed as the reactor material since it does not appear to catalyze surface reactions. The precolumn in the reactor assembly serves to purify the input sample. The packing for the gas chromatographic columns are the various Poropaks. Column lengths are 2–6 ft., and the temperature is between 100 to 150 °C. The gas chromatograph is a standard commercial instrument with flame ionization and helium ionization detectors. The last is necessary for formaldehyde detection. Peak areas are determined using an electronic integrator.

For pollution of applications, it is necessary to deliver to the detector submicrogram quantities of reactive species. Thus the use of previously diluted samples of the "parent" compound is essential. Alternatively, it would be necessary to work with microvolume samples or to carry out reactions at impractically low conversions. For introduction as a liquid sample the most convenient approach is to dissolve the "parent" compound in toluene. The concentration level is 0.2 percent or less on a mole basis. Standard gas chromatographic syringes and techniques can be used.

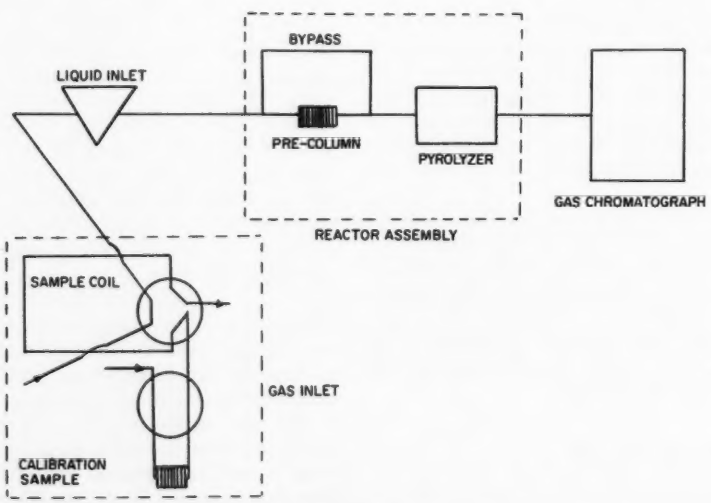

FIGURE 1. *Experimental apparatus.*

Note that a 5 μl sample yields about 1 cm^3 of toluene in the gas phase. The maximum possible reactive species concentration is that of the "parent" compound, while the lower limit is set by the impurities in the system and/or the detector sensitivity. An added advantage with regard to the use of toluene when the precolumn in the reactor assembly is not used is that it is an inhibitor for chain processes and thus provides an additional guarantee for the "cleanliness" of the reaction. The mixtures of alcohols in toluene appear to be stable for a period of at least six months. An adaptation of the standard bubbler technique is used for introduction as a gas. The "parent" compounds, in their pure state, are simply deposited on gas chromatographic packing (Chromosorb P, 100–200 mesh).[3] When swept out by helium the fractional molar concentration is the vapor pressure of the liquid divided by the total pressure. The two alcohols are particularly suitable since their vapor pressure at 0 °C is below 1 mm Hg and thus the mixtures produced are in the same concentration range as that from the liquid introduction. Overall, the present apparatus permits the introduction of dilute samples of various sizes in the pyrolyzer in the presence or absence of an inhibitor with or without preliminary purification. The subsequent section will demonstrate that the postulated stoichiometry is preserved under all reaction conditions.

[3] Certain commercial materials and equipment are identified in this paper in order to specify adequately the experimental procedure. In no case does such identification imply recommendations or endorsement by the National Bureau of Standards, nor does it imply that the material or equipment identified is necessarily the best available for the purpose.

3. Results

Several chromatograms from the pyrolysis experiments on oxacyclohexene-2 are shown in figure 2. They are the results of experiments with 5 μl samples of 1/500 (parts by volume) oxacyclohexene-2 in toluene (without precolumn) and are typical for this and the other two systems. The important factors are:

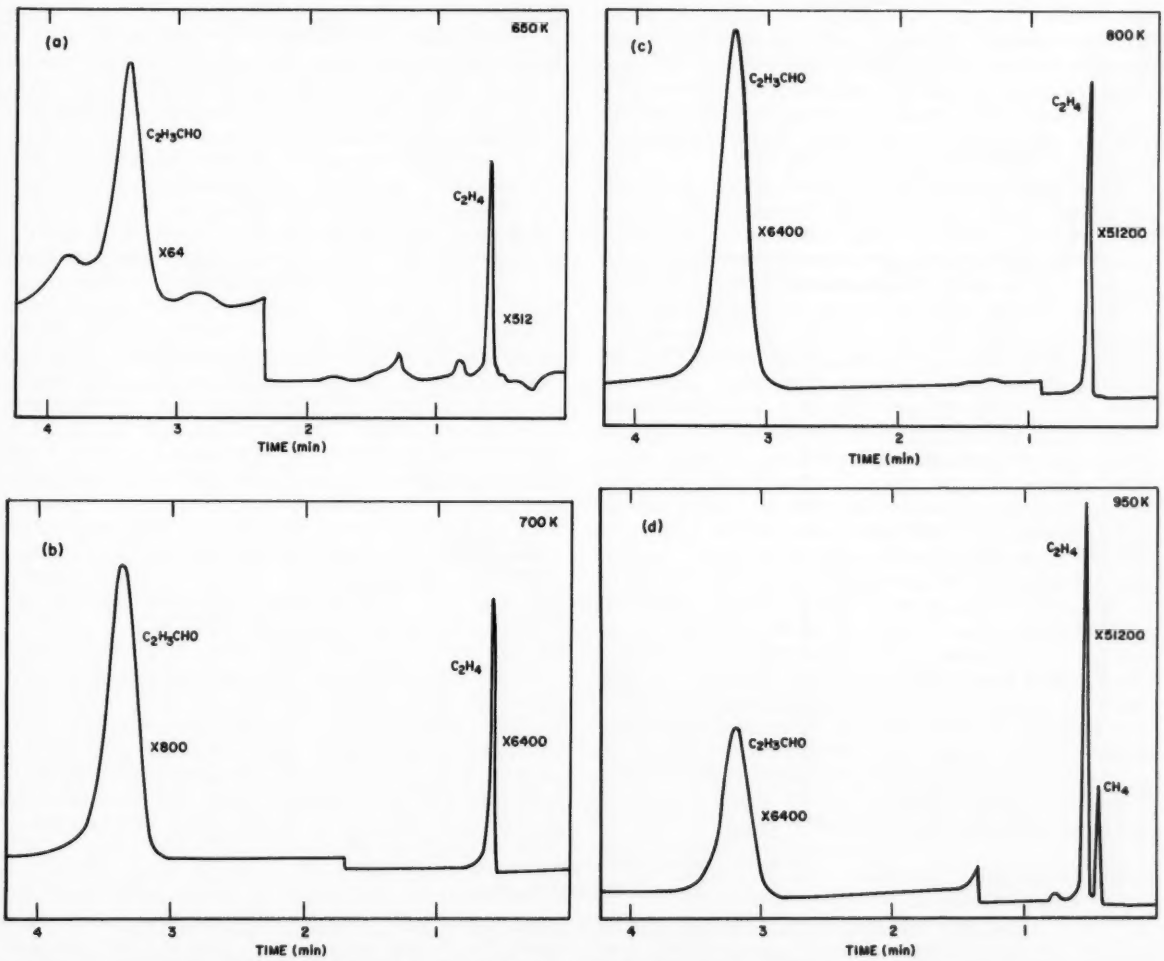

FIGURE 2. *Typical chromatograms ~ 5 μl of 1/500 oxacyclohexene-2 in toluene at various temperatures.*

530-326 OL - 74 - 5

(a) The concentration of reactive specie extends over two orders of magnitude.

(b) In the mid-range for this case 700 to 900 K, the chromatograms are essentially identical to each other. Note that since similar sized samples are used and the two components are created at the same time the ratio of peak heights should be a good measure of the relative concentrations and it can be seen that this is the case.

(c) At the lower limit of conversion and temperature the baseline is very noisy. With the present mode of operation this is unavoidable since the extraneous peaks represent trace impurities in the oxacyclohexene-2 and/or toluene. Presumably rigorous purification will bring about some improvement. The alternative possibility of using a precolumn did not prove worth while since removal of the impurities also entails the dilution of the oxacyclohexene as it moved down the precolumn thus degrading the detectability. The simplest way of going to lower quantity of substance deliv-

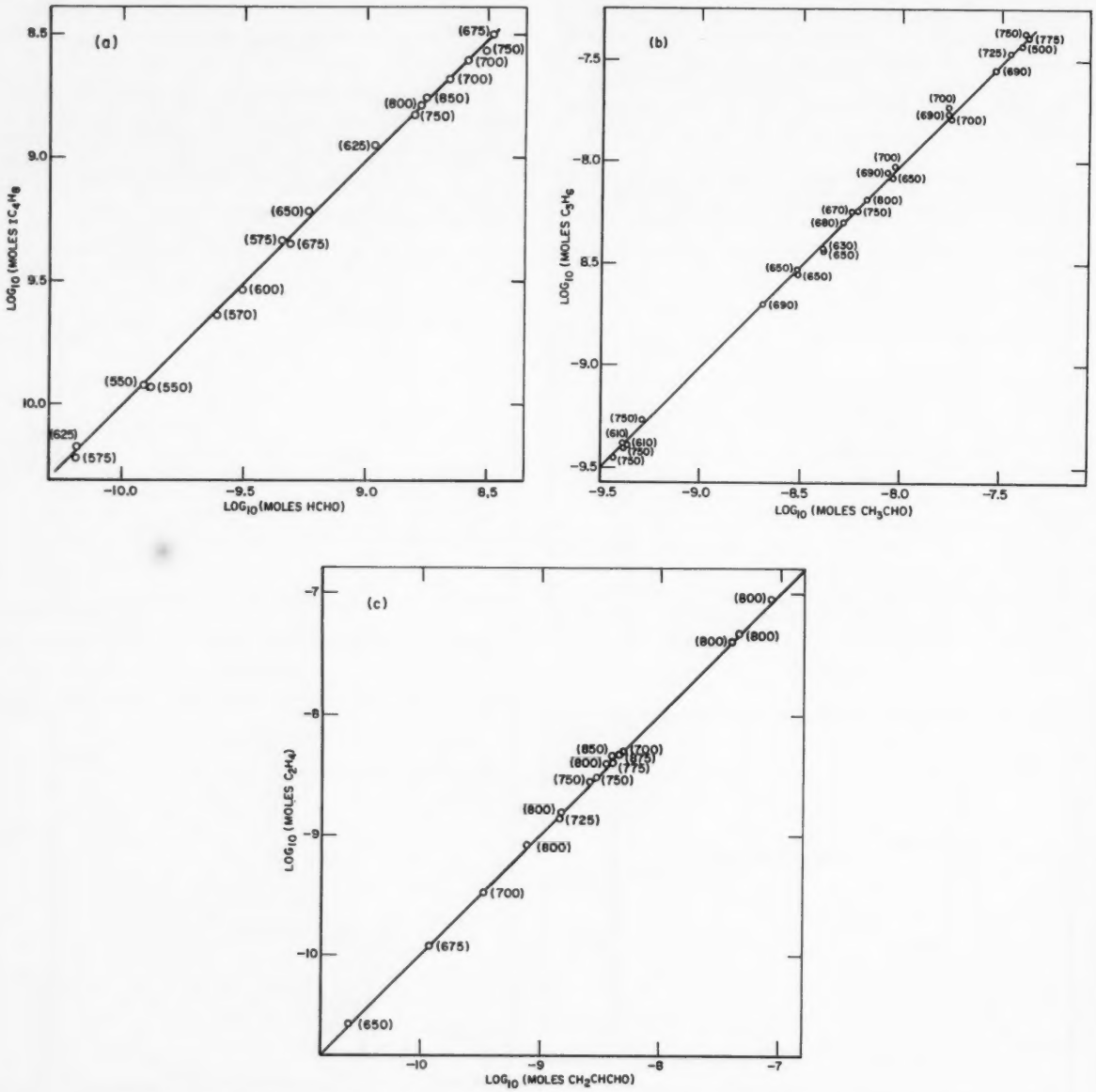

FIGURE 3. *Number of moles of olefin and aldehyde delivered to the director at a given pyrolyzer temperature.*

Liquid samples are from ~ .2–10 μl at concentrations of ~ .02–.2 percent (mole basis). Gas samples 1/2 cm³. (a) Formaldehyde and isobutene. (b) Acetaldehyde and propylene. (c) Acrolein and ethylene. Line represents 1–1 correspondence

ered to the detector is to use smaller samples at higher temperatures. Thus with a 0.5 μl sample at 700 K a chromatogram with areas similar to that of figure 2b, except on the 640 and 80 scale, can be obtained.

(d) At the highest temperatures an extraneous methane peak is present. Also, the peak height ratio has now changed considerably. It is quite clear that the conditions are now such that the unimolecular decomposition process is no longer the only process occurring. The presence of methane and the noisy baseline at the low conversions serve as a warning signal that the calibration procedure may be questionable. It should be noted that in dealing with hydrocarbons under the present conditions, formation of methane is a usual product in chain decomposition processes. The same phenomenon has been observed in the two alcohol systems.

In figure 3 the results are placed on a more quantitative basis by plotting the logarithms of the total number of moles of aldehyde produced versus the number of moles of olefins for a number of different experiments. It can be seen that within the scatter of 5–10 percent there is a one-to-one correspondence between aldehyde and olefin. Furthermore, this covers over 2 to 4 orders of magnitude in moles delivered and a temperature range of several hundred degrees. They range in extent of decomposition from less than 1 percent to complete reaction during the highest 25 to 50 degrees. It is possible to carry out reactions for another 50° or so before side reactions become important. In terms of a 10 cm^3 air pollution sample the numbers here represent a lowest concentration of a few ppm or less. It is also important to note that these results are independent of the means of delivery or size and concentration of samples. The calibration factors for acrolein and acetaldehyde have been determined using dilute samples of pure substances. For formaldehyde the calibration factor is derived from the pyrolysis of trioxane in toluene at a temperature of 900 K. This is a generally used technique for formaldehyde generation. The olefins are prepared as a 45 ppm mixture in He prepared by a commercial supplier and with a stated but unconfirmed accuracy of $\pm$ 5 percent. Checks on these calibrations have been carried out by pyrolyzing other "parent" compounds. For example, for acetaldehyde, the reaction $H_2C = CHOC_2H_5 \rightarrow C_2H_4 + CH_3CHO$ gives area ratios of $A(C_2H_4)/A(CH_3CHO) \cong 2$ on a chromatogram. This can be compared with the ratio of $A(C_3H_6)/AA(CH_3CHO) \cong 3$ from 4-pentene-2-ol or for that matter from allyl ethyl ether decomposition ($H_2C = CHCH_2OC_2H_5 \rightarrow C_3H_6 + CH_3CHO$). The 3 to 2 ratio is the relative sensitivity of the flame ionization detector of propylene as against ethylene and has been verified from the standard olefin mixture. With regard to acrolein the reaction $H_2C = CH_2CH_2OCH_2CH_3 = CH_2 \rightarrow C_3H_6 + H_2C = CHCHO$ gives an area ratio of $A(C_3H_6)/A(\text{acrolein}) = 3/2$ and can be compared with $A(C_2H_4)/A(\text{acrolein}) = 1$ from oxacyclohexene-2 pyrolysis. Here again one observes the required 3 to 2 propylene to ethylene ratio. The sensitivity of the aldehydes to the flame ionization detector is in accord with the observation that carbonyl groups are not detectable by this means while the rest of the molecule behaves as a hydrocarbon.

It did not prove feasible to carry out these checks for formaldehyde. The use of 3-butene-1-ol and allyl methyl ether as "parents" yields propylene and formaldehyde. Unfortunately, and unexpectedly these compounds are not separated by the Poropaks to an extent that permitted accurate area measurements.

4. Discussion

The scatter of these results is larger than can be accounted for by uncertainties in the area measurements. There does not appear to be any simple explanation since there are no perceptible trends. This sets a limit with respect to the precision of this type of gas generation. With respect to the dynamic range it should be emphasized that the lower limit could probably be lowered if greater efforts are made to "cleanup" the system by rigorous purification. The present data represents the results achieved with readily purchasable chemicals using standard general purpose instrumentation. The highest concentrations tested here are in the range of 2000 ppm. This is probably as high as one would want to go since it is only at the lower levels that sample integrity is a problem. Overall, the entire procedure makes the generation of reactive gases a simple matter. Thus, there is no need to control temperature, sample size or method of introduction. Indeed, there is no certainty that a gold reactor is need. This point will be tested.

Although all the present data have been obtained on the basis of the introduction of a pulse of the parent compound, it should be noted that the setup for gaseous introduction can, with minor modifications, be used to generate a constant stream of reactive gases. In so far as the pyrolytic technique is concerned no new problems are introducted. Indeed the experience from kinetic studies is that continuous pyrolysis may produce more satisfactory results that that using the pulse method. Continuous generation is necessary for toxicological and physical chemical investigations. Complications will arise from the multicomponent nature of the system. The parent compound can be eliminated by working at a temperature where reaction is complete. Another reason for working in this region is that if one carries out experiments in the kinetic region, the exponential dependence of the rate constant requires sensitive temperature control. With regard to the presence of the stable compound, it may be of no importance or one can select a parent molecule which will give a standard molecule which is easily separated from the reactive species of interest.

The success of this technique for generating the desired aldehydes implies that similar reactions can be used to generate a variety of other gases. Some of these include organic acids, alcohols, ketones, hydrogen halides, ammonia, etc. Some typical reactions

which might be utilized are as follows:

$$CH_3COOC_2H_5 \rightarrow CH_3COOH + C_2H_4$$

$$C_2H_5OCOOC_2H_5 \rightarrow C_2H_5OH + C_2H_4 + CO_2$$

$$tC_4H_9Cl \rightarrow iC_4H_8 + HCl$$

$$tC_4H_9F \rightarrow iC_4H_8 + HF$$

An examination of Benson and O'Neal's monograph [5], and a consideration of the criteria given here suggests that a large number of reactive gas molecules from an endless array of parent compounds may be made in this fashion. The only obvious exceptions are probably ozone and various highly oxygenated compounds.

The author is grateful to James R. McNesby for his encouragement and to the Measures for Air Quality program at the National Bureau of Standards for support.

5. References

[1] Nelson, G. O., Controlled Test Atmospheres. Principles and Techniques (Ann Arbor Science Publishers, Ann Arbor, Michigan, 1971).

[2] Dimitriades, B., Ellis, C. F., and Seizinger, D. E., in Advances in Chromatography, Vol. 7 (J. C. Giddings and R. A. Keller, Ed), (Dekker, New York, 1968).

[3] Altshuller, A. P., and Buffalini, J. J., Environmental Science and Technology **5**, 39 (1971).

[4] Walker, J., Formaldehyde (Reinhold Publishing Co., New York, 195 1964).

[5] Benson, S. W., and O'Neal, H. E., Kinetic Data on Gas Phase Unimolecular Reactions, Nat. Stand. Ref. Data Ser., Nat. Bur. Stand. (U.S.), 21, 645 pages (Feb. 1970).

(Paper 78A2–810)

JOURNAL OF RESEARCH of the National Bureau of Standards—A. Physics and Chemistry
Vol. 78A, No. 2, March–April 1974

Energy Levels and Classified Lines in the Second Spectrum of Thorium (Th II)

Romuald Zalubas and Charles H. Corliss

Institute for Basic Standards, National Bureau of Standards, Washington, D.C. 20234

(November 30, 1973)

The analysis of Th II has been extended with improved observations of the spectrum between 2000 and 25 000 Å. About 6500 lines are classified as transitions between 199 odd levels and 271 even levels. Of the 192 levels expected from the six odd configurations $5f(6d+7s)^2$ and $(6d+7s)^27p$, 188 are now known. In the even level system, all but one of the 37 levels of the three $(6d+7s)^3$ configurations are known. Of the 268 levels predicted for the configurations $5f^27s+5f7s7p+5f6d7p+5f^26d$, 235 are now known. The identifications are based on the theoretical calculations by N. Minsky.[1] New Zeeman effect observations have increased the number of levels with known g-values to 406 out of 470 known levels. The classifications will be useful in establishing secondary standards of wavelength.

Key words: Energy levels of Th II; g-values of Th II; spectrum of Th II; Th II spectrum; thorium; wavelengths of Th II.

1. Introduction

The first work published on the analysis of the second spectrum of thorium (Th II) was done by McNally, Harrison, and Park [1942][2] at the M.I.T. Spectroscopy Laboratory. Their analysis was based on the new thorium wavelengths reported in the M.I.T. Wavelength Tables of Harrison [1939] and new Zeeman effect observations made with the Bitter magnet at fields of about 9 teslas. With resolved Zeeman patterns for more than 700 lines, they classified 1100 Th II lines as arising from 219 levels. Measured g-values were provided for each level. Many levels were identified from the Zeeman effect. The levels belonged to two unconnected groups of terms. In one group, the low even configurations were identified as $(6d+7s)^3$ and the higher odd configurations as $6d^27p$, $6d7s7p$, and $5f6d7s$. In the other group the low odd levels were attributed to $5f7s^2$ and $5f6d7s$ and the higher evens to $5f7s7p$ and $5f6d7p$.

In a second paper, McNally [1945] investigated the infrared spectrum of Th II and established that the lowest odd level, $5f7s^2\ {}^2F^o_{2^1/_2}$, lay 4490 cm^{-1} above the ground state. His paper gives 301 levels on a unified scale relative to the ground state. Of these levels, 21 are credited to the first paper of de Bruin, Schuurmans, and Klinkenberg [1943] (v.i.) and 17 others have been rejected since.

In an investigation which, because of the war, was entirely independent, de Bruin, Schuurmans, and Klinkenberg [1943], [1944] at the Zeeman Laboratory in Amsterdam, classified about 1900 lines as arising from 232 levels. Measured g-values were published for every level but no list of classified lines could be printed. They found essentially the same two systems as those found at M.I.T. and in a note at the end of their second paper announced their discovery of the wavenumber difference between the two systems which later, and independently, was confirmed by McNally.

Their work was extended by Schuurmans [1946] with a discussion based on the theory of the configurations with 5f-electrons. He suggested tentative locations for the then undiscovered configuration $5f^27p$ and for $5f^3$. He found 31 new levels, all but one of which are here confirmed.

In 1958 G. W. Charles prepared a compilation of available data on the first four spectra of thorium. For Th II Charles listed 165 odd and 191 even levels (including some not previously published) and 2850 classified lines, together with all known Zeeman patterns and isotope shifts. We have rejected 5 even and 14 odd levels in his list.

Recently Minsky [1969] has calculated all 13 of the important configurations of Th II as three groups in intermediate coupling with configuration interaction. They are the low even group $(6d+7s)^3$, the high even group $5f^2\,7s+5f7s7p+5f6d7p+5f^26d$, and the six odd configurations $5f7s^2+5f6d7s+5f6d^2+6d7s7p+7s^27p+6d^27p$. Thus Minsky's work provides a modern theoretical analysis for all the important configurations of Th II.

In addition to his extensive theoretical analysis,

[1] N. Minsky, Dissertation, Hebrew University, Jerusalem (1969).

[2] Literature references are at the end of this paper.

Minsky discovered 29 new levels, all of which are confirmed in this paper. Furthermore, his predictions of the locations of the undiscovered levels of the thirteen configurations have been most helpful in guiding our searches and, of course, in identifying newly found levels.

Recently Brewer [1971] has predicted the position of the lowest terms of $5f^27p$ at 48 000 : 2000 cm^{-1}, $5f7p^2$ at 54 000 ± 4000 cm^{-1}, and $5f^3$ at 55 000 ± 5000 cm^{-1}. In this paper we have confirmed his predictions for f^2p and fp^2.

2. Observations

A summary of the observations of thorium spectra at NBS and elsewhere prior to 1960 has been given by Zalubas [1960]. His monograph presented new observations of wavelengths and intensities in electrodeless lamps and spark sources for 15 000 lines of Th I and Th II in the spectral range 2000 to 11 550 Å. It superseded all previous published descriptions of Th I and Th II in both accuracy and extent. The monograph was used by Minsky [1969] for his extension of the classification of Th II.

With the completion of the new description, work on the analysis of Th I was begun by Zalubas [1959]. As the work proceeded it became clear that the analysis could be carried on to a considerably more advanced state if the precision of the wavelengths could be improved still further. New observations were made at NBS over the period 1965–1970 with instruments of higher resolution and with improved standards. These observations will be described in detail in a forthcoming publication on thorium spectra by Zalubas.

In the region 9200 to 30 000 Å lines observed with the C.N.R.S. (Orsay) Fourier transform spectrometer of Connes et al. [1970] were generously furnished to us by Giacchetti. That list is discussed and published by Giacchetti, Blaise, Corliss, and Zalubas [1974]. Earlier work in the infrared region of the thorium spectra was done by Steers [1967] and by Bernage, Houdart, and Niay [1971].

The list of thorium lines now at hand has nearly 40 000 lines, of which about 14 000 are regarded as belonging to Th II. This list will be published to replace the earlier list of Zalubas [1960].

In addition to the wavelength observations described above, we have Zeeman effect plates taken at the Argonne National Laboratory in 1964 in the range 2690 to 9100 Å at a magnetic field of 2.4 teslas. These spectra, made with electrodeless thorium iodide lamps, provided Zeeman patterns mostly for Th I, but there were also many good resolved patterns for lines of Th II. These data were used to calculate g-values for Th II levels for which published values were not already available.

3. Searches for Energy Levels

Before we undertook searches for new energy levels in Th II, we had to improve the accuracy of the published level values, most of which were in error by more than 0.03 cm^{-1} and a few by more than 0.2 cm^{-1}. With the aid of the proposed secondary-standard wavelengths of Giacchetti, Stanley, and Zalubas [1970] and Giacchetti's Fourier transform infrared list, we determined three decimal wavenumber values (cm^{-1}) for 82 even and 110 odd levels. With these values and our new line list we then determined two decimal values for the remaining known levels.

The searches for new energy levels were carried out on the NBS Univac 1108 using the programs called "Combo," written by Jack Tech. They were guided by the predictions of Minsky [1969]. At the conclusion of the searchers we had found 71 new even and 37 new odd levels.

This paper incorporates the results of seven investigations, each of which increased the number of known energy levels in Th II. The contribution of each to the total number of levels now regarded as real is listed below.

Symbol		Even	Odd	Total
H	McNally et al. [1942]	112	102	214
B	de Bruin et al. [1943], [1944]	37	28	65
R	McNally [1945]	8	5	13
S	Schuurmans [1946]	21	10	31
C	Charles [1958]	7	3	10
M	Minsky [1969]	15	14	29
Z	Present paper	71	37	108
	Total	271	199	470

Although, as mentioned earlier, the results of McNally, Harrison and Park and of de Bruin, Schuurmans and Klinkenberg were for the most part the same, we have credited the levels in common to McNally et al. because of prior publication.

4. Results

4.1. Energy Levels

The known energy levels are listed in numerical order in two tables: (1) the even parity levels and (2) the odd levels. The relative positions of the configurations are illustrated by the energy diagram in figure 1.

The three low even configurations $(6d+7s)^3$ have 37 levels of which 31 were already known. We have found five of the remaining six levels, leaving only the highest level with $J=1/2$ undiscovered.

The four higher even configurations $4f^26s$, $5f7s7p$, $5f6d7p$ and $5f^26d$ start between 24 000 and 33 000 cm^{-1} and consist of 268 levels, of which 235 are now known. Most of the unknown levels are above 50 000 cm^{-1}. In these configurations Minsky's correlation of observed energy levels with the calculated ones appears to be in error above 42 000 cm^{-1} for $J=2\frac{1}{2}$, above 41 000 cm^{-1} for $J=3\frac{1}{2}$, and above 43 000 cm^{-1} for $J=4\frac{1}{2}$. No designations are given here for these levels, only the configurations. New calculations will

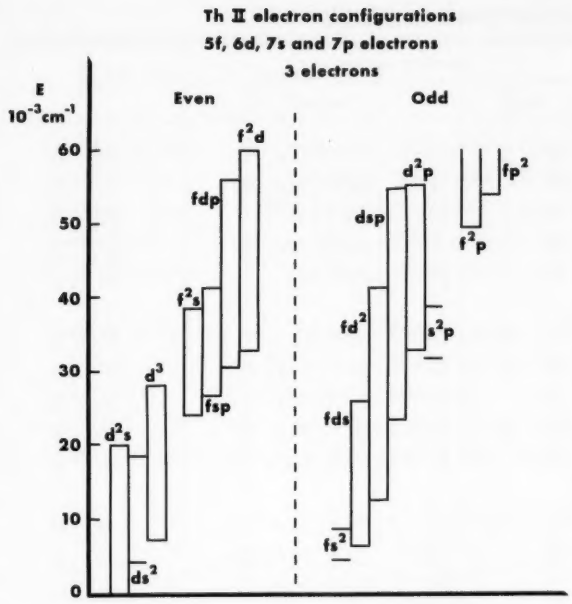

FIGURE 1. *Relative positions of the 15 known electron configurations of Th* II.

be needed before proper correlation of energy levels with eigenvectors can be made in these cases.

The three low odd configurations $5f(6d+7s)^2$, with 122 levels, are now all known. The lowest term, $5f7s^2$ ^{2}F°, was identified by McNally, Harrison, and Park [1942]. The three high odd configurations $(6d+7s)^2 7p$ give 70 levels, of which only the two highest $J=1/2$ and $J=1\,1/2$ levels have not been found.

The three higher odd configurations $5f^2 7p$, $5f7p^2$, and $5f^3$ are predicted by Brewer [1971] to start near 50 000 cm^{-1}. We have found eight likely $5f^2 7p$ levels. The lowest, at 49 495.57 cm^{-1}, may be $^4I^\circ_{4\,1/2}$, which lies lowest, according to Hund's rule.

In tables 1 and 2 the configuration of the largest component in the eigenvector of the level is listed in the first column. The compositions are from Minsky [1969]. If this component is at least 50 percent, the term symbol is listed in the second column and serves as a designation for the level. If the largest component in the eigenvector is less than 50 percent, no name is given and the term symbol for the major component appears in column seven.

For example, the leading component of the ground state is 43 percent $6d^2 7s$ $^4F_{1\,1/2}$ with a second component of 27 percent $6d7s^2$ $^2D_{1\,1/2}$. However, the level at 1859 cm^{-1} is 52 percent $6d^2 7s$ $^4F_{1\,1/2}$ and 36 percent $6d7s^2$ $^2D_{1\,1/2}$. Therefore, it is impossible to assign a meaningful *LS* designation to the ground level. In a spectrum with such strong intermediate coupling and configuration interactions, many levels have no meaningful names.

The *J*-value, observed level value, and observed *g*-value appear in the next three columns. The *g*-values are taken from Charles's [1958] compilation or from our own observations. The percentage contributed by the first component in the eigenvector of the level is given in the sixth column. In columns 8 and 9 appears the percentage and term for the second largest component. A very few of the levels of Th II have purity greater than 99 percent. In such cases the second component is omitted from the table.

The last columns show the approximate number of combinations observed for each level and a symbol (from the list in section 3) for the discoverer of the level.

The $6d^3$ configuration has two ^{2}D terms, which are theoretically differentiated by the seniority number of Racah [1943]. We use the notations of Nielson and Koster [1963] for these terms; the ^{2}D1 term has seniority 1 and the ^{2}D2 term has seniority 3.

TABLE 1. *Even energy levels of* Th II

Configuration	Term	*J*	Level (cm^{-1})	*g*	Leading percentages				*n*, ref.	
					First		Second			
$6d^2(^3F)7s$		$1\,1/2$	0.000	0.639	43	^{4}F	27	$6d(^2D)7s^2$ ^{2}D	74	H
$6d^2(^3F)7s$	^{4}F	$2\,1/2$	1521.893	1.076	65		17	(^{1}D) ^{2}D	82	H
$6d^2(^3F)7s$	^{4}F	$1\,1/2$	1859.936	0.586	52		36	$6d(^2D)7s^2$ ^{2}D	64	H
$6d(^2D)7s^2$		$2\,1/2$	4113.356	1.163	36	^{2}D	30	$6d^2(^3F)7s$ ^{4}F	78	H
$6d^2(^3F)7s$	^{4}F	$3\,1/2$	4146.575	1.232	96		2	(^{1}F) ^{2}F	68	H
$6d^2(^3F)7s$	^{4}F	$4\,1/2$	6213.488	1.312	89		9	(^{1}G) ^{2}G	43	H
$6d^2(^3P)7s$	^{4}P	$1/2$	6244.294	2.112	70		13	(^{1}P) ^{2}P	31	H
$6d^3$		$1\,1/2$	7001.425	0.800	41	^{4}F	16	$6d(^2D)7s^2$ ^{2}D	62	H
$6d^2(^1P)7s$		$1/2$	7828.562	1.254	36	^{2}P	36	$6d^3$ ^{2}P	33	H
$6d^2(^3P)7s$	^{4}P	$1\,1/2$	8018.191	1.608	89		3	$6d^3$ ^{4}F	51	H

TABLE 1. *Even energy levels of* Th II – Continued

Configuration	Term	J	Level (cm^{-1})	g	Leading percentages				n, ref.	
					First		Second			
$6d^3$		$1^1/_2$	8460.354	0.968	43	^{4}F	21	$6d(^2P)7s^2\ ^2P$	60	H
$6d^2(^1F)7s$	^{2}F	$2^1/_2$	8605.841	0.986	62		11	$6d(^2D)7s^2\ ^2D$	72	H
$6d^2(^3P)7s$	^{4}P	$2^1/_2$	9061.101	1.419	71		12	$(^1F)\ ^2F$	69	H
$6d^3$	^{4}F	$2^1/_2$	9400.967	1.034	84		6	$6d(^2D)7s^2\ ^2D$	69	H
$6d^2(^1G)7s$	^{2}G	$3^1/_2$	9711.961	0.953	54		27	$6d^3\ ^2G$	64	H
$6d^2(^1G)7s$		$4^1/_2$	10379.124	1.153	41	^{2}G	30	$6d^3\ ^2G$	45	B
$6d^3$		$3^1/_2$	10855.324	1.166	46	^{4}F	33	$6d^2(^1F)7s\ ^2F$	57	B
$6d^2(^1D)7s$	^{2}D	$1^1/_2$	12219.974	0.977	56		11	$6d(^2D)7s^2\ ^2D$	55	H
$6d^3$		$3^1/_2$	12570.492	1.131	40	^{4}F	34	$6d^2(^1F)7s\ ^2F$	56	B
$6d^3$	^{4}F	$4^1/_2$	13248.709	1.242	60		33	$6d^2(^1G)7s\ ^2G$	36	H
$6d^2(^1D)7s$		$2^1/_2$	13250.505	1.245	44	^{2}D	20	$6d(^2D)7s^2\ ^2D$	48	H
$6d^3$	^{4}P	$^1/_2$	14349.390	2.555	93		5	$6d^2(^1P)7s\ ^2P$	22	H
$6d^3$	^{4}P	$1^1/_2$	15236.639	1.592	71		19	$6d^2(^1P)7s\ ^2P$	36	H
$6d^3$	^{2}H	$4^1/_2$	15305.265	1.006	69		16	^{4}F	35	H
$6d^3$	^{4}P	$2^1/_2$	15786.986	1.571	91		4	^{2}D1	36	B
$6d^3$	^{2}G	$3^1/_2$	16818.067	0.916	58		32	$6d^2(^1G)7s\ ^2G$	45	B
$6d^3$	^{2}H	$5^1/_2$	17727.251	1.09	99				20	Z
$6d^3$		$1^1/_2$	18118.705	0.93	44	^{2}D2	20	^{2}D1	35	M
$6d^2(^1S)7s$	^{2}S	$^1/_2$	19594.350		80		10	$6d^3\ ^2P$	12	Z
$6d^3$	^{2}G	$4^1/_2$	19880.083	1.08	59		22	^{2}H	23	Z
$6d^3$	^{2}D2	$2^1/_2$	20158.744	1.19	67		12	$6d^2(^1D)7s\ ^2D$	38	M
$6d^3$	^{2}F	$2^1/_2$	22106.437	0.92	71		8	$6d^2(^1F)7s\ ^2F$	36	Z
$6d^3$	^{2}F	$3^1/_2$	22834.138	1.12	82		15	$6d^2(^1F)7s\ ^2F$	31	M
$5f^2(^3H)7s$	^{4}H	$3^1/_2$	24381.802	0.70	74		12	$5f6d(^3G°)7p\ ^4H$	21	M
$5f^2(^3H)7s$		$4^1/_2$	25246.298	0.96	45	^{4}H	33	$(^3H)\ ^2H$	20	R
$6d^3$		$1^1/_2$	25381.927	1.25	46	^{2}P	34	$6d^2(^1P)7s\ ^2P$	9	Z
$5f7s(^3F°)7p$		$2^1/_2$	26488.644	0.776	43	^{4}G	16	$(^3F°)\ ^4F$	18	H
$5f^2(^3F)7s$		$1^1/_2$	26762.272	0.47	42	^{4}F	17	$5f6d(^3F°)7p\ ^4F$	18	B
$5f7s(^3F°)7p$		$3^1/_2$	27257.144	1.032	32	^{4}G	15	$(^1F°)\ ^2G$	23	H
$5f^2(^3H)7s$		$4^1/_2$	27526.948	0.93	42	^{2}H	37	$(^3H)\ ^4H$	20	S
$5f^2(^3F)7s$		$2^1/_2$	27593.965	0.963	37	^{4}F	17	$5f7s(^3F°)7p\ ^4G$	23	B
$5f7s(^3F°)7p$		$1^1/_2$	27631.225	0.625	45	^{4}F	25	$5f^2(^3F)7s\ ^4F$	14	H
$5f^2(^3H)7s$	^{4}H	$5^1/_2$	27937.074	1.12	73		14	$(^3H)\ ^2H$	13	Z
$6d^3$	^{2}D1	$1^1/_2$	28011.159	0.717	52		36	^{2}D3	11	H
$6d^3$	^{2}D1	$2^1/_2$	28026.347	1.13	70		14	^{2}F	15	S

TABLE 1. *Even energy levels of* Th II – Continued

Configuration	Term	J	Level (cm^{-1})	g	Leading percentages				n, ref.	
					First		Second			
$5f7s(^3F°)7p$		$2^1/_2$	28823.649	0.987	26	^4F	15	$(^3F°)$ ^4D	18	H
$5f^2(^3F)7s$		$2^1/_2$	29345.894	0.935	39	^2F	29	(^3F) ^4F	24	B
$5f^2(^3F)7s$	^4F	$3^1/_2$	29431.847	1.1	63		11	$5f6d(^3F°)7p$ ^4F	23	M
$5f^2(^3F)7s$		$4^1/_2$	29515.132	1.030	32	^4F	13	(^1G) ^2G	25	H
$5f^2(^3F)7s$		$3^1/_2$	29873.948	1.10	44	^2F	18	(^3F) ^2G	19	B
$5f6d(^3H°)7p$		$4^1/_2$	30452.723	1.035	41	^4I	14	$(^3H°)$ ^2H	22	H
$5f^2(^3H)7s$	^2H	$5^1/_2$	30484.713	1.08	72		12	(^3H) ^4H	17	M
$5f^2(^3H)7s$	^4H	$6^1/_2$	30548.67	1.23	87		6	$5f6d(^3G°)7p$ ^4H	4	Z
$5f7s(^3F°)7p$		$3^1/_2$	30879.418	1.213	35	^4F	25	$(^3F°)$ ^4D	22	B
$5f6d(^3F°)7p$		$2^1/_2$	31259.295	0.781	27	^4G	15	$5f^2(^3F)7s$ ^2F	22	H
$5f7s(^1F°)7p$		$2^1/_2$	31754.210	0.948	36	^2F	23	$(^1F°)$ ^2D	21	H
$5f7s(^3F°)7p$		$4^1/_2$	31773.077	1.222	35	^4G	30	$(^3F°)$ ^4F	21	H
$5f7s(^1F°)7p$		$3^1/_2$	32576.745	1.024	22	^2G	18	$5f^2(^3F)7s$ ^2F	27	H
$5f^2(^3H)6d$	^4K	$5^1/_2$	32620.859	0.826	72		11	(^3H) ^2I	9	H
$5f6d(^3H°)7p$		$3^1/_2$	32736.186	0.904	24	^4H	13	$(^3H°)$ ^2G	24	H
$5f6d(^1D°)7p$		$1^1/_2$	32959.48	0.874	23	^2D	15	$(^1D°)$ ^2P	16	H
$5f7s(^3F°)7p$		$3^1/_2$	33209.40	1.051	15	^4G	13	$(^1F°)$ ^2F	29	H
$5f^2(^3F)7s$		$4^1/_2$	33384.444	1.14	26	^4F	16	(^1G) ^2G	24	B
$5f^2(^3F)6d$		$3^1/_2$	33637.228	0.830	17	^4H	11	(^3H) ^4H	22	H
$5f^2(^1D)7s$		$2^1/_2$	33730.94	1.031	13	^2D	8	$5f6d(^1D°)7p$ ^2D	23	H
$5f^2(^1D)7s$		$1^1/_2$	34019.240	0.823	25	^2D	21	$5f6d(^3F°)7p$ ^2D	18	B
$5f^2(^1D)7s$		$2^1/_2$	34174.540	0.986	22	^2D	12	$5f6d(^3F°)7p$ ^4G	27	H
$5f^2(^3H)6d$		$4^1/_2$	34270.25	0.938	42	^2H	11	(^3F) ^2H	22	H
$5f^2(^1G)7s$		$3^1/_2$	34279.321	1.047	26	^2G	14	$5f7s(^1F°)7p$ ^2G	34	H
$5f7s(^3F°)7p$		$2^1/_2$	34543.551	1.003	28	^4D	13	$(^3F°)$ ^4F	29	H
$5f7s(^3F°)7p$		$4^1/_2$	34553.950	1.069	19	^4G	15	$(^3F°)$ ^4F	28	H
$5f6d(^3H°)7p$	^4I	$5^1/_2$	34661.718	0.998	50		12	$(^3H°)$ ^2H	19	H
$5f6d(^3F°)7p$		$3^1/_2$	34726.58	0.950	29	^4G	18	$5f^2(^3F)6d$ ^4G	22	H
$5f^2(^3P)7s$	^4P	$^1/_2$	34782.74	1.67	57		14	$5f6d(^3P°)7p$ ^4P	6	S
$5f7s(^3F°)7p$	^4D	$1^1/_2$	35021.37	1.042	57		15	$(^3F°)$ ^4F	18	B
$5f^2(^3H)6d$	^4K	$6^1/_2$	35400.78	0.98	91		3	(^1G) ^2I	6	Z
$5f7s(^3F°)7p$	^4D	$^1/_2$	35425.627	0.265	88		2	$5f^2(^3F)6d$ ^4D	7	H
$5f6d(^1G°)7p$		$4^1/_2$	35456.181	1.054	23	^2H	13	$5f^2(^1G)7s$ ^2G	25	H
$5f^2(^3H)6d$		$5^1/_2$	35525.169	1.024	18	^2H	17	(^3H) ^4K	16	B
$5f^2(^3H)6d$	^4I	$4^1/_2$	35545.60	0.826	71		8	(^1G) ^2H	19	H

TABLE 1. *Even energy levels of* Th II – Continued

Configuration	Term	J	Level (cm^{-1})	g	Leading percentages				n, ref.	
					First		Second			
$5f6d(^3F^\circ)7p$		$2^1/_2$	35741.295	0.954	19	^4G	9	$(^3F^\circ)\ ^2D$	29	H
$5f6d(^1G^\circ)7p$		$3^1/_2$	35878.862	0.983	17	^2F	11	$(^3H^\circ)\ ^4H$	31	H
$5f^2(^3F)6d$		$^1/_2$	36040.85	1.210	29	^2P	28	$5f^2(^3P)7s\ ^2P$	11	H
$5f^2(^3F)6d$		$2^1/_2$	36065.729	0.887	42	^4G	10	$(^3H)\ ^4G$	26	H
$5f^2(^3F)6d$		$4^1/_2$	36125.335	1.035	22	^4H	19	$(^3H)\ ^4H$	24	H
$5f^2(^3P)7s$	^4P	$1^1/_2$	36328.61	1.615	64		10	$5f6d(^3P^\circ)7p\ ^4P$	17	H
$5f6d(^1G^\circ)7p$		$3^1/_2$	36809.279	1.022	13	^2F	13	$5f^2(^3F)6d\ ^4H$	33	H
$5f^2(^3P)7s$		$^1/_2$	36812.44	0.737	36	^2P	17	$5f6d(^3D^\circ)7p\ ^2P$	13	H
$5f7s(^3F^\circ)7p$		$5^1/_2$	37053.44		19	^4G	14	$5f^2(^3H)6d\ ^2I$	13	Z
$5f6d(^3H^\circ)7p$		$4^1/_2$	37063.308	0.999	29	^4H	13	$5f^2(^3F)6d\ ^4H$	27	H
$5f6d(^3F^\circ)7p$		$3^1/_2$	37277.368	0.881	16	^4G	13	$5f^2(^3H)6d\ ^4G$	26	H
$5f6d(^3F^\circ)7p$		$2^1/_2$	37465.46	1.048	18	^4D	15	$(^3F^\circ)\ ^2D$	28	H
$5f^2(^3P)7s$		$1^1/_2$	37542.17	1.003	21	^2P	13	$5f6d(^1D^\circ)7p\ ^2D$	22	H
$5f^2(^3H)6d$	^4I	$5^1/_2$	37562.27	1.008	61		14	$5f7s(^3F^\circ)7p\ ^4G$	13	R
$5f^2(^1I)7s$	^2I	$6^1/_2$	37575.24	1.088	77		6	$5f6d(^1H^\circ)7p\ ^2I$	10	R
$5f7s(^3F^\circ)7p$		$5^1/_2$	37679.71	1.13	31	^4G	11	$5f6d(^3H^\circ)7p\ ^4G$	18	R
$5f6d(^3G^\circ)7p$		$3^1/_2$	37787.89	1.062	26	^4H	11	$(^3G^\circ)\ ^4G$	27	B
$5f7s(^3F^\circ)7p$		$1^1/_2$	37821.97	1.15	13	^2D	7	$5f6d(^3F^\circ)7p\ ^4F$	17	B
$5f^2(^3F)6d$		$4^1/_2$	37840.845	1.07	35	^4G	15	$(^3H)\ ^4G$	21	S
$5f7s(^3F^\circ)7p$		$2^1/_2$	37945.104	0.893	32	^2F	16	$5f6d(^1G^\circ)7p\ ^2F$	28	H
$5f^2(^3P)7s$		$2^1/_2$	38105.065	1.172	33	^4P	9	$5f6d(^3D^\circ)7p\ ^4P$	25	H
$5f^2(^3H)6d$	^4K	$7^1/_2$	38107.11	1.08	99				2	Z
$5f7s(^1F^\circ)7p$		$3^1/_2$	38165.355	0.981	11	^2G	7	$5f6d(^3G^\circ)7p\ ^2F$	30	H
$5f6d(^3H^\circ)7p$		$4^1/_2$	38179.941	0.979	29	^2H	14	$(^3H^\circ)\ ^4I$	25	H
$5f7s(^3F^\circ)7p$		$3^1/_2$	38291.801	0.949	19	^2G	12	$5f^2(^3F)6d\ ^4G$	31	H
$5f^2(^3F)6d$		$1^1/_2$	38372.02	1.200	15	^4P	15	$5f6d(^1D^\circ)7p\ ^2P$	13	B
$5f7s(^3F^\circ)7p$		$3^1/_2$	38389.368	1.088	16	^4D	7	$5f6d(^3F^\circ)7p\ ^2G$	27	H
$5f^2(^3H)6d$	^4I	$6^1/_2$	38517.98	1.111	55		33	$5f6d(^3H^\circ)7p\ ^4I$	8	B
$5f7s(^1F^\circ)7p$		$4^1/_2$	38617.68	1.16	39	^2G	19	$(^3F^\circ)\ ^4F$	20	M
$5f6d(^1D^\circ)7p$		$2^1/_2$	38728.681	1.255	13	^2F	12	$5f^2(^3F)6d\ ^4P$	31	H
$5f^2(^3F)6d$		$5^1/_2$	38740.45	1.188	27	^4H	20	$(^3H)\ ^4H$	12	R
$5f^2(^1D)7s$		$1^1/_2$	38757.190	0.935	14	^2D	10	$(^1P)\ ^2P$	21	H
$5f6d(^3D^\circ)7p$		$1^1/_2$	38836.20	1.013	21	^4F	9	$5f^2(^3P)7s\ ^2P$	20	H
$5f^2(^1I)7s$		$5^1/_2$	38862.817	1.083	47	^2I	13	$5f6d(^3H^\circ)7p\ ^2I$	22	R
$5f6d(^3H^\circ)7p$		$2^1/_2$	38863.85	0.967	15	^4G	10	$(^3G^\circ)\ ^4G$	25	H

TABLE 1. *Even energy levels of* Th II – Continued

Configuration	Term	J	Level (cm^{-1})	g	Leading percentages				n, ref.	
					First		Second			
$5f6d(^3F^\circ)7p$		$1/2$	38867.170	0.947	34	^4D	25	$5f^2(^3F)6d\ ^4P$	12	H
$5f^2(^3F)6d$		$3^1/_2$	39068.691	1.114	23	^2F	7	$5f6d(^3F^\circ)7p\ ^4D$	30	H
$5f^2(^3H)6d$		$6^1/_2$	39085.55	1.10	33	^2I	25	$(^1I)\ ^2I$	8	S
$5f6d(^3F^\circ)7p$		$1^1/_2$	39150.679	0.739	18	^4D	12	$(^3D^\circ)\ ^4D$	21	H
$5f6d(^1G^\circ)7p$		$5^1/_2$	39352.294	1.05	20	^2H	10	$5f^2(^3F)6d\ ^4H$	15	S
$5f7s(^1F^\circ)7p$		$2^1/_2$	39366.90	1.140	22	^2D	13	$(^3F^\circ)\ ^4D$	24	H
$5f^2(^3F)6d$		$3^1/_2$	39458.272	0.979	15	^4G	9	$5f6d(^3G^\circ)7p\ ^4G$	24	H
$5f6d(^3F^\circ)7p$		$4^1/_2$	39552.244	1.100	13	^2G	10	$(^1G^\circ)\ ^2H$	29	H
$5f6d(^3H^\circ)7p$		$2^1/_2$	39700.583	1.090	16	^4G	10	$(^3F^\circ)\ ^4F$	29	H
$5f6d(^3G^\circ)7p$		$4^1/_2$	39895.42	1.024	13	^2G	12	$(^3F^\circ)\ ^4G$	29	H
$5f^2(^3F)6d$		$5^1/_2$	39939.115	1.12	25	^4G	14	$5f^2(^1I)7s\ ^2I$	17	B
$5f^2(^3F)6d$		$1/2$	39948.40	1.542	29	^4P	23	$5f6d(^3F^\circ)7p\ ^4D$	9	H
$5f6d(^3H^\circ)7p$		$2^1/_2$	40216.12	1.024	23	^4G	10	$5f^2(^1D)7s\ ^2D$	23	S
$5f7s(^1F^\circ)7p$		$1^1/_2$	40222.903	0.738	25	^2D	17	$(^3F^\circ)\ ^2D$	18	H
$5f7s(^1F^\circ)7p$		$1^1/_2$	40278.13	0.705	14	^2D	13	$5f^2(^3H)6d\ ^4F$	22	H
$5f6d(^3G^\circ)7p$		$4^1/_2$	40367.44	1.176	26	^4G	8	$(^3G^\circ)\ ^4F$	27	B
$5f6d(^1D^\circ)7p$		$3^1/_2$	40411.48	1.106	18	^2F	11	$(^3F^\circ)\ ^2G$	25	H
$5f6d(^3P^\circ)7p$		$1/2$	40523.74	0.50	41	^4D	12	$(^3D^\circ)\ ^4D$	11	S
$5f6d(^3F^\circ)7p$		$3^1/_2$	40570.63	1.1	19	^4D	12	$(^3G^\circ)\ ^4G$	28	M
$5f6d(^3H^\circ)7p$		$5^1/_2$	40574.76	1.140	14	^2H	11	$(^3H^\circ)\ ^4G$	19	B
$5f^2(^3F)6d$		$2^1/_2$	40644.331	0.856	11	^2F	10	$(^3F)\ ^4P$	35	H
$5f^2(^3H)6d$		$6^1/_2$	40724.74	1.129	32	^4I	26	$5f6d(^3H^\circ)7p\ ^4I$	11	B
$5f6d(^3D^\circ)7p$		$2^1/_2$	40923.62	0.988	24	^4F	9	$5f^2(^3H)6d\ ^4F$	30	H
$5f6d(^3F^\circ)7p$		$1^1/_2$	40991.58	1.036	10	^4D	9	$5f^2(^3H)6d\ ^4F$	23	S
$5f6d(^1G^\circ)7p$		$4^1/_2$	41047.209	1.112	30	^2G	20	$(^3F^\circ)\ ^4G$	29	B
$5f^2(^3H)6d$	^4I	$7^1/_2$	41099.07	1.17	83		6	$(^3H)\ ^2K$	5	B
$5f6d(^3H^\circ)7p$		$5^1/_2$	41223.56	1.11	35	^4H	26	$(^1G^\circ)\ ^2H$	19	B
$5f7s(^3F^\circ)7p$		$2^1/_2$	41328.341	1.101	22	^2D	7	$5f6d(^3F^\circ)7p\ ^4F$	32	H
$5f^2(^1G)6d$		$4^1/_2$	41398.51	0.983	25	^2H	10	$5f6d(^3G^\circ)7p\ ^4H$	28	S
$5f^26d+5f6d7p$		$3^1/_2$	41488.15	1.010					31	H
$5f^2(^3F)6d$		$1^1/_2$	41676.85	1.220	21	^4P	11	$5f6d(^3D^\circ)7p\ ^4D$	21	H
$5f^26d+5f6d7p$		$3^1/_2$	41688.44	0.940					29	H
$5f^2(^3F)6d$		$6^1/_2$	41882.39		37	^4H	23	$(^3H)\ ^4H$	8	Z
$5f6d(^3F^\circ)7p$		$4^1/_2$	41909.33	1.097	12	^2G	10	$(^3G^\circ)\ ^4F$	26	B
$5f^2(^3F)6d$		$1^1/_2$	41936.53	1.095	22	^4P	16	$(^3F)\ ^2D$	18	C

TABLE 1. *Even energy levels of* Th II – Continued

Configuration	Term	J	Level (cm^{-1})	g	Leading percentages				n, ref.	
					First		Second			
$5f^2(^3F)6d$		1/2	42008.16	0.8	24	^2P	17	$5f6d(^3D^\circ)7p$ ^4D	7	Z
$5f6d(^3G^\circ)7p$		5 1/2	42146.54	1.158	31	^4G	12	$(^3G^\circ)$ ^2H	22	B
$5f6d(^3F^\circ)7p$		4 1/2	42200.205	1.08	12	^4G	11	$(^3H^\circ)$ ^2G	32	B
$5f^26d+5f6d7p$		3 1/2	42222.31	0.935					30	S
$5f6d(^3P^\circ)7p$		1/2	42246.02	0.8	20	^4P	13	$5f^2(^3F)6d$ ^4D	7	Z
$5f^26d+5f6d7p$		2 1/2	42336.83	1.15					21	Z
$5f^26d+5f6d7p$		2 1/2	42352.13	1.126					27	H
$5f^26d+5f6d7p$		3 1/2	42518.907	1.080					31	H
$5f6d(^3H^\circ)7p$		6 1/2	42644.878	1.10	32	^4I	28	$(^3H^\circ)$ ^4H	10	B
$5f^26d+5f6d7p$		3 1/2	42751.324	1.09					31	S
$5f6d(^3H^\circ)7p$		4 1/2	42955.85	1.141	21	^4G	15	$(^2G^\circ)$ ^4F	29	B
$5f^2(^3H)6d$	^2K	6 1/2	43014.143	0.976	57		25	(^1I) ^2K	12	H
$5f^26d+5f6d7p$		2 1/2	43096.54	0.982					21	H
$5f6d(^3H^\circ)7p$	^2I	5 1/2	43127.21	1.037	53		9	$(^3H^\circ)$ ^4H	22	B
$5f^26d+5f6d7p$		2 1/2	43227.86	1.153					22	H
$5f^2(^3F)6d$		1 1/2	43244.86	1.08	28	^4F	13	(^3F) ^2P	16	Z
$5f^26d+5f6d7p$		3 1/2	43246.83	1.033					30	R
$5f^26d+5f6d7p$		2 1/2	43772.47	1.04					28	Z
$5f^26d+5f6d7p$		3 1/2	43803.975	1.026					32	H
$5f6d(^3F^\circ)7p$		1 1/2	43807.55	1.211	23	^4D	18	$(^3D^\circ)$ ^4D	21	H
$5f^26d+5f6d7p$		4 1/2	43809.26	1.102					27	B
$5f6d(^3P^\circ)7p$		1/2	43965.62	1.555	20	^4D	15	$5f^2(^3F)6d$ ^4D	12	S
$5f^26d+5f6d7p$		4 1/2	44096.26	1.14					27	Z
$5f6d(^3G^\circ)7p$		5 1/2	44177.26	1.12	18	^4H	17	$5f^2(^1G)6d$ ^2H	20	B
$5f^2(^3F)6d$		1 1/2	44300.548	1.342	19	^4F	9	$5f6d(^3F^\circ)7p$ ^2D	18	H
$5f^26d+5f6d7p$		2 1/2	44388.77	1.158					29	H
$5f^26d+5f6d7p$		4 1/2	44450.28	1.04					26	M
$5f^26d+5f6d7p$		3 1/2	44503.80	1.058					26	H
$5f^26d+5f6d7p$		2 1/2	44552.68	1.182					21	H
$5f6d(^3F^\circ)7p$		5 1/2	44727.24	1.2	43	^4G	10	$(^3H^\circ)$ ^4G	17	M
$5f6d(^1D^\circ)7p$		1/2	44789.30	0.84	24	^2P	18	$(^3F^\circ)$ ^4D	13	Z
$5f^26d+5f6d7p$		3 1/2	44807.95	1.078					29	B
$5f^2(^3F)6d$		1 1/2	44889.81	1.346	36	^4D	21	$5f6d(^3P^\circ)7p$ ^4D	19	C
$5f^26d+5f6d7p$		3 1/2	44898.77	1.181					29	H
$5f6d(^3H^\circ)7p$	^4I	7 1/2	45095.24		58		25	$5f^2(^3H)6d$ ^2K	5	Z

TABLE 1. *Even energy levels of* Th II – Continued

Configuration	Term	J	Level (cm^{-1})	g	Leading percentages				n, ref.	
					First		Second			
$5f^26d+5f6d7p$		$4^1/_2$	45126.24	1.21					24	B
$5f^26d+5f6d7p$		$2^1/_2$	45189.645	0.674					24	H
$5f6d(^3P^\circ)7p$		$1^1/_2$	45306.16	0.6	27	^4P	17	$(^3D^\circ)\ ^4P$	13	Z
$5f^26d+5f6d7p$		$3^1/_2$	45395.04	1.216					21	S
$5f^26d+5f6d7p$		$2^1/_2$	45610.63	1.075					23	H
$5f6d(^3H^\circ)7p$		$7^1/_2$	45646.25	1.13	35	^4I	29	$5f^2(^3H)6d\ ^2K$	3	Z
$5f^2(^3H)6d$		$5^1/_2$	45735.10	1.141	34	^4H	16	$(^3F)\ ^4H$	20	B
$5f^26d+5f6d7p$		$2^1/_2$	45800.27	1.3					26	Z
$5f^26d+5f6d7p$		$4^1/_2$	45904.40	1.02					17	S
$5f6d(^3F^\circ)7p$		$5^1/_2$	46216.583	1.16	14	^4G	14	$5f^2(^3F)6d\ ^4G$	21	S
$5f^26d+5f6d7p$		$4^1/_2$	46253.33	1.01					23	M
$5f6d(^1D^\circ)7p$		$1^1/_2$	46264.24	0.891	13	^2P	10	$(^3D^\circ)\ ^4D$	17	H
$5f^26d+5f6d7p$		$3^1/_2$	46352.23	1.1					34	C
$5f6d(^3H^\circ)7p$		$6^1/_2$	46378.86	1.13	29	^2I	25	$5f^2(^3H)6d\ ^4H$	11	B
$5f^26d+5f6d7p$		$3^1/_2$	46385.42	1.07					31	Z
$5f6d(^3G^\circ)7p$		$1^1/_2$	46395.98		23	^4F	17	$5f^2(^3H)6d\ ^4F$	15	Z
$5f6d(^3G^\circ)7p$		$5^1/_2$	46555.61		32	^4H	20	$(^3H^\circ)\ ^4G$	15	Z
$5f^26d+5f6d7p$		$2^1/_2$	46581.30	1.018					28	C
$5f^26d+5f6d7p$		$2^1/_2$	46603.20	1.112					28	H
$5f^26d+5f6d7p$		$3^1/_2$	46706.25	1.081					19	H
$5f6d(^3G^\circ)7p$		$5^1/_2$	46861.59	1.15	12	^4H	12	$5f^2(^1I)6d\ ^2I$	20	Z
$5f^26d+5f6d7p$		$2^1/_2$	46902.54	1.143					22	H
$5f6d(^3H^\circ)7p$		$6^1/_2$	46910.78	1.18	26	^4H	22	$(^3H^\circ)\ ^2I$	14	S
$5f^2(^1D)6d$		$1^1/_2$	46935.66	0.956	22	^2P	19	$(^3P)\ ^2P$	23	H
$5f6d(^3D^\circ)7p$		$^1/_2$	47145.77		19	^4D	18	$(^3D^\circ)\ ^4P$	8	C
$5f6d(^3P^\circ)7p$		$1^1/_2$	47148.60	1.09	11	^4S	9	$5f^2(^3F)6d\ ^4D$	19	H
$5f^26d+5f6d7p$		$4^1/_2$	47171.38	1.15					23	Z
$5f^26d+5f6d7p$		$2^1/_2$	47324.39	1.189					35	H
$5f6d(^3G^\circ)7p$		$5^1/_2$	47675.06	1.15	17	^2H	14	$5f^2(^3H)6d\ ^4G$	6	Z
$5f^26d+5f6d7p$		$4^1/_2$	47731.50	1.1					24	M
$5f^2(^3P)6d$		$1^1/_2$	47869.61		18	^4F	14	$(^3F)\ ^2D$	25	Z
$5f^26d+5f6d7p$		$3^1/_2$	47871.39	1.194					23	S
$5f^26d+5f6d7p$		$4^1/_2$	48006.87	1.13					25	Z
$5f^26d+5f6d7p$		$3^1/_2$	48298.50	1.07					22	S
$5f^26d+5f6d7p$		$2^1/_2$	48320.81						20	Z

TABLE 1. *Even energy levels of* Th II – Continued

Configuration	Term	J	Level (cm^{-1})	g	Leading percentages				n, ref.	
					First		Second			
$5f^26d+5f6d7p$		$3^1/_2$	48453.12						22	Z
$5f^26d+5f6d7p$		$2^1/_2$	48492.03						20	Z
$5f6d(^3G°)7p$		$6^1/_2$	48612.23	1.08	49	^4H	17	$5f^2(^1G)6d\ ^2I$	9	Z
$5f6d(^3D°)7p$		$1^1/_2$	48689.95	0.922	19	^2D	12	$5f^2(^3P)6d\ ^4F$	24	H
$5f^2(^3P)6d$		$1^1/_2$	48817.97	0.956	22	^4F	19	$5f6d(^3D°)7p\ ^2D$	17	H
$5f^26d+5f6d7p$		$4^1/_2$	48844.96	1.1					25	S
$5f^26d+5f6d7p$		$2^1/_2$	49068.82						22	Z
$5f^2(^1I)6d$		$5^1/_2$	49124.56		18	^2H	18	$5f6d(^3G°)7p\ ^4G$	18	Z
$5f6d(^3G°)7p$		$5^1/_2$	49357.99	1.15	30	^2H	28	$(^1H°)\ ^2H$	15	Z
$5f^26d+5f6d7p$		$3^1/_2$	49377.17	1.2					23	M
$5f6d(^3P°)7p$		$1^1/_2$	49414.65	1.003	18	^4S	14	$5f^2(^3P)6d\ ^4D$	14	H
$5f6d(^3D°)7p$		$^1/_2$	49485.52		17	^4P	16	$5f^2(^3P)6d\ ^4D$	10	Z
$5f^2(^1I)6d$		$6^1/_2$	49527.320	1.1	26	^2I	25	$5f6d(^3G°)7p\ ^4H$	7	Z
$5f^26d+5f6d7p$		$4^1/_2$	49837.66						19	Z
$5f^26d+5f6d7p$		$2^1/_2$	49873.098						23	Z
$5f^26d+5f6d7p$		$3^1/_2$	49960.57	1.248					27	R
$5f^26d+5f6d7p$		$3^1/_2$	50407.27						16	M
$5f^26d+5f6d7p$		$4^1/_2$	50470.04	1.18					30	S
$5f6d(^1H°)7p$		$5^1/_2$	50631.12		19	^2I	18	$5f^2(^3F)6d\ ^2H$	14	Z
$5f^26d+5f6d7p$		$2^1/_2$	50663.62						20	Z
$5f6d(^3D°)7p$		$1^1/_2$	50735.47	1.36	16	^2P	9	$(^3P°)\ ^4S$	23	C
$5f6d(^3D°)7p$		$1^1/_2$	50907.79	1.3	26	^4P	10	$5f^2(^3F)6d\ ^4P$	10	Z
$5f^2(^3P)6d$		$1^1/_2$	51024.846	1.270	24	^4D	15	$5f6d(^3P°)7p\ ^4P$	16	C
$5f^26d+5f6d7p$		$4^1/_2$	51224.27						19	Z
$5f^26d+5f6d7p$		$3^1/_2$	51268.12						21	Z
$5f^26d+5f6d7p$		$2^1/_2$	51362.89						21	Z
$5f^2(^3P)6d$		$^1/_2$	51653.96		24	^2P	17	$(^3P)\ ^4D$	10	Z
$5f6d(^1P°)7p$		$1^1/_2$	51676.08		25	^2D	11	$5f^2(^3P)6d\ ^4P$	15	Z
$5f^26d+5f6d7p$		$4^1/_2$	51681.99						17	Z
$5f^26d+5f6d7p$		$3^1/_2$	51830.53						25	Z
$5f^26d+5f6d7p$		$2^1/_2$	51865.14						25	Z
$5f^26d+5f6d7p$		$2^1/_2$	51935.68						22	Z
$5f^2(^1I)6d$	^2I	$5^1/_2$	52170.20	1.12	55		16	$5f6d(^1H°)7p\ ^2H$	16	Z
$5f^26d+5f6d7p$		$3^1/_2$	52272.33						19	Z
$5f6d(^1P°)7p$		$1^1/_2$	52307.48		22	^2D	12	$5f^2(^1G)6d\ ^2D$	15	Z

TABLE 1. *Even energy levels of* Th II – Continued

Configuration	Term	J	Level (cm^{-1})	g	Leading percentages				n, ref.	
					First		Second			
$5f^26d+5f6d7p$		$3^1/_2$	52562.52						19	Z
$5f6d(^3P^\circ)7p$		$1^1/_2$	52735.74		22	^2D	16	$(^3P^\circ)$ ^2P	17	Z
$5f^2(^1I)6d$		$6^1/_2$	52918.92		36	^2I	18	(^3H) ^2I	10	Z
$5f^26d+5f6d7p$		$4^1/_2$	53520.890						17	Z
$5f^26d+5f6d7p$		$2^1/_2$	53845.40						20	Z
$5f^26d+5f6d7p$		$3^1/_2$	54010.17						18	Z
$5f^26d+5f6d7p$		$3^1/_2$	54169.67						14	Z
$5f^26d+5f6d7p$		$2^1/_2$	54493.99						20	M
$5f^26d+5f6d7p$		$4^1/_2$	54845.32						15	Z
$5f6d(^1F^\circ)7p$		$1^1/_2$	54922.10		18	^2D	17	$5f^2(^3P)6d$ ^4P	15	Z
$5f^26d+5f6d7p$		$4^1/_2$	55496.83						18	Z
$5f6d(^1F^\circ)7p$		$1^1/_2$	56235.23		16	^2D	15	$5f^2(^3P)6d$ ^4P	14	Z
$5f^26d+5f6d7p$		$2^1/_2$	56391.01						16	Z
$5f^2(^1I)6d$		$5^1/_2$	56945.14	1.1	40	^2H	26	$5f6d(^1H^\circ)7p$ ^2H	11	Z
$5f^26d+5f6d7p$		$4^1/_2$	57078.52						13	Z
$5f^26d+5f6d7p$		$3^1/_2$	59387.31						14	Z

TABLE 2. *Odd energy levels of* Th II

Configuration	Term	J	Level (cm^{-1})	g	Leading percentages				n, ref.	
					First		Second			
$5f(^2F^\circ)7s^2$	$^2F^\circ$	$2^1/_2$	4490.256	0.856	89		3	$5f(^1S^\circ)6d^2$ $^2F^\circ$	74	H
$5f6d(^3H^\circ)7s$	$^4H^\circ$	$3^1/_2$	6168.351	0.718	78		17	$(^1G^\circ)$ $^2G^\circ$	76	H
$5f6d(^3F^\circ)7s$	$^4F^\circ$	$1^1/_2$	6691.386	0.492	74		20	$(^1D^\circ)$ $^2D^\circ$	60	H
$5f6d(^3H^\circ)7s$		$4^1/_2$	6700.183	1.018	37	$^4H^\circ$	27	$(^1G^\circ)$ $^2G^\circ$	70	H
$5f6d(^3F^\circ)7s$	$^4F^\circ$	$2^1/_2$	7331.485	1.061	54		25	$(^1D^\circ)$ $^2D^\circ$	77	H
$5f(^2F^\circ)7s^2$	$^2F^\circ$	$3^1/_2$	8378.853	1.132	85		3	$5f(^1S^\circ)6d^2$ $^2F^\circ$	91	H
$5f6d(^1G^\circ)7s$	$^2G^\circ$	$3^1/_2$	9202.264	0.911	50		17	$(^3F^\circ)$ $^4F^\circ$	86	H
$5f6d(^1G^\circ)7s$		$4^1/_2$	9238.018	1.086	44	$^2G^\circ$	31	$(^3H^\circ)$ $^4H^\circ$	76	H
$5f6d(^3G^\circ)7s$	$^4G^\circ$	$2^1/_2$	9585.404	0.601	83		6	$6d^2(^3F)7p$ $^4G^\circ$	87	H
$5f6d(^3F^\circ)7s$	$^4F^\circ$	$3^1/_2$	9720.296	1.173	60		11	$(^3G^\circ)$ $^4G^\circ$	84	H

TABLE 2. *Odd energy levels of* Th II—Continued

Configuration	Term	J	Level (cm^{-1})	g	Leading percentages				n, ref.	
					First		Second			
$5f6d(^3H°)7s$	$^4H°$	$5^1/_2$	10189.063	1.128	81		13	$(^3H°)\ ^2H°$	62	H
$5f6d(^3H°)7s$		$4^1/_2$	10572.042	0.931	45	$^2H°$	27	$(^3H°)\ ^4H°$	79	H
$5f6d(^3F°)7s$		$2^1/_2$	10673.137	1.088	40	$^4F°$	31	$(^1D°)\ ^2D°$	82	H
$5f6d(^3G°)7s$	$^4G°$	$3^1/_2$	11116.584	0.983	54		8	$(^1G°)\ ^2G°$	99	H
$5f6d(^1D°)7s$	$^2D°$	$1^1/_2$	11576.402	0.832	51		19	$(^3F°)\ ^4F°$	67	H
$5f6d(^3D°)7s$	$^4D°$	$^1/_2$	11725.431	0.255	53		12	$5f(^1D°)6d^2\ ^2P°$	33	H
$5f6d(^3F°)7s$	$^2F°$	$2^1/_2$	12472.178	0.982	55		17	$(^1D°)\ ^2D°$	89	H
$5f(^3F°)6d^2$		$3^1/_2$	12485.688	0.855	37	$^4H°$	20	$(^3F°)\ ^2G°$	90	B
$5f6d(^3F°)7s$	$^4F°$	$4^1/_2$	12488.288	1.245	53		30	$(^3G°)\ ^4G°$	82	B
$5f6d(^3D°)7s$		$1^1/_2$	12902.378	1.167	48	$^4D°$	9	$(^1D°)\ ^2D°$	71	H
$5f6d(^3H°)7s$	$^4H°$	$6^1/_2$	13406.439	1.231	96		2	$5f(^3F°)6d^2\ ^4H°$	28	B
$5f6d(^3G°)7s$	$^4G°$	$4^1/_2$	13468.969	1.185	57		20	$(^3F°)\ ^4F°$	68	B
$5f6d(^3F°)7s$		$3^1/_2$	13818.339	1.153	26	$^2F°$	17	$(^1F°)\ ^2F°$	94	B
$5f6d(^3D°)7s$		$^1/_2$	14101.800	0.523	33	$^4D°$	29	$5f(^1D°)6d^2\ ^2P°$	38	S
$5f(^3F°)6d^2$	$^4I°$	$4^1/_2$	14275.583	0.791	77		10	$5f6d(^3H°)7s\ ^2H°$	75	H
$5f6d(^3H°)7s$	$^2H°$	$5^1/_2$	14484.327	1.09	60		15	$5f(^1D°)6d^2\ ^2H°$	59	B
$5f6d(^3D°)7s$	$^4D°$	$2^1/_2$	14545.557	1.339	67		6	$(^1D°)\ ^2D°$	80	B
$5f6d(^3G°)7s$		$3^1/_2$	14790.996	0.862	40	$^2G°$	29	$5f(^3F°)6d^2\ ^4H°$	91	H
$5f6d(^3P°)7s$		$1^1/_2$	15144.738	1.366	41	$^4P°$	14	$(^3D°)\ ^4D°$	65	H
$5f(^3F°)6d^2$	$^4H°$	$4^1/_2$	15242.905	1.00	59		20	$(^3F°)\ ^2G°$	56	B
$5f6d(^3P°)7s$	$^4P°$	$^1/_2$	15324.239	2.565	87		5	$6d7s(^3D)7p\ ^4P°$	28	S
$5f6d(^3G°)7s$	$^4G°$	$5^1/_2$	15349.879	1.267	91		4	$6d^2(^3F)7p\ ^4G°$	50	B
$5f6d(^3D°)7s$	$^4D°$	$3^1/_2$	15453.036	1.296	55		17	$(^3F°)\ ^2F°$	92	B
$5f6d(^3D°)7s$	$^2D°$	$1^1/_2$	15710.843	0.643	52		21	$(^3P°)\ ^4P°$	67	R
$5f6d(^3D°)7s$		$2^1/_2$	16033.149	1.07	33	$^2D°$	32	$(^1F°)\ ^2F°$	77	B
$5f(^3F°)6d^2$	$^4I°$	$5^1/_2$	16564.633	0.98	86		4	$(^1G°)\ ^2I°$	47	B
$5f(^3F°)6d^2$		$3^1/_2$	16906.604	0.950	24	$^2G°$	17	$(^3F°)\ ^4H°$	82	S
$5f(^1D°)6d^2$		$1^1/_2$	17121.623	1.277	28	$^2P°$	28	$5f6d(^3P°)7s\ ^2P°$	60	H
$5f6d(^3G°)7s$	$^2G°$	$4^1/_2$	17272.252	1.083	58		12	$5f(^1D°)6d^2\ ^2G°$	79	B
$5f6d(^3P°)7s$	$^4P°$	$2^1/_2$	17460.625	1.51	73		8	$(^1D°)\ ^2D°$	83	B
$5f(^3F°)6d^2$		$4^1/_2$	17722.990	1.08	45	$^2G°$	30	$(^3F°)\ ^4H°$	59	M
$5f(^3F°)6d^2$	$^4H°$	$5^1/_2$	17771.06	1.10	69		13	$(^1G°)\ ^2I°$	45	B
$5f6d(^3P°)7s$		$^1/_2$	17837.804	1.080	30	$^2P°$	25	$5f(^3F°)6d^2\ ^4D°$	29	M
$5f(^3F°)6d^2$		$2^1/_2$	17983.388	0.995	25	$^2F°$	14	$(^3F°)\ ^4D°$	72	S
$5f(^3F°)6d^2$		$1^1/_2$	18214.423	0.876	31	$^4F°$	14	$(^3F°)\ ^4D°$	48	H

TABLE 2. *Odd energy levels of* Th II—Continued

Configuration	Term	J	Level (cm^{-1})	g	Leading percentages		n, ref.
					First	Second	
$5f(^3F^\circ)6d^2$		$^1/_2$	18568.27	1.007	44 $^2S^\circ$	25 $(^3F^\circ)\ ^4D^\circ$	31 Z
$5f(^3F^\circ)6d^2$	$^4I^\circ$	$6^1/_2$	18816.87	1.10	72	8 $(^1G^\circ)\ ^2I^\circ$	34 B
$5f6d(^1F^\circ)7s$		$3^1/_2$	18973.782	1.12	37 $^2F^\circ$	14 $5f(^3F^\circ)6d^2\ ^2G^\circ$	57 S
$5f(^3F^\circ)6d^2$		$1^1/_2$	19050.832	0.888	33 $^4F^\circ$	23 $(^3F^\circ)\ ^4D^\circ$	45 H
$5f6d(^3D^\circ)7s$		$2^1/_2$	19248.267	0.931	20 $^2D^\circ$	16 $(^1F^\circ)\ ^2F^\circ$	63 H
$5f(^3F^\circ)6d^2$	$^4H^\circ$	$6^1/_2$	19912.34	1.16	56	22 $(^3F^\circ)\ ^4I^\circ$	30 B
$5f6d(^1F^\circ)7s$		$3^1/_2$	20080.667	1.142	14 $^2F^\circ$	12 $5f(^3F^\circ)6d^2\ ^2F^\circ$	60 H
$5f(^3P^\circ)6d^2$		$2^1/_2$	20120.157	0.743	44 $^4G^\circ$	15 $(^3F^\circ)\ ^4F^\circ$	64 R
$5f(^1G^\circ)6d^2$		$5^1/_2$	20288.57	0.97	42 $^2I^\circ$	26 $(^3F^\circ)\ ^4H^\circ$	37 M
$5f(^3F^\circ)6d^2$		$2^1/_2$	20310.944	1.161	17 $^4D^\circ$	15 $(^3F^\circ)\ ^4G^\circ$	62 M
$5f(^3F^\circ)6d^2$		$2^1/_2$	20686.148	0.945	39 $^4F^\circ$	8 $(^3P^\circ)\ ^4G^\circ$	59 B
$5f(^3P^\circ)6d^2$		$3^1/_2$	20969.01	0.99	39 $^4G^\circ$	14 $(^3F^\circ)\ ^4G^\circ$	50 M
$5f(^1D^\circ)6d^2$		$4^1/_2$	20989.81	0.953	27 $^2H^\circ$	16 $5f6d(^3G^\circ)7s\ ^2G^\circ$	63 S
$5f6d(^1P^\circ)7s$		$1^1/_2$	21131.81	1.24	24 $^2P^\circ$	18 $5f(^3F^\circ)6d^2\ ^2P^\circ$	47 M
$5f(^3F^\circ)6d^2$		$2^1/_2$	21297.417	0.767	38 $^4G^\circ$	21 $(^3P^\circ)\ ^4G^\circ$	62 H
$5f(^3F^\circ)6d^2$		$3^1/_2$	21682.747	1.248	41 $^4F^\circ$	17 $(^3F^\circ)\ ^4D^\circ$	51 B
$5f6d(^1H^\circ)7s$	$^2H^\circ$	$5^1/_2$	22014.881	1.10	61	18 $5f(^1D^\circ)6d^2\ ^2H^\circ$	47 S
$5f(^3F^\circ)6d^2$	$^4I^\circ$	$7^1/_2$	22028.00	1.18	97	2 $(^1G^\circ)\ ^2K^\circ$	11 S
$5f(^1G^\circ)6d^2$		$4^1/_2$	22139.66	1.090	23 $^2G^\circ$	19 $(^1G^\circ)\ ^2H^\circ$	55 H
$5f6d(^1P^\circ)7s$		$^1/_2$	22355.208	0.77	35 $^2P^\circ$	16 $5f(^3F^\circ)6d^2\ ^2P^\circ$	23 M
$5f(^3P^\circ)6d^2$		$2^1/_2$	22513.290	1.17	43 $^2D^\circ$	21 $(^3F^\circ)\ ^4D^\circ$	40 C
$5f6d(^1H^\circ)7s$		$4^1/_2$	22642.107	1.043	42 $^2H^\circ$	9 $5f(^1D^\circ)6d^2\ ^2G^\circ$	50 H
$5f(^3F^\circ)6d^2$	$^4G^\circ$	$3^1/_2$	22685.447	0.981	65	12 $(^3P^\circ)\ ^4G^\circ$	45 B
$5f(^3P^\circ)6d^2$		$1^1/_2$	23012.060	1.017	25 $^4F^\circ$	13 $(^3P^\circ)\ ^2D^\circ$	30 H
$5f(^1G^\circ)6d^2$		$6^1/_2$	23187.02		31 $^2I^\circ$	31 $(^3F^\circ)\ ^4H^\circ$	23 Z
$6d7s(^3D)7p$		$1^1/_2$	23372.582	1.067	29 $^4F^\circ$	9 $5f(^3P^\circ)6d^2\ ^4F^\circ$	27 H
$5f(^3F^\circ)6d^2$		$3^1/_2$	23518.425	1.2	21 $^4F^\circ$	18 $(^3F^\circ)\ ^4D^\circ$	45 M
$5f(^3P^\circ)6d^2$		$3^1/_2$	23697.66	1.0	26 $^4G^\circ$	26 $(^1G^\circ)\ ^2G^\circ$	43 Z
$5f(^3F^\circ)6d^2$		$4^1/_2$	23730.656	1.186	45 $^4F^\circ$	13 $(^1G^\circ)\ ^2H^\circ$	35 H
$5f(^3F^\circ)6d^2$	$^4P^\circ$	$1^1/_2$	24132.037	1.429	60	5 $6d7s(^3D)7p\ ^4F^\circ$	30 H
$5f(^1G^\circ)6d^2$		$5^1/_2$	24309.226	1.11	25 $^2H^\circ$	25 $(^3F^\circ)\ ^2H^\circ$	31 M
$5f(^3F^\circ)6d^2$		$1^1/_2$	24414.643	1.105	24 $^4S^\circ$	17 $6d7s(^3D)7p\ ^4F^\circ$	29 H
$5f(^3F^\circ)6d^2$	$^4P^\circ$	$2^1/_2$	24463.792	1.396	64	7 $(^3F^\circ)\ ^2D^\circ$	43 H
$5f(^3F^\circ)6d^2$		$4^1/_2$	24757.507	1.13	45 $^4G^\circ$	40 $(^3P^\circ)\ ^4G^\circ$	37 S
$6d7s(^3D)7p$		$2^1/_2$	24873.981	1.081	26 $^4F^\circ$	20 $5f(^3P^\circ)6d^2\ ^4F^\circ$	25 H

530-326 OL - 74 - 6

TABLE 2. *Odd energy levels of* Th II – Continued

Configuration	Term	J	Level (cm^{-1})	g	Leading percentages		n, ref.
					First	Second	
$5f(^1G^\circ)6d^2$		$3^1/_2$	24982.451	0.990	30 $^2G^\circ$	24 $(^1D^\circ)\ ^2G^\circ$	37 H
$5f(^3P^\circ)6d^2$		$^1/_2$	25027.04	0.6	28 $^4D^\circ$	22 $(^3F^\circ)\ ^4P^\circ$	6 Z
$5f(^3P^\circ)6d^2$		$1^1/_2$	25188.124	0.937	19 $^4D^\circ$	16 $(^3P^\circ)\ ^4F^\circ$	23 H
$5f(^3F^\circ)6d^2$		$^1/_2$	25266.498	0.725	32 $^4P^\circ$	29 $(^3P^\circ)\ ^4D^\circ$	12 H
$5f(^3F^\circ)6d^2$		$5^1/_2$	25414.92	1.236	44 $^4G^\circ$	28 $(^1G^\circ)\ ^2H^\circ$	33 M
$5f(^3P^\circ)6d^2$		$2^1/_2$	25440.234	1.138	20 $^4F^\circ$	13 $(^3F^\circ)\ ^4P^\circ$	33 H
$5f6d(^1P^\circ)7s$		$^1/_2$	25594.88	1.27	17 $^2P^\circ$	14 $5f(^3F^\circ)6d^2\ ^2S^\circ$	7 Z
$5f(^3F^\circ)6d^2$		$4^1/_2$	25607.12	1.09	23 $^4G^\circ$	17 $(^3P^\circ)\ ^4G^\circ$	32 M
$5f(^3P^\circ)6d^2$		$2^1/_2$	26424.48	1.169	29 $^4F^\circ$	20 $(^3P^\circ)\ ^4D^\circ$	29 H
$5f(^3P^\circ)6d^2$		$1^1/_2$	26586.27	0.76	28 $^4F^\circ$	28 $(^3P^\circ)\ ^2D^\circ$	19 Z
$6d7s(^3D)7p$		$^1/_2$	26626.478	0.645	38 $^4D^\circ$	19 $(^3D)\ ^2P^\circ$	8 H
$5f(^1G^\circ)6d^2$	$^2K^\circ$	$6^1/_2$	26647.80		86	7 $(^1G^\circ)\ ^2I^\circ$	11 M
$5f(^3P^\circ)6d^2$	$^4G^\circ$	$5^1/_2$	26770.495	1.250	53	33 $(^3F^\circ)\ ^4G^\circ$	22 S
$5f(^3P^\circ)6d^2$	$^4F^\circ$	$3^1/_2$	26963.92	1.20	73	7 $(^3F^\circ)\ ^4F^\circ$	22 Z
$5f(^3F^\circ)6d^2$		$1^1/_2$	26965.202	1.384	35 $^4S^\circ$	17 $(^3F^\circ)\ ^2P^\circ$	24 B
$5f(^3P^\circ)6d^2$	$^4D^\circ$	$3^1/_2$	27249.543	1.382	50	18 $(^3F^\circ)\ ^4D^\circ$	24 R
$5f(^1G^\circ)6d^2$		$4^1/_2$	27357.36	1.02	25 $^2H^\circ$	14 $(^3P^\circ)\ ^4F^\circ$	35 M
$5f(^1D^\circ)6d^2$		$1^1/_2$	27403.18	1.002	20 $^2D^\circ$	20 $(^3P^\circ)\ ^4D^\circ$	11 H
$5f(^1G^\circ)6d^2$		4 /2	27787.84	1.16	31 $^2G^\circ$	18 $(^1D^\circ)\ ^2G^\circ$	23 M
$6d7s(^3D)7p$		$2^1/_2$	28243.812	0.922	25 $^4F^\circ$	17 $6d^2(^3F)7p\ ^4G^\circ$	22 H
$5f(^1G^\circ)6d^2$		$2^1/_2$	28587.36	1.0	42 $^2F^\circ$	17 $(^3F^\circ)\ ^2F^\circ$	26 Z
$6d7s(^3D)7p$		$1^1/_2$	28720.835	1.162	46 $^4D^\circ$	9 $(^3D)\ ^2P^\circ$	16 H
$5f(^3F^\circ)6d^2$		$2^1/_2$	28923.20	1.07	22 $^2D^\circ$	15 $(^1D^\circ)\ ^2D^\circ$	19 Z
$5f(^1D^\circ)6d^2$		$2^1/_2$	29095.467	0.998	24 $^2F^\circ$	11 $6d^2(^3F)7p\ ^4G^\circ$	26 H
$5f(^3F^\circ)6d^2$		$1^1/_2$	29720.32	0.990	21 $^2D^\circ$	15 $(^1D^\circ)\ ^2D^\circ$	21 H
$5f(^3P^\circ)6d^2$	$^4F^\circ$	$4^1/_2$	29788.45		67	13 $(^1D^\circ)\ ^2G^\circ$	18 Z
$5f(^1G^\circ)6d^2$	$^2F^\circ$	$3^1/_2$	30101.42	1.13	68	13 $(^3F^\circ)\ ^2F^\circ$	21 Z
$5f(^1G^\circ)6d^2$	$^2K^\circ$	$7^1/_2$	30223.14		97	2 $(^3F^\circ)\ ^4I^\circ$	4 Z
$5f(^1G^\circ)6d^2$		$5^1/_2$	30310.210	1.1	34 $^2H^\circ$	23 $(^1D^\circ)\ ^2H^\circ$	19 Z
$5f(^3F^\circ)6d^2$		$^1/_2$	30564.58	0.553	25 $^2P^\circ$	20 $(^1D^\circ)\ ^2P^\circ$	7 H
$5f(^3F^\circ)6d^2$	$^2H^\circ$	$4^1/_2$	30956.568	0.94	50	23 $(^1D^\circ)\ ^2H^\circ$	16 Z
$6d^2(^3F)7p$		$2^1/_2$	30972.166	1.217	16 $^4G^\circ$	15 $6d7s(^3D)7p\ ^2D^\circ$	16 H
$6d7s(^3D)7p$	$^4F^\circ$	$3^1/_2$	30994.263	1.199	53	8 $6d^2(^3F)7p\ ^4G^\circ$	19 H
$6d7s(^3D)7p$		$1^1/_2$	31353.127	0.863	17 $^4F^\circ$	9 $6d^2(^3F)7p\ ^2D^\circ$	15 H
$7s^2(^1S^\circ)7p$		$^1/_2$	31625.680	0.344	31 $^2P^\circ$	26 $6d7s(^3D)7p\ ^4D^\circ$	10 H

TABLE 2. *Odd energy levels of* Th II—Continued

Configuration	Term	J	Level (cm^{-1})	g	Leading percentages				n, ref.	
					First		Second			
$5f(^1D^\circ)6d^2$		$3^1/_2$	31800.192	1.168	37	$^2F^\circ$	11	$(^3P^\circ)\ ^2F^\circ$	24	H
$6d7s(^3D)7p$		$2^1/_2$	31810.548	1.118	36	$^4D^\circ$	12	$6d^2(^3F)7p\ ^2D^\circ$	19	H
$5f(^3F^\circ)6d^2$		$5^1/_2$	31924.599	0.99	26	$^2H^\circ$	22	$(^3F^\circ)\ ^2I^\circ$	16	Z
$5f(^3F^\circ)6d^2$		$1^1/_2$	31928.714	0.891	25	$^2D^\circ$	16	$(^1G^\circ)\ ^2D^\circ$	18	H
$5f(^1D^\circ)6d^2$		$2^1/_2$	32850.07	1.093	18	$^2D^\circ$	16	$(^3F^\circ)\ ^2D^\circ$	16	H
$6d^2(^3F)7p$	$^4G^\circ$	$3^1/_2$	32957.432	1.072	58		11	$6d7s(^3D)7p\ ^4F^\circ$	17	H
$5f(^1G^\circ)6d^2$		$1^1/_2$	33215.466	1.036	20	$^2D^\circ$	17	$6d^2(^3F)7p\ ^4F^\circ$	16	H
$5f(^1S^\circ)6d^2$		$2^1/_2$	33354.78	0.952	37	$^2F^\circ$	14	$(^3P^\circ)\ ^2F^\circ$	18	H
$5f(^1D^\circ)6d^2$		$1^1/_2$	33843.042	1.19	32	$^2P^\circ$	13	$5f6d(^3P^\circ)7s\ ^2P^\circ$	9	Z
$6d^2(^1G)7p$		$3^1/_2$	33902.085	1.0	19	$^2G^\circ$	15	$(^1G)\ ^2F^\circ$	17	Z
$6d7s(^3D)7p$		$2^1/_2$	34212.024	1.148	30	$^4D^\circ$	10	$(^1D)\ ^2F^\circ$	16	H
$6d^2(^3P)7p$		$^1/_2$	34330.500	1.503	29	$^2S^\circ$	24	$(^3P)\ ^4P^\circ$	9	H
$6d7s(^3D)7p$		$1^1/_2$	34986.606	1.298	27	$^4D^\circ$	22	$(^3D)\ ^4P^\circ$	13	R
$5f(^1G^\circ)6d^2$		$2^1/_2$	35156.916	1.079	29	$^2D^\circ$	13	$(^1G^\circ)\ ^2F^\circ$	16	H
$5f(^3F^\circ)6d^2$	$^2I^\circ$	$6^1/_2$	35165.36	1.08	58		41	$(^1G^\circ)\ ^2I^\circ$	5	Z
$6d^2(^3P)7p$	$^4D^\circ$	$^1/_2$	35198.99	0.972	54		16	$6d7s(^3D)7p\ ^4P^\circ$	9	H
$6d^2(^3F)7p$		$4^1/_2$	35593.436		38	$^4G^\circ$	18	$(^3F)\ ^4F^\circ$	8	Z
$6d7s(^3D)7p$		$3^1/_2$	35593.527	1.253	39	$^4D^\circ$	10	$5f(^3P^\circ)6d^2\ ^2G^\circ$	17	B
$5f(^3F^\circ)6d^2$		$5^1/_2$	35602.42	1.02	38	$^2I^\circ$	22	$(^1G^\circ)\ ^2I^\circ$	10	Z
$5f(^3P^\circ)6d^2$		$4^1/_2$	36193.437	1.149	34	$^2G^\circ$	18	$6d^2(^1G)7p\ ^2G^\circ$	14	H
$6d^2(^3F)7p$		$1^1/_2$	36390.527	0.829	21	$^4F^\circ$	21	$5f(^1G^\circ)6d^2\ ^2P^\circ$	14	H
$6d^2(^3P)7p$		$1^1/_2$	36444.815	1.182	47	$^4D^\circ$	9	$5f(^1G^\circ)6d^2\ ^2P^\circ$	13	H
$6d^2(^3F)7p$		$1^1/_2$	36581.568	1.107	21	$^4F^\circ$	14	$5f(^1G^\circ)6d^2\ ^2D^\circ$	14	H
$6d^2(^1D)7p$		$3^1/_2$	36583.82	1.140	21	$^2F^\circ$	19	$6d7s(^1D)7p\ ^2F^\circ$	16	H
$6d^2(^3F)7p$		$2^1/_2$	36687.992	1.049	41	$^4F^\circ$	8	$6d7s(^3D)7p\ ^4P^\circ$	14	H
$5f(^1G^\circ)6d^2$	$^2P^\circ$	$^1/_2$	37130.340	0.521	70		8	$6d^2(^3P)7p\ ^4D^\circ$	10	H
$6d7s(^3D)7p$	$^4F^\circ$	$4^1/_2$	37569.762	1.29	70		21	$6d^2(^3F)7p\ ^4G^\circ$	9	B
$6d7s(^3D)7p$		$1^1/_2$	37601.699	1.267	24	$^2D^\circ$	11	$6d^2(^1D)7p\ ^2P^\circ$	15	H
$6d7s(^3D)7p$		$^1/_2$	37607.989	2.239	43	$^4P^\circ$	33	$6d^2(^3P)7p\ ^2S^\circ$	7	H
$6d^2(^1D)7p$		$^1/_2$	37716.322	0.690	28	$^2P^\circ$	18	$(^3F)\ ^4D^\circ$	5	H
$5f(^1S^\circ)6d^2$		$3^1/_2$	37756.790	1.118	27	$^2F^\circ$	20	$(^3P^\circ)\ ^2F^\circ$	18	H
$6d^2(^3P)7p$		$2^1/_2$	37846.174	1.165	17	$^2D^\circ$	15	$(^3P)\ ^4D^\circ$	22	H
$6d7s(^3D)7p$		$1^1/_2$	38436.169	1.419	33	$^4P^\circ$	27	$7s^2(^1S)7p\ ^2P^\circ$	12	H
$6d^2(^3P)7p$		$2^1/_2$	38493.769	1.217	18	$^4D^\circ$	11	$6d7s(^1D)7p\ ^2D^\circ$	21	H
$6d^2(^3F)7p$		$2^1/_2$	38581.627	1.105	20	$^2F^\circ$	16	$6d7s(^3D)7p\ ^2F^\circ$	21	H

TABLE 2. *Odd energy levels of* Th II—Continued

Configuration	Term	J	Level (cm^{-1})	g	Leading percentages		n, ref.
					First	Second	
$6d^2(^3F)7p$		$3^1/_2$	38764.652	1.098	19 $^2G°$	18 (^3F) $^2F°$	14 B
$6d^2(^1G)7p$		$3^1/_2$	39396.55	1.131	24 $^2F°$	17 $5f(^1S°)6d^2$ $^2F°$	19 H
$6d^2(^3F)7p$		$4^1/_2$	39442.996	1.145	30 $^4G°$	16 (^3F) $^2G°$	11 H
$6d7s(^3D)7p$		$2^1/_2$	39861.642	1.172	26 $^4P°$	11 $6d^2(^1G)7p$ $^2F°$	19 H
$6d^2(^3F)7p$		$3^1/_2$	40184.111	1.230	20 $^4F°$	16 (^3F) $^4D°$	13 B
$6d^2(^3F)7p$		$1^1/_2$	40472.459	1.249	39 $^4D°$	14 $6d7s(^1D)7p$ $^2D°$	17 H
$5f(^3P°)6d^2$		$2^1/_2$	40654.460	0.943	21 $^2F°$	14 $(^1S°)$ $^2F°$	17 H
$6d^2(^1G)7p$		$3^1/_2$	40706.82	1.073	24 $^2G°$	15 $5f(^1S°)6d^2$ $^2F°$	15 H
$6d^2(^3F)7p$	$^4D°$	$^1/_2$	40825.607	0.261	51	8 $6d7s(^3D)7p$ $^2P°$	9 H
$6d^2(^3F)7p$	$^4G°$	$5^1/_2$	41447.968	1.267	88	4 $5f6d(^3G°)7s$ $^4G°$	6 R
$6d^2(^1D)7p$		$1^1/_2$	42112.94	1.467	21 $^2P°$	16 (^3P) $^4S°$	16 H
$6d^2(^3F)7p$		$2^1/_2$	42219.764	1.168	31 $^4D°$	15 (^1D) $^2F°$	21 H
$6d^2(^3F)7p$		$4^1/_2$	42319.024	1.165	38 $^4F°$	32 (^1G) $^2H°$	10 H
$6d^2(^3F)7p$		$1^1/_2$	42418.228	1.304	24 $^4D°$	14 (^3P) $^2D°$	16 H
$6d^2(^3F)7p$		$3^1/_2$	42944.467	1.246	25 $^4D°$	23 $6d7s(^3D)7p$ $^2F°$	16 H
$6d^2(^3P)7p$		$1^1/_2$	43287.642	1.564	40 $^4S°$	32 (^3P) $^4P°$	14 H
$6d^2(^3P)7p$		$2^1/_2$	43382.780	1.203	39 $^4D°$	18 (^3F) $^4D°$	16 H
$6d^2(^3P)7p$	$^4P°$	$^1/_2$	43744.11	2.219	54	19 (^3P) $^2S°$	9 H
$6d^2(^1G)7p$		$3^1/_2$	43773.64	1.052	18 $^2G°$	16 (^3P) $^4D°$	16 B
$6d^2(^3P)7p$		$3^1/_2$	44650.491	1.234	42 $^4D°$	11 (^3F) $^2G°$	17 H
$6d7s(^3D)7p$		$2^1/_2$	44821.897	0.999	30 $^2F°$	10 $5f(^3P°)6d^2$ $^2F°$	14 H
$6d^2(^3P)7p$		$2^1/_2$	45221.54	1.347	47 $^4P°$	10 $6d7s(^3D)7p$ $^2F°$	15 H
$6d^2(^3F)7p$	$^2G°$	$4^1/_2$	45489.129	1.089	61	18 (^3F) $^4F°$	12 H
$6d^2(^3F)7p$		$3^1/_2$	45689.325	1.261	18 $^2F°$	13 $6d7s(^1D)7p$ $^2F°$	11 H
$6d7s(^1D)7p$		$1^1/_2$	45697.78	1.18	30 $^2P°$	10 $6d^2(^3P)7p$ $^2D°$	10 B
$6d^2(^3P)7p$		$1^1/_2$	45838.437		31 $^2P°$	20 (^1D) $^2D°$	5 Z
$6d^2(^3P)7p$		$2^1/_2$	46155.54	1.152	33 $^2D°$	12 $6d7s(^3D)7p$ $^2D°$	16 H
$6d^2(^1G)7p$	$^2G°$	$4^1/_2$	46368.21	1.088	51	29 (^1G) $^2H°$	8 H
$6d7s(^3D)7p$		$1^1/_2$	46423.76	1.118	20 $^2P°$	14 $6s^2(^1S)7p$ $^2P°$	14 H
$6d^2(^1S)7p$		$^1/_2$	46426.05	0.9	16 $^2P°$	14 $6d7s(^3D)7p$ $^2P°$	6 Z
$6d^2(^1G)7p$	$^2H°$	$5^1/_2$	47466.262	1.13	83	6 $5f6d(^1H°)7s$ $^2H°$	4 Z
$6d7s(^1D)7p$		$^1/_2$	48532.05		30 $^2P°$	24 (^3D) $^2P°$	8 Z
$6d^2(^1D)7p$		$3^1/_2$	49121.92	1.11	36 $^2F°$	24 $6d7s(^1D)7p$ $^2F°$	9 Z
$6d^2(^1D)7p$		$2^1/_2$	49289.524	1.208	47 $^2D°$	10 (^3P) $^4P°$	9 H
$5f^27p$?		$4^1/_2$	49495.57				14 Z
$6d^2(^3P)7p$		$1^1/_2$	51528.46	0.925	25 $^2D°$	16 $6d7s(^1D)7p$ $^2D°$	11 C
$6d^2(^1G)7p$		$2^1/_2$	51946.84	0.937	37 $^2F°$	11 $6d7s(^3D)7p$ $^2F°$	12 B
$5f^2$ $7p$?		$2^1/_2$	52678.41				11 Z

TABLE 2. *Odd energy levels of* Th II—Continued

Configuration	Term	J	Level (cm^{-1})	g	Leading percentages				n, ref.	
					First		Second			
$5f\,7p^2?$		$4^1/_2$	54360.46						12	Z
$6d7s(^3D)7p$		$3^1/_2$	54497.69	1.126	28	$^2F°$	27	$6d^2(^1G)7p\ ^2F°$	10	C
$6d^2(^3F)7p$		$2^1/_2$	54648.28		21	$^2D°$	15	$(^1G)\ ^2F°$	12	Z
$5f^2\ 7p?$		$4^1/_2$	55038.943						11	Z
$5f^2\ 7p?$		$4^1/_2$	56086.24						17	Z
$5f^2\ 7p?$		$3^1/_2$	56683.43						17	Z
$5f^2\ 7p?$		$2^1/_2$	56892.09						15	Z
$5f^2\ 7p?$		$2^1/_2$	59299.15						15	Z
		$1^1/_2$	59616.61	1.1					13	Z
$5f\,7p^2?$		$1^1/_2$	59987.43						11	Z
$5f^2\ 7p?$		$4^1/_2$	59993.66						11	Z

4.2. Classified Lines

The classified lines of Th II (table 3) consist of 6500 lines in the wavelength range 2000 to 25 000 Å. Following the measured wavelength in table 3, the visually estimated intensities in electrodeless lamp and sliding spark spectra are given. Lines not observed as single sharp lines are described with the following symbols:

b = blend (two wavelengths measured)
d = double (one wavelength measured)
h = hazy
l = shaded to long wavelength
r = reversed
s = shaded to short wavelengths
w = wide

In column 4 is the wavenumber in vacuum in units of cm^{-1}. The classification is given by the values of the energy levels responsible for the transition, with their J-values as subscripts, and a superscript degree symbol to indicate odd parity.

The average absolute value of O–C in cm^{-1} for 100 lines at each of seven wavelengths is shown below.

Wavelength	O–C
3 000	0.007
3 500	.009
4 000	.010
4 500	.012
6 000	.012
9 000	.018
15 000	.002

The general precision of the wave numbers of the lines was determined by measuring the precision of repeating differences between three pairs of odd levels. The average deviation of 180 differences from the means was 0.015 cm^{-1}. Therefore the average deviation for a single wavenumber is about 0.011 cm^{-1}.

The Th II lines that have not been classified will be published in an improved complete description of thorium spectra.

The authors express their appreciation for the help of Mrs. Ruth Peterson in handling the data during this work.

5. References

Bernage, P., Houdart, R., and Niay, P. [1971], Spectrochim. Acta **26B**, 261.
Brewer. L. [1971], J. Opt. Soc. Am. **61**, 1674.
Charles. G. W. [1958], Oak Ridge Nat. Lab., ORNL–2319.
Connes. J., Delouis. H., Connes. P., Guelachvili. G., Maillard. J., and Michel. G. [1970], Nouv. Rev. d'Optique Appl. **1**, 3.
de Bruin, T. L., Schuurmans. P., and Klinkenberg, P. F. A. [1943], Z. Phys. **121**, 667.
de Bruin, T. L., Klinkenberg, P. F. A., and Schuurmans. P. [1944], Z. Phys. **122**, 23.
Giacchetti. A., Blaise, J., Corliss, C. H., and Zalubas. R. [1974], J. Res. Nat. Bur. Stand. (U.S. **78A** (Phys. and Chem.) No. 2, 247.
Giacchetti. A., Stanley, R. W., and Zalubas. R. [1970], J. Opt. Soc. Am. **60**, 474.
Harrison, G. R. [1939], MIT Wavelength Tables (John Wiley & Sons. N.Y.).
McNally, J. R., Harrison, G. R., and Park, H. B. [1942], J. Opt. Soc. Am. **32**, 334.
McNally, J. R. [1945], J. Opt. Soc. Am. **35**, 390.
Minsky, N. [1969], Dissertation, Hebrew Univ., Jerusalem.
Nielson, C. W. and Koster. G. F., Spectroscopic Coefficients for the p^n, d^n, f^n Configurations. p, 2 (MIT Press, Cambridge, Mass., 1963).
Racah. G. [1943], Phys. Rev. **63**, 367.
Schuurmans. P. [1946], Dissertation, Univ. Amsterdam (N.V. Noord-Hollandsche Uitgevers Maatschappij. Amsterdam).
Steers. E. B. M. [1967], Spectrochim. Acta **23B**, 135.
Zalubas. R. [1959], J. Res. Nat. Bur. Stand. (U.S.) **63A** (Phys. and Chem.), No. 3. 275.
Zalubas. R. [1960], Nat. Bur. Stand. (U.S.), Monogr. 17. 103 pages.

(Paper 78A2–811)

TABLE 3. *Classified lines of* Th II

Wavelength Å	Intensity		Wavenumber cm^{-1}	Classification	Wavelength Å	Intensity		Wavenumber cm^{-1}	Classification
	Lamp	Spark				Lamp	Spark		
29068.481	1		3439.214	$10379_{9/2} - 13818^{\circ}_{7/2}$	21121.474	1		4733.226	$10572^{\circ}_{9/2} - 15305_{9/2}$
25401.710	1		3935.669	$10855_{7/2} - 14790^{\circ}_{7/2}$	21046.638	0		4750.056	$23187^{\circ}_{13/2} - 27937_{11/2}$
25181.424	1		3970.098	$4490^{\circ}_{5/2} - 8460_{3/2}$	21014.864	2		4757.238	$9061_{5/2} - 13818^{\circ}_{7/2}$
24926.551	3		4010.692	$9238^{\circ}_{9/2} - 13248_{9/2}$	20934.926	0		4775.403	$15305_{9/2} - 20080^{\circ}_{7/2}$
24887.997	2		4016.905	$14101^{\circ}_{1/2} - 18118_{3/2}$	20692.063	6		4831.452	$1859_{3/2} - 6691^{\circ}_{3/2}$
24352.698	0		4105.201	$10379_{9/2} - 14484^{\circ}_{11/2}$	20682.889	4		4833.595	$9711_{7/2} - 14545^{\circ}_{5/2}$
24345.717	0		4106.378	$9711_{7/2} - 13818^{\circ}_{7/2}$	20649.114	1		4841.501	$22685^{\circ}_{7/2} - 27526_{9/2}$
24291.248	3		4115.586	$4490^{\circ}_{5/2} - 8605_{5/2}$	20609.747	1		4850.749	$17983^{\circ}_{5/2} - 22834_{7/2}$
24060.000	1		4155.142	$6700^{\circ}_{9/2} - 10855_{7/2}$	20575.702	0		4858.775	$22106_{5/2} - 26965^{\circ}_{3/2}$
23964.262	3		4171.742	$16818_{7/2} - 20989^{\circ}_{9/2}$	20554.521	3		4863.782	$10379_{9/2} - 15242^{\circ}_{9/2}$
23850.490	2		4191.642	$8378^{\circ}_{7/2} - 12570_{7/2}$	20528.880	4		4869.857	$8378^{\circ}_{7/2} - 13248_{9/2}$
23745.817	1		4210.119	$13250_{5/2} - 17460^{\circ}_{5/2}$	20521.311	2		4871.653	$8378^{\circ}_{7/2} - 13250_{5/2}$
23742.146	4		4210.770	$6168^{\circ}_{7/2} - 10379_{9/2}$	20468.653	4		4884.186	$8018_{3/2} - 12902^{\circ}_{3/2}$
23696.506	1		4218.880	$14349_{1/2} - 18568^{\circ}_{1/2}$	20450.627	1		4888.491	$7331^{\circ}_{5/2} - 12219_{3/2}$
23621.480	2		4232.280	$4146_{7/2} - 8378^{\circ}_{7/2}$	20443.773	2		4890.130	$12570_{7/2} - 17460^{\circ}_{5/2}$
23597.934	1		4236.503	$18118_{3/2} - 22355^{\circ}_{1/2}$	20430.283	0		4893.359	$18118_{3/2} - 23012^{\circ}_{3/2}$
23477.236	1		4258.283	$13468^{\circ}_{9/2} - 17727_{11/2}$	20395.738	3		4901.647	$12219_{3/2} - 17121^{\circ}_{3/2}$
23458.743	0		4261.640	$20120^{\circ}_{5/2} - 24381_{7/2}$	20389.710	4		4903.096	$6213_{9/2} - 11116^{\circ}_{7/2}$
23437.525	5		4265.498	$4113_{5/2} - 8378^{\circ}_{7/2}$	20358.092	0		4910.711	$4490^{\circ}_{5/2} - 9400_{5/2}$
23372.954	0		4277.282	$20969^{\circ}_{7/2} - 25246_{9/2}$	20165.057	3		4957.720	$20288^{\circ}_{11/2} - 25246_{9/2}$
23316.550	1		4287.629	$17727_{11/2} - 22014^{\circ}_{11/2}$	20139.866	1		4963.921	$13250_{5/2} - 18214^{\circ}_{3/2}$
23222.202	1		4305.049	$20158_{5/2} - 24463^{\circ}_{5/2}$	20061.498	0		4983.312	$15305_{9/2} - 20288^{\circ}_{11/2}$
23075.703	2		4332.380	$12485^{\circ}_{7/2} - 16818_{7/2}$	19998.121	1		4999.105	$23012^{\circ}_{3/2} - 28011_{3/2}$
23003.968	2		4345.890	$12472^{\circ}_{5/2} - 16818_{7/2}$	19984.221	0		5002.582	$26770^{\circ}_{11/2} - 31773_{9/2}$
22937.124	2		4358.555	$6213_{9/2} - 10572^{\circ}_{9/2}$	19844.520	0		5037.799	$25414^{\circ}_{11/2} - 30452_{9/2}$
22911.403	0		4363.448	$24982^{\circ}_{7/2} - 29345_{5/2}$	19774.295	6		5055.690	$4146_{7/2} - 9202^{\circ}_{7/2}$
22785.383	1		4387.581	$10855_{7/2} - 15242^{\circ}_{9/2}$	19719.303	1		5069.789	$25414^{\circ}_{11/2} - 30484_{11/2}$
22733.218	0		4397.649	$27526_{9/2} - 31924^{\circ}_{11/2}$	19703.648	1		5073.817	$7828_{1/2} - 12902^{\circ}_{3/2}$
22631.728	0		4417.370	$9400_{5/2} - 13818^{\circ}_{7/2}$	19703.283	1		5073.911	$10379_{9/2} - 15453^{\circ}_{7/2}$
22582.257	1		4427.047	$15453^{\circ}_{7/2} - 19880_{9/2}$	19701.761	0		5074.303	$15236_{3/2} - 20310^{\circ}_{5/2}$
22571.571	1		4429.143	$19880_{9/2} - 24309^{\circ}_{11/2}$	19683.409	5		5079.034	$9711_{7/2} - 14790^{\circ}_{7/2}$
22506.128	4		4442.022	$8460_{3/2} - 12902^{\circ}_{3/2}$	19644.523	4		5089.088	$14790^{\circ}_{7/2} - 19880_{9/2}$
22467.732	1		4449.613	$15144^{\circ}_{3/2} - 19594_{1/2}$	19593.390	0		5102.369	$19880_{9/2} - 24982^{\circ}_{7/2}$
22445.678	2		4453.985	$8018_{3/2} - 12472^{\circ}_{5/2}$	19540.414	1		5116.202	$10189^{\circ}_{11/2} - 15305_{9/2}$
22343.861	3		4474.281	$13248_{9/2} - 17722^{\circ}_{9/2}$	19535.499	0		5117.489	$22139^{\circ}_{9/2} - 27257_{7/2}$
22264.353	6		4490.259	$0_{3/2} - 4490^{\circ}_{5/2}$	19503.105	1		5125.989	$23697^{\circ}_{7/2} - 28823_{5/2}$
22098.511	0		4523.957	$15786_{5/2} - 20310^{\circ}_{5/2}$	19474.463	2		5133.528	$19248^{\circ}_{5/2} - 24381_{7/2}$
21907.002	1		4563.505	$10673^{\circ}_{5/2} - 15236_{3/2}$	19473.652	1		5133.742	$25414^{\circ}_{11/2} - 30548_{13/2}$
21906.445	1		4563.621	$9711_{7/2} - 14275^{\circ}_{9/2}$	19432.597	3		5144.588	$9400_{5/2} - 14545^{\circ}_{5/2}$
21871.813	1		4570.847	$4490^{\circ}_{5/2} - 9061_{5/2}$	19402.768	2		5152.497	$12570_{7/2} - 17722^{\circ}_{9/2}$
21852.069	2		4574.977	$7001_{3/2} - 11576^{\circ}_{3/2}$	19353.457	0		5165.625	$20080^{\circ}_{7/2} - 25246_{9/2}$
21743.999	5		4597.715	$10855_{7/2} - 15453^{\circ}_{7/2}$	19338.976	7		5169.493	$1521_{5/2} - 6691^{\circ}_{3/2}$
21662.376	0		4615.039	$22642^{\circ}_{9/2} - 27257_{7/2}$	19307.868	2		5177.822	$10855_{7/2} - 16033^{\circ}_{5/2}$
21558.955	2		4637.178	$15242^{\circ}_{9/2} - 19880_{9/2}$	19179.419	3		5212.499	$8605_{5/2} - 13818^{\circ}_{7/2}$
21387.561	1		4674.339	$24757^{\circ}_{9/2} - 29431_{7/2}$	19165.340	1		5216.328	$12902^{\circ}_{3/2} - 18118_{3/2}$
21329.914	1		4686.972	$6168^{\circ}_{7/2} - 10855_{7/2}$	19145.601	7		5221.706	$4490^{\circ}_{5/2} - 9711_{7/2}$
21264.265	0		4701.442	$14349_{1/2} - 19050^{\circ}_{3/2}$	19082.536	3		5238.963	$12488^{\circ}_{9/2} - 17727_{11/2}$
21262.841	1		4701.757	$12570_{7/2} - 17272^{\circ}_{9/2}$	19076.390	0		5240.651	$12219_{3/2} - 17460^{\circ}_{5/2}$
21162.697	5		4724.006	$7001_{3/2} - 11725^{\circ}_{1/2}$	18961.873	1		5272.301	$25607^{\circ}_{9/2} - 30879_{7/2}$
21123.018	0		4732.880	$13250_{5/2} - 17983^{\circ}_{5/2}$	18880.700	0		5294.968	$22642^{\circ}_{9/2} - 27937_{11/2}$

TABLE 3. *Classified lines of* Th II—Continued

Wavelength Å	Intensity		Wavenumber cm^{-1}	Classification	Wavelength Å	Intensity		Wavenumber cm^{-1}	Classification
	Lamp	Spark				Lamp	Spark		
18624.701	0		5367.748	$14790^{\circ}_{7/2} - 20158_{5/2}$	16433.049	2		6083.636	$9061_{5/2} - 15144^{\circ}_{5/2}$
18557.117	1		5387.297	$22139^{\circ}_{9/2} - 27526_{9/2}$	16428.820	2		6085.202	$8460_{3/2} - 14545^{\circ}_{5/2}$
18547.718	3		5390.027	$9400_{5/2} - 14790^{\circ}_{7/2}$	16380.898	6		6103.004	$9202^{\circ}_{7/2} - 15305_{9/2}$
18469.362	1		5412.894	$12570_{7/2} - 17983^{\circ}_{5/2}$	16269.133	3		6144.930	$10673^{\circ}_{5/2} - 16818_{7/2}$
18402.093	0		5432.681	$19594_{1/2} - 25027^{\circ}_{1/2}$	16182.835	0		6177.699	$20310^{\circ}_{5/2} - 26488_{5/2}$
18381.291	3		5438.829	$4146_{7/2} - 9585^{\circ}_{5/2}$	16163.327	3		6185.155	$8605_{5/2} - 14790^{\circ}_{7/2}$
18293.755	1		5464.854	$21297^{\circ}_{5/2} - 26762_{3/2}$	15951.379	0		6267.338	$20989^{\circ}_{9/2} - 27257_{7/2}$
18271.367	5		5471.550	$1859_{3/2} - 7331^{\circ}_{5/2}$	15939.011	1		6272.201	$6213_{9/2} - 12485^{\circ}_{7/2}$
18269.704	3		5472.048	$4113_{5/2} - 9585^{\circ}_{5/2}$	15936.374	4		6273.239	$7828_{1/2} - 14101^{\circ}_{1/2}$
18239.409	5		5481.137	$6244_{1/2} - 11725^{\circ}_{1/2}$	15932.409	6		6274.800	$6213_{9/2} - 12488^{\circ}_{9/2}$
18228.371	4		5484.456	$9061_{5/2} - 14545^{\circ}_{5/2}$	15927.216	0		6276.846	$24982^{\circ}_{7/2} - 31259_{5/2}$
18112.220	1		5519.627	$20969^{\circ}_{7/2} - 26488_{5/2}$	15898.637	1		6288.129	$20969^{\circ}_{7/2} - 27257_{7/2}$
18082.856	4		5528.590	$6691^{\circ}_{3/2} - 12219_{3/2}$	15877.380	0		6296.548	$21297^{\circ}_{5/2} - 27593_{5/2}$
18075.163	1		5530.943	$9711_{7/2} - 15242^{\circ}_{9/2}$	15843.848	0		6309.874	$9400_{5/2} - 15710^{\circ}_{3/2}$
17936.434	7		5573.722	$4146_{7/2} - 9720^{\circ}_{7/2}$	15815.492	6		6321.187	$9711_{7/2} - 16033^{\circ}_{5/2}$
17900.307	4		5584.971	$9720^{\circ}_{7/2} - 15305_{9/2}$	15767.555	3		6340.405	$13818^{\circ}_{7/2} - 20158_{5/2}$
17837.933	1		5604.500	$14275^{\circ}_{9/2} - 19880_{9/2}$	15747.955	1		6348.296	$12219_{3/2} - 18568^{\circ}_{7/2}$
17830.167	5		5606.941	$4113_{5/2} - 9720^{\circ}_{7/2}$	15706.454	2		6365.070	$4490^{\circ}_{5/2} - 10855_{7/2}$
17795.604	3		5617.831	$12219_{3/2} - 17837^{\circ}_{1/2}$	15698.032	0		6368.485	$20120^{\circ}_{5/2} - 26488_{5/2}$
17721.115	4		5641.445	$8460_{3/2} - 14101^{\circ}_{1/2}$	15640.438	5		6391.936	$9061_{5/2} - 15453^{\circ}_{7/2}$
17705.162	3		5646.528	$12472^{\circ}_{5/2} - 18118_{3/2}$	15637.160	3		6393.276	$11725^{\circ}_{1/2} - 18118_{3/2}$
17699.808	0		5648.236	$23697^{\circ}_{7/2} - 29345_{5/2}$	15631.483	1		6395.598	$15710^{\circ}_{3/2} - 22106_{5/2}$
17535.396	0		5701.194	$23730^{\circ}_{9/2} - 29431_{7/2}$	15624.606	1		6398.413	$17983^{\circ}_{5/2} - 24381_{7/2}$
17534.504	5		5701.484	$11116^{\circ}_{7/2} - 16818_{7/2}$	15615.505	1		6402.142	$6168^{\circ}_{7/2} - 12570_{7/2}$
17507.525	0		5710.270	$25246_{9/2} - 30956^{\circ}_{9/2}$	15612.710	0		6403.288	$12570_{7/2} - 18973^{\circ}_{7/2}$
17462.260	3		5725.072	$13248_{9/2} - 18973^{\circ}_{7/2}$	15593.649	1		6411.115	$13468^{\circ}_{9/2} - 19880_{9/2}$
17456.286	0		5727.031	$19880_{9/2} - 25607^{\circ}_{9/2}$	15558.814	2		6425.469	$4146_{7/2} - 10572^{\circ}_{9/2}$
17455.753	0		5727.206	$24757^{\circ}_{9/2} - 30484_{11/2}$	15425.673	2		6480.928	$22106_{5/2} - 28587^{\circ}_{5/2}$
17447.564	3		5729.894	$9061_{5/2} - 14790^{\circ}_{7/2}$	15317.814	3		6526.563	$4146_{7/2} - 10673^{\circ}_{5/2}$
17413.587	2		5741.074	$9711_{7/2} - 15453^{\circ}_{7/2}$	15315.929	5		6527.366	$8018_{3/2} - 14545^{\circ}_{5/2}$
17405.417	3		5743.769	$9400_{5/2} - 15144^{\circ}_{3/2}$	15315.660	2		6527.481	$10379_{9/2} - 16906^{\circ}_{7/2}$
17346.089	1		5763.414	$12219_{3/2} - 17983^{\circ}_{5/2}$	15293.025	0		6537.142	$20989^{\circ}_{9/2} - 27526_{9/2}$
17244.366	1		5797.412	$22139^{\circ}_{9/2} - 27937_{11/2}$	15288.921	4		6538.897	$8605_{5/2} - 15144^{\circ}_{3/2}$
17235.699	1		5800.327	$13250_{5/2} - 19050^{\circ}_{3/2}$	15280.959	2		6542.304	$11576^{\circ}_{3/2} - 18118_{3/2}$
17229.251	0		5802.498	$20686^{\circ}_{5/2} - 26488_{5/2}$	15266.440	4		6548.526	$6700^{\circ}_{9/2} - 13248_{9/2}$
17208.215	8		5809.591	$1521_{5/2} - 7331^{\circ}_{5/2}$	15241.775	1		6559.123	$6691^{\circ}_{3/2} - 13250_{5/2}$
17155.413	1		5827.472	$23518^{\circ}_{7/2} - 29345_{5/2}$	15240.242	7		6559.783	$4113_{5/2} - 10673^{\circ}_{5/2}$
17030.220	3		5870.311	$6700^{\circ}_{9/2} - 12570_{7/2}$	15214.240	1		6570.994	$20686^{\circ}_{5/2} - 27257_{7/2}$
16958.427	1		5895.163	$15236_{3/2} - 21131^{\circ}_{3/2}$	15188.855	5		6581.976	$17727_{11/2} - 24309^{\circ}_{11/2}$
16956.701	2		5895.763	$15786_{5/2} - 21682^{\circ}_{7/2}$	15135.223	0		6605.299	$10855_{7/2} - 17460^{\circ}_{5/2}$
16941.790	0		5900.952	$7001_{3/2} - 12902^{\circ}_{3/2}$	15034.068	3		6649.742	$9061_{5/2} - 15710^{\circ}_{3/2}$
16912.370	1		5911.217	$21682^{\circ}_{7/2} - 27593_{5/2}$	15015.230	2		6658.085	$6244_{1/2} - 12902^{\circ}_{3/2}$
16906.064	0		5913.422	$23518^{\circ}_{7/2} - 29431_{7/2}$	15013.595	0		6658.810	$17722^{\circ}_{9/2} - 24381_{7/2}$
16890.066	5		5919.023	$7331^{\circ}_{5/2} - 13250_{5/2}$	15009.909	2		6660.445	$22685^{\circ}_{7/2} - 29345_{5/2}$
16520.919	3		6051.279	$10855_{7/2} - 16906^{\circ}_{7/2}$	14970.942	1		6677.781	$12570_{7/2} - 19248^{\circ}_{5/2}$
16518.765	3		6052.068	$9400_{5/2} - 15453^{\circ}_{7/2}$	14969.772	1		6678.303	$25246_{9/2} - 31924^{\circ}_{11/2}$
16495.017	0		6060.781	$15236_{3/2} - 21297^{\circ}_{5/2}$	14940.492	7		6691.391	$0_{3/2} - 6691^{\circ}_{3/2}$
16492.394	2		6061.745	$13818^{\circ}_{7/2} - 19880_{9/2}$	14939.197	1		6691.971	$12902^{\circ}_{3/2} - 19594_{1/2}$
16477.433	2		6067.249	$9238^{\circ}_{9/2} - 15305_{9/2}$	14920.495	3		6700.359	$16818_{7/2} - 23518^{\circ}_{7/2}$
16453.368	0		6076.123	$20686^{\circ}_{5/2} - 26762_{3/2}$	14899.905	2		6709.618	$15305_{9/2} - 22014^{\circ}_{11/2}$

TABLE 3. *Classified lines of* Th II—Continued

Wavelength Å	Intensity		Wavenumber cm^{-1}	Classification	Wavelength Å	Intensity		Wavenumber cm^{-1}	Classification
	Lamp	Spark				Lamp	Spark		
14739.988	0		6782.412	$14349_{1/2} - 21131^{\circ}_{3/2}$	13395.691	4		7463.046	$4113_{3/2} - 11576^{\circ}_{3/2}$
14699.723	2		6800.990	$16033^{\circ}_{3/2} - 22834_{7/2}$	13376.396	0		7473.811	$20120^{\circ}_{5/2} - 27593_{5/2}$
14690.666	0		6805.183	$20158_{5/2} - 26963^{\circ}_{7/2}$	13373.859	3		7475.229	$17771^{\circ}_{11/2} - 25246_{9/2}$
14672.400	0		6813.655	$18568^{\circ}_{1/2} - 25381_{3/2}$	13370.190	2		7477.280	$19880_{9/2} - 27357^{\circ}_{9/2}$
14633.086	3		6831.961	$13248_{9/2} - 20080^{\circ}_{7/2}$	13319.676	1		7505.637	$9400_{3/2} - 16906^{\circ}_{7/2}$
14627.874	4		6834.395	$15305_{9/2} - 22139^{\circ}_{9/2}$	13311.623	2		7510.178	$12570_{7/2} - 20080^{\circ}_{7/2}$
14579.735	6		6856.961	$1521_{5/2} - 8378^{\circ}_{7/2}$	13310.052	1		7511.064	$20120^{\circ}_{5/2} - 27631_{3/2}$
14565.023	0		6863.887	$8460_{3/2} - 15324^{\circ}_{1/2}$	13306.095	2		7513.298	$20080^{\circ}_{7/2} - 27593_{5/2}$
14557.004	4		6867.668	$10855_{7/2} - 17722^{\circ}_{9/2}$	13304.846	2		7514.003	$19248^{\circ}_{5/2} - 26762_{3/2}$
14508.948	1		6890.415	$19880_{9/2} - 26770^{\circ}_{11/2}$	13288.387	1		7523.310	$17722^{\circ}_{9/2} - 25246_{9/2}$
14503.235	6		6893.129	$10379_{9/2} - 17272^{\circ}_{9/2}$	13283.226	1		7526.233	$21297^{\circ}_{5/2} - 28823_{5/2}$
14472.395	1		6907.818	$20686^{\circ}_{5/2} - 27593_{5/2}$	13262.164	2		7538.186	$10189^{\circ}_{11/2} - 17727_{11/2}$
14462.402	0		6912.591	$16818_{7/2} - 23730^{\circ}_{9/2}$	13251.713	2		7544.131	$7001_{3/2} - 14545^{\circ}_{5/2}$
14433.541	1		6926.413	$8378^{\circ}_{7/2} - 15305_{9/2}$	13251.713	2		7544.131	$17837^{\circ}_{1/2} - 25381_{3/2}$
14360.388	0		6961.697	$15144^{\circ}_{3/2} - 22106_{5/2}$	13241.997	0		7549.666	$12570_{7/2} - 20120^{\circ}_{5/2}$
14343.260	6		6970.010	$4146_{7/2} - 11116^{\circ}_{7/2}$	13223.385	3		7560.292	$9711_{7/2} - 17272^{\circ}_{9/2}$
14339.066	2		6972.049	$9061_{5/2} - 16033^{\circ}_{5/2}$	13222.361	0		7560.878	$14545^{\circ}_{5/2} - 22106_{5/2}$
14275.223	0		7003.230	$4113_{5/2} - 11116^{\circ}_{7/2}$	13188.919	2		7580.049	$9238^{\circ}_{9/2} - 16818_{7/2}$
14224.305	0		7028.299	$12219_{3/2} - 19248^{\circ}_{5/2}$	13179.277	0		7585.595	$15786_{5/2} - 23372^{\circ}_{3/2}$
14159.556	0		7060.438	$13250_{5/2} - 20310^{\circ}_{5/2}$	13145.904	7		7604.852	$6213_{9/2} - 13818^{\circ}_{7/2}$
14070.742	5		7105.003	$8605_{5/2} - 15710^{\circ}_{3/2}$	13130.308	1		7613.885	$22106_{5/2} - 29720^{\circ}_{3/2}$
14043.929	1		7118.568	$15236_{3/2} - 22355^{\circ}_{1/2}$	13126.998	1		7615.805	$9202^{\circ}_{7/2} - 16818_{7/2}$
14028.205	3		7126.547	$8018_{3/2} - 15144^{\circ}_{3/2}$	13029.053	0		7673.056	$12485^{\circ}_{7/2} - 20158_{5/2}$
14025.216	2		7128.066	$10855_{7/2} - 17983^{\circ}_{5/2}$	13016.640	5		7680.373	$1521_{5/2} - 9202^{\circ}_{7/2}$
14007.683	1		7136.988	$20120^{\circ}_{5/2} - 27257_{7/2}$	13006.151	2		7686.567	$12472^{\circ}_{5/2} - 20158_{5/2}$
13972.014	1		7155.208	$10572^{\circ}_{9/2} - 17727_{11/2}$	13004.273	4		7687.677	$17727_{11/2} - 25414^{\circ}_{11/2}$
13895.433	3		7194.642	$9711_{7/2} - 16906^{\circ}_{7/2}$	12983.105	0		7700.211	$20310^{\circ}_{5/2} - 28011_{3/2}$
13836.909	0		7225.072	$15786_{5/2} - 23012^{\circ}_{3/2}$	12964.195	2		7711.443	$19050^{\circ}_{3/2} - 26762_{3/2}$
13822.377	0		7232.668	$9585^{\circ}_{5/2} - 16818_{7/2}$	12940.654	7		7725.471	$1859_{3/2} - 9585^{\circ}_{5/2}$
13811.481	4		7238.374	$20288^{\circ}_{11/2} - 27526_{9/2}$	12933.539	5		7729.721	$4490^{\circ}_{5/2} - 12219_{3/2}$
13788.405	1		7250.488	$8460_{3/2} - 15710^{\circ}_{3/2}$	12930.664	1		7731.440	$15786_{5/2} - 23518^{\circ}_{7/2}$
13778.916	6		7255.481	$6213_{9/2} - 13468^{\circ}_{9/2}$	12925.892	3		7734.294	$22139^{\circ}_{9/2} - 29873_{7/2}$
13777.235	1		7256.366	$12902^{\circ}_{3/2} - 20158_{5/2}$	12901.919	2		7748.665	$9711_{7/2} - 17460^{\circ}_{5/2}$
13756.558	2		7267.273	$22834_{7/2} - 30101^{\circ}_{7/2}$	12742.669	1		7845.503	$9061_{5/2} - 16906^{\circ}_{7/2}$
13709.552	1		7292.190	$22139^{\circ}_{9/2} - 29431_{7/2}$	12684.798	3		7881.296	$13250_{5/2} - 21131^{\circ}_{3/2}$
13699.211	3		7297.695	$23187^{\circ}_{13/2} - 30484_{11/2}$	12683.213	4		7882.281	$7828_{1/2} - 15710^{\circ}_{3/2}$
13665.979	0		7315.441	$14790^{\circ}_{7/2} - 22106_{5/2}$	12642.339	3		7907.765	$19880_{9/2} - 27787^{\circ}_{9/2}$
13664.604	3		7316.177	$7828_{1/2} - 15144^{\circ}_{3/2}$	12591.895	1		7939.444	$16818_{7/2} - 24757^{\circ}_{9/2}$
13654.606	0		7321.534	$18118_{3/2} - 25440^{\circ}_{5/2}$	12479.376	1		8011.029	$9711_{7/2} - 17722^{\circ}_{9/2}$
13636.063	5		7331.490	$0_{3/2} - 7331^{\circ}_{5/2}$	12468.606	1		8017.949	$11576^{\circ}_{3/2} - 19594_{1/2}$
13626.116	4		7336.842	$15305_{9/2} - 22642^{\circ}_{9/2}$	12458.068	1		8024.731	$19912^{\circ}_{13/2} - 27937_{11/2}$
13582.026	0		7360.659	$22513^{\circ}_{5/2} - 29873_{7/2}$	12421.310	1		8048.478	$21297^{\circ}_{5/2} - 29345_{5/2}$
13544.406	1		7381.103	$15453^{\circ}_{7/2} - 22834_{7/2}$	12402.749	1		8060.523	$9061_{5/2} - 17121^{\circ}_{3/2}$
13524.811	1		7391.797	$12488^{\circ}_{9/2} - 19880_{9/2}$	12400.331	3		8062.095	$6213_{9/2} - 14275^{\circ}_{9/2}$
13520.057	1		7394.396	$12485^{\circ}_{7/2} - 19880_{9/2}$	12398.153	2		8063.511	$1521_{5/2} - 9585^{\circ}_{5/2}$
13494.985	0		7408.134	$8378^{\circ}_{7/2} - 15786_{5/2}$	12372.484	4		8080.240	$4490^{\circ}_{5/2} - 12570_{7/2}$
13460.143	3		7427.310	$8605_{5/2} - 16033^{\circ}_{5/2}$	12356.076	2		8090.970	$12219_{3/2} - 20310^{\circ}_{5/2}$
13445.057	0		7435.644	$13250_{5/2} - 20686^{\circ}_{5/2}$	12318.487	1		8115.659	$12570_{7/2} - 20686^{\circ}_{5/2}$
13427.136	3		7445.568	$10673^{\circ}_{5/2} - 18118_{3/2}$	12285.424	1		8137.500	$20686^{\circ}_{5/2} - 28823_{5/2}$
13425.849	0		7446.282	$20080^{\circ}_{7/2} - 27526_{9/2}$	12276.652	1		8143.315	$7001_{3/2} - 15144^{\circ}_{3/2}$

TABLE 3. *Classified lines of* Th II—Continued

Wavelength Å	Intensity		Wavenumber cm^{-1}	Classification	Wavelength Å	Intensity		Wavenumber cm^{-1}	Classification
	Lamp	Spark				Lamp	Spark		
12251.360	0		8160.126	$22834_{7/2} - 30994^{\circ}_{7/2}$	11071.877	1		9029.419	$6213_{9/2} - 15242^{\circ}_{9/2}$
12244.970	3		8164.384	$16818_{7/2} - 24982^{\circ}_{7/2}$	11069.049	3		9031.726	$7001_{3/2} - 16033^{\circ}_{5/2}$
12200.702	1		8194.007	$18568^{\circ}_{1/2} - 26762_{3/2}$	11013.293	1		9077.450	$12219_{3/2} - 21297^{\circ}_{5/2}$
12194.157	8		8198.405	$1521_{5/2} - 9720^{\circ}_{7/2}$	11010.266	1		9079.946	$6244_{1/2} - 15324^{\circ}_{1/2}$
12170.869	0		8214.092	$21131^{\circ}_{3/2} - 29345_{5/2}$	10981.861	1		9103.431	$8018_{3/2} - 17121^{\circ}_{3/2}$
12136.565	1		8237.309	$22642^{\circ}_{9/2} - 30879_{7/2}$	10942.244	8		9136.391	$6213_{9/2} - 15349^{\circ}_{11/2}$
12102.779	1		8260.304	$17121^{\circ}_{3/2} - 25381_{3/2}$	10941.617	4		9136.914	$6168^{\circ}_{7/2} - 15305_{9/2}$
12087.362	2		8270.840	$6213_{9/2} - 14484^{\circ}_{11/2}$	10924.483	4		9151.245	$1521_{5/2} - 10673^{\circ}_{5/2}$
12086.503	3		8271.428	$9711_{7/2} - 17983^{\circ}_{5/2}$	10892.630	0		9178.005	$15236_{3/2} - 24414^{\circ}_{3/2}$
12043.786	1		8300.765	$8605_{5/2} - 16906^{\circ}_{7/2}$	10861.797	1		9204.059	$12902^{\circ}_{3/2} - 22106_{5/2}$
12011.883	0		8322.811	$7001_{3/2} - 15324^{\circ}_{1/2}$	10835.309	2w		9226.559	$20288^{\circ}_{11/2} - 29515_{9/2}$
12007.854	5		8325.604	$4146_{7/2} - 12472^{\circ}_{5/2}$	10834.611	2		9227.153	$15236_{3/2} - 24463^{\circ}_{5/2}$
11984.664	8		8341.714	$4146_{7/2} - 12488^{\circ}_{9/2}$	10820.075	5		9239.549	$6213_{9/2} - 15453^{\circ}_{7/2}$
11979.873	2		8345.050	$22139^{\circ}_{9/2} - 30484_{11/2}$	10794.056	3		9261.821	$9711_{7/2} - 18973^{\circ}_{7/2}$
11979.873	2		8345.050	$15786_{5/2} - 24132^{\circ}_{3/2}$	10790.541	0		9264.838	$10855_{7/2} - 20120^{\circ}_{5/2}$
11974.695	1		8348.658	$16033^{\circ}_{5/2} - 24381_{7/2}$	10757.771	0		9293.060	$7828_{1/2} - 17121^{\circ}_{3/2}$
11960.136	3		8358.821	$4113_{5/2} - 12472^{\circ}_{5/2}$	10740.457	1		9308.041	$10572^{\circ}_{9/2} - 19880_{9/2}$
11940.834	2		8372.333	$4113_{5/2} - 12485^{\circ}_{7/2}$	10723.921	7		9322.394	$4146_{7/2} - 13468^{\circ}_{9/2}$
11934.349	1		8376.882	$20969^{\circ}_{7/2} - 29345_{5/2}$	10660.847	3		9377.549	$8605_{5/2} - 17983^{\circ}_{5/2}$
11911.501	4		8392.950	$10855_{7/2} - 19248^{\circ}_{5/2}$	10658.585	1		9379.539	$18214^{\circ}_{3/2} - 27593_{5/2}$
11903.594	0		8398.525	$12570_{7/2} - 20969^{\circ}_{7/2}$	10642.859	1		9393.398	$13248_{9/2} - 22642^{\circ}_{9/2}$
11874.199	3		8419.316	$12570_{7/2} - 20989^{\circ}_{9/2}$	10605.455	4		9426.527	$25594^{\circ}_{1/2} - 35021_{3/2}$
11865.636	4		8425.392	$15305_{9/2} - 23730^{\circ}_{9/2}$	10595.992	0		9434.946	$13250_{5/2} - 22685^{\circ}_{7/2}$
11846.202	2		8439.214	$8378^{\circ}_{7/2} - 16818_{7/2}$	10587.588	1		9442.435	$8018_{3/2} - 17460^{\circ}_{5/2}$
11842.232	0		8442.043	$20989^{\circ}_{9/2} - 29431_{7/2}$	10576.600	1		9452.244	$15305_{9/2} - 24757^{\circ}_{9/2}$
11808.476	0		8466.176	$12219_{3/2} - 20686^{\circ}_{5/2}$	10572.824	1		9455.620	$10855_{7/2} - 20310^{\circ}_{5/2}$
11776.403	5		8489.233	$9238^{\circ}_{9/2} - 17727_{11/2}$	10560.617	1		9466.550	$6244_{1/2} - 15710^{\circ}_{3/2}$
11739.687	2		8515.783	$8605_{5/2} - 17121^{\circ}_{3/2}$	10539.400	1		9485.607	$10673^{\circ}_{5/2} - 20158_{5/2}$
11715.587	1		8533.301	$9585^{\circ}_{5/2} - 18118_{3/2}$	10538.316	2		9486.583	$7331^{\circ}_{5/2} - 16818_{7/2}$
11695.652	0		8547.846	$18214^{\circ}_{3/2} - 26762_{3/2}$	10483.360	4		9536.313	$9711_{7/2} - 19248^{\circ}_{5/2}$
11655.207	1		8577.508	$6213_{9/2} - 14790^{\circ}_{7/2}$	10429.665	6		9585.409	$0_{3/2} - 9585^{\circ}_{5/2}$
11648.639	1		8582.344	$11576^{\circ}_{3/2} - 20158_{5/2}$	10423.795	2		9590.807	$14790^{\circ}_{7/2} - 24381_{7/2}$
11631.948	3		8594.659	$10379_{9/2} - 18973^{\circ}_{7/2}$	10419.574	7		9594.692	$1521_{5/2} - 11116^{\circ}_{7/2}$
11594.834	0		8622.170	$16818_{7/2} - 25440^{\circ}_{5/2}$	10404.502	3		9608.591	$8605_{5/2} - 18214^{\circ}_{3/2}$
11542.494	3		8661.268	$8460_{3/2} - 17121^{\circ}_{3/2}$	10402.349	1		9610.580	$17983^{\circ}_{5/2} - 27593_{5/2}$
11521.827	2		8676.804	$15786_{5/2} - 24463^{\circ}_{5/2}$	10391.352	0		9620.750	$12485^{\circ}_{7/2} - 22106_{5/2}$
11515.375	0		8681.665	$16564^{\circ}_{11/2} - 25246_{9/2}$	10373.462	0		9637.342	$15236_{3/2} - 24873^{\circ}_{5/2}$
11478.678	2		8709.420	$7001_{3/2} - 15710^{\circ}_{3/2}$	10359.998	3		9649.867	$9400_{5/2} - 19050^{\circ}_{3/2}$
11455.648	1u		8726.929	$12570_{7/2} - 21297^{\circ}_{5/2}$	10356.372	2		9653.246	$15786_{5/2} - 25440^{\circ}_{5/2}$
11412.071	2		8760.253	$4490^{\circ}_{5/2} - 13250_{5/2}$	10316.006	1		9691.018	$10189^{\circ}_{11/2} - 19880_{9/2}$
11387.846	1		8778.888	$17983^{\circ}_{5/2} - 26762_{3/2}$	10304.810	2		9701.547	$10379_{9/2} - 20080^{\circ}_{7/2}$
11374.713	6		8789.024	$4113_{5/2} - 12902^{\circ}_{3/2}$	10301.161	6		9704.984	$4113_{5/2} - 13818^{\circ}_{7/2}$
11290.238	0		8854.785	$8605_{5/2} - 17460^{\circ}_{5/2}$	10288.987	4		9716.467	$1859_{3/2} - 11576^{\circ}_{3/2}$
11252.925	1		8884.146	$20989^{\circ}_{9/2} - 29873_{7/2}$	10249.314	1		9754.077	$8460_{3/2} - 18214^{\circ}_{3/2}$
11244.310	2d		8890.952	$13248_{9/2} - 22139^{\circ}_{9/2}$	10247.419	1		9755.881	$17771^{\circ}_{11/2} - 27526_{9/2}$
11232.320	2		8900.443	$6244_{1/2} - 15144^{\circ}_{3/2}$	10244.986	1		9758.198	$22014^{\circ}_{11/2} - 31773_{9/2}$
11204.818	2		8922.289	$9061_{5/2} - 17983^{\circ}_{5/2}$	10241.463	2		9761.555	$13250_{5/2} - 23012^{\circ}_{3/2}$
11202.078	1		8924.471	$17837^{\circ}_{1/2} - 26762_{3/2}$	10219.382	2		9782.646	$14349_{1/2} - 24132^{\circ}_{3/2}$
11186.716	0		8936.727	$20158_{5/2} - 29095^{\circ}_{5/2}$	10208.285	0		9793.281	$20080^{\circ}_{7/2} - 29873_{7/2}$
11107.735	0		9000.271	$8460_{3/2} - 17460^{\circ}_{5/2}$	10197.163	0		9803.962	$17722^{\circ}_{9/2} - 27526_{9/2}$

TABLE 3. *Classified lines of* Th II—Continued

Wavelength Å	Intensity		Wavenumber cm^{-1}	Classification	Wavelength Å	Intensity		Wavenumber cm^{-1}	Classification
	Lamp	Spark				Lamp	Spark		
10180.909	0		9819.614	$8018_{3/2} - 17837^{\circ}_{1/2}$	9362.640	1		10677.819	$9202^{\circ}_{7/2} - 19880_{9/2}$
10169.296	2		9830.828	$10855_{7/2} - 20686^{\circ}_{5/2}$	9360.989	2		10679.702	$9400_{5/2} - 20080^{\circ}_{7/2}$
10133.559	7		9865.497	$1859_{3/2} - 11725^{\circ}_{1/2}$	9349.246	1		10693.116	$6213_{9/2} - 16906^{\circ}_{7/2}$
10085.323	1		9912.681	$9061_{5/2} - 18973^{\circ}_{7/2}$	9346.644	1	2	10696.092	$22513^{\circ}_{5/2} - 33209_{7/2}$
10045.996	0		9951.486	$15236_{3/2} - 25188^{\circ}_{3/2}$	9311.053	2	4	10736.978	$30310^{\circ}_{11/2} - 41047_{9/2}$
10032.174	1		9965.197	$8018_{3/2} - 17983^{\circ}_{5/2}$	9292.242	2	2	10758.713	$35593^{\circ}_{7/2} - 46352_{7/2}$
9993.866	2		10003.395	$15242^{\circ}_{9/2} - 25246_{9/2}$	9267.686	2		10787.220	$7331^{\circ}_{5/2} - 18118_{3/2}$
9988.024	2		10009.246	$7828_{1/2} - 17837^{\circ}_{1/2}$	9267.082	3		10787.923	$8460_{3/2} - 19248^{\circ}_{5/2}$
9943.061	6		10054.508	$1521_{5/2} - 11576^{\circ}_{3/2}$	9253.268	1	3	10804.028	$20969^{\circ}_{7/2} - 31773_{9/2}$
9926.172	0		10071.616	$12570_{7/2} - 22642^{\circ}_{9/2}$	9252.860	0		10804.504	$18118_{3/2} - 28923^{\circ}_{5/2}$
9892.187	0		10106.217	$14275^{\circ}_{9/2} - 24381_{7/2}$	9249.887	5	4	10807.977	$27357^{\circ}_{9/2} - 38165_{7/2}$
9890.522	1		10107.918	$8460_{3/2} - 18568^{\circ}_{1/2}$	9245.253	10	5	10813.394	$20158_{5/2} - 30972^{\circ}_{5/2}$
9888.819	0		10109.659	$15305_{9/2} - 25414^{\circ}_{11/2}$	9233.267	3	75	10827.431	$10855_{7/2} - 21682^{\circ}_{7/2}$
9880.782	2		10117.882	$6700^{\circ}_{9/2} - 16818_{7/2}$	9226.409	0	5	10835.479	$20158_{5/2} - 30994^{\circ}_{7/2}$
9878.520	2		10120.199	$7001_{3/2} - 17121^{\circ}_{3/2}$	9225.657	1	2	10836.363	$14545^{\circ}_{5/2} - 25381_{3/2}$
9876.688	0		10122.076	$13250_{5/2} - 23372^{\circ}_{3/2}$					$7001_{3/2} - 17837^{\circ}_{1/2}$
9869.929	0		10129.008	$4146_{7/2} - 14275^{\circ}_{9/2}$	9164.081	0	8	10909.175	$26770^{\circ}_{11/2} - 37679_{11/2}$
9864.597	2	8	10134.483	$10855_{7/2} - 20989^{\circ}_{9/2}$	9157.414	2	20	10917.117	$14349_{1/2} - 25266^{\circ}_{1/2}$
9863.866	1		10135.234	$12219_{3/2} - 22355^{\circ}_{1/2}$	9133.422	0	5	10945.794	$33354^{\circ}_{5/2} - 44300_{3/2}$
9834.008	3		10166.006	$17771^{\circ}_{11/2} - 27937_{11/2}$					$30101^{\circ}_{7/2} - 41047_{9/2}$
9817.034	3h	3	10183.583	$19248^{\circ}_{5/2} - 29431_{7/2}$	9129.691	3	5	10950.268	$1521_{5/2} - 12472^{\circ}_{5/2}$
9780.808	1	1	10221.301	$19880_{9/2} - 30101^{\circ}_{7/2}$	9124.513	2	4	10956.482	$9202^{\circ}_{7/2} - 20158_{5/2}$
9734.696	1		10269.718	$13248_{9/2} - 23518^{\circ}_{7/2}$	9119.627	200	100	10962.352	$16564^{\circ}_{11/2} - 27526_{9/2}$
9663.062	0		10345.849	$12488^{\circ}_{9/2} - 22834_{7/2}$	9118.418	4	5	10963.805	$1521_{5/2} - 12485^{\circ}_{7/2}$
9651.502	4	2	10358.241	$15236_{3/2} - 25594^{\circ}_{1/2}$	9113.459	2	10	10969.771	$16818_{7/2} - 27787^{\circ}_{9/2}$
9642.471	4		10367.942	$8605_{5/2} - 18973^{\circ}_{7/2}$	9112.672	2	15	10970.718	$14275^{\circ}_{9/2} - 25246_{9/2}$
9613.689	5		10398.982	$4146_{7/2} - 14545^{\circ}_{5/2}$	9109.777	2	10	10974.205	$9711_{7/2} - 20686^{\circ}_{5/2}$
9583.076	3		10432.201	$4113_{5/2} - 14545^{\circ}_{5/2}$	9107.667	2	15	10976.747	$18118_{3/2} - 29095^{\circ}_{5/2}$
9578.636	0	5	10437.037	$22139^{\circ}_{9/2} - 32576_{7/2}$	9103.998	1	4	10981.171	$26963^{\circ}_{7/2} - 37945_{5/2}$
9577.344	3		10438.445	$9720^{\circ}_{7/2} - 20158_{5/2}$	9103.341	3	5	10981.964	$7001_{3/2} - 17983^{\circ}_{5/2}$
9560.574	1	2	10456.755	$21297^{\circ}_{5/2} - 31754_{5/2}$	9096.811	1	3	10989.847	$11116^{\circ}_{7/2} - 22106_{5/2}$
9558.370	1	2	10459.166	$7001_{3/2} - 17460^{\circ}_{5/2}$	9072.260	5	40	11019.587	$9061_{5/2} - 20080^{\circ}_{7/2}$
9519.819	0	5	10501.521	$26963^{\circ}_{7/2} - 37465_{5/2}$	9066.096	20	40	11027.079	$6700^{\circ}_{9/2} - 17727_{11/2}$
9494.041	1		10530.034	$11576^{\circ}_{3/2} - 22106_{3/2}$	9062.545	100	150	11031.400	$4113_{3/2} - 15144^{\circ}_{3/2}$
9483.850	0		10541.349	$18973^{\circ}_{7/2} - 29515_{9/2}$	9053.468	150	75	11042.460	$1859_{3/2} - 12902^{\circ}_{3/2}$
9477.269	1	10	10548.669	$23730^{\circ}_{9/2} - 34279_{7/2}$	9046.321	0	5	11051.184	$35165^{\circ}_{13/2} - 46216_{11/2}$
9456.023	0		10572.370	$19912^{\circ}_{13/2} - 30484_{11/2}$	9040.106	50	75	11058.781	$6213_{9/2} - 17272^{\circ}_{9/2}$
9455.297	0	15w	10573.182	$20686^{\circ}_{5/2} - 31259_{5/2}$	9038.675	4	15	11060.532	$13248_{9/2} - 24309^{\circ}_{11/2}$
9439.854	0		10590.479	$8460_{3/2} - 19050^{\circ}_{3/2}$	9032.634	0	8	11067.929	$22834_{7/2} - 33902^{\circ}_{7/2}$
9432.280	3		10598.983	$9711_{7/2} - 20310^{\circ}_{3/2}$	8974.923	1		11139.099	$20120^{\circ}_{5/2} - 31259_{5/2}$
9420.493	2d		10612.244	$1859_{3/2} - 12472^{\circ}_{5/2}$	8974.326	0	5	11139.840	$27249^{\circ}_{7/2} - 38389_{7/2}$
9398.155	2	4	10637.468	$15786_{5/2} - 26424^{\circ}_{5/2}$	8964.041	2	20	11152.621	$12219_{3/2} - 23372^{\circ}_{3/2}$
9394.096	0		10642.064	$9238^{\circ}_{9/2} - 19880_{9/2}$	8957.972	10	100	11160.177	$12570_{7/2} - 23730^{\circ}_{9/2}$
9393.770	1		10642.433	$8605_{5/2} - 19248^{\circ}_{5/2}$	8954.817	1	2	11164.109	$13250_{5/2} - 24414^{\circ}_{3/2}$
9392.016	1		10644.421	$4146_{7/2} - 14790^{\circ}_{7/2}$	8935.812	1	10	11187.853	$15236_{3/2} - 26424^{\circ}_{5/2}$
9374.051	0		10664.821	$17272^{\circ}_{9/2} - 27937_{11/2}$	8929.834	0	5	11195.343	$35156^{\circ}_{5/2} - 46352_{7/2}$
9366.743	0d		10673.141	$0_{3/2} - 10673^{\circ}_{5/2}$	8928.630	3	2	11196.852	$32576_{7/2} - 43773^{\circ}_{7/2}$
9362.794	0		10677.643	$4113_{3/2} - 14790^{\circ}_{7/2}$	8902.210	1	3	11230.082	$8018_{3/2} - 19248^{\circ}_{5/2}$
9362.794	0		10677.643	$14349_{1/2} - 25027^{\circ}_{1/2}$	8887.781	1	3	11248.314	$22106_{5/2} - 33354^{\circ}_{5/2}$
9362.685	2	20	10677.767	$34212^{\circ}_{5/2} - 44889_{3/2}$	8880.875	1	2	11257.061	$9711_{7/2} - 20969^{\circ}_{7/2}$

TABLE 3. *Classified lines of* Th II—Continued

Wavelength Å	Intensity		Wavenumber cm^{-1}	Classification	Wavelength Å	Intensity		Wavenumber cm^{-1}	Classification
	Lamp	Spark				Lamp	Spark		
8864.494	2	3	11277.863	$9711_{7/2} - 20989^{\circ}_{9/2}$	8403.787	100	300	11896.128	$12485^{\circ}_{7/2} - 24381_{7/2}$
8842.067	15	2	11306.468	$4146_{7/2} - 15453^{\circ}_{7/2}$	8403.556	15	15	11896.455	$9400_{5/2} - 21297^{\circ}_{5/2}$
8826.334	0	5	11326.622	$24414^{\circ}_{3/2} - 35741_{5/2}$	8399.688	5s	2	11901.933	$26965^{\circ}_{3/2} - 38867_{1/2}$
8816.161	8	40	11339.692	$4113_{5/2} - 15453^{\circ}_{7/2}$	8397.074	2	5	11905.638	$18973^{\circ}_{7/2} - 30879_{7/2}$
8798.457	1	5	11362.509	$17983^{\circ}_{5/2} - 29345_{5/2}$	8394.722	0	8	11908.974	$44177_{11/2} - 56086^{\circ}_{9/2}$
8784.553	40	50	11380.493	$1521_{5/2} - 12902^{\circ}_{3/2}$	8392.547	2	50	11912.060	$12219_{3/2} - 24132^{\circ}_{3/2}$
8777.333	1	3	11389.854	$15236_{3/2} - 26626^{\circ}_{1/2}$	8391.218	0	8	11913.947	$24414^{\circ}_{3/2} - 36328_{3/2}$
8757.977	0	5	11415.027	$24463^{\circ}_{3/2} - 35878_{7/2}$	8387.089	150	200	11919.812	$4113_{5/2} - 16033^{\circ}_{5/2}$
8749.761	1	1	11425.746	$16818_{7/2} - 28243^{\circ}_{5/2}$	8351.367	3	8	11970.798	$9711_{7/2} - 21682^{\circ}_{7/2}$
8745.509	2	2	11431.301	$32957^{\circ}_{7/2} - 44388_{5/2}$	8351.052	2	8	11971.249	$17460^{\circ}_{5/2} - 29431_{7/2}$
8736.376	1	3	11443.251	$20310^{\circ}_{5/2} - 31754_{5/2}$	8342.686	2	5	11983.254	$28587^{\circ}_{5/2} - 40570_{7/2}$
8721.653	8	100	11462.568	$15786_{5/2} - 27249^{\circ}_{7/2}$	8321.156	0	10	12014.259	$15242^{\circ}_{9/2} - 27257_{7/2}$
8719.623	5	50	11465.237	$15305_{9/2} - 26770^{\circ}_{11/2}$	8313.535	4	2	12025.272	$25440^{\circ}_{5/2} - 37465_{5/2}$
8698.591	10	4	11492.958	$33902^{\circ}_{7/2} - 45395_{7/2}$	8310.076	1	10	12030.278	$22513^{\circ}_{5/2} - 34543_{5/2}$
8695.106	2	1	11497.564	$22139^{\circ}_{9/2} - 33637_{7/2}$	8302.576	2	15	12041.145	$22685^{\circ}_{7/2} - 34726_{7/2}$
8688.761	2w	1	11505.960	$22513^{\circ}_{5/2} - 34019_{3/2}$	8295.021	4	15	12052.112	$15305_{9/2} - 27357^{\circ}_{9/2}$
8686.605	3	10	11508.816	$13248_{9/2} - 24757^{\circ}_{9/2}$	8282.232	5	15	12070.722	$9061_{5/2} - 21131^{\circ}_{3/2}$
8686.074	10	25	11509.520	$6213_{9/2} - 17722^{\circ}_{9/2}$	8280.974	1	8	12072.556	$25607^{\circ}_{9/2} - 37679_{11/2}$
8682.441	3	8	11514.336	$8605_{5/2} - 20120^{\circ}_{5/2}$	8263.029	0	8	12098.774	$30101^{\circ}_{7/2} - 42200_{9/2}$
8629.132	8	40w	11585.469	$9711_{7/2} - 21297^{\circ}_{5/2}$	8258.994	4	3	12104.685	$33384_{9/2} - 45489^{\circ}_{9/2}$
8628.062	1	4	11586.905	$20989^{\circ}_{9/2} - 32576_{7/2}$	8242.406	0	8	12129.045	$35602^{\circ}_{11/2} - 47731_{9/2}$
8621.818	2	1	11595.297	$32957^{\circ}_{7/2} - 44552_{5/2}$	8241.355	2	15	12130.592	$22139^{\circ}_{9/2} - 34270_{9/2}$
8620.179	10	15	11597.501	$4113_{5/2} - 15710^{\circ}_{3/2}$	8236.320	5	2	12138.008	$35593^{\circ}_{7/2} - 47731_{9/2}$
8617.110	2	8	11601.632	$18118_{3/2} - 29720^{\circ}_{3/2}$	8235.216	0	5	12139.635	$22139^{\circ}_{9/2} - 34279_{7/2}$
8600.910	3	10	11623.484	$13250_{5/2} - 24873^{\circ}_{5/2}$	8221.233	0	5	12160.282	$25414^{\circ}_{11/2} - 37575_{13/2}$
8599.731	10	25	11625.077	$9061_{5/2} - 20686^{\circ}_{5/2}$	8220.764	3	10	12160.976	$10673^{\circ}_{5/2} - 22834_{7/2}$
8597.434	5	10	11628.183	$22642^{\circ}_{9/2} - 34270_{9/2}$	8217.219	75	150	12166.223	$13248_{9/2} - 25414^{\circ}_{11/2}$
8591.828	200	300	11635.770	$10379_{9/2} - 22014^{\circ}_{11/2}$	8216.352	0	15	12167.506	$35156^{\circ}_{5/2} - 47324_{5/2}$
8590.751	2	40	11637.229	$22642^{\circ}_{9/2} - 34279_{7/2}$	8203.190	200	100	12187.029	$12570_{7/2} - 24757^{\circ}_{9/2}$
8587.629	5	50	11641.459	$20158_{5/2} - 31800^{\circ}_{7/2}$	8198.067	1	1	12194.645	$12219_{3/2} - 24414^{\circ}_{3/2}$
8582.539	2		11648.364	$25414^{\circ}_{11/2} - 37063_{9/2}$	8184.393	1	10	12215.019	$26647^{\circ}_{13/2} - 38862_{11/2}$
8580.560	2	1	11651.050	$24414^{\circ}_{3/2} - 36065_{5/2}$	8182.265	5	8	12218.196	$37277_{7/2} - 49495^{\circ}_{9/2}$
8568.203	10	150	11667.853	$18816^{\circ}_{13/2} - 30484_{11/2}$	8181.307	2	10	12219.626	$20989^{\circ}_{9/2} - 33209_{7/2}$
8531.872	3	5	11717.538	$11116^{\circ}_{7/2} - 22834_{7/2}$	8178.203	4	20	12224.264	$17121^{\circ}_{3/2} - 29345_{5/2}$
8523.848	2	4	11728.568	$15236_{3/2} - 26965^{\circ}_{3/2}$	8177.169	5	15	12225.810	$8460_{3/2} - 20686^{\circ}_{5/2}$
8522.191	2	5	11730.849	$9400_{5/2} - 21131^{\circ}_{3/2}$	8170.181	3	5	12236.267	$9061_{5/2} - 21297^{\circ}_{5/2}$
8521.409	2	25	11731.925	$13250_{5/2} - 24982^{\circ}_{7/2}$	8166.441	150	100	12241.871	$1859_{3/2} - 14101^{\circ}_{1/2}$
8512.591	5h	50	11744.078	$17771^{\circ}_{11/2} - 29515_{9/2}$	8165.733	4	4	12242.932	$17272^{\circ}_{9/2} - 29515_{9/2}$
8500.667	50	75	11760.551	$10379_{9/2} - 22139^{\circ}_{9/2}$	8165.153	8h	8	12243.802	$12219_{3/2} - 24463^{\circ}_{5/2}$
8498.514	2	5	11763.531	$26965^{\circ}_{3/2} - 38728_{5/2}$	8163.117	100	150	12246.855	$7001_{3/2} - 19248^{\circ}_{5/2}$
8496.718	8	4	11766.017	$22513^{\circ}_{5/2} - 34279_{7/2}$	8152.391	8	40	12262.968	$10379_{9/2} - 22642^{\circ}_{9/2}$
8481.756	2	4	11786.773	$10855_{7/2} - 22642^{\circ}_{9/2}$	8150.530	0	8	12265.768	$20310^{\circ}_{5/2} - 32576_{7/2}$
8477.916	20	150	11792.111	$43246_{7/2} - 55038^{\circ}_{9/2}$	8145.474	2	5	12273.382	$20686^{\circ}_{5/2} - 32959_{3/2}$
8453.046	2h	1	11826.805	$24982^{\circ}_{7/2} - 36809_{7/2}$	8139.896	75	100	12281.792	$9400_{5/2} - 21682^{\circ}_{7/2}$
8452.387	4	2	11827.727	$39396^{\circ}_{7/2} - 51224_{9/2}$	8130.213	15	8	12296.420	$1521_{5/2} - 13818^{\circ}_{7/2}$
8450.675	75b	150	11830.123	$10855_{7/2} - 22685^{\circ}_{7/2}$	8127.630	2	8	12300.327	$15710^{\circ}_{3/2} - 28011_{3/2}$
8436.118	0	5	11850.537	$32957^{\circ}_{7/2} - 44807_{7/2}$	8125.514	1	3	12303.531	$12570_{7/2} - 24873^{\circ}_{5/2}$
8412.973	4	25	11883.139	$15710^{\circ}_{3/2} - 27593_{5/2}$	8123.655	2	5	12306.346	$10379_{9/2} - 22685^{\circ}_{7/2}$
8410.532	25	25	11886.588	$4146_{7/2} - 16033^{\circ}_{5/2}$	8112.024	1	1	12323.991	$6244_{1/2} - 18568^{\circ}_{1/2}$
8405.770	3	8	11893.322	$12570_{7/2} - 24463^{\circ}_{5/2}$	8082.673	5	4	12368.743	$23372^{\circ}_{3/2} - 35741_{5/2}$

TABLE 3. *Classified lines of* Th II—Continued

Wavelength Å	Intensity		Wavenumber cm^{-1}	Classification	Wavelength Å	Intensity		Wavenumber cm^{-1}	Classification
	Lamp	Spark				Lamp	Spark		
8054.524	10	50	12411.970	$12570_{7/2}-24982^{\circ}_{7/2}$	7743.934	5	25	12909.780	$12472^{\circ}_{5/2}-25381_{3/2}$
8053.584	1	8	12413.418	$35593^{\circ}_{9/2}-48006_{9/2}$	7731.716	75	100	12930.181	$9711_{7/2}-22642^{\circ}_{9/2}$
8053.010	1	10	12414.303	$22139^{\circ}_{9/2}-34553_{9/2}$	7729.542	2	4	12933.818	$15786_{5/2}-28720^{\circ}_{3/2}$
8036.828	20	10	12439.299	$16906^{\circ}_{7/2}-29345_{5/2}$	7701.101	15	20	12981.583	$14275^{\circ}_{9/2}-27257_{7/2}$
8020.742	2	2	12464.246	$25381_{3/2}-37846^{\circ}_{5/2}$	7676.212	100	15	13023.674	$1521_{5/2}-14545^{\circ}_{5/2}$
8015.626	25	300	12472.202	$0_{3/2}-12472^{\circ}_{5/2}$	7637.767	1	3	13089.229	$20120^{\circ}_{5/2}-33209_{7/2}$
7984.363	8	10	12521.037	$9585^{\circ}_{5/2}-22106_{5/2}$	7633.890	2	4	13095.876	$20288^{\circ}_{11/2}-33384_{9/2}$
7983.722	1	10	12522.042	$22139^{\circ}_{9/2}-34661_{11/2}$	7624.311	5	8	13112.330	$9400_{5/2}-22513^{\circ}_{5/2}$
7981.670	5	50	12525.261	$16906^{\circ}_{7/2}-29431_{7/2}$	7623.565	5	5	13113.613	$8018_{3/2}-21131^{\circ}_{3/2}$
7981.213	75	1	12525.978	$8605_{5/2}-21131^{\circ}_{3/2}$	7623.440	1	1	13113.828	$9720^{\circ}_{7/2}-22834_{7/2}$
7973.517	5	4	12538.068	$27357^{\circ}_{9/2}-39895_{9/2}$	7620.586	3	4	13118.739	$7001_{3/2}-20120^{\circ}_{5/2}$
7972.881	4h	50	12539.069	$22014^{\circ}_{11/2}-34553_{9/2}$	7616.576	1	2	13125.646	$4146_{7/2}-17272^{\circ}_{9/2}$
7945.845	0	5	12581.733	$27357^{\circ}_{9/2}-39939_{11/2}$	7614.810	3	8	13128.690	$20080^{\circ}_{7/2}-33209_{7/2}$
7945.057	5	50	12582.981	$17727_{11/2}-30310^{\circ}_{11/2}$	7608.659	2	3	13139.303	$10379^{\circ}_{9/2}-23518^{\circ}_{7/2}$
7936.475	2	15	12596.587	$21682^{\circ}_{7/2}-34279_{7/2}$	7566.526	5	20	13212.467	$17272^{\circ}_{9/2}-30484_{11/2}$
7934.889	0	8	12599.105	$21131^{\circ}_{3/2}-33730_{5/2}$	7556.892	1	4	13229.311	$17727_{11/2}-30956^{\circ}_{9/2}$
7933.275	2	4	12601.668	$17272^{\circ}_{9/2}-29873_{7/2}$	7547.309	1	8	13246.108	$21297^{\circ}_{3/2}-34543_{5/2}$
7928.939	4	40	12608.559	$16906^{\circ}_{7/2}-29515_{9/2}$	7536.407	50	10	13265.270	$11116^{\circ}_{7/2}-24381_{7/2}$
7914.333	0	5	12631.829	$29720^{\circ}_{3/2}-42352_{5/2}$	7536.011	0	8	13265.967	$24309^{\circ}_{11/2}-37575_{13/2}$
7896.427	5c	40	12660.472	$14101^{\circ}_{1/2}-26762_{3/2}$	7534.224	3	2	13269.113	$1521_{5/2}-14790^{\circ}_{7/2}$
7894.776	4	20	12663.120	$10855_{7/2}-23518^{\circ}_{7/2}$	7525.507	200	150	13284.483	$9400_{5/2}-22685^{\circ}_{7/2}$
7892.892	3	5	12666.143	$22355^{\circ}_{1/2}-35021_{3/2}$	7525.329	10	5	13284.797	$1859_{3/2}-15144^{\circ}_{3/2}$
7891.743	3	8	12667.987	$8018_{3/2}-20686^{\circ}_{5/2}$	7522.654	2	10	13289.521	$20989^{\circ}_{9/2}-34279_{7/2}$
7883.986	1	8	12680.451	$28026_{5/2}-40706^{\circ}_{7/2}$	7514.891	4	4	13303.250	$7828^{\circ}_{1/2}-21131^{\circ}_{3/2}$
7880.761	4	8	12685.640	$1859_{3/2}-14545^{\circ}_{3/2}$	7514.604	1	4	13303.758	$20080^{\circ}_{7/2}-33384_{9/2}$
7877.057	15	50	12691.605	$8605_{3/2}-21297^{\circ}_{5/2}$	7511.346	50	25	13309.528	$7001_{3/2}-20310^{\circ}_{5/2}$
7875.448	8	100	12694.198	$15242^{\circ}_{9/2}-27937_{11/2}$	7509.517	1	1	13312.770	$16033^{\circ}_{5/2}-29345_{5/2}$
7871.284	4	1	12700.913	$39861^{\circ}_{5/2}-52562_{7/2}$	7508.791	3		13314.057	$4146_{7/2}-17460^{\circ}_{5/2}$
7853.482	0	15	12729.703	$17722^{\circ}_{9/2}-30452_{9/2}$	7497.882	4	8	13333.428	$24132^{\circ}_{3/2}-37465_{5/2}$
7849.616	8	150	12735.972	$14790^{\circ}_{7/2}-27526_{9/2}$	7490.104	8	5	13347.274	$4113_{5/2}-17460^{\circ}_{5/2}$
7836.703	0	5	12756.958	$25188^{\circ}_{3/2}-37945_{5/2}$	7488.169	2	2	13350.723	$15236_{3/2}-28587^{\circ}_{5/2}$
7836.081	1	5	12757.971	$12488^{\circ}_{9/2}-25246_{9/2}$	7487.713	5	5	13351.536	$10379_{9/2}-23730^{\circ}_{9/2}$
7835.266	2	40	12759.298	$22834_{7/2}-35593^{\circ}_{9/2}$	7484.002	1	3	13358.156	$24463^{\circ}_{5/2}-37821_{3/2}$
7834.805	2	10h	12760.049	$4146_{7/2}-16906^{\circ}_{7/2}$	7483.374	2	8	13359.277	$22834_{7/2}-36193^{\circ}_{9/2}$
7834.446	100	200	12760.633	$12485^{\circ}_{7/2}-25246_{9/2}$	7479.821	3	15	13365.623	$23697^{\circ}_{7/2}-37063_{9/2}$
7824.041	2	10	12777.603	$17771^{\circ}_{11/2}-30548_{13/2}$	7454.096	2	4	13411.749	$21131^{\circ}_{3/2}-34543_{5/2}$
7818.331	4	40	12786.935	$27787^{\circ}_{9/2}-40574_{11/2}$	7439.086	8	8	13438.810	$13818^{\circ}_{7/2}-27257_{7/2}$
7815.866	1	2	12790.968	$30223^{\circ}_{15/2}-43014_{13/2}$	7438.494	2	8	13439.880	$22685^{\circ}_{7/2}-36125_{9/2}$
7811.159	2	40	12798.676	$20158_{5/2}-32957^{\circ}_{7/2}$					$23372^{\circ}_{3/2}-36812_{1/2}$
7807.026	5	4	12805.451	$24982^{\circ}_{7/2}-37787_{7/2}$	7437.708	2	5	13441.300	$22014^{\circ}_{11/2}-35456_{9/2}$
7806.029	4	3	12807.087	$12219_{3/2}-25027^{\circ}_{1/2}$	7431.680	4	2	13452.202	$9061_{3/2}-22513^{\circ}_{5/2}$
7787.793	75b	200	12837.076	$8460_{3/2}-21297^{\circ}_{5/2}$	7431.378	5	3	13452.749	$14484^{\circ}_{11/2}-27937_{11/2}$
7786.444	2	5	12839.300	$20120^{\circ}_{5/2}-32959_{3/2}$	7423.311	10	4	13467.368	$6691^{\circ}_{3/2}-20158_{5/2}$
7784.608	2	50	12842.328	$10855_{7/2}-23697^{\circ}_{7/2}$	7414.052	5	4	13484.187	$15236_{3/2}-28720^{\circ}_{3/2}$
7777.302	0	5	12854.392	$30101^{\circ}_{7/2}-42955_{9/2}$	7412.008	4	5	13487.905	$19248^{\circ}_{5/2}-32736_{7/2}$
7773.429	2	1	12860.796	$21682^{\circ}_{7/2}-34543_{5/2}$	7399.724	2	4	13510.296	$22014^{\circ}_{11/2}-35525_{11/2}$
7767.173	0	8	12871.155	$21682^{\circ}_{7/2}-34553_{9/2}$	7396.009	8	8	13517.082	$20120^{\circ}_{5/2}-33637_{7/2}$
7764.645	3	10	12875.346	$10855_{7/2}-23730^{\circ}_{9/2}$	7393.434	200	150	13521.790	$13248_{9/2}-26770^{\circ}_{11/2}$
7748.368	2	3	12902.393	$0_{3/2}-12902^{\circ}_{5/2}$	7389.264	20	3	13529.421	$14101^{\circ}_{1/2}-27631_{3/2}$
7747.415	5	4	12903.980	$36581^{\circ}_{3/2}-49485_{1/2}$	7380.156	8	8	13546.117	$16906^{\circ}_{7/2}-30452_{9/2}$

TABLE 3. *Classified lines of* Th II—Continued

Wavelength Å	Intensity		Wavenumber cm^{-1}	Classification	Wavelength Å	Intensity		Wavenumber cm^{-1}	Classification
	Lamp	Spark				Lamp	Spark		
7359.069	2	8	13584.933	$20969^{\circ}_{7/2} - 34553_{9/2}$	7098.675	1	3	14083.253	$26963^{\circ}_{7/2} - 41047_{9/2}$
7358.347	50	20	13586.266	$12902^{\circ}_{3/2} - 26488_{5/2}$	7089.699	4		14101.083	$4113_{5/2} - 18214^{\circ}_{3/2}$
7354.610	2	3	13593.169	$20686^{\circ}_{5/2} - 34279_{7/2}$	7089.334	400	100	14101.809	$0_{3/2} - 14101^{\circ}_{1/2}$
7353.034	8		13596.083	$9238^{\circ}_{9/2} - 22834_{7/2}$	7087.595	0	5	14105.269	$24757^{\circ}_{9/2} - 38862_{11/2}$
7353.007	15	8	13596.133	$9238^{\circ}_{9/2} - 22834_{7/2}$	7084.983	2	10	14110.469	$22014^{\circ}_{11/2} - 36125_{9/2}$
7352.581	5		13596.920	$26770^{\circ}_{11/2} - 40367_{9/2}$	7078.262	5	4	14123.867	$22685^{\circ}_{7/2} - 36809_{7/2}$
7349.315	3	8	13602.963	$18973^{\circ}_{7/2} - 32576_{7/2}$	7075.331	200	150	14129.718	$11116^{\circ}_{7/2} - 25246_{9/2}$
7347.048	8	15	13607.160	$17272^{\circ}_{9/2} - 30879_{7/2}$	7075.003	5	4	14130.373	$7001_{3/2} - 21131^{\circ}_{3/2}$
7346.341	15	15	13608.469	$10855_{7/2} - 24463^{\circ}_{5/2}$	7053.614	300	75	14173.221	$1859_{3/2} - 16033^{\circ}_{5/2}$
7338.591	5	3	13622.841	$1521_{5/2} - 15144^{\circ}_{3/2}$	7045.795	400	150	14188.950	$15242^{\circ}_{9/2} - 29431_{7/2}$
									$1521_{5/2} - 15710^{\circ}_{3/2}$
7337.775	15	8	13624.356	$9061_{5/2} - 22685^{\circ}_{7/2}$					
7332.015	3	3	13635.059	$15710^{\circ}_{3/2} - 29345_{5/2}$	7008.051	2	5	14265.368	$20288^{\circ}_{11/2} - 34553_{9/2}$
7323.851	4	5	13650.258	$20080^{\circ}_{7/2} - 33730_{5/2}$	6995.930	2	5	14290.084	$12472^{\circ}_{5/2} - 26762_{3/2}$
7312.255	2	4	13671.905	$20989^{\circ}_{9/2} - 34661_{11/2}$	6993.034	300	200	14296.002	$22513^{\circ}_{5/2} - 36809_{7/2}$
7308.515	5	8	13678.901	$15144^{\circ}_{3/2} - 28823_{5/2}$					$7001_{3/2} - 21297^{\circ}_{5/2}$
7305.397	100	75	13684.739	$7001_{3/2} - 20686^{\circ}_{5/2}$	6992.692	50	40	14296.701	$9400_{5/2} - 23697^{\circ}_{7/2}$
7292.669	5	5	13708.623	$13818^{\circ}_{7/2} - 27526_{9/2}$	6985.467	20	40	14311.488	$9061_{5/2} - 23372^{\circ}_{3/2}$
7289.438	3	8	13714.700	$13250_{5/2} - 26965^{\circ}_{3/2}$	6975.478	1	5	14331.982	$25607^{\circ}_{9/2} - 39939_{11/2}$
7257.189	4	4	13775.644	$13818^{\circ}_{7/2} - 27593_{5/2}$	6973.043	0	5	14336.987	$8018_{3/2} - 22355^{\circ}_{1/2}$
7250.587	15	20	13788.187	$13468^{\circ}_{9/2} - 27257_{7/2}$	6973.020	4	5	14337.034	$8018_{3/2} - 22355^{\circ}_{1/2}$
7240.981	5	2	13806.479	$9711_{7/2} - 23518^{\circ}_{7/2}$	6965.415	2	5	14352.687	$16906^{\circ}_{7/2} - 31259_{5/2}$
7225.125	20	5	13836.778	$4146_{7/2} - 17983^{\circ}_{5/2}$	6956.332	1	8	14371.428	$14349_{1/2} - 28720^{\circ}_{3/2}$
7217.759	150	50	13850.898	$1859_{3/2} - 15710^{\circ}_{3/2}$	6955.504	2	20	14373.139	$20288^{\circ}_{11/2} - 34661_{11/2}$
7216.158	4	4	13853.971	$12570_{7/2} - 26424^{\circ}_{5/2}$	6953.230	0	5	14377.839	$22685^{\circ}_{7/2} - 37063_{9/2}$
7195.955	5	5	13892.867	$15453^{\circ}_{7/2} - 29345_{5/2}$	6952.961	50	50	14378.396	$10379_{9/2} - 24757^{\circ}_{9/2}$
7194.925	3	5	13894.856	$8460_{3/2} - 22355^{\circ}_{1/2}$	6946.781	1	5	14391.187	$18568^{\circ}_{1/2} - 32959_{3/2}$
7191.128	500	300	13902.192	$10855_{7/2} - 24757^{\circ}_{9/2}$	6938.967	0	5	14407.393	$23697^{\circ}_{7/2} - 38105_{5/2}$
7188.415	3	2	13907.439	$8605_{5/2} - 22513^{\circ}_{5/2}$	6937.080	0	25	14411.312	$22642^{\circ}_{9/2} - 37053_{11/2}$
7187.438	2	4	13909.330	$14101^{\circ}_{1/2} - 28011_{3/2}$	6932.458	2	5	14420.920	$15453^{\circ}_{7/2} - 29873_{7/2}$
7181.902	1	3	13920.051	$16564^{\circ}_{11/2} - 30484_{11/2}$	6929.689	2	3	14426.682	$23518^{\circ}_{7/2} - 37945_{5/2}$
7179.048	1	8	13925.585	$24463^{\circ}_{5/2} - 38389_{7/2}$	6921.432	2	20	14443.893	$21297^{\circ}_{5/2} - 35741_{5/2}$
7176.719	25	25	13930.104	$10379^{\circ}_{9/2} - 24309_{11/2}$	6917.036	3	3	14453.072	$26770^{\circ}_{11/2} - 41223_{11/2}$
7176.184	20	10	13931.143	$1521_{5/2} - 15453^{\circ}_{7/2}$	6915.001	2b	8	14457.325	$9061_{5/2} - 23518^{\circ}_{7/2}$
7172.987	1	2	13937.352	$25414^{\circ}_{11/2} - 39352_{11/2}$	6910.690	1	3	14466.344	$20989^{\circ}_{9/2} - 35456_{9/2}$
7166.514	0	8	13949.940	$35545_{9/2} - 49495^{\circ}_{9/2}$	6909.845	100	200	14468.113	$13468^{\circ}_{9/2} - 27937_{11/2}$
7165.988	20	10	13950.964	$9061_{5/2} - 23012^{\circ}_{3/2}$	6907.384	2	5	14473.268	$20080^{\circ}_{7/2} - 34553_{9/2}$
7160.764	1	3	13961.142	$19248^{\circ}_{5/2} - 33209_{7/2}$	6903.086	2	40	14482.279	$23697^{\circ}_{7/2} - 38179_{9/2}$
7157.067	0	5	13968.353	$20310^{\circ}_{3/2} - 34279_{7/2}$	6902.652	5	2	14483.190	$15305_{9/2} - 29788^{\circ}_{9/2}$
7151.197	3	3	13979.819	$31924^{\circ}_{11/2} - 45904_{9/2}$	6898.146	0	8	14492.650	$23187^{\circ}_{13/2} - 37679_{11/2}$
7148.191	5	5	13985.698	$9711_{7/2} - 23697^{\circ}_{7/2}$	6891.087	1	3	14507.496	$28243^{\circ}_{5/2} - 42751_{7/2}$
7145.793	3	2	13990.391	$6168^{\circ}_{7/2} - 20158_{5/2}$	6889.297	300	200	14511.265	$1521_{5/2} - 16033^{\circ}_{5/2}$
7140.454	10	15	14000.852	$13248_{9/2} - 27249^{\circ}_{7/2}$	6888.720	10	3	14512.481	$25188^{\circ}_{3/2} - 39700_{5/2}$
7139.861	5	25	14002.015	$17771^{\circ}_{11/2} - 31773_{9/2}$	6877.881	1	10	14535.351	$20989^{\circ}_{9/2} - 35525_{11/2}$
7132.509	4h		14016.448	$12472^{\circ}_{5/2} - 26488_{5/2}$	6873.051	10	3	14545.566	$0_{3/2} - 14545^{\circ}_{5/2}$
7124.286	0	5	14032.626	$14790^{\circ}_{7/2} - 28823_{5/2}$	6870.154	2	2	14551.699	$8460_{3/2} - 23012^{\circ}_{3/2}$
7120.334	1	2	14040.414	$20686^{\circ}_{5/2} - 34726_{7/2}$	6869.274	2	5	14553.564	$24309^{\circ}_{11/2} - 38862_{11/2}$
7119.977	0	5	14041.118	$27357^{\circ}_{9/2} - 41398_{9/2}$	6868.638	2	3	14554.911	$14790^{\circ}_{7/2} - 29345_{5/2}$
7113.983	8	10	14052.949	$8460_{3/2} - 22513^{\circ}_{5/2}$	6854.496	10	15	14584.940	$10855_{7/2} - 25440^{\circ}_{5/2}$
7109.371	0	5	14062.065	$15453^{\circ}_{7/2} - 29515_{9/2}$	6851.210	1	5	14591.935	$22685^{\circ}_{7/2} - 37277_{7/2}$
7100.507	150	75	14079.619	$8605_{5/2} - 22685^{\circ}_{7/2}$	6850.531	5	40	14593.382	$17983^{\circ}_{5/2} - 32576_{7/2}$

TABLE 3. *Classified lines of* Th II—Continued

Wavelength Å	Intensity		Wavenumber cm^{-1}	Classification	Wavelength Å	Intensity		Wavenumber cm^{-1}	Classification
	Lamp	Spark				Lamp	Spark		
6845.852	3	4	14603.356	$10379_{9/2} - 24982^{\circ}_{7/2}$	6628.169	1	3	15082.957	$14790^{\circ}_{7/2} - 29873_{7/2}$
6845.132	1	2	14604.892	$24463^{\circ}_{5/2} - 39068_{7/2}$	6622.127	1	5	15096.719	$20969^{\circ}_{7/2} - 36065_{5/2}$
6832.885	5	20	14631.069	$15242^{\circ}_{9/2} - 29873_{7/2}$	6619.940	200	200	15101.706	$4146_{7/2} - 19248^{\circ}_{5/2}$
6832.196	2	3	14632.544	$17121^{\circ}_{3/2} - 31754_{5/2}$	6619.616	3	40	15102.445	$22685^{\circ}_{7/2} - 37787_{7/2}$
6812.762	40	750	14674.285	$10572^{\circ}_{9/2} - 25246_{9/2}$	6617.054	25	50	15108.293	$12485^{\circ}_{7/2} - 27593_{5/2}$
6810.539	40	100	14679.075	$12570_{7/2} - 27249^{\circ}_{7/2}$	6616.863	2	2	15108.729	$12902^{\circ}_{3/2} - 28011_{3/2}$
6804.731	8	20	14691.603	$12902^{\circ}_{3/2} - 27593_{5/2}$	6615.482	1	10	15111.883	$26770^{\circ}_{11/2} - 41882_{13/2}$
6796.776	10	10	14708.798	$10673^{\circ}_{5/2} - 25381_{3/2}$	6615.345	3	5	15112.196	$20288^{\circ}_{11/2} - 35400_{13/2}$
6792.470	1	2	14718.123	$24982^{\circ}_{7/2} - 39700_{5/2}$	6611.194	3	15	15121.684	$17837^{\circ}_{7/2} - 32959_{3/2}$
6789.687	1	3	14724.155	$14790^{\circ}_{7/2} - 29515_{9/2}$	6610.306	1	8	15123.716	$19050^{\circ}_{3/2} - 34174_{5/2}$
6786.360	2	8	14731.374	$18118_{3/2} - 32850^{\circ}_{5/2}$	6605.406	200	150	15134.935	$4113_{5/2} - 19248^{\circ}_{5/2}$
6784.629	1	2	14735.132	$24132^{\circ}_{3/2} - 38867_{1/2}$	6604.106	2	20	15137.914	$24757^{\circ}_{9/2} - 39895_{9/2}$
6784.159	1	2	14736.153	$19594_{1/2} - 34330^{\circ}_{1/2}$	6601.537	5	2	15143.805	$9238^{\circ}_{9/2} - 24381_{7/2}$
6779.987	15	10	14745.221	$12219_{3/2} - 26965^{\circ}_{3/2}$	6601.124	5	3	15144.752	$0_{3/2} - 15144^{\circ}_{3/2}$
6771.323	3	3	14764.088	$22513^{\circ}_{5/2} - 37277_{7/2}$	6594.891	2	4	15159.066	$12472^{\circ}_{5/2} - 27631_{3/2}$
6770.101	150	100	14766.752	$8605_{5/2} - 23372^{\circ}_{3/2}$	6593.606	3	10	15162.020	$9711_{7/2} - 24873^{\circ}_{5/2}$
6769.385	3l	15	14768.314	$21297^{\circ}_{5/2} - 36065_{5/2}$	6592.555	0	8	15164.437	$31259_{5/2} - 46423^{\circ}_{3/2}$
6769.126	4h	5	14768.879	$12488^{\circ}_{9/2} - 27257_{7/2}$	6591.790	0	8	15166.197	$23697^{\circ}_{7/2} - 38863_{5/2}$
6768.164	1	3	14770.979	$19248^{\circ}_{5/2} - 34019_{3/2}$	6585.996	3	8	15179.539	$9202^{\circ}_{7/2} - 24381_{7/2}$
6767.945	2	5	14771.456	$12485^{\circ}_{7/2} - 27257_{7/2}$	6584.276	8	3	15183.505	$7828_{1/2} - 23012^{\circ}_{3/2}$
6766.341	8	10	14774.958	$7331^{\circ}_{5/2} - 22106_{5/2}$	6583.585	5	4	15185.098	$28587^{\circ}_{5/2} - 43772_{5/2}$
6760.888	25	25	14786.875	$12570_{7/2} - 27357^{\circ}_{9/2}$	6583.310	8	100	15185.733	$44807_{7/2} - 59993^{\circ}_{9/2}$
6757.310	0	5	14794.704	$24757^{\circ}_{9/2} - 39552_{9/2}$	6578.923	2	2	15195.859	$25027^{\circ}_{1/2} - 40222_{3/2}$
6756.540	100b	75	14796.390	$9585^{\circ}_{5/2} - 24381_{7/2}$	6577.651	20	100	15198.797	$15349^{\circ}_{11/2} - 30548_{13/2}$
6742.493	8	5	14827.216	$4146_{7/2} - 18973^{\circ}_{7/2}$	6576.800	0	5	15200.764	$18973^{\circ}_{7/2} - 34174_{5/2}$
6737.643	50	8	14837.889	$25440^{\circ}_{5/2} - 40278_{3/2}$	6573.986	2	10	15207.271	$15786_{5/2} - 30994^{\circ}_{7/2}$
6732.242	3	3	14849.793	$17771^{\circ}_{11/2} - 32620_{11/2}$	6573.482	2	10	15208.437	$16564^{\circ}_{11/2} - 31773_{9/2}$
6725.376	3	1	14864.953	$27357^{\circ}_{9/2} - 42222_{7/2}$	6572.883	5	40	15209.823	$15242^{\circ}_{9/2} - 30452_{9/2}$
6715.181	25	8	14887.521	$6244_{1/2} - 21131^{\circ}_{3/2}$	6570.097	1	2	15216.272	$34279_{7/2} - 49495^{\circ}_{9/2}$
6704.048	50	25	14912.244	$8460_{3/2} - 23372^{\circ}_{3/2}$	6569.628	8	50	15217.358	$12570_{7/2} - 27787^{\circ}_{9/2}$
				$11576^{\circ}_{3/2} - 26488_{5/2}$					
					6569.057	5	2	15218.681	$29431_{7/2} - 44650^{\circ}_{7/2}$
6703.883	10	8	14912.611	$8605_{5/2} - 23518^{\circ}_{7/2}$	6566.192	0	8	15225.321	$34270_{9/2} - 49495^{\circ}_{9/2}$
6703.348	5		14913.801	$22139^{\circ}_{9/2} - 37053_{11/2}$	6565.909	3	8	15225.978	$17983^{\circ}_{5/2} - 33209_{7/2}$
6700.487	2	5	14920.169	$22642^{\circ}_{9/2} - 37562_{11/2}$	6561.566	1	4	15236.055	$18118_{3/2} - 33354^{\circ}_{5/2}$
6692.717	100	25	14937.491	$4113_{5/2} - 19050^{\circ}_{3/2}$	6561.462	0	5	15236.297	$26963^{\circ}_{7/2} - 42200_{9/2}$
6664.956	4h	5	14999.708	$15453^{\circ}_{7/2} - 30452_{9/2}$	6561.244	0	8	15236.803	$24463^{\circ}_{5/2} - 39700_{5/2}$
6662.624	10h	8	15004.958	$15305_{9/2} - 30310^{\circ}_{11/2}$	6560.055	15	200	15239.565	$14275^{\circ}_{9/2} - 29515_{9/2}$
6659.496	1h	2	15012.006	$22834_{7/2} - 37846^{\circ}_{5/2}$	6559.088	2	50	15241.811	$15242^{\circ}_{9/2} - 30484_{11/2}$
6651.164	2	3	15030.812	$14484^{\circ}_{11/2} - 29515_{9/2}$	6558.576	1	8	15243.001	$24309^{\circ}_{11/2} - 39552_{9/2}$
6651.058	2	3	15031.051	$19248^{\circ}_{5/2} - 34279_{7/2}$	6550.542	8	5	15261.696	$1859_{3/2} - 17121^{\circ}_{3/2}$
6651.000	1	2	15031.182	$21297^{\circ}_{5/2} - 36328_{3/2}$	6544.596	2	8	15275.562	$17460^{\circ}_{5/2} - 32736_{7/2}$
6648.956	50	50	15035.803	$10379_{9/2} - 25414^{\circ}_{11/2}$	6540.141	4	1	15285.967	$24414^{\circ}_{3/2} - 39700_{5/2}$
6648.496	50	50	15036.843	$11725^{\circ}_{1/2} - 26762_{3/2}$	6535.645	1	5	15296.483	$18973^{\circ}_{7/2} - 34270_{9/2}$
6647.693	2	5l	15038.660	$12488^{\circ}_{9/2} - 27526_{9/2}$	6532.223	5	20	15304.496	$17272^{\circ}_{9/2} - 32576_{7/2}$
6646.542	40	50	15041.264	$12485^{\circ}_{7/2} - 27526_{9/2}$	6531.769	0	8	15305.560	$18973^{\circ}_{7/2} - 34279_{7/2}$
6644.661	200	150	15045.522	$9711_{7/2} - 24757^{\circ}_{9/2}$	6529.947	0	40	15309.830	$25414^{\circ}_{11/2} - 40724_{13/2}$
6643.374	1	8	15048.436	$22014^{\circ}_{11/2} - 37063_{9/2}$	6520.938	4	8	15330.981	$23187^{\circ}_{13/2} - 38517_{13/2}$
6637.032	1	2	15062.816	$9400_{5/2} - 24463^{\circ}_{5/2}$	6518.963	1	5	15335.626	$25188^{\circ}_{3/2} - 40523_{1/2}$
6633.453	10	20	15070.943	$9061_{5/2} - 24132^{\circ}_{3/2}$	6518.439	3	5	15336.859	$13250_{5/2} - 28587^{\circ}_{5/2}$
6631.806	1	3	15074.686	$36193^{\circ}_{9/2} - 51268_{7/2}$	6511.356	5	15	15353.542	$9061_{5/2} - 24414^{\circ}_{3/2}$

TABLE 3. *Classified lines of* Th II—Continued

Wavelength Å	Intensity		Wavenumber cm^{-1}	Classification	Wavelength Å	Intensity		Wavenumber cm^{-1}	Classification
	Lamp	Spark				Lamp	Spark		
6511.256	3	10	15353.778	$7001_{3/2}^{\circ} - 22355_{5/2}^{\circ}$	6381.966	1	10l	15664.822	$22014_{11/2}^{\circ} - 37679_{11/2}$
6510.997	5	15	15354.388	$8018_{3/2}^{\circ} - 23372_{5/2}^{\circ}$	6379.795	2	10	15670.153	$16906_{7/2}^{\circ} - 32576_{7/2}$
6503.997	4	2	15370.914	$14349_{1/2}^{\circ} - 29720_{3/2}^{\circ}$	6379.170	5	10	15671.688	$8460_{3/2}^{\circ} - 24132_{3/2}^{\circ}$
6503.898	5	2	15371.148	$31800_{7/2}^{\circ} - 47171_{9/2}$	6378.756	4	10	15672.705	$13250_{5/2}^{\circ} - 28923_{5/2}^{\circ}$
6503.512	50	75	15372.060	$11116_{7/2}^{\circ} - 26488_{5/2}^{\circ}$	6378.494	1	5	15673.349	$12570_{7/2}^{\circ} - 28243_{5/2}^{\circ}$
6501.819	0	8	15376.063	$26770_{11/2}^{\circ} - 42146_{11/2}$	6377.495	2	50	15675.804	$23187_{13/2}^{\circ} - 38862_{11/2}$
6493.531	3	3	15395.688	$30956_{9/2}^{\circ} - 46352_{7/2}$	6368.957	8	8	15696.818	$13818_{7/2}^{\circ} - 29515_{9/2}$
				$31928_{3/2}^{\circ} - 47324_{5/2}$	6363.271	8	5	15710.844	$0_{3/2}^{\circ} - 15710_{3/2}^{\circ}$
6491.269	0	8	15401.053	$37277_{7/2}^{\circ} - 52678_{5/2}^{\circ}$	6359.132	15	100	15721.070	$16033_{5/2}^{\circ} - 31754_{5/2}$
6490.583	5	10	15402.680	$9061_{5/2}^{\circ} - 24463_{5/2}^{\circ}$	6358.623	8	100	15722.328	$19880_{9/2}^{\circ} - 35602_{11/2}^{\circ}$
6485.370	4	5	15415.061	$6691_{3/2}^{\circ} - 22106_{5/2}$	6356.218	2	8	15728.277	$9711_{7/2}^{\circ} - 25440_{5/2}^{\circ}$
6481.226	0	5	15424.917	$30310_{11/2}^{\circ} - 45735_{11/2}$	6353.285	1	5	15735.538	$15236_{3/2}^{\circ} - 30972_{5/2}^{\circ}$
6480.607	3	10	15426.390	$15453_{7/2}^{\circ} - 30879_{7/2}$	6348.559	2	50	15747.252	$22642_{9/2}^{\circ} - 38389_{7/2}$
6479.558	0	5	15428.888	$30956_{9/2}^{\circ} - 46385_{7/2}$	6348.435	1	5	15747.559	$17983_{5/2}^{\circ} - 33730_{5/2}$
6478.940	2	10	15430.360	$20310_{5/2}^{\circ} - 35741_{5/2}$	6347.103	8	40	15750.864	$35156_{5/2}^{\circ} - 50907_{3/2}$
6471.345	0	8	15448.469	$32850_{3/2}^{\circ} - 48298_{7/2}$	6343.157	0	5	15760.663	$23697_{7/2}^{\circ} - 39458_{7/2}$
6471.205	20	50	15448.803	$12488_{9/2}^{\circ} - 27937_{11/2}$	6339.442	0	40	15769.898	$27357_{9/2}^{\circ} - 43127_{11/2}$
6470.289	1	4	15450.990	$18568_{1/2}^{\circ} - 34019_{3/2}$	6332.510	5	20	15787.161	$35741_{5/2}^{\circ} - 51528_{3/2}^{\circ}$
6468.090	0	5	15456.243	$25188_{3/2}^{\circ} - 40644_{5/2}$					$9400_{5/2}^{\circ} - 25188_{3/2}^{\circ}$
6467.558	2	1	15457.515	$26762_{3/2}^{\circ} - 42219_{5/2}^{\circ}$	6330.804	0	5	15791.415	$25607_{9/2}^{\circ} - 41398_{9/2}$
6462.622	200b	200b	15469.321	$29720_{3/2}^{\circ} - 45189_{5/2}$	6328.754	4	3	15796.530	$9585_{5/2}^{\circ} - 25381_{3/2}$
6455.482	1	5	15486.430	$17722_{9/2}^{\circ} - 33209_{7/2}$	6325.432	1	10	15804.826	$18214_{3/2}^{\circ} - 34019_{3/2}$
6450.369	15	10	15498.706	$26647_{13/2}^{\circ} - 42146_{11/2}$	6324.598	0	8	15806.910	$31924_{11/2}^{\circ} - 47731_{9/2}$
6448.726	3	8	15502.654	$7331_{5/2}^{\circ} - 22834_{7/2}$	6323.837	5	8	15808.813	$8605_{5/2}^{\circ} - 24414_{3/2}^{\circ}$
6438.372	2	8	15527.585	$13818_{7/2}^{\circ} - 29345_{5/2}$	6322.204	2	4	15812.896	$9061_{3/2}^{\circ} - 24873_{3/2}^{\circ}$
6432.950	1	4	15540.672	$12485_{7/2}^{\circ} - 28026_{5/2}$	6321.159	3	10	15815.510	$10673_{5/2}^{\circ} - 26488_{5/2}$
6430.229	2	10	15547.248	$22028_{15/2}^{\circ} - 37575_{13/2}$	6315.533	0	8	15829.599	$16906_{7/2}^{\circ} - 32736_{7/2}$
6428.524	1	2	15551.372	$25440_{5/2}^{\circ} - 40991_{3/2}$	6312.668	0	5	15836.783	$20288_{11/2}^{\circ} - 36125_{9/2}$
6427.011	0	8	15555.033	$26963_{7/2}^{\circ} - 42518_{7/2}$	6311.278	1	5	15840.271	$20969_{7/2}^{\circ} - 36809_{7/2}$
6424.809	5	200	15560.364	$22014_{11/2}^{\circ} - 37575_{13/2}$	6309.451	1	4	15844.858	$18816_{13/2}^{\circ} - 34661_{11/2}$
6423.402	1	2	15563.772	$28243_{5/2}^{\circ} - 43807_{3/2}$	6309.414	2	4	15844.951	$13250_{5/2}^{\circ} - 29095_{5/2}^{\circ}$
6421.673	1	3	15567.963	$20310_{5/2}^{\circ} - 35878_{7/2}$	6304.239	20	40	15857.957	$8605_{5/2}^{\circ} - 24463_{5/2}^{\circ}$
6421.417	0	8	15568.583	$24132_{3/2}^{\circ} - 39700_{5/2}$	6304.087	0	5	15858.340	$33637_{7/2}^{\circ} - 49495_{9/2}^{\circ}$
6416.097	25	75	15581.492	$9400_{5/2}^{\circ} - 24982_{7/2}^{\circ}$	6299.795	1	1	15869.144	$36809_{7/2}^{\circ} - 52678_{5/2}^{\circ}$
6408.869	0	8	15599.065	$30956_{9/2}^{\circ} - 46555_{11/2}$	6289.483	5	20	15895.162	$9711_{7/2}^{\circ} - 25607_{9/2}^{\circ}$
6408.193	2	4	15600.711	$1859_{3/2}^{\circ} - 17460_{5/2}^{\circ}$	6285.277	40	100	15905.799	$11725_{1/2}^{\circ} - 27631_{3/2}$
6406.278	4	3	15605.374	$37130_{1/2}^{\circ} - 52735_{3/2}$	6279.164	100	200	15921.283	$12902_{3/2}^{\circ} - 28823_{3/2}$
6405.870	0	8	15606.368	$22685_{7/2}^{\circ} - 38291_{7/2}$	6277.232	25	50	15926.183	$6213_{9/2}^{\circ} - 22139_{9/2}^{\circ}$
6404.390	0	8	15609.974	$24757_{9/2}^{\circ} - 40367_{9/2}$	6274.115	300	200	15934.096	$4146_{7/2}^{\circ} - 20080_{7/2}^{\circ}$
6402.932	3	8	15613.529	$13818_{7/2}^{\circ} - 29431_{7/2}$	6269.591	2	8	15945.593	$20120_{5/2}^{\circ} - 36065_{5/2}$
6401.729	0	40	15616.463	$25607_{9/2}^{\circ} - 41223_{11/2}$	6269.172	0	5	15946.659	$29788_{9/2}^{\circ} - 45735_{11/2}$
6399.797	0	10	15621.177	$20120_{5/2}^{\circ} - 35741_{5/2}$	6268.765	0	8	15947.694	$24463_{5/2}^{\circ} - 40411_{7/2}$
6388.731	0	8	15648.235	$22139_{9/2}^{\circ} - 37787_{7/2}$	6266.172	75	50	15954.294	$8460_{3/2}^{\circ} - 24414_{3/2}^{\circ}$
6388.136	2	8	15649.692	$22642_{9/2}^{\circ} - 38291_{7/2}$	6261.060	200	200	15967.320	$4113_{5/2}^{\circ} - 20080_{7/2}^{\circ}$
6387.865	2	15	15650.356	$22106_{5/2}^{\circ} - 37756_{7/2}^{\circ}$	6258.600	20	50	15973.596	$4146_{7/2}^{\circ} - 20120_{5/2}^{\circ}$
6387.473	0	8	15651.317	$15305_{9/2}^{\circ} - 30956_{9/2}^{\circ}$	6256.923	2	4	15977.877	$1859_{3/2}^{\circ} - 17837_{1/2}^{\circ}$
6386.386	0	40	15653.981	$24757_{9/2}^{\circ} - 40411_{7/2}$	6256.112	3	2	15979.948	$21297_{5/2}^{\circ} - 37277_{7/2}$
6384.094	5	5	15659.601	$22834_{7/2}^{\circ} - 38493_{5/2}^{\circ}$	6248.115	2	10	16000.401	$14484_{11/2}^{\circ} - 30484_{11/2}$
6383.342	5	40	15661.445	$17722_{9/2}^{\circ} - 33384_{9/2}$	6247.117	3	5	16002.957	$8378_{7/2}^{\circ} - 24381_{7/2}$
6383.222	5	40	15661.740	$14790_{7/2}^{\circ} - 30452_{9/2}$	6246.924	4	5	16003.451	$8460_{3/2}^{\circ} - 24463_{5/2}^{\circ}$

TABLE 3. *Classified lines of* Th II—Continued

Wavelength Å	Intensity		Wavenumber cm^{-1}	Classification	Wavelength Å	Intensity		Wavenumber cm^{-1}	Classification
	Lamp	Spark				Lamp	Spark		
6245.601	50	15	16006.841	$4113_{5/2} - 20120^{\circ}_{5/2}$	6163.249	1	10	16220.719	$22642^{\circ}_{9/2} - 38862_{11/2}$
6245.034	5	15	16008.295	$9238^{\circ}_{9/2} - 25246_{9/2}$	6159.840	0	10	16229.696	$24414^{\circ}_{5/2} - 40644_{5/2}$
6244.117	1	1	16010.646	$7001_{3/2} - 23012^{\circ}_{3/2}$	6154.119	0	8b	16244.784	$21297^{\circ}_{5/2} - 37542_{3/2}$
6243.103	0	5	16013.246	$15786_{5/2} - 31800^{\circ}_{7/2}$	6147.454	3	2	16262.396	$21682^{\circ}_{7/2} - 37945_{5/2}$
6241.694	2	4	16016.861	$12570_{7/2} - 28587^{\circ}_{5/2}$	6146.272	1	3	16265.523	$24309^{\circ}_{11/2} - 40574_{11/2}$
6241.408	2	8	16017.595	$11576^{\circ}_{3/2} - 27593_{5/2}$	6145.287	20	50	16268.131	$8605_{5/2} - 24873^{\circ}_{5/2}$
6239.543	2	2	16022.382	$33354^{\circ}_{5/2} - 49377_{7/2}$	6138.650	3	40	16285.719	$11725^{\circ}_{1/2} - 28011_{3/2}$
6239.083	3	15	16023.564	$15786_{5/2} - 31810^{\circ}_{5/2}$	6138.526	0	8	16286.048	$20158_{3/2} - 36444^{\circ}_{3/2}$
6238.970	1	5	16023.854	$12219_{3/2} - 28243^{\circ}_{5/2}$	6134.794	2	5	16295.955	$17983^{\circ}_{5/2} - 34279_{7/2}$
6238.244	0	5	16025.719	$22139^{\circ}_{9/2} - 38165_{7/2}$	6132.228	2	5	16302.774	$16906^{\circ}_{7/2} - 33209_{7/2}$
6235.793	1	8	16032.018	$16818_{7/2} - 32850^{\circ}_{5/2}$	6131.967	3	1	16303.468	$7828_{1/2} - 24132^{\circ}_{3/2}$
6235.346	2	2	16033.167	$0_{3/2} - 16033^{\circ}_{5/2}$	6125.749	25	150	16320.017	$15453^{\circ}_{7/2} - 31773_{9/2}$
6234.295	1	10	16035.870	$17983^{\circ}_{5/2} - 34019_{3/2}$	6124.675	1	3	16322.879	$22513^{\circ}_{5/2} - 38836_{3/2}$
6232.970	25	50	16039.279	$9400_{5/2} - 25440^{\circ}_{5/2}$	6122.337	0	15	16329.112	$18214^{\circ}_{3/2} - 34543_{5/2}$
6231.380	4	40	16043.371	$15710^{\circ}_{3/2} - 31754_{5/2}$	6120.563	250	300	16333.845	$14545^{\circ}_{5/2} - 30879_{7/2}$
6231.116	4	10	16044.051	$9202^{\circ}_{7/2} - 25246_{9/2}$	6113.969	3	10	16351.461	$12472^{\circ}_{5/2} - 28823_{5/2}$
6229.597	5	3	16047.963	$25440^{\circ}_{5/2} - 41488_{7/2}$	6112.838	150	200	16354.486	$1859_{3/2} - 18214^{\circ}_{3/2}$
6226.927	2	4	16054.844	$11576^{\circ}_{5/2} - 27631_{3/2}$	6108.922	3	2	16364.970	$17272^{\circ}_{9/2} - 33637_{7/2}$
6226.619	0	5	16055.638	$13818^{\circ}_{7/2} - 29873_{7/2}$	6108.411	10	20	16366.339	$26647^{\circ}_{13/2} - 43014_{13/2}$
6223.516	2	25	16063.643	$20989^{\circ}_{9/2} - 37053_{11/2}$	6106.613	5	4	16371.158	$7001_{3/2} - 23372^{\circ}_{3/2}$
6221.575	2	50	16068.655	$30310^{\circ}_{11/2} - 46378_{13/2}$	6104.572	300	200	16376.631	$8605_{5/2} - 24982^{\circ}_{7/2}$
6216.441	4	1	16081.925	$25594^{\circ}_{7/2} - 41676_{3/2}$	6103.640	15	50	16379.132	$9061_{5/2} - 25440^{\circ}_{5/2}$
6213.650	2	5	16089.149	$10673^{\circ}_{5/2} - 26762_{3/2}$	6100.578	1	1	16387.353	$22106_{5/2} - 38493^{\circ}_{5/2}$
6211.663	3	75	16094.295	$20969^{\circ}_{7/2} - 37063_{9/2}$	6099.804	3	5	16389.432	$27787^{\circ}_{9/2} - 44177_{11/2}$
6211.607	0	5	16094.441	$26424^{\circ}_{3/2} - 42518_{7/2}$	6099.083	100	200	16391.370	$10379_{9/2} - 26770^{\circ}_{11/2}$
6207.477	2	2	16105.149	$21682^{\circ}_{7/2} - 37787_{7/2}$	6097.194	10	10	16396.448	$8018_{3/2} - 24414^{\circ}_{3/2}$
6206.820	0	5	16106.853	$24463^{\circ}_{5/2} - 40570_{7/2}$	6094.023	4	4	16404.980	$34330^{\circ}_{1/2} - 50735_{3/2}$
6205.254	3	5	16110.918	$6244_{1/2} - 22355^{\circ}_{1/2}$					$13468^{\circ}_{9/2} - 29873_{7/2}$
6204.767	1	8	16112.183	$17272^{\circ}_{9/2} - 33384_{9/2}$	6092.033	8	8	16410.338	$21131^{\circ}_{3/2} - 37542_{3/2}$
6204.123	4	8	16113.855	$8018_{3/2} - 24132^{\circ}_{3/2}$					$25266^{\circ}_{7/2} - 41676_{3/2}$
									$11116^{\circ}_{7/2} - 27526_{9/2}$
6200.551	0	10	16123.138	$20686^{\circ}_{5/2} - 36809_{7/2}$					
6200.427	40	40	16123.460	$1859_{3/2} - 17983^{\circ}_{3/2}$	6090.816	8	8	16413.617	$8460_{3/2} - 24873^{\circ}_{5/2}$
6199.054	2	5	16127.031	$9061_{5/2} - 25188^{\circ}_{3/2}$	6090.109	15	25	16415.523	$24309^{\circ}_{11/2} - 40724_{13/2}$
6196.396	5	10	16133.949	$6700^{\circ}_{9/2} - 22834_{7/2}$	6087.576	0	8	16422.353	$21682^{\circ}_{7/2} - 38105_{5/2}$
6194.315	0	5	16139.369	$16818_{7/2} - 32957^{\circ}_{7/2}$	6087.387	3	3	16422.863	$20158_{5/2} - 36581^{\circ}_{3/2}$
6193.978	0	5	16140.247	$25188^{\circ}_{5/2} - 41328_{5/2}$	6087.262	75	300	16423.200	$15349^{\circ}_{11/2} - 31773_{9/2}$
6193.858	50	200	16140.560	$11116^{\circ}_{7/2} - 27257_{7/2}$	6085.998	4	5	16426.611	$22642^{\circ}_{9/2} - 39068_{7/2}$
6189.417	0	50	16152.141	$22139^{\circ}_{9/2} - 38291_{7/2}$	6085.430	2	40	16428.144	$29788^{\circ}_{9/2} - 46216_{11/2}$
6188.051	20b	150	16155.707	$30223^{\circ}_{13/2} - 46378_{13/2}$	6085.257	40	75	16428.611	$6213_{9/2} - 22642^{\circ}_{9/2}$
6184.737	10b	8	16164.363	$4146_{7/2} - 20310^{\circ}_{5/2}$	6078.968	40	8	16445.607	$8018_{3/2} - 24463^{\circ}_{5/2}$
6184.469	2	15	16165.064	$22014^{\circ}_{11/2} - 38179_{9/2}$	6078.588	5	8	16446.636	$27357^{\circ}_{9/2} - 43803_{7/2}$
6184.390	8	10	16165.270	$23187^{\circ}_{13/2} - 39352_{11/2}$	6077.358	15	10	16449.964	$11576^{\circ}_{3/2} - 28026_{5/2}$
6179.847	8	50	16177.154	$14275^{\circ}_{9/2} - 30452_{9/2}$	6076.639	3	3	16451.911	$27357^{\circ}_{9/2} - 43809_{9/2}$
6178.885	3	2	16179.672	$27593_{5/2} - 43773^{\circ}_{7/2}$	6076.195	8	5	16453.113	$18568^{\circ}_{1/2} - 35021_{3/2}$
6178.549	0	8	16180.552	$24463^{\circ}_{5/2} - 40644_{5/2}$	6073.710	3	3	16459.844	$24463^{\circ}_{5/2} - 40923_{5/2}$
6172.044	1	2	16197.606	$4113_{5/2} - 20310^{\circ}_{5/2}$	6073.100	100	150	16461.498	$1521_{5/2} - 17983^{\circ}_{5/2}$
6168.580	2	2	16206.701	$31800^{\circ}_{7/2} - 48006_{9/2}$	6071.415	2	2	16466.066	$24757^{\circ}_{9/2} - 41223_{11/2}$
6167.907	0	5	16208.470	$20120^{\circ}_{5/2} - 36328_{3/2}$	6070.892	3	4	16467.485	$25414^{\circ}_{11/2} - 41882_{13/2}$
				$23730^{\circ}_{9/2} - 39939_{11/2}$	6070.034	4	10	16469.812	$13250_{5/2} - 29720^{\circ}_{3/2}$
6167.059	0	5	16210.698	$29095^{\circ}_{5/2} - 45306_{3/2}$	6068.043	2	2	16475.216	$22106_{5/2} - 38581^{\circ}_{5/2}$

TABLE 3. *Classified lines of* Th II—Continued

Wavelength Å	Intensity		Wavenumber cm^{-1}	Classification	Wavelength Å	Intensity		Wavenumber cm^{-1}	Classification
	Lamp	Spark				Lamp	Spark		
6067.077	20	100	16477.839	$16906^{\circ}_{7/2} - 33384_{9/2}$	6015.424	50	200	16619.329	$15305_{9/2} - 31924^{\circ}_{11/2}$
6066.496	40	200	16479.417	$26647^{\circ}_{13/2} - 43127_{11/2}$	6011.349	25	20	16630.595	$19248^{\circ}_{5/2} - 35878_{7/2}$
6066.330	4h	3	16479.868	$30101^{\circ}_{7/2} - 46581_{5/2}$	6009.113	5	8	16636.783	$23730^{\circ}_{9/2} - 40367_{9/2}$
6063.355	2	2	16487.954	$31810^{\circ}_{5/2} - 48298_{7/2}$	6007.591	4	8	16640.998	$24757^{\circ}_{9/2} - 41398_{9/2}$
6063.068	8	15	16488.735	$25188^{\circ}_{3/2} - 41676_{3/2}$	5998.655	3	8	16665.787	$6168^{\circ}_{7/2} - 22834_{7/2}$
6062.614	15	40	16489.969	$22028^{\circ}_{15/2} - 38517_{13/2}$	5993.268	3	8	16680.767	$37679_{11/2} - 54360^{\circ}_{9/2}$
6062.431	3	2	16490.467	$21297^{\circ}_{5/2} - 37787_{7/2}$	5991.711	2	2	16685.102	$10572^{\circ}_{9/2} - 27257_{7/2}$
6061.486	3	25	16493.038	$19248^{\circ}_{5/2} - 35741_{5/2}$	5990.792	0	20	16687.661	$30223^{\circ}_{15/2} - 46910_{13/2}$
6060.230	3	2	16496.456	$20969^{\circ}_{7/2} - 37465_{5/2}$					$31924^{\circ}_{11/2} - 48612_{13/2}$
6059.975	4		16497.150	$21682^{\circ}_{7/2} - 38179_{9/2}$	5990.267	3	40	16689.124	$20120^{\circ}_{5/2} - 36809_{7/2}$
6059.535	2	3	16498.348	$20310^{\circ}_{5/2} - 36809_{7/2}$	5989.987	1	4	16689.904	$20989^{\circ}_{9/2} - 37679_{11/2}$
6058.612	15	20	16500.862	$12219_{3/2} - 28720^{\circ}_{3/2}$	5989.893	1	8	16690.166	$21131^{\circ}_{3/2} - 37821_{3/2}$
6058.273	3	2	16501.785	$30101^{\circ}_{7/2} - 46603_{5/2}$	5989.200	0	5	16692.097	$15236_{3/2} - 31928^{\circ}_{3/2}$
6058.180	15	20	16502.038	$10855_{7/2} - 27357^{\circ}_{9/2}$	5989.045	400s	500	16692.529	$1521_{3/2} - 18214^{\circ}_{3/2}$
6055.160	3	3	16510.269	$31810^{\circ}_{5/2} - 48320_{5/2}$	5985.204	2	8	16703.242	$12219_{3/2} - 28923^{\circ}_{5/2}$
				$26586^{\circ}_{3/2} - 43096_{5/2}$	5983.991	4	75	16706.627	$21682^{\circ}_{7/2} - 38389_{7/2}$
6054.535	2	4	16511.973	$22355^{\circ}_{7/2} - 38867_{1/2}$	5983.378	5	15	16708.339	$1859_{3/2} - 18568^{\circ}_{1/2}$
6052.173	2	1	16518.417	$23697^{\circ}_{7/2} - 40216_{5/2}$	5981.880	15	20	16712.523	$9711_{7/2} - 26424^{\circ}_{5/2}$
6049.925	8	10	16524.555	$21297^{\circ}_{5/2} - 37821_{3/2}$	5981.385	1	5	16713.906	$17460^{\circ}_{5/2} - 34174_{5/2}$
6049.771	15	25	16524.975	$12570_{7/2} - 29095^{\circ}_{5/2}$	5978.069	5	15	16723.177	$22139^{\circ}_{9/2} - 38862_{11/2}$
6048.174	3	1	16529.339	$39861^{\circ}_{5/2} - 56391_{5/2}$	5976.437	3	3	16727.744	$8460_{3/2} - 25188^{\circ}_{3/2}$
6045.467	2	2	16536.740	$16818_{7/2} - 33354^{\circ}_{7/2}$	5976.118	1	4	16728.637	$20080^{\circ}_{7/2} - 36809_{7/2}$
6044.430	100	200	16539.577	$4146_{7/2} - 20686^{\circ}_{5/2}$	5975.404	5	50	16730.636	$16906^{\circ}_{7/2} - 33637_{7/2}$
6042.962	25	50	16543.595	$16033^{\circ}_{5/2} - 32576_{7/2}$					$24757^{\circ}_{9/2} - 41488_{7/2}$
6041.628	5h	3	16547.248	$17722^{\circ}_{9/2} - 34270_{9/2}$	5972.789	4l	75	16737.960	$24309^{\circ}_{11/2} - 41047_{9/2}$
6040.120	3	10	16551.379	$30310^{\circ}_{11/2} - 46861_{11/2}$	5972.436	15	15	16738.950	$27357^{\circ}_{9/2} - 44096_{9/2}$
6039.665	2	1	16552.626	$37945_{5/2} - 54497^{\circ}_{7/2}$	5961.970	25	50	16768.334	$9720^{\circ}_{7/2} - 26488_{5/2}$
6038.308	3	2	16556.346	$17722^{\circ}_{9/2} - 34279_{7/2}$	5960.372	4d	40	16772.830	$22685^{\circ}_{7/2} - 39458_{7/2}$
6036.088	2	3	16562.435	$27403^{\circ}_{3/2} - 43965_{1/2}$	5958.072	3	20	16779.304	$20686^{\circ}_{5/2} - 37465_{5/2}$
				$22834_{7/2} - 39396^{\circ}_{7/2}$	5957.736	5	2	16780.251	$42518_{7/2} - 59299^{\circ}_{5/2}$
6034.545	10	10	16566.670	$8460_{3/2} - 25027^{\circ}_{1/2}$	5957.091	2	15	16782.067	$25440^{\circ}_{5/2} - 42222_{7/2}$
6034.139	1	4	16567.785	$35602^{\circ}_{11/2} - 52170_{11/2}$	5956.813	2	5	16782.851	$17771^{\circ}_{11/2} - 34553_{9/2}$
6032.665	0	8	16571.833	$18973^{\circ}_{7/2} - 35545_{9/2}$	5955.952	2	10	16785.277	$25414^{\circ}_{11/2} - 42200_{9/2}$
6032.432	0	5	16572.473	$20989^{\circ}_{9/2} - 37562_{11/2}$	5952.350	5	8	16795.434	$22355^{\circ}_{1/2} - 39150_{3/2}$
6032.320	25b	15	16572.780	$4113_{5/2} - 20686^{\circ}_{5/2}$	5950.888	2	2	16799.560	$35878_{7/2} - 52678^{\circ}_{5/2}$
6031.911	10	25	16573.904	$15236_{3/2} - 31810^{\circ}_{5/2}$	5948.557	3	3	16806.143	$8460_{3/2} - 25266^{\circ}_{1/2}$
6030.808	1	2	16576.935	$24414^{\circ}_{3/2} - 40991_{3/2}$	5946.922	1	1	16810.764	$28011_{3/2} - 44821^{\circ}_{5/2}$
6028.863	10	5	16582.283	$8605_{3/2} - 25188^{\circ}_{3/2}$	5945.616	1	5	16814.456	$24873^{\circ}_{3/2} - 41688_{7/2}$
6028.273	10	3	16583.906	$18816^{\circ}_{13/2} - 35400_{13/2}$	5945.012	1	2	16816.165	$22642^{\circ}_{9/2} - 39458_{7/2}$
6028.240	2	10	16583.997	$10673^{\circ}_{5/2} - 27257_{7/2}$	5944.112	1	5	16818.711	$17460^{\circ}_{5/2} - 34279_{7/2}$
6027.952	2	2	16584.789	$10379_{9/2} - 26963^{\circ}_{7/2}$	5944.054	2	8	16818.875	$20969^{\circ}_{7/2} - 37787_{7/2}$
6027.481	5s	2	16586.085	$7828_{1/2} - 24414^{\circ}_{3/2}$	5942.792	40	50	16822.447	$4146_{7/2} - 20969^{\circ}_{7/2}$
6025.616	4	5	16591.219	$20686^{\circ}_{5/2} - 37277_{7/2}$	5942.120	3	40	16824.349	$16906^{\circ}_{7/2} - 33730_{5/2}$
6024.934	8	10	16593.097	$25607^{\circ}_{9/2} - 42200_{9/2}$	5938.571	20	40	16834.403	$8605_{3/2} - 25440^{\circ}_{5/2}$
6022.223	8	10	16600.566	$30310^{\circ}_{11/2} - 46910_{13/2}$	5936.602	1	15	16839.987	$23730^{\circ}_{9/2} - 40570_{7/2}$
6022.149	4	4	16600.771	$22139^{\circ}_{9/2} - 38740_{11/2}$	5934.714	1	25	16845.344	$26963^{\circ}_{7/2} - 43809_{9/2}$
6021.409	40	200	16602.811	$22014^{\circ}_{11/2} - 38617_{9/2}$	5932.701	0	5	16851.060	$20989^{\circ}_{9/2} - 37840_{9/2}$
6019.215	1	2	16608.862	$22834_{7/2} - 39443^{\circ}_{9/2}$	5932.128	4	10	16852.687	$13248_{9/2} - 30101^{\circ}_{7/2}$
6018.998	20	100	16609.461	$15144^{\circ}_{3/2} - 31754_{3/2}$	5930.957	2	10	16856.015	$20686^{\circ}_{5/2} - 37542_{3/2}$
6015.769	1	1	16618.376	$26626^{\circ}_{1/2} - 43244_{3/2}$	5929.479	8	40	16860.216	$12485^{\circ}_{7/2} - 29345_{5/2}$

530-326 OL - 74 - 7

TABLE 3. *Classified lines of* Th II—Continued

Wavelength Å	Intensity		Wavenumber cm^{-1}	Classification	Wavelength Å	Intensity		Wavenumber cm^{-1}	Classification
	Lamp	Spark				Lamp	Spark		
5929.141	1	8	16861.178	$30310^{\circ}_{11/2} - 47171_{9/2}$	5849.999	1	4	17089.283	$24309^{\circ}_{11/2} - 41398_{9/2}$
5927.949	1	15	16864.568	$24463^{\circ}_{3/2} - 41328_{5/2}$	5849.077	2	10	17091.976	$21297^{\circ}_{5/2} - 38389_{7/2}$
5926.933	3	8	16867.459	$8378^{\circ}_{7/2} - 25246_{9/2}$	5838.945	75	20	17121.635	$0_{3/2} - 17121^{\circ}_{3/2}$
5926.780	3	10	16867.894	$18118_{3/2} - 34986^{\circ}_{3/2}$	5837.485	0	5	17125.917	$23518^{\circ}_{7/2} - 40644_{5/2}$
5924.389	3	150	16874.702	$32620_{11/2} - 49495^{\circ}_{9/2}$	5836.674	2	2	17128.297	$6244_{1/2} - 23372^{\circ}_{3/2}$
5918.808	15	5	16890.613	$17771^{\circ}_{11/2} - 34661_{11/2}$	5835.881	5	5	17130.624	$7001_{3/2} - 24132^{\circ}_{3/2}$
5916.347	1	4	16897.639	$17121^{\circ}_{3/2} - 34019_{3/2}$	5832.941	1	1	17139.259	$27249^{\circ}_{7/2} - 44388_{5/2}$
5914.387	200	200	16903.239	$9585^{\circ}_{5/2} - 26488_{5/2}$	5830.492	10	20	17146.457	$27357^{\circ}_{9/2} - 44503_{7/2}$
5912.104	4	5	16909.766	$11116^{\circ}_{7/2} - 28026_{5/2}$	5822.522	10	5	17169.928	$8018_{3/2} - 25188^{\circ}_{3/2}$
5911.360	5	5	16911.894	$25440^{\circ}_{5/2} - 42352_{5/2}$	5820.381	15	25	17176.244	$16033^{\circ}_{5/2} - 33209_{7/2}$
5910.507	5	40	16914.335	$24309^{\circ}_{11/2} - 41223_{11/2}$	5820.168	5	10	17176.872	$9585^{\circ}_{5/2} - 26762_{3/2}$
5910.041	5	2	16915.669	$32957^{\circ}_{7/2} - 49873_{5/2}$	5817.733	15	5	17184.061	$4113_{5/2} - 21297^{\circ}_{5/2}$
5908.403	25l	50	16920.358	$31924^{\circ}_{11/2} - 48844_{9/2}$	5817.326	10	5	17185.264	$9400_{5/2} - 26586^{\circ}_{3/2}$
5908.244	5	8	16920.814	$10673^{\circ}_{5/2} - 27593_{5/2}$	5816.994	8	10	17186.244	$26586^{\circ}_{3/2} - 43772_{5/2}$
5906.316	5	40	16926.337	$16033^{\circ}_{5/2} - 32959_{3/2}$	5815.422	100	150	17190.890	$1859_{3/2} - 19050^{\circ}_{3/2}$
5902.560	0	8b	16937.108	$36583^{\circ}_{7/2} - 53520_{9/2}$	5812.107	1	1	17200.695	$27249^{\circ}_{7/2} - 44450_{9/2}$
				$35741_{5/2} - 52678^{\circ}_{5/2}$	5810.973	8	10	17204.052	$23012^{\circ}_{3/2} - 40216_{5/2}$
5901.995	3	20	16938.729	$17722^{\circ}_{9/2} - 34661_{11/2}$	5809.430	8	5	17208.621	$14545^{\circ}_{5/2} - 31754_{5/2}$
5901.754	0	5	16939.421	$27787^{\circ}_{9/2} - 44727_{11/2}$	5808.978	4	5	17209.960	$22685^{\circ}_{7/2} - 39895_{9/2}$
5899.407	5	50	16946.160	$12485^{\circ}_{7/2} - 29431_{7/2}$	5808.079	20	50	17212.624	$22139^{\circ}_{9/2} - 39352_{11/2}$
5896.361	15	40	16954.914	$10572^{\circ}_{9/2} - 27526_{9/2}$	5806.279	40	40	17217.960	$12570_{7/2} - 29788^{\circ}_{9/2}$
5893.476	10	50	16963.214	$14790^{\circ}_{7/2} - 31754_{5/2}$	5804.589	1	2	17222.973	$30101^{\circ}_{7/2} - 47324_{5/2}$
5888.260	15	15	16978.240	$10379_{9/2} - 27357^{\circ}_{9/2}$	5802.239	25	50	17229.948	$25414^{\circ}_{11/2} - 42644_{13/2}$
5887.815	1	5	16979.523	$25266^{\circ}_{7/2} - 42246_{1/2}$	5801.813	10	15	17231.214	$20310^{\circ}_{5/2} - 37542_{3/2}$
5886.741	8	50	16982.621	$20080^{\circ}_{7/2} - 37063_{9/2}$	5798.910	2	3	17239.840	$24982^{\circ}_{7/2} - 42222_{7/2}$
5886.346	5	10	16983.761	$13468^{\circ}_{9/2} - 30452_{9/2}$	5796.417	100	100	17247.254	$11576^{\circ}_{3/2} - 28823_{5/2}$
5884.178	2	8	16990.018	$19050^{\circ}_{3/2} - 36040_{1/2}$	5795.963	15	20	17248.605	$15710^{\circ}_{3/2} - 32959_{3/2}$
5881.414	2	5	16998.003	$17272^{\circ}_{9/2} - 34270_{9/2}$	5794.377	20	25	17253.326	$22642^{\circ}_{9/2} - 39895_{9/2}$
5879.479	5h	15	17003.597	$17722^{\circ}_{9/2} - 34726_{7/2}$	5793.209	5	15	17256.805	$29095^{\circ}_{5/2} - 46352_{7/2}$
5879.049	0	15	17004.841	$35165^{\circ}_{13/2} - 52170_{11/2}$	5790.136	3	4	17265.963	$17460^{\circ}_{5/2} - 34726_{7/2}$
5878.279	8		17007.068	$17272^{\circ}_{9/2} - 34279_{7/2}$	5788.193	10	15	17271.759	$23372^{\circ}_{3/2} - 40644_{5/2}$
5875.501	2		17015.109	$22685^{\circ}_{7/2} - 39700_{5/2}$	5787.541	10	10	17273.705	$20288^{\circ}_{11/2} - 37562_{11/2}$
5875.279	1	4	17015.752	$13468^{\circ}_{9/2} - 30484_{11/2}$	5786.678	15	10	17276.281	$14349_{1/2} - 31625^{\circ}_{1/2}$
5874.348	20	10	17018.449	$4113_{5/2} - 21131^{\circ}_{3/2}$	5785.498	3	8	17279.805	$42336_{3/2} - 59616^{\circ}_{3/2}$
5872.604	15	40	17023.503	$9400_{5/2} - 26424^{\circ}_{3/2}$	5784.866	75b	50	17281.692	$17272^{\circ}_{9/2} - 34553_{9/2}$
5872.312	0	5	17024.349	$24463^{\circ}_{5/2} - 41488_{7/2}$	5784.373	4	5	17283.165	$15453^{\circ}_{7/2} - 32736_{7/2}$
5871.447	2	4	17026.857	$12488^{\circ}_{9/2} - 29515_{9/2}$	5783.757	1	1	17285.006	$26488_{5/2} - 43773^{\circ}_{7/2}$
5870.554	25	150	17029.447	$12485^{\circ}_{7/2} - 29515_{9/2}$	5783.205	15l	200	17286.656	$20288^{\circ}_{11/2} - 37575_{13/2}$
5867.621	2	5	17037.960	$17983^{\circ}_{5/2} - 35021_{3/2}$	5782.499	1	1	17288.766	$14484^{\circ}_{11/2} - 31773_{9/2}$
5867.348	0	5	17038.752	$26770^{\circ}_{11/2} - 43809_{9/2}$	5782.047	5	10	17290.118	$22106_{5/2} - 39396^{\circ}_{7/2}$
5864.882	1	4	17045.916	$21682^{\circ}_{7/2} - 38728_{5/2}$	5778.082	15h	15	17301.983	$20989^{\circ}_{9/2} - 38291_{7/2}$
5860.879	1h	1	17057.559	$22028^{\circ}_{5/2} - 39085_{13/2}$	5777.094	10	4	17304.942	$6213_{9/2} - 23518^{\circ}_{7/2}$
5859.666	50	150	17061.090	$13818^{\circ}_{7/2} - 30879_{7/2}$	5775.795	1	2	17308.834	$33354^{\circ}_{5/2} - 50663_{5/2}$
5859.524	15	40	17061.503	$13248_{9/2} - 30310^{\circ}_{11/2}$	5775.035	2	5	17311.111	$25440^{\circ}_{5/2} - 42751_{7/2}$
5856.379	2	5	17070.665	$22014^{\circ}_{11/2} - 39085_{13/2}$	5773.204	3	4	17316.602	$23730^{\circ}_{9/2} - 41047_{9/2}$
5855.032	2	8	17074.593	$21297^{\circ}_{5/2} - 38372_{3/2}$	5772.529	4	4	17318.626	$22139^{\circ}_{9/2} - 39458_{7/2}$
5853.762	3	4	17078.297	$13406^{\circ}_{13/2} - 30484_{11/2}$	5771.144	20	25	17322.783	$20969^{\circ}_{7/2} - 38291_{7/2}$
5853.059	5	20	17080.348	$19248^{\circ}_{5/2} - 36328_{3/2}$	5770.145	15b	50	17325.782	$26770^{\circ}_{11/2} - 44096_{9/2}$
5852.188	8	15	17082.890	$17460^{\circ}_{5/2} - 34543_{5/2}$	5767.459	4	2	17333.851	$15242^{\circ}_{9/2} - 32576_{7/2}$
5850.258	1	8	17088.526	$37756^{\circ}_{7/2} - 54845_{9/2}$	5766.470	3	8	17336.824	$31353^{\circ}_{3/2} - 48689_{3/2}$

TABLE 3. *Classified lines of* Th II—Continued

Wavelength Å	Intensity		Wavenumber cm^{-1}	Classification	Wavelength Å	Intensity		Wavenumber cm^{-1}	Classification
	Lamp	Spark				Lamp	Spark		
5766.101	20	10	17337.933	$10189^{\circ}_{11/2}-27526_{9/2}$	5709.102	3	3	17511.031	$20310^{\circ}_{5/2}-37821_{3/2}$
5765.947	10	15	17338.396	$27787^{\circ}_{9/2}-45126_{9/2}$	5707.100	300	200	17517.174	$6213_{9/2}-23730^{\circ}_{9/2}$
5765.697	1	2	17339.148	$26626^{\circ}_{1/2}-43965_{1/2}$	5706.145	5	8	17520.105	$25607^{\circ}_{9/2}-43127_{11/2}$
5764.766	1	2	17341.948	$30956^{\circ}_{9/2}-48298_{7/2}$	5703.942	50	40	17526.872	$18214^{\circ}_{3/2}-35741_{5/2}$
5763.645	10	15	17345.321	$20120^{\circ}_{5/2}-37465_{5/2}$	5703.268	10	20	17528.943	$1521_{3/2}-19050^{\circ}_{3/2}$
5762.237	3	5	17349.559	$23697^{\circ}_{7/2}-41047_{9/2}$	5700.914	200b	200	17536.181	$4146_{7/2}-21682^{\circ}_{7/2}$
5762.096	3b	5	17349.984	$22834_{7/2}-40184^{\circ}_{7/2}$	5700.698	100	100	17536.846	$9720^{\circ}_{7/2}-27257_{7/2}$
5761.018	4	3	17353.230	$10673^{\circ}_{5/2}-28026_{5/2}$	5700.521	0	10	17537.390	$22014^{\circ}_{11/2}-39552_{9/2}$
5758.920	10	5	17359.552	$7828_{1/2}-25188^{\circ}_{3/2}$	5700.453	100	100	17537.599	$9711_{7/2}-27249^{\circ}_{7/2}$
5757.648	5	4	17363.387	$9061_{5/2}-26424^{\circ}_{5/2}$	5700.060	3	3	17538.809	$21297^{\circ}_{5/2}-38836_{3/2}$
5757.551	5	5	17363.680	$16906^{\circ}_{7/2}-34270_{9/2}$	5699.370	10	20	17540.932	$25414^{\circ}_{11/2}-42955_{9/2}$
5757.099	15	10	17365.043	$10572^{\circ}_{9/2}-27937_{11/2}$	5699.220	5	10	17541.394	$27357^{\circ}_{9/2}-44898_{7/2}$
5754.551	50	40	17372.732	$16906^{\circ}_{7/2}-34279_{7/2}$	5696.084	2	2	17551.051	$23372^{\circ}_{3/2}-40923_{5/2}$
5752.303	5	8	17379.521	$26424^{\circ}_{5/2}-43803_{7/2}$	5692.936	2	4	17560.756	$17460^{\circ}_{5/2}-35021_{3/2}$
5751.173	2	4	17382.936	$29788^{\circ}_{9/2}-47171_{9/2}$	5692.853	5	5	17561.012	$19248^{\circ}_{3/2}-36809_{7/2}$
5750.556	25	20	17384.801	$20080^{\circ}_{7/2}-37465_{5/2}$	5691.804	2	2	17564.248	$9400_{5/2}-26965^{\circ}_{5/2}$
5750.268	15	10	17385.671	$12488^{\circ}_{9/2}-29873_{7/2}$	5691.628	15	100	17564.792	$27257_{7/2}-44821^{\circ}_{5/2}$
5750.117	2	3	17386.128	$27403^{\circ}_{3/2}-44789_{1/2}$	5691.092	20	10	17566.446	$21297^{\circ}_{5/2}-38863_{5/2}$
5749.582	40	50	17387.746	$23187^{\circ}_{13/2}-40574_{11/2}$	5688.931	20	10	17573.119	$24309^{\circ}_{11/2}-41882_{13/2}$
5749.383	200	200d	17388.348	$1859_{3/2}-19248^{\circ}_{5/2}$	5687.682	10	20c	17576.978	$31800^{\circ}_{7/2}-49377_{7/2}$
5749.157	3	8	17389.031	$24757^{\circ}_{9/2}-42146_{11/2}$	5684.171	2h	2	17587.834	$17837^{\circ}_{1/2}-35425_{1/2}$
5749.012	15	15	17389.470	$17272^{\circ}_{9/2}-34661_{11/2}$	5682.436	5	5	17593.204	$22355^{\circ}_{1/2}-39948_{1/2}$
5747.521	15	15	17393.981	$16818_{7/2}-34212^{\circ}_{5/2}$	5681.249	8	8	17596.880	$21131^{\circ}_{3/2}-38728_{5/2}$
5745.676	75	100	17399.566	$20989^{\circ}_{9/2}-38389_{7/2}$	5680.489	2	2	17599.234	$25414^{\circ}_{11/2}-43014_{13/2}$
5743.810	2	2	17405.219	$23518^{\circ}_{7/2}-40923_{5/2}$	5680.211	8	5	17600.096	$24309^{\circ}_{11/2}-41909_{9/2}$
5742.651	10	5	17408.731	$10379_{9/2}-27787^{\circ}_{9/2}$	5678.920	15	20	17604.097	$31810^{\circ}_{3/2}-49414_{3/2}$
5742.084	150	150	17410.450	$13468^{\circ}_{9/2}-30879_{7/2}$					$16033^{\circ}_{5/2}-33637_{7/2}$
5741.379	15	25	17412.588	$22139^{\circ}_{9/2}-39552_{9/2}$	5676.763	1	3	17610.786	$29095^{\circ}_{5/2}-46706_{7/2}$
5741.170	150	100	17413.222	$7001_{3/2}-24414^{\circ}_{3/2}$	5675.019	75b	25	17616.198	$4490^{\circ}_{5/2}-22106_{5/2}$
5738.819	3	4	17420.356	$20969^{\circ}_{7/2}-38389_{7/2}$	5674.119	2	2	17618.992	$23372^{\circ}_{3/2}-40991_{3/2}$
5738.515	1	2	17421.278	$30310^{\circ}_{11/2}-47731_{9/2}$	5670.666	5	3	17629.720	$17771^{\circ}_{11/2}-35400_{13/2}$
5738.306	25d	100b	17421.913	$17121^{\circ}_{3/2}-34543_{5/2}$	5669.842	20	25	17632.283	$23012^{\circ}_{3/2}-40644_{5/2}$
5738.271	1	10b	17422.019	$20120^{\circ}_{5/2}-37542_{3/2}$	5669.232	1	1	17634.180	$20310^{\circ}_{5/2}-37945_{5/2}$
				$8018_{3/2}-25440^{\circ}_{5/2}$	5668.890	3	3	17635.243	$15324^{\circ}_{1/2}-32959_{3/2}$
5736.142	4	3	17428.485	$15786_{5/2}-33215^{\circ}_{3/2}$	5668.792	1	1	17635.548	$39443^{\circ}_{9/2}-57078_{9/2}$
5734.526	1	2	17433.397	$31924^{\circ}_{11/2}-49357_{11/2}$	5668.340	20	15	17636.955	$16906^{\circ}_{7/2}-34543_{5/2}$
5732.977	200	200	17438.107	$17727_{11/2}-35165^{\circ}_{13/2}$	5665.772	2	2	17644.949	$24873^{\circ}_{5/2}-42518_{7/2}$
5732.043	8	8	17440.948	$13818^{\circ}_{7/2}-31259_{5/2}$	5665.625	100	100	17645.406	$9711_{7/2}-27357^{\circ}_{9/2}$
5731.466	10	15	17442.704	$24757^{\circ}_{9/2}-42200_{9/2}$	5664.999	25	15	17647.356	$16906^{\circ}_{7/2}-34553_{9/2}$
5726.151	2l	1	17458.894	$30994^{\circ}_{7/2}-48453_{7/2}$	5663.441	0	20	17652.211	$15305_{9/2}-32957^{\circ}_{7/2}$
5725.579	50	75	17460.639	$0_{3/2}-17460^{\circ}_{5/2}$	5661.551	1	1	17658.104	$28923^{\circ}_{5/2}-46581_{5/2}$
5725.011	40	40	17462.371	$7001_{3/2}-24463^{\circ}_{5/2}$	5660.015	15	15	17662.896	$19912^{\circ}_{13/2}-37575_{13/2}$
5721.655	1	1	17472.613	$18568^{\circ}_{1/2}-36040_{1/2}$	5657.295	2	3	17671.388	$28026_{5/2}-45697^{\circ}_{5/2}$
5721.618	2	1	17472.726	$24463^{\circ}_{5/2}-41936_{3/2}$	5657.183	20	20	17671.738	$9585^{\circ}_{5/2}-27257_{7/2}$
5719.847	3	5	17478.136	$24873^{\circ}_{5/2}-42352_{5/2}$	5654.607	1	2	17679.788	$26770^{\circ}_{11/2}-44450_{9/2}$
5717.328	5	10	17485.837	$29095^{\circ}_{5/2}-46581_{5/2}$	5654.022	50	40	17681.617	$6700^{\circ}_{9/2}-24381_{7/2}$
5714.894	8	10	17493.284	$15242^{\circ}_{9/2}-32736_{7/2}$	5653.915	1	2	17681.952	$39396^{\circ}_{7/2}-57078_{9/2}$
5713.828	1	2	17496.548	$30956^{\circ}_{9/2}-48453_{7/2}$	5653.209	2	3	17684.160	$21682^{\circ}_{7/2}-39366_{5/2}$
5713.519	3	2	17497.494	$14275^{\circ}_{9/2}-31773_{9/2}$	5652.904	50	100	17685.114	$17771^{\circ}_{11/2}-35456_{9/2}$
5712.588	40	20	17500.345	$12219_{3/2}-29720^{\circ}_{3/2}$	5652.664	4	5	17685.865	$20686^{\circ}_{5/2}-38372_{3/2}$

TABLE 3. *Classified lines of* Th II—Continued

Wavelength Å	Intensity		Wavenumber cm^{-1}	Classification	Wavelength Å	Intensity		Wavenumber cm^{-1}	Classification
	Lamp	Spark				Lamp	Spark		
5652.433	2	3	17686.588	$28011_{3/2} - 45697^{\circ}_{5/2}$	5611.775	3	2	17814.728	$15144^{\circ}_{3/2} - 32959_{3/2}$
5652.164	5	4	17687.430	$20158_{5/2} - 37846^{\circ}_{5/2}$	5611.144	1	2	17816.731	$36193^{\circ}_{9/2} - 54010_{7/2}$
5651.446	2	2	17689.677	$19880_{9/2} - 37569^{\circ}_{9/2}$	5609.300	20	15	17822.588	$17722^{\circ}_{9/2} - 35545_{9/2}$
5649.218	2	8	17696.653	$30310^{\circ}_{11/2} - 48006_{9/2}$	5608.100	8	10	17826.402	$18214^{\circ}_{5/2} - 36040_{1/2}$
5648.862	20	20	17697.769	$16033^{\circ}_{5/2} - 33730_{5/2}$	5606.539	8	10	17831.365	$24414^{\circ}_{3/2} - 42246_{1/2}$
5647.878	1	1	17700.852	$23697^{\circ}_{7/2} - 41398_{9/2}$	5605.247	15	10	17835.475	$18973^{\circ}_{7/2} - 36809_{7/2}$
5647.108	2	1	17703.266	$20686^{\circ}_{5/2} - 38389_{7/2}$	5604.666	15	20	17837.324	$24309^{\circ}_{11/2} - 42146_{11/2}$
5646.359	8	5	17705.614	$16564^{\circ}_{11/2} - 34270_{9/2}$	5604.514	100	40	17837.808	$0_{3/2} - 17837^{\circ}_{1/2}$
5645.894	100b	200d	17707.072	$11116^{\circ}_{7/2} - 28823_{5/2}$	5601.136	3	1	17848.566	$9400_{5/2} - 27249^{\circ}_{7/2}$
5645.856	20b	25b	17707.191	$20080^{\circ}_{7/2} - 37787_{7/2}$	5599.300	15b	15	17854.418	$20310^{\circ}_{5/2} - 38165_{7/2}$
5645.084	2	2	17709.613	$22513^{\circ}_{5/2} - 40222_{3/2}$	5596.152	10	15	17864.462	$20080^{\circ}_{7/2} - 37945_{5/2}$
5644.231	1	1	17712.289	$25414^{\circ}_{11/2} - 43127_{11/2}$	5595.610	50	75	17866.192	$17727_{11/2} - 35593^{\circ}_{9/2}$
5643.596	1	1	17714.282	$26586^{\circ}_{3/2} - 44300_{3/2}$	5594.583	20	25	17869.472	$21682^{\circ}_{7/2} - 39552_{9/2}$
5640.081	50	75	17725.322	$22642^{\circ}_{9/2} - 40367_{9/2}$	5593.612	100	50	17872.574	$7001_{3/2} - 24873^{\circ}_{5/2}$
5639.849	4	8	17726.051	$22685^{\circ}_{7/2} - 40411_{7/2}$	5593.480	15	25	17872.995	$20989^{\circ}_{9/2} - 38862_{11/2}$
5639.746	300	300	17726.375	$1521_{3/2} - 19248^{\circ}_{5/2}$	5593.266	25	15	17873.679	$9720^{\circ}_{7/2} - 27593_{5/2}$
5637.947	3	2	17732.031	$21131^{\circ}_{3/2} - 38863_{5/2}$	5592.796	5	5	17875.181	$17727_{11/2} - 35602^{\circ}_{11/2}$
				$10855_{7/2} - 28587^{\circ}_{5/2}$	5592.510	8	10	17876.095	$26424^{\circ}_{5/2} - 44300_{3/2}$
5635.409	2	8	17740.017	$37756^{\circ}_{7/2} - 55496_{9/2}$	5592.321	15	15	17876.700	$27249^{\circ}_{7/2} - 45126_{9/2}$
5634.221	15	15	17743.757	$13250_{5/2} - 30994^{\circ}_{7/2}$					$19880_{9/2} - 37756^{\circ}_{7/2}$
5633.649	20b	25	17745.559	$13248_{9/2} - 30994^{\circ}_{7/2}$	5592.125	3	5	17877.326	$24873^{\circ}_{5/2} - 42751_{7/2}$
5632.872	25l	20	17748.007	$10189^{\circ}_{11/2} - 27937_{11/2}$	5591.270	3	4	17880.060	$23518^{\circ}_{7/2} - 41398_{9/2}$
5632.036	15	25	17750.641	$20989^{\circ}_{9/2} - 38740_{11/2}$	5591.124	1	2	17880.527	$22014^{\circ}_{11/2} - 39895_{9/2}$
5631.111	3	8	17753.557	$35165^{\circ}_{13/2} - 52918_{13/2}$	5589.671	15	15	17885.174	$22685^{\circ}_{7/2} - 40570_{7/2}$
5630.922	8	4	17754.153	$17771^{\circ}_{11/2} - 35525_{11/2}$	5588.867	40	20	17887.747	$6244_{1/2} - 24132^{\circ}_{3/2}$
5630.589	3	3	17755.203	$22106_{5/2} - 39861^{\circ}_{5/2}$	5588.662	4	8l	17888.404	$30956^{\circ}_{9/2} - 48844_{9/2}$
5630.411	10	40	17755.764	$22139^{\circ}_{9/2} - 39895_{9/2}$	5587.857	25	25	17890.981	$24309^{\circ}_{11/2} - 42200_{9/2}$
5630.231	5	4	17756.332	$15453^{\circ}_{7/2} - 33209_{7/2}$	5587.734	75	10	17891.374	$20288^{\circ}_{11/2} - 38179_{9/2}$
5629.856	2	4	17757.514	$23730^{\circ}_{9/2} - 41488_{7/2}$	5586.658	8	10	17894.820	$20969^{\circ}_{7/2} - 38863_{5/2}$
5629.731	2	1	17757.909	$17983^{\circ}_{5/2} - 35741_{5/2}$	5586.453	40	20	17895.477	$17983^{\circ}_{5/2} - 35878_{7/2}$
5629.174	3	4	17759.666	$20969^{\circ}_{7/2} - 38728_{5/2}$	5585.610	20	4	17898.178	$22513^{\circ}_{5/2} - 40411_{7/2}$
5628.963	1	2	17760.331	$18568^{\circ}_{1/2} - 36328_{3/2}$	5585.121	4	1	17899.745	$17121^{\circ}_{3/2} - 35021_{3/2}$
5628.624	3	5	17761.401	$24757^{\circ}_{9/2} - 42518_{7/2}$	5584.161	15	75	17902.822	$9061_{5/2} - 26963^{\circ}_{7/2}$
5628.568	1	2	17761.578	$37277_{7/2} - 55038^{\circ}_{9/2}$	5583.758	100	15	17904.114	$9061_{5/2} - 26965^{\circ}_{3/2}$
5626.734	40	50	17767.367	$19912^{\circ}_{13/2} - 37679_{11/2}$	5583.073	2	15	17906.311	$38179_{9/2} - 56086^{\circ}_{9/2}$
5626.256	5	15	17768.877	$27357^{\circ}_{9/2} - 45126_{9/2}$	5581.283	20	20	17912.053	$23187^{\circ}_{13/2} - 41099_{15/2}$
				$24982^{\circ}_{7/2} - 42751_{7/2}$	5577.905	25	40	17922.901	$22355^{\circ}_{1/2} - 40278_{3/2}$
5626.085	3b	4b	17769.416	$22642^{\circ}_{9/2} - 40411_{7/2}$	5577.489	20	40	17924.238	$22014^{\circ}_{11/2} - 39939_{11/2}$
5626.057	10b	25b	17769.505	$11576^{\circ}_{5/2} - 29345_{5/2}$	5576.510	2	4	17927.384	$35593^{\circ}_{7/2} - 53520_{9/2}$
5625.495	1	1	17771.280	$21297^{\circ}_{5/2} - 39068_{7/2}$	5575.264	2	4	17931.391	$15453^{\circ}_{7/2} - 33384_{9/2}$
5624.146	10	10	17775.543	$21682^{\circ}_{7/2} - 39458_{7/2}$	5574.876	5b	50	17932.639	$22642^{\circ}_{9/2} - 40574_{11/2}$
5620.918	15	10	17785.751	$14790^{\circ}_{7/2} - 32576_{7/2}$	5573.873	40	25	17935.866	$13818^{\circ}_{7/2} - 31754_{5/2}$
5619.422	2	2	17790.486	$23697^{\circ}_{7/2} - 41488_{7/2}$	5568.000	300b	150	17954.784	$13818^{\circ}_{7/2} - 31773_{9/2}$
5615.728	75	100	17802.188	$17722^{\circ}_{9/2} - 35525_{11/2}$	5567.395	20	40	17956.735	$26770^{\circ}_{11/2} - 44727_{11/2}$
5615.635	15	20	17802.483	$26586^{\circ}_{3/2} - 44388_{5/2}$	5566.730	3	3	17958.880	$22685^{\circ}_{7/2} - 40644_{5/2}$
5615.008	10	8	17804.471	$24132^{\circ}_{5/2} - 41936_{3/2}$	5565.105	5	4	17964.124	$8460_{3/2} - 26424^{\circ}_{5/2}$
5614.515	5	1	17806.034	$36687^{\circ}_{5/2} - 54493_{5/2}$	5565.005	50	75	17964.447	$12488^{\circ}_{9/2} - 30452_{9/2}$
5614.337	3	5	17806.599	$25440^{\circ}_{5/2} - 43246_{7/2}$	5564.371	50	50	17966.494	$15242^{\circ}_{9/2} - 33209_{7/2}$
5614.187	3	4	17807.074	$29095^{\circ}_{5/2} - 46902_{5/2}$	5564.201	200	200	17967.043	$12485^{\circ}_{7/2} - 30452_{9/2}$
5613.471	1	4	17809.346	$33215^{\circ}_{3/2} - 51024_{3/2}$	5563.375	5	4	17969.710	$23518^{\circ}_{7/2} - 41488_{7/2}$

TABLE 3. *Classified lines of* Th II—Continued

Wavelength Å	Intensity		Wavenumber cm^{-1}	Classification	Wavelength Å	Intensity		Wavenumber cm^{-1}	Classification
	Lamp	Spark				Lamp	Spark		
5560.556	6	5	17978.820	$15236_{3/2} - 33215^{\circ}_{3/2}$	5495.806	75	75	18190.639	$14545^{\circ}_{5/2} - 32736_{7/2}$
5560.339	5	8	17979.522	$23012^{\circ}_{3/2} - 40991_{3/2}$	5494.556	50	50	18194.777	$19912^{\circ}_{13/2} - 38107_{15/2}$
5560.054	15	10	17980.443	$8605_{5/2} - 26586^{\circ}_{3/2}$	5493.931	2	4	18196.847	$25607^{\circ}_{9/2} - 43803_{7/2}$
5559.141	8	2	17983.396	$0_{3/2} - 17983^{\circ}_{5/2}$	5493.478	3	4	18198.348	$24757^{\circ}_{9/2} - 42955_{9/2}$
5557.311	75	75	17989.318	$16564^{\circ}_{11/2} - 34553_{9/2}$	5492.332	40	20	18202.145	$25607^{\circ}_{9/2} - 43809_{9/2}$
5556.146	40	10	17993.090	$4146_{7/2} - 22139^{\circ}_{9/2}$	5492.061	20	25	18203.043	$26586^{\circ}_{3/2} - 44789_{1/2}$
5555.115	2	1	17996.429	$12488^{\circ}_{9/2} - 30484_{11/2}$					$17837^{\circ}_{1/2} - 36040_{1/2}$
5551.515	3	4	18008.099	$33354^{\circ}_{5/2} - 51362_{5/2}$	5491.528	20	25	18204.810	$24132^{\circ}_{3/2} - 42336_{5/2}$
5551.370	100	75	18008.570	$9585^{\circ}_{5/2} - 27593_{5/2}$	5489.623	10	10	18211.127	$20080^{\circ}_{7/2} - 38291_{7/2}$
5548.516	20	25	18017.833	$21682^{\circ}_{7/2} - 39700_{5/2}$	5489.452	3	3	18211.694	$23697^{\circ}_{7/2} - 41909_{9/2}$
5547.824	3	2	18020.080	$15710^{\circ}_{3/2} - 33730_{5/2}$	5488.922	50	40	18213.453	$6168^{\circ}_{7/2} - 24381_{7/2}$
5546.490	20	20	18024.414	$20080^{\circ}_{7/2} - 38105_{5/2}$	5488.622	75	15	18214.448	$0_{3/2} - 18214^{\circ}_{3/2}$
5545.323	4	5	18028.207	$38863_{5/2} - 56892^{\circ}_{5/2}$	5488.518	2	3	18214.793	$28720^{\circ}_{3/2} - 46935_{3/2}$
5545.051	5	3	18029.092	$19248^{\circ}_{5/2} - 37277_{7/2}$	5487.426	1	3	18218.418	$29788^{\circ}_{9/2} - 48006_{9/2}$
5544.405	4	3	18031.192	$14545^{\circ}_{5/2} - 32576_{7/2}$	5487.133	2	4	18219.391	$30101^{\circ}_{7/2} - 48320_{5/2}$
5543.672	2	2	18033.576	$33902^{\circ}_{7/2} - 51935_{5/2}$	5486.917	20	40	18220.108	$24132^{\circ}_{3/2} - 42352_{5/2}$
5543.375	5	5	18034.543	$15349^{\circ}_{11/2} - 33384_{9/2}$	5486.180	2	2	18222.556	$24873^{\circ}_{5/2} - 43096_{5/2}$
5542.766	50	75	18036.524	$23187^{\circ}_{13/2} - 41223_{11/2}$	5484.615	3b	2	18227.756	$22139^{\circ}_{9/2} - 40367_{9/2}$
5542.472	5	5	18037.481	$31800^{\circ}_{7/2} - 49837_{9/2}$	5484.268	15h	15	18228.909	$29095^{\circ}_{3/2} - 47324_{5/2}$
5540.102	8	4	18045.197	$20120^{\circ}_{5/2} - 38165_{7/2}$	5484.138	150	200	18229.341	$11116^{\circ}_{7/2} - 29345_{5/2}$
5539.909	300	3000	18045.826	$9585^{\circ}_{5/2} - 27631_{3/2}$	5482.406	20	75	18235.100	$21131^{\circ}_{3/2} - 39366_{5/2}$
5538.500	50	20	18050.416	$7331^{\circ}_{5/2} - 25381_{3/2}$	5481.961	20	20	18236.580	$18816^{\circ}_{13/2} - 37053_{11/2}$
5537.663	1	1	18053.145	$29095^{\circ}_{3/2} - 47148_{3/2}$	5481.477	75	100	18238.190	$22685^{\circ}_{7/2} - 40923_{5/2}$
5537.131	75	50	18054.879	$9202^{\circ}_{7/2} - 27257_{7/2}$	5480.886	50	25	18240.157	$10855_{7/2} - 29095^{\circ}_{5/2}$
5533.146	20	10	18067.882	$10855_{7/2} - 28923^{\circ}_{5/2}$	5479.680	15	15	18244.171	$18568^{\circ}_{1/2} - 36812_{1/2}$
5532.179	15h	15	18071.040	$20686^{\circ}_{5/2} - 38757_{3/2}$	5479.310	1	2	18245.403	$24982^{\circ}_{7/2} - 43227_{5/2}$
5530.693	50	150	18075.896	$9711_{7/2} - 27787^{\circ}_{9/2}$	5477.380	2	1	18251.832	$20120^{\circ}_{5/2} - 38372_{3/2}$
5529.782	10	8	18078.874	$20989^{\circ}_{9/2} - 39068_{7/2}$	5477.046	50	50	18252.945	$17272^{\circ}_{9/2} - 35525_{11/2}$
5529.651	5	8	18079.302	$26424^{\circ}_{5/2} - 44503_{7/2}$	5474.856	50	20	18260.246	$1859_{3/2} - 20120^{\circ}_{5/2}$
5528.001	50	50	18084.698	$20080^{\circ}_{7/2} - 38165_{7/2}$	5473.616	3	4	18264.383	$24982^{\circ}_{7/2} - 43246_{7/2}$
5524.219	100	100	18097.079	$16564^{\circ}_{11/2} - 34661_{11/2}$	5473.404	25	40	18265.090	$7001_{3/2} - 25266^{\circ}_{1/2}$
5523.431	20	15	18099.661	$20969^{\circ}_{7/2} - 39068_{7/2}$	5471.387	50	75	18271.824	$22139^{\circ}_{9/2} - 40411_{7/2}$
5520.753	10	5	18108.441	$28243^{\circ}_{5/2} - 46352_{7/2}$					$18118_{3/2} - 36390^{\circ}_{3/2}$
5520.341	15	8	18109.792	$8378^{\circ}_{7/2} - 26488_{5/2}$	5470.937	15	20	18273.327	$17272^{\circ}_{9/2} - 35545_{9/2}$
5518.722	15	15	18115.105	$15786_{3/2} - 33902^{\circ}_{7/2}$	5469.708	2	2	18277.432	$20158_{5/2} - 38436^{\circ}_{3/2}$
5517.791	10	8	18118.161	$15236_{3/2} - 33354^{\circ}_{5/2}$	5468.742	20	15	18280.661	$17460^{\circ}_{5/2} - 35741_{3/2}$
5514.743	10	15	18128.175	$26424^{\circ}_{5/2} - 44552_{5/2}$	5466.685	2	2	18287.539	$24463^{\circ}_{3/2} - 42751_{7/2}$
5514.438	4	8	18129.178	$28026_{5/2} - 46155^{\circ}_{5/2}$	5466.266	4	2	18288.941	$9238^{\circ}_{9/2} - 27526_{9/2}$
5513.871	8	15	18131.042	$22513^{\circ}_{5/2} - 40644_{5/2}$	5464.784	5	5	18293.901	$19248^{\circ}_{5/2} - 37542_{3/2}$
5512.699	20	15	18134.897	$38757_{3/2} - 56892^{\circ}_{5/2}$	5462.611	150	150	18301.178	$14275^{\circ}_{9/2} - 32576_{7/2}$
5512.191	8h	5	18136.568	$14484^{\circ}_{11/2} - 32620_{11/2}$	5461.890	20	25	18303.594	$18973^{\circ}_{7/2} - 37277_{7/2}$
5510.680	50	40	18141.541	$15242^{\circ}_{9/2} - 33384_{9/2}$	5461.735	100	100	18304.113	$13468^{\circ}_{9/2} - 31773_{9/2}$
5507.948	50s	25	18150.539	$10673^{\circ}_{5/2} - 28823_{5/2}$	5461.151	10	8	18306.071	$9720^{\circ}_{7/2} - 28026_{5/2}$
5506.334	3	2	18155.859	$17722^{\circ}_{9/2} - 35878_{7/2}$	5458.403	4	2	18315.287	$11116^{\circ}_{7/2} - 29431_{7/2}$
5504.964	3	8	18160.378	$31800^{\circ}_{7/2} - 49960_{7/2}$	5458.105	20	40	18316.287	$23012^{\circ}_{3/2} - 41328_{5/2}$
5502.034	2	4	18170.049	$23518^{\circ}_{7/2} - 41688_{7/2}$	5453.355	2	3	18332.240	$25440^{\circ}_{5/2} - 43772_{5/2}$
5501.944	50	50	18170.346	$6244_{1/2} - 24414^{\circ}_{3/2}$	5452.518	5	4	18335.055	$20158_{3/2} - 38493^{\circ}_{5/2}$
5501.543	25	25	18171.670	$20120^{\circ}_{5/2} - 38291_{7/2}$	5452.334	15	20	18335.673	$24309^{\circ}_{11/2} - 42644_{13/2}$
5497.752	15	15	18184.200	$15453^{\circ}_{7/2} - 33637_{7/2}$	5449.895	20	10	18343.879	$4490^{\circ}_{5/2} - 22834_{7/2}$
5496.464	2	1	18188.461	$9061_{5/2} - 27249^{\circ}_{7/2}$	5449.479	200	200	18345.279	$14275^{\circ}_{9/2} - 32620_{11/2}$

TABLE 3. *Classified lines of* Th II—Continued

Wavelength Å	Intensity		Wavenumber cm^{-1}	Classification	Wavelength Å	Intensity		Wavenumber cm^{-1}	Classification
	Lamp	Spark				Lamp	Spark		
5448.568	4h	5	18348.347	$28587^{\circ}_{5/2} - 46935_{3/2}$	5396.538	8	20	18525.248	$20310^{\circ}_{5/2} - 38836_{3/2}$
5447.313	50	20	18352.574	$22014^{\circ}_{11/2} - 40367_{9/2}$	5393.113	15b	75	18537.013	$20080^{\circ}_{7/2} - 38617_{9/2}$
5446.021	25	8	18356.928	$12902^{\circ}_{3/2} - 31259_{5/2}$	5392.569	200	75	18538.883	$4146_{7/2} - 22685^{\circ}_{7/2}$
5445.295	4	2	18359.375	$28243^{\circ}_{5/2} - 46603_{5/2}$	5392.356	20	40	18539.615	$19248^{\circ}_{5/2} - 37787_{7/2}$
				$8605_{5/2} - 26965^{\circ}_{5/2}$	5391.942	2	3	18541.038	$25266^{\circ}_{1/2} - 43807_{3/2}$
5444.792	5	4	18361.071	$27249^{\circ}_{7/2} - 45610_{5/2}$	5391.071	20	10	18544.034	$6213_{9/2} - 24757^{\circ}_{9/2}$
5444.589	2	4	18361.756	$22685^{\circ}_{7/2} - 41047_{9/2}$	5390.658	1	4	18545.454	$31924^{\circ}_{11/2} - 50470_{9/2}$
5444.371	3	4	18362.491	$20989^{\circ}_{9/2} - 39352_{11/2}$	5390.458	150b	75	18546.142	$6700^{\circ}_{9/2} - 25246_{9/2}$
5443.999	3	5	18363.746	$25440^{\circ}_{5/2} - 43803_{7/2}$	5390.197	10	25	18547.040	$27357^{\circ}_{9/2} - 45904_{9/2}$
5443.114	100	50	18366.731	$4146_{7/2} - 22513^{\circ}_{5/2}$	5389.913	2	2	18548.018	$22106_{5/2} - 40654^{\circ}_{5/2}$
5442.943	1	3	18367.308	$25440^{\circ}_{5/2} - 43807_{3/2}$	5389.453	50h	50	18549.601	$16906^{\circ}_{7/2} - 35456_{9/2}$
5441.298	5	15	18372.861	$24873^{\circ}_{5/2} - 43246_{7/2}$	5389.126	15	50	18550.726	$27249^{\circ}_{7/2} - 45800_{5/2}$
5437.385	50	50	18386.083	$12570_{7/2} - 30956^{\circ}_{9/2}$	5388.903	20	15	18551.494	$13248_{9/2} - 31800^{\circ}_{7/2}$
5436.499	20	75	18389.079	$30223^{\circ}_{13/2} - 48612_{13/2}$	5386.783	15	10	18558.795	$1521_{5/2} - 20080^{\circ}_{7/2}$
5435.893	150	200	18391.129	$12488^{\circ}_{9/2} - 30879_{7/2}$	5386.476	8b	10b	18559.853	$22014^{\circ}_{11/2} - 40574_{11/2}$
5435.722	20	25	18391.708	$9202^{\circ}_{7/2} - 27593_{5/2}$	5386.425	8g	10b	18560.029	$13250_{5/2} - 31810^{\circ}_{5/2}$
5435.126	100	100	18393.725	$12485^{\circ}_{7/2} - 30879_{7/2}$	5385.731	8	10	18562.420	$20989^{\circ}_{9/2} - 39552_{9/2}$
5434.947	25	50	18394.330	$25414^{\circ}_{11/2} - 43809_{9/2}$	5384.031	50	15	18568.281	$0_{3/2} - 18568^{\circ}_{1/2}$
				$15242^{\circ}_{9/2} - 33637_{7/2}$	5383.899	2	1	18568.736	$21131^{\circ}_{3/2} - 39700_{5/2}$
5433.699	75	75	18398.555	$11116^{\circ}_{7/2} - 29515_{9/2}$	5383.746	2	2	18569.264	$18118_{3/2} - 36687^{\circ}_{5/2}$
5433.287	20	8	18399.950	$4113_{5/2} - 22513^{\circ}_{5/2}$	5382.923	100	50	18572.103	$4113_{5/2} - 22685^{\circ}_{7/2}$
5432.580	10	25	18402.345	$17722^{\circ}_{9/2} - 36125_{9/2}$	5380.211	8	20	18581.465	$22642^{\circ}_{9/2} - 41223_{11/2}$
5431.774	10	25	18405.076	$22642^{\circ}_{9/2} - 41047_{9/2}$	5379.700	8	15	18583.229	$20969^{\circ}_{7/2} - 39552_{9/2}$
5431.418	8	4	18406.282	$8018_{3/2} - 26424^{\circ}_{5/2}$	5379.374	2	10	18584.356	$25188^{\circ}_{3/2} - 43772_{5/2}$
5428.961	10	20	18414.612	$19050^{\circ}_{3/2} - 37465_{5/2}$	5375.767	100	100	18596.825	$15305_{9/2} - 33902^{\circ}_{7/2}$
5428.048	8	10	18417.709	$20310^{\circ}_{5/2} - 38728_{5/2}$	5375.349	200	100	18598.271	$1521_{5/2} - 20120^{\circ}_{5/2}$
5426.526	1	1	18422.875	$20158_{5/2} - 38581^{\circ}_{5/2}$	5373.223	8	15	18605.630	$19912^{\circ}_{13/2} - 38517_{13/2}$
5426.261	15	15	18423.775	$12570_{7/2} - 30994^{\circ}_{7/2}$	5373.148	4	8	18605.890	$20158_{5/2} - 38764^{\circ}_{7/2}$
5425.678	300	300	18425.754	$9585^{\circ}_{5/2} - 28011_{5/2}$	5372.938	20	50l	18606.617	$17272^{\circ}_{9/2} - 35878_{7/2}$
5424.793	3	2	18428.760	$27787^{\circ}_{9/2} - 46216_{11/2}$	5372.456	10	8	18608.286	$8018_{3/2} - 26626^{\circ}_{1/2}$
5424.135	50	75	18430.996	$22139^{\circ}_{9/2} - 40570_{7/2}$	5372.397	2	3	18608.491	$20120^{\circ}_{5/2} - 38728_{5/2}$
5421.837	75	75	18438.808	$7001_{3/2} - 25440^{\circ}_{5/2}$	5369.170	40h	50	18619.675	$17121^{\circ}_{3/2} - 35741_{5/2}$
5421.205	10	10	18440.957	$9585^{\circ}_{5/2} - 28026_{5/2}$	5364.363	5	10	18636.359	$22355^{\circ}_{1/2} - 40991_{3/2}$
5419.658	3	4	18446.221	$20310^{\circ}_{5/2} - 38757_{3/2}$	5364.175	20	50	18637.013	$20120^{\circ}_{5/2} - 38757_{3/2}$
5415.434	200b	200	18460.609	$33215^{\circ}_{3/2} - 51676_{3/2}$	5363.611	25	40	18638.972	$16906^{\circ}_{7/2} - 35545_{9/2}$
				$14275^{\circ}_{9/2} - 32736_{7/2}$	5362.257	20	20	18643.679	$8605_{5/2} - 27249^{\circ}_{7/2}$
5414.530	40h	40	18463.691	$15710^{\circ}_{3/2} - 34174_{5/2}$	5361.766	2	4	18645.386	$26965^{\circ}_{3/2} - 45610_{5/2}$
5413.805	20	25	18466.163	$17727_{11/2} - 36193^{\circ}_{9/2}$	5361.409	75	100	18646.627	$24309^{\circ}_{11/2} - 42955_{9/2}$
5413.128	3	4	18468.473	$20989^{\circ}_{9/2} - 39458_{7/2}$	5360.998	15	15	18648.057	$20080^{\circ}_{7/2} - 38728_{5/2}$
5412.808	15	50	18469.565	$23730^{\circ}_{9/2} - 42200_{9/2}$	5357.832	5	2	18659.076	$41328_{5/2} - 59987^{\circ}_{3/2}$
5411.005	2	10	18475.719	$33354^{\circ}_{5/2} - 51830_{7/2}$	5357.446	1	3	18660.421	$33902^{\circ}_{7/2} - 52562_{7/2}$
5410.258	10b	15	18478.270	$22513^{\circ}_{5/2} - 40991_{3/2}$	5356.471	10h	10	18663.817	$14545^{\circ}_{5/2} - 33209_{7/2}$
5407.078	2b	2	18489.137	$25607^{\circ}_{9/2} - 44096_{9/2}$	5356.199	3b	10	18664.765	$23012^{\circ}_{3/2} - 41676_{3/2}$
5406.336	20	50	18491.674	$23730^{\circ}_{9/2} - 42222_{7/2}$	5354.747	2	5	18669.826	$31800^{\circ}_{7/2} - 50470_{9/2}$
				$18973^{\circ}_{7/2} - 37465_{5/2}$	5352.334	3b	3	18678.243	$13250_{5/2} - 31928^{\circ}_{5/2}$
5405.207	10	3	18495.537	$4146_{7/2} - 22642^{\circ}_{9/2}$	5351.614	4	10	18680.756	$20686^{\circ}_{5/2} - 39366_{5/2}$
5402.780	1	8	18503.845	$34174_{3/2} - 52678^{\circ}_{5/2}$	5351.452	8	40	18681.321	$25414^{\circ}_{11/2} - 44096_{9/2}$
5400.872	4	4	18510.382	$33354^{\circ}_{5/2} - 51865_{5/2}$	5351.325	10	20	18681.765	$23518^{\circ}_{7/2} - 42200_{9/2}$
				$16033^{\circ}_{5/2} - 34543_{5/2}$	5350.495	2	10	18684.663	$21682^{\circ}_{7/2} - 40367_{9/2}$
5396.705	3	3	18524.674	$23697^{\circ}_{7/2} - 42222_{7/2}$	5349.401	1	10	18688.484	$35156^{\circ}_{5/2} - 53845_{5/2}$

TABLE 3. *Classified lines of* Th II—Continued

Wavelength Å	Intensity		Wavenumber cm^{-1}	Classification	Wavelength Å	Intensity		Wavenumber cm^{-1}	Classification
	Lamp	Spark				Lamp	Spark		
5347.432	10	15	18695.365	$23187^{\circ}_{13/2} - 41882_{13/2}$	5292.919	15	20	18887.911	$21682^{\circ}_{7/2} - 40570_{7/2}$
5347.036	100w	150	18696.750	$22028^{\circ}_{15/2} - 40724_{13/2}$	5291.895	10	8	18891.565	$16564^{\circ}_{11/2} - 35456_{9/2}$
5346.375	50	40	18699.061	$9238^{\circ}_{9/2} - 27937_{11/2}$	5291.133	3	3	18894.286	$19050^{\circ}_{3/2} - 37945_{5/2}$
5345.000	15	25	18703.871	$23518^{\circ}_{7/2} - 42222_{7/2}$	5290.665	4	5	18895.958	$27357^{\circ}_{9/2} - 46253_{9/2}$
5344.244	4	20	18706.517	$31924^{\circ}_{11/2} - 50631_{11/2}$	5289.895	50	25	18898.708	$4113_{5/2} - 23012^{\circ}_{3/2}$
5343.297	15	50	18709.833	$22014^{\circ}_{11/2} - 40724_{13/2}$	5289.503	5h	5	18900.109	$14484^{\circ}_{11/2} - 33384_{9/2}$
5342.373	2	3	18713.069	$22685^{\circ}_{7/2} - 41398_{9/2}$	5287.963	3	3	18905.613	$20989^{\circ}_{9/2} - 39895_{9/2}$
5339.960	10b	10	18721.524	$15453^{\circ}_{7/2} - 34174_{5/2}$	5284.758	8	15	18917.078	$19248^{\circ}_{5/2} - 38165_{7/2}$
5333.163	15	10	18745.384	$18816^{\circ}_{13/2} - 37562_{11/2}$	5284.542	50	50	18917.851	$13818^{\circ}_{7/2} - 32736_{7/2}$
5331.226	2	1	18752.195	$12219_{3/2} - 30972^{\circ}_{5/2}$	5284.305	4	5	18918.700	$21297^{\circ}_{5/2} - 40216_{5/2}$
5329.758	25	25	18757.360	$11116^{\circ}_{7/2} - 29873_{7/2}$	5280.286	5	5	18933.099	$10855_{7/2} - 29788^{\circ}_{9/2}$
5329.651	5	8	18757.737	$20310^{\circ}_{5/2} - 39068_{7/2}$	5278.375	3	5	18939.954	$14790^{\circ}_{7/2} - 33730_{5/2}$
5329.476	40	50	18758.352	$18816^{\circ}_{13/2} - 37575_{13/2}$	5278.228	2b	10	18940.481	$26963^{\circ}_{7/2} - 45904_{9/2}$
5329.373	50	50	18758.715	$10673^{\circ}_{5/2} - 29431_{7/2}$	5277.500	300	200	18943.094	$10572^{\circ}_{9/2} - 29515_{9/2}$
5328.339	5	15	18762.355	$25414^{\circ}_{11/2} - 44177_{11/2}$	5277.219	10	50	18944.103	$17121^{\circ}_{3/2} - 36065_{5/2}$
5325.559	3	4	18772.149	$20686^{\circ}_{5/2} - 39458_{7/2}$	5276.407	40	15	18947.018	$8018_{3/2} - 26965^{\circ}_{3/2}$
5325.145	200	200	18773.609	$12485^{\circ}_{7/2} - 31259_{5/2}$	5276.293	1	10	18947.427	$33730_{5/2} - 52678^{\circ}_{5/2}$
5324.650	20b	20	18775.354	$16818_{7/2} - 35593^{\circ}_{9/2}$	5275.775	3	4	18949.287	$20989^{\circ}_{9/2} - 39939_{11/2}$
5324.043	3	20	18777.494	$25188^{\circ}_{3/2} - 43965_{1/2}$	5275.447	3	5	18950.466	$19912^{\circ}_{13/2} - 38862_{11/2}$
5322.464	3b	10b	18783.065	$24463^{\circ}_{5/2} - 43246_{7/2}$	5272.643	75	75	18960.543	$16564^{\circ}_{11/2} - 35525_{11/2}$
5322.432	4	20b	18783.178	$20080^{\circ}_{7/2} - 38863_{5/2}$	5271.614	8	15	18964.244	$23372^{\circ}_{3/2} - 42336_{5/2}$
5321.315	15	75	18787.121	$12472^{\circ}_{5/2} - 31259_{5/2}$	5270.744	5	50	18967.375	$30101^{\circ}_{7/2} - 49068_{5/2}$
5320.991	8	15	18788.265	$23730^{\circ}_{9/2} - 42518_{7/2}$	5270.124	2	8	18969.606	$29720^{\circ}_{5/2} - 48689_{3/2}$
5320.494	2	4	18790.020	$24982^{\circ}_{7/2} - 43772_{5/2}$	5269.650	15	20	18971.312	$18973^{\circ}_{7/2} - 37945_{5/2}$
5318.423	50	20	18797.337	$8605_{5/2} - 27403^{\circ}_{3/2}$	5269.385	40	50	18972.266	$16906^{\circ}_{7/2} - 35878_{7/2}$
5315.755	1	3	18806.771	$31928^{\circ}_{3/2} - 50735_{3/2}$	5268.932	15	20	18973.898	$18568^{\circ}_{1/2} - 37542_{3/2}$
5313.671	10	15b	18814.147	$18973^{\circ}_{7/2} - 37787_{7/2}$	5268.737	15	25	18974.600	$17837^{\circ}_{1/2} - 36812_{1/2}$
5313.612	8	20	18814.356	$30310^{\circ}_{11/2} - 49124_{11/2}$	5268.716	2c	8	18974.675	$17837^{\circ}_{1/2} - 36812_{1/2}$
5310.864	15	15	18824.091	$9202^{\circ}_{7/2} - 28026_{5/2}$	5267.365	10	40	18979.542	$23372^{\circ}_{3/2} - 42352_{5/2}$
5310.260	200	100	18826.232	$1859_{3/2} - 20686^{\circ}_{5/2}$	5267.030	4b	5	18980.749	$21297^{\circ}_{5/2} - 40278_{3/2}$
5310.103	4	15	18826.788	$24982^{\circ}_{7/2} - 43809_{9/2}$	5264.956	50	50	18988.226	$16033^{\circ}_{5/2} - 35021_{3/2}$
5309.728	15	20	18828.118	$19912^{\circ}_{13/2} - 38740_{11/2}$	5263.118	8	25	18994.857	$27357^{\circ}_{9/2} - 46352_{7/2}$
5308.430	20	50	18832.722	$15710^{\circ}_{3/2} - 34543_{5/2}$	5260.867	20	20	19002.985	$22685^{\circ}_{7/2} - 41688_{7/2}$
5308.154	15	40	18833.701	$23518^{\circ}_{7/2} - 42352_{5/2}$	5258.471	8	4	19011.643	$18118_{3/2} - 37130^{\circ}_{1/2}$
5307.710	2	200	18835.276	$35525_{11/2} - 54360^{\circ}_{9/2}$	5255.972	50	50	19020.682	$23730^{\circ}_{9/2} - 42751_{7/2}$
5307.466	100	150	18836.142	$16564^{\circ}_{11/2} - 35400_{13/2}$	5253.939	2	4	19028.042	$27357^{\circ}_{9/2} - 46385_{7/2}$
5306.033	1	5	18841.229	$27526_{9/2} - 46368^{\circ}_{9/2}$	5253.443	100	75	19029.839	$15144^{\circ}_{3/2} - 34174_{5/2}$
5305.577	75	50	18842.849	$9400_{5/2} - 28243^{\circ}_{5/2}$	5253.249	5	75	19030.541	$20120^{\circ}_{5/2} - 39150_{3/2}$
5305.495	4	5	18843.140	$25607^{\circ}_{9/2} - 44450_{9/2}$	5252.766	50	75	19032.291	$22014^{\circ}_{11/2} - 41047_{9/2}$
5304.675	15b	20b	18846.053	$22642^{\circ}_{9/2} - 41488_{7/2}$	5252.280	3	10	19034.052	$25266^{\circ}_{1/2} - 44300_{3/2}$
5304.620	25	25	18846.248	$14790^{\circ}_{7/2} - 33637_{7/2}$	5251.930	4	10	19035.321	$25414^{\circ}_{11/2} - 44450_{9/2}$
5303.048	50	40	18851.835	$12902^{\circ}_{3/2} - 31754_{5/2}$	5249.853	2	8	19042.852	$30452_{9/2} - 49495^{\circ}_{9/2}$
5302.698	3	4	18853.079	$31810^{\circ}_{5/2} - 50663_{5/2}$	5249.657	3	2	19043.563	$19248^{\circ}_{5/2} - 38291_{7/2}$
				$17272^{\circ}_{9/2} - 36125_{9/2}$	5248.855	3		19046.472	$24757^{\circ}_{9/2} - 43803_{7/2}$
5301.649	3	3	18856.809	$19248^{\circ}_{5/2} - 38105_{5/2}$	5247.654	500	100	19050.831	$0_{3/2} - 19050^{\circ}_{3/2}$
5301.403	100	100	18857.684	$14101^{\circ}_{1/2} - 32959_{3/2}$	5242.091	3	200	19071.048	$22028^{\circ}_{15/2} - 41099_{15/2}$
5300.969	2	5	18859.228	$27357^{\circ}_{9/2} - 46216_{11/2}$	5240.200	8	75	19077.930	$6168^{\circ}_{7/2} - 25246_{9/2}$
5296.676	10	40	18874.513	$15144^{\circ}_{3/2} - 34019_{3/2}$	5237.907	5	500	19086.282	$17722^{\circ}_{9/2} - 36809_{7/2}$
5295.617	20h	15	18878.288	$8378^{\circ}_{7/2} - 27257_{7/2}$	5237.626	2	300	19087.306	$26647^{\circ}_{13/2} - 45735_{11/2}$
5294.826	2	3	18881.108	$30956^{\circ}_{9/2} - 49837_{9/2}$	5236.425	4	10	19091.684	$14545^{\circ}_{5/2} - 33637_{7/2}$

TABLE 3. *Classified lines of* Th II—Continued

Wavelength Å	Intensity		Wavenumber cm^{-1}	Classification	Wavelength Å	Intensity		Wavenumber cm^{-1}	Classification
	Lamp	Spark				Lamp	Spark		
5233.225	150	175	19103.358	$9720^{\circ}_{7/2} - 28823_{5/2}$	5148.212	200	1500	19418.810	$15242^{\circ}_{9/2} - 34661_{11/2}$
5232.985	0	25	19104.234	$37787_{7/2} - 56892^{\circ}_{5/2}$	5145.035	150s	200	19430.800	$26965^{\circ}_{3/2} - 46395_{3/2}$
5231.715	3	4	19108.871	$14275^{\circ}_{9/2} - 33384_{9/2}$					$7331^{\circ}_{5/2} - 26762_{3/2}$
5227.642	2	10	19123.759	$19248^{\circ}_{5/2} - 38372_{3/2}$	5143.268	300l	500	19437.476	$1859_{3/2} - 21297^{\circ}_{5/2}$
5225.579	3	75	19131.309	$18973^{\circ}_{7/2} - 38105_{5/2}$	5137.708	20	25	19458.511	$25440^{\circ}_{5/2} - 44898_{7/2}$
5225.074	3	2	19133.158	$12219_{3/2} - 31353^{\circ}_{3/2}$	5135.232	10	10	19467.893	$31800^{\circ}_{7/2} - 51268_{7/2}$
5224.116	5	2	19136.666	$7828_{1/2} - 26965^{\circ}_{3/2}$	5132.236	8	8	19479.257	$14790^{\circ}_{7/2} - 34270_{9/2}$
5219.960	4	8	19151.902	$13468^{\circ}_{9/2} - 32620_{11/2}$	5131.490	4	5	19482.089	$17983^{\circ}_{5/2} - 37465_{5/2}$
5218.527	75	100	19157.162	$7331^{\circ}_{5/2} - 26488_{5/2}$	5131.072	25	250	19483.676	$15242^{\circ}_{9/2} - 34726_{7/2}$
5216.593	200	1	19164.264	$1521_{5/2} - 20686^{\circ}_{5/2}$	5129.844	5h	20	19488.340	$14790^{\circ}_{7/2} - 34279_{7/2}$
5214.156	5	100	19173.221	$19912^{\circ}_{13/2} - 39085_{13/2}$	5124.430	3h	10	19508.929	$19248^{\circ}_{5/2} - 38757_{3/2}$
5211.574	5	8	19182.720	$9061_{5/2} - 28243^{\circ}_{5/2}$	5123.477	2	10	19512.558	$21131^{\circ}_{3/2} - 40644_{5/2}$
5210.572	3	1	19186.408	$9400_{5/2} - 28587^{\circ}_{5/2}$	5122.896	3	3	19514.771	$24873^{\circ}_{5/2} - 44388_{5/2}$
5206.659	15	50	19200.828	$25607^{\circ}_{9/2} - 44807_{7/2}$					$22685^{\circ}_{7/2} - 42200_{9/2}$
				$10673^{\circ}_{5/2} - 29873_{7/2}$	5119.564	0	15	19527.472	$30310^{\circ}_{11/2} - 49837_{9/2}$
5206.489	25	20	19201.454	$6213_{9/2} - 25414^{\circ}_{11/2}$	5113.379	15	25	19551.091	$4146_{7/2} - 23697^{\circ}_{7/2}$
5205.776	20	400	19204.084	$15349^{\circ}_{11/2} - 34553_{9/2}$	5110.863	15	300	19560.716	$16564^{\circ}_{11/2} - 36125_{9/2}$
5204.998	5	20	19206.955	$17121^{\circ}_{3/2} - 36328_{3/2}$	5108.743	0	25	19568.833	$28923^{\circ}_{5/2} - 48492_{5/2}$
5196.042	15	15	19240.060	$12570_{7/2} - 31810^{\circ}_{5/2}$	5107.235	3	2	19574.611	$7828_{1/2} - 27403^{\circ}_{3/2}$
5194.250	0	10	19246.698	$20120^{\circ}_{5/2} - 39366_{5/2}$	5104.778	2	1	19584.032	$4146_{7/2} - 23730^{\circ}_{9/2}$
5193.822	75	100	19248.284	$0_{3/2} - 19248^{\circ}_{5/2}$	5104.563	3b	2	19584.857	$7001_{3/2} - 26586^{\circ}_{3/2}$
5190.867	100	100	19259.241	$4113_{5/2} - 23372^{\circ}_{3/2}$	5103.765	5	100	19587.919	$19248^{\circ}_{5/2} - 38836_{3/2}$
5189.674	10	300	19263.668	$20288^{\circ}_{11/2} - 39552_{9/2}$	5098.657	4h	2	19607.543	$18214^{\circ}_{3/2} - 37821_{3/2}$
5188.721	2	25	19267.206	$22642^{\circ}_{9/2} - 41909_{9/2}$	5098.039	100	75	19609.920	$1521_{5/2} - 21131^{\circ}_{3/2}$
				$13468^{\circ}_{9/2} - 32736_{7/2}$	5093.086	3	20	19628.990	$14545^{\circ}_{5/2} - 34174_{5/2}$
5188.364	20	150	19268.532	$12485^{\circ}_{7/2} - 31754_{5/2}$	5090.752	300	400	19637.989	$26965^{\circ}_{3/2} - 46603_{5/2}$
5184.730	10	75	19282.037	$12472^{\circ}_{5/2} - 31754_{5/2}$					$8605_{5/2} - 28243^{\circ}_{5/2}$
5184.660	0	10	19282.298	$28587^{\circ}_{5/2} - 47869_{3/2}$	5089.224	3	1	19643.886	$18973^{\circ}_{7/2} - 38617_{9/2}$
5183.987	100	250	19284.801	$12488^{\circ}_{9/2} - 31773_{9/2}$	5087.503	2	50	19650.531	$20288^{\circ}_{11/2} - 39939_{11/2}$
5183.601	3	2	19286.237	$20080^{\circ}_{7/2} - 39366_{5/2}$	5085.117	2	10	19659.751	$9061_{5/2} - 28720^{\circ}_{3/2}$
5182.527	20	30	19290.234	$18816^{\circ}_{13/2} - 38107_{13/2}$	5079.138	8	15	19682.893	$11576^{\circ}_{3/2} - 31259_{5/2}$
5178.988	2	1	19303.415	$36193^{\circ}_{9/2} - 55496_{9/2}$	5076.600	5	50	19692.734	$24757^{\circ}_{9/2} - 44450_{9/2}$
5177.097	0	25	19310.466	$31353^{\circ}_{3/2} - 50663_{5/2}$	5076.196	0	5	19694.301	$29720^{\circ}_{3/2} - 49414_{3/2}$
5176.735	4	8	19311.816	$15349^{\circ}_{11/2} - 34661_{11/2}$	5075.470	15	150	19697.118	$15324^{\circ}_{1/2} - 35021_{3/2}$
5175.073	2	5	19318.018	$18973^{\circ}_{7/2} - 38291_{7/2}$	5073.981	4	5	19702.898	$20158_{5/2} - 39861^{\circ}_{5/2}$
5172.912	10	25	19326.088	$10189^{\circ}_{11/2} - 29515_{9/2}$	5073.080	5s	25	19706.397	$19050^{\circ}_{3/2} - 38757_{3/2}$
5170.220	10	100	19336.151	$11116^{\circ}_{7/2} - 30452_{9/2}$	5072.930	0	1	19706.980	$13250^{\circ}_{5/2} - 32957^{\circ}_{7/2}$
5169.684	2h	1	19338.155	$20120^{\circ}_{3/2} - 39458_{7/2}$	5072.627	10	150	19708.157	$16033^{\circ}_{5/2} - 35741_{5/2}$
5169.160	1	25	19340.116	$23012^{\circ}_{3/2} - 42352_{5/2}$	5072.480	3	125	19708.728	$12219_{3/2} - 31928^{\circ}_{3/2}$
5166.923	2b	25	19348.489	$29720^{\circ}_{3/2} - 49068_{5/2}$					$13248_{9/2} - 32957^{\circ}_{7/2}$
				$22139^{\circ}_{9/2} - 41488_{7/2}$					
					5072.331	0	25	19709.307	$40278_{3/2} - 59987^{\circ}_{3/2}$
5166.875	3	20	19348.669	$17460^{\circ}_{5/2} - 36809_{7/2}$	5068.239	0	15	19725.220	$31928^{\circ}_{3/2} - 51653_{1/2}$
5160.678	50	25	19371.903	$4146_{7/2} - 23518^{\circ}_{7/2}$	5064.330	20b	50	19740.445	$13468^{\circ}_{9/2} - 33209_{7/2}$
5159.781	0	25	19375.270	$28923^{\circ}_{5/2} - 48298_{7/2}$	5061.219	25	200	19752.579	$14790^{\circ}_{7/2} - 34543_{5/2}$
5159.153	3		19377.629	$20989^{\circ}_{9/2} - 40367_{9/2}$	5058.589	1b	2	19762.848	$11116^{\circ}_{7/2} - 30879_{7/2}$
				$20080^{\circ}_{7/2} - 39458_{7/2}$	5058.563	40h	200	19762.950	$14790^{\circ}_{7/2} - 34553_{9/2}$
5154.893	8	8	19393.642	$6213_{9/2} - 25607^{\circ}_{9/2}$	5057.848	2		19765.743	$16818_{7/2} - 36583^{\circ}_{7/2}$
5154.867	0	5	19393.740	$40222_{3/2} - 59616^{\circ}_{3/2}$	5056.331	0	15	19771.673	$30101^{\circ}_{7/2} - 49873_{5/2}$
5153.516	4	25	19398.824	$15144^{\circ}_{3/2} - 34543_{3/2}$	5055.338	300	50	19775.557	$1521_{5/2} - 21297^{\circ}_{5/2}$
5151.855	50	20	19405.078	$4113_{5/2} - 23518^{\circ}_{7/2}$	5053.309	4	2	19783.497	$8460_{3/2} - 28243^{\circ}_{5/2}$

TABLE 3. *Classified lines of* Th II—Continued

Wavelength Å	Intensity		Wavenumber cm^{-1}	Classification	Wavelength Å	Intensity		Wavenumber cm^{-1}	Classification
	Lamp	Spark				Lamp	Spark		
5051.331	5	75	19791.244	$17771^{\circ}_{11/2}-37562_{11/2}$	4979.135	5	15	20078.207	$20969^{\circ}_{7/2}-41047_{9/2}$
5049.799	500	300	19797.248	$6691^{\circ}_{3/2}-26488_{5/2}$	4978.308	2	8	20081.543	$17460^{\circ}_{3/2}-37542_{3/2}$
5047.431	3	100	19806.536	$15786_{5/2}-35593^{\circ}_{7/2}$	4978.034	10	50	20082.648	$22139^{\circ}_{9/2}-42222_{7/2}$
5044.935	2	10	19816.335	$19050^{\circ}_{3/2}-38867_{1/2}$	4976.591	50	75	20088.471	$12488^{\circ}_{9/2}-32576_{7/2}$
5040.555	8	5	19833.554	$24132^{\circ}_{3/2}-43965_{1/2}$	4975.947	100	100	20091.071	$12485^{\circ}_{7/2}-32576_{7/2}$
5037.729	2	3	19844.680	$36390^{\circ}_{3/2}-56235_{3/2}$	4975.572	3	4	20092.585	$15453^{\circ}_{7/2}-35545_{9/2}$
5037.285	1	4	19846.429	$9585^{\circ}_{5/2}-29431_{7/2}$	4974.998	4	5	20094.903	$18973^{\circ}_{7/2}-39068_{7/2}$
5033.902	1	10	19859.767	$21131^{\circ}_{3/2}-40991_{3/2}$	4974.737	1	5	20095.958	$20120^{\circ}_{5/2}-40216_{5/2}$
5029.632	5	75	19876.627	$15144^{\circ}_{3/2}-35021_{3/2}$	4974.441	1	3	20097.154	$28720^{\circ}_{3/2}-48817_{3/2}$
5028.613	150b	200b	19880.655	$10572^{\circ}_{9/2}-30452_{9/2}$	4973.769	5	10	20099.869	$19050^{\circ}_{3/2}-39150_{3/2}$
5023.049	3	50	19902.676	$16906^{\circ}_{7/2}-36809_{7/2}$	4973.596	5	10	20100.568	$20310^{\circ}_{5/2}-40411_{7/2}$
5021.758	4	25	19907.793	$26647^{\circ}_{13/2}-46555_{11/2}$	4973.384	100l	150	20101.425	$15324^{\circ}_{1/2}-35425_{1/2}$
5020.541	50	40	19912.618	$13818^{\circ}_{7/2}-33730_{5/2}$	4973.092	5b	20b	20102.605	$28587^{\circ}_{3/2}-48689_{3/2}$
5019.614	2	10	19916.296	$24982^{\circ}_{7/2}-44898_{7/2}$	4973.050	8	50	20102.775	$20120^{\circ}_{5/2}-40222_{3/2}$
5019.324	150	150	19917.446	$14101^{\circ}_{1/2}-34019_{3/2}$	4972.668	5	10	20104.319	$13250_{5/2}-33354^{\circ}_{5/2}$
5018.220	2	10	19921.828	$27249^{\circ}_{7/2}-47171_{9/2}$	4972.174	50	150	20106.316	$23697^{\circ}_{7/2}-43803_{7/2}$
5017.255	300	400	19925.660	$7331^{\circ}_{5/2}-27257_{7/2}$					$15349^{\circ}_{11/2}-35456_{9/2}$
5015.888	100	100	19931.090	$10379_{9/2}-30310^{\circ}_{11/2}$	4971.186	2	3	20110.312	$22834_{7/2}-42944^{\circ}_{7/2}$
5014.751	50	50	19935.609	$30972^{\circ}_{5/2}-50907_{3/2}$	4970.029	15b	75	20114.994	$8605_{5/2}-28720^{\circ}_{5/2}$
5013.994	1	3	19938.619	$26963^{\circ}_{7/2}-46902_{5/2}$	4968.377	2l	3	20121.682	$17983^{\circ}_{5/2}-38105_{5/2}$
5013.600	20l	50	19940.186	$23187^{\circ}_{13/2}-43127_{11/2}$	4967.058	5	3	20127.025	$8460_{3/2}-28587^{\circ}_{5/2}$
5012.729	2	5	19943.650	$27787^{\circ}_{9/2}-47731_{9/2}$	4964.982	15	20b	20135.441	$20080^{\circ}_{7/2}-40216_{5/2}$
5009.976	50b	100	19954.609	$20969^{\circ}_{7/2}-40923_{5/2}$	4964.116	100	150	20138.953	$10855_{7/2}-30994^{\circ}_{7/2}$
5009.442	10	20	19956.736	$17722^{\circ}_{9/2}-37679_{11/2}$	4963.791	0	5	20140.272	$26770^{\circ}_{11/2}-46910_{13/2}$
5009.078	2	3	19958.187	$20686^{\circ}_{5/2}-40644_{5/2}$	4963.550	3	25	20141.250	$24757^{\circ}_{9/2}-44898_{7/2}$
5008.377	1	3	19960.980	$26424^{\circ}_{5/2}-46385_{7/2}$	4963.184	75	100	20142.735	$11116^{\circ}_{7/2}-31259_{5/2}$
5008.190	100	150	19961.725	$17983^{\circ}_{5/2}-37945_{5/2}$	4962.959	25b	100b	20143.648	$9202^{\circ}_{7/2}-29345_{5/2}$
5007.377	8	8	19964.966	$13250_{3/2}-33215^{\circ}_{3/2}$	4962.925	40b	75b	20143.786	$24982^{\circ}_{7/2}-45126_{9/2}$
5006.821	3	5	19967.183	$20310^{\circ}_{5/2}-40278_{3/2}$	4960.492	25b	20	20153.666	$9720^{\circ}_{7/2}-29873_{7/2}$
5005.738	2	2	19971.503	$26424^{\circ}_{5/2}-46395_{3/2}$	4959.738	1	1	20156.730	$16906^{\circ}_{7/2}-37063_{9/2}$
5003.503	2	10	19980.424	$29515_{9/2}-49495^{\circ}_{9/2}$	4959.438	3	10	20157.949	$20120^{\circ}_{5/2}-40278_{3/2}$
5002.567	15	20	19984.162	$17837^{\circ}_{1/2}-37821_{3/2}$	4958.974	1	8	20159.835	$30310^{\circ}_{11/2}-50470_{9/2}$
4999.937	100	100	19994.674	$14275^{\circ}_{9/2}-34270_{9/2}$	4958.717	10	5	20160.880	$1521_{3/2}-21682^{\circ}_{7/2}$
4999.105	20	20	19998.002	$14545^{\circ}_{5/2}-34543_{5/2}$	4956.836	5b	75	20168.531	$24132^{\circ}_{3/2}-44300_{3/2}$
4997.669	40	50	20003.748	$14275^{\circ}_{9/2}-34279_{7/2}$	4956.370	1	2	20170.427	$25440^{\circ}_{5/2}-45610_{5/2}$
4997.326	40	50	20005.121	$17272^{\circ}_{9/2}-37277_{7/2}$	4955.960	2	10	20172.096	$29788^{\circ}_{9/2}-49960_{7/2}$
4996.982	3	4	20006.498	$22106_{3/2}-42112^{\circ}_{3/2}$	4954.657	150b	200	20177.401	$14484^{\circ}_{11/2}-34661_{11/2}$
4996.873	5	10	20006.934	$31928^{\circ}_{3/2}-51935_{5/2}$	4954.555	50	150	20177.816	$11576^{\circ}_{3/2}-31754_{5/2}$
4992.275	2	4	20025.361	$20158_{5/2}-40184^{\circ}_{7/2}$	4954.336	3	10	20178.708	$26424^{\circ}_{5/2}-46603_{5/2}$
4991.925	3	5	20026.765	$19912^{\circ}_{13/2}-39939_{11/2}$	4951.826	8	15	20188.936	$18568^{\circ}_{1/2}-38757_{3/2}$
4991.007	10b	20	20030.448	$15710^{\circ}_{3/2}-35741_{5/2}$	4951.385	8	15	20190.734	$21297^{\circ}_{5/2}-41488_{7/2}$
4990.472	5	4	20032.596	$16033^{\circ}_{5/2}-36065_{5/2}$	4950.621	150	100	20193.850	$9238^{\circ}_{9/2}-29431_{7/2}$
4990.030	20	15	20034.370	$9061_{5/2}-29095^{\circ}_{5/2}$	4950.167	10	20	20195.702	$15349^{\circ}_{11/2}-35545_{9/2}$
4987.149	200	300	20045.944	$18816^{\circ}_{13/2}-38862_{11/2}$	4949.961	8	40	20196.542	$21131^{\circ}_{3/2}-41328_{5/2}$
4986.029	4	25	20050.446	$24757^{\circ}_{9/2}-44807_{7/2}$	4947.315	4	10	20207.344	$35878_{7/2}-56086^{\circ}_{9/2}$
4984.301	1	1	20057.397	$20989^{\circ}_{9/2}-41047_{9/2}$	4946.661	100	100	20210.016	$19248^{\circ}_{5/2}-39458_{7/2}$
4981.228	3b	4	20069.771	$17771^{\circ}_{11/2}-37840_{9/2}$	4945.863	15	20	20213.277	$15242^{\circ}_{9/2}-35456_{9/2}$
4980.949	50	40	20070.895	$6691^{\circ}_{3/2}-26762_{3/2}$	4945.249	2	3b	20215.786	$23012^{\circ}_{3/2}-43227_{5/2}$
4979.976	3	10	20074.817	$23697^{\circ}_{7/2}-43772_{5/2}$	4942.844	15	15	20225.622	$8018_{3/2}-28243^{\circ}_{5/2}$
4979.438	1	4	20076.986	$28243^{\circ}_{5/2}-48320_{5/2}$	4942.616	3	15	20226.555	$21682^{\circ}_{7/2}-41909_{9/2}$

TABLE 3. *Classified lines of* Th II—Continued

Wavelength Å	Intensity		Wavenumber cm^{-1}	Classification	Wavelength Å	Intensity		Wavenumber cm^{-1}	Classification
	Lamp	Spark				Lamp	Spark		
4941.621	1	2h	20230.628	$28587^{\circ}_{5/2} - 48817_{3/2}$	4885.985	2b	3	20460.988	$13818^{\circ}_{7/2} - 34279_{7/2}$
4939.948	8	15	20237.479	$20686^{\circ}_{5/2} - 40923_{5/2}$	4885.529	1	3	20462.898	$18118_{3/2} - 38581^{\circ}_{5/2}$
4939.808	5	15	20238.053	$22513^{\circ}_{5/2} - 42751_{7/2}$	4884.684	2	3	20466.437	$27403^{\circ}_{3/2} - 47869_{3/2}$
4937.962	2	5	20245.618	$31924^{\circ}_{11/2} - 52170_{11/2}$	4882.446	4	10	20475.819	$14545^{\circ}_{5/2} - 35021_{3/2}$
4937.405	2	2b	20247.902	$12488^{\circ}_{9/2} - 32736_{7/2}$	4881.106	0	1	20481.440	$28587^{\circ}_{5/2} - 49068_{5/2}$
4934.534	3	4	20259.683	$20310^{\circ}_{5/2} - 40570_{7/2}$	4880.230	3b	4	20485.116	$22642^{\circ}_{9/2} - 43127_{11/2}$
4933.850	15b	75	20262.491	$7331^{\circ}_{5/2} - 27593_{5/2}$	4879.349	5	20	20488.815	$16564^{\circ}_{11/2} - 37053_{11/2}$
4933.563	4b	5b	20263.670	$10189^{\circ}_{11/2} - 30452_{9/2}$	4879.186	0	1	20489.499	$25414^{\circ}_{11/2} - 45904_{9/2}$
4933.480	3b	5b	20264.011	$12472^{\circ}_{5/2} - 32736_{7/2}$	4879.154	5	4	20489.634	$8605_{3/2} - 29095^{\circ}_{5/2}$
4932.587	0	3	20267.680	$30956^{\circ}_{9/2} - 51224_{9/2}$	4877.809	15	5	20495.283	$1859_{3/2} - 22355^{\circ}_{1/2}$
4932.532	8h	5h	20267.906	$18568^{\circ}_{1/2} - 38836_{3/2}$	4877.704	1	2	20495.725	$20158_{5/2} - 40654^{\circ}_{5/2}$
4932.345	1	2	20268.674	$18816^{\circ}_{13/2} - 39085_{13/2}$	4877.002	25	150	20498.675	$16564^{\circ}_{11/2} - 37063_{9/2}$
				$24381_{7/2} - 44650^{\circ}_{7/2}$	4874.152	2	3	20510.661	$27787^{\circ}_{9/2} - 48298_{7/2}$
4929.985	10	100	20278.377	$14275^{\circ}_{9/2} - 34553_{9/2}$	4874.030	1	2	20511.174	$26424^{\circ}_{5/2} - 46935_{3/2}$
4929.378	2	15	20280.874	$15144^{\circ}_{3/2} - 35425_{1/2}$	4873.351	2	3	20514.032	$27357^{\circ}_{9/2} - 47871_{7/2}$
4927.587	4	15	20288.245	$15453^{\circ}_{7/2} - 35741_{5/2}$	4872.971	0	8	20515.631	$17272^{\circ}_{9/2} - 37787_{7/2}$
				$15305_{9/2} - 35593^{\circ}_{7/2}$	4872.537	1	1	20517.459	$21682^{\circ}_{7/2} - 42200_{9/2}$
4926.969	1	1	20290.790	$23518^{\circ}_{7/2} - 43809_{9/2}$	4872.138	3	5	20519.139	$20969^{\circ}_{7/2} - 41488_{7/2}$
4925.795	2b	3	20295.626	$10189^{\circ}_{11/2} - 30484_{11/2}$	4868.274	5	25	20535.425	$18816^{\circ}_{13/2} - 39352_{11/2}$
4925.418	5	50	20297.179	$15305_{9/2} - 35602^{\circ}_{11/2}$	4863.163	300d	1000	20557.006	$6213_{9/2} - 26770^{\circ}_{11/2}$
4925.002	3	75	20298.893	$18568^{\circ}_{1/2} - 38867_{1/2}$	4862.203	0	2	20561.065	$35525_{11/2} - 56086^{\circ}_{9/2}$
4924.798	2	8	20299.734	$7331^{\circ}_{5/2} - 27631_{3/2}$	4862.128	1	3	20561.382	$22685^{\circ}_{7/2} - 43246_{7/2}$
4924.420	15	50	20301.293	$4113_{5/2} - 24414^{\circ}_{3/2}$	4861.932	1	5	20562.211	$30101^{\circ}_{7/2} - 50663_{5/2}$
4923.421	1	2	20305.412	$20686^{\circ}_{5/2} - 40991_{3/2}$	4860.421	3	200	20568.603	$17272^{\circ}_{9/2} - 37840_{9/2}$
4922.946	15	100	20307.371	$10572^{\circ}_{9/2} - 30879_{7/2}$	4858.332	40	500	20577.448	$10379_{9/2} - 30956^{\circ}_{9/2}$
4921.876	0	2	20311.786	$22106_{5/2} - 42418^{\circ}_{5/2}$	4858.241	0	5	20577.833	$23518^{\circ}_{7/2} - 44096_{9/2}$
4921.612	50b	150	20312.875	$9202^{\circ}_{7/2} - 29515_{9/2}$	4858.096	5	300	20578.447	$18973^{\circ}_{7/2} - 39552_{9/2}$
4920.554	2b	3	20317.243	$4146_{7/2} - 24463^{\circ}_{5/2}$	4857.159	2	75	20582.417	$18568^{\circ}_{1/2} - 39150_{3/2}$
4920.526	10b	100	20317.358	$8605_{3/2} - 28923^{\circ}_{5/2}$	4856.957	1	2	20583.273	$22513^{\circ}_{5/2} - 43096_{5/2}$
4919.816	500	500	20320.290	$6168^{\circ}_{7/2} - 26488_{5/2}$	4856.273	3	40	20586.172	$10673^{\circ}_{5/2} - 31259_{5/2}$
4917.468	2	2b	20329.993	$15710^{\circ}_{3/2} - 36040_{1/2}$	4854.647	1	1	20593.067	$23372^{\circ}_{3/2} - 43965_{1/2}$
4914.119	5	100	20343.847	$17121^{\circ}_{3/2} - 37465_{5/2}$	4851.898	2	40	20604.734	$22642^{\circ}_{9/2} - 43246_{7/2}$
4912.526	50	100	20350.444	$4113_{5/2} - 24463^{\circ}_{5/2}$	4850.437	100	300	20610.941	$4146_{7/2} - 24757^{\circ}_{9/2}$
4911.447	2	4	20354.915	$15710^{\circ}_{3/2} - 36065_{5/2}$	4850.263	0	2	20611.680	$22139^{\circ}_{9/2} - 42751_{7/2}$
4911.147	8	75	20356.159	$13818^{\circ}_{7/2} - 34174_{5/2}$	4850.024	3	100	20612.696	$20310^{\circ}_{5/2} - 40923_{5/2}$
4910.418	0	1	20359.180	$26965^{\circ}_{3/2} - 47324_{5/2}$					$15453^{\circ}_{7/2} - 36065_{5/2}$
4910.312	1	1	20359.620	$10189^{\circ}_{11/2} - 30548_{13/2}$	4849.439	3	15	20615.182	$10379_{9/2} - 30994^{\circ}_{7/2}$
4906.680	3	1	20374.690	$24414^{\circ}_{5/2} - 44789_{1/2}$	4849.043	20	500	20616.866	$22028^{\circ}_{15/2} - 42644_{13/2}$
4903.122	1	1	20389.475	$9711_{7/2} - 30101^{\circ}_{7/2}$	4848.826	1	2	20617.789	$15710^{\circ}_{3/2} - 36328_{3/2}$
4899.158	2	8	20405.972	$17983^{\circ}_{5/2} - 38389_{7/2}$	4847.887	2	3	20621.782	$18214^{\circ}_{3/2} - 38836_{3/2}$
4898.802	5l	75	20407.455	$17272^{\circ}_{9/2} - 37679_{11/2}$	4845.936	3	100	20630.084	$12219_{3/2} - 32850^{\circ}_{5/2}$
4898.457	8	100	20408.893	$17771^{\circ}_{11/2} - 38179_{9/2}$	4844.755	4	100	20635.113	$8460_{3/2} - 29095^{\circ}_{5/2}$
4897.928	2	10	20411.097	$22685^{\circ}_{7/2} - 43096_{5/2}$	4844.559	8	200	20635.948	$15242^{\circ}_{9/2} - 35878_{7/2}$
4895.660	2	5	20420.553	$17121^{\circ}_{3/2} - 37542_{3/2}$					$9238^{\circ}_{9/2} - 29873_{7/2}$
4894.397	1	1	20425.822	$15453^{\circ}_{7/2} - 35878_{7/2}$	4844.257	3	100b	20637.234	$14349_{1/2} - 34986^{\circ}_{3/2}$
4894.351	0	1	20426.014	$24463^{\circ}_{5/2} - 44889_{3/2}$	4844.164	50	300b	20637.631	$11116^{\circ}_{7/2} - 31754_{5/2}$
4893.517	1	2	20429.495	$20969^{\circ}_{7/2} - 41398_{9/2}$	4843.815	0	1	20639.118	$21297^{\circ}_{5/2} - 41936_{3/2}$
4889.853	8	5	20444.803	$8378^{\circ}_{7/2} - 28823_{5/2}$	4842.562	1	1	20644.458	$17460^{\circ}_{5/2} - 38105_{5/2}$
4888.498	2	2	20450.470	$20120^{\circ}_{5/2} - 40570_{7/2}$	4841.385	1	3	20649.477	$27357^{\circ}_{9/2} - 48006_{9/2}$
4888.365	2	2	20451.026	$14275^{\circ}_{9/2} - 34726_{7/2}$	4841.320	2	20	20649.754	$19050^{\circ}_{3/2} - 39700_{5/2}$

TABLE 3. *Classified lines of* Th II—Continued

Wavelength Å	Intensity		Wavenumber cm^{-1}	Classification	Wavelength Å	Intensity		Wavenumber cm^{-1}	Classification
	Lamp	Spark				Lamp	Spark		
4841.037	0	3	20650.961	$33843^{\circ}_{3/2} - 54493_{5/2}$	4800.921	0	1	20823.516	$17121^{\circ}_{3/2} - 37945_{5/2}$
4840.471	40	300	20653.376	$13248_{9/2} - 33902^{\circ}_{7/2}$	4800.168	20	200	20826.782	$6700^{\circ}_{5/2} - 27526_{9/2}$
				$1859_{3/2} - 22513^{\circ}_{5/2}$	4800.050	0	2	20827.295	$28587^{\circ}_{5/2} - 49414_{3/2}$
4839.738	3	75	20656.504	$11116^{\circ}_{7/2} - 31773_{9/2}$	4799.756	3	40	20828.570	$12902^{\circ}_{3/2} - 33730_{3/2}$
4839.563	0	1	20657.251	$24132^{\circ}_{3/2} - 44789_{1/2}$	4799.158	0	1	20831.165	$17460^{\circ}_{5/2} - 38291_{7/2}$
4838.353	8	300	20662.417	$19912^{\circ}_{13/2} - 40574_{11/2}$	4797.569	2	10	20838.065	$22106_{5/2} - 42944^{\circ}_{7/2}$
4837.701	3	100	20665.202	$14790^{\circ}_{7/2} - 35456_{9/2}$	4796.511	0	2	20842.661	$29788^{\circ}_{9/2} - 50631_{11/2}$
4836.725	0	2	20669.372	$25594^{\circ}_{1/2} - 46264_{3/2}$	4796.448	0	2	20842.935	$20080^{\circ}_{7/2} - 40923_{5/2}$
				$21682^{\circ}_{7/2} - 42352_{5/2}$	4794.918	2	4	20849.585	$14349_{1/2} - 35198^{\circ}_{1/2}$
4836.179	2	15	20671.705	$9202^{\circ}_{7/2} - 29873_{7/2}$	4794.175	1	2	20852.817	$17983^{\circ}_{5/2} - 38836_{3/2}$
4833.872	0	3	20681.571	$29788^{\circ}_{9/2} - 50470_{9/2}$	4793.669	2	40	20855.018	$23697^{\circ}_{7/2} - 44552_{5/2}$
4833.826	25	40b	20681.767	$31625^{\circ}_{1/2} - 52307_{3/2}$	4792.910	4	2	20858.321	$30972^{\circ}_{5/2} - 51830_{7/2}$
4832.799	75	300	20686.162	$0_{3/2} - 20686^{\circ}_{5/2}$	4790.434	5	40	20869.101	$4113_{5/2} - 24982^{\circ}_{7/2}$
4831.645	0	3	20691.103	$23697^{\circ}_{7/2} - 44388_{5/2}$	4790.148	0	2	20870.347	$23518^{\circ}_{7/2} - 44388_{5/2}$
4829.884	1	25	20698.647	$20989^{\circ}_{9/2} - 41688_{7/2}$	4789.903	2	40	20871.415	$20120^{\circ}_{5/2} - 40991_{3/2}$
4828.952	2	8	20702.642	$8018_{3/2} - 28720^{\circ}_{3/2}$	4788.375	2	2	20878.075	$19594_{1/2} - 40472^{\circ}_{3/2}$
4828.463	4	200	20704.738	$17460^{\circ}_{5/2} - 38165_{7/2}$	4787.827	2	50	20880.464	$17983^{\circ}_{3/2} - 38863_{3/2}$
4824.647	5	100	20721.114	$12488^{\circ}_{9/2} - 33209_{7/2}$	4787.372	4	150	20882.449	$15242^{\circ}_{9/2} - 36125_{9/2}$
4824.044	1	2	20723.704	$12485^{\circ}_{7/2} - 33209_{7/2}$	4785.721	1	2	20889.653	$22355^{\circ}_{1/2} - 43244_{3/2}$
4823.692	2	5	20725.217	$13818^{\circ}_{7/2} - 34543_{5/2}$	4785.295	0	4b	20891.513	$24414^{\circ}_{3/2} - 45306_{3/2}$
4823.319	3	75	20726.820	$18973^{\circ}_{7/2} - 39700_{5/2}$	4784.929	5	200	20893.110	$17272^{\circ}_{9/2} - 38165_{7/2}$
4823.179	8b	200	20727.421	$4146_{7/2} - 24873^{\circ}_{5/2}$	4784.565	2	8	20894.700	$17722^{\circ}_{9/2} - 38617_{9/2}$
4821.272	10	500	20735.620	$13818^{\circ}_{7/2} - 34553_{9/2}$	4784.237	1	3	20896.132	$15144^{\circ}_{3/2} - 36040_{1/2}$
4821.035	0	2	20736.639	$24873^{\circ}_{5/2} - 45610_{5/2}$					$12488^{\circ}_{9/2} - 33384_{9/2}$
4820.693	0	3	20738.110	$26586^{\circ}_{3/2} - 47324_{5/2}$	4783.904	8	15	20897.587	$19050^{\circ}_{3/2} - 39948_{1/2}$
4819.017	3	40	20745.322	$17983^{\circ}_{5/2} - 38728_{5/2}$	4783.636	3	200	20898.758	$12485^{\circ}_{7/2} - 33384_{9/2}$
4818.644	50	500	20746.928	$17771^{\circ}_{11/2} - 38517_{13/2}$	4783.167	0	2	20900.807	$27631_{3/2} - 48532^{\circ}_{1/2}$
4817.826	2	8	20750.451	$6213_{9/2} - 26963^{\circ}_{7/2}$	4782.759	20	200	20902.590	$6691^{\circ}_{5/2} - 27593_{5/2}$
4817.320	2	40	20752.630	$23697^{\circ}_{7/2} - 44450_{9/2}$	4782.204	2	2	20905.016	$8018_{3/2} - 28923^{\circ}_{5/2}$
4816.859	3b	100	20754.616	$14790^{\circ}_{7/2} - 35545_{9/2}$	4781.584	3	5	20907.726	$17272^{\circ}_{9/2} - 38179_{9/2}$
4816.129	1	10	20757.762	$24132^{\circ}_{3/2} - 44889_{3/2}$	4779.587	5	2	20916.462	$14484^{\circ}_{11/2} - 35400_{13/2}$
4815.927	0	2	20758.633	$20288^{\circ}_{11/2} - 41047_{9/2}$	4778.921	1	4	20919.377	$17837^{\circ}_{1/2} - 38757_{3/2}$
4815.460	8	3	20760.646	$4113_{5/2} - 24873^{\circ}_{5/2}$	4778.883	4	200	20919.543	$20989^{\circ}_{9/2} - 41909_{9/2}$
4813.591	0	1	20768.707	$34270_{9/2} - 55038^{\circ}_{9/2}$	4778.547	1	3	20921.014	$15144^{\circ}_{3/2} - 36065_{5/2}$
4812.562	1	3	20773.147	$23730^{\circ}_{9/2} - 44503_{7/2}$	4777.649	3	75	20924.946	$39068_{7/2} - 59993^{\circ}_{9/2}$
4812.449	1	5	20773.635	$25381_{3/2} - 46155^{\circ}_{5/2}$	4777.350	0	2	20926.256	$24873^{\circ}_{5/2} - 45800_{5/2}$
4812.020	3	50	20775.487	$15349^{\circ}_{11/2} - 36125_{9/2}$	4776.779	50	150	20928.757	$17460^{\circ}_{5/2} - 38389_{7/2}$
4811.867	4	75	20776.147	$16033^{\circ}_{5/2} - 36809_{7/2}$	4776.076	0	2	20931.838	$23518^{\circ}_{7/2} - 44450_{9/2}$
4811.369	2	25	20778.298	$25607^{\circ}_{9/2} - 46385_{7/2}$	4775.357	3b	40	20934.989	$20288^{\circ}_{11/2} - 41223_{11/2}$
4810.874	2	1	20780.436	$38836_{3/2} - 59616^{\circ}_{3/2}$	4775.067	2	50	20936.261	$18214^{\circ}_{3/2} - 39150_{3/2}$
4807.079	3	50	20796.841	$15786_{3/2} - 36583^{\circ}_{7/2}$	4774.499	2	50	20938.751	$16818_{7/2} - 37756^{\circ}_{7/2}$
4806.050	3	75	20801.294	$13468^{\circ}_{9/2} - 34270_{9/2}$	4774.331	2	5	20939.488	$22834_{7/2} - 43773^{\circ}_{7/2}$
4805.963	4	200	20801.670	$25414^{\circ}_{11/2} - 46216_{11/2}$	4774.254	50b	200	20939.826	$6691^{\circ}_{3/2} - 27631_{3/2}$
4805.880	2	15b	20802.029	$20686^{\circ}_{5/2} - 41488_{7/2}$	4773.991	1	3	20940.979	$22014^{\circ}_{11/2} - 42955_{9/2}$
4805.547	3	50	20803.471	$20120^{\circ}_{5/2} - 40923_{5/2}$	4773.955	1	3	20941.137	$27357^{\circ}_{9/2} - 48298_{7/2}$
4805.290	0	2	20804.583	$35878_{7/2} - 56683^{\circ}_{7/2}$	4773.482	0	1	20943.212	$33902^{\circ}_{7/2} - 54845_{9/2}$
4803.954	8	200	20810.369	$13468^{\circ}_{9/2} - 34279_{7/2}$	4773.104	3	50	20944.871	$10855_{7/2} - 31800^{\circ}_{7/2}$
4803.483	50	300	20812.410	$19912^{\circ}_{13/2} - 40724_{13/2}$	4771.952	1	4	20949.927	$28923^{\circ}_{5/2} - 49873_{5/2}$
4802.612	0	3	20816.184	$22139^{\circ}_{9/2} - 42955_{9/2}$	4771.862	2	10	20950.322	$14790^{\circ}_{7/2} - 35741_{5/2}$
4802.422	1	3	20817.008	$24309^{\circ}_{11/2} - 45126_{9/2}$	4771.123	1h	2	20953.567	$23012^{\circ}_{3/2} - 43965_{1/2}$

TABLE 3. *Classified lines of* Th II—Continued

Wavelength Å	Intensity		Wavenumber cm^{-1}	Classification	Wavelength Å	Intensity		Wavenumber cm^{-1}	Classification
	Lamp	Spark				Lamp	Spark		
4770.945	0	2	20954.349	$31353^{\circ}_{3/2} - 52307_{3/2}$	4726.254	2	4	21152.488	$18214^{\circ}_{3/2} - 39366_{5/2}$
4770.744	2b	100	20955.232	$10855_{7/2} - 31810^{\circ}_{5/2}$	4725.943	5	100	21153.880	$15236_{3/2} - 36390^{\circ}_{5/2}$
4769.429	1	3	20961.009	$26770^{\circ}_{11/2} - 47731_{9/2}$	4725.305	3	15	21156.736	$20989^{\circ}_{9/2} - 42146_{11/2}$
4768.761	3	100	20963.945	$25414^{\circ}_{11/2} - 46378_{13/2}$	4724.822	5b	40b	21158.899	$6244_{1/2} - 27403^{\circ}_{3/2}$
4768.170	3	75	20966.544	$20080^{\circ}_{7/2} - 41047_{9/2}$	4724.771	40b	300	21159.127	$9720^{\circ}_{7/2} - 30879_{7/2}$
4768.054	5	100	20967.054	$8378^{\circ}_{7/2} - 29345_{5/2}$	4724.553	2	8	21160.104	$32850^{\circ}_{5/2} - 54010_{7/2}$
4767.871	1	10	20967.859	$19248^{\circ}_{5/2} - 40216_{5/2}$	4724.155	2	50	21161.886	$22642^{\circ}_{9/2} - 43803_{7/2}$
4766.961	5	150	20971.861	$14484^{\circ}_{11/2} - 35456_{9/2}$	4723.783	300	500	21163.553	$1521_{5/2} - 22685^{\circ}_{7/2}$
4766.016	0b	25	20976.020	$33384_{9/2} - 54360^{\circ}_{9/2}$	4722.974	2b	25	21167.178	$22642^{\circ}_{9/2} - 43809_{9/2}$
4765.655	5b	25	20977.608	$24757^{\circ}_{9/2} - 45735_{11/2}$	4722.948	1b	10b	21167.294	$17983^{\circ}_{5/2} - 39150_{3/2}$
4763.890	1	5	20985.380	$23518^{\circ}_{7/2} - 44503_{7/2}$	4721.882	3	100	21172.073	$19050^{\circ}_{3/2} - 40222_{3/2}$
4763.718	2	20	20986.138	$22028^{\circ}_{15/2} - 43014_{13/2}$	4719.979	20l	400	21180.609	$14275^{\circ}_{9/2} - 35456_{9/2}$
4763.398	0	2	20987.548	$22139^{\circ}_{9/2} - 43127_{11/2}$	4719.251	3	50	21183.877	$15144^{\circ}_{3/2} - 36328_{3/2}$
4762.519	5	20	20991.422	$1521_{5/2} - 22513^{\circ}_{5/2}$	4718.616	25	300	21186.727	$19912^{\circ}_{13/2} - 41099_{15/2}$
4761.854	4	100	20994.353	$31924^{\circ}_{11/2} - 52918_{13/2}$	4717.277	1	5	21192.741	$13468^{\circ}_{9/2} - 34661_{11/2}$
4761.631	0	1	20995.336	$32850^{\circ}_{5/2} - 53845_{5/2}$	4716.606	2	8	21195.756	$14545^{\circ}_{5/2} - 35741_{5/2}$
4761.353	1	3	20996.562	$23730^{\circ}_{9/2} - 44727_{11/2}$	4715.998	3b	75	21198.488	$16906^{\circ}_{7/2} - 38105_{5/2}$
4761.106	75	500	20997.651	$16564^{\circ}_{11/2} - 37562_{11/2}$	4715.429	20	200	21201.046	$10572^{\circ}_{9/2} - 31773_{9/2}$
4760.937	3	75	20998.396	$17837^{\circ}_{1/2} - 38836_{3/2}$	4714.867	3	50	21203.573	$27249^{\circ}_{7/2} - 48453_{7/2}$
4760.052	2	20	21002.301	$20686^{\circ}_{5/2} - 41688_{7/2}$	4713.839	2	8	21208.198	$20120^{\circ}_{5/2} - 41328_{5/2}$
									$15236_{3/2} - 36444^{\circ}_{3/2}$
4759.582	3	75	21004.375	$15324^{\circ}_{1/2} - 36328_{3/2}$					
4756.619	3	50	21017.458	$17722^{\circ}_{9/2} - 38740_{11/2}$	4712.393	50b	150	21214.705	$9238^{\circ}_{9/2} - 30452_{9/2}$
4754.403	3	2	21027.254	$26647^{\circ}_{13/2} - 47675_{11/2}$	4711.141	2	10	21220.343	$21131^{\circ}_{3/2} - 42352_{5/2}$
4754.208	2	40	21028.117	$16818_{7/2} - 37846^{\circ}_{5/2}$	4709.598	2	8	21227.295	$19050^{\circ}_{3/2} - 40278_{3/2}$
4753.810	2	25	21029.877	$19248^{\circ}_{5/2} - 40278_{3/2}$	4708.102	50	200	21234.040	$11725^{\circ}_{1/2} - 32959_{3/2}$
4752.414	200	500	21036.055	$6213_{9/2} - 27249^{\circ}_{7/2}$	4707.581	2	25	21236.390	$26770^{\circ}_{11/2} - 48006_{9/2}$
4751.328	2	20	21040.863	$14484^{\circ}_{11/2} - 35525_{11/2}$	4706.250	50	200b	21242.396	$7001_{3/2} - 28243^{\circ}_{5/2}$
4751.117	2	1	21041.797	$25381_{3/2} - 46423^{\circ}_{3/2}$	4705.758	200	500	21244.617	$9711_{7/2} - 30956^{\circ}_{5/2}$
4748.585	3b	75	21053.017	$8378^{\circ}_{7/2} - 29431_{7/2}$	4705.615	50	200	21245.262	$12485^{\circ}_{7/2} - 33730_{5/2}$
4747.550	2	2	21057.606	$24132^{\circ}_{5/2} - 45189_{5/2}$	4705.294	2	10	21246.712	$9238^{\circ}_{9/2} - 30484_{11/2}$
4743.693	150w	300	21074.728	$4113_{5/2} - 25188^{\circ}_{3/2}$	4705.084	1	4	21247.660	$20080^{\circ}_{7/2} - 41328_{5/2}$
4743.112	2	10	21077.309	$23730^{\circ}_{9/2} - 44807_{7/2}$	4704.657	2	25	21249.589	$14275^{\circ}_{9/2} - 35525_{11/2}$
4742.259	10s	100	21081.100	$10673^{\circ}_{3/2} - 31754_{5/2}$	4703.844	2	5	21253.261	$20969^{\circ}_{7/2} - 42222_{7/2}$
4741.384	5	200	21084.991	$13468^{\circ}_{9/2} - 34553_{9/2}$	4703.577	1	3	21254.467	$25607^{\circ}_{9/2} - 46861_{11/2}$
4740.529	500	500	21088.793	$6168^{\circ}_{7/2} - 27257_{7/2}$	4703.404	3	4	21255.249	$13406^{\circ}_{13/2} - 34661_{11/2}$
4739.860	5	100	21091.770	$17771^{\circ}_{11/2} - 38862_{11/2}$	4702.624	3	25	21258.775	$16906^{\circ}_{7/2} - 38165_{7/2}$
4737.656	4	100	21101.582	$15710^{\circ}_{3/2} - 36812_{1/2}$					$12472^{\circ}_{5/2} - 33730_{5/2}$
4736.399	4	200	21107.182	$22139^{\circ}_{9/2} - 43246_{7/2}$	4702.359	3	25b	21259.973	$8460_{3/2} - 29720^{\circ}_{3/2}$
4735.780	2	5	21109.941	$20288^{\circ}_{11/2} - 41398_{9/2}$	4702.309	8	200	21260.199	$9711_{7/2} - 30972^{\circ}_{5/2}$
4735.702	2	8	21110.288	$23697^{\circ}_{7/2} - 44807_{7/2}$	4700.574	1	4	21268.046	$17460^{\circ}_{5/2} - 38728_{5/2}$
4735.245	2	15	21112.326	$22014^{\circ}_{11/2} - 43127_{11/2}$	4700.137	75	200	21270.023	$14275^{\circ}_{9/2} - 35545_{9/2}$
4734.757	2	10	21114.502	$8605_{3/2} - 29720^{\circ}_{3/2}$	4699.460	1	10	21273.087	$21682^{\circ}_{7/2} - 42955_{9/2}$
4734.626	2	10	21115.086	$16564^{\circ}_{11/2} - 37679_{11/2}$	4699.091	2	20	21274.758	$14790^{\circ}_{7/2} - 36065_{5/2}$
4733.023	3	50h	21122.237	$18816^{\circ}_{13/2} - 39939_{11/2}$	4698.767	4	100	21276.225	$16564^{\circ}_{11/2} - 37840_{9/2}$
4732.668	8	200	21123.821	$22685^{\circ}_{7/2} - 43809_{9/2}$	4698.270	2	50	21278.475	$33215^{\circ}_{3/2} - 54493_{5/2}$
4730.877	4	10	21131.818	$0_{3/2} - 21131^{\circ}_{3/2}$	4695.835	1	5	21289.509	$23518^{\circ}_{7/2} - 44807_{7/2}$
4729.875	50	200	21136.295	$8378^{\circ}_{7/2} - 29515_{9/2}$	4694.921	10	200	21293.654	$4146_{7/2} - 25440^{\circ}_{5/2}$
4729.084	50b	40	21139.830	$17722^{\circ}_{9/2} - 38862_{11/2}$	4694.844	1	3	21294.003	$9585^{\circ}_{5/2} - 30879_{7/2}$
4726.462	4	200	21151.558	$12485^{\circ}_{7/2} - 33637_{7/2}$	4694.783	5l	40l	21294.280	$22513^{\circ}_{5/2} - 43807_{3/2}$
4726.333	5	40	21152.135	$1859_{3/2} - 23012^{\circ}_{3/2}$	4694.282	1	25	21296.552	$17460^{\circ}_{5/2} - 38757_{3/2}$

TABLE 3. *Classified lines of* Th II—Continued

Wavelength Å	Intensity		Wavenumber cm^{-1}	Classification	Wavelength Å	Intensity		Wavenumber cm^{-1}	Classification
	Lamp	Spark				Lamp	Spark		
4694.090	400	300	21297.423	$0_{3/2} - 21297^{\circ}_{5/2}$	4647.913	2	4	21509.010	$16033^{\circ}_{5/2} - 37542_{3/2}$
4691.050	10	400	21311.225	$19912^{\circ}_{13/2} - 41223_{11/2}$	4646.140	1	3	21517.218	$23372^{\circ}_{3/2} - 44889_{3/2}$
4690.680	10	200	21312.906	$17837^{\circ}_{1/2} - 39150_{3/2}$	4645.495	2	20	21520.205	$14545^{\circ}_{5/2} - 36065_{5/2}$
4690.331	3	100	21314.492	$17771^{\circ}_{11/2} - 39085_{13/2}$	4642.889	1	5	21532.284	$34553_{9/2} - 56086^{\circ}_{9/2}$
4689.596	1	5	21317.832	$20080^{\circ}_{7/2} - 41398_{9/2}$	4642.272	1	5	21535.146	$22642^{\circ}_{9/2} - 44177_{11/2}$
4689.170	100	300b	21319.769	$6691^{\circ}_{3/2} - 28011_{3/2}$	4642.055	3	75	21536.153	$20686^{\circ}_{5/2} - 42222_{7/2}$
4688.276	3	100	21323.834	$14101^{\circ}_{1/2} - 35425_{1/2}$	4641.435	2	3	21539.029	$9720^{\circ}_{7/2} - 31259_{5/2}$
4686.568	4	75	21331.605	$12570_{7/2} - 33902^{\circ}_{7/2}$	4641.181	50	200	21540.208	$23187^{\circ}_{13/2} - 44727_{11/2}$
4685.963	3	50	21334.359	$14790^{\circ}_{7/2} - 36125_{9/2}$	4640.045	50	200b	21545.482	$10379_{9/2} - 31924^{\circ}_{11/2}$
4685.827	3	8	21334.979	$6691^{\circ}_{3/2} - 28026_{5/2}$	4639.704	75	300	21547.065	$12472^{\circ}_{3/2} - 34019_{3/2}$
4685.494	2	200	21336.495	$24463^{\circ}_{5/2} - 45800_{3/2}$	4639.094	3	100	21549.898	$20969^{\circ}_{7/2} - 42518_{7/2}$
4685.448	1	5	21336.704	$27787^{\circ}_{9/2} - 49124_{11/2}$	4633.830	40b	40	21574.378	$6213_{9/2} - 27787^{\circ}_{9/2}$
4684.127	2	25	21342.722	$35602^{\circ}_{11/2} - 56945_{11/2}$	4631.760	150	400	21584.020	$10189^{\circ}_{11/2} - 31773_{9/2}$
4683.533	1	2	21345.428	$17272^{\circ}_{9/2} - 38617_{9/2}$	4631.348	2	4	21585.940	$7001_{3/2} - 28587^{\circ}_{5/2}$
4683.484	2	3	21345.652	$17722^{\circ}_{9/2} - 39068_{7/2}$	4630.353	2	50	21590.579	$17272^{\circ}_{9/2} - 38862_{11/2}$
4681.649	2	2	21354.018	$37945_{5/2} - 59299^{\circ}_{5/2}$	4629.769	10	75	21593.302	$9400_{5/2} - 30994^{\circ}_{7/2}$
4681.163	2	20	21356.235	$15453^{\circ}_{7/2} - 36809_{7/2}$	4629.375	25	200	21595.140	$24309^{\circ}_{11/2} - 45904_{9/2}$
4680.640	40b	150b	21358.621	$6168^{\circ}_{7/2} - 27526_{9/2}$	4629.005	2	75	21596.866	$18973^{\circ}_{7/2} - 40570_{7/2}$
4679.045	1	20	21365.902	$20310^{\circ}_{5/2} - 41676_{3/2}$	4627.628	3	75	21603.292	$14275^{\circ}_{9/2} - 35878_{7/2}$
4678.594	1	2	21367.962	$20120^{\circ}_{5/2} - 41488_{7/2}$	4626.818	1	2	21607.074	$17121^{\circ}_{3/2} - 38728_{5/2}$
4678.200	4	10	21369.761	$24982^{\circ}_{7/2} - 46352_{7/2}$	4626.666	2	50	21607.784	$20080^{\circ}_{7/2} - 41688_{7/2}$
4676.936	3	5	21375.537	$17460^{\circ}_{5/2} - 38836_{3/2}$	4626.604	2	10	21608.074	$17460^{\circ}_{3/2} - 39068_{7/2}$
4676.680	1	5	21376.707	$23012^{\circ}_{3/2} - 44388_{5/2}$	4626.133	2	4	21610.274	$15453^{\circ}_{7/2} - 37063_{9/2}$
4676.502	2	75	21377.520	$20310^{\circ}_{5/2} - 41688_{7/2}$	4625.054	10	300	21615.315	$16564^{\circ}_{11/2} - 38179_{9/2}$
4675.934	2	75	21380.117	$18568^{\circ}_{1/2} - 39948_{1/2}$	4624.136	10	200	21619.606	$11116^{\circ}_{7/2} - 32736_{7/2}$
4675.290	2	15	21383.062	$11576^{\circ}_{3/2} - 32959_{3/2}$	4623.892	5	400	21620.747	$24982^{\circ}_{7/2} - 46603_{5/2}$
4674.816	1	3	21385.230	$16906^{\circ}_{7/2} - 38291_{7/2}$					$20288^{\circ}_{11/2} - 41909_{9/2}$
4674.730	1	3	21385.624	$24414^{\circ}_{3/2} - 45800_{5/2}$	4623.397	1	5	21623.062	$12219_{3/2} - 33843^{\circ}_{3/2}$
4670.889	1	2	21403.209	$17460^{\circ}_{5/2} - 38863_{5/2}$	4622.065	2	5	21629.293	$28243^{\circ}_{5/2} - 49873_{5/2}$
4666.991	4	20	21421.085	$10379_{9/2} - 31800^{\circ}_{7/2}$					$17722^{\circ}_{9/2} - 39352_{11/2}$
4666.002	40	200	21425.626	$6168^{\circ}_{7/2} - 27593_{5/2}$	4620.725	3	20	21635.565	$17121^{\circ}_{3/2} - 38757_{3/2}$
4665.955	2	25	21425.842	$24309^{\circ}_{11/2} - 45735_{11/2}$	4619.561	50	300	21641.017	$14484^{\circ}_{11/2} - 36125_{9/2}$
4664.542	1	3	21432.332	$16033^{\circ}_{5/2} - 37465_{5/2}$	4619.480	100b	400	21641.396	$9238^{\circ}_{9/2} - 30879_{7/2}$
4663.372	1	5	21437.709	$18973^{\circ}_{7/2} - 40411_{7/2}$	4613.978	2	100	21667.202	$22106_{5/2} - 43773^{\circ}_{7/2}$
4661.423	2	100	21446.672	$25414^{\circ}_{11/2} - 46861_{11/2}$	4613.875	2	25	21667.686	$15144^{\circ}_{3/2} - 36812_{1/2}$
4659.846	1	3	21453.930	$21297^{\circ}_{5/2} - 42751_{7/2}$	4613.762	2	50	21668.217	$24132^{\circ}_{3/2} - 45800_{5/2}$
4659.799	5	3	21454.147	$22642^{\circ}_{9/2} - 44096_{9/2}$	4613.468	3	100	21669.598	$22139^{\circ}_{9/2} - 43809_{9/2}$
4658.727	2	15	21459.083	$24757^{\circ}_{9/2} - 46216_{11/2}$	4613.263	2	8	21670.561	$18973^{\circ}_{7/2} - 40644_{5/2}$
4658.492	10b	10b	21460.166	$11116^{\circ}_{7/2} - 32576_{7/2}$	4612.544	200	150	21673.938	$9585^{\circ}_{5/2} - 31259_{5/2}$
4656.748	2	8	21468.203	$17272^{\circ}_{9/2} - 38740_{11/2}$	4612.168	2	20	21675.705	$16818_{7/2} - 38493^{\circ}_{5/2}$
4655.727	1	3	21472.911	$19050^{\circ}_{3/2} - 40523_{1/2}$	4611.859	50	300	21677.158	$9202^{\circ}_{7/2} - 30879_{7/2}$
4654.272	2	2	21479.623	$29788^{\circ}_{9/2} - 51268_{7/2}$	4609.370	50	400	21688.863	$12485^{\circ}_{7/2} - 34174_{5/2}$
4653.084	2	15	21485.107	$35593^{\circ}_{9/2} - 57078_{9/2}$	4606.501	25	200	21702.371	$12472^{\circ}_{5/2} - 34174_{5/2}$
4652.851	2	15	21486.183	$18214^{\circ}_{3/2} - 39700_{5/2}$	4606.299	2	50	21703.322	$22685^{\circ}_{7/2} - 44388_{5/2}$
4652.415	3	8	21488.197	$15324^{\circ}_{1/2} - 36812_{1/2}$	4605.232	2	75	21708.351	$25440^{\circ}_{5/2} - 47148_{3/2}$
4651.986	75	200	21490.178	$1521_{5/2} - 23012^{\circ}_{3/2}$	4604.651	2	25	21711.090	$16906^{\circ}_{7/2} - 38617_{9/2}$
4651.554	150b	500	21492.174	$7331^{\circ}_{5/2} - 28823_{5/2}$	4604.160	2	8	21713.405	$15349^{\circ}_{11/2} - 37063_{9/2}$
4650.918	8	75	21495.113	$8378^{\circ}_{7/2} - 29873_{7/2}$	4603.907	2	100	21714.599	$17121^{\circ}_{3/2} - 38836_{3/2}$
4650.815	50	75	21495.589	$8605_{5/2} - 30101^{\circ}_{7/2}$	4602.885	75	300	21719.420	$7001_{3/2} - 28720^{\circ}_{3/2}$
4650.757	2	75	21495.857	$25414^{\circ}_{11/2} - 46910_{13/2}$	4601.952	2	50	21723.823	$24982^{\circ}_{7/2} - 46706_{7/2}$

TABLE 3. *Classified lines of* Th II—Continued

Wavelength Å	Intensity		Wavenumber cm^{-1}	Classification	Wavelength Å	Intensity		Wavenumber cm^{-1}	Classification
	Lamp	Spark				Lamp	Spark		
4599.522	2	5	21735.300	$17722^{\circ}_{9/2} - 39458_{7/2}$	4556.806	2	10	21939.046	$14101^{\circ}_{1/2} - 36040_{1/2}$
4599.353	8	10	21736.099	$13250_{5/2} - 34986^{\circ}_{5/2}$	4555.063	2	50	21947.441	$21297^{\circ}_{5/2} - 43244_{3/2}$
4598.055	1	5	21742.235	$17121^{\circ}_{3/2} - 38863_{5/2}$	4554.792	3	75	21948.747	$24757^{\circ}_{9/2} - 46706_{7/2}$
4597.915	1	50	21742.897	$30564^{\circ}_{1/2} - 52307_{3/2}$	4554.657	2	50	21949.397	$21297^{\circ}_{5/2} - 43246_{7/2}$
4597.357	1	3	21745.536	$17121^{\circ}_{3/2} - 38867_{1/2}$	4554.565	3	25	21949.840	$18973^{\circ}_{7/2} - 40923_{5/2}$
4596.937	1	5	21747.522	$25188^{\circ}_{3/2} - 46935_{3/2}$	4554.082	3	10	21952.169	$9400_{5/2} - 31353^{\circ}_{3/2}$
4594.749	1	3	21757.878	$18816^{\circ}_{13/2} - 40574_{11/2}$	4553.837	4	100	21953.350	$16564^{\circ}_{11/2} - 38517_{13/2}$
4593.979	3	75	21761.525	$20989^{\circ}_{9/2} - 42751_{7/2}$	4553.162	2	15	21956.604	$22139^{\circ}_{9/2} - 44096_{9/2}$
4593.553	5	75	21763.543	$16818_{7/2} - 38581^{\circ}_{5/2}$	4553.118	2	40	21956.816	$34726_{7/2} - 56683^{\circ}_{7/2}$
4593.283	3	200	21764.822	$22685^{\circ}_{7/2} - 44450_{9/2}$	4553.027	3b	200	21957.255	$16906^{\circ}_{7/2} - 38863_{5/2}$
4592.781	8	25	21767.201	$27357^{\circ}_{9/2} - 49124_{11/2}$	4552.359	2	20	21960.477	$25188^{\circ}_{3/2} - 47148_{3/2}$
4589.835	2	100	21781.172	$17771^{\circ}_{11/2} - 39552_{9/2}$	4551.541	3	20	21964.423	$26647^{\circ}_{13/2} - 48612_{13/2}$
4589.667	50b	150	21781.970	$12488^{\circ}_{9/2} - 34270_{9/2}$	4551.205	1	8	21966.045	$20989^{\circ}_{9/2} - 42955_{9/2}$
4589.445	1	3	21783.023	$14545^{\circ}_{5/2} - 36328_{3/2}$	4550.429	2	4	21969.791	$15786_{5/2} - 37756^{\circ}_{7/2}$
4589.121	20	200	21784.561	$12485^{\circ}_{7/2} - 34270_{9/2}$	4550.377	1	4	21970.042	$19912^{\circ}_{13/2} - 41882_{13/2}$
4588.226	10	300	21788.810	$16033^{\circ}_{5/2} - 37821_{3/2}$	4546.832	25	15	21987.171	$13468^{\circ}_{9/2} - 35456_{9/2}$
4587.756	20	75	21791.043	$12488^{\circ}_{9/2} - 34279_{7/2}$	4546.132	10	40	21990.556	$22513^{\circ}_{5/2} - 44503_{7/2}$
4587.209	3	50	21793.641	$12485^{\circ}_{7/2} - 34279_{7/2}$	4545.824	2	25	21992.046	$12219_{3/2} - 34212^{\circ}_{5/2}$
4586.620	3	75	21796.440	$17272^{\circ}_{9/2} - 39068_{7/2}$	4545.348	3b	3	21994.349	$13406^{\circ}_{13/2} - 35400_{13/2}$
4586.267	4	200	21798.117	$24757^{\circ}_{9/2} - 46555_{11/2}$	4545.270	2	4	21994.727	$10855_{7/2} - 32850^{\circ}_{5/2}$
4586.061	50b	50	21799.097	$21297^{\circ}_{5/2} - 43096_{5/2}$	4544.895	8	15	21996.541	$1521_{5/2} - 23518^{\circ}_{7/2}$
4584.368	8	200	21807.147	$12472^{\circ}_{5/2} - 34279_{7/2}$	4544.512	150	200	21998.395	$4490^{\circ}_{5/2} - 26488_{5/2}$
4584.159	1	5	21808.141	$22642^{\circ}_{9/2} - 44450_{9/2}$	4543.208	4	20	22004.709	$10572^{\circ}_{9/2} - 32576_{7/2}$
4583.654	2	40	21810.544	$15242^{\circ}_{9/2} - 37053_{11/2}$	4542.427	2	15	22008.493	$18214^{\circ}_{3/2} - 40222_{3/2}$
4582.778	2	50	21814.712	$15786_{5/2} - 37601^{\circ}_{5/2}$	4541.615	3	40	22012.427	$15453^{\circ}_{7/2} - 37465_{5/2}$
4582.436	3	50	21816.341	$22834_{7/2} - 44650^{\circ}_{7/2}$	4541.204	4	10	22014.420	$7331^{\circ}_{5/2} - 29345_{5/2}$
4581.815	1	1	21819.297	$27249^{\circ}_{7/2} - 49068_{5/2}$	4540.403	40	200	22018.303	$14790^{\circ}_{7/2} - 36809_{7/2}$
4581.581	20	200	21820.412	$15242^{\circ}_{9/2} - 37063_{9/2}$	4540.087	4	15	22019.836	$27357^{\circ}_{9/2} - 49377_{7/2}$
4581.229	25b	150	21822.088	$16906^{\circ}_{7/2} - 38728_{5/2}$	4538.844	4	25	22025.866	$20310^{\circ}_{5/2} - 42336_{5/2}$
4580.758	2	15	21824.332	$15453^{\circ}_{7/2} - 37277_{7/2}$	4538.182	1	2	22029.079	$17121^{\circ}_{3/2} - 39150_{3/2}$
4579.292	3	75	21831.319	$15710^{\circ}_{3/2} - 37542_{3/2}$	4537.072	20	200	22034.468	$15242^{\circ}_{9/2} - 37277_{7/2}$
4578.995	3	25	21832.735	$20686^{\circ}_{5/2} - 42518_{7/2}$	4536.427	1	4	22037.601	$22139^{\circ}_{9/2} - 44177_{11/2}$
4575.425	10	200	21849.770	$14275^{\circ}_{9/2} - 36125_{9/2}$	4535.708	2b	5	22041.094	$14349_{1/2} - 36390^{\circ}_{3/2}$
4573.703	25	150	21857.996	$6168^{\circ}_{7/2} - 28026_{5/2}$	4534.117	75	200	22048.828	$10572^{\circ}_{9/2} - 32620_{11/2}$
4572.935	1	8	21861.667	$22642^{\circ}_{9/2} - 44503_{7/2}$	4533.302	50	300	22052.792	$9720^{\circ}_{7/2} - 31773_{9/2}$
4570.614	2	75	21872.768	$19050^{\circ}_{3/2} - 40923_{5/2}$	4533.240	50	40b	22053.094	$16564^{\circ}_{11/2} - 38617_{9/2}$
4569.812	2	5	21876.607	$23518^{\circ}_{7/2} - 45395_{7/2}$	4532.430	3	50	22057.035	$9202^{\circ}_{7/2} - 31259_{5/2}$
4568.236	2	10	21884.154	$25440^{\circ}_{5/2} - 47324_{5/2}$	4532.256	50	300	22057.882	$12485^{\circ}_{7/2} - 34543_{5/2}$
4566.650	20	200	21891.754	$7828_{1/2} - 29720^{\circ}_{3/2}$	4531.713	8	300	22060.525	$13818^{\circ}_{7/2} - 35878_{7/2}$
4566.282	1	50	21893.519	$29788^{\circ}_{9/2} - 51681_{9/2}$	4531.611	2	10	22061.021	$20158_{5/2} - 42219^{\circ}_{5/2}$
4566.247	2		21893.686	$15236_{3/2} - 37130^{\circ}_{1/2}$	4531.196	3b	50	22063.042	$10673^{\circ}_{5/2} - 32736_{7/2}$
4564.178	15	200	21903.611	$10673^{\circ}_{7/2} - 32576_{7/2}$	4530.656	1	1	22065.671	$12488^{\circ}_{9/2} - 34553_{9/2}$
4563.727	3	8	21905.775	$26586^{\circ}_{3/2} - 48492_{5/2}$	4529.484	4	200	22071.381	$12472^{\circ}_{5/2} - 34543_{5/2}$
4563.291	50	500b	21907.868	$18816^{\circ}_{13/2} - 40724_{13/2}$	4529.376	2	3	22071.907	$16033^{\circ}_{5/2} - 38105_{5/2}$
4563.219	10	300	21908.214	$23187^{\circ}_{13/2} - 45095_{13/2}$	4528.973	3	50	22073.871	$8378^{\circ}_{7/2} - 30452_{9/2}$
4562.632	2	5	21911.032	$9061_{5/2} - 30972^{\circ}_{5/2}$	4528.409	2	50	22076.620	$13468^{\circ}_{9/2} - 35545_{9/2}$
4562.565	2	15	21911.354	$20310^{\circ}_{5/2} - 42222_{7/2}$	4527.710	2b	150	22080.028	$17272^{\circ}_{9/2} - 39352_{11/2}$
4562.439	3	25	21911.959	$16033^{\circ}_{5/2} - 37945_{5/2}$	4526.028	4	50	22088.234	$9711_{7/2} - 31800^{\circ}_{7/2}$
4560.394	3	10	21921.785	$7001_{3/2} - 28923^{\circ}_{5/2}$	4525.090	10	200	22092.812	$11116^{\circ}_{7/2} - 33209_{7/2}$
4558.029	2	10	21933.159	$9061_{3/2} - 30994^{\circ}_{7/2}$	4524.838	25	150	22094.043	$7001_{3/2} - 29095^{\circ}_{5/2}$

TABLE 3. *Classified lines of* Th II—Continued

Wavelength Å	Intensity		Wavenumber cm^{-1}	Classification	Wavelength Å	Intensity		Wavenumber cm^{-1}	Classification
	Lamp	Spark				Lamp	Spark		
4524.560	1	2	22095.400	$14349_{1/2} - 36444^{\circ}_{3/2}$	4471.978	8	20	22355.196	$0_{3/2} - 22355^{\circ}_{1/2}$
4524.432	1	2	22096.025	$21131^{\circ}_{5/2} - 43227_{5/2}$	4471.764	2	200	22356.266	$16033^{\circ}_{5/2} - 38389_{7/2}$
4522.783	2	150	22104.081	$24757^{\circ}_{9/2} - 46861_{11/2}$					$20288^{\circ}_{11/2} - 42644_{13/2}$
4521.458	1	5	22110.559	$12219_{3/2} - 34330^{\circ}_{1/2}$	4470.005	2	75	22365.063	$15236_{3/2} - 37601^{\circ}_{3/2}$
				$17837^{\circ}_{1/2} - 39948_{1/2}$	4469.754	2	3	22366.319	$8605_{5/2} - 30972^{\circ}_{5/2}$
4520.949	2	75	22113.048	$21131^{\circ}_{3/2} - 43244_{3/2}$	4465.931	2	2	22385.465	$22513^{\circ}_{5/2} - 44898_{7/2}$
4520.034	3	15	22117.524	$24463^{\circ}_{5/2} - 46581_{5/2}$	4465.341	200	200	22388.423	$8605_{5/2} - 30994^{\circ}_{7/2}$
4519.621	1	2	22119.546	$20080^{\circ}_{7/2} - 42200_{9/2}$	4463.190	2	20	22399.213	$9400_{5/2} - 31800^{\circ}_{7/2}$
4518.636	3b	100	22124.367	$25607^{\circ}_{9/2} - 47731_{9/2}$	4463.080	1	25	22399.765	$25607^{\circ}_{9/2} - 48006_{9/2}$
				$17771^{\circ}_{11/2} - 39895_{9/2}$	4461.705	4	200	22406.668	$18816^{\circ}_{13/2} - 41223_{11/2}$
4517.036	4b	200	22132.204	$24132^{\circ}_{3/2} - 46264_{3/2}$	4461.125	4	150	22409.581	$9400_{5/2} - 31810^{\circ}_{5/2}$
				$16033^{\circ}_{5/2} - 38165_{7/2}$	4461.065	4	200	22409.882	$13468^{\circ}_{9/2} - 35878_{7/2}$
4512.483	8	200	22154.535	$11576^{\circ}_{3/2} - 33730_{5/2}$	4457.082	2	4	22429.908	$18214^{\circ}_{3/2} - 40644_{5/2}$
4510.946	2	3	22162.083	$16906^{\circ}_{7/2} - 39068_{7/2}$	4456.708	4	150	22431.790	$10189^{\circ}_{11/2} - 32620_{11/2}$
4510.526	200	600	22164.147	$10572^{\circ}_{9/2} - 32736_{7/2}$	4455.715	2	100	22436.789	$15242^{\circ}_{9/2} - 37679_{11/2}$
4509.581	2		22168.791	$9585^{\circ}_{5/2} - 31754_{5/2}$	4455.576	3	2	22437.489	$28587^{\circ}_{3/2} - 51024_{3/2}$
4508.841	1	2	22172.429	$17722^{\circ}_{9/2} - 39895_{9/2}$	4455.424	2	2	22438.255	$20080^{\circ}_{7/2} - 42518_{7/2}$
4508.639	1	2	22173.423	$12488^{\circ}_{9/2} - 34661_{11/2}$	4455.294	5	20	22438.909	$19880_{9/2} - 42319^{\circ}_{9/2}$
4508.163	5	40	22175.764	$1521_{5/2} - 23697^{\circ}_{7/2}$	4455.045	3	200	22440.164	$19248^{\circ}_{5/2} - 41688_{7/2}$
4506.071	2	2	22186.059	$17272^{\circ}_{9/2} - 39458_{7/2}$	4455.005	2	10	22440.365	$20310^{\circ}_{5/2} - 42751_{7/2}$
4498.108	1	1	22225.335	$15349^{\circ}_{11/2} - 37575_{13/2}$	4454.513	8	300	22442.844	$11576^{\circ}_{3/2} - 34019_{3/2}$
4496.315	8	200	22234.197	$19912^{\circ}_{13/2} - 42146_{11/2}$	4452.791	1	8	22451.522	$15305_{9/2} - 37756^{\circ}_{7/2}$
4495.489	3	100	22238.282	$12488^{\circ}_{9/2} - 34726_{7/2}$	4451.268	5	4	22459.204	$23187^{\circ}_{13/2} - 45646_{13/2}$
4495.241	3	150	22239.509	$17983^{\circ}_{5/2} - 40222_{3/2}$	4451.051	2	100	22460.299	$16906^{\circ}_{7/2} - 39366_{5/2}$
4494.964	4	200	22240.880	$12485^{\circ}_{7/2} - 34726_{7/2}$	4448.555	5	100	22472.901	$4113_{5/2} - 26586^{\circ}_{3/2}$
4494.076	4	40	22245.274	$17121^{\circ}_{3/2} - 39366_{5/2}$	4448.133	1	2	22475.033	$21297^{\circ}_{5/2} - 43772_{5/2}$
4493.651	1	2	22247.378	$13818^{\circ}_{7/2} - 36065_{5/2}$	4447.834	100	400	22476.544	$6244_{1/2} - 28720^{\circ}_{5/2}$
4492.236	4	200	22254.386	$12472^{\circ}_{5/2} - 34726_{7/2}$	4447.787	8	20	22476.781	$26647^{\circ}_{13/2} - 49124_{11/2}$
4491.884	2	100	22256.130	$20080^{\circ}_{7/2} - 42336_{5/2}$	4444.987	4	150	22490.940	$15349^{\circ}_{11/2} - 37840_{9/2}$
4491.708	2	100	22257.002	$20989^{\circ}_{9/2} - 43246_{7/2}$	4443.086	20	300	22500.562	$8378^{\circ}_{7/2} - 30879_{7/2}$
4491.378	2	100	22258.637	$16033^{\circ}_{5/2} - 38291_{7/2}$	4442.370	1	15	22504.189	$22685^{\circ}_{7/2} - 45189_{5/2}$
4490.354	2	50	22263.713	$14545^{\circ}_{3/2} - 36809_{7/2}$	4441.905	2	25	22506.545	$21297^{\circ}_{5/2} - 43803_{7/2}$
4490.198	2	150	22264.486	$15305_{9/2} - 37569^{\circ}_{9/2}$	4440.866	200	200	22511.810	$8460_{3/2} - 30972^{\circ}_{5/2}$
4489.611	2	2	22267.397	$29095^{\circ}_{5/2} - 51362_{3/2}$	4440.574	150	200	22513.291	$0_{3/2} - 22513^{\circ}_{5/2}$
4489.527	2	40	22267.814	$11116^{\circ}_{7/2} - 33384_{9/2}$	4439.124	150	400	22520.644	$11116^{\circ}_{7/2} - 33637_{7/2}$
4488.678	100	500	22272.026	$4490^{\circ}_{3/2} - 26762_{3/2}$	4437.722	20	20	22527.759	$9400_{5/2} - 31928^{\circ}_{3/2}$
4488.628	3	20	22272.274	$14790^{\circ}_{7/2} - 37063_{9/2}$	4436.553	75	8	22533.695	$14275^{\circ}_{9/2} - 36809_{7/2}$
4487.495	100	300	22277.897	$4146_{7/2} - 26424^{\circ}_{5/2}$	4436.375	1	8	22534.599	$22355^{\circ}_{1/2} - 44889_{3/2}$
4486.631	15	300	22282.187	$18816^{\circ}_{13/2} - 41099_{15/2}$	4436.286	50	200	22535.051	$9238^{\circ}_{9/2} - 31773_{9/2}$
4485.795	8	200	22286.340	$10673^{\circ}_{5/2} - 32959_{3/2}$	4436.145	1	15	22535.767	$18118_{3/2} - 40654^{\circ}_{5/2}$
4484.291	4	75	22293.814	$11725^{\circ}_{1/2} - 34019_{3/2}$	4436.049	20	200	22536.255	$10673^{\circ}_{5/2} - 33209_{7/2}$
4484.235	2	2	22294.092	$23012^{\circ}_{3/2} - 45306_{3/2}$	4434.829	4	50	22542.455	$7331^{\circ}_{3/2} - 29873_{7/2}$
4484.106	2	25	22294.734	$17983^{\circ}_{3/2} - 40278_{3/2}$	4434.516	1	5	22544.046	$22106_{5/2} - 44650^{\circ}_{7/2}$
4481.640	3	150	22307.001	$13818^{\circ}_{7/2} - 36125_{9/2}$	4434.332	4	75	22544.981	$15242^{\circ}_{9/2} - 37787_{7/2}$
4481.178	2	150	22309.301	$18214^{\circ}_{3/2} - 40523_{1/2}$	4433.723	2	75	22548.078	$23187^{\circ}_{13/2} - 45735_{11/2}$
4480.909	2	2	22310.640	$22139^{\circ}_{9/2} - 44450_{9/2}$	4432.962	500	800	22551.948	$9202^{\circ}_{7/2} - 31754_{5/2}$
4479.158	3	150	22319.362	$15242^{\circ}_{9/2} - 37562_{11/2}$	4432.420	2	4	22554.706	$1859_{3/2} - 24414^{\circ}_{3/2}$
4474.073	20	200	22344.728	$13248_{9/2} - 35593^{\circ}_{9/2}$	4431.628	1	5	22558.737	$20686^{\circ}_{5/2} - 43244_{3/2}$
4472.275	5	200	22353.711	$13248_{9/2} - 35602^{\circ}_{11/2}$	4429.594	3	75	22569.095	$14484^{\circ}_{11/2} - 37053_{11/2}$
4472.105	1	1	22354.561	$18973^{\circ}_{7/2} - 41328_{5/2}$	4429.258	50	100	22570.807	$9202^{\circ}_{7/2} - 31773_{9/2}$

TABLE 3. *Classified lines of* Th II – Continued

Wavelength Å	Intensity		Wavenumber cm^{-1}	Classification	Wavelength Å	Intensity		Wavenumber cm^{-1}	Classification
	Lamp	Spark				Lamp	Spark		
4427.786	4	50	22578.311	$10379_{9/2} - 32957^{\circ}_{7/2}$	4396.477	75	300	22739.097	$9061_{5/2} - 31800^{\circ}_{7/2}$
4427.655	50	300	22578.979	$17121^{\circ}_{3/2} - 39700_{5/2}$	4394.894	100	300	22747.287	$8605_{5/2} - 31353^{\circ}_{3/2}$
				$14484^{\circ}_{11/2} - 37063_{9/2}$	4393.059	40l	400	22756.788	$26770^{\circ}_{11/2} - 49527_{13/2}$
4426.050	1	50	22587.166	$29720^{\circ}_{3/2} - 52307_{3/2}$	4392.611	1	8	22759.109	$22139^{\circ}_{9/2} - 44898_{7/2}$
4425.983	8	200	22587.508	$26770^{\circ}_{11/2} - 49357_{11/2}$	4391.110	600	1000	22766.889	$4490^{\circ}_{5/2} - 27257_{7/2}$
4425.114	2	25	22591.944	$25414^{\circ}_{11/2} - 48006_{9/2}$	4390.580	1	50	22769.637	$29095^{\circ}_{5/2} - 51865_{5/2}$
4423.933	25b	50b	22597.975	$15242^{\circ}_{9/2} - 37840_{9/2}$	4390.409	2	15	22770.524	$24132^{\circ}_{3/2} - 46902_{5/2}$
4423.903	20b	40b	22598.128	$11576^{\circ}_{3/2} - 34174_{5/2}$	4389.438	1		22775.561	$28587^{\circ}_{5/2} - 51362_{5/2}$
4422.781	50	100	22603.861	$1859_{3/2} - 24463^{\circ}_{5/2}$	4388.999	3		22777.839	$14275^{\circ}_{9/2} - 37053_{11/2}$
4421.831	5	100	22608.717	$30310^{\circ}_{11/2} - 52918_{13/2}$	4388.402	10	150	22780.938	$14349_{1/2} - 37130^{\circ}_{1/2}$
4421.664	1	5	22609.571	$15236_{3/2} - 37846^{\circ}_{5/2}$	4387.502	2	50	22785.611	$20310^{\circ}_{5/2} - 43096_{5/2}$
4421.544	400l	200	22610.184	$1521_{5/2} - 24132^{\circ}_{3/2}$	4387.479	3		22785.730	$20158_{5/2} - 42944^{\circ}_{7/2}$
4420.737	5	4	22614.312	$11116^{\circ}_{7/2} - 33730_{5/2}$	4387.104	5	100	22787.678	$16564^{\circ}_{11/2} - 39352_{11/2}$
4419.322	2	10	22621.552	$23730^{\circ}_{9/2} - 46352_{7/2}$	4386.107	2		22792.857	$22513^{\circ}_{5/2} - 45306_{3/2}$
4419.006	5	200	22623.170	$17272^{\circ}_{9/2} - 39895_{9/2}$	4384.019	5	5	22803.713	$17771^{\circ}_{11/2} - 40574_{11/2}$
4418.661	40	200	22624.936	$16818_{7/2} - 39443^{\circ}_{9/2}$	4383.933	1	3	22804.160	$36812_{1/2} - 59616^{\circ}_{3/2}$
4416.236	100	300	22637.360	$10572^{\circ}_{9/2} - 33209_{7/2}$	4382.007	2		22814.183	$20989^{\circ}_{9/2} - 43803_{7/2}$
4415.592	3	10h	22640.662	$21131^{\circ}_{3/2} - 43772_{5/2}$	4381.860	800	1000	22814.949	$6700^{\circ}_{9/2} - 29515_{9/2}$
4414.853	1	8	22644.451	$17722^{\circ}_{9/2} - 40367_{9/2}$	4381.402	75	200	22817.333	$4146_{7/2} - 26963^{\circ}_{7/2}$
4414.623	15	200	22645.631	$16906^{\circ}_{7/2} - 39552_{9/2}$	4380.144	2		22823.887	$19594_{1/2} - 42418^{\circ}_{3/2}$
4413.373	5b	150	22652.045	$15453^{\circ}_{7/2} - 38105_{5/2}$	4379.941	2	1	22824.944	$23730^{\circ}_{9/2} - 46555_{11/2}$
4412.891	100	200	22654.519	$6691^{\circ}_{3/2} - 29345_{5/2}$	4379.587	3	8	22826.789	$17121^{\circ}_{3/2} - 39948_{1/2}$
4412.797	50	100	22655.001	$22834_{7/2} - 45489^{\circ}_{9/2}$	4378.957	3	4	22830.073	$15349^{\circ}_{11/2} - 38179_{9/2}$
4412.739	300	400	22655.299	$6168^{\circ}_{7/2} - 28823_{5/2}$	4378.833	4	15	22830.720	$16033^{\circ}_{5/2} - 38863_{5/2}$
4412.533	50b	400b	22656.357	$13468^{\circ}_{9/2} - 36125_{9/2}$	4377.313	40	200	22838.647	$20288^{\circ}_{11/2} - 43127_{11/2}$
4411.641	3	50	22660.938	$17983^{\circ}_{5/2} - 40644_{5/2}$	4377.261	3	25	22838.919	$12902^{\circ}_{3/2} - 35741_{5/2}$
4410.488	20	200	22666.862	$17272^{\circ}_{9/2} - 39939_{11/2}$	4375.588	10	100	22847.651	$17722^{\circ}_{9/2} - 40570_{7/2}$
4410.410	5	200	22667.263	$20288^{\circ}_{11/2} - 42955_{9/2}$	4375.022	8	15	22850.607	$4113_{3/2} - 26963^{\circ}_{7/2}$
4409.005	15	50	22674.486	$14790^{\circ}_{7/2} - 37465_{5/2}$	4374.785	150	400	22851.845	$4113_{3/2} - 26965^{\circ}_{3/2}$
4408.769	1	8	22675.700	$21131^{\circ}_{3/2} - 43807_{3/2}$	4373.901	100	200	22856.463	$9720^{\circ}_{7/2} - 32576_{7/2}$
4407.510	1	4	22682.177	$27787^{\circ}_{9/2} - 50470_{9/2}$	4372.814	2	20	22862.145	$24309^{\circ}_{11/2} - 47171_{9/2}$
4406.997	1	8	22684.817	$24463^{\circ}_{5/2} - 47148_{3/2}$	4371.767	4	4	22867.620	$9061_{3/2} - 31928^{\circ}_{3/2}$
4406.785	2	20	22685.908	$17837^{\circ}_{1/2} - 40523_{1/2}$	4370.773	4	2	22872.820	$34019_{3/2} - 56892^{\circ}_{5/2}$
4406.429	2	50	22687.741	$23697^{\circ}_{7/2} - 46385_{7/2}$	4370.011	4	2	22876.809	$33209_{7/2} - 56086^{\circ}_{9/2}$
4406.329	1	10	22688.256	$19248^{\circ}_{5/2} - 41936_{3/2}$	4369.317	50b	200b	22880.442	$33354^{\circ}_{5/2} - 56235_{3/2}$
4405.724	1	25	22691.371	$25607^{\circ}_{9/2} - 48298_{7/2}$					$8378^{\circ}_{7/2} - 31259_{5/2}$
4404.917	2	25	22695.529	$16033^{\circ}_{5/2} - 38728_{5/2}$	4369.061	5	20	22881.783	$22513^{\circ}_{5/2} - 45395_{7/2}$
4402.736	4	100	22706.771	$15786_{5/2} - 38493^{\circ}_{5/2}$	4368.706	2		22883.642	$23697^{\circ}_{7/2} - 46581_{5/2}$
4401.992	2	25	22710.609	$14101^{\circ}_{1/2} - 36812_{1/2}$	4368.314	1		22885.695	$19050^{\circ}_{3/2} - 41936_{3/2}$
4401.658	10	200	22712.332	$15453^{\circ}_{7/2} - 38165_{7/2}$	4366.961	75	50	22892.786	$8460_{3/2} - 31353^{\circ}_{3/2}$
4401.209	3	100	22714.649	$18973^{\circ}_{7/2} - 41688_{7/2}$	4364.187	2	25	22907.337	$28923^{\circ}_{5/2} - 51830_{7/2}$
4401.050	1	8	22715.470	$22106_{5/2} - 44821^{\circ}_{5/2}$	4362.361	5	25	22916.925	$20310^{\circ}_{5/2} - 43227_{5/2}$
4400.646	1	2	22717.555	$34174_{5/2} - 56892^{\circ}_{5/2}$	4361.792	10	100	22919.915	$14545^{\circ}_{5/2} - 37465_{5/2}$
4400.384	20	150	22718.908	$7001_{3/2} - 29720^{\circ}_{3/2}$	4361.307	100l	200	22922.464	$15242^{\circ}_{9/2} - 38165_{7/2}$
4399.093	10	300	22725.575	$20288^{\circ}_{11/2} - 43014_{13/2}$	4359.804	1		22930.366	$37063_{9/2} - 59993^{\circ}_{9/2}$
4398.837	1	5	22726.897	$15453^{\circ}_{7/2} - 38179_{9/2}$	4359.127	5	25	22933.927	$20310^{\circ}_{5/2} - 43244_{3/2}$
4398.020	1	25	22731.119	$24414^{\circ}_{5/2} - 47145_{1/2}$	4358.815	5	40	22935.569	$18973^{\circ}_{7/2} - 41909_{9/2}$
4397.914	75	300	22731.667	$6700^{\circ}_{9/2} - 29431_{7/2}$	4358.668	4		22936.342	$15453^{\circ}_{7/2} - 38389_{7/2}$
4397.752	2	1	22732.504	$19912^{\circ}_{13/2} - 42644_{13/2}$	4358.549	50s	100	22936.968	$12219_{3/2} - 35156^{\circ}_{5/2}$
4397.260	1	15	22735.048	$29095^{\circ}_{5/2} - 51830_{7/2}$	4357.928	2		22940.237	$17983^{\circ}_{5/2} - 40923_{5/2}$
									$37053_{11/2} - 59993^{\circ}_{9/2}$

TABLE 3. *Classified lines of* Th II—Continued

Wavelength Å	Intensity		Wavenumber cm^{-1}	Classification	Wavelength Å	Intensity		Wavenumber cm^{-1}	Classification
	Lamp	Spark				Lamp	Spark		
4357.614	100b	150	22941.890	$1521_{5/2} - 24463^{\circ}_{5/2}$	4327.228	50	75	23102.986	$4146_{7/2} - 27249^{\circ}_{7/2}$
4357.074	4	8	22944.733	$13248^{\circ}_{9/2} - 36193^{\circ}_{9/2}$	4327.091	25	75	23103.717	$4490^{\circ}_{5/2} - 27593_{5/2}$
4355.911	2	8	22950.859	$17460^{\circ}_{5/2} - 40411_{7/2}$	4326.576	2	2	23106.467	$20989^{\circ}_{9/2} - 44096_{9/2}$
4355.320	100	300	22953.973	$8018_{3/2} - 30972^{\circ}_{5/2}$	4326.341	2	5	23107.722	$20120^{\circ}_{3/2} - 43227_{5/2}$
4353.405	75b	200	22964.070	$10673^{\circ}_{5/2} - 33637_{7/2}$	4326.179	3	8	23108.588	$18568^{\circ}_{1/2} - 41676_{3/2}$
4352.818	40	75	22967.167	$11576^{\circ}_{3/2} - 34543_{5/2}$	4325.920	2		23109.971	$17460^{\circ}_{5/2} - 40570_{7/2}$
4352.677	50	200	22967.911	$12488^{\circ}_{9/2} - 35456_{9/2}$	4325.663	2		23111.344	$22014^{\circ}_{11/2} - 45126_{9/2}$
4352.182	5	10	22970.523	$36328_{3/2} - 59299^{\circ}_{5/2}$	4325.189	2		23113.877	$24757^{\circ}_{9/2} - 47871_{7/2}$
4351.073	3		22976.378	$20120^{\circ}_{5/2} - 43096_{5/2}$	4324.958	4		23115.112	$22106_{5/2} - 45221^{\circ}_{5/2}$
					4324.442	4	4	23117.870	$20686^{\circ}_{5/2} - 43803_{7/2}$
4350.572	4	8	22979.024	$12219_{3/2} - 35198^{\circ}_{1/2}$	4323.165	1		23124.698	$20120^{\circ}_{5/2} - 43244_{3/2}$
4348.943	4s	8	22987.631	$16564^{\circ}_{11/2} - 39552_{9/2}$	4323.043	8	25	23125.351	$15710^{\circ}_{3/2} - 38836_{3/2}$
4348.713	3		22988.847	$16906^{\circ}_{7/2} - 39895_{9/2}$	4322.788	1	1	23126.715	$20120^{\circ}_{5/2} - 43246_{7/2}$
4348.312	20	40	22990.967	$13818^{\circ}_{7/2} - 36809_{7/2}$	4322.386	2	1	23128.866	$20158_{5/2} - 43287^{\circ}_{5/2}$
4348.236	5	8	22991.368	$9585^{\circ}_{5/2} - 32576_{7/2}$	4322.001	3	10	23130.926	$23730^{\circ}_{9/2} - 46861_{11/2}$
4347.430	1		22995.631	$24873^{\circ}_{5/2} - 47869_{3/2}$	4321.012	8	20	23136.220	$4113_{3/2} - 27249^{\circ}_{7/2}$
4347.239	25h	200	22996.641	$26963^{\circ}_{7/2} - 49960_{7/2}$	4320.657	3	20	23138.121	$9711_{7/2} - 32850^{\circ}_{5/2}$
4347.193	20	200	22996.885	$14790^{\circ}_{7/2} - 37787_{7/2}$	4320.590	50	300	23138.480	$12902^{\circ}_{3/2} - 36040_{1/2}$
4347.092	1		22997.419	$24873^{\circ}_{5/2} - 47871_{7/2}$	4320.449	5	200	23139.235	$17272^{\circ}_{9/2} - 40411_{7/2}$
4346.262	5	15	23001.811	$14275^{\circ}_{9/2} - 37277_{7/2}$	4320.126	200	500	23140.965	$4490^{\circ}_{3/2} - 27631_{3/2}$
4345.052	10	40	23008.216	$17983^{\circ}_{5/2} - 40991_{3/2}$	4319.097	10	300	23146.478	$15242^{\circ}_{9/2} - 38389_{7/2}$
4344.984	3	20	23008.576	$23697^{\circ}_{7/2} - 46706_{7/2}$	4318.959	2	50	23147.218	$20080^{\circ}_{7/2} - 43227_{5/2}$
4344.326	400	300	23012.061	$0_{3/2} - 23012^{\circ}_{3/2}$	4318.293	50	300	23150.787	$9585^{\circ}_{5/2} - 32736_{7/2}$
4343.951	200	300	23014.048	$1859_{3/2} - 24873^{\circ}_{5/2}$	4317.756	2	8	23153.667	$11116^{\circ}_{7/2} - 34270_{9/2}$
4343.602	50	200	23015.897	$30994^{\circ}_{7/2} - 54010_{7/2}$	4317.670	2	10	23154.128	$14790^{\circ}_{7/2} - 37945_{3/2}$
				$9720^{\circ}_{7/2} - 32736_{7/2}$	4317.222	3	20	23156.531	$17121^{\circ}_{3/2} - 40278_{3/2}$
4343.238	10	20	23017.826	$15710^{\circ}_{3/2} - 38728_{5/2}$	4315.946	25	100	23163.377	$12902^{\circ}_{3/2} - 36065_{3/2}$
4342.255	100	200	23023.036	$12570_{7/2} - 35593^{\circ}_{7/2}$	4315.706	4	25	23164.665	$15453^{\circ}_{7/2} - 38617_{9/2}$
4341.992	1		23024.431	$24982^{\circ}_{7/2} - 48006_{9/2}$	4315.579	4	8	23165.347	$8460_{3/2} - 31625^{\circ}_{1/2}$
4341.030	50	300	23029.533	$23187^{\circ}_{13/2} - 46216_{11/2}$	4314.010	5	8	23173.771	$6700^{\circ}_{9/2} - 29873_{7/2}$
4339.650	4h	8	23036.856	$12488^{\circ}_{9/2} - 35525_{11/2}$	4313.308	15	50	23177.543	$6168^{\circ}_{7/2} - 29345_{5/2}$
4338.383	4	10	23043.584	$16818_{7/2} - 39861^{\circ}_{5/2}$	4312.156	3	5	23183.735	$17460^{\circ}_{5/2} - 40644_{5/2}$
4337.860	5	10	23046.362	$15710^{\circ}_{3/2} - 38757_{3/2}$	4310.644	2	40	23191.867	$23187^{\circ}_{13/2} - 46378_{13/2}$
4337.384	100	800	23048.891	$15242^{\circ}_{9/2} - 38291_{7/2}$	4310.550	1		23192.372	$24132^{\circ}_{3/2} - 47324_{5/2}$
4336.494	3		23053.621	$30956^{\circ}_{9/2} - 54010_{7/2}$	4310.179	5	25	23194.369	$8605_{5/2} - 31800^{\circ}_{7/2}$
4335.797	50	200	23057.327	$12488^{\circ}_{9/2} - 35545_{9/2}$	4309.991	100	800	23195.380	$14484^{\circ}_{11/2} - 37679_{11/2}$
4335.687	25b	200b	23057.912	$11116^{\circ}_{7/2} - 34174_{5/2}$					$10189^{\circ}_{11/2} - 33384_{9/2}$
4335.312	25b	200	23059.907	$12485^{\circ}_{7/2} - 35545_{9/2}$	4309.215	1		23199.557	$15236_{3/2} - 38436^{\circ}_{3/2}$
4334.316	5	5	23065.206	$10572^{\circ}_{9/2} - 33637_{7/2}$	4308.255	8	15	23204.727	$8605_{5/2} - 31810^{\circ}_{3/2}$
4334.254	5	5	23065.536	$18816^{\circ}_{13/2} - 41882_{13/2}$	4307.956	2	10	23206.337	$21297^{\circ}_{5/2} - 44503_{7/2}$
4333.933	50	150	23067.244	$22028^{\circ}_{15/2} - 45095_{13/2}$	4306.365	200b	200b	23214.911	$19912^{\circ}_{13/2} - 43127_{11/2}$
4331.924	75l	200	23077.942	$14484^{\circ}_{11/2} - 37562_{11/2}$	4306.159	1	5	23216.021	$21682^{\circ}_{7/2} - 44898_{7/2}$
4330.351	2		23086.325	$20686^{\circ}_{5/2} - 43772_{5/2}$	4305.328	2	100	23220.502	$27249^{\circ}_{7/2} - 50470_{9/2}$
4329.907	3	10	23088.692	$28587^{\circ}_{5/2} - 51676_{3/2}$	4304.070	2	5	23227.289	$15144^{\circ}_{3/2} - 38372_{3/2}$
4329.489	40	100	23090.921	$14484^{\circ}_{11/2} - 37575_{13/2}$	4302.109	2	40	23237.876	$25607^{\circ}_{9/2} - 48844_{9/2}$
4329.107	10	50	23092.959	$22642^{\circ}_{9/2} - 45735_{11/2}$	4301.280	3	10	23242.355	$14545^{\circ}_{5/2} - 37787_{7/2}$
4328.686	40	100	23095.205	$17272^{\circ}_{9/2} - 40367_{9/2}$	4300.793	8	150	23244.987	$13818^{\circ}_{7/2} - 37063_{9/2}$
4328.286	15	50	23097.339	$22513^{\circ}_{5/2} - 45610_{5/2}$	4300.700	2	3	23245.489	$9711_{7/2} - 32957^{\circ}_{7/2}$
4327.546	5	50	23101.288	$17121^{\circ}_{3/2} - 40222_{3/2}$	4300.135	2	10	23248.544	$18973^{\circ}_{7/2} - 42222_{7/2}$
4327.448	4	50	23101.811	$19912^{\circ}_{13/2} - 43014_{13/2}$	4299.435	3	50	23252.329	$14349_{1/2} - 37601^{\circ}_{3/2}$

530-326 OL - 74 - 8

TABLE 3. *Classified lines of* Th II—Continued

Wavelength Å	Intensity		Wavenumber cm^{-1}	Classification	Wavelength Å	Intensity		Wavenumber cm^{-1}	Classification
	Lamp	Spark				Lamp	Spark		
4298.891	25	50	23255.271	$21297^{\circ}_{5/2} - 44552_{5/2}$	4271.546	3	20	23404.141	$14275^{\circ}_{9/2} - 37679_{11/2}$
4298.826	20	200b	23255.623	$12485^{\circ}_{7/2} - 35741_{5/2}$	4271.240	3	50	23405.818	$24463^{\circ}_{3/2} - 47869_{3/2}$
4298.283	1		23258.560	$14349_{1/2} - 37607^{\circ}_{1/2}$	4271.103	40b	200	23406.568	$1859_{3/2} - 25266^{\circ}_{1/2}$
4297.365	25b	75	23263.529	$6168^{\circ}_{7/2} - 29431_{7/2}$	4271.084	20b		23406.672	$12472^{\circ}_{5/2} - 35878_{7/2}$
4296.580	3	10	23267.779	$15349^{\circ}_{11/2} - 38617_{9/2}$	4270.911	1	10	23407.620	$24463^{\circ}_{5/2} - 47871_{7/2}$
4295.125	8	100	23275.661	$15453^{\circ}_{7/2} - 38728_{5/2}$	4270.326	50	200	23410.827	$15453^{\circ}_{7/2} - 38863_{5/2}$
4295.035	20		23276.149	$17771^{\circ}_{11/2} - 41047_{9/2}$	4267.716	4	15	23425.144	$16033^{\circ}_{5/2} - 39458_{7/2}$
4293.218	1		23286.000	$19050^{\circ}_{3/2} - 42336_{5/2}$	4267.518	20	50	23426.231	$12902^{\circ}_{3/2} - 36328_{3/2}$
4293.089	1	3	23286.700	$14275^{\circ}_{9/2} - 37562_{11/2}$	4267.381	2	5	23426.983	$11116^{\circ}_{7/2} - 34543_{5/2}$
4292.509	10b	8	23289.846	$4113_{5/2} - 27403^{\circ}_{3/2}$	4266.823	1		23430.047	$25414^{\circ}_{11/2} - 48844_{9/2}$
4291.382	4	40	23295.962	$11725^{\circ}_{1/2} - 35021_{3/2}$	4265.661	1		23436.429	$27787^{\circ}_{9/2} - 51224_{9/2}$
4290.829	1		23298.965	$33384_{9/2} - 56683^{\circ}_{7/2}$	4265.488	8	15	23437.380	$11116^{\circ}_{7/2} - 34553_{9/2}$
4290.169	15	50	23302.549	$17272^{\circ}_{9/2} - 40574_{11/2}$	4265.034	5	25	23439.874	$18568^{\circ}_{1/2} - 42008_{1/2}$
4288.047	20	200	23314.080	$14790^{\circ}_{7/2} - 38105_{5/2}$	4264.943	5		23440.375	$14101^{\circ}_{1/2} - 37542_{3/2}$
4287.683	4	75	23316.059	$24982^{\circ}_{7/2} - 48298_{7/2}$	4264.374	4l	100	23443.502	$21682^{\circ}_{7/2} - 45126_{9/2}$
4286.699	5	200	23321.411	$22834_{7/2} - 46155^{\circ}_{5/2}$	4264.105	20	50	23444.981	$11576^{\circ}_{3/2} - 35021_{3/2}$
4286.187	15b	200b	23324.197	$17722^{\circ}_{9/2} - 41047_{9/2}$	4263.355	200	75	23449.105	$9400_{5/2} - 32850^{\circ}_{5/2}$
4285.450	3	8	23328.208	$1859_{3/2} - 25188^{\circ}_{3/2}$	4262.739	5	3	23452.494	$17771^{\circ}_{11/2} - 41223_{11/2}$
4285.181	15	200	23329.672	$18816^{\circ}_{13/2} - 42146_{11/2}$	4261.273	50	4	23460.562	$1521_{5/2} - 24982^{\circ}_{7/2}$
4284.975	50	200	23330.794	$16564^{\circ}_{11/2} - 39895_{9/2}$	4260.936	4		23462.418	$18214^{\circ}_{3/2} - 41676_{3/2}$
4284.927	3	5	23331.056	$13250_{5/2} - 36581^{\circ}_{3/2}$	4259.857	3		23468.360	$8460_{3/2} - 31928^{\circ}_{3/2}$
4284.514	10b	10	23333.305	$13250_{5/2} - 36583^{\circ}_{7/2}$	4258.828	2		23474.031	$33209_{7/2} - 56683^{\circ}_{7/2}$
4284.431	3	8	23333.756	$16033^{\circ}_{5/2} - 39366_{5/2}$	4258.466	3		23476.026	$6244_{1/2} - 29720^{\circ}_{3/2}$
4284.215	2	8	23334.933	$8018_{3/2} - 31353^{\circ}_{3/2}$	4256.094	50	10	23489.109	$9720^{\circ}_{7/2} - 33209_{7/2}$
4284.181	3	1	23335.118	$13248_{9/2} - 36583^{\circ}_{7/2}$	4254.739	1		23496.590	$20310^{\circ}_{5/2} - 43807_{3/2}$
4283.519	150	400	23338.724	$9238^{\circ}_{9/2} - 32576_{7/2}$	4254.451	75	8	23498.180	$9238^{\circ}_{9/2} - 32736_{7/2}$
4282.370	10l	200	23344.986	$17983^{\circ}_{5/2} - 41328_{5/2}$	4254.169	1		23499.738	$30994^{\circ}_{7/2} - 54493_{5/2}$
				$15236_{3/2} - 38581^{\circ}_{3/2}$	4254.021	5		23500.555	$17722^{\circ}_{9/2} - 41223_{11/2}$
4282.042	300b	500b	23346.774	$6168^{\circ}_{7/2} - 29515_{9/2}$	4253.975	2		23500.810	$14790^{\circ}_{7/2} - 38291_{7/2}$
4281.758	2	2	23348.323	$28587^{\circ}_{5/2} - 51935_{5/2}$	4253.867	15	8	23501.406	$10673^{\circ}_{5/2} - 34174_{5/2}$
4281.416	150	400	23350.188	$8460_{3/2} - 31810^{\circ}_{5/2}$	4253.259	3b		23504.766	$17983^{\circ}_{5/2} - 41488_{7/2}$
4281.068	200	500	23352.086	$1521_{5/2} - 24873^{\circ}_{5/2}$	4253.239	2b		23504.876	$16906^{\circ}_{7/2} - 40411_{7/2}$
4280.253	3	8	23356.532	$14484^{\circ}_{11/2} - 37840_{9/2}$	4253.017	1		23506.103	$26963^{\circ}_{7/2} - 50470_{9/2}$
4280.221	5	8	23356.707	$10855_{7/2} - 34212^{\circ}_{5/2}$	4252.876	1		23506.883	$21682^{\circ}_{7/2} - 45189_{5/2}$
4278.507	5	50	23366.064	$16818_{7/2} - 40184^{\circ}_{7/2}$	4251.958	1		23511.957	$15324^{\circ}_{1/2} - 38836_{3/2}$
4278.110	1		23368.232	$18568^{\circ}_{1/2} - 41936_{3/2}$	4251.781	1		23512.936	$15349^{\circ}_{11/2} - 38862_{11/2}$
4277.313	600	500	23372.586	$0_{3/2} - 23372^{\circ}_{3/2}$	4251.592	2		23513.982	$20989^{\circ}_{9/2} - 44503_{7/2}$
4277.039	40	100	23374.083	$9585^{\circ}_{5/2} - 32959_{3/2}$	4250.341	100b		23520.902	$4490^{\circ}_{5/2} - 28011_{3/2}$
4276.966	100l	300	23374.482	$16564^{\circ}_{11/2} - 39939_{11/2}$	4250.014	1		23522.712	$17121^{\circ}_{3/2} - 40644_{5/2}$
				$9202^{\circ}_{7/2} - 32576_{7/2}$	4249.969	3		23522.961	$10379_{9/2} - 33902^{\circ}_{7/2}$
4276.909	4		23374.794	$15242^{\circ}_{9/2} - 38617_{9/2}$	4249.678	75	10	23524.572	$7828_{1/2} - 31353^{\circ}_{3/2}$
4276.808	100	400	23375.346	$8378^{\circ}_{7/2} - 31754_{5/2}$	4247.989	150	100	23533.925	$9202^{\circ}_{7/2} - 32736_{7/2}$
4275.439	3	3	23382.830	$9238^{\circ}_{9/2} - 32620_{11/2}$	4247.598	50	5	23536.091	$4490^{\circ}_{5/2} - 28026_{5/2}$
4275.240	2		23383.919	$23012^{\circ}_{3/2} - 46395_{3/2}$	4246.363	3		23542.936	$15324^{\circ}_{1/2} - 38867_{1/2}$
4275.203	2		23384.121	$23518^{\circ}_{7/2} - 46902_{5/2}$	4244.824	2		23551.472	$25266^{\circ}_{1/2} - 48817_{3/2}$
4274.321	50		23388.947	$14790^{\circ}_{7/2} - 38179_{9/2}$	4243.925	75	15	23556.461	$9400_{5/2} - 32957^{\circ}_{7/2}$
4274.024	100	300	23390.572	$12488^{\circ}_{9/2} - 35878_{7/2}$	4243.674	1		23557.854	$35741_{5/2} - 59299^{\circ}_{5/2}$
				$15349^{\circ}_{11/2} - 38740_{11/2}$	4243.375	2		23559.514	$14545^{\circ}_{5/2} - 38105_{5/2}$
4273.357	300	800	23394.223	$8378^{\circ}_{7/2} - 31773_{9/2}$	4242.720	15	4	23563.151	$7001_{3/2} - 30564^{\circ}_{1/2}$
4271.913	3	25	23402.130	$17121^{\circ}_{3/2} - 40523_{1/2}$	4242.338	5	3	23565.272	$14275^{\circ}_{9/2} - 37840_{9/2}$

TABLE 3. *Classified lines of* Th II—Continued

Wavelength Å	Intensity		Wavenumber cm^{-1}	Classification	Wavelength Å	Intensity		Wavenumber cm^{-1}	Classification
	Lamp	Spark				Lamp	Spark		
4241.865	2		23567.900	$22685^{\circ}_{7/2} - 46253_{9/2}$	4214.073	1		23723.329	$20080^{\circ}_{7/2} - 43803_{7/2}$
4240.676	4	1	23574.508	$22642^{\circ}_{9/2} - 46216_{11/2}$	4213.994	3		23723.773	$23187^{\circ}_{13/2} - 46910_{13/2}$
4240.594	40	5	23574.964	$6213_{9/2} - 29788^{\circ}_{9/2}$	4213.146	1	2	23728.548	$20080^{\circ}_{7/2} - 43809_{9/2}$
4239.673	5	1	23580.085	$12485^{\circ}_{7/2} - 36065_{5/2}$	4212.452	2		23732.457	$29788^{\circ}_{9/2} - 53520_{9/2}$
4239.030	2		23583.662	$20969^{\circ}_{7/2} - 44552_{5/2}$	4211.514	10	10	23737.743	$16906^{\circ}_{7/2} - 40644_{5/2}$
4238.978	5	4	23583.951	$15144^{\circ}_{3/2} - 38728_{5/2}$	4210.400	1		23744.023	$30101^{\circ}_{7/2} - 53845_{5/2}$
4238.884	1		23584.474	$13468^{\circ}_{9/2} - 37053_{11/2}$	4208.890	200b	200	23752.542	$6700^{\circ}_{9/2} - 30452_{9/2}$
4237.685	2		23591.147	$23012^{\circ}_{3/2} - 46603_{3/2}$	4207.922	1		23758.006	$21131^{\circ}_{3/2} - 44889_{3/2}$
4237.657	1		23591.303	$22106_{5/2} - 45697^{\circ}_{3/2}$	4206.656	5	10	23765.156	$17722^{\circ}_{9/2} - 41488_{7/2}$
4237.113	5	5	23594.332	$13468^{\circ}_{9/2} - 37063_{9/2}$	4201.847	20	100	23792.354	$8018_{3/2} - 31810^{\circ}_{5/2}$
4236.915	2		23595.434	$22139^{\circ}_{9/2} - 45735_{11/2}$	4201.602	8	8	23793.742	$18214^{\circ}_{3/2} - 42008_{1/2}$
4236.390	8	3	23598.358	$14790^{\circ}_{7/2} - 38389_{7/2}$	4201.005	1		23797.123	$7828_{1/2} - 31625^{\circ}_{1/2}$
4235.849	1		23601.372	$21297^{\circ}_{5/2} - 44898_{7/2}$	4199.015	3	10	23808.401	$13468^{\circ}_{9/2} - 37277_{7/2}$
4234.984	25	5	23606.193	$10673^{\circ}_{5/2} - 34279_{7/2}$	4197.936	2	2	23814.520	$9400_{5/2} - 33215^{\circ}_{3/2}$
4234.752	5		23607.486	$8018_{3/2} - 31625^{\circ}_{1/2}$	4195.949	3	15	23825.797	$15242^{\circ}_{9/2} - 39068_{7/2}$
4234.375	3		23609.588	$15786_{5/2} - 39396^{\circ}_{7/2}$	4195.832	4	75	23826.462	$14545^{\circ}_{5/2} - 38372_{3/2}$
4234.302	8	3	23609.995	$11116^{\circ}_{7/2} - 34726_{7/2}$	4195.557	4	75	23828.023	$18816^{\circ}_{13/2} - 42644_{13/2}$
4234.083	1		23611.216	$22642^{\circ}_{9/2} - 46253_{9/2}$	4194.082	2	4	23836.403	$16818^{\circ}_{7/2} - 40654^{\circ}_{5/2}$
4233.511	2		23614.406	$20686^{\circ}_{3/2} - 44300_{3/2}$	4191.995	1		23848.270	$19248^{\circ}_{5/2} - 43096_{3/2}$
4233.287	25	20	23615.656	$15453^{\circ}_{7/2} - 39068_{7/2}$	4191.826	5	10	23849.231	$11576^{\circ}_{3/2} - 35425_{1/2}$
4232.525	3b		23619.907	$15242^{\circ}_{9/2} - 38862_{11/2}$	4190.562	1		23856.425	$12472^{\circ}_{5/2} - 36328_{3/2}$
4231.983	3		23622.932	$12570_{7/2} - 36193^{\circ}_{9/2}$	4188.580	2	5	23867.713	$17460^{\circ}_{5/2} - 41328_{5/2}$
4231.794	4		23623.987	$9585^{\circ}_{5/2} - 33209_{7/2}$	4188.103	1	2	23870.432	$10673^{\circ}_{5/2} - 34543_{5/2}$
4231.174	3		23627.449	$17771^{\circ}_{11/2} - 41398_{9/2}$	4185.035	1	2	23887.931	$6213_{9/2} - 30101^{\circ}_{7/2}$
4229.454	75	15	23637.057	$12488^{\circ}_{9/2} - 36125_{9/2}$	4184.903	3	4	23888.684	$20288^{\circ}_{11/2} - 44177_{11/2}$
4228.988	5	4	23639.662	$12485^{\circ}_{7/2} - 36125_{9/2}$	4184.709	4	25	23889.791	$14275^{\circ}_{9/2} - 38165_{7/2}$
4228.701	10b		23641.266	$4146_{7/2} - 27787^{\circ}_{9/2}$	4184.282	2		23892.229	$21297^{\circ}_{5/2} - 45189_{5/2}$
4227.654	4b	5	23647.121	$13818^{\circ}_{7/2} - 37465_{5/2}$	4183.562	5	15	23896.341	$9061_{3/2} - 32957^{\circ}_{7/2}$
4226.726	3		23652.312	$20120^{\circ}_{5/2} - 43772_{5/2}$	4183.414	1		23897.186	$27631_{3/2} - 51528^{\circ}_{3/2}$
4225.803	5		23657.479	$21131^{\circ}_{3/2} - 44789_{1/2}$	4182.155	5	50	23904.380	$14275^{\circ}_{9/2} - 38179_{9/2}$
4224.614	15	5	23664.137	$9720^{\circ}_{7/2} - 33384_{9/2}$	4181.348	2	4	23908.994	$22355^{\circ}_{1/2} - 46264_{3/2}$
4224.238	10	5	23666.243	$1521_{5/2} - 25188^{\circ}_{3/2}$					$20989^{\circ}_{9/2} - 44898_{7/2}$
4224.142	2		23666.781	$22685^{\circ}_{7/2} - 46352_{7/2}$	4181.161	2	5	23910.063	$12902^{\circ}_{3/2} - 36812_{1/2}$
4222.749	4		23674.588	$23187^{\circ}_{13/2} - 46861_{11/2}$	4181.077	2	3	23910.543	$8018_{3/2} - 31928^{\circ}_{3/2}$
4222.579	3		23675.541	$17722^{\circ}_{9/2} - 41398_{9/2}$	4181.041	2	1	23910.749	$27357^{\circ}_{9/2} - 51268_{7/2}$
4222.185	2		23677.750	$18568^{\circ}_{1/2} - 42246_{1/2}$	4179.958	75	150	23916.944	$9720^{\circ}_{7/2} - 33637_{7/2}$
4219.678	4		23691.818	$20080^{\circ}_{7/2} - 43772_{5/2}$	4179.713	100	150	23918.346	$1521_{5/2} - 25440^{\circ}_{5/2}$
4219.414	2		23693.300	$19594_{1/2} - 43287^{\circ}_{3/2}$	4178.060	150	300	23927.809	$7331^{\circ}_{5/2} - 31259_{5/2}$
4219.380	5	5	23693.491	$17983^{\circ}_{3/2} - 41676_{3/2}$	4176.895	2		23934.483	$27593_{5/2} - 51528^{\circ}_{3/2}$
4218.998	3		23695.636	$14484^{\circ}_{11/2} - 38179_{9/2}$	4176.333	2	5	23937.703	$14790^{\circ}_{7/2} - 38728_{5/2}$
				$24757^{\circ}_{9/2} - 48453_{7/2}$					
					4175.482	1		23942.582	$26965^{\circ}_{3/2} - 50907_{3/2}$
4218.820	1		23696.636	$31800^{\circ}_{7/2} - 55496_{9/2}$	4173.959	1		23951.318	$17272^{\circ}_{9/2} - 41223_{11/2}$
4218.636	2		23697.669	$24309^{\circ}_{11/2} - 48006_{9/2}$	4173.530	4l	4	23953.780	$9400_{3/2} - 33354^{\circ}_{5/2}$
4218.539	10	10	23698.214	$10572^{\circ}_{9/2} - 34270_{9/2}$	4170.783	4	25	23969.556	$13818^{\circ}_{7/2} - 37787_{7/2}$
4218.224	3		23699.984	$22685^{\circ}_{7/2} - 46385_{7/2}$	4170.469	25	50	23971.361	$9238^{\circ}_{9/2} - 33209_{7/2}$
4218.187	8	5	23700.192	$11725^{\circ}_{1/2} - 35425_{1/2}$	4168.633	10	100	23981.919	$10572^{\circ}_{9/2} - 34553_{9/2}$
4217.759	4	1	23702.597	$20686^{\circ}_{3/2} - 44388_{5/2}$	4167.275	2	15	23989.733	$15710^{\circ}_{3/2} - 39700_{5/2}$
4214.629	4		23720.199	$22014^{\circ}_{11/2} - 45735_{11/2}$	4166.493	2h	2	23994.236	$18118_{3/2} - 42112^{\circ}_{3/2}$
4214.537	5	8	23720.717	$17727_{11/2} - 41447^{\circ}_{11/2}$	4165.070	3	10	24002.434	$15349^{\circ}_{11/2} - 39352_{11/2}$
4214.227	1		23722.462	$15144^{\circ}_{3/2} - 38867_{1/2}$	4164.253	10	50	24007.143	$9202^{\circ}_{7/2} - 33209_{7/2}$

TABLE 3. *Classified lines of* Th II—Continued

Wavelength Å	Intensity		Wavenumber cm^{-1}	Classification	Wavelength Å	Intensity		Wavenumber cm^{-1}	Classification
	Lamp	Spark				Lamp	Spark		
4163.733	5	75	24010.141	$16564^{\circ}_{11/2}-40574_{11/2}$	4132.979	1		24188.800	$24132^{\circ}_{3/2}-48320_{5/2}$
4163.645	20	200	24010.648	$9720^{\circ}_{7/2}-33730_{5/2}$	4132.754	150	200	24190.116	$9711_{7/2}-33902^{\circ}_{7/2}$
4163.179	3	15	24013.336	$12570_{7/2}-36583^{\circ}_{7/2}$	4132.287	2		24192.850	$20310^{\circ}_{5/2}-44503_{7/2}$
4162.678	10	100	24016.226	$14275^{\circ}_{9/2}-38291_{7/2}$	4132.090	2		24194.003	$19050^{\circ}_{3/2}-43244_{3/2}$
4161.587	2	5	24022.522	$13818^{\circ}_{7/2}-37840_{9/2}$	4131.529	5	10	24197.289	$18816^{\circ}_{13/2}-43014_{13/2}$
4159.657	10	100	24033.668	$14484^{\circ}_{11/2}-38517_{13/2}$	4131.425	50	100	24197.898	$8378^{\circ}_{7/2}-32576_{7/2}$
4156.987	1		24049.104	$22106_{5/2}-46155^{\circ}_{5/2}$	4130.663	5	3	24202.361	$15349^{\circ}_{11/2}-39552_{9/2}$
4156.512	100b	150	24051.852	$9585^{\circ}_{5/2}-33637_{7/2}$	4129.914	3b	4	24206.751	$17121^{\circ}_{3/2}-41328_{3/2}$
4156.235	50	100	24053.455	$10673^{\circ}_{5/2}-34726_{7/2}$	4128.912	1		24212.625	$20686^{\circ}_{5/2}-44898_{7/2}$
4155.474	1		24057.860	$21131^{\circ}_{3/2}-45189_{5/2}$	4128.300	3	3	24216.215	$17460^{\circ}_{5/2}-41676_{3/2}$
4153.722	2		24068.007	$22513^{\circ}_{5/2}-46581_{5/2}$	4127.289	3		24222.146	$15144^{\circ}_{3/2}-39366_{5/2}$
4151.447	4	5	24081.196	$10189^{\circ}_{11/2}-34270_{9/2}$	4126.607	1		24226.149	$24463^{\circ}_{5/2}-48689_{3/2}$
4150.482	4	5	24086.795	$14349_{1/2}-38436^{\circ}_{3/2}$	4124.666	5	15	24237.549	$15710^{\circ}_{3/2}-39948_{1/2}$
4150.369	4	8	24087.451	$24757^{\circ}_{9/2}-48844_{9/2}$	4124.513	5	10	24238.449	$22014^{\circ}_{11/2}-46253_{9/2}$
4149.986	200b	300	24089.674	$10572^{\circ}_{9/2}-34661_{11/2}$	4123.953	2		24241.740	$20310^{\circ}_{5/2}-44552_{5/2}$
4149.711	4	5	24091.270	$15305_{9/2}-39396^{\circ}_{7/2}$	4123.530	40	25	24244.226	$8605_{5/2}-32850^{\circ}_{5/2}$
4148.773	2		24096.717	$6213_{9/2}-30310^{\circ}_{11/2}$	4123.401	2		24244.985	$16033^{\circ}_{5/2}-40278_{3/2}$
4148.684	4		24097.234	$4146_{7/2}-28243^{\circ}_{5/2}$	4123.270	2		24245.755	$22139^{\circ}_{9/2}-46385_{7/2}$
4148.425	2		24098.738	$17837^{\circ}_{1/2}-41936_{3/2}$	4122.965	8	15	24247.549	$15453^{\circ}_{7/2}-39700_{5/2}$
4148.344	20	50	24099.209	$15453^{\circ}_{7/2}-39552_{9/2}$	4122.673	5b		24249.266	$25246_{9/2}-49495^{\circ}_{9/2}$
4148.180	200	150	24100.162	$7828_{1/2}-31928^{\circ}_{3/2}$	4121.857	5	10	24254.067	$18973^{\circ}_{7/2}-43227_{5/2}$
4148.026	4	10	24101.056	$18118_{3/2}-42219^{\circ}_{5/2}$	4120.014	3	4	24264.916	$19912^{\circ}_{13/2}-44177_{11/2}$
4146.664	2		24108.972	$26626^{\circ}_{1/2}-50735_{3/2}$	4119.390	2	2	24268.592	$20120^{\circ}_{5/2}-44388_{5/2}$
4146.256	1		24111.345	$17771^{\circ}_{11/2}-41882_{13/2}$	4118.594	5	10	24273.282	$13406^{\circ}_{13/2}-37679_{11/2}$
4146.069	2		24112.432	$25414^{\circ}_{11/2}-49527_{13/2}$	4117.839	4	4	24277.732	$35021_{3/2}-59299^{\circ}_{5/2}$
4145.836	2b		24113.787	$14275^{\circ}_{9/2}-38389_{7/2}$					$14790^{\circ}_{7/2}-39068_{7/2}$
4145.664	1		24114.788	$35878_{7/2}-59993^{\circ}_{9/2}$	4116.714	500b	400	24284.367	$6168^{\circ}_{7/2}-30452_{9/2}$
4145.197	1		24117.504	$12570_{7/2}-36687^{\circ}_{5/2}$	4116.311	4	4	24286.744	$13818^{\circ}_{7/2}-38105_{5/2}$
4144.453	5	2	24121.834	$20686^{\circ}_{5/2}-44807_{7/2}$	4115.144	8l		24293.632	$9061_{5/2}-33354^{\circ}_{5/2}$
4143.603	3	5	24126.782	$13818^{\circ}_{7/2}-37945_{5/2}$	4114.145	2		24299.530	$18118_{3/2}-42418^{\circ}_{3/2}$
4142.970	5	3	24130.468	$4113_{5/2}-28243^{\circ}_{5/2}$	4113.557	5		24303.004	$24309^{\circ}_{11/2}-48612_{13/2}$
4142.700	300	100	24132.041	$0_{3/2}-24132^{\circ}_{3/2}$	4112.485	1		24309.339	$15242^{\circ}_{9/2}-39552_{9/2}$
4142.475	50	150	24133.352	$14484^{\circ}_{11/2}-38617_{9/2}$	4112.313	5	15	24310.355	$18816^{\circ}_{13/2}-43127_{11/2}$
4141.947	1		24136.428	$20989^{\circ}_{9/2}-45126_{9/2}$	4111.986	3		24312.288	$23012^{\circ}_{3/2}-47324_{5/2}$
4141.631	50	75	24138.269	$17771^{\circ}_{11/2}-41909_{9/2}$	4111.458	3		24315.411	$11725^{\circ}_{1/2}-36040_{1/2}$
4141.225	2		24140.636	$16906^{\circ}_{7/2}-41047_{9/2}$	4111.427	3	2	24315.594	$27631_{3/2}-51946^{\circ}_{5/2}$
4140.385	50	100	24145.533	$9585^{\circ}_{5/2}-33730_{5/2}$	4111.133	4	5	24317.333	$22106_{3/2}-46423^{\circ}_{3/2}$
4140.235	200	150	24146.408	$9238^{\circ}_{9/2}-33384_{9/2}$	4110.968	4	4	24318.309	$14545^{\circ}_{5/2}-38863_{5/2}$
4139.934	2		24148.164	$25266^{\circ}_{1/2}-49414_{3/2}$	4110.633	15	15	24320.291	$6244_{1/2}-30564^{\circ}_{1/2}$
4139.758	1		24149.190	$26586^{\circ}_{3/2}-50735_{3/2}$	4110.512	40	25	24321.006	$12488^{\circ}_{9/2}-36809_{7/2}$
4138.841	5	5	24154.541	$10572^{\circ}_{9/2}-34726_{7/2}$	4110.075	5	4	24323.592	$12485^{\circ}_{7/2}-36809_{7/2}$
4137.886	2		24160.115	$16564^{\circ}_{11/2}-40724_{13/2}$	4108.420	500	150	24333.391	$4490^{\circ}_{5/2}-28823_{5/2}$
4137.612	2		24161.715	$20288^{\circ}_{11/2}-44450_{9/2}$	4107.793	5	8	24337.105	$12472^{\circ}_{5/2}-36809_{7/2}$
4137.068	2		24164.892	$11576^{\circ}_{3/2}-35741_{5/2}$	4107.370	20	8	24339.611	$11116^{\circ}_{7/2}-35456_{9/2}$
4136.393	75b	20b	24168.836	$13406^{\circ}_{13/2}-37575_{13/2}$	4106.950	4		24342.100	$14275^{\circ}_{9/2}-38617_{9/2}$
4136.101	2		24170.542	$12219_{3/2}-36390^{\circ}_{3/2}$	4106.120	5b	5b	24347.020	$13818^{\circ}_{7/2}-38165_{7/2}$
4134.989	2		24177.042	$19050^{\circ}_{3/2}-43227_{5/2}$	4105.911	25b	50	24348.260	$10673^{\circ}_{5/2}-35021_{3/2}$
4134.414	1		24180.404	$20120^{\circ}_{5/2}-44300_{3/2}$	4105.037	2b		24353.444	$17983^{\circ}_{3/2}-42336_{5/2}$
4134.106	100b	100b	24182.205	$9202^{\circ}_{7/2}-33384_{9/2}$					$25607^{\circ}_{9/2}-49960_{7/2}$
4133.396	2		24186.359	$17722^{\circ}_{9/2}-41909_{9/2}$	4104.381	150	75	24357.336	$8378^{\circ}_{7/2}-32736_{7/2}$

TABLE 3. *Classified lines of* Th II—Continued

Wavelength Å	Intensity		Wavenumber cm^{-1}	Classification	Wavelength Å	Intensity		Wavenumber cm^{-1}	Classification
	Lamp	Spark				Lamp	Spark		
4103.669	5b		24361.562	$13818^{\circ}_{7/2} - 38179_{9/2}$	4075.709	5	8	24528.682	$9202^{\circ}_{7/2} - 33730_{5/2}$
				$12219^{\circ}_{3/2} - 36581^{\circ}_{5/2}$	4074.642	1		24535.106	$30310^{\circ}_{11/2} - 54845_{9/2}$
4103.264	5	15	24363.966	$22014^{\circ}_{11/2} - 46378_{13/2}$	4074.245	2	4	24537.496	$35456_{9/2} - 59993^{\circ}_{9/2}$
4103.112	4		24364.869	$10189^{\circ}_{11/2} - 34553_{9/2}$					$16033^{\circ}_{5/2} - 40570_{7/2}$
4102.462	2		24368.729	$17983^{\circ}_{5/2} - 42352_{5/2}$	4073.708	10	40	24540.731	$22014^{\circ}_{11/2} - 46555_{11/2}$
4101.326	4	5	24375.479	$17771^{\circ}_{11/2} - 42146_{11/2}$	4072.907	10	5	24545.557	$15349^{\circ}_{11/2} - 39895_{9/2}$
4100.847	10b		24378.326	$16033^{\circ}_{5/2} - 40411_{7/2}$	4072.178	3	1	24549.951	$9720^{\circ}_{7/2} - 34270_{9/2}$
4100.820	50b	75	24378.486	$14484^{\circ}_{11/2} - 38862_{11/2}$	4071.466	5		24554.244	$30484_{11/2} - 55038^{\circ}_{9/2}$
4098.932	50	20	24389.715	$8460_{3/2} - 32850^{\circ}_{5/2}$	4071.302	1		24555.233	$17121^{\circ}_{3/2} - 41676_{3/2}$
4098.093	2		24394.708	$24982^{\circ}_{7/2} - 49377_{7/2}$	4070.671	15	3	24559.040	$9720^{\circ}_{7/2} - 34279_{7/2}$
4097.691	15b	10	24397.102	$15786_{5/2} - 40184^{\circ}_{7/2}$	4069.757	15	3	24564.555	$1859_{3/2} - 26424^{\circ}_{5/2}$
4096.332	8	2	24405.196	$20989^{\circ}_{9/2} - 45395_{7/2}$	4069.299	4		24567.320	$15710^{\circ}_{3/2} - 40278_{3/2}$
4094.747	500	200	24414.642	$0_{3/2} - 24414^{\circ}_{3/2}$	4069.202	300	200	24567.905	$6691^{\circ}_{3/2} - 31259_{5/2}$
4094.490	3		24416.174	$17272^{\circ}_{9/2} - 41688_{7/2}$	4068.025	5	3	24575.013	$12488^{\circ}_{9/2} - 37063_{9/2}$
4093.556	3	3	24421.745	$16906^{\circ}_{7/2} - 41328_{5/2}$	4067.876	10		24575.913	$14790^{\circ}_{7/2} - 39366_{5/2}$
4093.392	20	10	24422.724	$7331^{\circ}_{5/2} - 31754_{5/2}$	4067.594	15	4	24577.617	$12485^{\circ}_{7/2} - 37063_{9/2}$
4093.327	2		24423.111	$20080^{\circ}_{7/2} - 44503_{7/2}$	4066.169	1		24586.230	$30452_{9/2} - 55038^{\circ}_{9/2}$
4093.255	2		24423.541	$17722^{\circ}_{9/2} - 42146_{11/2}$	4066.003	8	4	24587.234	$14275^{\circ}_{9/2} - 38862_{11/2}$
4092.338	2s		24429.014	$11116^{\circ}_{7/2} - 35545_{9/2}$	4065.687	40l	8	24589.145	$9585^{\circ}_{5/2} - 34174_{5/2}$
4092.314	1		24429.157	$17771^{\circ}_{11/2} - 42200_{9/2}$	4065.254	4	4	24591.764	$17727_{11/2} - 42319^{\circ}_{9/2}$
4091.530	5	4	24433.838	$9585^{\circ}_{5/2} - 34019_{3/2}$	4064.610	4	2	24595.660	$13250_{5/2} - 37846^{\circ}_{5/2}$
4091.347	50	8	24434.931	$9202^{\circ}_{7/2} - 33637_{7/2}$	4063.755	3		24600.835	$23697^{\circ}_{7/2} - 48298_{7/2}$
4090.367	3		24440.785	$4146_{7/2} - 28587^{\circ}_{5/2}$	4063.691	5	4	24601.222	$14484^{\circ}_{11/2} - 39085_{13/2}$
4090.103	2l		24442.362	$15453^{\circ}_{7/2} - 39895_{9/2}$	4063.054	100		24605.079	$14545^{\circ}_{5/2} - 39150_{3/2}$
4088.108	1		24454.290	$9720^{\circ}_{7/2} - 34174_{5/2}$	4062.661	20		24607.459	$4113_{5/2} - 28720^{\circ}_{3/2}$
4086.520	500	150	24463.793	$0_{3/2} - 24463^{\circ}_{5/2}$	4062.305	8		24609.616	$8605_{5/2} - 33215^{\circ}_{3/2}$
4086.412	5	8	24464.439	$11576^{\circ}_{3/2} - 36040_{1/2}$	4059.888	50		24624.267	$7001_{3/2} - 31625^{\circ}_{1/2}$
4086.336	3		24464.894	$14275^{\circ}_{9/2} - 38740_{11/2}$	4059.815	4		24624.709	$11116^{\circ}_{7/2} - 35741_{5/2}$
4085.815	8	8	24468.014	$12219_{3/2} - 36687^{\circ}_{5/2}$	4059.766	3		24625.007	$15236_{3/2} - 39861^{\circ}_{5/2}$
4085.042	300	200	24472.644	$10189^{\circ}_{11/2} - 34661_{11/2}$	4057.776	25	50	24637.083	$17272^{\circ}_{9/2} - 41909_{9/2}$
4084.953	10	10	24473.177	$27357^{\circ}_{9/2} - 51830_{7/2}$	4057.327	50		24639.809	$12902^{\circ}_{3/2} - 37542_{3/2}$
4084.815	2b		24474.004	$4113_{5/2} - 28587^{\circ}_{5/2}$	4057.034	4		24641.589	$20969^{\circ}_{7/2} - 45610_{5/2}$
4084.499	2	2	24475.897	$17460^{\circ}_{5/2} - 41936_{3/2}$	4054.765	3	2	24655.377	$14101^{\circ}_{1/2} - 38757_{3/2}$
4084.278	3	3	24477.221	$17722^{\circ}_{9/2} - 42200_{9/2}$	4054.185	4	20	24658.905	$16564^{\circ}_{11/2} - 41223_{11/2}$
4084.008	1		24478.840	$21131^{\circ}_{3/2} - 45610_{5/2}$	4052.443	8	10	24669.504	$21682^{\circ}_{7/2} - 46352_{7/2}$
4083.388	4b	8	24482.556	$16564^{\circ}_{11/2} - 41047_{9/2}$	4051.277	2		24676.604	$18568^{\circ}_{1/2} - 43244_{3/2}$
4082.256	20		24489.345	$11576^{\circ}_{3/2} - 36065_{5/2}$	4049.825	8	8	24685.452	$15786_{5/2} - 40472^{\circ}_{3/2}$
4081.853	3	20h	24491.763	$20158_{5/2} - 44650^{\circ}_{7/2}$	4049.747	10	2	24685.927	$24132^{\circ}_{3/2} - 48817_{3/2}$
4081.829	4		24491.907	$16906^{\circ}_{7/2} - 41398_{9/2}$	4048.030	15	50	24696.398	$13468^{\circ}_{9/2} - 38165_{7/2}$
4080.975	3		24497.032	$20310^{\circ}_{5/2} - 44807_{7/2}$	4045.627	75	50	24711.066	$6168^{\circ}_{7/2} - 30879_{7/2}$
				$23372^{\circ}_{3/2} - 47869_{3/2}$					
					4043.852	1		24721.913	$22139^{\circ}_{9/2} - 46861_{11/2}$
4080.590	2		24499.343	$17722^{\circ}_{9/2} - 42222_{7/2}$	4043.128	200	40	24726.340	$1859_{3/2} - 26586^{\circ}_{3/2}$
4080.470	2		24500.064	$9711_{7/2} - 34212^{\circ}_{5/2}$	4042.973	8	75	24727.288	$20080^{\circ}_{7/2} - 44807_{7/2}$
4080.297	5	4	24501.102	$9400_{5/2} - 33902^{\circ}_{7/2}$	4041.811	10	15	24734.396	$14101^{\circ}_{1/2} - 38836_{3/2}$
4079.900	4	8	24503.486	$20686^{\circ}_{5/2} - 45189_{5/2}$	4041.207	200	400	24738.093	$10855_{7/2} - 35593^{\circ}_{9/2}$
4079.603	4	5	24505.270	$15710^{\circ}_{3/2} - 40216_{5/2}$	4040.391	40	20	24743.089	$6213_{9/2} - 30956^{\circ}_{9/2}$
4079.434	1		24506.286	$13250_{5/2} - 37756^{\circ}_{7/2}$	4039.431	40	15	24748.969	$8605_{5/2} - 33354^{\circ}_{5/2}$
4079.135	4	4	24508.082	$13248_{9/2} - 37756^{\circ}_{7/2}$	4038.903	1		24752.205	$11576^{\circ}_{3/2} - 36328_{3/2}$
4077.103	1		24520.296	$25440^{\circ}_{3/2} - 49960_{7/2}$	4038.427	8		24755.122	$8460_{3/2} - 33215^{\circ}_{3/2}$
4076.633	2		24523.123	$14545^{\circ}_{5/2} - 39068_{7/2}$	4038.351	50	25	24755.588	$34543_{5/2} - 59299^{\circ}_{5/2}$

TABLE 3. *Classified lines of* Th II – Continued

Wavelength Å	Intensity		Wavenumber cm^{-1}	Classification	Wavelength Å	Intensity		Wavenumber cm^{-1}	Classification
	Lamp	Spark				Lamp	Spark		
4037.434	4	4	24761.210	$14790^{\circ}_{7/2} - 39552_{9/2}$	4007.019	200	300	24949.155	$11116^{\circ}_{7/2} - 36065_{5/2}$
4037.259	25	50	24762.284	$11116^{\circ}_{7/2} - 35878_{7/2}$	4006.874	1		24950.058	$17272^{\circ}_{9/2} - 42222_{7/2}$
4037.132	8	4	24763.063	$15453^{\circ}_{7/2} - 40216_{5/2}$	4006.378	200	100	24953.146	$10572^{\circ}_{9/2} - 35525_{11/2}$
4036.565	300b	300	24766.541	$1859_{3/2} - 26626^{\circ}_{1/2}$	4005.571	50	100	24958.173	$9585^{\circ}_{5/2} - 34543_{5/2}$
4035.236	3		24774.698	$27787^{\circ}_{9/2} - 52562_{7/2}$	4005.528	50	500b	24958.441	$15453^{\circ}_{7/2} - 40411_{7/2}$
4034.919	75	25	24776.644	$4146_{7/2} - 28923^{\circ}_{5/2}$					$16033^{\circ}_{5/2} - 40991_{3/2}$
4034.364	2		24780.052	$23518^{\circ}_{7/2} - 48298_{7/2}$	4003.307	300	600	24972.288	$9202^{\circ}_{7/2} - 34174_{5/2}$
4034.246	200	200	24780.777	$6213_{9/2} - 30994^{\circ}_{7/2}$	4003.104	100	200	24973.554	$10572^{\circ}_{9/2} - 35545_{9/2}$
4032.893	10	10	24789.091	$12488^{\circ}_{9/2} - 37277_{7/2}$	4002.106	3	2	24979.782	$12485^{\circ}_{7/2} - 37465_{5/2}$
4032.238	2		24793.117	$14275^{\circ}_{9/2} - 39068_{7/2}$	4001.732	100	20	24982.116	$4113_{5/2} - 29095^{\circ}_{5/2}$
4032.035	2		24794.366	$23697^{\circ}_{7/2} - 48492_{5/2}$	3999.944	20	10	24993.283	$12472^{\circ}_{5/2} - 37465_{5/2}$
4031.781	3		24795.928	$17722^{\circ}_{9/2} - 42518_{7/2}$	3997.977	15	15	25005.580	$8378^{\circ}_{7/2} - 33384_{9/2}$
4031.225	3		24799.347	$13818^{\circ}_{7/2} - 38617_{9/2}$	3997.865	200	200	25006.280	$9720^{\circ}_{7/2} - 34726_{7/2}$
4029.518	20	10	24809.853	$4113_{5/2} - 28923^{\circ}_{5/2}$	3997.467	40b	100	25008.770	$11116^{\circ}_{7/2} - 36125_{9/2}$
4029.322	25	40	24811.060	$9400_{5/2} - 34212^{\circ}_{5/2}$	3996.061	150	300	25017.569	$15349^{\circ}_{11/2} - 40367_{9/2}$
4029.025	10	50	24812.889	$15710^{\circ}_{3/2} - 40523_{1/2}$	3995.701	2		25019.823	$34279_{7/2} - 59299^{\circ}_{5/2}$
4028.629	50	40	24815.328	$24309^{\circ}_{11/2} - 49124_{11/2}$	3995.030	2		25024.025	$25607^{\circ}_{9/2} - 50631_{11/2}$
4027.651	15	75	24821.353	$14545^{\circ}_{5/2} - 39366_{5/2}$	3994.549	600	200	25027.038	$0_{3/2} - 25027^{\circ}_{1/2}$
4027.412	8	25	24822.826	$13468^{\circ}_{9/2} - 38291_{7/2}$	3994.341	10	200	25028.341	$17722^{\circ}_{9/2} - 42751_{7/2}$
4027.341	50	75	24823.264	$9720^{\circ}_{7/2} - 34543_{5/2}$	3993.722	20l	10	25032.221	$9238^{\circ}_{9/2} - 34270_{9/2}$
4026.043	10		24831.267	$20969^{\circ}_{7/2} - 45800_{5/2}$	3992.273	100h	150	25041.306	$9238^{\circ}_{9/2} - 34279_{7/2}$
4025.944	10	3	24831.877	$8018_{3/2} - 32850^{\circ}_{5/2}$	3992.046	8	20	25042.730	$12902^{\circ}_{3/2} - 37945_{5/2}$
4025.654	100b	300b	24833.666	$9720^{\circ}_{7/2} - 34553_{9/2}$	3991.601	4b		25045.521	$13818^{\circ}_{7/2} - 38863_{5/2}$
4025.620	25	8b	24833.876	$16564^{\circ}_{11/2} - 41398_{9/2}$	3991.066	10	15	25048.879	$14101^{\circ}_{1/2} - 39150_{3/2}$
4024.467	25	40	24840.990	$9061_{5/2} - 33902^{\circ}_{7/2}$	3990.118	2		25054.830	$21297^{\circ}_{5/2} - 46352_{7/2}$
4023.765	1		24845.324	$29515_{9/2} - 54360^{\circ}_{9/2}$	3989.568	2		25058.284	$17460^{\circ}_{5/2} - 42518_{7/2}$
4023.542	2b		24846.701	$22014^{\circ}_{11/2} - 46861_{11/2}$	3988.845	200	200	25062.826	$6691^{\circ}_{3/2} - 31754_{5/2}$
4022.091	100b	75	24855.665	$4490^{\circ}_{5/2} - 29345_{5/2}$	3988.599	100	25	25064.371	$1521_{3/2} - 26586^{\circ}_{3/2}$
4020.915	3		24862.934	$25607^{\circ}_{9/2} - 50470_{9/2}$	3988.025	200b	500b	25067.979	$9202^{\circ}_{7/2} - 34270_{9/2}$
4020.100	5	10	24867.974	$14484^{\circ}_{11/2} - 39352_{11/2}$	3987.706	50	50	25069.984	$12472^{\circ}_{5/2} - 37542_{3/2}$
4019.129	1000b	800	24873.982	$0_{3/2} - 24873^{\circ}_{5/2}$	3987.483	10	15	25071.386	$15144^{\circ}_{3/2} - 40216_{5/2}$
4018.768	5	50	24876.216	$17460^{\circ}_{5/2} - 42336_{5/2}$	3987.219	200b	75	25073.046	$34543_{3/2} - 59616^{\circ}_{5/2}$
4017.709	2		24882.773	$22028^{\circ}_{13/2} - 46910_{13/2}$	3987.071	5	3	25073.977	$12488^{\circ}_{9/2} - 37562_{11/2}$
4017.486	75	50	24884.155	$10572^{\circ}_{9/2} - 35456_{9/2}$	3985.464	15	40	25084.087	$20310^{\circ}_{5/2} - 45395_{7/2}$
4016.459	1		24890.517	$16033^{\circ}_{5/2} - 40923_{3/2}$	3985.408	2		25084.439	$27593_{5/2} - 52678^{\circ}_{5/2}$
4016.438	1		24890.647	$24982^{\circ}_{7/2} - 49873_{5/2}$	3985.065	2	8	25086.598	$24873^{\circ}_{5/2} - 49960$
4016.299	5	50	24891.509	$17460^{\circ}_{5/2} - 42352_{5/2}$	3984.620	10		25089.400	$22642^{\circ}_{9/2} - 47731_{9/2}$
4015.826	15	15	24894.441	$8460_{3/2} - 33354^{\circ}_{5/2}$	3984.373	50	25	25090.955	$6168^{\circ}_{7/2} - 31259_{5/2}$
4015.589	2	10	24895.910	$22014^{\circ}_{11/2} - 46910_{13/2}$	3982.232	75	25	25104.445	$14790^{\circ}_{7/2} - 39895_{9/2}$
4015.142	2l		24898.681	$15324^{\circ}_{1/2} - 40222_{3/2}$	3982.100	200	40	25105.277	$1859_{3/2} - 26965^{\circ}_{5/2}$
4014.937	1		24899.952	$26965^{\circ}_{3/2} - 51865_{5/2}$	3981.534	10	20	25108.846	$6244_{1/2} - 31353^{\circ}_{5/2}$
4014.511	75	25	24902.595	$1521_{5/2} - 26424^{\circ}_{5/2}$	3981.105	150	200	25111.551	$13406^{\circ}_{13/2} - 38517_{13/2}$
4013.257	15	40	24910.376	$12219_{3/2} - 37130^{\circ}_{1/2}$	3980.753	8	100	25113.772	$24381_{7/2} - 49495^{\circ}_{9/2}$
4011.775	50b	100b	24919.578	$12902^{\circ}_{3/2} - 37821_{3/2}$	3980.143	5	15	25117.621	$15453^{\circ}_{7/2} - 40570_{7/2}$
4010.984	2		24924.492	$20686^{\circ}_{7/2} - 45610_{5/2}$	3979.038	200	200	25124.596	$34174_{5/2} - 59299^{\circ}_{5/2}$
4010.531	15	8	24927.307	$7001_{3/2} - 31928^{\circ}_{3/2}$	3977.795	3	15	25132.447	$21131^{\circ}_{3/2} - 46264_{3/2}$
4010.427	4	20	24927.954	$17272^{\circ}_{9/2} - 42200_{9/2}$	3976.414	100	200	25141.175	$9585^{\circ}_{5/2} - 34726_{7/2}$
4010.326	1		24928.582	$29431_{7/2} - 54360^{\circ}_{9/2}$	3975.222	20	75	25148.714	$13468^{\circ}_{9/2} - 38617_{9/2}$
4009.535	4	10	24933.499	$15710^{\circ}_{3/2} - 40644_{3/2}$	3974.873	1		25150.922	$9061_{5/2} - 34212^{\circ}_{5/2}$
4008.743	2		24938.425	$26424^{\circ}_{3/2} - 51362_{5/2}$	3974.391	20	50	25153.972	$31924^{\circ}_{11/2} - 57078_{9/2}$

TABLE 3. *Classified lines of* Th II—Continued

Wavelength Å	Intensity		Wavenumber cm^{-1}	Classification	Wavelength Å	Intensity		Wavenumber cm^{-1}	Classification
	Lamp	Spark				Lamp	Spark		
3974.224	15	100	25155.029	$14545^{\circ}_{5/2} - 39700_{5/2}$	3945.818	75	300	25336.116	$10189^{\circ}_{11/2} - 35525_{11/2}$
3973.993	1		25156.491	$22014^{\circ}_{11/2} - 47171_{9/2}$	3945.506	200	300	25338.120	$10855_{7/2} - 36193^{\circ}_{9/2}$
3969.854	5	50	25182.719	$14275^{\circ}_{9/2} - 39458_{7/2}$	3943.688	100	200	25349.800	$12472^{\circ}_{5/2} - 37821_{5/2}$
3969.826	3	10	25182.896	$19912^{\circ}_{13/2} - 45095_{15/2}$	3943.395	100	300	25351.684	$9202^{\circ}_{7/2} - 34553_{9/2}$
3969.561	75	50	25184.577	$26762_{3/2} - 51946^{\circ}_{5/2}$	3943.258	20	100	25352.564	$12488^{\circ}_{9/2} - 37840_{9/2}$
3969.529	5	50	25184.780	$17771^{\circ}_{11/2} - 42955_{9/2}$	3942.855	8	40	25355.155	$12485^{\circ}_{7/2} - 37840_{9/2}$
3969.337	5	50	25185.999	$20120^{\circ}_{5/2} - 45306_{3/2}$	3942.700	5b	10	25356.152	$17771^{\circ}_{11/2} - 43127_{11/2}$
3969.289	10	10	25186.303	$12570_{7/2} - 37756^{\circ}_{7/2}$	3942.668	100b	50	25356.358	$22513^{\circ}_{5/2} - 47869_{5/2}$
3969.002	200	150	25188.124	$0_{3/2} - 25188^{\circ}_{5/2}$	3942.639	50	50	25356.544	$10189^{\circ}_{11/2} - 35545_{9/2}$
3968.484	100	400	25191.412	$12488^{\circ}_{9/2} - 37679_{11/2}$	3942.042	5b	10	25360.385	$18816^{\circ}_{13/2} - 44177_{11/2}$
3967.212	50	200	25199.489	$15324^{\circ}_{1/2} - 40523_{1/2}$	3941.725	25	25	25362.424	$20989^{\circ}_{9/2} - 46352_{7/2}$
3966.707	3		25202.697	$12902^{\circ}_{3/2} - 38105_{5/2}$	3941.360	3	40	25364.773	$22642^{\circ}_{9/2} - 48006_{9/2}$
3966.231	15	25	25205.722	$10673^{\circ}_{5/2} - 35878_{7/2}$	3940.369	2	25	25371.152	$23697^{\circ}_{7/2} - 49068_{5/2}$
3966.054	1		25206.847	$30879_{7/2} - 56086^{\circ}_{9/2}$	3939.793	15	50	25374.861	$15349^{\circ}_{11/2} - 40724_{13/2}$
3964.865	40	75	25214.406	$10379_{9/2} - 35593^{\circ}_{7/2}$	3938.779	100	100	25381.393	$6244_{1/2} - 31625^{\circ}_{1/2}$
3964.738	200	200d	25215.213	$17121^{\circ}_{3/2} - 42336_{5/2}$	3938.726	20	100	25381.735	$12219_{3/2} - 37601^{\circ}_{3/2}$
3963.468	40	100	25223.293	$10379_{9/2} - 35602^{\circ}_{11/2}$	3938.580	5b		25382.676	$8460_{3/2} - 33843^{\circ}_{3/2}$
3963.220	40	200	25224.871	$15349^{\circ}_{11/2} - 40574_{11/2}$	3938.421	15	15	25383.701	$4490^{\circ}_{5/2} - 29873_{7/2}$
3962.921	3	20	25226.774	$20989^{\circ}_{9/2} - 46216_{11/2}$	3937.923	100	200	25386.910	$7828_{1/2} - 33215^{\circ}_{3/2}$
3962.336	50	200b	25230.498	$17121^{\circ}_{3/2} - 42352_{5/2}$	3937.040	200s	300	25392.604	$10673^{\circ}_{5/2} - 36065_{5/2}$
3961.966	4	75	25232.855	$17722^{\circ}_{7/2} - 42955_{9/2}$	3936.838	1		25393.907	$23730^{\circ}_{9/2} - 49124_{11/2}$
3961.503	2		25235.804	$15236_{3/2} - 40472^{\circ}_{3/2}$	3936.604	75	40	25395.416	$30101^{\circ}_{7/2} - 55496_{9/2}$
3960.955	2b		25239.295	$18568^{\circ}_{1/2} - 43807_{3/2}$	3936.125	1		25398.507	$29095^{\circ}_{5/2} - 54493_{5/2}$
3960.360	4b	25b	25243.087	$17771^{\circ}_{11/2} - 43014_{13/2}$	3935.945	10h	200	25399.668	$26770^{\circ}_{11/2} - 52170_{11/2}$
3960.333	100b	200b	25243.259	$13250_{5/2} - 38493^{\circ}_{5/2}$	3935.631	20	200	25401.695	$16818_{7/2} - 42219^{\circ}_{5/2}$
3960.019	8	8	25245.260	$7331^{\circ}_{5/2} - 32576_{7/2}$	3935.240	2	20	25404.219	$17722^{\circ}_{9/2} - 43127_{11/2}$
3959.222	8	40	25250.342	$13818^{\circ}_{7/2} - 39068_{7/2}$	3934.175	5	50	25411.096	$14484^{\circ}_{11/2} - 39895_{9/2}$
3959.024	1	10	25251.605	$26424^{\circ}_{3/2} - 51676_{3/2}$	3933.571	2b		25414.997	$18973^{\circ}_{7/2} - 44388_{5/2}$
3958.014	1		25258.049	$28587^{\circ}_{5/2} - 53845_{5/2}$	3933.353	5	50	25416.406	$20969^{\circ}_{7/2} - 46385_{7/2}$
3957.480	2		25261.457	$17983^{\circ}_{5/2} - 43244_{3/2}$	3932.226	200	250	25423.690	$9238^{\circ}_{9/2} - 34661_{11/2}$
3957.157	10		25263.519	$20989^{\circ}_{9/2} - 46253_{9/2}$	3932.002	15	300	25425.138	$14790^{\circ}_{7/2} - 40216_{5/2}$
3956.690	300	300	25266.500	$0_{3/2} - 25266^{\circ}_{1/2}$	3931.257	2	100	25429.957	$25594^{\circ}_{7/2} - 51024_{3/2}$
3956.593	100	500	25267.120	$10189^{\circ}_{11/2} - 35456_{9/2}$	3929.669	800	500	25440.233	$0_{3/2} - 25440^{\circ}_{5/2}$
3955.252	25		25275.686	$12570_{7/2} - 37846^{\circ}_{5/2}$	3929.192	2		25443.321	$1521_{5/2} - 26965^{\circ}_{3/2}$
3955.101	5	15	25276.651	$14275^{\circ}_{9/2} - 39552_{9/2}$	3928.940	5b		25444.953	$9711_{7/2} - 35156^{\circ}_{5/2}$
3954.591	1		25279.911	$34019_{3/2} - 59299^{\circ}_{5/2}$	3928.698	4	20	25446.520	$20288^{\circ}_{11/2} - 45735_{11/2}$
3954.464	10	25	25280.723	$15710^{\circ}_{3/2} - 40991_{3/2}$	3928.239	1		25449.493	$21131^{\circ}_{3/2} - 46581_{5/2}$
3953.970	2		25283.881	$21297^{\circ}_{5/2} - 46581_{5/2}$	3927.421	50	300	25454.794	$14484^{\circ}_{11/2} - 39939_{11/2}$
3953.900	2		25284.329	$20969^{\circ}_{7/2} - 46253_{9/2}$	3927.176	100	300	25456.382	$13406^{\circ}_{13/2} - 38862_{11/2}$
3952.901	2		25290.719	$17460^{\circ}_{5/2} - 42751_{7/2}$	3926.706	50	200	25459.429	$12485^{\circ}_{7/2} - 37945_{5/2}$
3952.448	3	8	25293.617	$16906^{\circ}_{7/2} - 42200_{9/2}$	3924.987	20	40	25470.579	$15453^{\circ}_{7/2} - 40923_{5/2}$
3951.515	300	400	25299.589	$12488^{\circ}_{9/2} - 37787_{7/2}$	3924.628	3	2	25472.909	$12472^{\circ}_{3/2} - 37945_{5/2}$
3951.107	40	200	25302.202	$12485^{\circ}_{7/2} - 37787_{7/2}$	3922.218	50	50	25488.560	$9238^{\circ}_{9/2} - 34726_{7/2}$
3950.088	1		25308.729	$23012^{\circ}_{3/2} - 48320_{5/2}$	3922.098	8	40	25489.340	$20310^{\circ}_{3/2} - 45800_{5/2}$
3949.206	4	25	25314.381	$20080^{\circ}_{7/2} - 45395_{7/2}$	3921.019	5	10	25496.354	$12219_{3/2} - 37716^{\circ}_{1/2}$
3948.999	8b		25315.708	$16906^{\circ}_{7/2} - 42222_{7/2}$	3920.951	15	25	25496.796	$24463^{\circ}_{3/2} - 49960_{7/2}$
				$12472^{\circ}_{5/2} - 37787_{7/2}$	3920.520	5b		25499.599	$15144^{\circ}_{3/2} - 40644_{5/2}$
3948.964	200b	500	25315.932	$9238^{\circ}_{9/2} - 34553_{9/2}$	3920.312	50	300	25500.952	$16818_{7/2} - 42319^{\circ}_{9/2}$
3946.596	2		25331.122	$13250_{5/2} - 38581^{\circ}_{5/2}$	3920.170	1		25501.876	$19050^{\circ}_{3/2} - 44552_{5/2}$
3946.144	150	500	25334.023	$13406^{\circ}_{13/2} - 38740_{11/2}$	3918.285	10	75	25514.144	$13250_{5/2} - 38764^{\circ}_{7/2}$

TABLE 3. *Classified lines of* Th II—Continued

Wavelength Å	Intensity		Wavenumber cm^{-1}	Classification	Wavelength Å	Intensity		Wavenumber cm^{-1}	Classification
	Lamp	Spark				Lamp	Spark		
3918.011	20	100	25515.928	$13248_{9/2} - 38764^{\circ}_{7/2}$	3888.460	3b	8	25709.836	$20686^{\circ}_{5/2} - 46395_{3/2}$
3916.796	50	300	25523.843	$17722^{\circ}_{9/2} - 43246_{7/2}$	3888.048	2		25712.561	$24757^{\circ}_{9/2} - 50470_{9/2}$
3916.724	75	200	25524.312	$9202^{\circ}_{7/2} - 34726_{7/2}$	3887.434	3	15	25716.622	$22014^{\circ}_{11/2} - 47731_{9/2}$
3915.770	8	40	25530.531	$20158_{5/2} - 45689^{\circ}_{7/2}$	3885.766	75	50	25727.661	$1521_{3/2} - 27249^{\circ}_{7/2}$
3914.470	10	75	25539.009	$20158_{5/2} - 45697^{\circ}_{3/2}$	3885.639	8	20	25728.501	$10855_{7/2} - 36583^{\circ}_{7/2}$
3913.823	75	20	25543.231	$1859_{3/2} - 27403^{\circ}_{3/2}$	3885.151	3	50	25731.733	$22139^{\circ}_{9/2} - 47871_{7/2}$
3913.195	1		25547.330	$25188^{\circ}_{3/2} - 50735_{3/2}$	3884.949	2		25733.071	$27787^{\circ}_{9/2} - 53520_{9/2}$
3913.005	75	300	25548.571	$13818^{\circ}_{7/2} - 39366_{5/2}$	3884.819	500	500	25733.932	$19912^{\circ}_{13/2} - 45646_{13/2}$
3912.282	75	200	25553.292	$10572^{\circ}_{9/2} - 36125_{9/2}$	3884.523	50	200	25735.893	$9720^{\circ}_{7/2} - 35456_{9/2}$
3911.299	15	25	25559.714	$19248^{\circ}_{5/2} - 44807_{7/2}$	3884.318	2	10	25737.251	$20969^{\circ}_{7/2} - 46706_{7/2}$
3908.488	3	50	25578.096	$20686^{\circ}_{5/2} - 46264_{3/2}$	3882.214	1		25751.199	$18214^{\circ}_{3/2} - 43965_{1/2}$
3907.905	10	50	25581.912	$16564^{\circ}_{11/2} - 42146_{11/2}$	3882.142	100	150	25751.677	$8460_{3/2} - 34212^{\circ}_{5/2}$
3907.336	10	10	25585.637	$9400_{5/2} - 34986^{\circ}_{3/2}$	3881.497	50		25755.956	$9400_{5/2} - 35156^{\circ}_{5/2}$
3906.828	3		25588.964	$15236_{3/2} - 40825^{\circ}_{1/2}$	3879.796	15	15	25767.248	$17460^{\circ}_{5/2} - 43227_{5/2}$
3906.033	3		25594.172	$15453^{\circ}_{7/2} - 41047_{9/2}$	3878.047	20	15	25778.869	$15144^{\circ}_{3/2} - 40923_{5/2}$
3905.924	15	25	25594.886	$0_{3/2} - 25594^{\circ}_{1/2}$	3877.238	5	15	25784.247	$17460^{\circ}_{5/2} - 43244_{3/2}$
3905.356	3	50	25598.609	$26963^{\circ}_{7/2} - 52562_{7/2}$	3876.946	1		25786.189	$17460^{\circ}_{5/2} - 43246_{7/2}$
3905.186	150	300	25599.723	$13468^{\circ}_{9/2} - 39068_{7/2}$	3876.510	2		25789.089	$17983^{\circ}_{5/2} - 43772_{5/2}$
3904.200	10	15	25606.188	$8605_{5/2} - 34212^{\circ}_{5/2}$	3875.518	4	5	25795.690	$8378^{\circ}_{7/2} - 34174_{5/2}$
3904.082	200	200	25606.962	$4113_{5/2} - 29720^{\circ}_{3/2}$	3873.981	1	10	25805.925	$23012^{\circ}_{3/2} - 48817_{3/2}$
3903.764	2		25609.048	$19880_{9/2} - 45489^{\circ}_{9/2}$	3873.950	5	10	25806.131	$12485^{\circ}_{7/2} - 38291_{7/2}$
3902.731	3		25615.826	$20288^{\circ}_{11/2} - 45904_{9/2}$	3872.721	200	600	25814.320	$10379_{9/2} - 36193^{\circ}_{9/2}$
3902.474	8	40	25617.513	$15710^{\circ}_{9/2} - 41328_{5/2}$	3872.358	25	100	25816.740	$11725^{\circ}_{1/2} - 37542_{3/2}$
3902.120	20	100	25619.837	$14275^{\circ}_{9/2} - 39895_{9/2}$	3871.925	3	10	25819.627	$12472^{\circ}_{5/2} - 38291_{7/2}$
3901.152	75	200	25626.194	$12219_{3/2} - 37846^{\circ}_{5/2}$	3871.781	1		25820.587	$17983^{\circ}_{5/2} - 43803_{7/2}$
3900.878	400	400	25627.994	$7331^{\circ}_{3/2} - 32959_{3/2}$	3871.455	8	200	25822.762	$19912^{\circ}_{13/2} - 45735_{11/2}$
3900.131	50a	100	25632.902	$12472^{\circ}_{5/2} - 38105_{5/2}$	3871.245	5	25	25824.163	$17983^{\circ}_{5/2} - 43807_{3/2}$
3900.037	1	40b	25633.520	$30452_{9/2} - 56086^{\circ}_{9/2}$	3871.142	3		25824.850	$8018_{3/2} - 33843^{\circ}_{5/2}$
3899.674	2		25635.906	$17460^{\circ}_{5/2} - 43096_{5/2}$	3871.073	25	15	25825.310	$9720^{\circ}_{7/2} - 35545_{9/2}$
3899.318	1		25638.247	$21297^{\circ}_{5/2} - 46935_{3/2}$	3870.923	5	8	25826.311	$12902^{\circ}_{3/2} - 38728_{5/2}$
3898.488	4b		25643.705	$16033^{\circ}_{5/2} - 41676_{3/2}$	3869.971	75	100	25832.664	$10855_{7/2} - 36687^{\circ}_{5/2}$
3898.062	1		25646.507	$23730^{\circ}_{9/2} - 49377_{7/2}$	3868.161	1		25844.751	$16906^{\circ}_{7/2} - 42751_{7/2}$
3897.456	1		25650.495	$19248^{\circ}_{5/2} - 44898_{7/2}$	3867.883	2		25846.609	$14101^{\circ}_{1/2} - 39948_{1/2}$
3895.982	1		25660.199	$22014^{\circ}_{11/2} - 47675_{11/2}$	3867.849	20	300	25846.836	$15144^{\circ}_{3/2} - 40991_{3/2}$
3895.854	1		25661.042	$25607^{\circ}_{9/2} - 51268_{7/2}$	3867.696	1	8	25847.858	$26424^{\circ}_{5/2} - 52272_{7/2}$
3894.899	15	40	25667.334	$15324^{\circ}_{1/2} - 40991_{3/2}$	3867.577	50	75	25848.654	$7001_{3/2} - 32850^{\circ}_{5/2}$
3894.408	10	40	25670.570	$14545^{\circ}_{5/2} - 40216_{5/2}$	3867.197	1		25851.193	$21297^{\circ}_{5/2} - 47148_{3/2}$
3893.423	10	75	25677.064	$12488^{\circ}_{9/2} - 38165_{7/2}$	3866.876	15b	50	25853.339	$14790^{\circ}_{7/2} - 40644_{5/2}$
3893.111	20	75	25679.122	$13406^{\circ}_{13/2} - 39085_{13/2}$	3866.657	1		25854.803	$12902^{\circ}_{3/2} - 38757_{3/2}$
3893.046	1b		25679.551	$23697^{\circ}_{7/2} - 49377_{7/2}$	3866.632	3	5	25854.971	$17272^{\circ}_{9/2} - 43127_{11/2}$
3893.026	20	75	25679.683	$20158_{3/2} - 45838^{\circ}_{5/2}$	3866.064	5	200	25858.769	$23518^{\circ}_{7/2} - 49377_{7/2}$
				$12485^{\circ}_{7/2} - 38165_{7/2}$	3864.993	3b		25865.935	$14545^{\circ}_{5/2} - 40411_{7/2}$
3892.432	4	15	25683.601	$17272^{\circ}_{9/2} - 42955_{9/2}$	3864.370	25b	75	25870.105	$8460_{3/2} - 34330^{\circ}_{1/2}$
3892.307	75	100	25684.426	$6244_{1/2} - 31928^{\circ}_{3/2}$	3864.118	2	25	25871.792	$20989^{\circ}_{9/2} - 46861_{11/2}$
3891.053	75	100	25692.704	$11116^{\circ}_{7/2} - 36809_{7/2}$	3863.593	4		25875.307	$15453^{\circ}_{7/2} - 41328_{5/2}$
3890.981	10	50	25693.179	$12472^{\circ}_{5/2} - 38165_{7/2}$	3863.405	500	600	25876.566	$6700^{\circ}_{9/2} - 32576_{7/2}$
3890.821	15l	25	25694.236	$12485^{\circ}_{7/2} - 38179_{9/2}$	3863.205	5	5	25877.906	$7331^{\circ}_{5/2} - 33209_{7/2}$
3890.351	4b	10	25697.340	$15349^{\circ}_{11/2} - 41047_{9/2}$	3862.701	20b	25	25881.282	$1521_{5/2} - 27403^{\circ}_{3/2}$
3890.057	1		25699.282	$20686^{\circ}_{5/2} - 46385_{7/2}$	3862.654	200b	200	25881.597	$9711_{7/2} - 35593^{\circ}_{7/2}$
3888.673	50	100h	25708.428	$25027^{\circ}_{1/2} - 50735_{3/2}$	3862.557	5		25882.247	$13818^{\circ}_{7/2} - 39700_{5/2}$

TABLE 3. *Classified lines of* Th II—Continued

Wavelength Å	Intensity		Wavenumber cm^{-1}	Classification	Wavelength Å	Intensity		Wavenumber cm^{-1}	Classification
	Lamp	Spark				Lamp	Spark		
3862.398	100b	150b	25883.312	$13468^{\circ}_{9/2} - 39352_{11/2}$	3826.022	10	75	26129.393	$12488^{\circ}_{9/2} - 38617_{9/2}$
3862.052	2	100	25885.631	$33730_{5/2} - 59616^{\circ}_{3/2}$	3825.546	2		26132.644	$14790^{\circ}_{7/2} - 40923_{5/2}$
3861.540	25b	50	25889.063	$11576^{\circ}_{3/2} - 37465_{5/2}$	3825.034	150	400	26136.142	$10673^{\circ}_{5/2} - 36809_{7/2}$
3859.931	50	200	25899.855	$12472^{\circ}_{5/2} - 38372_{3/2}$	3824.759	5	50	26138.021	$26424^{\circ}_{5/2} - 52562_{7/2}$
3859.840	300	500	25900.466	$8378^{\circ}_{7/2} - 34279_{7/2}$	3824.645	5	25	26138.800	$19050^{\circ}_{3/2} - 45189_{5/2}$
3859.747	50	200	25901.090	$12488^{\circ}_{9/2} - 38389_{7/2}$	3823.873	1		26144.077	$20120^{\circ}_{3/2} - 46264_{3/2}$
3857.507	4	200	25916.130	$26762_{3/2} - 52678^{\circ}_{5/2}$	3823.584	75	300	26146.053	$13250_{5/2} - 39396^{\circ}_{7/2}$
3857.347	10	50	25917.205	$12472^{\circ}_{5/2} - 38389_{7/2}$	3823.321	15	100	26147.852	$13248_{9/2} - 39396^{\circ}_{7/2}$
3856.188	3	25	25924.994	$18973^{\circ}_{7/2} - 44898_{7/2}$	3822.149	300b	200b	26155.869	$9585^{\circ}_{5/2} - 35741_{5/2}$
3856.113	5	10	25925.498	$9061_{5/2} - 34986^{\circ}_{3/2}$	3821.755	20	50	26158.566	$9720^{\circ}_{7/2} - 35878_{7/2}$
3856.060	2		25925.855	$28243^{\circ}_{5/2} - 54169_{7/2}$	3821.431	200	500	26160.784	$11116^{\circ}_{7/2} - 37277_{7/2}$
3854.920	3		25933.521	$20969^{\circ}_{7/2} - 46902_{5/2}$	3821.032	2		26163.515	$27357^{\circ}_{9/2} - 53520_{9/2}$
3854.876	10	150	25933.817	$12902^{\circ}_{3/2} - 38836_{3/2}$	3819.941	3b	40	26170.988	$23187^{\circ}_{13/2} - 49357_{11/2}$
3854.510	300	600	25936.280	$10189^{\circ}_{11/2} - 36125_{9/2}$	3819.339	8	8	26175.113	$8378^{\circ}_{7/2} - 34553_{9/2}$
3854.319	2b	8	25937.565	$23187^{\circ}_{13/2} - 49124_{11/2}$	3819.286	3	8	26175.476	$23697^{\circ}_{7/2} - 49873_{5/2}$
3853.437	1		25943.502	$24463^{\circ}_{5/2} - 50407_{7/2}$	3819.161	2		26176.332	$14101^{\circ}_{1/2} - 40278_{3/2}$
3853.083	2		25945.885	$13406^{\circ}_{13/2} - 39352_{11/2}$	3818.099	5	25	26183.613	$15144^{\circ}_{3/2} - 41328_{5/2}$
3852.958	40	200	25946.727	$11116^{\circ}_{7/2} - 37063_{9/2}$	3817.366	8	100	26188.641	$21682^{\circ}_{7/2} - 47871_{7/2}$
3850.768	2		25961.483	$12902^{\circ}_{3/2} - 38863_{5/2}$	3817.291	5	40	26189.155	$16033^{\circ}_{5/2} - 42222_{7/2}$
3850.281	20	150	25964.767	$20288^{\circ}_{11/2} - 46253_{9/2}$	3816.793	10	40	26192.572	$9400_{5/2} - 35593^{\circ}_{7/2}$
				$12902^{\circ}_{3/2} - 38867_{1/2}$					$21131^{\circ}_{3/2} - 47324_{5/2}$
3850.132	75	200	25965.771	$11576^{\circ}_{3/2} - 37542_{3/2}$	3816.607	5	10	26193.849	$8018_{3/2} - 34212^{\circ}_{5/2}$
3850.092	2		25966.041	$15710^{\circ}_{3/2} - 41676_{3/2}$	3816.561	8	75	26194.164	$12570_{7/2} - 38764^{\circ}_{7/2}$
3849.542	1		25969.751	$17837^{\circ}_{1/2} - 43807_{3/2}$	3815.026	75	200	26204.704	$10379_{9/2} - 36583^{\circ}_{7/2}$
3848.823	2		25974.602	$17272^{\circ}_{9/2} - 43246_{7/2}$	3813.666	100	150	26214.048	$7001_{3/2} - 33215^{\circ}_{3/2}$
3846.832	10	8	25988.046	$4113_{3/2} - 30101^{\circ}_{7/2}$	3813.400	1		26215.877	$18973^{\circ}_{7/2} - 45189_{5/2}$
3846.753	2		25988.579	$30956^{\circ}_{9/2} - 56945_{11/2}$	3813.324	5	200	26216.399	$20686^{\circ}_{5/2} - 46902_{5/2}$
3846.247	10	200	25991.998	$22014^{\circ}_{11/2} - 48006_{9/2}$	3813.068	400	500	26218.159	$9238^{\circ}_{9/2} - 35456_{9/2}$
3845.535	8	300	25996.810	$20158_{5/2} - 46155^{\circ}_{5/2}$	3812.300	1		26223.441	$25607_{9/2} - 51830^{\circ}_{7/2}$
3845.223	10	15	25998.920	$28923^{\circ}_{5/2} - 54922_{3/2}$	3811.975	3		26225.677	$15710^{\circ}_{3/2} - 41936_{3/2}$
3843.415	4	10	26011.150	$12570_{7/2} - 38581^{\circ}_{5/2}$	3811.355	3	20	26229.943	$23730^{\circ}_{9/2} - 49960_{7/2}$
3842.919	25b		26014.507	$7828_{1/2} - 33843^{\circ}_{3/2}$	3810.558	2		26235.429	$15453^{\circ}_{7/2} - 41688_{7/2}$
3841.960	300	800	26021.000	$9720^{\circ}_{7/2} - 35741_{5/2}$	3810.497	2		26235.849	$25440^{\circ}_{5/2} - 51676_{3/2}$
3841.358	4b	10	26025.078	$14545^{\circ}_{5/2} - 40570_{7/2}$	3810.295	15	5	26237.239	$10572^{\circ}_{9/2} - 36809_{7/2}$
3839.744	1000b	800b	26036.017	$6700^{\circ}_{9/2} - 32736_{7/2}$	3809.834	75	300	26240.414	$14484^{\circ}_{11/2} - 40724_{13/2}$
3838.964	1		26041.307	$20310^{\circ}_{5/2} - 46352_{7/2}$	3809.629	1		26241.826	$24982^{\circ}_{7/2} - 51224_{9/2}$
3838.850	2		26042.080	$23372^{\circ}_{3/2} - 49414_{3/2}$	3809.457	1		26243.011	$12485^{\circ}_{7/2} - 38728_{5/2}$
3837.794	2		26049.246	$16906^{\circ}_{7/2} - 42955_{9/2}$	3809.132	3	25	26245.250	$15242^{\circ}_{9/2} - 41488_{7/2}$
3834.080	2		26074.479	$20310^{\circ}_{5/2} - 46385_{7/2}$	3809.081	1		26245.601	$11576^{\circ}_{3/2} - 37821_{3/2}$
3833.693	50	100	26077.111	$13818^{\circ}_{7/2} - 39895_{9/2}$	3808.688	4		26248.310	$12902^{\circ}_{3/2} - 39150_{3/2}$
3833.231	10	50	26080.254	$16564^{\circ}_{11/2} - 42644_{13/2}$	3808.512	3		26249.523	$20686^{\circ}_{5/2} - 46935_{3/2}$
3832.789	25	200	26083.261	$13468^{\circ}_{9/2} - 39552_{9/2}$	3808.128	50	200	26252.169	$12488^{\circ}_{9/2} - 38740_{11/2}$
3832.347	2		26086.270	$17722^{\circ}_{9/2} - 43809_{9/2}$	3807.875	300	800	26253.914	$9202^{\circ}_{7/2} - 35456_{9/2}$
3831.737	100	500	26090.422	$14484^{\circ}_{11/2} - 40574_{11/2}$	3807.671	3	100	26255.320	$19050^{\circ}_{3/2} - 45306_{3/2}$
3831.525	8	25	26091.866	$14275^{\circ}_{9/2} - 40367_{9/2}$	3807.500	3		26256.499	$12472^{\circ}_{5/2} - 38728_{5/2}$
3830.946	25	50	26095.809	$9061_{5/2} - 35156^{\circ}_{5/2}$	3806.266	5	75	26265.011	$20158_{5/2} - 46423^{\circ}_{3/2}$
3830.836	25b	100	26096.558	$11725^{\circ}_{1/2} - 37821_{3/2}$	3806.230	2		26265.260	$20120^{\circ}_{5/2} - 46385_{7/2}$
3830.511	25	100	26098.773	$14545^{\circ}_{3/2} - 40644_{5/2}$	3805.969	8	200	26267.061	$20288^{\circ}_{11/2} - 46555_{11/2}$
3829.415	50b	40	26106.242	$17121^{\circ}_{3/2} - 43227_{5/2}$					$25414^{\circ}_{11/2} - 51681_{9/2}$
3826.949	100	400	26123.064	$14349_{1/2} - 40472^{\circ}_{3/2}$	3805.820	200	400	26268.089	$6691^{\circ}_{3/2} - 32959_{3/2}$

TABLE 3. *Classified lines of* Th II—Continued

Wavelength Å	Intensity		Wavenumber cm^{-1}	Classification	Wavelength Å	Intensity		Wavenumber cm^{-1}	Classification
	Lamp	Spark				Lamp	Spark		
3805.341	2b	50b	26271.396	$27249^{\circ}_{7/2} - 53520_{9/2}$	3783.012	150	400	26426.457	$13468^{\circ}_{9/2} - 39895_{9/2}$
3805.314	500l	400b	26271.582	$20080^{\circ}_{7/2} - 46352_{7/2}$	3782.108	5		26432.774	$15786_{5/2} - 42219^{\circ}_{5/2}$
3804.995	100	200	26273.785	$12219_{3/2} - 38493^{\circ}_{5/2}$	3780.282	3		26445.541	$15242^{\circ}_{9/2} - 41688_{7/2}$
3804.335	8h	20	26278.343	$18816^{\circ}_{13/2} - 45095_{13/2}$	3779.712	1		26449.529	$16564^{\circ}_{11/2} - 43014_{13/2}$
3803.369	2		26285.017	$12472^{\circ}_{5/2} - 38757_{3/2}$	3778.744	10	75	26456.305	$15453^{\circ}_{7/2} - 41909_{9/2}$
3802.320	1		26292.268	$20310^{\circ}_{5/2} - 46603_{5/2}$	3777.286	3	40	26466.516	$19912^{\circ}_{13/2} - 46378_{13/2}$
3802.147	25	75	26293.465	$9585^{\circ}_{5/2} - 35878_{7/2}$	3775.901	8	200	26476.224	$14349_{1/2} - 40825^{\circ}_{1/2}$
3801.916	10	50	26295.062	$14275^{\circ}_{9/2} - 40570_{7/2}$	3775.312	10	25	26480.354	$9585^{\circ}_{5/2} - 36065_{5/2}$
3801.324	15	150	26299.157	$14275^{\circ}_{9/2} - 40574_{11/2}$	3774.924	1		26483.076	$20120^{\circ}_{5/2} - 46603_{5/2}$
3800.588	10	400	26304.250	$19912^{\circ}_{13/2} - 46216_{11/2}$	3774.202	100b	500	26488.142	$19880_{9/2} - 46368^{\circ}_{9/2}$
3800.371	75	200	26305.752	$7331^{\circ}_{5/2} - 33637_{7/2}$	3773.758	300	400	26491.259	$10572^{\circ}_{9/2} - 37063_{9/2}$
3800.113	20	20	26307.538	$9238^{\circ}_{9/2} - 35545_{9/2}$	3772.429	1		26500.591	$20080^{\circ}_{7/2} - 46581_{5/2}$
3799.489	3		26311.858	$17460^{\circ}_{5/2} - 43772_{5/2}$	3772.236	100	200	26501.947	$7828_{1/2} - 34330^{\circ}_{1/2}$
3799.422	2		26312.322	$8018_{3/2} - 34330^{\circ}_{1/2}$	3771.201	1		26509.220	$6700^{\circ}_{9/2} - 33209_{7/2}$
3798.459	4	15	26318.993	$16033^{\circ}_{5/2} - 42352_{5/2}$	3768.778	3	10	26526.263	$8460_{3/2} - 34986^{\circ}_{3/2}$
3798.426	200	75	26319.221	$23518^{\circ}_{7/2} - 49837_{9/2}$	3768.435	20	100	26528.677	$11576^{\circ}_{3/2} - 38105_{5/2}$
3797.718	2		26324.128	$21682^{\circ}_{7/2} - 48006_{9/2}$	3768.003	3	5	26531.719	$17272^{\circ}_{9/2} - 43803_{7/2}$
3797.564	2		26325.195	$17771^{\circ}_{11/2} - 44096_{9/2}$	3767.946	8b	50	26532.120	$15144^{\circ}_{3/2} - 41676_{3/2}$
3797.453	15	200	26325.965	$15786_{5/2} - 42112^{\circ}_{3/2}$	3767.898	300s	500	26532.458	$9061_{5/2} - 35593^{\circ}_{7/2}$
3796.185	1	5	26334.758	$28587^{\circ}_{5/2} - 54922_{3/2}$	3767.868	4		26532.669	$13406^{\circ}_{13/2} - 39939_{11/2}$
				$22355^{\circ}_{1/2} - 48689_{3/2}$					
					3767.513	2		26535.169	$15710^{\circ}_{3/2} - 42246_{1/2}$
3795.678	3	75	26338.276	$18214^{\circ}_{3/2} - 44552_{5/2}$	3767.252	2		26537.007	$17272^{\circ}_{9/2} - 43809_{9/2}$
3794.951	2		26343.321	$9202^{\circ}_{7/2} - 35545_{9/2}$	3767.201	10	200	26537.367	$14790^{\circ}_{7/2} - 41328_{5/2}$
3794.646	4	20	26345.438	$9720^{\circ}_{7/2} - 36065_{5/2}$	3765.535	8h	20	26549.108	$13818^{\circ}_{7/2} - 40367_{9/2}$
3794.428	2		26346.952	$17460^{\circ}_{5/2} - 43807_{3/2}$	3765.129	3	10	26551.970	$19248^{\circ}_{3/2} - 45800_{5/2}$
3794.316	150	100	26347.730	$8378^{\circ}_{7/2} - 34726_{7/2}$	3764.070	2	50	26559.440	$15349^{\circ}_{11/2} - 41909_{9/2}$
3794.150	100	200	26348.882	$11116^{\circ}_{7/2} - 37465_{5/2}$	3763.581	15	300b	26562.891	$14484^{\circ}_{11/2} - 41047_{9/2}$
3793.309	2		26354.724	$23518^{\circ}_{7/2} - 49873_{5/2}$	3763.554	2	25	26563.082	$25607^{\circ}_{9/2} - 52170_{11/2}$
3792.312	15b	200	26361.652	$12219_{3/2} - 38581^{\circ}_{5/2}$	3763.320	40	300	26564.733	$16818_{7/2} - 43382^{\circ}_{5/2}$
3791.972	15	100	26364.016	$12472^{\circ}_{5/2} - 38836_{3/2}$	3762.885	400b	600	26567.804	$6168^{\circ}_{7/2} - 32736_{7/2}$
3791.296	100	300	26368.717	$11576^{\circ}_{3/2} - 37945_{5/2}$	3762.679	1		26569.259	$17983^{\circ}_{5/2} - 44552_{5/2}$
3790.459	3		26374.539	$12488^{\circ}_{9/2} - 38862_{11/2}$	3762.417	1	20	26571.109	$29515_{9/2} - 56086^{\circ}_{9/2}$
3789.951	25	200	26378.075	$14545^{\circ}_{3/2} - 40923_{5/2}$	3762.012	1		26573.969	$21297^{\circ}_{5/2} - 47871_{7/2}$
3789.610	2	15	26380.448	$24982^{\circ}_{7/2} - 51362_{5/2}$	3761.887	2		26574.852	$18214^{\circ}_{3/2} - 44789_{1/2}$
3789.563	4		26380.775	$8605_{5/2} - 34986^{\circ}_{3/2}$	3761.101	50	200	26580.406	$12488^{\circ}_{9/2} - 39068_{7/2}$
3789.413	2		26381.819	$27787^{\circ}_{9/2} - 54169_{7/2}$	3760.733	1		26583.007	$12485^{\circ}_{7/2} - 39068_{7/2}$
3789.122	500b	400	26383.845	$1859_{3/2} - 28243^{\circ}_{5/2}$	3760.295	3b		26586.103	$20120^{\circ}_{5/2} - 46706_{7/2}$
3788.358	50	100	26389.166	$4490^{\circ}_{5/2} - 30879_{7/2}$	3760.271	50b	25b	26586.273	$0_{3/2} - 26586^{\circ}_{3/2}$
3788.062	1		26391.228	$16564^{\circ}_{11/2} - 42955_{9/2}$	3758.822	4	40	26596.521	$12472^{\circ}_{5/2} - 39068_{7/2}$
3787.995	1		26391.695	$12472^{\circ}_{5/2} - 38863_{5/2}$	3757.276	1		26607.465	$14790^{\circ}_{7/2} - 41398_{9/2}$
3787.478	10	100	26395.297	$20310^{\circ}_{5/2} - 46706_{7/2}$	3756.889	1		26610.205	$24414^{\circ}_{3/2} - 51024_{3/2}$
3787.116	8	200	26397.820	$13818^{\circ}_{7/2} - 40216_{5/2}$	3756.757	8	50	26611.141	$13250_{3/2} - 39861^{\circ}_{5/2}$
3786.881	100	200	26399.458	$7331^{\circ}_{5/2} - 33730_{3/2}$	3754.843	1		26624.705	$20310^{\circ}_{5/2} - 46935_{3/2}$
3786.076	2		26405.071	$9720^{\circ}_{7/2} - 36125_{9/2}$	3754.592	200	200	26626.485	$0_{3/2} - 26626^{\circ}_{1/2}$
3785.913	100	300	26406.208	$17771^{\circ}_{11/2} - 44177_{11/2}$	3752.568	500	800	26640.846	$9238^{\circ}_{9/2} - 35878_{7/2}$
3785.600	500	500	26408.391	$6168^{\circ}_{7/2} - 32576_{7/2}$	3751.758	8	40	26646.597	$11725^{\circ}_{1/2} - 38372_{3/2}$
3785.428	2		26409.591	$25266^{\circ}_{1/2} - 51676_{3/2}$	3750.658	2	40	26654.412	$29431_{7/2} - 56086^{\circ}_{9/2}$
3783.752	4	10	26421.289	$18973^{\circ}_{7/2} - 45395_{7/2}$	3748.975	200	100	26666.378	$15242^{\circ}_{9/2} - 41909_{9/2}$
3783.660	100b	100	26421.932	$14101^{\circ}_{1/2} - 40523_{1/2}$	3748.282	50	200	26671.308	$11116^{\circ}_{7/2} - 37787_{7/2}$
3783.295	200	300	26424.481	$0_{3/2} - 26424^{\circ}_{3/2}$	3747.706	2	20	26675.407	$18214^{\circ}_{3/2} - 44889_{3/2}$

TABLE 3. *Classified lines of* Th II—Continued

Wavelength Å	Intensity		Wavenumber cm^{-1}	Classification	Wavelength Å	Intensity		Wavenumber cm^{-1}	Classification
	Lamp	Spark				Lamp	Spark		
3747.539	300	500	26676.595	$9202^{\circ}_{7/2} - 35878_{7/2}$	3721.824	800b	500	26860.906	$1859_{3/2} - 28720^{\circ}_{3/2}$
3747.270	1		26678.511	$12472^{\circ}_{3/2} - 39150_{3/2}$	3721.344	8	40	26864.371	$10189^{\circ}_{11/2} - 37053_{11/2}$
3747.170	3	10	26679.222	$17771^{\circ}_{11/2} - 44450_{9/2}$	3721.137	2b	2	26865.865	$16906^{\circ}_{7/2} - 43772_{5/2}$
3746.463	25	50	26684.257	$6700^{\circ}_{9/2} - 33384_{9/2}$	3720.700	10	75	26869.020	$10673^{\circ}_{5/2} - 37542_{3/2}$
3746.227	5	75	26685.938	$17121^{\circ}_{3/2} - 43807_{3/2}$	3720.307	200s	400	26871.859	$9711_{7/2} - 36583^{\circ}_{7/2}$
3745.968	400	500	26687.783	$7331^{\circ}_{5/2} - 34019_{3/2}$	3720.214	150	100	26872.530	$12570_{7/2} - 39443^{\circ}_{9/2}$
3744.735	200	200	26696.570	$8460_{3/2} - 35156^{\circ}_{5/2}$	3719.976	300b	500	26874.249	$10189^{\circ}_{11/2} - 37063_{9/2}$
3744.652	15	200	26697.162	$14790^{\circ}_{7/2} - 41488_{7/2}$	3719.693	20	200	26876.294	$15236_{3/2} - 42112^{\circ}_{3/2}$
3743.806	100	200	26703.194	$18118_{3/2} - 44821^{\circ}_{5/2}$	3719.152	1	1	26880.204	$26965^{\circ}_{5/2} - 53845_{5/2}$
3743.506	20	200	26705.334	$10572^{\circ}_{9/2} - 37277_{7/2}$	3719.057	10	5	26880.890	$4113_{5/2} - 30994^{\circ}_{7/2}$
3742.228	5	200	26714.454	$10855_{7/2} - 37569^{\circ}_{9/2}$	3719.012	3	5	26881.215	$12485^{\circ}_{7/2} - 39366_{5/2}$
3741.183	1000r	600	26721.916	$1521_{5/2} - 28243^{\circ}_{5/2}$	3718.806	1	2	26882.704	$24982^{\circ}_{7/2} - 51865_{5/2}$
3740.854	40o	300	26724.266	$11116^{\circ}_{7/2} - 37840_{9/2}$	3718.656	10	200	26883.789	$15453^{\circ}_{7/2} - 42336_{5/2}$
3740.411	15	20	26727.431	$1859_{3/2} - 28587^{\circ}_{5/2}$	3718.168	75	200	26887.317	$9238^{\circ}_{9/2} - 36125_{9/2}$
3738.847	300	300	26738.611	$8460_{3/2} - 35198^{\circ}_{1/2}$	3717.830	15	200	26889.762	$14101^{\circ}_{7/2} - 40991_{3/2}$
3738.758	3b	400	26739.248	$14484^{\circ}_{11/2} - 41223_{11/2}$	3716.773	4	5	26897.408	$16906^{\circ}_{7/2} - 43803_{7/2}$
3738.103	8b		26743.933	$6213_{9/2} - 32957^{\circ}_{7/2}$	3716.542	2b		26899.080	$15453^{\circ}_{7/2} - 42352_{5/2}$
3737.647	3		26747.196	$15453^{\circ}_{7/2} - 42200_{9/2}$	3716.214	4	2	26901.454	$10855_{7/2} - 37756^{\circ}_{7/2}$
3737.334	1		26749.435	$19050^{\circ}_{5/2} - 45800_{5/2}$	3716.088	1		26902.366	$20969^{\circ}_{7/2} - 47871_{7/2}$
3736.936	15	200	26752.284	$13818^{\circ}_{7/2} - 40570_{7/2}$	3715.911	3	2	26903.648	$15242^{\circ}_{9/2} - 42146_{11/2}$
3735.511	3	15	26762.490	$20969^{\circ}_{7/2} - 47731_{9/2}$	3715.721	3	25	26905.023	$17272^{\circ}_{9/2} - 44177_{11/2}$
3734.698	1	2	26768.315	$30310^{\circ}_{11/2} - 57078_{9/2}$	3714.455	1		26914.193	$14484^{\circ}_{11/2} - 41398_{9/2}$
3734.598	100b	200b	26769.032	$4490^{\circ}_{5/2} - 31259_{5/2}$	3714.338	2	3	26915.041	$24309^{\circ}_{11/2} - 51224_{9/2}$
3734.566	3b	10b	26769.261	$15453^{\circ}_{7/2} - 42222_{7/2}$	3714.291	8b	200	26915.382	$17983^{\circ}_{5/2} - 44898_{7/2}$
3734.414	1		26770.351	$21682^{\circ}_{7/2} - 48453_{7/2}$	3712.533	40b	25b	26928.127	$17460^{\circ}_{5/2} - 44388_{5/2}$
3734.232	1		26771.656	$14275^{\circ}_{9/2} - 41047_{9/2}$	3711.780	3	2	26933.589	$13250_{5/2} - 40184^{\circ}_{7/2}$
3734.128	1		26772.401	$23697^{\circ}_{7/2} - 50470_{9/2}$	3711.304	300	500	26937.044	$6700^{\circ}_{9/2} - 33637_{7/2}$
3732.736	2		26782.385	$20120^{\circ}_{5/2} - 46902_{5/2}$	3710.552	5	50	26942.503	$13468^{\circ}_{9/2} - 40411_{7/2}$
3732.679	3	20	26782.794	$14545^{\circ}_{5/2} - 41328_{5/2}$	3709.817	3	8	26947.841	$7331^{\circ}_{5/2} - 34279_{7/2}$
3732.473	1		26784.272	$33209_{7/2} - 59993^{\circ}_{9/2}$	3709.624	5	200	26949.242	$19912^{\circ}_{13/2} - 46861_{11/2}$
3731.425	8	75	26791.794	$15144^{\circ}_{5/2} - 41936_{3/2}$	3709.310	2		26951.524	$17837^{\circ}_{7/2} - 44789_{1/2}$
3731.354	4b		26792.304	$10673^{\circ}_{5/2} - 37465_{5/2}$	3708.754	5	150	26955.564	$16818_{7/2} - 43773^{\circ}_{7/2}$
3730.748	75	500	26796.656	$15349^{\circ}_{11/2} - 42146_{11/2}$	3708.671	5b	75	26956.167	$17771^{\circ}_{11/2} - 44727_{11/2}$
3730.532	2		26798.207	$12902^{\circ}_{3/2} - 39700_{5/2}$	3707.428	75	75	26965.205	$0_{3/2} - 26965^{\circ}_{3/2}$
3729.678	25	50	26804.343	$24463^{\circ}_{5/2} - 51268_{7/2}$	3706.046	8	200	26975.260	$18214^{\circ}_{3/2} - 45189_{5/2}$
3728.990	1		26809.289	$21682^{\circ}_{7/2} - 48492_{5/2}$	3705.942	5	50	26976.017	$9711_{7/2} - 36687^{\circ}_{5/2}$
3728.965	1		26809.468	$29873_{7/2} - 56683^{\circ}_{7/2}$	3704.966	25	200	26983.123	$15236_{3/2} - 42219^{\circ}_{3/2}$
3726.946	1		26823.991	$17272^{\circ}_{9/2} - 44096_{9/2}$	3704.342	20h	100	26987.668	$8605_{5/2} - 35593^{\circ}_{7/2}$
3726.724	200	200	26825.589	$4146_{7/2} - 30972^{\circ}_{5/2}$	3704.085	100	200	26989.541	$9400_{3/2} - 36390^{\circ}_{3/2}$
3726.659	25	50	26826.057	$12570_{7/2} - 39396^{\circ}_{7/2}$	3703.990	100	300	26990.233	$10572^{\circ}_{9/2} - 37562_{11/2}$
3726.197	3	50	26829.383	$18816^{\circ}_{13/2} - 45646_{13/2}$	3703.907	75	200	26990.838	$10855_{7/2} - 37846^{\circ}_{5/2}$
3726.099	2	1	26830.089	$22014^{\circ}_{11/2} - 48844_{9/2}$	3702.864	10	300	26998.440	$19912^{\circ}_{13/2} - 46910_{13/2}$
3725.875	3	100	26831.702	$19594_{1/2} - 46426^{\circ}_{1/2}$	3702.067	3	15	27004.252	$17722^{\circ}_{9/2} - 44727_{11/2}$
3725.822	1	3	26832.084	$25440^{\circ}_{5/2} - 52272_{7/2}$	3700.766	50	500	27013.745	$15305_{9/2} - 42319^{\circ}_{9/2}$
3724.733	40	200	26839.928	$17460^{\circ}_{5/2} - 44300_{3/2}$	3700.526	1	2	27015.497	$22106_{5/2} - 49121^{\circ}_{7/2}$
3724.498	75	50	26841.622	$7001_{3/2} - 33843^{\circ}_{3/2}$	3700.462	25	75	27015.964	$19248^{\circ}_{5/2} - 46264_{3/2}$
3724.299	3	1	26843.056	$7331^{\circ}_{5/2} - 34174_{5/2}$	3698.755	5	200	27028.432	$20120^{\circ}_{5/2} - 47148_{3/2}$
3723.657	100	200	26847.684	$4146_{7/2} - 30994^{\circ}_{7/2}$	3698.301	10b	8	27031.750	$11725^{\circ}_{7/2} - 38757_{3/2}$
3723.291	20	200	26850.323	$15349^{\circ}_{11/2} - 42200_{9/2}$	3697.234	2		27039.551	$6691^{\circ}_{3/2} - 33730_{5/2}$
3722.115	300b	500	26858.806	$4113_{5/2} - 30972^{\circ}_{5/2}$	3697.030	100	200	27041.043	$6168^{\circ}_{7/2} - 33209_{7/2}$

TABLE 3. *Classified lines of* Th II—Continued

Wavelength Å	Intensity		Wavenumber cm^{-1}	Classification	Wavelength Å	Intensity		Wavenumber cm^{-1}	Classification
	Lamp	Spark				Lamp	Spark		
3696.647	50	200	27043.845	$9400_{5/2} - 36444^{\circ}_{3/2}$	3672.205	2		27223.842	$9585^{\circ}_{5/2} - 36809_{7/2}$
3696.316	1	1	27046.266	$26963^{\circ}_{7/2} - 54010_{7/2}$	3671.164	10	50	27231.562	$17272^{\circ}_{9/2} - 44503_{7/2}$
3695.974	100	300	27048.769	$11116^{\circ}_{7/2} - 38165_{7/2}$	3670.057	300	150	27239.775	$4113_{5/2} - 31353^{\circ}_{3/2}$
3694.785	1	2	27057.473	$27787^{\circ}_{9/2} - 54845_{9/2}$	3669.403	4	10l	27244.630	$16564^{\circ}_{11/2} - 43809_{9/2}$
3693.901	50	300	27063.948	$12488^{\circ}_{9/2} - 39552_{9/2}$	3666.373	3b	2	27267.146	$17121^{\circ}_{3/2} - 44388_{5/2}$
3693.693	100	100	27065.472	$1521_{5/2} - 28587^{\circ}_{5/2}$	3666.150	2	2	27268.804	$10572^{\circ}_{9/2} - 37840_{9/2}$
3693.640	1		27065.860	$15453^{\circ}_{7/2} - 42518_{7/2}$	3665.723	20	100	27271.980	$10673^{\circ}_{5/2} - 37945_{5/2}$
3693.544	4b		27066.564	$12485^{\circ}_{7/2} - 39552_{9/2}$	3665.181	15	100	27276.013	$15242^{\circ}_{9/2} - 42518_{7/2}$
3692.075	50	200	27077.333	$8378^{\circ}_{7/2} - 35456_{9/2}$	3663.702	300b	500b	27287.024	$9400_{5/2} - 36687^{\circ}_{5/2}$
3690.486	150	300	27088.991	$9720^{\circ}_{7/2} - 36809_{7/2}$	3663.318	2	3	27289.884	$24982^{\circ}_{7/2} - 52272_{7/2}$
3690.070	5b	20	27092.045	$17460^{\circ}_{5/2} - 44552_{5/2}$	3662.631	2	1	27295.003	$15349^{\circ}_{11/2} - 42644_{13/2}$
3688.812	8	40	27101.284	$15144^{\circ}_{3/2} - 42246_{1/2}$	3662.562	2	3	27295.517	$25440^{\circ}_{5/2} - 52735_{3/2}$
3688.756	100b	150b	27101.695	$13468^{\circ}_{9/2} - 40570_{7/2}$	3662.191	15l	25	27298.282	$15453^{\circ}_{7/2} - 42751_{7/2}$
3688.266	3	2	27105.296	$13818^{\circ}_{7/2} - 40923_{5/2}$	3660.117	4b	3	27313.750	$12902^{\circ}_{3/2} - 40216_{5/2}$
3688.198	4	10	27105.796	$13468^{\circ}_{9/2} - 40574_{11/2}$	3659.508	300l	500s	27318.296	$13406^{\circ}_{13/2} - 40724_{13/2}$
3687.671	10h	75	27109.669	$22014^{\circ}_{11/2} - 49124_{11/2}$	3659.208	1		27320.535	$12902^{\circ}_{3/2} - 40222_{3/2}$
3687.524	100b	100	27110.750	$11725^{\circ}_{1/2} - 38836_{3/2}$	3658.226	100	200	27327.869	$6691^{\circ}_{3/2} - 34019_{3/2}$
3686.980	20	100	27114.750	$10673^{\circ}_{5/2} - 37787_{7/2}$	3658.063	100b	200b	27329.087	$7001_{3/2} - 34330^{\circ}_{1/2}$
3686.494	1		27118.325	$14790^{\circ}_{7/2} - 41909_{9/2}$	3656.199	50	300	27343.019	$9720^{\circ}_{7/2} - 37063_{9/2}$
3685.867	8	100	27122.937	$14275^{\circ}_{9/2} - 41398_{9/2}$	3655.624	1		27347.320	$17460^{\circ}_{5/2} - 44807_{7/2}$
3683.936	5	75	27137.154	$19248^{\circ}_{5/2} - 46385_{7/2}$	3655.027	2	2	27351.786	$20969^{\circ}_{7/2} - 48320_{5/2}$
3683.723	5	1	27138.723	$8018_{3/2} - 35156^{\circ}_{5/2}$	3654.605	2	2	27354.945	$19248^{\circ}_{3/2} - 46603_{5/2}$
3683.313	20	200	27141.744	$11725^{\circ}_{1/2} - 38867_{1/2}$	3654.572	4	20	27355.192	$17771^{\circ}_{11/2} - 45126_{9/2}$
3682.846	2	2	27145.185	$23518^{\circ}_{7/2} - 50663_{5/2}$	3653.602	50	50	27362.454	$8378^{\circ}_{7/2} - 35741_{5/2}$
3682.350	25	200	27148.842	$10673^{\circ}_{5/2} - 37821_{3/2}$	3652.536	100	300	27370.440	$7828_{1/2} - 35198^{\circ}_{1/2}$
3681.880	100	200	27152.307	$11576^{\circ}_{3/2} - 38728_{5/2}$	3652.224	1	20	27372.778	$32620_{11/2} - 59993^{\circ}_{9/2}$
3681.180	10	200	27157.470	$15786_{5/2} - 42944^{\circ}_{7/2}$					$24309^{\circ}_{11/2} - 51681_{9/2}$
3681.103	5	10	27158.038	$7828_{1/2} - 34986^{\circ}_{3/2}$	3652.167	200	500	27373.205	$10189^{\circ}_{11/2} - 37562_{11/2}$
3680.540	2	3	27162.192	$21682^{\circ}_{7/2} - 48844_{9/2}$	3651.825	5	50	27375.768	$12902^{\circ}_{3/2} - 40278_{3/2}$
3679.710	200	500	27168.319	$29515_{9/2} - 56683^{\circ}_{7/2}$	3651.468	4	75	27378.445	$18973^{\circ}_{7/2} - 46352_{7/2}$
				$13406^{\circ}_{13/2} - 40574_{11/2}$					
					3650.765	100	300	27383.717	$9061_{5/2} - 36444^{\circ}_{3/2}$
3678.776	4	2	27175.217	$11116^{\circ}_{7/2} - 38291_{7/2}$	3650.502	4b	3	27385.689	$15710^{\circ}_{3/2} - 43096_{5/2}$
3678.273	5	20	27178.933	$17121^{\circ}_{3/2} - 44300_{3/2}$	3649.249	200	400	27395.092	$7331^{\circ}_{5/2} - 34726_{7/2}$
3678.047	150	150	27180.603	$9400_{5/2} - 36581^{\circ}_{3/2}$	3648.634	5	300	27399.710	$18816^{\circ}_{13/2} - 46216_{11/2}$
3678.021	150	150	27180.795	$8018_{3/2} - 35198^{\circ}_{1/2}$	3648.420	100b	150	27401.317	$1521_{5/2} - 28923^{\circ}_{5/2}$
				$11576^{\circ}_{3/2} - 38757_{3/2}$	3648.172	150	200	27403.180	$0_{3/2} - 27403^{\circ}_{3/2}$
3677.915	200	300	27181.578	$15236_{3/2} - 42418^{\circ}_{3/2}$	3647.646	200b	200	27407.131	$12488^{\circ}_{9/2} - 39895_{9/2}$
3677.742	100	200	27182.857	$9400_{5/2} - 36583^{\circ}_{7/2}$	3647.369	10	100	27409.213	$14790^{\circ}_{7/2} - 42200_{9/2}$
3677.089	2	2	27187.684	$22685^{\circ}_{7/2} - 49873_{5/2}$	3647.299	15	100	27409.739	$12485^{\circ}_{7/2} - 39895_{9/2}$
3676.823	2	2	27189.651	$16906^{\circ}_{7/2} - 44096_{9/2}$	3647.046	10	40	27411.640	$18973^{\circ}_{7/2} - 46385_{7/2}$
									$17983^{\circ}_{5/2} - 45395_{7/2}$
3676.690	20	100	27190.634	$10379_{9/2} - 37569^{\circ}_{9/2}$					
3675.567	500	500	27198.942	$1521_{5/2} - 28720^{\circ}_{3/2}$	3646.883	15	100	27412.865	$14275^{\circ}_{9/2} - 41688_{7/2}$
3674.648	2	2	27205.744	$26963^{\circ}_{7/2} - 54169_{7/2}$	3645.268	1	2	27425.010	$14484^{\circ}_{11/2} - 41909_{9/2}$
3673.793	150	300	27212.075	$7331^{\circ}_{5/2} - 34543_{5/2}$	3645.235	2		27425.258	$11725^{\circ}_{1/2} - 39150_{3/2}$
3673.615	2		27213.394	$19050^{\circ}_{3/2} - 46264_{3/2}$	3644.714	8	200	27429.178	$17460^{\circ}_{5/2} - 44889_{3/2}$
3673.411	2		27214.905	$12485^{\circ}_{7/2} - 39700_{5/2}$	3644.461	1		27431.082	$17121^{\circ}_{3/2} - 44552_{5/2}$
3673.283	400b	300b	27215.853	$10572^{\circ}_{9/2} - 37787_{7/2}$	3644.431	15	5	27431.308	$14790^{\circ}_{7/2} - 42222_{7/2}$
3673.255	40b	75b	27216.061	$6168^{\circ}_{7/2} - 33384_{9/2}$	3644.348	20	150	27431.933	$10673^{\circ}_{5/2} - 38105_{5/2}$
3672.950	5	20	27218.321	$22139^{\circ}_{9/2} - 49357_{11/2}$	3642.888	3	8	27442.927	$20288^{\circ}_{11/2} - 47731_{9/2}$
3672.466	1	2	27221.908	$13250_{5/2} - 40472^{\circ}_{3/2}$	3641.882	1	10	27450.507	$24414^{\circ}_{3/2} - 51865_{5/2}$

TABLE 3. *Classified lines of* Th II—Continued

Wavelength Å	Intensity		Wavenumber cm^{-1}	Classification	Wavelength Å	Intensity		Wavenumber cm^{-1}	Classification
	Lamp	Spark				Lamp	Spark		
3641.841	10	300	27450.816	$12488^{\circ}_{9/2} - 39939_{11/2}$	3617.731	8b	2	27633.755	$14275^{\circ}_{9/2} - 41909_{9/2}$
3641.287	3	20	27454.993	$17272^{\circ}_{9/2} - 44727_{11/2}$	3617.615	1	2	27634.641	$20686^{\circ}_{5/2} - 48320_{5/2}$
3641.113	15	200	27456.305	$13250_{5/2} - 40706^{\circ}_{7/2}$	3617.117	200	500	27638.445	$10855_{7/2} - 38493^{\circ}_{5/2}$
3640.873	3	2	27458.115	$13248_{9/2} - 40706^{\circ}_{7/2}$	3617.017	100	500	27639.209	$15305_{9/2} - 42944^{\circ}_{7/2}$
3640.184	1	1	27463.312	$20989^{\circ}_{9/2} - 48453_{7/2}$	3616.697	8	200	27641.655	$12219_{3/2} - 39861^{\circ}_{5/2}$
3639.587	2	3	27467.816	$28923^{\circ}_{5/2} - 56391_{5/2}$	3615.372	25	150	27651.785	$10189^{\circ}_{11/2} - 37840_{9/2}$
3639.446	300	500	27468.880	$6168^{\circ}_{7/2} - 33637_{7/2}$	3615.132	400	500	27653.621	$4146_{7/2} - 31800^{\circ}_{7/2}$
3637.686	5	100	27482.170	$16906^{\circ}_{7/2} - 44388_{5/2}$	3615.040	2		27654.324	$19248^{\circ}_{5/2} - 46902_{5/2}$
3637.555	75	200	27483.160	$6691^{\circ}_{3/2} - 34174_{5/2}$	3614.009	75	500	27662.213	$14484^{\circ}_{11/2} - 42146_{11/2}$
3636.918	1	2	27487.973	$27357^{\circ}_{9/2} - 54845_{9/2}$	3613.778	100	150	27663.981	$4146_{7/2} - 31810^{\circ}_{5/2}$
3636.566	20	200	27490.634	$10189^{\circ}_{11/2} - 37679_{11/2}$	3613.611	2	3	27665.260	$23697^{\circ}_{7/2} - 51362_{5/2}$
3636.357	4	2	27492.214	$10673^{\circ}_{5/2} - 38165_{7/2}$	3612.113	4	25	27676.733	$14545^{\circ}_{5/2} - 42222_{7/2}$
3636.172	5	50	27493.613	$23730^{\circ}_{9/2} - 51224_{9/2}$	3610.793	100	200	27686.850	$4113_{5/2} - 31800^{\circ}_{7/2}$
3635.420	15	400	27499.299	$22028^{\circ}_{13/2} - 49527_{13/2}$	3610.562	2		27688.622	$6213_{9/2} - 33902^{\circ}_{7/2}$
3635.327	8	10	27500.003	$8378^{\circ}_{7/2} - 35878_{7/2}$	3610.398	75	200	27689.879	$7331^{\circ}_{5/2} - 35021_{3/2}$
3635.242	20	400	27500.646	$15786_{5/2} - 43287^{\circ}_{3/2}$	3610.125	50	200	27691.973	$9585^{\circ}_{5/2} - 37277_{7/2}$
3634.953	1		27502.832	$15453^{\circ}_{7/2} - 42955_{9/2}$	3610.036	200b	300	27692.656	$13406^{\circ}_{13/2} - 41099_{13/2}$
3634.214	10		27508.425	$15242^{\circ}_{9/2} - 42751_{7/2}$	3609.444	1000	600	27697.198	$4113_{5/2} - 31810^{\circ}_{5/2}$
3634.002	1		27510.029	$13818^{\circ}_{7/2} - 41328_{5/2}$	3609.224	100	300	27698.886	$10673^{\circ}_{5/2} - 38372_{3/2}$
3633.740	1	2	27512.013	$27526_{9/2} - 55038^{\circ}_{9/2}$	3607.910	2		27708.974	$27787^{\circ}_{9/2} - 55496_{9/2}$
3633.683	1	2	27512.445	$22014^{\circ}_{11/2} - 49527_{13/2}$	3607.392	10	150	27712.952	$15242^{\circ}_{9/2} - 42955_{9/2}$
3633.369	2	15	27514.822	$24757^{\circ}_{9/2} - 52272_{7/2}$	3607.009	2		27715.895	$14484^{\circ}_{11/2} - 42200_{9/2}$
3633.077	3	2	27517.034	$15710^{\circ}_{3/2} - 43227_{3/2}$	3606.963	2		27716.248	$10673^{\circ}_{3/2} - 38389_{7/2}$
3632.625	75	100	27520.457	$9061_{5/2} - 36581^{\circ}_{3/2}$	3606.696	3		27718.300	$20288^{\circ}_{11/2} - 48006_{9/2}$
3631.151	4	5	27531.629	$16564^{\circ}_{11/2} - 44096_{9/2}$	3606.505	2		27719.768	$10572^{\circ}_{9/2} - 38291_{7/2}$
3630.677	2		27535.223	$23372^{\circ}_{3/2} - 50907_{3/2}$	3605.654	20	200	27726.310	$10855_{7/2} - 38581^{\circ}_{5/2}$
3630.613	15	15	27535.708	$17272^{\circ}_{9/2} - 44807_{7/2}$	3605.440	15	20	27727.956	$14790^{\circ}_{7/2} - 42518_{7/2}$
3629.278	4	2	27545.837	$14790^{\circ}_{7/2} - 42336_{5/2}$	3605.296	2		27729.063	$17460^{\circ}_{5/2} - 45189_{5/2}$
3627.799	5	40	27557.066	$9720^{\circ}_{7/2} - 37277_{7/2}$	3605.117	3		27730.440	$12485^{\circ}_{7/2} - 40216_{3/2}$
3627.658	2	1	27558.138	$21131^{\circ}_{3/2} - 48689_{3/2}$	3604.039	8b		27738.734	$18816^{\circ}_{13/2} - 46555_{11/2}$
3627.591	4	50	27558.646	$20310^{\circ}_{5/2} - 47869_{3/2}$	3603.620	10	100	27741.959	$12902^{\circ}_{3/2} - 40644_{5/2}$
3627.265	10	50	27561.123	$14790^{\circ}_{7/2} - 42352_{5/2}$	3603.362	50	200	27743.946	$12472^{\circ}_{3/2} - 40216_{3/2}$
3627.150	8	75	27561.997	$18816^{\circ}_{13/2} - 46378_{13/2}$	3603.204	300	300	27745.162	$9720^{\circ}_{7/2} - 37465_{5/2}$
3627.073	15	20	27562.582	$6168^{\circ}_{7/2} - 33730_{5/2}$	3603.031	20	50	27746.494	$8378^{\circ}_{7/2} - 36125_{9/2}$
3626.090	25	50	27570.054	$6700^{\circ}_{9/2} - 34270_{9/2}$	3602.936	5		27747.226	$11116^{\circ}_{7/2} - 38863_{3/2}$
3625.931	75b	75b	27571.263	$9238^{\circ}_{9/2} - 36809_{7/2}$	3602.646	1		27749.459	$20120^{\circ}_{3/2} - 47869_{3/2}$
3625.628	500	300	27573.567	$1521_{5/2} - 29095^{\circ}_{5/2}$	3602.478	4	5	27750.754	$12472^{\circ}_{3/2} - 40222_{3/2}$
3625.536	5	20	27574.267	$11576^{\circ}_{3/2} - 39150_{3/2}$	3601.980	5	50	27754.590	$13468^{\circ}_{9/2} - 41223_{11/2}$
3624.896	300	400	27579.135	$6700^{\circ}_{9/2} - 34279_{7/2}$	3601.034	100	500	27761.881	$17727_{11/2} - 45489^{\circ}_{9/2}$
3624.776	2	2	27580.048	$24982^{\circ}_{7/2} - 52562_{7/2}$	3600.816	8	100	27763.562	$14349_{1/2} - 42112^{\circ}_{3/2}$
3624.014	3	4	27585.847	$18214^{\circ}_{3/2} - 45800_{5/2}$	3600.606	2	3	27765.181	$22642^{\circ}_{9/2} - 50407_{7/2}$
3623.847	1	3	27587.118	$31800^{\circ}_{7/2} - 59387_{7/2}$	3599.872	5	75	27770.842	$16033^{\circ}_{5/2} - 43803_{7/2}$
3623.034	8	20	27593.308	$10572^{\circ}_{9/2} - 38165_{7/2}$	3599.355	10	100	27774.831	$15453^{\circ}_{7/2} - 43227_{5/2}$
3621.168	3	5	27607.527	$18973^{\circ}_{7/2} - 46581_{5/2}$	3599.030	5	50	27777.339	$15349^{\circ}_{11/2} - 43127_{11/2}$
3621.118	200	500	27607.908	$10572^{\circ}_{9/2} - 38179_{9/2}$	3596.901	8	20	27793.780	$15453^{\circ}_{7/2} - 43246_{7/2}$
3620.569	4	1	27612.094	$11116^{\circ}_{7/2} - 38728_{5/2}$	3595.326	20	100	27805.955	$12472^{\circ}_{3/2} - 40278_{3/2}$
3620.502	25b	4	27612.605	$16564^{\circ}_{11/2} - 44177_{11/2}$	3594.110	50	75	27815.363	$4113_{5/2} - 31928^{\circ}_{3/2}$
3620.370	100	200	27613.612	$12570_{7/2} - 40184^{\circ}_{7/2}$	3593.880	25	300	27817.143	$13406^{\circ}_{13/2} - 41223_{11/2}$
3619.709	20	100	27618.654	$10673^{\circ}_{5/2} - 38291_{7/2}$	3593.855	8b		27817.336	$10572^{\circ}_{9/2} - 38389_{7/2}$
3619.356	4	40	27621.348	$12902^{\circ}_{3/2} - 40523_{1/2}$	3593.392	1	2	27820.920	$22139^{\circ}_{9/2} - 49960_{7/2}$

TABLE 3. *Classified lines of* Th II—Continued

Wavelength Å	Intensity		Wavenumber cm^{-1}	Classification	Wavelength Å	Intensity		Wavenumber cm^{-1}	Classification
	Lamp	Spark				Lamp	Spark		
3593.150	2	3	27822.794	$22014^{\circ}_{11/2} - 49837_{9/2}$	3559.964	50b	25b	28082.151	$8605_{5/2} - 36687^{\circ}_{5/2}$
3592.826	150b	100	27825.303	$9238^{\circ}_{9/2} - 37063_{9/2}$	3559.940	50b	500	28082.340	$12488^{\circ}_{9/2} - 40570_{7/2}$
3592.487	2	50	27827.929	$22642^{\circ}_{9/2} - 50470_{9/2}$	3559.730	25	100	28083.997	$12570^{\circ}_{7/2} - 40654_{5/2}$
3591.906	3		27832.430	$16818^{\circ}_{7/2} - 44650_{7/2}$	3559.614	150	200	28084.912	$12485^{\circ}_{7/2} - 40570_{7/2}$
3591.607	3	3	27834.747	$14101^{\circ}_{1/2} - 41936_{3/2}$	3559.450	300b	500	28086.206	$6244_{1/2} - 34330^{\circ}_{1/2}$
3589.358	150	300	27852.187	$6691^{\circ}_{3/2} - 34543_{5/2}$	3559.415	25b	50b	28086.482	$4490^{\circ}_{5/2} - 32576_{7/2}$
3589.153	50b	200	27853.777	$6700^{\circ}_{9/2} - 34553_{9/2}$					$12488^{\circ}_{9/2} - 40574_{11/2}$
3589.127	5b		27853.979	$17272^{\circ}_{9/2} - 45126_{9/2}$	3558.842	3	25	28091.004	$13818^{\circ}_{7/2} - 41909_{9/2}$
3588.974	1		27855.167	$20989^{\circ}_{9/2} - 48844_{9/2}$	3558.471	2	50	28093.933	$18816^{\circ}_{13/2} - 46910_{13/2}$
3588.640	3	2	27857.759	$9711_{7/2} - 37569^{\circ}_{9/2}$	3558.344	2	3	28094.935	$19050^{\circ}_{3/2} - 47145_{1/2}$
3588.300	50	75	27860.399	$1859_{3/2} - 29720^{\circ}_{3/2}$	3558.120	1		28096.704	$15710^{\circ}_{3/2} - 43807_{3/2}$
3588.216	20	75	27861.051	$9202^{\circ}_{7/2} - 37063_{9/2}$	3557.898	1		28098.457	$12472^{\circ}_{5/2} - 40570_{7/2}$
3587.051	2		27870.099	$13818^{\circ}_{7/2} - 41688_{7/2}$	3557.727	2		28099.808	$20969^{\circ}_{7/2} - 49068_{5/2}$
3586.941	4	50	27870.954	$14275^{\circ}_{9/2} - 42146_{11/2}$	3557.464	100	300	28101.885	$6168^{\circ}_{7/2} - 34270_{9/2}$
3585.884	10	40	27879.169	$12488^{\circ}_{9/2} - 40367_{9/2}$	3556.313	15	100	28110.980	$6168^{\circ}_{7/2} - 34279_{7/2}$
3585.769	40	75	27880.063	$9585^{\circ}_{5/2} - 37465_{5/2}$	3555.101	75	100	28120.563	$9720^{\circ}_{7/2} - 37840_{9/2}$
3585.549	5	20	27881.774	$12485^{\circ}_{7/2} - 40367_{9/2}$	3554.823	5	15b	28122.762	$17272^{\circ}_{9/2} - 45395_{7/2}$
3585.050	20	40	27885.655	$16564^{\circ}_{11/2} - 44450_{9/2}$	3554.644	4	8	28124.178	$11576^{\circ}_{3/2} - 39700_{5/2}$
3583.036	8	200	27901.328	$16906^{\circ}_{7/2} - 44807_{7/2}$	3553.377	50	200	28134.206	$9711_{7/2} - 37846^{\circ}_{5/2}$
3582.391	3	2	27906.352	$14101^{\circ}_{1/2} - 42008_{1/2}$	3553.110	100	300	28136.320	$12570_{7/2} - 40706^{\circ}_{7/2}$
3582.217	1		27907.707	$26586^{\circ}_{3/2} - 54493_{5/2}$	3551.869	8	150	28146.151	$15236_{3/2} - 43382^{\circ}_{5/2}$
3582.006	100	300	27909.351	$10855_{7/2} - 38764^{\circ}_{7/2}$	3550.292	50	200	28158.653	$12485^{\circ}_{7/2} - 40644_{5/2}$
3580.226	25b	200	27923.227	$12488^{\circ}_{9/2} - 40411_{7/2}$	3549.736	40	200	28163.063	$10673^{\circ}_{3/2} - 38836_{3/2}$
3580.043	3	10	27924.654	$14275^{\circ}_{9/2} - 42200_{9/2}$	3549.179	1		28167.483	$23697^{\circ}_{7/2} - 51865_{5/2}$
3579.414	5		27929.561	$13468^{\circ}_{9/2} - 41398_{9/2}$	3548.589	2		28172.166	$12472^{\circ}_{5/2} - 40644_{5/2}$
3579.334	100l	200	27930.185	$8460^{\circ}_{3/2} - 36390_{3/2}$	3548.175	1		28175.453	$24132^{\circ}_{3/2} - 52307_{3/2}$
3578.164	20	200	27939.318	$12472^{\circ}_{5/2} - 40411_{7/2}$	3545.390	50	200	28197.585	$7001_{3/2} - 35198^{\circ}_{1/2}$
3577.214	10	5	27946.737	$14275^{\circ}_{9/2} - 42222_{7/2}$					$18973^{\circ}_{7/2} - 47171_{9/2}$
3575.930	2	4	27956.772	$9585^{\circ}_{5/2} - 37542_{3/2}$	3545.284	100	75	28198.428	$1521_{5/2} - 29720^{\circ}_{3/2}$
3575.320	300b	400	27961.541	$6700^{\circ}_{9/2} - 34661_{11/2}$	3545.180	50	200	28199.255	$13248_{9/2} - 41447^{\circ}_{11/2}$
3573.811	2	2	27973.347	$14545^{\circ}_{5/2} - 42518_{7/2}$	3544.993	40b	75	28200.742	$9400_{5/2} - 37601^{\circ}_{3/2}$
3573.508	40	100	27975.719	$8605_{3/2} - 36581^{\circ}_{3/2}$	3544.775	10	40	28202.477	$9585^{\circ}_{5/2} - 37787_{7/2}$
3573.220	100	300	27977.974	$8605_{3/2} - 36583^{\circ}_{7/2}$	3544.361	10	50	28205.771	$14545^{\circ}_{5/2} - 42751_{7/2}$
3572.392	150	400	27984.459	$8460_{3/2} - 36444^{\circ}_{3/2}$	3542.639	40b	50	28219.481	$13468^{\circ}_{9/2} - 41688_{7/2}$
3572.299	40	150	27985.187	$7001_{3/2} - 34986^{\circ}_{3/2}$	3542.620	40b	50	28219.632	$16906^{\circ}_{7/2} - 45126_{9/2}$
3571.810	2	2	27989.018	$22642^{\circ}_{9/2} - 50631_{11/2}$	3542.301	4		28222.173	$22513^{\circ}_{5/2} - 50735_{3/2}$
3571.572	40	200	27990.883	$10189^{\circ}_{11/2} - 38179_{9/2}$	3542.201	15	25	28222.970	$11725^{\circ}_{1/2} - 39948_{1/2}$
3569.918	3	4	28003.852	$16818^{\circ}_{7/2} - 44821_{5/2}$	3541.969	10	4	28224.818	$9720^{\circ}_{7/2} - 37945_{5/2}$
3569.620	50	150	28006.189	$6168^{\circ}_{7/2} - 34174_{5/2}$	3541.615	100	200	28227.640	$8460_{3/2} - 36687^{\circ}_{5/2}$
3567.965	10	150	28019.180	$13468^{\circ}_{9/2} - 41488_{7/2}$	3540.312	1		28238.028	$23697^{\circ}_{7/2} - 51935_{3/2}$
3567.701	50b	75	28021.253	$12902^{\circ}_{3/2} - 40923_{5/2}$	3540.047	5	2	28240.142	$20080^{\circ}_{7/2} - 48320_{5/2}$
3567.047	40	150	28026.390	$6700^{\circ}_{9/2} - 34726_{7/2}$	3539.587	1000	500	28243.812	$0_{3/2} - 28243^{\circ}_{5/2}$
3565.721	10	5	28036.812	$18118_{3/2} - 46155^{\circ}_{5/2}$	3539.322	800	400	28245.927	$4490^{\circ}_{5/2} - 32736_{7/2}$
3565.398	75b	200	28039.352	$9238^{\circ}_{9/2} - 37277_{7/2}$	3538.501	15	10	28252.480	$12219_{3/2} - 40472^{\circ}_{3/2}$
3564.712	25b		28044.748	$18816^{\circ}_{13/2} - 46861_{11/2}$	3538.211	50	100	28254.796	$15710^{\circ}_{3/2} - 43965_{1/2}$
3564.706	50	200	28044.795	$9711_{7/2} - 37756^{\circ}_{7/2}$	3537.158	400	300	28263.207	$9202^{\circ}_{7/2} - 37465_{5/2}$
3564.599	8	40	28045.637	$10572^{\circ}_{9/2} - 38617_{9/2}$	3536.632	50b	100	28267.410	$16033^{\circ}_{5/2} - 44300_{3/2}$
3561.571	10	4	28069.480	$26424^{\circ}_{3/2} - 54493_{5/2}$	3536.609	3		28267.594	$22139^{\circ}_{9/2} - 50407_{7/2}$
3560.857	5		28075.109	$9202^{\circ}_{7/2} - 37277_{7/2}$	3535.863	1		28273.558	$19050^{\circ}_{3/2} - 47324_{5/2}$
3560.264	2	2	28079.785	$21297^{\circ}_{5/2} - 49377_{7/2}$	3535.329	8	2	28277.828	$21682^{\circ}_{7/2} - 49960_{7/2}$

TABLE 3. *Classified lines of* Th II—Continued

Wavelength Å	Intensity		Wavenumber cm^{-1}	Classification	Wavelength Å	Intensity		Wavenumber cm^{-1}	Classification
	Lamp	Spark				Lamp	Spark		
3533.710	50	25	28290.784	$10572^{\circ}_{9/2} - 38862_{11/2}$	3512.351	10	25	28462.818	$17272^{\circ}_{9/2} - 45735_{11/2}$
3532.984	10	100	28296.597	$24381_{7/2} - 52678^{\circ}_{5/2}$	3511.562	400	150	28469.213	$4490^{\circ}_{5/2} - 32959_{3/2}$
3531.928	50	300	28305.057	$18118_{3/2} - 46423^{\circ}_{5/2}$	3511.387	3		28470.632	$16033^{\circ}_{5/2} - 44503_{7/2}$
3531.867	40	4	28305.546	$14790^{\circ}_{7/2} - 43096_{5/2}$	3511.277	20	50	28471.524	$14484^{\circ}_{11/2} - 42955_{9/2}$
3531.645	100	150	28307.325	$18118_{3/2} - 46426^{\circ}_{1/2}$	3510.755	8b		28475.757	$14275^{\circ}_{9/2} - 42751_{7/2}$
3531.049	3		28312.103	$23518^{\circ}_{7/2} - 51830_{7/2}$	3510.535	50	40	28477.542	$10673^{\circ}_{5/2} - 39150_{3/2}$
3530.134	8		28319.441	$15453^{\circ}_{7/2} - 43772_{5/2}$	3509.953	10	25	28482.263	$17771^{\circ}_{11/2} - 46253_{9/2}$
3529.922	2		28321.142	$24414^{\circ}_{3/2} - 52735_{3/2}$	3509.824	5		28483.310	$15324^{\circ}_{1/2} - 43807_{3/2}$
3528.953	300	400	28328.918	$10189^{\circ}_{11/2} - 38517_{13/2}$	3509.189	25	40	28488.464	$16906^{\circ}_{7/2} - 45395_{7/2}$
3528.819	150	40	28329.994	$6691^{\circ}_{3/2} - 35021_{3/2}$	3509.123	10		28489.000	$17121^{\circ}_{3/2} - 45610_{5/2}$
3528.092	8	2	28335.831	$26586^{\circ}_{3/2} - 54922_{3/2}$	3508.819	1		28491.468	$22139^{\circ}_{9/2} - 50631_{11/2}$
3527.361	10		28341.704	$11116^{\circ}_{7/2} - 39458_{7/2}$	3508.687	5	25	28492.540	$23372^{\circ}_{3/2} - 51865_{5/2}$
3526.253	25	75	28350.609	$18973^{\circ}_{7/2} - 47324_{5/2}$	3508.180	20	40	28496.658	$10572^{\circ}_{9/2} - 39068_{7/2}$
3525.868	5h	75	28353.704	$21131^{\circ}_{3/2} - 49485_{1/2}$	3506.903	8		28507.034	$20310^{\circ}_{5/2} - 48817_{3/2}$
3525.629	40h	75	28355.626	$16033^{\circ}_{9/2} - 44388_{5/2}$	3506.852	50	300	28507.449	$15236_{3/2} - 43744^{\circ}_{1/2}$
3525.605	8b		28355.819	$9400_{5/2} - 37756^{\circ}_{7/2}$	3505.493	100	200	28518.500	$13818^{\circ}_{7/2} - 42336_{5/2}$
3525.551	8h	4h	28356.254	$15453^{\circ}_{7/2} - 43809_{9/2}$	3505.384	10	15	28519.387	$12472^{\circ}_{5/2} - 40991_{3/2}$
3525.122	25		28359.704	$9585^{\circ}_{5/2} - 37945_{5/2}$	3505.350	5	10	28519.663	$9585^{\circ}_{5/2} - 38105_{5/2}$
3524.230	3		28366.882	$18214^{\circ}_{5/2} - 46581_{5/2}$	3504.100	2		28529.837	$14484^{\circ}_{11/2} - 43014_{13/2}$
3524.068	2		28368.186	$20989^{\circ}_{9/2} - 49357_{11/2}$	3504.037	25	75	28530.350	$17722^{\circ}_{9/2} - 46253_{9/2}$
3523.615	8	8	28371.833	$20120^{\circ}_{5/2} - 48492_{5/2}$	3503.615	100	200	28533.786	$13818^{\circ}_{7/2} - 42352_{5/2}$
3523.196	10	8	28375.207	$6168^{\circ}_{7/2} - 34543_{5/2}$	3502.778	100b	200	28540.604	$9061_{5/2} - 37601^{\circ}_{5/2}$
3522.569	3		28380.258	$22355^{\circ}_{7/2} - 50735_{3/2}$	3502.701	10	10	28541.232	$10855_{7/2} - 39396^{\circ}_{7/2}$
3522.367	5b		28381.885	$13818^{\circ}_{7/2} - 42200_{9/2}$	3502.648	1		28541.663	$23730^{\circ}_{9/2} - 52272_{7/2}$
3521.912	800	300	28385.552	$10379_{9/2} - 38764^{\circ}_{7/2}$	3501.945	25	25	28547.393	$7331^{\circ}_{5/2} - 35878_{7/2}$
3521.688	4		28387.357	$20989^{\circ}_{9/2} - 49377_{7/2}$	3501.642	15	25	28549.863	$9238^{\circ}_{9/2} - 37787_{7/2}$
3521.514	4		28388.760	$18214^{\circ}_{3/2} - 46603_{5/2}$	3501.455	200	200	28551.388	$10189^{\circ}_{11/2} - 38740_{11/2}$
3520.801	1		28394.509	$22513^{\circ}_{5/2} - 50907_{3/2}$	3500.843	20	100	28556.379	$20288^{\circ}_{11/2} - 48844_{9/2}$
3519.869	1		28402.027	$17983^{\circ}_{5/2} - 46385_{7/2}$	3500.531	40	75	28558.924	$12488^{\circ}_{9/2} - 41047_{9/2}$
3519.741	5		28403.060	$25607^{\circ}_{9/2} - 54010_{7/2}$	3500.267	25	200	28561.078	$15242^{\circ}_{9/2} - 43803_{7/2}$
3519.688	50	200	28403.488	$16818_{7/2} - 45221^{\circ}_{5/2}$	3500.206	10	4	28561.575	$16564^{\circ}_{11/2} - 45126_{9/2}$
3519.482	1		28405.150	$25440^{\circ}_{5/2} - 53845_{5/2}$	3499.986	200	200	28563.371	$8018_{3/2} - 36581^{\circ}_{3/2}$
3518.902	25b		28409.832	$7331^{\circ}_{5/2} - 35741_{5/2}$	3498.989	75b	100b	28571.509	$9720^{\circ}_{7/2} - 38291_{7/2}$
3518.713	4		28411.357	$20080^{\circ}_{7/2} - 48492_{5/2}$	3498.478	1		28575.682	$21297^{\circ}_{5/2} - 49873_{5/2}$
3518.558	4s		28412.609	$17983^{\circ}_{5/2} - 46395_{3/2}$	3498.008	100	75	28579.522	$1521_{5/2} - 30101^{\circ}_{7/2}$
3516.903	15		28425.979	$12902^{\circ}_{3/2} - 41328_{5/2}$	3497.955	15	50	28579.955	$9585^{\circ}_{5/2} - 38165_{7/2}$
3516.823	200	75	28426.626	$8018_{3/2} - 36444^{\circ}_{3/2}$	3497.686	15	200	28582.153	$22642^{\circ}_{9/2} - 51224_{9/2}$
3516.576	50	40	28428.623	$10189^{\circ}_{11/2} - 38617_{9/2}$	3497.460	8	40	28584.000	$11116^{\circ}_{7/2} - 39700_{5/2}$
3516.354	200	300	28430.417	$8378^{\circ}_{7/2} - 36809_{7/2}$	3497.262	50	200	28585.618	$9202^{\circ}_{7/2} - 37787_{7/2}$
3515.849	15	25	28434.501	$12219_{3/2} - 40654^{\circ}_{5/2}$	3497.010	40	200	28587.678	$10855_{7/2} - 39443^{\circ}_{9/2}$
3515.706	75	100	28435.657	$11116^{\circ}_{7/2} - 39552_{9/2}$	3496.762	8	15	28589.705	$15710^{\circ}_{3/2} - 44300_{3/2}$
3515.555	8		28436.879	$14790^{\circ}_{7/2} - 43227_{5/2}$	3495.158	25	4	28602.825	$9238^{\circ}_{9/2} - 37840_{9/2}$
3515.424	10		28437.938	$12485^{\circ}_{7/2} - 40923_{5/2}$	3494.815	25	10	28605.632	$12219_{3/2} - 40825^{\circ}_{1/2}$
3515.224	15		28439.556	$23730^{\circ}_{9/2} - 52170_{11/2}$	3493.518	500	200	28616.252	$7828_{1/2} - 36444^{\circ}_{3/2}$
3514.960	100	100	28441.692	$9238^{\circ}_{9/2} - 37679_{11/2}$	3493.084	8	20	28619.807	$17983^{\circ}_{5/2} - 46603_{5/2}$
3514.526	300b	200	28445.204	$9400_{5/2} - 37846^{\circ}_{5/2}$	3492.898	5	10	28621.331	$19248^{\circ}_{5/2} - 47869_{3/2}$
3513.755	20	75	28451.445	$12472^{\circ}_{5/2} - 40923_{5/2}$	3492.680	8	25	28623.118	$19248^{\circ}_{5/2} - 47871_{7/2}$
3513.299	15	40	28455.138	$22014^{\circ}_{11/2} - 50470_{9/2}$	3492.327	4	5	28626.011	$22642^{\circ}_{9/2} - 51268_{7/2}$
3513.213	50	75	28455.835	$14790^{\circ}_{7/2} - 43246_{7/2}$	3492.117	4	3	28627.732	$15144^{\circ}_{3/2} - 43772_{5/2}$
3512.742	100b	200	28459.650	$9720^{\circ}_{7/2} - 38179_{9/2}$	3491.580	75	100	28632.135	$17272^{\circ}_{9/2} - 45904_{9/2}$

TABLE 3. *Classified lines of* Th II—Continued

Wavelength Å	Intensity		Wavenumber cm^{-1}	Classification	Wavelength Å	Intensity		Wavenumber cm^{-1}	Classification
	Lamp	Spark				Lamp	Spark		
3490.795	1b		28638.574	$9202^{\circ}_{7/2} - 37840_{9/2}$	3473.092	4		28784.545	$17771^{\circ}_{11/2} - 46555_{11/2}$
3490.656	5	4	28639.714	$11576^{\circ}_{3/2} - 40216_{5/2}$	3473.027	150b	100	28785.084	$9061_{5/2} - 37846^{\circ}_{5/2}$
3490.504	8	25	28640.961	$17727_{11/2} - 46368^{\circ}_{9/2}$	3472.842	15	10	28786.618	$9585^{\circ}_{5/2} - 38372_{3/2}$
3490.452	50	100	28641.388	$15324^{\circ}_{1/2} - 43965_{1/2}$	3472.759	3		28787.306	$21682^{\circ}_{7/2} - 50470_{9/2}$
3490.389	2		28641.905	$23012^{\circ}_{3/2} - 51653_{1/2}$	3470.788	4		28803.653	$17460^{\circ}_{5/2} - 46264_{3/2}$
3490.269	20	100	28642.889	$14484^{\circ}_{11/2} - 43127_{11/2}$	3469.919	2000h	800	28810.866	$4146_{7/2} - 32957^{\circ}_{7/2}$
3490.230	8	10	28643.209	$15453^{\circ}_{7/2} - 44096_{9/2}$	3468.966	3	8	28818.781	$19050^{\circ}_{3/2} - 47869_{3/2}$
3489.829	25	20	28646.501	$11576^{\circ}_{3/2} - 40222_{3/2}$	3468.714	25	10	28820.875	$15144^{\circ}_{3/2} - 43965_{1/2}$
3487.884	5		28662.475	$17722^{\circ}_{9/2} - 46385_{7/2}$	3468.219	800	300	28824.988	$6700^{\circ}_{9/2} - 35525_{11/2}$
3487.845	75	100	28662.795	$15144^{\circ}_{3/2} - 43807_{3/2}$	3467.301	3		28832.619	$17722^{\circ}_{9/2} - 46555_{11/2}$
3487.805	1		28663.124	$21297^{\circ}_{5/2} - 49960_{7/2}$	3466.896	20	15	28835.987	$20288^{\circ}_{11/2} - 49124_{11/2}$
3487.700	3		28663.987	$23012^{\circ}_{3/2} - 51676_{3/2}$	3465.924	200	15	28844.074	$4113_{5/2} - 32957^{\circ}_{7/2}$
3487.081	20	75	28669.075	$9720^{\circ}_{7/2} - 38389_{7/2}$	3465.764	1000	200	28845.406	$6700^{\circ}_{9/2} - 35545_{9/2}$
3486.971	40	100	28669.979	$8460_{3/2} - 37130^{\circ}_{1/2}$	3465.471	8	15	28847.844	$20989^{\circ}_{9/2} - 49837_{9/2}$
3486.841	8		28671.048	$16818^{\circ}_{7/2} - 45489_{9/2}$	3465.262	3	10	28849.584	$22513^{\circ}_{3/2} - 51362_{5/2}$
3486.514	500b	200	28673.737	$10189^{\circ}_{11/2} - 38862_{11/2}$	3465.017	50b	75	28851.624	$14275^{\circ}_{9/2} - 43127_{11/2}$
3486.050	3l		28677.554	$13468^{\circ}_{9/2} - 42146_{11/2}$	3464.841	8	20h	28853.090	$23012^{\circ}_{3/2} - 51865_{5/2}$
3485.917	4		28678.648	$17121^{\circ}_{3/2} - 45800_{5/2}$	3464.471	15	8	28856.171	$12472^{\circ}_{3/2} - 41328_{3/2}$
3485.721	5	5	28680.260	$14275^{\circ}_{9/2} - 42955_{9/2}$	3464.409	40	50	28856.687	$16033^{\circ}_{5/2} - 44889_{3/2}$
3485.473	15	50	28682.301	$14545^{\circ}_{5/2} - 43227_{5/2}$	3464.228	2		28858.195	$18816^{\circ}_{13/2} - 47675_{11/2}$
3485.212	100b	150	28684.449	$8378^{\circ}_{7/2} - 37063_{9/2}$	3463.719	500	400	28862.436	$13250_{5/2} - 42112^{\circ}_{3/2}$
3484.414	5	25	28691.018	$20686^{\circ}_{3/2} - 49377_{7/2}$	3463.592	20	8	28863.494	$15786_{5/2} - 44650^{\circ}_{7/2}$
3484.080	100	100	28693.768	$10673^{\circ}_{3/2} - 39366_{5/2}$	3463.424	1		28864.894	$23697^{\circ}_{7/2} - 52562_{7/2}$
3483.589	3		28697.813	$20120^{\circ}_{5/2} - 48817_{3/2}$	3462.850	800	400	28869.678	$9711_{7/2} - 38581^{\circ}_{5/2}$
3483.409	20b	50	28699.295	$14545^{\circ}_{5/2} - 43244_{3/2}$	3460.223	3		28891.596	$17460^{\circ}_{5/2} - 46352_{7/2}$
3483.254	10	25	28700.572	$13818^{\circ}_{7/2} - 42518_{7/2}$	3459.974	5	15	28893.675	$16906^{\circ}_{7/2} - 45800_{5/2}$
3483.169	15	100	28701.273	$14545^{\circ}_{5/2} - 43246_{7/2}$	3459.641	75b	10	28896.456	$10189^{\circ}_{11/2} - 39085_{13/2}$
3483.113	8	5	28701.734	$11576^{\circ}_{3/2} - 40278_{3/2}$	3459.397	5	4	28898.494	$8378^{\circ}_{7/2} - 37277_{7/2}$
3482.834	20	150	28704.033	$16906^{\circ}_{7/2} - 45610_{5/2}$	3458.882	5	8	28902.797	$9202^{\circ}_{7/2} - 38105_{5/2}$
3482.761	100	100	28704.635	$1859_{3/2} - 30564^{\circ}_{1/2}$	3458.724	3		28904.117	$20969^{\circ}_{7/2} - 49873_{5/2}$
3482.547	200	100	28706.399	$9585^{\circ}_{5/2} - 38291_{7/2}$	3457.683	15	8	28912.819	$12485^{\circ}_{7/2} - 41398_{9/2}$
3481.003	20	200	28719.131	$4490^{\circ}_{5/2} - 33209_{7/2}$	3456.928	8	3	28919.133	$17983^{\circ}_{5/2} - 46902_{5/2}$
3480.798	50	4	28720.822	$0_{3/2} - 28720^{\circ}_{3/2}$	3456.253	1		28924.781	$17460^{\circ}_{5/2} - 46385_{7/2}$
3480.750	2		28721.219	$18214^{\circ}_{3/2} - 46935_{3/2}$	3455.951	20	40	28927.308	$9238^{\circ}_{9/2} - 38165_{7/2}$
3480.549	5l	5	28722.877	$17983^{\circ}_{5/2} - 46706_{7/2}$	3455.469	1		28931.343	$18214^{\circ}_{3/2} - 47145_{1/2}$
3480.350	4	4	28724.519	$21682^{\circ}_{7/2} - 50407_{7/2}$	3455.273	20	5	28932.984	$13818^{\circ}_{7/2} - 42751_{7/2}$
3479.912	1		28728.135	$31259_{5/2} - 59987^{\circ}_{3/2}$	3455.131	4b		28934.173	$18214^{\circ}_{3/2} - 47148_{3/2}$
3479.172	500b	200	28734.245	$6691^{\circ}_{3/2} - 35425_{1/2}$	3455.112	4b	20	28934.332	$15242^{\circ}_{9/2} - 44177_{11/2}$
				$7331^{\circ}_{5/2} - 36065_{5/2}$	3455.044	3		28934.902	$23372^{\circ}_{3/2} - 52307_{3/2}$
3478.463	150	150	28740.101	$13406^{\circ}_{13/2} - 42146_{11/2}$	3454.992	8	25b	28935.337	$17460^{\circ}_{5/2} - 46395_{3/2}$
3478.131	150	150	28742.845	$9202^{\circ}_{7/2} - 37945_{5/2}$	3454.946	8	20	28935.723	$15453^{\circ}_{7/2} - 44388_{5/2}$
3477.704	100	150	28746.374	$15349^{\circ}_{11/2} - 44096_{9/2}$	3454.715	50	20	28937.657	$19594_{1/2} - 48532^{\circ}_{1/2}$
3476.902	15	8	28753.004	$7828_{1/2} - 36581^{\circ}_{3/2}$	3454.646	10	15	28938.235	$14349_{1/2} - 43287^{\circ}_{3/2}$
3476.540	150b	100	28755.998	$6700^{\circ}_{9/2} - 35456_{9/2}$	3454.206	200	15	28941.921	$9238^{\circ}_{9/2} - 38179_{9/2}$
3476.332	5	8	28757.719	$18973^{\circ}_{7/2} - 47731_{9/2}$	3453.920	15	5	28944.318	$17272^{\circ}_{9/2} - 46216_{11/2}$
3475.537	25	10	28764.297	$20080^{\circ}_{7/2} - 48844_{9/2}$	3453.559	50b	50	28947.343	$11576^{\circ}_{3/2} - 40523_{1/2}$
3474.270	10	50b	28774.786	$16033^{\circ}_{5/2} - 44807_{7/2}$	3453.404	5		28948.643	$20120^{\circ}_{5/2} - 49068_{5/2}$
3473.780	20	8	28778.845	$11116^{\circ}_{7/2} - 39895_{9/2}$	3452.970	4		28952.281	$17983^{\circ}_{5/2} - 46935_{3/2}$
3473.610	5	3	28780.253	$10572^{\circ}_{9/2} - 39352_{11/2}$	3452.682	400	200	28954.696	$6244_{1/2} - 35198^{\circ}_{1/2}$
3473.422	150	150	28781.811	$9711_{7/2} - 38493^{\circ}_{5/2}$	3450.948	100	15	28969.244	$13250_{5/2} - 42219^{\circ}_{5/2}$

TABLE 3. *Classified lines of* Th II—Continued

Wavelength Å	Intensity		Wavenumber cm^{-1}	Classification	Wavelength Å	Intensity		Wavenumber cm^{-1}	Classification
	Lamp	Spark				Lamp	Spark		
3450.769	1		28970.747	$20989^{\circ}_{9/2} - 49960_{7/2}$	3430.124	20	8	29145.109	$22685^{\circ}_{7/2} - 51830_{7/2}$
3450.710	15	4	28971.242	$14275^{\circ}_{9/2} - 43246_{7/2}$	3429.903	100b	200	29146.987	$4490^{\circ}_{5/2} - 33637_{7/2}$
3450.108	5	10	28976.297	$15324^{\circ}_{1/2} - 44300_{3/2}$	3429.827	5		29147.633	$8460_{3/2} - 37607^{\circ}_{1/2}$
3449.949	200	5	28977.633	$9202^{\circ}_{7/2} - 38179_{9/2}$	3429.433	4		29150.981	$8605_{3/2} - 37756^{\circ}_{7/2}$
3449.566	2b		28980.850	$21682^{\circ}_{7/2} - 50663_{5/2}$	3429.390	75	100	29151.347	$9238^{\circ}_{9/2} - 38389_{7/2}$
3449.543	3b		28981.043	$17272^{\circ}_{9/2} - 46253_{9/2}$	3427.993	25	50	29163.226	$10189^{\circ}_{11/2} - 39352_{11/2}$
3449.493	8	4	28981.463	$14790^{\circ}_{7/2} - 43772_{5/2}$	3427.464	8	40	29167.727	$13250_{5/2} - 42418^{\circ}_{5/2}$
3449.286	50	300	28983.202	$23187^{\circ}_{13/2} - 52170_{11/2}$	3426.988	10	25	29171.778	$9585^{\circ}_{5/2} - 38757_{5/2}$
3448.737	5		28987.816	$27403^{\circ}_{3/2} - 56391_{5/2}$	3426.177	2		29178.683	$6700^{\circ}_{9/2} - 35878_{7/2}$
3448.296	1		28991.523	$20969^{\circ}_{7/2} - 49960_{7/2}$	3426.144	8	75	29178.964	$15710^{\circ}_{3/2} - 44889_{3/2}$
3447.632	8	2	28997.107	$7331^{\circ}_{5/2} - 36328_{3/2}$	3426.058	4	10	29179.697	$22685^{\circ}_{7/2} - 51865_{5/2}$
3446.997	8	4	29002.448	$12485^{\circ}_{7/2} - 41488_{7/2}$	3425.944	100	100	29180.668	$9400_{5/2} - 38581^{\circ}_{5/2}$
3446.288	8	2	29008.415	$9720^{\circ}_{7/2} - 38728_{5/2}$	3425.185	100b	200	29187.134	$9202^{\circ}_{7/2} - 38389_{7/2}$
3445.743	300	200	29013.003	$14790^{\circ}_{7/2} - 43803_{7/2}$	3423.356	5	3	29202.727	$12485^{\circ}_{7/2} - 41688_{7/2}$
3445.389	150l	150	29015.984	$12472^{\circ}_{5/2} - 41488_{7/2}$	3423.129	150	150	29204.664	$12472^{\circ}_{5/2} - 41676_{3/2}$
3445.217	200	100	29017.432	$10379_{9/2} - 39396^{\circ}_{7/2}$	3422.809	3		29207.394	$15242^{\circ}_{9/2} - 44450_{9/2}$
3445.121	8	3	29018.241	$14790^{\circ}_{7/2} - 43809_{9/2}$	3422.576	25		29209.382	$22014^{\circ}_{11/2} - 51224_{9/2}$
3444.028	25	100	29027.450	$10673^{\circ}_{5/2} - 39700_{5/2}$	3422.306	2		29211.687	$24309^{\circ}_{11/2} - 53520_{9/2}$
3443.139	50b	20b	29034.944	$15786_{3/2} - 44821^{\circ}_{5/2}$	3422.245	1		29212.207	$19912^{\circ}_{13/2} - 49124_{11/2}$
3443.110	40b	75b	29035.189	$9400_{5/2} - 38436^{\circ}_{5/2}$	3421.770	3		29216.262	$12472^{\circ}_{3/2} - 41688_{7/2}$
3441.365	200	25	29049.911	$6691^{\circ}_{3/2} - 35741_{5/2}$	3419.173	500	300	29238.453	$13406^{\circ}_{13/2} - 42644_{13/2}$
3441.036	100	20	29052.688	$9711_{7/2} - 38764^{\circ}_{7/2}$	3418.952	150b	40b	29240.342	$8605_{5/2} - 37846^{\circ}_{5/2}$
3440.909	10	20	29053.761	$9238^{\circ}_{9/2} - 38291_{7/2}$	3418.914	100b	40b	29240.667	$4490^{\circ}_{5/2} - 33730_{5/2}$
				$25440^{\circ}_{5/2} - 54493_{5/2}$	3418.776	200	300	29241.848	$19880_{9/2} - 49121^{\circ}_{7/2}$
3439.711	500b	400	29063.879	$10379_{9/2} - 39443^{\circ}_{9/2}$	3418.523	4		29244.012	$15144^{\circ}_{3/2} - 44388_{3/2}$
3439.232	10	5	29067.927	$11576^{\circ}_{3/2} - 40644_{5/2}$	3418.333	3		29245.637	$17460^{\circ}_{5/2} - 46706_{7/2}$
3439.056	10	4	29069.415	$20288^{\circ}_{11/2} - 49357_{11/2}$	3417.794	1		29250.249	$22685^{\circ}_{7/2} - 51935_{5/2}$
3438.951	500	300	29070.302	$13248_{9/2} - 42319^{\circ}_{9/2}$	3417.724	50	75	29250.848	$11116^{\circ}_{7/2} - 40367_{9/2}$
3438.689	4	10	29072.517	$19248^{\circ}_{5/2} - 48320_{5/2}$	3417.126	15	15	29255.967	$8460_{3/2} - 37716^{\circ}_{1/2}$
3437.808	8	20	29079.967	$17272^{\circ}_{9/2} - 46352_{7/2}$	3417.001	1		29257.037	$20120^{\circ}_{5/2} - 49377_{7/2}$
3437.024	100	150b	29086.600	$8378^{\circ}_{7/2} - 37465_{5/2}$	3416.551	1		29260.891	$15242^{\circ}_{9/2} - 44503_{7/2}$
3436.679	75b	100b	29089.520	$9202^{\circ}_{7/2} - 38291_{7/2}$	3416.421	40b	50	29262.004	$14545^{\circ}_{5/2} - 43807_{3/2}$
3436.288	3	2	29092.830	$9400_{5/2} - 38493^{\circ}_{5/2}$	3415.487	3b		29270.006	$19050^{\circ}_{3/2} - 48320_{5/2}$
3435.975	800b	200	29095.480	$0_{3/2} - 29095^{\circ}_{3/2}$					$26965^{\circ}_{3/2} - 56235_{3/2}$
3435.695	3l	5	29097.851	$17837^{\circ}_{1/2} - 46935_{3/2}$	3414.979	3		29274.360	$17121^{\circ}_{3/2} - 46395_{3/2}$
3435.193	15	10	29102.103	$4113_{3/2} - 33215^{\circ}_{3/2}$	3414.503	100	200	29278.441	$9585^{\circ}_{5/2} - 38863_{5/2}$
3435.004	2		29103.705	$20310^{\circ}_{5/2} - 49414_{3/2}$	3413.634	3b		29285.894	$30101^{\circ}_{7/2} - 59387_{7/2}$
3434.759	100b	40	29105.780	$12902^{\circ}_{3/2} - 42008_{1/2}$	3413.408	100	75	29287.833	$6168^{\circ}_{7/2} - 35456_{9/2}$
3434.266	4	8	29109.959	$18214^{\circ}_{3/2} - 47324_{5/2}$	3412.632	4		29294.492	$20120^{\circ}_{5/2} - 49414_{3/2}$
3433.999	1000h	300	29112.222	$1859_{3/2} - 30972^{\circ}_{5/2}$	3412.521	3		29295.445	$23012^{\circ}_{3/2} - 52307_{3/2}$
3433.946	40	15	29112.671	$22834_{7/2} - 51946^{\circ}_{5/2}$	3412.399	25	4	29296.493	$20080^{\circ}_{7/2} - 49377_{7/2}$
3433.890	15	100	29113.146	$17272^{\circ}_{9/2} - 46385_{7/2}$	3411.785	200b	100	29301.765	$7828_{1/2} - 37130^{\circ}_{1/2}$
3432.085	5	40	29128.457	$22139^{\circ}_{9/2} - 51268_{7/2}$	3411.312	2	5	29305.827	$25188^{\circ}_{3/2} - 54493_{3/2}$
3431.811	50	200	29130.782	$20158^{\circ}_{5/2} - 49289^{\circ}_{5/2}$	3411.061	3		29307.984	$17837^{\circ}_{1/2} - 47145_{1/2}$
3431.019	15	75	29137.506	$13818^{\circ}_{7/2} - 42955_{9/2}$	3409.986	3		29317.223	$22513^{\circ}_{5/2} - 51830_{7/2}$
3430.761	5	2	29139.698	$17771^{\circ}_{11/2} - 46910_{13/2}$	3409.562	3		29320.868	$22355^{\circ}_{1/2} - 51676_{3/2}$
3430.567	15	75	29141.345	$8460_{3/2} - 37601^{\circ}_{5/2}$	3409.270	400	200	29323.380	$10572^{\circ}_{9/2} - 39895_{9/2}$
3430.419	8	75	29142.603	$17460^{\circ}_{5/2} - 46603_{3/2}$	3409.112	3b		29324.739	$18973^{\circ}_{7/2} - 48298_{7/2}$
				$17121^{\circ}_{3/2} - 46264_{3/2}$	3408.644	200	150	29328.765	$10855_{7/2} - 40184^{\circ}_{7/2}$
3430.339	8b	15	29143.282	$9585^{\circ}_{5/2} - 38728_{5/2}$	3407.631	40	200	29337.483	$16818_{7/2} - 46155^{\circ}_{5/2}$

530-326 OL - 74 - 9

TABLE 3. *Classified lines of* Th II—Continued

Wavelength Å	Intensity		Wavenumber cm^{-1}	Classification	Wavelength Å	Intensity		Wavenumber cm^{-1}	Classification
	Lamp	Spark				Lamp	Spark		
3407.221	3s		29341.013	$17983^{\circ}_{5/2} - 47324_{5/2}$	3387.532	2		29511.544	$24982^{\circ}_{7/2} - 54493_{5/2}$
3406.730	3		29345.242	$15305_{9/2} - 44650^{\circ}_{7/2}$	3386.763	10	75	29518.244	$18973^{\circ}_{7/2} - 48492_{5/2}$
3406.365	8	8	29348.386	$9720^{\circ}_{7/2} - 39068_{7/2}$	3386.500	500	300	29520.537	$9061_{5/2} - 38581^{\circ}_{5/2}$
3406.242	150	100	29349.446	$6691^{\circ}_{3/2} - 36040_{1/2}$	3385.825	8	15	29526.422	$9202^{\circ}_{7/2} - 38728_{5/2}$
3405.607	50		29354.918	$15453^{\circ}_{7/2} - 44807_{7/2}$	3385.596	8	2	29528.419	$14275^{\circ}_{9/2} - 43803_{7/2}$
3404.798	8	15	29361.893	$16033^{\circ}_{5/2} - 45395_{7/2}$	3385.531	800	200	29528.986	$4490^{\circ}_{5/2} - 34019_{3/2}$
3404.651	200	100	29363.161	$10189^{\circ}_{11/2} - 39552_{9/2}$	3385.206	2		29531.821	$21131^{\circ}_{3/2} - 50663_{5/2}$
				$23372^{\circ}_{3/2} - 52735_{3/2}$	3384.991	100	100	29533.696	$14275^{\circ}_{9/2} - 43809_{9/2}$
3404.592	40	40	29363.669	$9400_{5/2} - 38764^{\circ}_{7/2}$	3384.095	2		29541.516	$21682^{\circ}_{7/2} - 51224_{9/2}$
3404.198	4		29367.068	$10572^{\circ}_{9/2} - 39939_{11/2}$	3384.001	8	40	29542.336	$22139^{\circ}_{9/2} - 51681_{9/2}$
3403.353	100	25	29374.359	$6691^{\circ}_{3/2} - 36065_{5/2}$	3383.149	25b	25b	29549.776	$10673^{\circ}_{5/2} - 40222_{3/2}$
3403.271	200	200b	29375.067	$9061_{5/2} - 38436^{\circ}_{3/2}$	3383.107	100b	200	29550.143	$16818_{7/2} - 46368^{\circ}_{9/2}$
3403.006	15	40	29377.354	$15349^{\circ}_{11/2} - 44727_{11/2}$	3381.374	50b	40b	29565.287	$9585^{\circ}_{5/2} - 39150_{3/2}$
3402.698	800b	400b	29380.013	$6213_{9/2} - 35593^{\circ}_{7/2}$	3381.343	50b	50b	29565.558	$15324^{\circ}_{1/2} - 44889_{3/2}$
3402.027	200	200	29385.808	$8460_{3/2} - 37846^{\circ}_{5/2}$	3380.500	3	2	29572.931	$6168^{\circ}_{7/2} - 35741_{5/2}$
3401.647	150	150	29389.090	$7001_{3/2} - 36390^{\circ}_{3/2}$	3379.981	8	15	29577.472	$16033^{\circ}_{5/2} - 45610_{5/2}$
3400.998	10	15	29394.699	$14349_{1/2} - 43744^{\circ}_{1/2}$	3379.292	8		29583.502	$8018_{3/2} - 37601^{\circ}_{3/2}$
3400.350	8		29400.300	$17771^{\circ}_{11/2} - 47171_{9/2}$	3379.090	15	50	29585.270	$15236_{3/2} - 44821^{\circ}_{5/2}$
3399.466	5	2	29407.945	$15144^{\circ}_{3/2} - 44552_{5/2}$	3378.905	4		29586.890	$22685^{\circ}_{7/2} - 52272_{7/2}$
3399.344	25b	75b	29409.001	$8378^{\circ}_{7/2} - 37787_{7/2}$	3378.803	5	3	29587.783	$27357^{\circ}_{9/2} - 56945_{11/2}$
3399.284	20	40	29409.520	$13818^{\circ}_{7/2} - 43227_{5/2}$	3378.573	500	300	29589.797	$8018_{3/2} - 37607^{\circ}_{1/2}$
3397.953	15	25	29421.039	$12488^{\circ}_{9/2} - 41909_{9/2}$	3377.943	2b		29595.316	$15710^{\circ}_{3/2} - 45306_{3/2}$
3397.844	20	150	29421.983	$22106_{5/2} - 51528^{\circ}_{3/2}$	3377.661	10b	15	29597.786	$14790^{\circ}_{7/2} - 44388_{5/2}$
3397.255	3		29427.084	$26963^{\circ}_{7/2} - 56391_{5/2}$	3377.538	3		29598.864	$29788^{\circ}_{9/2} - 59387_{7/2}$
3397.092	15b	40	29428.496	$13818^{\circ}_{7/2} - 43246_{7/2}$	3376.840	75	50	29604.982	$10673^{\circ}_{5/2} - 40278_{3/2}$
3396.874	2		29430.384	$25414^{\circ}_{11/2} - 54845_{9/2}$	3376.529	4	5	29607.709	$13406^{\circ}_{13/2} - 43014_{13/2}$
3396.612	100	100	29432.654	$9061_{5/2} - 38493^{\circ}_{5/2}$	3376.411	2		29608.744	$26626^{\circ}_{1/2} - 56235_{3/2}$
3396.456	50	100	29434.006	$17272^{\circ}_{9/2} - 46706_{7/2}$	3376.049	3	3	29611.918	$14484^{\circ}_{11/2} - 44096_{9/2}$
3396.394	50	100	29434.543	$15786_{5/2} - 45221^{\circ}_{5/2}$	3374.582	300	300	29624.791	$9238^{\circ}_{9/2} - 38862_{11/2}$
3395.966	8b		29438.253	$20969^{\circ}_{7/2} - 50407_{7/2}$	3373.964	2		29630.217	$22642^{\circ}_{9/2} - 52272_{7/2}$
3395.628	8	50	29441.183	$19050^{\circ}_{3/2} - 48492_{5/2}$	3373.165	2		29637.235	$6691^{\circ}_{3/2} - 36328_{3/2}$
3395.573	3		29441.660	$19248^{\circ}_{5/2} - 48689_{3/2}$	3372.955	8	20	29639.081	$19050^{\circ}_{3/2} - 48689_{3/2}$
3395.545	2		29441.903	$17460^{\circ}_{5/2} - 46902_{5/2}$	3372.702	50	100	29641.304	$20989^{\circ}_{9/2} - 50631_{11/2}$
3395.372	100	150	29443.403	$7001_{3/2} - 36444^{\circ}_{3/2}$	3372.334	10	15	29644.538	$15144^{\circ}_{3/2} - 44789_{1/2}$
3395.112	20	100	29445.658	$19912^{\circ}_{13/2} - 49357_{11/2}$	3372.097	1		29646.622	$9720^{\circ}_{7/2} - 39366_{5/2}$
3394.797	150	200	29448.390	$17722^{\circ}_{9/2} - 47171_{9/2}$	3371.795	500b	300	29649.277	$12570_{7/2} - 42219^{\circ}_{5/2}$
3394.640	8	10	29449.752	$12902^{\circ}_{3/2} - 42352_{5/2}$	3371.492	10	50	29651.941	$16564^{\circ}_{11/2} - 46216_{11/2}$
3394.583	15	3	29450.246	$1521_{5/2} - 30972^{\circ}_{5/2}$	3371.123	2		29655.187	$18214^{\circ}_{3/2} - 47869_{3/2}$
3394.145	150	200	29454.047	$11116^{\circ}_{7/2} - 40570_{7/2}$	3371.043	1		29655.891	$15242^{\circ}_{9/2} - 44898_{7/2}$
3393.500	5	3	29459.645	$17121^{\circ}_{3/2} - 46581_{5/2}$	3370.656	2		29659.296	$14790^{\circ}_{7/2} - 44450_{9/2}$
3393.230	50	100	29461.989	$8378^{\circ}_{7/2} - 37840_{9/2}$	3370.397	10		29661.575	$9202^{\circ}_{7/2} - 38863_{5/2}$
3392.958	150b	50b	29464.350	$12472^{\circ}_{5/2} - 41936_{3/2}$	3369.077	8		29673.196	$15453^{\circ}_{7/2} - 45126_{9/2}$
3392.878	3		29465.045	$15324^{\circ}_{1/2} - 44789_{1/2}$	3368.908	5	10	29674.684	$16906^{\circ}_{7/2} - 46581_{5/2}$
3392.035	1000d	1000	29472.368	$1521_{5/2} - 30994^{\circ}_{7/2}$	3367.819	500b	150b	29684.279	$4490^{\circ}_{5/2} - 34174_{5/2}$
3391.296	5	8	29478.790	$15710^{\circ}_{3/2} - 45189_{3/2}$	3367.784	100b	50b	29684.588	$9711_{7/2} - 39396^{\circ}_{7/2}$
3391.131	2		29480.224	$20989^{\circ}_{9/2} - 50470_{9/2}$	3367.399	8	5	29687.982	$17460^{\circ}_{5/2} - 47148_{3/2}$
3390.780	25	50	29483.276	$9585^{\circ}_{5/2} - 39068_{7/2}$	3367.318	5		29688.696	$16564^{\circ}_{11/2} - 46253_{9/2}$
3389.640	500	300	29493.191	$1859_{3/2} - 31353^{\circ}_{3/2}$	3367.073	2h	12	29690.856	$22139^{\circ}_{9/2} - 51830_{7/2}$
3388.578	100	75	29502.434	$9238^{\circ}_{9/2} - 38740_{11/2}$	3366.721	40	100	29693.960	$13250_{5/2} - 42944^{\circ}_{7/2}$
3387.834	4		29508.913	$30484_{11/2} - 59993^{\circ}_{9/2}$	3366.649	8	200	29694.595	$20969^{\circ}_{7/2} - 50663_{5/2}$

TABLE 3. *Classified lines of* Th II—Continued

Wavelength Å	Intensity		Wavenumber cm^{-1}	Classification
	Lamp	Spark		
3366.517	200	200	29695.759	$13248^{\circ}_{9/2} - 42944^{\circ}_{7/2}$
3366.423	10	20	29696.588	$16906^{\circ}_{7/2} - 46603_{5/2}$
3365.633	15	15	29703.559	$9061_{5/2} - 38764^{\circ}_{7/2}$
3365.318	25b		29706.339	$10189^{\circ}_{11/2} - 39895_{9/2}$
3364.846	15	15	29710.506	$6168^{\circ}_{7/2} - 35878_{7/2}$
3364.685	75b	200b	29711.928	$12488^{\circ}_{9/2} - 42200_{9/2}$
3364.587	20	75	29712.793	$14790^{\circ}_{7/2} - 44503_{7/2}$
3364.388	15	25	29714.550	$12485^{\circ}_{7/2} - 42200_{9/2}$
3363.733	50	10	29720.336	$0_{3/2} - 29720^{\circ}_{3/2}$
3363.682	200	100	29720.787	$13406^{\circ}_{13/2} - 43127_{11/2}$
3363.066	100	100	29726.231	$8378^{\circ}_{7/2} - 38105_{5/2}$
3362.674	100	50	29729.696	$4113_{5/2} - 33843^{\circ}_{3/2}$
3362.521	50b	100	29731.049	$9711_{7/2} - 39443^{\circ}_{9/2}$
3362.427	15b	5	29731.880	$23187^{\circ}_{13/2} - 52918_{13/2}$
3362.184	75	200	29734.029	$12488^{\circ}_{9/2} - 42222_{7/2}$
3361.890	10	40	29736.628	$15453^{\circ}_{7/2} - 45189_{5/2}$
				$12485^{\circ}_{7/2} - 42222_{7/2}$
3361.734	150	150	29738.008	$9720^{\circ}_{7/2} - 39458_{7/2}$
3361.617	100	200	29739.043	$17727_{11/2} - 47466^{\circ}_{11/2}$
3360.937	3b		29745.060	$15144^{\circ}_{3/2} - 44889_{3/2}$
3360.371	150	100	29750.070	$10189^{\circ}_{11/2} - 39939_{11/2}$
3360.156	100	50	29751.974	$11576^{\circ}_{3/2} - 41328_{5/2}$
3360.043	3		29752.974	$20120^{\circ}_{5/2} - 49873_{5/2}$
3359.755	20	40	29755.524	$4146_{7/2} - 33902^{\circ}_{7/2}$
3359.059	15	25	29761.690	$14790^{\circ}_{7/2} - 44552_{5/2}$
3358.602	500	300	29765.739	$1859_{3/2} - 31625^{\circ}_{5/2}$
3358.446	10	15	29767.122	$16033^{\circ}_{5/2} - 45800_{5/2}$
				$19050^{\circ}_{3/2} - 48817_{3/2}$
3357.765	8	10	29773.159	$7828_{1/2} - 37601^{\circ}_{3/2}$
3357.403	15	40	29776.369	$15349^{\circ}_{11/2} - 45126_{9/2}$
3357.233	50b	50	29777.877	$13468^{\circ}_{9/2} - 43246_{7/2}$
3357.056	25	40	29779.447	$7828_{1/2} - 37607^{\circ}_{1/2}$
3356.888	10	40	29780.937	$17121^{\circ}_{3/2} - 46902_{3/2}$
3356.821	75	75	29781.531	$9585^{\circ}_{5/2} - 39366_{5/2}$
3356.262	8		29786.491	$8378^{\circ}_{7/2} - 38165_{7/2}$
3356.005	4		29788.772	$4113_{5/2} - 33902^{\circ}_{7/2}$
3355.970	10	10	29789.083	$4490^{\circ}_{3/2} - 34279_{7/2}$
3355.567	50	200	29792.661	$25246_{9/2} - 55038^{\circ}_{9/2}$
3355.256	100	100	29795.422	$10572^{\circ}_{9/2} - 40367_{9/2}$
3354.836	5	5	29799.152	$10855_{7/2} - 40654^{\circ}_{5/2}$
3354.780	8	10	29799.649	$16906^{\circ}_{7/2} - 46706_{7/2}$
3354.616	150	100	29801.106	$8378^{\circ}_{7/2} - 38179_{9/2}$
3354.180	500	200	29804.980	$10379_{9/2} - 40184^{\circ}_{7/2}$
3353.948	100	100	29807.041	$11116^{\circ}_{7/2} - 40923_{5/2}$
3353.160	4b		29814.046	$17121^{\circ}_{3/2} - 46935_{3/2}$
3353.141	25b	50b	29814.215	$16564^{\circ}_{11/2} - 46378_{13/2}$
3352.415	5	2	29820.671	$14275^{\circ}_{9/2} - 44096_{9/2}$
3351.594	20s	25	29827.976	$8018_{3/2} - 37846^{\circ}_{5/2}$
3351.288	50	25	29830.699	$9238^{\circ}_{9/2} - 39068_{7/2}$
3351.228	800b	200b	29831.233	$1521_{5/2} - 31353^{\circ}_{3/2}$
3351.150	50b	50b	29831.928	$9720^{\circ}_{7/2} - 39552_{9/2}$
3350.308	5	4	29839.425	$10572^{\circ}_{9/2} - 40411_{7/2}$
3350.202	5h	4	29840.369	$22106_{5/2} - 51946^{\circ}_{5/2}$
3349.883	10	8	29843.210	$14545^{\circ}_{5/2} - 44388_{5/2}$
3348.992	5b		29851.150	$12485^{\circ}_{7/2} - 42336_{5/2}$
3348.953	100	400	29851.497	$10855_{7/2} - 40706^{\circ}_{7/2}$
3347.678	2		29862.866	$24982^{\circ}_{7/2} - 54845_{9/2}$
3347.576	15	15	29863.776	$17460^{\circ}_{5/2} - 47324_{5/2}$
3347.478	3		29864.651	$12472^{\circ}_{5/2} - 42336_{5/2}$
3346.746	8	10	29871.182	$18973^{\circ}_{7/2} - 48844_{9/2}$
3346.555	150	150	29872.887	$9585^{\circ}_{5/2} - 39458_{7/2}$
3345.384	5	8	29883.343	$15242^{\circ}_{9/2} - 45126_{9/2}$
3345.060	5h	8	29886.238	$17983^{\circ}_{5/2} - 47869_{3/2}$
3344.872	50b	50	29887.917	$8605_{5/2} - 38493^{\circ}_{5/2}$
3344.670	1	3	29889.722	$25607^{\circ}_{9/2} - 55496_{9/2}$
3343.813	75s	20	29897.383	$6168^{\circ}_{7/2} - 36065_{5/2}$
3343.617	100	150	29899.135	$17272^{\circ}_{9/2} - 47171_{9/2}$
3343.545	3	5b	29899.779	$15710^{\circ}_{3/2} - 45610_{5/2}$
3343.258	25b	50b	29902.346	$15786_{3/2} - 45689^{\circ}_{7/2}$
3342.069	200	10	29912.984	$8378^{\circ}_{7/2} - 38291_{7/2}$
3340.097	2		29930.644	$11116^{\circ}_{7/2} - 41047_{9/2}$
3338.828	10	40	29942.019	$15453^{\circ}_{7/2} - 45395_{7/2}$
3338.396	150	200	29945.894	$7331^{\circ}_{5/2} - 37277_{7/2}$
3337.870	800	150	29950.613	$1859_{3/2} - 31810^{\circ}_{5/2}$
3337.780	10	10	29951.420	$11725^{\circ}_{1/2} - 41676_{3/2}$
3337.684	2b		29952.282	$22355^{\circ}_{1/2} - 52307_{3/2}$
3337.478	5	50	29954.130	$13818^{\circ}_{7/2} - 43772_{5/2}$
3337.159	50	20	29956.994	$6168^{\circ}_{7/2} - 36125_{9/2}$
3337.019	1		29958.250	$14545^{\circ}_{5/2} - 44503_{7/2}$
3336.775	8	25	29960.441	$17771^{\circ}_{11/2} - 47731_{9/2}$
3336.161	50	40	29965.955	$14484^{\circ}_{11/2} - 44450_{9/2}$
3335.576	2	2	29971.210	$10673^{\circ}_{5/2} - 40644_{5/2}$
3335.064	100b	100	29975.811	$8460_{3/2} - 38436^{\circ}_{5/2}$
				$8605_{5/2} - 38581^{\circ}_{5/2}$
3334.879	4	20	29977.474	$20686^{\circ}_{5/2} - 50663_{5/2}$
3334.603	600l	300	29979.955	$6213_{9/2} - 36193^{\circ}_{9/2}$
3334.053	10	25	29984.900	$15236_{3/2} - 45221^{\circ}_{3/2}$
3333.969	8	10	29985.656	$13818^{\circ}_{7/2} - 43803_{7/2}$
3333.383	15	15	29990.927	$13818^{\circ}_{7/2} - 43809_{9/2}$
3332.532	5	3b	29998.585	$10572^{\circ}_{9/2} - 40570_{7/2}$
3332.460	3b	8	29999.234	$21682^{\circ}_{7/2} - 51681_{9/2}$
3332.399	75	50	29999.783	$12219_{3/2} - 42219^{\circ}_{5/2}$
3332.074	20	5	30002.709	$10572^{\circ}_{9/2} - 40574_{11/2}$
3331.429	2	1	30008.517	$17722^{\circ}_{9/2} - 47731_{9/2}$
3331.207	15	15	30010.517	$8378^{\circ}_{7/2} - 38389_{7/2}$
3330.379	0	2	30017.978	$19050^{\circ}_{3/2} - 49068_{3/2}$
3329.380	3	15	30026.985	$17121^{\circ}_{3/2} - 47148_{3/2}$
3328.976	20	20	30030.629	$12488^{\circ}_{9/2} - 42518_{7/2}$
3328.845	2	3	30031.811	$17837^{\circ}_{1/2} - 47869_{3/2}$
3328.688	1b		30033.227	$12485^{\circ}_{7/2} - 42518_{7/2}$

TABLE 3. *Classified lines of* Th II—Continued

Wavelength Å	Intensity		Wavenumber cm^{-1}	Classification	Wavelength Å	Intensity		Wavenumber cm^{-1}	Classification
	Lamp	Spark				Lamp	Spark		
3328.668	5	8	30033.407	$8460_{3/2} - 38493^{\circ}_{5/2}$	3303.481	100	100	30262.386	$14545^{\circ}_{5/2} - 44807_{7/2}$
3328.255	100	75	30037.134	$13250_{5/2} - 43287^{\circ}_{3/2}$	3303.410	5	5	30263.036	$12488^{\circ}_{9/2} - 42751_{7/2}$
3327.392	4	5	30044.924	$15144^{\circ}_{3/2} - 45189_{5/2}$	3303.126	3	4	30265.638	$12485^{\circ}_{7/2} - 42751_{7/2}$
3327.041	2		30048.094	$24873^{\circ}_{5/2} - 54922_{3/2}$	3301.823	2		30277.582	$18214^{\circ}_{3/2} - 48492_{5/2}$
3326.913	5	15	30049.250	$22513^{\circ}_{5/2} - 52562_{7/2}$	3301.785	10	50	30277.930	$13818^{\circ}_{7/2} - 44096_{9/2}$
3326.670	1	5	30051.445	$15786_{3/2} - 45838^{\circ}_{3/2}$	3301.743	15	20	30278.315	$1521_{5/2} - 31800^{\circ}_{7/2}$
3326.465	150	40	30053.297	$4490^{\circ}_{5/2} - 34543_{5/2}$					$20989^{\circ}_{9/2} - 51268_{7/2}$
3325.120	1000	500	30065.453	$4146_{7/2} - 34212^{\circ}_{5/2}$	3301.651	1500r	150	30279.159	$12472^{\circ}_{5/2} - 42751_{7/2}$
3324.752	800	400	30068.780	$1859_{3/2} - 31928^{\circ}_{3/2}$	3301.349	300	300	30281.929	$11116^{\circ}_{7/2} - 41398_{9/2}$
3323.583	2	5	30079.356	$24414^{\circ}_{3/2} - 54493_{5/2}$	3301.264	100	100	30282.708	$11725^{\circ}_{1/2} - 42008_{1/2}$
3322.470	10	15	30089.432	$15710^{\circ}_{3/2} - 45800_{5/2}$	3300.616	100b	5b	30288.653	$1521_{5/2} - 31810^{\circ}_{5/2}$
3321.707	4	5	30096.344	$20310^{\circ}_{5/2} - 50407_{7/2}$	3299.707	2		30296.997	$16564^{\circ}_{11/2} - 46861_{11/2}$
3321.451	800	800	30098.663	$4113_{5/2} - 34212^{\circ}_{5/2}$	3299.670	50	200	30297.337	$26647^{\circ}_{13/2} - 56945_{11/2}$
3321.254	10	15	30100.448	$11576^{\circ}_{3/2} - 41676_{3/2}$	3299.478	1		30299.100	$20969^{\circ}_{7/2} - 51268_{7/2}$
3320.301	600	500	30109.088	$6700^{\circ}_{9/2} - 36809_{7/2}$	3298.542	1		30307.697	$18816^{\circ}_{13/2} - 49124_{11/2}$
3319.629	25	100	30115.183	$9585^{\circ}_{5/2} - 39700_{5/2}$	3298.019	8	10	30312.503	$23697^{\circ}_{7/2} - 54010_{7/2}$
3318.984	75	200	30121.035	$6691^{\circ}_{3/2} - 36812_{1/2}$	3297.833	200	500	30314.213	$9238^{\circ}_{9/2} - 39552_{9/2}$
3318.958	50	50	30121.271	$8460_{3/2} - 38581^{\circ}_{5/2}$	3297.735	3h	3	30315.114	$17983^{\circ}_{5/2} - 48298_{7/2}$
3318.915	4	10b	30121.661	$18568^{\circ}_{7/2} - 48689_{3/2}$	3297.374	150	300	30318.432	$10673^{\circ}_{3/2} - 40991_{3/2}$
3318.118	5h	8	30128.896	$19248^{\circ}_{5/2} - 49377_{7/2}$	3297.305	5	8	30319.067	$16033^{\circ}_{5/2} - 46352_{7/2}$
3318.018	2l	1	30129.804	$26762_{3/2} - 56892^{\circ}_{5/2}$	3296.607	150	200	30325.486	$12902^{\circ}_{3/2} - 43227_{5/2}$
3317.746	75	200	30132.274	$13250_{5/2} - 43382^{\circ}_{5/2}$	3296.485	5	10	30326.609	$20080^{\circ}_{7/2} - 50407_{7/2}$
3317.560	50	100	30133.963	$7331^{\circ}_{5/2} - 37465_{5/2}$	3296.445	4	8	30326.976	$23518^{\circ}_{7/2} - 53845_{5/2}$
3316.215	100	40	30146.185	$6244_{1/2} - 36390^{\circ}_{3/2}$	3295.571	10b	20	30335.019	$13468^{\circ}_{9/2} - 43803_{7/2}$
3316.042	3	5	30147.757	$23697^{\circ}_{7/2} - 53845_{5/2}$	3295.523	75l	100l	30335.461	$9061_{5/2} - 39396^{\circ}_{7/2}$
3315.971	4	10	30148.403	$17722^{\circ}_{9/2} - 47871_{7/2}$	3295.325	200b	500	30337.283	$6244_{1/2} - 36581^{\circ}_{3/2}$
3315.832	25	20	30149.667	$9711_{7/2} - 39861^{\circ}_{5/2}$	3294.998	100	300	30340.294	$13468^{\circ}_{9/2} - 43809_{9/2}$
3315.560	10	50	30152.140	$15242^{\circ}_{9/2} - 45395_{7/2}$	3294.753	40	100	30342.550	$20288^{\circ}_{11/2} - 50631_{11/2}$
3315.210	5	10	30155.323	$22014^{\circ}_{11/2} - 52170_{11/2}$	3294.568	75	50	30344.254	$14545^{\circ}_{5/2} - 44889_{3/2}$
3314.827	300b	300	30158.807	$8605_{5/2} - 38764^{\circ}_{7/2}$	3294.362	4	8	30346.151	$16564^{\circ}_{11/2} - 46910_{13/2}$
3314.541	3		30161.410	$15144^{\circ}_{3/2} - 45306_{3/2}$	3294.244	100	200	30347.238	$15453^{\circ}_{7/2} - 45800_{5/2}$
3314.187	2h	1	30164.631	$9202^{\circ}_{7/2} - 39366_{5/2}$	3293.948	500	500	30349.965	$9202^{\circ}_{7/2} - 39552_{9/2}$
3313.996	10h	50	30166.369	$19248^{\circ}_{5/2} - 49414_{3/2}$	3293.698	100	200	30352.269	$16033^{\circ}_{5/2} - 46385_{7/2}$
3313.036	8	5b	30175.110	$9720^{\circ}_{7/2} - 39895_{9/2}$	3293.654	3		30352.674	$20310^{\circ}_{5/2} - 50663_{5/2}$
3312.680	20	15	30178.353	$10189^{\circ}_{11/2} - 40367_{9/2}$	3293.595	100	300	30353.218	$14545^{\circ}_{5/2} - 44898_{7/2}$
3312.076	20	150	30183.856	$15305_{9/2} - 45489^{\circ}_{9/2}$	3292.844	5	4	30360.140	$11576^{\circ}_{5/2} - 41936_{3/2}$
3310.946	5	8	30194.157	$12902^{\circ}_{3/2} - 43096_{5/2}$	3292.551	50b	5w	30362.842	$16033^{\circ}_{5/2} - 46395_{3/2}$
3310.497	75	100	30198.252	$12219_{3/2} - 42418^{\circ}_{3/2}$	3292.520	1000b	1000b	30363.128	$6700^{\circ}_{9/2} - 37063_{9/2}$
3310.249	150b	200	30200.515	$6244_{1/2} - 36444^{\circ}_{3/2}$	3291.932	15	40	30368.551	$15786_{5/2} - 46155^{\circ}_{5/2}$
3310.001	4	8	30202.777	$17121^{\circ}_{3/2} - 47324_{3/2}$	3291.739	1000	800	30370.331	$6213_{9/2} - 36583^{\circ}_{7/2}$
3309.135	150	200	30210.681	$7331^{\circ}_{5/2} - 37542_{3/2}$	3291.606	50	15	30371.559	$11116^{\circ}_{7/2} - 41488_{7/2}$
3309.016	8	15	30211.768	$11116^{\circ}_{7/2} - 41328_{5/2}$	3291.343	8	100	30373.986	$12570_{7/2} - 42944^{\circ}_{7/2}$
3308.085	10b	40	30220.270	$9238^{\circ}_{9/2} - 39458_{7/2}$	3290.633	2		30380.539	$22355^{\circ}_{1/2} - 52735_{3/2}$
3307.215	3h	8	30228.219	$14275^{\circ}_{9/2} - 44503_{7/2}$	3290.250	15	15	30384.075	$15305_{9/2} - 45689^{\circ}_{7/2}$
3306.389	1b	40	30235.771	$17771^{\circ}_{11/2} - 48006_{9/2}$	3290.126	150	40	30385.220	$15349^{\circ}_{11/2} - 45735_{11/2}$
3306.054	10	20	30238.835	$8378^{\circ}_{7/2} - 38617_{9/2}$	3289.675	0	2	30389.386	$20080^{\circ}_{7/2} - 50470_{9/2}$
3305.607	8	20	30242.923	$14484^{\circ}_{11/2} - 44727_{11/2}$	3288.159	50	400	30403.396	$18973^{\circ}_{7/2} - 49377_{7/2}$
3304.780	3	4	30250.491	$10673^{\circ}_{5/2} - 40923_{5/2}$	3287.789	800	1000	30406.818	$1521_{5/2} - 31928^{\circ}_{3/2}$
3304.512	4	10	30252.945	$21682^{\circ}_{7/2} - 51935_{5/2}$	3287.363	4		30410.758	$17460^{\circ}_{5/2} - 47871_{7/2}$
3304.176	50b	25	30256.021	$9202^{\circ}_{7/2} - 39458_{7/2}$	3287.083	50	50	30413.348	$18118_{3/2} - 48532^{\circ}_{1/2}$

TABLE 3. *Classified lines of* Th II – Continued

Wavelength Å	Intensity		Wavenumber cm^{-1}	Classification	Wavelength Å	Intensity		Wavenumber cm^{-1}	Classification
	Lamp	Spark				Lamp	Spark		
3286.583	400	500	30417.975	$8018_{3/2} - 38436^{\circ}_{3/2}$	3263.626	15	150	30631.934	$13818^{\circ}_{7/2} - 44450_{9/2}$
3284.776	3		30434.708	$19050^{\circ}_{3/2} - 49485_{1/2}$	3263.111	4		30636.768	$15786_{3/2} - 46423^{\circ}_{3/2}$
3284.310	2		30439.026	$23730^{\circ}_{9/2} - 54169_{7/2}$	3263.032	100	200	30637.510	$9585^{\circ}_{5/2} - 40222_{3/2}$
3282.979	100	500	30451.366	$15453^{\circ}_{7/2} - 45904_{9/2}$	3262.952	8	15	30638.261	$21297^{\circ}_{5/2} - 51935_{5/2}$
3282.948	5		30451.654	$14275^{\circ}_{9/2} - 44727_{11/2}$	3262.882	5	5	30638.918	$12488^{\circ}_{9/2} - 43127_{11/2}$
3282.231	2	50	30458.306	$24463^{\circ}_{3/2} - 54922_{3/2}$	3262.669	800	800	30640.918	$6168^{\circ}_{7/2} - 36809_{7/2}$
3282.130	15	50	30459.243	$17272^{\circ}_{9/2} - 47731_{9/2}$	3262.564	15	50	30641.905	$14484^{\circ}_{11/2} - 45126_{9/2}$
3281.976	25		30460.672	$9400_{5/2} - 39861^{\circ}_{5/2}$	3262.005	2	5	30647.155	$9720^{\circ}_{7/2} - 40367_{9/2}$
3281.604	2		30464.125	$28923^{\circ}_{5/2} - 59387_{7/2}$	3261.541	100	200	30651.515	$10572^{\circ}_{9/2} - 41223_{11/2}$
3281.414	100b		30465.889	$15144^{\circ}_{3/2} - 45610_{5/2}$	3261.148	4	20	30655.209	$10673^{\circ}_{5/2} - 41328_{5/2}$
3281.234	5		30467.560	$12488^{\circ}_{9/2} - 42955_{9/2}$	3261.114	10	100	30655.528	$15144^{\circ}_{3/2} - 45800_{5/2}$
3281.000	3		30469.733	$17983^{\circ}_{5/2} - 48453_{7/2}$	3260.941	20b		30657.155	$24381_{7/2} - 55038^{\circ}_{9/2}$
3280.954	10	25	30470.160	$12485^{\circ}_{7/2} - 42955_{9/2}$	3260.915	50b	200b	30657.399	$9238^{\circ}_{9/2} - 39895_{9/2}$
3280.740	25	40	30472.148	$9711_{7/2} - 40184^{\circ}_{7/2}$	3260.478	4		30661.508	$15242^{\circ}_{9/2} - 45904_{9/2}$
3280.415	50b	75	30475.166	$10572^{\circ}_{9/2} - 41047_{9/2}$	3259.616	100	200	30669.616	$11576^{\circ}_{3/2} - 42246_{1/2}$
3280.372	150	500	30475.566	$8018_{3/2} - 38493^{\circ}_{5/2}$	3259.245	50b	50	30673.107	$16033^{\circ}_{5/2} - 46706_{7/2}$
3279.357	10	25	30484.998	$8378^{\circ}_{7/2} - 38863_{3/2}$	3257.934	100	200	30685.450	$13818^{\circ}_{7/2} - 44503_{7/2}$
3278.767	150	75	30490.484	$7331^{\circ}_{5/2} - 37821_{3/2}$	3257.718	4	5	30687.484	$14101^{\circ}_{1/2} - 44789_{1/2}$
3278.630	3		30491.758	$23518^{\circ}_{7/2} - 54010_{7/2}$	3257.162	300	400	30692.722	$9585^{\circ}_{5/2} - 40278_{3/2}$
3278.193	10	25	30495.822	$9720^{\circ}_{7/2} - 40216_{5/2}$	3256.274	800	800	30701.092	$9238^{\circ}_{9/2} - 39939_{11/2}$
3277.925	20	25	30498.316	$9202^{\circ}_{7/2} - 39700_{5/2}$	3255.691	3		30706.589	$17983^{\circ}_{3/2} - 48689_{3/2}$
3276.941	8		30507.473	$24414^{\circ}_{3/2} - 54922_{3/2}$	3255.509	200	200	30708.306	$13468^{\circ}_{9/2} - 44177_{11/2}$
3276.814	3h		30508.656	$17983^{\circ}_{5/2} - 48492_{5/2}$	3255.283	8	400	30710.438	$18816^{\circ}_{13/2} - 49527_{13/2}$
3275.365	1		30522.152	$21131^{\circ}_{3/2} - 51653_{1/2}$	3255.014	3		30712.976	$20969^{\circ}_{7/2} - 51681_{9/2}$
3275.261	25	40	30523.121	$13250_{5/2} - 43773^{\circ}_{7/2}$	3254.810	150	200	30714.901	$7001_{3/2} - 37716^{\circ}_{1/2}$
3275.068	300b	800	30524.920	$13248_{9/2} - 43773^{\circ}_{7/2}$	3254.398	3		30718.789	$19912^{\circ}_{13/2} - 50631_{11/2}$
3274.404	50	25	30531.110	$4490^{\circ}_{5/2} - 35021_{3/2}$	3252.750	15	75	30734.352	$13818^{\circ}_{7/2} - 44552_{5/2}$
3274.266	4		30532.396	$14275^{\circ}_{9/2} - 44807_{7/2}$	3252.721	15	100	30734.626	$17272^{\circ}_{9/2} - 48006_{9/2}$
3274.192	4		30533.086	$21297^{\circ}_{5/2} - 51830_{7/2}$	3251.308	5	20	30747.983	$17121^{\circ}_{3/2} - 47869_{3/2}$
3273.916	400	800	30535.660	$10189^{\circ}_{11/2} - 40724_{13/2}$	3250.494	2		30755.683	$12472^{\circ}_{5/2} - 43227_{5/2}$
3272.995	2		30544.252	$21131^{\circ}_{3/2} - 51676_{3/2}$	3250.191	10	50	30758.550	$12488^{\circ}_{9/2} - 43246_{7/2}$
3272.577	8	100	30548.154	$16033^{\circ}_{5/2} - 46581_{5/2}$	3249.973	10b	40	30760.613	$14545^{\circ}_{5/2} - 45306_{3/2}$
3271.121	20	150	30561.750	$29431_{7/2} - 59993^{\circ}_{9/2}$	3249.916	75b	100	30761.152	$12485^{\circ}_{7/2} - 43246_{7/2}$
3270.940	5		30563.441	$8018_{3/2} - 38581^{\circ}_{5/2}$	3248.893	100b	200	30770.838	$13406^{\circ}_{13/2} - 44177_{11/2}$
3270.818	150	100	30564.582	$0_{3/2} - 30564^{\circ}_{1/2}$	3248.602	40	40	30773.594	$7331^{\circ}_{5/2} - 38105_{3/2}$
3270.234	15	100	30570.039	$16033^{\circ}_{5/2} - 46603_{5/2}$	3248.490	75	100	30774.655	$12472^{\circ}_{5/2} - 43246_{7/2}$
3270.193	3	8	30570.423	$13818^{\circ}_{7/2} - 44388_{5/2}$	3248.376	50	100	30775.735	$11576^{\circ}_{3/2} - 42352_{5/2}$
3270.041	1		30571.844	$11116^{\circ}_{7/2} - 41688_{7/2}$	3247.594	150	300	30783.146	$9400_{3/2} - 40184^{\circ}_{7/2}$
3269.470	100	100	30577.183	$6700^{\circ}_{9/2} - 37277_{7/2}$	3247.081	4		30788.009	$14101^{\circ}_{1/2} - 44889_{3/2}$
3268.855	5		30582.935	$20080^{\circ}_{7/2} - 50663_{5/2}$	3246.795	15b	25	30790.720	$8605_{3/2} - 39396^{\circ}_{7/2}$
3268.146	2		30589.570	$21682^{\circ}_{7/2} - 52272_{7/2}$	3246.581	20	50	30792.750	$11116^{\circ}_{7/2} - 41909_{9/2}$
3267.368	1		30596.853	$20310^{\circ}_{5/2} - 50907_{3/2}$	3246.558	1b		30792.968	$28823_{5/2} - 59616^{\circ}_{5/2}$
3267.003	200	300	30600.272	$7001_{3/2} - 37601^{\circ}_{3/2}$	3246.345	5		30794.989	$25440^{\circ}_{5/2} - 56235_{3/2}$
3266.601	5		30604.037	$14790^{\circ}_{7/2} - 45395_{7/2}$	3245.761	200b	1000	30800.529	$9061_{5/2} - 39861^{\circ}_{5/2}$
3266.330	5b		30606.576	$7001_{3/2} - 37607^{\circ}_{1/2}$	3244.522	15		30812.291	$12570_{7/2} - 43382^{\circ}_{5/2}$
3266.313	40b	100	30606.736	$16564^{\circ}_{11/2} - 47171_{9/2}$	3244.236	10	25	30815.007	$10673^{\circ}_{5/2} - 41488_{7/2}$
3265.578	150l	200	30613.624	$7331^{\circ}_{5/2} - 37945_{5/2}$	3243.748	5	50	30819.643	$14790^{\circ}_{7/2} - 45610_{5/2}$
3264.434	100	500	30624.352	$12472^{\circ}_{5/2} - 43096_{5/2}$	3243.469	1		30822.294	$19050^{\circ}_{3/2} - 49873_{5/2}$
3264.121	100	200	30627.289	$13468^{\circ}_{9/2} - 44096_{9/2}$	3243.195	2		30824.898	$16906^{\circ}_{7/2} - 47731_{9/2}$
3263.756	40	40	30630.714	$9585^{\circ}_{5/2} - 40216_{5/2}$	3243.070	10	25	30826.086	$9585^{\circ}_{5/2} - 40411_{7/2}$

TABLE 3. *Classified lines of* Th II—Continued

Wavelength Å	Intensity		Wavenumber cm^{-1}	Classification	Wavelength Å	Intensity		Wavenumber cm^{-1}	Classification
	Lamp	Spark				Lamp	Spark		
3243.029	50	25	30826.475	$10572^{\circ}_{9/2} - 41398_{9/2}$	3224.488	3	3	31003.723	$10673^{\circ}_{5/2} - 41676_{3/2}$
3242.251	75l	800	30833.872	$7331^{\circ}_{5/2} - 38165_{7/2}$	3223.911	5	20	31009.272	$14790^{\circ}_{7/2} - 45800_{5/2}$
3242.176	4		30834.585	$17983^{\circ}_{5/2} - 48817_{3/2}$	3223.800	25	20	31010.340	$4146_{7/2} - 35156^{\circ}_{5/2}$
3241.830	4		30837.876	$17460^{\circ}_{5/2} - 48298_{7/2}$	3223.435	4	5	31013.851	$9202^{\circ}_{7/2} - 40216_{3/2}$
3241.612	5	25	30839.950	$25246_{9/2} - 56086^{\circ}_{9/2}$	3223.285	20	15	31015.294	$10673^{\circ}_{5/2} - 41688_{7/2}$
3241.533	15l	200	30840.702	$20989^{\circ}_{9/2} - 51830_{7/2}$	3221.864	20	150	31028.973	$15349^{\circ}_{11/2} - 46378_{13/2}$
3241.484	5	3	30841.168	$17771^{\circ}_{11/2} - 48612_{13/2}$	3221.291	400b	40	31034.492	$10189^{\circ}_{11/2} - 41223_{11/2}$
3241.108	400	500	30844.746	$7001_{3/2} - 37846^{\circ}_{5/2}$	3220.351	200	300	31043.550	$4113_{5/2} - 35156^{\circ}_{5/2}$
3240.521	15	75	30850.333	$9720^{\circ}_{7/2} - 40570_{7/2}$	3218.866	75	150	31057.872	$7331^{\circ}_{5/2} - 38389_{7/2}$
3240.475	100	150	30850.771	$6691^{\circ}_{3/2} - 37542_{3/2}$	3218.755	100	40	31058.943	$9585^{\circ}_{5/2} - 40644_{5/2}$
3240.330	8	75	30852.151	$17837^{\circ}_{1/2} - 48689_{3/2}$	3218.340	4		31062.948	$15305_{9/2} - 46368^{\circ}_{9/2}$
3240.090	8	3	30854.436	$18214^{\circ}_{3/2} - 49068_{5/2}$	3218.309	10	40	31063.247	$12902^{\circ}_{3/2} - 43965_{1/2}$
3239.700	4		30858.150	$10189^{\circ}_{11/2} - 41047_{9/2}$	3218.123	5	15	31065.042	$14545^{\circ}_{5/2} - 45610_{5/2}$
3239.288	100	200	30862.075	$6700^{\circ}_{9/2} - 37562_{11/2}$	3217.853	40	100	31067.649	$12219_{3/2} - 43287^{\circ}_{5/2}$
3238.802	10	75	30866.706	$15349^{\circ}_{11/2} - 46216_{11/2}$	3217.730	75	150	31068.836	$10379_{9/2} - 41447^{\circ}_{11/2}$
3238.445	4	5	30870.109	$12902^{\circ}_{3/2} - 43772_{5/2}$	3217.456	100b	300	31071.482	$9400_{5/2} - 40472^{\circ}_{3/2}$
3238.408	5	4	30870.461	$15710^{\circ}_{3/2} - 46581_{5/2}$	3217.432	15b		31071.714	$15324^{\circ}_{1/2} - 46395_{3/2}$
3238.116	1000	800	30873.245	$4113_{5/2} - 34986^{\circ}_{5/2}$	3216.634	20		31079.422	$8378^{\circ}_{7/2} - 39458_{7/2}$
3237.534	2b		30878.795	$22642^{\circ}_{9/2} - 53520_{9/2}$	3216.530	8		31080.427	$13818^{\circ}_{7/2} - 44898_{7/2}$
3236.773	8	100	30886.054	$6244_{1/2} - 37130^{\circ}_{1/2}$	3216.013	5	10	31085.423	$17983^{\circ}_{5/2} - 49068_{5/2}$
3236.261	8		30890.941	$22028^{\circ}_{13/2} - 52918_{13/2}$	3215.778	100	100	31087.694	$6700^{\circ}_{9/2} - 37787_{7/2}$
3236.113	5	5	30892.353	$15710^{\circ}_{3/2} - 46603_{5/2}$	3214.478	2		31100.267	$16906^{\circ}_{7/2} - 48006_{9/2}$
3235.841	800r	500	30894.950	$6168^{\circ}_{7/2} - 37063_{9/2}$	3213.574	200	300	31109.015	$6168^{\circ}_{7/2} - 37277_{7/2}$
3235.397	5b	50	30899.190	$15453^{\circ}_{7/2} - 46352_{7/2}$	3212.812	10	15b	31116.393	$10572^{\circ}_{9/2} - 41688_{7/2}$
3235.381	2b		30899.342	$18973^{\circ}_{7/2} - 49873_{5/2}$	3212.494	3		31119.473	$14275^{\circ}_{9/2} - 45395_{7/2}$
3234.888	10	100	30904.051	$22014^{\circ}_{11/2} - 52918_{13/2}$	3212.241	2		31121.924	$17722^{\circ}_{9/2} - 48844_{9/2}$
3234.771	2		30905.169	$12902^{\circ}_{3/2} - 43807_{3/2}$	3212.131	20	75	31122.990	$9061_{5/2} - 40184^{\circ}_{7/2}$
3233.626	10	25	30916.112	$10572^{\circ}_{9/2} - 41488_{7/2}$	3211.467	8	50	31129.424	$9238^{\circ}_{9/2} - 40367_{9/2}$
3233.506	3		30917.259	$18568^{\circ}_{1/2} - 49485_{1/2}$	3210.309	300	300	31140.653	$6700^{\circ}_{9/2} - 37840_{9/2}$
3233.334	20	50	30918.904	$15236_{3/2} - 46155^{\circ}_{5/2}$	3209.332	10	50	31150.132	$15453^{\circ}_{7/2} - 46603_{5/2}$
3232.797	50l	100	30924.040	$9720^{\circ}_{7/2} - 40644_{5/2}$	3208.418	2		31159.006	$19248^{\circ}_{5/2} - 50407_{7/2}$
3231.925	5		30932.383	$15453^{\circ}_{7/2} - 46385_{7/2}$	3208.026	100	150	31162.813	$12219_{3/2} - 43382^{\circ}_{5/2}$
3231.579	2		30935.695	$20288^{\circ}_{11/2} - 51224_{9/2}$	3207.784	100	200	31165.164	$9202^{\circ}_{7/2} - 40367_{9/2}$
3230.867	500	400	30942.512	$9711_{7/2} - 40654^{\circ}_{5/2}$	3207.202	5	15	31170.819	$18118_{3/2} - 49289^{\circ}_{5/2}$
3229.336	4		30957.181	$20310^{\circ}_{5/2} - 51268_{7/2}$	3206.933	75b	100	31173.434	$9238^{\circ}_{9/2} - 40411_{7/2}$
3229.010	1000	1000	30960.306	$7331^{\circ}_{5/2} - 38291_{7/2}$					$8378^{\circ}_{7/2} - 39552_{9/2}$
3228.542	5		30964.794	$16906^{\circ}_{7/2} - 47871_{7/2}$	3206.218	8	20	31180.386	$20989^{\circ}_{9/2} - 52170_{11/2}$
3228.342	5	15	30966.712	$20969^{\circ}_{7/2} - 51935_{5/2}$	3206.170	10	50	31180.852	$17272^{\circ}_{9/2} - 48453_{7/2}$
3227.774	150b	100b	30972.161	$0_{3/2} - 30972^{\circ}_{3/2}$	3205.480	5	50	31187.564	$24309^{\circ}_{11/2} - 55496_{9/2}$
3227.488	2b		30974.906	$21297^{\circ}_{5/2} - 52272_{7/2}$	3205.290	25	150	31189.412	$15236_{3/2} - 46426^{\circ}_{1/2}$
3227.419	2		30975.568	$23518^{\circ}_{7/2} - 54493_{5/2}$	3205.056	5		31191.690	$15710^{\circ}_{3/2} - 46902_{5/2}$
3227.008	100	200	30979.513	$6700^{\circ}_{9/2} - 37679_{11/2}$	3204.180	10	50	31200.217	$18214^{\circ}_{3/2} - 49414_{3/2}$
3226.940	3		30980.166	$17837^{\circ}_{7/2} - 48817_{3/2}$	3203.881	50	200	31203.128	$12570_{7/2} - 43773^{\circ}_{7/2}$
3226.817	1		30981.347	$13468^{\circ}_{9/2} - 44450_{9/2}$	3203.755	1		31204.356	$14101^{\circ}_{1/2} - 45306_{3/2}$
3226.413	100	200	30985.226	$9585^{\circ}_{5/2} - 40570_{7/2}$	3203.616	10	150	31205.710	$15349^{\circ}_{11/2} - 46555_{11/2}$
3226.119	100	200	30988.050	$8378^{\circ}_{7/2} - 39366_{5/2}$	3203.255	8b	20b	31209.226	$9202^{\circ}_{7/2} - 40411_{7/2}$
3225.957	3		30989.606	$13818^{\circ}_{7/2} - 44807_{7/2}$	3203.233	20b	100b	31209.441	$10189^{\circ}_{11/2} - 41398_{9/2}$
3225.902	50	50	30990.134	$1859_{3/2} - 32850^{\circ}_{5/2}$	3202.125	10	15	31220.239	$11116^{\circ}_{7/2} - 42336_{5/2}$
3225.657	75	100	30992.488	$17460^{\circ}_{5/2} - 48453_{7/2}$	3201.655	2b		31224.822	$15710^{\circ}_{3/2} - 46935_{3/2}$
3225.412	400	400	30994.842	$9711_{7/2} - 40706^{\circ}_{7/2}$	3201.194	8	20	31229.319	$17460^{\circ}_{5/2} - 48689_{3/2}$

TABLE 3. *Classified lines of* Th II—Continued

Wavelength Å	Intensity		Wavenumber cm^{-1}	Classification	Wavelength Å	Intensity		Wavenumber cm^{-1}	Classification
	Lamp	Spark				Lamp	Spark		
3200.556	10	25	31235.544	$11116^{\circ}_{7/2} - 42352_{5/2}$	3181.758	8	50	31420.078	$14484^{\circ}_{11/2} - 45904_{9/2}$
3199.123	2		31249.535	$20686^{\circ}_{5/2} - 51935_{5/2}$	3181.189	200	300	31425.698	$7331^{\circ}_{5/2} - 38757_{3/2}$
3198.969	75s		31251.039	$4490^{\circ}_{5/2} - 35741_{5/2}$	3180.773	3	8	31429.808	$13468^{\circ}_{9/2} - 44898_{7/2}$
3198.694	50b		31253.726	$6691^{\circ}_{3/2} - 37945_{5/2}$	3180.194	1000r	1500	31435.530	$1521_{5/2} - 32957^{\circ}_{7/2}$
3198.596	4	4	31254.683	$14545^{\circ}_{5/2} - 45800_{5/2}$	3179.969	40	100	31437.754	$15710^{\circ}_{5/2} - 47148_{3/2}$
3198.482	100	100	31255.797	$8605_{5/2} - 39861^{\circ}_{5/2}$	3179.531	2	5	31442.085	$9202^{\circ}_{7/2} - 40644_{5/2}$
3198.229	100	200	31258.270	$13468^{\circ}_{9/2} - 44727_{11/2}$	3179.048	500s	500	31446.862	$4146_{7/2} - 35593^{\circ}_{9/2}$
3197.704	8	2	31263.401	$10673^{\circ}_{3/2} - 41936_{3/2}$	3178.781	20	200	31449.503	$15453^{\circ}_{7/2} - 46902_{5/2}$
3197.530	3		31265.103	$21297^{\circ}_{3/2} - 52562_{7/2}$	3177.876	20	100	31458.459	$15144^{\circ}_{3/2} - 46603_{5/2}$
3195.313	25		31286.795	$12485^{\circ}_{7/2} - 43772_{5/2}$	3177.769	8	75	31459.518	$14275^{\circ}_{9/2} - 45735_{11/2}$
3194.859	4		31291.240	$16033^{\circ}_{5/2} - 47324_{5/2}$	3177.485	8	100	31462.330	$14790^{\circ}_{7/2} - 46253_{9/2}$
3194.260	5	40	31297.108	$6168^{\circ}_{7/2} - 37465_{5/2}$	3177.382	3		31463.350	$15242^{\circ}_{9/2} - 46706_{7/2}$
3193.624	1		31303.340	$20969^{\circ}_{7/2} - 52272_{7/2}$	3177.346	2		31463.706	$10855_{7/2} - 42319^{\circ}_{9/2}$
3193.368	50	200	31305.850	$9400_{5/2} - 40706^{\circ}_{7/2}$	3177.198	50		31465.172	$6700^{\circ}_{9/2} - 38165_{7/2}$
3193.159	75	200	31307.899	$13818^{\circ}_{7/2} - 45126_{9/2}$	3176.568	5		31471.412	$25607^{\circ}_{9/2} - 57078_{9/2}$
3192.364	8	20	31315.695	$12488^{\circ}_{9/2} - 43803_{7/2}$	3176.506	100	150	31472.026	$6244_{1/2} - 37716^{\circ}_{1/2}$
3192.099	50	150	31318.295	$12485^{\circ}_{7/2} - 43803_{7/2}$	3175.726	400	500	31479.756	$6700^{\circ}_{9/2} - 38179_{9/2}$
3191.843	10b	150	31320.807	$13406^{\circ}_{13/2} - 44727_{11/2}$	3175.057	5	50	31486.388	$12902^{\circ}_{3/2} - 44388_{5/2}$
3191.749	5	5	31321.729	$8378^{\circ}_{7/2} - 39700_{5/2}$	3174.975	2	2	31487.201	$19248^{\circ}_{3/2} - 50735_{3/2}$
3191.560	2	4	31323.584	$12485^{\circ}_{7/2} - 43809_{9/2}$	3174.457	100	200	31492.339	$7001_{3/2} - 38493^{\circ}_{5/2}$
3191.221	150	300	31326.911	$9720^{\circ}_{7/2} - 41047_{9/2}$	3174.204	300	200	31494.849	$1859_{3/2} - 33354^{\circ}_{5/2}$
3191.093	300	200	31328.168	$1521_{5/2} - 32850^{\circ}_{5/2}$	3174.062	2		31496.258	$18973^{\circ}_{7/2} - 50470_{9/2}$
3190.360	75	200	31335.365	$12472^{\circ}_{5/2} - 43807_{3/2}$	3173.211	15	100	31504.705	$7331^{\circ}_{5/2} - 38836_{3/2}$
3190.220	10	100	31336.740	$9238^{\circ}_{9/2} - 40574_{11/2}$	3173.078	4		31506.025	$22014^{\circ}_{11/2} - 53520_{9/2}$
3190.164	200	400	31337.290	$10572^{\circ}_{9/2} - 41909_{9/2}$	3172.506	10	100	31511.705	$15349^{\circ}_{11/2} - 46861_{11/2}$
3190.070	300	300	31338.213	$9585^{\circ}_{5/2} - 40923_{5/2}$	3172.017	5	8	31516.563	$8378^{\circ}_{7/2} - 39895_{9/2}$
3189.038	5	25	31348.355	$14349_{1/2} - 45697^{\circ}_{3/2}$	3171.727	15b	200	31519.445	$11725^{\circ}_{1/2} - 43244_{3/2}$
3188.552	10	20	31353.132	$0_{3/2} - 31353^{\circ}_{3/2}$	3171.658	10	100	31520.130	$11576^{\circ}_{3/2} - 43096_{5/2}$
3188.515	5		31353.496	$17771^{\circ}_{11/2} - 49124_{11/2}$	3170.428	200l	150l	31532.358	$7331^{\circ}_{5/2} - 38863_{3/2}$
3188.307	500	800	31355.542	$1859_{3/2} - 33215^{\circ}_{3/2}$	3169.328	300	300	31543.302	$6213_{9/2} - 37756^{\circ}_{7/2}$
3188.234	500b	1000	31356.259	$6213_{9/2} - 37569^{\circ}_{9/2}$	3168.705	4		31549.504	$23372^{\circ}_{3/2} - 54922_{3/2}$
3188.118	300	300	31357.400	$6244_{1/2} - 37601^{\circ}_{3/2}$	3168.234	1		31554.194	$20310^{\circ}_{5/2} - 51865_{5/2}$
3187.478	50	50	31363.696	$6244_{1/2} - 37607^{\circ}_{1/2}$	3167.560	50b	400b	31560.908	$15349^{\circ}_{11/2} - 46910_{13/2}$
3187.403	100	150	31364.434	$10855_{7/2} - 42219^{\circ}_{5/2}$	3167.529	8b	100b	31561.217	$14790^{\circ}_{7/2} - 46352_{7/2}$
3187.332	3		31365.133	$20310^{\circ}_{5/2} - 51676_{3/2}$	3166.816	5	25	31568.322	$17121^{\circ}_{3/2} - 48689_{3/2}$
3187.033	5b		31368.076	$22642^{\circ}_{9/2} - 54010_{7/2}$	3166.376	5	5	31572.709	$17272^{\circ}_{9/2} - 48844_{9/2}$
3187.003	50	100	31368.371	$9202^{\circ}_{7/2} - 40570_{7/2}$					$20989^{\circ}_{9/2} - 52562_{7/2}$
3186.704	3		31371.314	$13818^{\circ}_{7/2} - 45189_{5/2}$	3166.197	10	50	31574.494	$10572^{\circ}_{9/2} - 42146_{11/2}$
3184.949	400	800	31388.600	$4490^{\circ}_{5/2} - 35878_{7/2}$	3166.098	300	300	31575.481	$4490^{\circ}_{5/2} - 36065_{5/2}$
3184.615	10	150	31391.892	$16906^{\circ}_{7/2} - 48298_{7/2}$	3165.819	200	500	31578.264	$8605_{5/2} - 40184^{\circ}_{7/2}$
3183.977	15	150	31398.182	$12902^{\circ}_{3/2} - 44300_{3/2}$	3165.624	150	200	31580.209	$7001_{3/2} - 38581^{\circ}_{5/2}$
3183.795	200	200	31399.976	$13250_{3/2} - 44650^{\circ}_{7/2}$	3164.952	3	25	31586.914	$17771^{\circ}_{11/2} - 49357_{11/2}$
3183.611	3	40	31401.791	$13248_{9/2} - 44650^{\circ}_{7/2}$	3164.482	200	200	31591.605	$6700^{\circ}_{9/2} - 38291_{7/2}$
3183.556	75	200	31402.334	$11116^{\circ}_{7/2} - 42518_{7/2}$	3164.306	20	50	31593.362	$9061_{5/2} - 40654^{\circ}_{5/2}$
3183.167	4	8	31406.171	$9585^{\circ}_{5/2} - 40991_{3/2}$	3164.201	2		31594.411	$14790^{\circ}_{7/2} - 46385_{7/2}$
3182.924	1		31408.568	$24982^{\circ}_{7/2} - 56391_{5/2}$	3163.510	4	8	31601.311	$20080^{\circ}_{7/2} - 51681_{9/2}$
3182.642	100	200	31411.351	$9061_{5/2} - 40472^{\circ}_{3/2}$	3163.248	5	20	31603.929	$21131^{\circ}_{3/2} - 52735_{3/2}$
3182.405	200b	200	31413.691	$6691^{\circ}_{5/2} - 38105_{5/2}$	3163.096	5	100	31605.447	$28011_{3/2} - 59616^{\circ}_{3/2}$
3182.357	8b	40	31414.164	$16906^{\circ}_{7/2} - 48320_{5/2}$	3162.839	150w	300	31608.015	$9720^{\circ}_{7/2} - 41328_{5/2}$
3182.236	2		31415.359	$19248^{\circ}_{5/2} - 50663_{3/2}$					$12488^{\circ}_{9/2} - 44096_{9/2}$

TABLE 3. *Classified lines of* Th II—Continued

Wavelength Å	Intensity		Wavenumber cm^{-1}	Classification	Wavelength Å	Intensity		Wavenumber cm^{-1}	Classification
	Lamp	Spark				Lamp	Spark		
3162.583	20	50	31610.574	$12485^{\circ}_{7/2} - 44096_{9/2}$	3140.064	15	75	31837.261	$8378^{\circ}_{7/2} - 40216_{5/2}$
3162.362	2		31612.783	$19050^{\circ}_{3/2} - 50663_{5/2}$	3139.964	2s		31838.275	$16033^{\circ}_{5/2} - 47871_{7/2}$
3162.286	2		31613.542	$15710^{\circ}_{5/2} - 47324_{5/2}$	3139.866	15		31839.268	$11116^{\circ}_{7/2} - 42955_{9/2}$
3161.687	75	200	31619.531	$6168^{\circ}_{7/2} - 37787_{7/2}$	3139.306	500b	800	31844.948	$9202^{\circ}_{7/2} - 41047_{9/2}$
3161.511	1		31621.292	$20686^{\circ}_{5/2} - 52307_{3/2}$	3139.225	100b	200	31845.769	$10673^{\circ}_{5/2} - 42518_{7/2}$
3161.072	10	15	31625.683	$0_{3/2} - 31625^{\circ}_{1/2}$	3138.767	5	10	31850.416	$14545^{\circ}_{5/2} - 46395_{3/2}$
3160.823	15	50	31628.174	$10572^{\circ}_{9/2} - 42200_{9/2}$	3138.580	3	8	31852.314	$17272^{\circ}_{9/2} - 49124_{11/2}$
3160.758	2	4	31628.825	$14275^{\circ}_{9/2} - 45904_{9/2}$	3138.314	10	100	31855.013	$20080^{\circ}_{7/2} - 51935_{5/2}$
3160.167	15	100	31634.740	$11116^{\circ}_{7/2} - 42751_{7/2}$	3137.172	25	100	31866.609	$8605_{5/2} - 40472^{\circ}_{3/2}$
3159.071	50	200	31645.714	$9061_{5/2} - 40706^{\circ}_{7/2}$	3136.705	40	150	31871.353	$15453^{\circ}_{7/2} - 47324_{5/2}$
3158.871	5	10	31647.718	$17837^{\circ}_{1/2} - 49485_{1/2}$	3135.696	1		31881.608	$20288^{\circ}_{11/2} - 52170_{11/2}$
3158.617	75b	100b	31650.263	$10572^{\circ}_{9/2} - 42222_{7/2}$	3134.896	5h	10	31889.744	$17983^{\circ}_{5/2} - 49873_{5/2}$
3157.918	20	100	31657.268	$13468^{\circ}_{9/2} - 45126_{9/2}$	3134.425	150	500	31894.536	$14484^{\circ}_{11/2} - 46378_{13/2}$
3157.296	8b		31663.505	$22834_{7/2} - 54497^{\circ}_{7/2}$	3133.618	150	200	31902.749	$9585^{\circ}_{5/2} - 41488_{7/2}$
3157.277	3b		31663.695	$10673^{\circ}_{5/2} - 42336_{5/2}$	3132.902	2b		31910.040	$23012^{\circ}_{3/2} - 54922_{3/2}$
3156.400	150	200	31672.493	$6168^{\circ}_{7/2} - 37840_{9/2}$	3132.389	8	20	31915.266	$14790^{\circ}_{7/2} - 46706_{7/2}$
3155.830	200	500	31678.213	$9720^{\circ}_{7/2} - 41398_{9/2}$	3132.259	50	25	31916.590	$12472^{\circ}_{5/2} - 44388_{5/2}$
3155.754	2		31678.976	$10673^{\circ}_{5/2} - 42352_{5/2}$	3132.169	8b	8	31917.507	$6700^{\circ}_{9/2} - 38617_{9/2}$
3155.589	10		31680.632	$6691^{\circ}_{3/2} - 38372_{3/2}$	3131.093	15b		31928.475	$15242^{\circ}_{9/2} - 47171_{9/2}$
3155.189	4s	10	31684.649	$19050^{\circ}_{3/2} - 50735_{3/2}$	3131.069	300b	200b	31928.720	$0_{3/2} - 31928^{\circ}_{3/2}$
3154.774	300b	500	31688.816	$13406^{\circ}_{13/2} - 45095_{13/2}$	3130.539	2		31934.125	$19594_{1/2} - 51528^{\circ}_{3/2}$
3154.760	200b	300	31688.957	$12488^{\circ}_{9/2} - 44177_{11/2}$	3130.284	5	50	31936.727	$6168^{\circ}_{7/2} - 38105_{5/2}$
3154.325	15b		31693.327	$10189^{\circ}_{11/2} - 41882_{13/2}$	3130.124	2		31938.359	$16906^{\circ}_{7/2} - 48844_{9/2}$
3154.301	500b	600	31693.568	$1521_{5/2} - 33215^{\circ}_{3/2}$	3129.973	150	200	31939.900	$10379_{9/2} - 42319^{\circ}_{9/2}$
3154.024	8	20	31696.352	$17121^{\circ}_{3/2} - 48817_{3/2}$	3129.863	2h		31941.022	$14275^{\circ}_{9/2} - 46216_{11/2}$
3153.218	25	50	31704.453	$24381_{7/2} - 56086^{\circ}_{9/2}$	3129.289	10	100	31946.881	$10572^{\circ}_{9/2} - 42518_{7/2}$
3152.631	1		31710.356	$20120^{\circ}_{5/2} - 51830_{7/2}$	3129.258	3		31947.197	$17121^{\circ}_{3/2} - 49068_{5/2}$
3151.836	5h	25b	31718.354	$15453^{\circ}_{7/2} - 47171_{9/2}$	3128.588	5	100	31954.039	$17460^{\circ}_{5/2} - 49414_{3/2}$
3151.647	100	200	31720.256	$10189^{\circ}_{11/2} - 41909_{9/2}$	3128.251	2h		31957.481	$10189^{\circ}_{11/2} - 42146_{11/2}$
3151.538	8b	25	31721.353	$9202^{\circ}_{7/2} - 40923_{5/2}$	3127.872	8	20	31961.353	$20310^{\circ}_{5/2} - 52272_{7/2}$
3150.455	200	400	31732.257	$14484^{\circ}_{11/2} - 46216_{11/2}$	3127.554	15	100	31964.603	$12485^{\circ}_{7/2} - 44450_{9/2}$
3149.963	20	100	31737.213	$7331^{\circ}_{5/2} - 39068_{7/2}$	3127.207	150	300	31968.149	$9720^{\circ}_{7/2} - 41688_{7/2}$
3149.395	3	2	31742.937	$9585^{\circ}_{5/2} - 41328_{5/2}$	3126.924	5	10	31971.042	$13250_{5/2} - 45221^{\circ}_{5/2}$
3146.926	2		31767.841	$9720^{\circ}_{7/2} - 41488_{7/2}$	3126.635	3	8	31973.998	$19050^{\circ}_{3/2} - 51024_{3/2}$
3146.880	3b		31768.305	$17727_{11/2} - 49495^{\circ}_{9/2}$	3126.267	5	15	31977.761	$14275^{\circ}_{9/2} - 46253_{9/2}$
3146.811	10	50	31769.002	$14484^{\circ}_{11/2} - 46253_{9/2}$	3126.204	1		31978.405	$23518^{\circ}_{7/2} - 55496_{9/2}$
3146.043	500	500	31776.757	$6168^{\circ}_{7/2} - 37945_{5/2}$	3126.052	50	150	31979.960	$11116^{\circ}_{7/2} - 43096_{5/2}$
3145.281	5	50	31784.455	$20080^{\circ}_{7/2} - 51865_{5/2}$	3125.982	1		31980.677	$22513^{\circ}_{5/2} - 54493_{5/2}$
3144.702	10	25	31790.307	$14790^{\circ}_{7/2} - 46581_{5/2}$	3125.858	10	40	31981.945	$13818^{\circ}_{7/2} - 45800_{5/2}$
3144.641	1		31790.924	$15144^{\circ}_{3/2} - 46935_{3/2}$	3125.745	200	200	31983.101	$1859_{3/2} - 33843^{\circ}_{3/2}$
3144.506	10		31792.288	$13818^{\circ}_{7/2} - 45610_{5/2}$	3125.507	500	1000	31985.537	$9238^{\circ}_{9/2} - 41223_{11/2}$
3143.084	8	20	31806.671	$14545^{\circ}_{5/2} - 46352_{7/2}$	3125.321	4	5	31987.440	$12902^{\circ}_{3/2} - 44889_{3/2}$
3142.836	400	600	31809.181	$9238^{\circ}_{9/2} - 41047_{9/2}$	3125.208	300	600	31988.597	$8378^{\circ}_{7/2} - 40367_{9/2}$
3142.701	50	40	31810.548	$0_{3/2} - 31810^{\circ}_{3/2}$	3124.387	500	600	31997.002	$6168^{\circ}_{7/2} - 38165_{7/2}$
3142.538	10	100	31812.197	$14790^{\circ}_{7/2} - 46603_{5/2}$	3123.994	8		32001.027	$15144^{\circ}_{3/2} - 47145_{1/2}$
3142.209	1		31815.528	$20120^{\circ}_{5/2} - 51935_{5/2}$	3123.004	100b	150	32011.171	$10189^{\circ}_{11/2} - 42200_{9/2}$
3141.847	200	300	31819.194	$7331^{\circ}_{5/2} - 39150_{3/2}$	3122.963	600b	800b	32011.591	$6168^{\circ}_{7/2} - 38179_{9/2}$
3141.337	10	100	31824.359	$15324^{\circ}_{1/2} - 47148_{3/2}$	3122.914	8g		32012.094	$8460_{3/2} - 40472^{\circ}_{3/2}$
3140.940	50	150	31828.382	$12472^{\circ}_{5/2} - 44300_{3/2}$	3122.582	3		32015.497	$12488^{\circ}_{9/2} - 44503_{7/2}$
3140.494	10	8	31832.902	$1521_{5/2} - 33354^{\circ}_{3/2}$	3122.327	10		32018.112	$12485^{\circ}_{7/2} - 44503_{7/2}$

TABLE 3. *Classified lines of* Th II—Continued

Wavelength Å	Intensity		Wavenumber cm^{-1}	Classification	Wavelength Å	Intensity		Wavenumber cm^{-1}	Classification
	Lamp	Spark				Lamp	Spark		
3122.158	2		32019.845	$19248^{\circ}_{5/2} - 51268_{7/2}$	3100.937	300	500	32238.961	$12488^{\circ}_{9/2} - 44727_{11/2}$
3121.888	1		32022.614	$27593_{5/2} - 59616^{\circ}_{3/2}$	3100.797	200b	200	32240.417	$13248_{9/2} - 45489^{\circ}_{9/2}$
3121.169	1		32029.990	$22139^{\circ}_{9/2} - 54169_{7/2}$	3099.863	150	200	32250.131	$9238^{\circ}_{9/2} - 41488_{7/2}$
3121.011	25	100	32031.612	$12472^{\circ}_{3/2} - 44503_{7/2}$	3099.740	100	200	32251.410	$12570_{7/2} - 44821^{\circ}_{5/2}$
3120.912	5		32032.628	$8378^{\circ}_{7/2} - 40411_{7/2}$	3099.118	1		32257.883	$19912^{\circ}_{13/2} - 52170_{11/2}$
3120.639	5	10	32035.430	$7331^{\circ}_{5/2} - 39366_{5/2}$	3098.387	40	100	32265.493	$8378^{\circ}_{7/2} - 40644_{5/2}$
3120.607	1		32035.759	$14545^{\circ}_{5/2} - 46581_{5/2}$	3098.325	20	75	32266.139	$13468^{\circ}_{9/2} - 45735_{11/2}$
3120.455	75	8	32037.319	$6691^{\circ}_{3/2} - 38728_{5/2}$	3097.267	200	300	32277.160	$4113_{5/2} - 36390^{\circ}_{3/2}$
3120.168	8		32040.266	$6700^{\circ}_{9/2} - 38740_{11/2}$	3097.142	20		32278.463	$15453^{\circ}_{7/2} - 47731_{9/2}$
3119.526	600b	100	32046.859	$4146_{7/2} - 36193^{\circ}_{9/2}$	3096.991	5	10b	32280.037	$14275^{\circ}_{9/2} - 46555_{11/2}$
3119.354	150	200	32048.626	$8605_{5/2} - 40654^{\circ}_{5/2}$	3096.963	5	10b	32280.328	$16564^{\circ}_{11/2} - 48844_{9/2}$
3118.478	25b		32057.629	$14545^{\circ}_{5/2} - 46603_{5/2}$	3096.430	150	200	32285.885	$9202^{\circ}_{7/2} - 41488_{7/2}$
3117.683	400	300	32065.803	$6691^{\circ}_{3/2} - 38757_{3/2}$	3096.295	10b	15b	32287.292	$12902^{\circ}_{3/2} - 45189_{3/2}$
3117.150	15	50	32071.286	$14484^{\circ}_{11/2} - 46555_{11/2}$	3096.260	40b	100	32287.657	$16033^{\circ}_{5/2} - 48320_{5/2}$
3116.626	2	3	32076.678	$14275^{\circ}_{9/2} - 46352_{7/2}$	3095.744	10	75	32293.039	$17121^{\circ}_{3/2} - 49414_{3/2}$
				$14349_{1/2} - 46426^{\circ}_{1/2}$	3095.634	3b		32294.186	$14101^{\circ}_{1/2} - 46395_{3/2}$
3116.478	200	150	32078.201	$10673^{\circ}_{5/2} - 42751_{7/2}$	3095.620	10b	75	32294.333	$18973^{\circ}_{7/2} - 51268_{7/2}$
3116.303	150b	400	32080.002	$12570_{7/2} - 44650^{\circ}_{7/2}$	3094.706	40b	100	32303.870	$16818_{7/2} - 49121^{\circ}_{7/2}$
3115.745	40	200	32085.747	$17272^{\circ}_{9/2} - 49357_{11/2}$	3093.254	8p	8	32319.033	$4490^{\circ}_{5/2} - 36809_{7/2}$
3115.715	2		32086.056	$13818^{\circ}_{7/2} - 45904_{9/2}$	3093.196	5	8	32319.639	$12488^{\circ}_{9/2} - 44807_{7/2}$
3115.415	8	40	32089.146	$10855_{7/2} - 42944^{\circ}_{7/2}$	3093.051	150	100	32321.154	$1521_{5/2} - 33843^{\circ}_{3/2}$
3115.191	5	8	32091.453	$9585^{\circ}_{5/2} - 41676_{3/2}$	3092.945	40	100	32322.262	$12485^{\circ}_{7/2} - 44807_{7/2}$
3114.744	3h		32096.059	$24982^{\circ}_{7/2} - 57078_{9/2}$	3092.452	2		32327.414	$21682^{\circ}_{7/2} - 54010_{7/2}$
3114.266	100	200	32100.985	$8605_{5/2} - 40706^{\circ}_{7/2}$	3092.332	20	100	32328.669	$13406^{\circ}_{13/2} - 45735_{11/2}$
3114.067	100	100	32103.036	$9585^{\circ}_{5/2} - 41688_{7/2}$	3091.653	50b	75	32335.769	$12472^{\circ}_{5/2} - 44807_{7/2}$
3113.408	8		32109.831	$14275^{\circ}_{9/2} - 46385_{7/2}$	3091.290	1		32339.566	$18568^{\circ}_{1/2} - 50907_{3/2}$
3113.242	8		32111.543	$14790^{\circ}_{7/2} - 46902_{5/2}$	3090.184	20	25	32351.140	$9585^{\circ}_{5/2} - 41936_{3/2}$
3112.941	4	10	32114.647	$19248^{\circ}_{5/2} - 51362_{5/2}$	3090.094	300	300	32352.082	$1859_{3/2} - 34212^{\circ}_{5/2}$
				$17722^{\circ}_{9/2} - 49837_{9/2}$	3089.699	1		32356.218	$27631_{3/2} - 59987^{\circ}_{3/2}$
3112.088	75	100	32123.449	$6168^{\circ}_{7/2} - 38291_{7/2}$	3089.626	75	75	32356.982	$14545^{\circ}_{5/2} - 46902_{5/2}$
3111.832	50	100	32126.092	$9202^{\circ}_{7/2} - 41328_{5/2}$	3088.967	4		32363.885	$17121^{\circ}_{3/2} - 49485_{1/2}$
3111.762	50	100	32126.815	$7331^{\circ}_{5/2} - 39458_{7/2}$	3088.839	100	100	32365.226	$8460_{3/2} - 40825^{\circ}_{1/2}$
3111.429	15	75	32130.253	$11116^{\circ}_{7/2} - 43246_{7/2}$	3088.526	25b		32368.506	$6700^{\circ}_{9/2} - 39068_{7/2}$
3110.020	600	500	32144.809	$6691^{\circ}_{3/2} - 38836_{3/2}$	3088.470	500	500	32369.093	$7331^{\circ}_{5/2} - 39700_{5/2}$
3108.671	5		32158.758	$15710^{\circ}_{3/2} - 47869_{3/2}$	3087.691	15	10	32377.259	$14484^{\circ}_{11/2} - 46861_{11/2}$
3108.454	40b	200	32161.003	$15305_{9/2} - 47466^{\circ}_{11/2}$	3087.275	8	15	32381.622	$15349^{\circ}_{11/2} - 47731_{9/2}$
3108.297	1000	1000	32162.627	$6700^{\circ}_{9/2} - 38862_{11/2}$	3087.067	2		32383.803	$10572^{\circ}_{9/2} - 42955_{9/2}$
3107.855	2		32167.201	$18568^{\circ}_{1/2} - 50735_{3/2}$	3086.466	3	2	32390.109	$14545^{\circ}_{5/2} - 46935_{3/2}$
3107.345	20	25	32172.480	$6691^{\circ}_{3/2} - 38863_{3/2}$	3086.361	8		32391.211	$22106_{3/2} - 54497^{\circ}_{7/2}$
3107.026	500	500	32175.783	$6691^{\circ}_{3/2} - 38867_{1/2}$	3086.147	2		32393.457	$27593_{5/2} - 59987^{\circ}_{3/2}$
3106.687	50	200b	32179.294	$10572^{\circ}_{9/2} - 42751_{7/2}$	3085.165	4		32403.767	$12902^{\circ}_{3/2} - 45306_{3/2}$
3106.652	8	100	32179.657	$15144^{\circ}_{3/2} - 47324_{5/2}$	3084.689	1		32408.767	$22513^{\circ}_{5/2} - 54922_{3/2}$
3105.747	800b	600	32189.033	$9720^{\circ}_{7/2} - 41909_{9/2}$	3084.524	2b		32410.501	$12488^{\circ}_{9/2} - 44898_{7/2}$
3105.473	100	150	32191.874	$6244_{1/2} - 38436^{\circ}_{3/2}$	3084.335	3		32412.487	$17460^{\circ}_{5/2} - 49873_{5/2}$
3105.257	8	5	32194.113	$8460_{3/2} - 40654^{\circ}_{5/2}$	3084.279	2		32413.075	$12485^{\circ}_{7/2} - 44898_{7/2}$
3105.050	100	150	32196.259	$9202^{\circ}_{7/2} - 41398_{9/2}$	3083.845	20	20	32417.637	$12472^{\circ}_{5/2} - 44889_{3/2}$
3104.381	5	25	32203.197	$22642^{\circ}_{9/2} - 54845_{9/2}$	3083.777	1		32418.351	$15453^{\circ}_{7/2} - 47871_{7/2}$
3102.664	500	500	32221.017	$6168^{\circ}_{7/2} - 38389_{7/2}$	3083.624	8	15	32419.960	$16033^{\circ}_{5/2} - 48453_{7/2}$
3101.688	100	200	32231.156	$11576^{\circ}_{3/2} - 43807_{3/2}$	3083.298	400	200	32423.387	$10673^{\circ}_{5/2} - 43096_{5/2}$
3101.069	2		32237.589	$17722^{\circ}_{9/2} - 49960_{7/2}$	3082.995	100b	200	32426.574	$12472^{\circ}_{5/2} - 44898_{7/2}$

TABLE 3. *Classified lines of* Th II—Continued

Wavelength Å	Intensity		Wavenumber cm^{-1}	Classification	Wavelength Å	Intensity		Wavenumber cm^{-1}	Classification
	Lamp	Spark				Lamp	Spark		
3082.606	2		32430.666	$14275^{\circ}_{9/2} - 46706_{7/2}$	3063.126	200b	100	32636.901	$9585^{\circ}_{5/2} - 42222_{7/2}$
3082.194	75	150	32435.001	$13818^{\circ}_{7/2} - 46253_{9/2}$	3063.029	300	150	32637.934	$12488^{\circ}_{9/2} - 45126_{9/2}$
3082.153	75	100	32435.432	$13468^{\circ}_{9/2} - 45904_{9/2}$	3062.784	5	3	32640.545	$12485^{\circ}_{7/2} - 45126_{9/2}$
3081.982	400	200	32437.232	$4146_{7/2} - 36583^{\circ}_{7/2}$	3061.700	800	200	32652.101	$6700^{\circ}_{9/2} - 39352_{11/2}$
3081.660	150	100	32440.621	$13248_{9/2} - 45689^{\circ}_{7/2}$	3061.345	40	25	32655.887	$11116^{\circ}_{7/2} - 43772_{5/2}$
3080.834	50		32449.318	$6168^{\circ}_{7/2} - 38617_{9/2}$	3061.259	10b		32656.805	$16033^{\circ}_{5/2} - 48689_{3/2}$
3080.730	8		32450.413	$9238^{\circ}_{9/2} - 41688_{7/2}$	3061.241	50b	40l	32656.997	$15349^{\circ}_{11/2} - 48006_{9/2}$
3080.217	800	600	32455.818	$10189^{\circ}_{11/2} - 42644_{13/2}$	3060.178	400	200	32668.340	$8378^{\circ}_{7/2} - 41047_{9/2}$
3079.888	150	75	32459.285	$6691^{\circ}_{3/2} - 39150_{3/2}$	3059.899	3		32671.319	$9238^{\circ}_{9/2} - 41909_{9/2}$
3079.042	20		32468.203	$4113_{5/2} - 36581^{\circ}_{3/2}$	3059.505	3		32675.526	$6691^{\circ}_{3/2} - 39366_{5/2}$
3078.829	100w	200	32470.449	$4113_{5/2} - 36583^{\circ}_{7/2}$	3059.321	3		32677.491	$16818_{7/2} - 49495^{\circ}_{9/2}$
3078.734	50	15b	32471.451	$16818_{7/2} - 49289^{\circ}_{5/2}$	3059.063	8b		32680.247	$17983^{\circ}_{5/2} - 50663_{5/2}$
3077.932	200	150	32479.911	$9720^{\circ}_{7/2} - 42200_{9/2}$	3058.685	3		32684.285	$17722^{\circ}_{9/2} - 50407_{7/2}$
3077.339	300	200	32486.170	$9202^{\circ}_{7/2} - 41688_{7/2}$	3058.426	100b	100b	32687.053	$14484^{\circ}_{11/2} - 47171_{9/2}$
3077.271	4		32486.888	$21682^{\circ}_{7/2} - 54169_{7/2}$	3058.395	8b	4b	32687.385	$11116^{\circ}_{7/2} - 43803_{7/2}$
3076.035	75	100	32499.941	$17460^{\circ}_{5/2} - 49960_{7/2}$	3058.307	8	5	32688.325	$17272^{\circ}_{9/2} - 49960_{7/2}$
3075.840	75		32502.001	$9720^{\circ}_{7/2} - 42222_{7/2}$	3058.139	50	8	32690.121	$1521_{5/2} - 34212^{\circ}_{5/2}$
3075.293	8		32507.782	$9711_{7/2} - 42219^{\circ}_{5/2}$	3057.901	25	10	32692.665	$11116^{\circ}_{7/2} - 43809_{9/2}$
3075.057	50	150	32510.277	$24381^{\circ}_{7/2} - 56892^{\circ}_{5/2}$	3057.837	4		32693.349	$18214^{\circ}_{3/2} - 50907_{3/2}$
3074.171	1		32519.647	$20158_{5/2} - 52678^{\circ}_{5/2}$					$23697^{\circ}_{7/2} - 56391_{5/2}$
3074.041	1		32521.022	$18214^{\circ}_{3/2} - 50735_{3/2}$	3057.637	100	50	32695.488	$6168^{\circ}_{7/2} - 38863_{5/2}$
3073.432	50	15	32527.465	$10855_{7/2} - 43382^{\circ}_{5/2}$	3057.311	2		32698.974	$17771^{\circ}_{11/2} - 50470_{9/2}$
3073.089	2		32531.096	$20989^{\circ}_{9/2} - 53520_{9/2}$	3056.845	15	10	32703.958	$12485^{\circ}_{7/2} - 45189_{5/2}$
3072.825	400	200	32533.890	$13818^{\circ}_{7/2} - 46352_{7/2}$	3056.555	5	2	32707.061	$9202^{\circ}_{7/2} - 41909_{9/2}$
3072.115	800	300	32541.409	$4146_{7/2} - 36687^{\circ}_{5/2}$	3056.445	20	10	32708.238	$12902^{\circ}_{3/2} - 45610_{3/2}$
3071.798	5	10	32544.767	$8378^{\circ}_{7/2} - 40923_{3/2}$	3056.097	50	15	32711.963	$9400_{5/2} - 42112^{\circ}_{3/2}$
3071.496	1		32547.967	$21297^{\circ}_{3/2} - 53845_{3/2}$	3056.024	2		32712.744	$21297^{\circ}_{3/2} - 54010_{7/2}$
3071.195	15	5	32551.157	$6213_{9/2} - 38764^{\circ}_{7/2}$	3055.944	4		32713.600	$21131^{\circ}_{3/2} - 53845_{5/2}$
3071.124	1		32551.909	$20969^{\circ}_{7/2} - 53520_{9/2}$	3055.582	5		32717.476	$12472^{\circ}_{3/2} - 45189_{5/2}$
3070.943	150	150	32553.828	$15453^{\circ}_{7/2} - 48006_{9/2}$	3054.959	10	8	32724.147	$11576^{\circ}_{3/2} - 44300_{3/2}$
3070.817	800	400	32555.164	$10572^{\circ}_{9/2} - 43127_{11/2}$	3054.892	5	4	32724.865	$15144^{\circ}_{3/2} - 47869_{3/2}$
3070.330	5		32560.327	$6168^{\circ}_{7/2} - 38728_{5/2}$	3052.771	8	5	32747.601	$13468^{\circ}_{9/2} - 46216_{11/2}$
3069.851	5	5	32565.407	$17272^{\circ}_{9/2} - 49837_{9/2}$	3052.414	10	4	32751.431	$9585^{\circ}_{5/2} - 42336_{5/2}$
3069.694	5		32567.073	$13818^{\circ}_{7/2} - 46385_{7/2}$	3052.353	1b		32752.085	$17983^{\circ}_{5/2} - 50735_{3/2}$
3069.255	150	150	32571.731	$10673^{\circ}_{5/2} - 43244_{3/2}$	3051.792	150	40	32758.106	$6700^{\circ}_{9/2} - 39458_{7/2}$
3069.070	50s	15	32573.694	$10673^{\circ}_{5/2} - 43246_{7/2}$	3051.340	2		32762.958	$13818^{\circ}_{7/2} - 46581_{5/2}$
3068.981	300b	150	32574.639	$4113_{3/2} - 36687^{\circ}_{5/2}$	3050.985	150b	100	32766.770	$10189^{\circ}_{11/2} - 42955_{9/2}$
3068.935	20b		32575.127	$11725^{\circ}_{1/2} - 44300_{3/2}$	3049.863	100	50	32778.824	$14545^{\circ}_{3/2} - 47324_{5/2}$
3068.263	15b	15b	32582.261	$19248^{\circ}_{5/2} - 51830_{7/2}$	3049.643	100	100	32781.188	$15710^{\circ}_{3/2} - 48492_{5/2}$
3067.909	5	4	32586.021	$14275^{\circ}_{9/2} - 46861_{11/2}$	3049.347	5	3	32784.370	$13468^{\circ}_{9/2} - 46253_{9/2}$
3067.729	800	500	32587.932	$13250_{5/2} - 45838^{\circ}_{3/2}$	3049.302	10	5	32784.854	$13818^{\circ}_{7/2} - 46603_{5/2}$
3066.412	150	100	32601.928	$12219_{3/2} - 44821^{\circ}_{5/2}$	3049.092	500b	200	32787.112	$4490^{\circ}_{5/2} - 37277_{7/2}$
3066.307	4	50	32603.044	$14545^{\circ}_{5/2} - 47148_{3/2}$	3048.023	5	3	32798.611	$9720^{\circ}_{7/2} - 42518_{7/2}$
3065.930	300	150	32607.053	$9711_{7/2} - 42319^{\circ}_{9/2}$	3047.206	5	3	32807.404	$8018_{3/2} - 40825^{\circ}_{1/2}$
3065.038	50	10	32616.543	$9720^{\circ}_{7/2} - 42336_{5/2}$	3046.952	300	200	32810.139	$13406^{\circ}_{13/2} - 46216_{11/2}$
3063.916	2		32628.486	$15242^{\circ}_{9/2} - 47871_{7/2}$	3046.745	5	2	32812.368	$11576^{\circ}_{3/2} - 44388_{5/2}$
3063.744	1		32630.318	$20288^{\circ}_{11/2} - 52918_{13/2}$	3046.564	1		32814.317	$19050^{\circ}_{3/2} - 51865_{5/2}$
3063.602	8b		32631.830	$9720^{\circ}_{7/2} - 42352_{5/2}$	3046.149	15	5	32818.788	$9400_{5/2} - 42219^{\circ}_{5/2}$
3063.217	5		32635.931	$24309^{\circ}_{11/2} - 56945_{11/2}$	3045.565	200	100	32825.080	$10189^{\circ}_{11/2} - 43014_{13/2}$
3063.185	10		32636.272	$8018_{3/2} - 40654^{\circ}_{5/2}$	3045.069	8	15	32830.427	$22014^{\circ}_{11/2} - 54845_{9/2}$

TABLE 3. *Classified lines of* Th II—Continued

Wavelength Å	Intensity		Wavenumber cm^{-1}	Classification	Wavelength Å	Intensity		Wavenumber cm^{-1}	Classification
	Lamp	Spark				Lamp	Spark		
3044.750	20	8	32833.867	$14101^{\circ}_{1/2} - 46935_{3/2}$	3025.845	10	2	33038.999	$15453^{\circ}_{7/2} - 48492_{5/2}$
3043.671	2		32845.506	$15453^{\circ}_{7/2} - 48298_{7/2}$	3025.647	4	4	33041.161	$20969^{\circ}_{7/2} - 54010_{7/2}$
3043.248	100	5	32850.071	$0_{3/2} - 32850^{\circ}_{5/2}$	3025.623	2		33041.423	$17983^{\circ}_{5/2} - 51024_{3/2}$
3043.065	200	100	32852.046	$6700^{\circ}_{9/2} - 39552_{9/2}$	3025.391	40b	25	33043.957	$14101^{\circ}_{1/2} - 47145_{1/2}$
3042.630	4	4	32856.743	$18973^{\circ}_{7/2} - 51830_{7/2}$	3025.131	10	5	33046.796	$14101^{\circ}_{1/2} - 47148_{3/2}$
3042.308	10	4	32860.220	$7001_{3/2} - 39861^{\circ}_{5/2}$	3024.669	50b	20	33051.844	$9061_{5/2} - 42112^{\circ}_{3/2}$
3042.086	1		32862.618	$23372^{\circ}_{3/2} - 56235_{3/2}$	3024.475	5	2	33053.964	$16906^{\circ}_{7/2} - 49960_{7/2}$
3041.608	2		32867.783	$15453^{\circ}_{7/2} - 48320_{5/2}$	3023.570	8	3	33063.857	$11725^{\circ}_{1/2} - 44789_{1/2}$
3041.163	2		32872.592	$23518^{\circ}_{7/2} - 56391_{5/2}$	3022.095	200	100	33079.994	$7331^{\circ}_{5/2} - 40411_{7/2}$
3040.177	8	4	32883.253	$13468^{\circ}_{9/2} - 46352_{7/2}$	3022.062	1		33080.355	$14790^{\circ}_{7/2} - 47871_{7/2}$
3040.049	150	50	32884.637	$7331^{\circ}_{5/2} - 40216_{5/2}$	3021.709	2		33084.219	$13818^{\circ}_{7/2} - 46902_{5/2}$
3039.425	8	5	32891.388	$7331^{\circ}_{5/2} - 40222_{3/2}$	3021.488	100b	20	33086.639	$13468^{\circ}_{9/2} - 46555_{11/2}$
				$18973^{\circ}_{7/2} - 51865_{5/2}$	3020.329	3	2	33099.335	$10673^{\circ}_{5/2} - 43772_{5/2}$
3039.017	2		32895.804	$14275^{\circ}_{9/2} - 47171_{9/2}$	3019.421	200	100	33109.289	$8378^{\circ}_{7/2} - 41488_{7/2}$
3038.825	40	20	32897.882	$12902^{\circ}_{3/2} - 45800_{5/2}$	3018.549	4	3	33118.853	$12570_{7/2} - 45689^{\circ}_{7/2}$
3038.598	200	75	32900.340	$6168^{\circ}_{7/2} - 39068_{7/2}$	3018.490	150	150	33119.500	$13248_{9/2} - 46368^{\circ}_{9/2}$
3038.164	2		32905.039	$13250_{5/2} - 46155^{\circ}_{5/2}$	3017.457	4	2	33130.838	$10673^{\circ}_{5/2} - 43803_{7/2}$
3038.007	40	25	32906.740	$12488^{\circ}_{9/2} - 45395_{7/2}$	3017.132	100	75	33134.406	$10673^{\circ}_{5/2} - 43807_{3/2}$
3037.842	2		32908.527	$9238^{\circ}_{9/2} - 42146_{11/2}$	3016.763	4	2	33138.459	$12472^{\circ}_{5/2} - 45610_{5/2}$
3037.766	3	3	32909.350	$12485^{\circ}_{7/2} - 45395_{7/2}$	3015.725	100	40	33149.865	$9202^{\circ}_{7/2} - 42352_{5/2}$
3037.111	8	5	32916.448	$13468^{\circ}_{9/2} - 46385_{7/2}$	3014.926	75	10	33158.650	$9061_{5/2} - 42219^{\circ}_{5/2}$
3036.938	8b	3b	32918.323	$10855_{7/2} - 43773^{\circ}_{7/2}$	3014.405	10	5	33164.380	$11725^{\circ}_{1/2} - 44889_{3/2}$
3036.910	25	8b	32918.626	$12570_{7/2} - 45489^{\circ}_{9/2}$	3013.599	100	50	33173.250	$13250_{5/2} - 46423^{\circ}_{3/2}$
3035.764	20	20	32931.052	$16906^{\circ}_{7/2} - 49837_{9/2}$	3013.343	2	2	33176.068	$15144^{\circ}_{3/2} - 48320_{5/2}$
3035.536	100	20	32933.526	$9585^{\circ}_{5/2} - 42518_{7/2}$	3013.000	5	4	33179.845	$20989^{\circ}_{9/2} - 54169_{7/2}$
3035.110	300	150	32938.148	$10189^{\circ}_{11/2} - 43127_{11/2}$	3012.707	100	75	33183.071	$6213_{9/2} - 39396^{\circ}_{7/2}$
3034.893	10	10	32940.503	$14790^{\circ}_{7/2} - 47731_{9/2}$	3012.347	2		33187.037	$17837^{\circ}_{1/2} - 51024_{3/2}$
3034.327	40	15	32946.647	$7331^{\circ}_{5/2} - 40278_{3/2}$	3012.014	1		33190.706	$14484^{\circ}_{11/2} - 47675_{11/2}$
				$17460^{\circ}_{5/2} - 50407_{7/2}$	3011.602	200	40	33195.246	$6700^{\circ}_{9/2} - 39895_{9/2}$
3034.065	500	300	32949.492	$8378^{\circ}_{7/2} - 41328_{5/2}$	3011.481	2		33196.580	$21297^{\circ}_{5/2} - 54493_{5/2}$
3032.895	15	5	32962.203	$9238^{\circ}_{9/2} - 42200_{9/2}$	3011.370	1		33197.804	$17272^{\circ}_{9/2} - 50470_{9/2}$
3032.834	2		32962.865	$26424^{\circ}_{5/2} - 59387_{7/2}$	3011.302	5	8	33198.553	$6168^{\circ}_{7/2} - 39366_{5/2}$
3031.955	100	75	32972.422	$13406^{\circ}_{13/2} - 46378_{13/2}$	3010.899	8b	8	33202.997	$17460^{\circ}_{5/2} - 50663_{5/2}$
3031.699	50b	8	32975.205	$4490^{\circ}_{5/2} - 37465_{5/2}$	3010.245	2		33210.210	$15242^{\circ}_{9/2} - 48453_{7/2}$
3031.600	5	2	32976.282	$11576^{\circ}_{3/2} - 44552_{5/2}$	3010.002	20	20	33212.891	$11576^{\circ}_{3/2} - 44789_{1/2}$
3031.339	10	4	32979.122	$15710^{\circ}_{3/2} - 48689_{3/2}$	3009.857	5		33214.491	$23730^{\circ}_{9/2} - 56945_{11/2}$
3031.287	75	10	32979.687	$11116^{\circ}_{7/2} - 44096_{9/2}$	3009.768	200	50	33215.473	$0_{3/2} - 33215^{\circ}_{3/2}$
3030.864	50b	15	32984.290	$9238^{\circ}_{9/2} - 42222_{7/2}$	3009.733	2		33215.859	$14790^{\circ}_{7/2} - 48006_{9/2}$
3029.692	5	2	32997.049	$7828_{1/2} - 40825^{\circ}_{1/2}$	3008.497	300	150	33229.505	$6213_{9/2} - 39443^{\circ}_{9/2}$
3029.609	10		32997.953	$9202^{\circ}_{7/2} - 42200_{9/2}$	3008.277	75	75	33231.935	$10572^{\circ}_{9/2} - 43803_{7/2}$
3029.414	8	4	33000.077	$15453^{\circ}_{7/2} - 48453_{7/2}$	3008.226	3	3	33232.498	$9711_{7/2} - 42944^{\circ}_{7/2}$
3029.278	2		33001.558	$12219_{3/2} - 45221^{\circ}_{5/2}$	3007.950	100	50	33235.547	$9720^{\circ}_{7/2} - 42955_{9/2}$
3028.577	200	150	33009.197	$6691^{\circ}_{3/2} - 39700_{5/2}$	3007.799	75	100	33237.216	$10572^{\circ}_{9/2} - 43809_{9/2}$
3027.837	2		33017.263	$9400_{5/2} - 42418^{\circ}_{3/2}$	3007.643	50b	40b	33238.940	$6700^{\circ}_{9/2} - 39939_{11/2}$
3027.617	15	5	33019.663	$8378^{\circ}_{7/2} - 41398_{9/2}$	3007.625	100b	50b	33239.139	$7331^{\circ}_{5/2} - 40570_{7/2}$
3027.583	8	3	33020.033	$9202^{\circ}_{7/2} - 42222_{7/2}$	3006.932	200	150	33246.799	$12488^{\circ}_{9/2} - 45735_{11/2}$
3027.554	1		33020.350	$20989^{\circ}_{9/2} - 54010_{7/2}$	3006.008	50	15	33257.018	$6691^{\circ}_{3/2} - 39948_{1/2}$
3027.216	4b		33024.036	$19248^{\circ}_{5/2} - 52272_{7/2}$	3005.527	10	8	33262.340	$15349^{\circ}_{11/2} - 48612_{13/2}$
3026.575	300	200	33031.030	$9720^{\circ}_{7/2} - 42751_{7/2}$	3004.637	20	5	33272.192	$11116^{\circ}_{7/2} - 44388_{5/2}$
3026.150	20	20	33035.669	$16033^{\circ}_{5/2} - 49068_{5/2}$	3004.562	2		33273.023	$16564^{\circ}_{11/2} - 49837_{9/2}$

TABLE 3. *Classified lines of* Th II—Continued

Wavelength Å	Intensity		Wavenumber cm^{-1}	Classification	Wavelength Å	Intensity		Wavenumber cm^{-1}	Classification
	Lamp	Spark				Lamp	Spark		
3004.398	2		33274.839	$17460^{\circ}_{5/2} - 50735_{3/2}$	2983.817	300	150	33504.344	$13406^{\circ}_{13/2} - 46910_{13/2}$
3003.851	8	3	33280.898	$9238^{\circ}_{9/2} - 42518_{7/2}$	2983.664	50	25	33506.062	$13818^{\circ}_{7/2} - 47324_{5/2}$
3003.036	8	5	33289.930	$6168^{\circ}_{7/2} - 39458_{7/2}$	2983.572	150b	75	33507.095	$8605_{5/2} - 42112^{\circ}_{5/2}$
3002.401	200b	100	33296.970	$1859_{3/2} - 35156^{\circ}_{5/2}$	2983.531	10b	3	33507.555	$9720^{\circ}_{7/2} - 43227_{5/2}$
3002.259	2	3	33298.545	$18973^{\circ}_{7/2} - 52272_{7/2}$	2983.213	15	4	33511.127	$9585^{\circ}_{5/2} - 43096_{5/2}$
3001.264	200	100	33309.584	$8378^{\circ}_{7/2} - 41688_{7/2}$	2983.018	100	25	33513.317	$9238^{\circ}_{9/2} - 42751_{7/2}$
3000.969	10	8	33312.858	$7331^{\circ}_{5/2} - 40644_{5/2}$	2982.198	10	5	33522.532	$14484^{\circ}_{11/2} - 48006_{9/2}$
3000.920	15	10	33313.402	$11576^{\circ}_{3/2} - 44889_{3/2}$	2982.048	50	8	33524.218	$10572^{\circ}_{9/2} - 44096_{9/2}$
3000.845	15	3	33314.235	$19248^{\circ}_{5/2} - 52562_{7/2}$	2982.003	40	5	33524.724	$6691^{\circ}_{3/2} - 40216_{5/2}$
3000.814	3		33314.579	$12485^{\circ}_{7/2} - 45800_{5/2}$	2981.843	100	25	33526.523	$9720^{\circ}_{7/2} - 43246_{7/2}$
3000.627	3	2	33316.655	$9202^{\circ}_{7/2} - 42518_{7/2}$	2981.550	15g	4	33529.818	$14790^{\circ}_{7/2} - 48320_{5/2}$
2999.962	1		33324.040	$20686^{\circ}_{5/2} - 54010_{7/2}$	2981.492	200	100	33530.470	$8378^{\circ}_{7/2} - 41909_{9/2}$
				$14545^{\circ}_{5/2} - 47869_{3/2}$	2981.399	100	25	33531.516	$6691^{\circ}_{3/2} - 40222_{3/2}$
2999.801	100	100	33325.828	$14545^{\circ}_{5/2} - 47871_{7/2}$	2981.337	100	40	33532.213	$6168^{\circ}_{7/2} - 39700_{5/2}$
2999.272	75	10	33331.706	$4490^{\circ}_{5/2} - 37821_{3/2}$	2981.139	3		33534.440	$20310^{\circ}_{5/2} - 53845_{5/2}$
2999.094	400	150	33333.684	$11116^{\circ}_{7/2} - 44450_{9/2}$	2980.335	150	25	33543.486	$9400_{5/2} - 42944^{\circ}_{7/2}$
2998.611	8		33339.053	$1859_{3/2} - 35198^{\circ}_{1/2}$	2980.185	15		33545.174	$15144^{\circ}_{3/2} - 48689_{3/2}$
2997.871	1	1	33347.282	$15144^{\circ}_{3/2} - 48492_{5/2}$					$17722^{\circ}_{9/2} - 51268_{7/2}$
2997.819	2	3	33347.861	$23730^{\circ}_{9/2} - 57078_{9/2}$	2979.837	8	2	33549.092	$9202^{\circ}_{7/2} - 42751_{7/2}$
2997.354	2		33353.034	$13818^{\circ}_{7/2} - 47171_{9/2}$	2978.860	2		33560.094	$23518^{\circ}_{7/2} - 57078_{9/2}$
2997.327	1		33353.334	$18816^{\circ}_{13/2} - 52170_{11/2}$	2978.564	2		33563.429	$16906^{\circ}_{7/2} - 50470_{9/2}$
2996.986	200s	100	33357.129	$9061_{5/2} - 42418^{\circ}_{3/2}$	2978.497	3		33564.184	$17460^{\circ}_{5/2} - 51024_{3/2}$
2996.911	5	4	33357.964	$15710^{\circ}_{3/2} - 49068_{5/2}$	2977.030	8	2	33580.723	$11725^{\circ}_{1/2} - 45306_{3/2}$
2996.829	1		33358.877	$17272^{\circ}_{9/2} - 50631_{11/2}$	2976.648	100	10	33585.032	$12570_{7/2} - 46155^{\circ}_{5/2}$
2996.561	1		33361.860	$12902^{\circ}_{3/2} - 46264_{3/2}$	2976.497	8b		33586.736	$6691^{\circ}_{3/2} - 40278_{3/2}$
2996.216	8		33365.701	$15324^{\circ}_{1/2} - 48689_{3/2}$	2976.320	2		33588.733	$18973^{\circ}_{7/2} - 52562_{7/2}$
2995.270	50	15	33376.239	$9720^{\circ}_{7/2} - 43096_{5/2}$	2976.019	200	75	33592.130	$7331^{\circ}_{5/2} - 40923_{5/2}$
2994.980	1		33379.470	$17983^{\circ}_{5/2} - 51362_{5/2}$	2974.860	4		33605.217	$10572^{\circ}_{9/2} - 44177_{11/2}$
2994.585	8	2	33383.873	$6168^{\circ}_{7/2} - 39552_{9/2}$	2974.418	10	1	33610.211	$4146_{7/2} - 37756^{\circ}_{7/2}$
2994.283	1		33387.240	$11116^{\circ}_{7/2} - 44503_{7/2}$	2974.091	75	20	33613.906	$8605_{5/2} - 42219^{\circ}_{5/2}$
2993.801	400	200	33392.615	$13468^{\circ}_{9/2} - 46861_{11/2}$	2974.011	500	100	33614.810	$4490^{\circ}_{5/2} - 38105_{5/2}$
2993.631	150	100	33394.511	$10379_{9/2} - 43773^{\circ}_{7/2}$	2973.926	2	2	33615.771	$15453^{\circ}_{7/2} - 49068_{5/2}$
2991.696	100	75	33416.110	$12488^{\circ}_{9/2} - 45904_{9/2}$	2973.536	400	100	33620.180	$10189^{\circ}_{11/2} - 43809_{9/2}$
2991.461	1		33418.735	$12485^{\circ}_{7/2} - 45904_{9/2}$	2972.895	8b	4	33627.429	$10673^{\circ}_{5/2} - 44300_{3/2}$
2991.062	400b	75	33423.192	$4146_{7/2} - 37569^{\circ}_{9/2}$	2972.224	400b	100	33635.020	$1521_{3/2} - 35156^{\circ}_{5/2}$
2989.907	50	15	33436.103	$11116^{\circ}_{7/2} - 44552_{5/2}$	2971.481	400	40	33643.430	$4113_{3/2} - 37756^{\circ}_{7/2}$
2989.599	1		33439.548	$18214^{\circ}_{3/2} - 51653_{1/2}$	2970.632	20		33653.045	$7001_{3/2} - 40654^{\circ}_{5/2}$
2989.537	3		33440.241	$20080^{\circ}_{7/2} - 53520_{9/2}$	2970.066	10	3	33659.457	$9585^{\circ}_{5/2} - 43244_{3/2}$
2988.232	500b	200	33454.845	$4490^{\circ}_{5/2} - 37945_{5/2}$	2970.011	10	2	33660.081	$7331^{\circ}_{5/2} - 40991_{3/2}$
2987.350	8	2	33464.721	$1521_{3/2} - 34986^{\circ}_{5/2}$	2969.892	50b	8	33661.429	$9585^{\circ}_{5/2} - 43246_{7/2}$
2986.786	100b	40	33471.040	$7001_{3/2} - 40472^{\circ}_{5/2}$	2969.378	100	8	33667.256	$6700^{\circ}_{9/2} - 40367_{9/2}$
2985.815	2		33481.925	$22014^{\circ}_{11/2} - 55496_{9/2}$	2969.064	75	8	33670.816	$9711_{7/2} - 43382^{\circ}_{5/2}$
2985.321	1b		33487.465	$19248^{\circ}_{5/2} - 52735_{3/2}$	2968.687	800	150	33675.092	$4490^{\circ}_{5/2} - 38165_{7/2}$
2985.243	400	75	33488.340	$4113_{3/2} - 37601^{\circ}_{3/2}$	2968.348	10l	1	33678.938	$12902^{\circ}_{3/2} - 46581_{5/2}$
2984.774	10b		33493.602	$12902^{\circ}_{3/2} - 46395_{3/2}$	2967.823	10l	4	33684.895	$19050^{\circ}_{3/2} - 52735_{3/2}$
2984.765	8b	8	33493.703	$15324^{\circ}_{1/2} - 48817_{3/2}$	2967.254	8	2	33691.354	$11116^{\circ}_{7/2} - 44807_{7/2}$
2984.642	8	3	33495.083	$15349^{\circ}_{11/2} - 48844_{9/2}$	2966.561	2		33699.224	$20310^{\circ}_{5/2} - 54010_{7/2}$
2984.145	3	2	33500.661	$16906^{\circ}_{7/2} - 50407_{7/2}$	2966.530	5		33699.576	$4146_{7/2} - 37846^{\circ}_{5/2}$
2984.090	4	3	33501.279	$17722^{\circ}_{9/2} - 51224_{9/2}$	2966.423	5		33700.792	$12902^{\circ}_{3/2} - 46603_{5/2}$
2983.979	2		33502.525	$15786_{5/2} - 49289^{\circ}_{5/2}$	2966.405	2		33700.996	$14790^{\circ}_{7/2} - 48492_{5/2}$

TABLE 3. *Classified lines of* Th II—Continued

Wavelength Å	Intensity		Wavenumber cm^{-1}	Classification	Wavelength Å	Intensity		Wavenumber cm^{-1}	Classification
	Lamp	Spark				Lamp	Spark		
2966.282	2		33702.394	$13468^{\circ}_{9/2} - 47171_{9/2}$	2950.576	10	50	33881.785	$4490^{\circ}_{5/2} - 38372_{3/2}$
2966.005	4		33705.541	$22685^{\circ}_{7/2} - 56391_{5/2}$	2950.437	200	300	33883.381	$9061_{5/2} - 42944^{\circ}_{7/2}$
2965.500	300	75	33711.281	$6700^{\circ}_{9/2} - 40411_{7/2}$	2950.150	1		33886.677	$9400_{5/2} - 43287^{\circ}_{3/2}$
2965.118	75	10	33715.624	$10673^{\circ}_{5/2} - 44388_{3/2}$	2949.930	300	300	33889.204	$9238^{\circ}_{9/2} - 43127_{11/2}$
2964.924	200	50	33717.829	$9238^{\circ}_{9/2} - 42955_{9/2}$	2949.487	10	25	33894.294	$9202^{\circ}_{7/2} - 43096_{5/2}$
2964.624	2		33721.242	$18214^{\circ}_{3/2} - 51935_{5/2}$	2949.240	50	150	33897.133	$12488^{\circ}_{9/2} - 46385_{7/2}$
2964.112	100b	20	33727.066	$6168^{\circ}_{7/2} - 39895_{9/2}$	2949.068	500	300	33899.109	$4490^{\circ}_{5/2} - 38389_{7/2}$
2964.005	75	15	33728.283	$12488^{\circ}_{9/2} - 46216_{11/2}$	2948.793	8	100	33902.271	$17460^{\circ}_{5/2} - 51362_{5/2}$
2963.876	50	20	33729.751	$11576^{\circ}_{3/2} - 45306_{3/2}$	2948.711	1		33903.213	$17121^{\circ}_{3/2} - 51024_{3/2}$
2963.608	75	8	33732.801	$4113_{5/2} - 37846^{\circ}_{5/2}$	2948.518	2	2	33905.432	$16564^{\circ}_{11/2} - 50470_{9/2}$
2963.046	5	2	33739.199	$18568^{\circ}_{7/2} - 52307_{3/2}$	2948.362	5	50	33907.226	$10189^{\circ}_{11/2} - 44096_{9/2}$
2961.842	1		33752.914	$14545^{\circ}_{5/2} - 48298_{7/2}$	2948.332	4	1	33907.571	$14545^{\circ}_{5/2} - 48453_{7/2}$
2961.783	4b		33753.586	$9202^{\circ}_{7/2} - 42955_{9/2}$	2947.843	8	150	33913.196	$12472^{\circ}_{5/2} - 46385_{7/2}$
2961.273	8		33759.399	$8460_{3/2} - 42219^{\circ}_{5/2}$					$13818^{\circ}_{7/2} - 47731_{9/2}$
2960.806	5		33764.724	$20080^{\circ}_{7/2} - 53845_{5/2}$	2946.922	2		33923.794	$12472^{\circ}_{3/2} - 46395_{3/2}$
2960.779	15	5	33765.032	$12488^{\circ}_{9/2} - 46253_{9/2}$	2946.896	4	25	33924.094	$15144^{\circ}_{3/2} - 49068_{5/2}$
2960.549	2b		33767.654	$12485^{\circ}_{7/2} - 46253_{9/2}$	2946.607	20	200	33927.421	$16033^{\circ}_{5/2} - 49960_{7/2}$
2960.536	5b		33767.803	$14101^{\circ}_{7/2} - 47869_{3/2}$	2946.231	10		33931.750	$10572^{\circ}_{9/2} - 44503_{7/2}$
2959.934	8		33774.670	$15710^{\circ}_{3/2} - 49485_{1/2}$	2945.899	5		33935.574	$12219_{3/2} - 46155^{\circ}_{5/2}$
				$15349^{\circ}_{11/2} - 49124_{11/2}$	2944.950	75	150	33946.509	$14545^{\circ}_{5/2} - 48492_{5/2}$
2959.883	15	100b	33775.252	$14545^{\circ}_{5/2} - 48320_{5/2}$	2944.471	10	150b	33952.031	$17272^{\circ}_{9/2} - 51224_{9/2}$
2959.449	4		33780.205	$25607^{\circ}_{5/2} - 59387_{7/2}$	2944.448	4		33952.297	$17983^{\circ}_{5/2} - 51935_{5/2}$
2959.275	10	75	33782.191	$11116^{\circ}_{7/2} - 44898_{7/2}$	2944.391	5	3	33952.954	$6691^{\circ}_{3/2} - 40644_{5/2}$
2958.565	8	200	33790.298	$21131^{\circ}_{3/2} - 54922_{3/2}$	2943.962	25	75	33957.901	$8460_{3/2} - 42418^{\circ}_{5/2}$
2958.409	10	50	33792.080	$12472^{\circ}_{5/2} - 46264_{3/2}$	2943.867	3		33958.997	$17722^{\circ}_{9/2} - 51681_{9/2}$
2958.139	200b	200	33795.164	$10855_{7/2} - 44650^{\circ}_{7/2}$	2943.210	8	10	33966.577	$10855_{7/2} - 44821^{\circ}_{5/2}$
2957.916	300	400	33797.712	$12570_{7/2} - 46368^{\circ}_{9/2}$	2942.860	800h	500h	33970.617	$6213_{9/2} - 40184^{\circ}_{7/2}$
2957.580	500	500	33801.551	$4490^{\circ}_{5/2} - 38291_{7/2}$	2942.628	200b	200	33973.295	$8378^{\circ}_{7/2} - 42352_{5/2}$
2957.059	10	150	33807.506	$17460^{\circ}_{5/2} - 51268_{7/2}$	2941.890	75	200	33981.817	$9400_{5/2} - 43382^{\circ}_{5/2}$
2956.631	40	150	33812.400	$8605_{5/2} - 42418^{\circ}_{3/2}$	2941.337	100	200	33988.206	$10189^{\circ}_{11/2} - 44177_{11/2}$
2956.484	1		33814.081	$21682^{\circ}_{7/2} - 55496_{9/2}$	2940.674	100	300	33995.868	$17272^{\circ}_{9/2} - 51268_{7/2}$
2956.257	8	2	33816.678	$15305_{9/2} - 49121^{\circ}_{7/2}$	2940.587	100	300	33996.874	$7331^{\circ}_{5/2} - 41328_{5/2}$
2955.847	100	200	33821.368	$8378^{\circ}_{7/2} - 42200_{9/2}$	2940.303	10	50	34000.158	$12902^{\circ}_{3/2} - 46902_{5/2}$
2955.601	100s	300	33824.183	$7001_{3/2} - 40825^{\circ}_{7/2}$	2939.616	75b	300	34008.103	$15349^{\circ}_{11/2} - 49357_{11/2}$
2955.255	2		33828.143	$18118_{3/2} - 51946^{\circ}_{5/2}$	2939.555	100b	300	34008.809	$9238^{\circ}_{9/2} - 43246_{7/2}$
2955.036	150	300	33830.650	$10673^{\circ}_{5/2} - 44503_{7/2}$	2938.336	10	75	34022.917	$14275^{\circ}_{9/2} - 48298_{7/2}$
2954.887	100	200	33832.356	$6691^{\circ}_{3/2} - 40523_{1/2}$	2938.104	100	150	34025.604	$9202^{\circ}_{7/2} - 43227_{5/2}$
2954.369	8h	2	33838.287	$17837^{\circ}_{1/2} - 51676_{3/2}$	2937.441	100b	300	34033.283	$12902^{\circ}_{3/2} - 46935_{3/2}$
2954.218	3		33840.017	$16033^{\circ}_{5/2} - 49873_{5/2}$	2937.361	20	200	34034.210	$11576^{\circ}_{3/2} - 45610_{5/2}$
2953.917	5	1	33843.465	$8378^{\circ}_{7/2} - 42222_{7/2}$	2936.467	400b	500b	34044.571	$9202^{\circ}_{7/2} - 43246_{7/2}$
2953.595	10	100	33847.154	$17983^{\circ}_{5/2} - 51830_{7/2}$	2936.192	400	300	34047.760	$6168^{\circ}_{7/2} - 40216_{5/2}$
2952.584	4	2	33858.743	$20310^{\circ}_{5/2} - 54169_{7/2}$	2935.812	40	200	34052.166	$9720^{\circ}_{7/2} - 43772_{5/2}$
2952.129	50	200	33863.962	$12488^{\circ}_{9/2} - 46352_{7/2}$	2935.752	20	100	34052.862	$15236_{3/2} - 49289^{\circ}_{5/2}$
2951.902	20	50	33866.566	$12485^{\circ}_{7/2} - 46352_{7/2}$	2935.658	50	200	34053.953	$14790^{\circ}_{7/2} - 48844_{9/2}$
2951.562	25	150	33870.467	$6700^{\circ}_{9/2} - 40570_{7/2}$	2934.992	150	200	34061.680	$9711_{7/2} - 43773^{\circ}_{7/2}$
2951.203	200	300	33874.587	$6700^{\circ}_{9/2} - 40574_{11/2}$	2934.578	5	20	34066.485	$16564^{\circ}_{11/2} - 50631_{11/2}$
2951.052	4	75l	33876.320	$20969^{\circ}_{7/2} - 54845_{9/2}$	2934.507	5	50	34067.309	$12488^{\circ}_{9/2} - 46555_{11/2}$
2950.883	4		33878.260	$10572^{\circ}_{9/2} - 44450_{9/2}$	2934.135	200	200	34071.628	$1521_{3/2} - 35593^{\circ}_{7/2}$
2950.769	10	50	33879.569	$10673^{\circ}_{5/2} - 44552_{5/2}$	2934.012	10	100	34073.056	$11116^{\circ}_{7/2} - 45189_{5/2}$
2950.725	10	50	33880.074	$12472^{\circ}_{5/2} - 46352_{7/2}$	2933.099	200b	200	34083.662	$9720^{\circ}_{7/2} - 43803_{7/2}$

TABLE 3. *Classified lines of* Th II—Continued

Wavelength Å	Intensity		Wavenumber cm^{-1}	Classification	Wavelength Å	Intensity		Wavenumber cm^{-1}	Classification
	Lamp	Spark				Lamp	Spark		
2932.644	100	400	34088.950	$9720^{\circ}_{7/2} - 43809_{9/2}$	2916.429	10		34278.472	$11116^{\circ}_{7/2} - 45395_{7/2}$
2932.293	3		34093.030	$18214^{\circ}_{3/2} - 52307_{3/2}$	2915.926	3	2	34284.385	$7828_{1/2} - 42112^{\circ}_{3/2}$
2932.147	50	100	34094.727	$8018_{3/2} - 42112^{\circ}_{3/2}$	2915.536	3		34288.970	$17983^{\circ}_{5/2} - 52272_{7/2}$
2932.073	3	3	34095.588	$12485^{\circ}_{7/2} - 46581_{5/2}$	2914.582	50	20	34300.193	$6691^{\circ}_{3/2} - 40991_{3/2}$
2931.519	4		34102.031	$18816^{\circ}_{13/2} - 52918_{13/2}$	2914.342	300	100	34303.018	$22642^{\circ}_{9/2} - 56945_{11/2}$
2931.045	4h	2	34107.546	$17722^{\circ}_{9/2} - 51830_{7/2}$	2913.097	3		34317.678	$16906^{\circ}_{7/2} - 51224_{9/2}$
2930.911	300*	300	34109.105	$12472^{\circ}_{5/2} - 46581_{5/2}$	2912.756	150	200	34321.695	$9061_{5/2} - 43382^{\circ}_{5/2}$
2930.190	5	10	34117.497	$12485^{\circ}_{7/2} - 46603_{5/2}$	2912.661	100	75	34322.814	$4113_{3/2} - 38436^{\circ}_{3/2}$
2929.297	100	150	34127.898	$14484^{\circ}_{11/2} - 48612_{13/2}$	2912.328	3		34326.739	$10572^{\circ}_{9/2} - 44898_{7/2}$
2929.027	1		34131.044	$12472^{\circ}_{5/2} - 46603_{5/2}$	2912.009	400b	200	34330.499	$0_{3/2} - 34330^{\circ}_{1/2}$
2928.254	600	500	34140.053	$8378^{\circ}_{7/2} - 42518_{7/2}$	2911.321	200	150	34338.611	$8605_{5/2} - 42944^{\circ}_{7/2}$
2927.883	5b	25	34144.379	$14545^{\circ}_{5/2} - 48689_{3/2}$	2911.137	4	3	34340.782	$15144^{\circ}_{5/2} - 49485_{1/2}$
2926.956	15	50	34155.192	$10572^{\circ}_{9/2} - 44727_{11/2}$	2910.747	20	20	34345.383	$7331^{\circ}_{5/2} - 41676_{3/2}$
2926.831	10		34156.651	$7331^{\circ}_{5/2} - 41488_{7/2}$	2910.596	400l	300	34347.164	$4146_{7/2} - 38493^{\circ}_{5/2}$
2926.435	10	50	34161.273	$15324^{\circ}_{1/2} - 49485_{1/2}$	2909.767	25	40	34356.950	$7331^{\circ}_{5/2} - 41688_{7/2}$
2926.349	5	3	34162.277	$15710^{\circ}_{3/2} - 49873_{3/2}$	2909.456	8	15	34360.622	$14484^{\circ}_{11/2} - 48844_{9/2}$
2925.903	3		34167.484	$18568^{\circ}_{1/2} - 52735_{3/2}$	2909.378	8	5	34361.543	$16906^{\circ}_{7/2} - 51268_{7/2}$
2925.051	600b	600	34177.436	$15349^{\circ}_{11/2} - 49527_{13/2}$	2908.984	10	50	34366.197	$10855_{7/2} - 45221^{\circ}_{5/2}$
2924.604	1		34182.659	$14349_{1/2} - 48532^{\circ}_{1/2}$	2908.672	4	10	34369.883	$17460^{\circ}_{5/2} - 51830_{7/2}$
2924.572	8	50b	34183.033	$20310^{\circ}_{5/2} - 54493_{5/2}$	2908.436	2g		34372.672	$9400_{5/2} - 43773^{\circ}_{7/2}$
2924.228	5	8	34187.054	$9585^{\circ}_{5/2} - 43772_{5/2}$	2908.383	10b		34373.298	$12488^{\circ}_{9/2} - 46861_{11/2}$
2924.103	75	100	34188.516	$13818^{\circ}_{7/2} - 48006_{9/2}$	2908.359	150b	100	34373.582	$4490^{\circ}_{5/2} - 38863_{5/2}$
2923.950	5b		34190.304	$15305_{9/2} - 49495^{\circ}_{9/2}$	2908.314	10b	50b	34374.114	$16033^{\circ}_{5/2} - 50407_{7/2}$
2923.199	4	3	34199.088	$6168^{\circ}_{7/2} - 40367_{9/2}$	2908.156	8	4	34375.981	$9720^{\circ}_{7/2} - 44096_{9/2}$
2922.990	100	100	34201.533	$8018_{3/2} - 42219^{\circ}_{5/2}$	2907.781	40	10	34380.414	$4113_{3/2} - 38493^{\circ}_{5/2}$
2922.799	150	150	34203.768	$12219_{3/2} - 46423^{\circ}_{3/2}$	2906.122	50	200	34400.040	$8018_{3/2} - 42418^{\circ}_{3/2}$
2922.602	300	300	34206.073	$12219_{3/2} - 46426^{\circ}_{1/2}$	2905.931	75	100	34402.301	$6168^{\circ}_{7/2} - 40570_{7/2}$
				$13468^{\circ}_{9/2} - 47675_{11/2}$	2905.745	4	8	34404.503	$17460^{\circ}_{5/2} - 51865_{5/2}$
2922.094	10	3	34212.020	$0_{3/2} - 34212^{\circ}_{5/2}$	2905.303	4	8	34409.737	$17272^{\circ}_{9/2} - 51681_{9/2}$
2921.802	3		34215.439	$17460^{\circ}_{5/2} - 51676_{3/2}$	2904.999	50	40	34413.338	$20080^{\circ}_{7/2} - 54493_{5/2}$
2921.622	200	300	34217.546	$13248_{9/2} - 47466^{\circ}_{11/2}$	2904.702	5	15	34416.856	$12485^{\circ}_{7/2} - 46902_{5/2}$
2921.534	100b	150	34218.58	$9585^{\circ}_{5/2} - 43803_{7/2}$	2904.429	5		34420.091	$15453^{\circ}_{7/2} - 49873_{5/2}$
2921.365	100	200	34220.56	$12485^{\circ}_{7/2} - 46706_{7/2}$	2904.267	10	50b	34422.011	$12902^{\circ}_{3/2} - 47324_{3/2}$
2921.083	75	100	34223.860	$11576^{\circ}_{3/2} - 45800_{5/2}$	2903.166	200	150	34435.064	$4146_{7/2} - 38581^{\circ}_{5/2}$
2920.932	200	200	34225.629	$10673^{\circ}_{5/2} - 44898_{7/2}$	2903.052	8	20	34436.416	$22642^{\circ}_{9/2} - 57078_{9/2}$
2920.856	5	3	34226.520	$9061_{5/2} - 43287^{\circ}_{3/2}$	2902.144	2	5	34447.190	$17722^{\circ}_{9/2} - 52170_{11/2}$
2920.717	8	5	34228.148	$6244_{1/2} - 40472^{\circ}_{3/2}$	2901.378	3		34456.284	$16906^{\circ}_{7/2} - 51362_{5/2}$
2920.369	150b	100	34232.227	$6691^{\circ}_{3/2} - 40923_{3/2}$	2900.772	4	10	34463.482	$12472^{\circ}_{5/2} - 46935_{3/2}$
2920.212	8	5	34234.067	$12472^{\circ}_{5/2} - 46706_{7/2}$	2900.367	5	8	34468.294	$4113_{3/2} - 38581^{\circ}_{5/2}$
2920.056	40	40	34235.896	$10572^{\circ}_{9/2} - 44807_{7/2}$	2899.720	600	400	34475.985	$6168^{\circ}_{7/2} - 40644_{5/2}$
2919.841	400	300	34238.417	$4490^{\circ}_{5/2} - 38728_{5/2}$	2899.369	50	150	34480.158	$13818^{\circ}_{7/2} - 48298_{7/2}$
2919.597	1		34241.279	$17121^{\circ}_{3/2} - 51362_{5/2}$	2898.729	1		34487.771	$15349^{\circ}_{11/2} - 49837_{9/2}$
2919.439	15b	8	34243.132	$6168^{\circ}_{7/2} - 40411_{7/2}$	2898.262	20	40	34493.327	$6213_{9/2} - 40706^{\circ}_{7/2}$
2919.175	20	100b	34246.228	$12902^{\circ}_{3/2} - 47148_{3/2}$	2898.202	10	15	34494.042	$11116^{\circ}_{7/2} - 45610_{5/2}$
2917.898	150	200	34261.215	$10189^{\circ}_{11/2} - 44450_{9/2}$	2897.493	3	5	34502.481	$13818^{\circ}_{7/2} - 48320_{5/2}$
2917.787	150	150b	34262.519	$13468^{\circ}_{9/2} - 47731_{9/2}$	2897.112	40b	20b	34507.019	$20989^{\circ}_{9/2} - 55496_{9/2}$
2917.411	800r	300	34266.934	$4490^{\circ}_{5/2} - 38757_{3/2}$	2897.069	75b	100b	34507.531	$15453^{\circ}_{7/2} - 49960_{7/2}$
2917.034	150	200	34271.363	$10379_{9/2} - 44650^{\circ}_{7/2}$	2896.315	4	10	34516.514	$10673^{\circ}_{5/2} - 45189_{5/2}$
2916.945	10	15	34272.408	$14545^{\circ}_{5/2} - 48817_{3/2}$	2895.913	2	5	34521.305	$18214^{\circ}_{3/2} - 52735_{3/2}$
2916.484	40	50	34277.825	$14790^{\circ}_{7/2} - 49068_{5/2}$	2895.747	4	10	34523.284	$14545^{\circ}_{5/2} - 49068_{5/2}$

TABLE 3. *Classified lines of* Th II – Continued

Wavelength Å	Intensity		Wavenumber cm^{-1}	Classification	Wavelength Å	Intensity		Wavenumber cm^{-1}	Classification
	Lamp	Spark				Lamp	Spark		
2895.370	1		34527.779	$20969^{\circ}_{9/2} - 55496_{9/2}$	2874.753	2	3	34775.392	$16906^{\circ}_{7/2} - 51681_{9/2}$
2895.136	300	150	34530.570	$1859_{3/2} - 36390^{\circ}_{3/2}$	2874.624	15	40	34776.952	$8605_{5/2} - 43382^{\circ}_{5/2}$
2894.988	3	75	34532.335	$17121^{\circ}_{3/2} - 51653_{1/2}$	2873.714	25b	75	34787.965	$6700^{\circ}_{9/2} - 41488_{7/2}$
2894.501	25b	20b	34538.145	$10189^{\circ}_{11/2} - 44727_{11/2}$	2873.168	2		34794.575	$19050^{\circ}_{3/2} - 53845_{5/2}$
2894.446	10	8	34538.801	$11725^{\circ}_{1/2} - 46264_{3/2}$	2872.441	2l		34803.381	$9585^{\circ}_{5/2} - 44388_{5/2}$
2893.747	2	5	34547.143	$18973^{\circ}_{7/2} - 53520_{9/2}$	2872.267	2		34805.489	$22139^{\circ}_{9/2} - 56945_{11/2}$
2893.157	3	5	34554.188	$10572^{\circ}_{9/2} - 45126_{9/2}$	2871.754	3		34811.706	$17460^{\circ}_{5/2} - 52272_{7/2}$
2892.815	1		34558.273	$17272^{\circ}_{9/2} - 51830_{7/2}$	2871.105	5	10	34819.575	$11576^{\circ}_{3/2} - 46395_{3/2}$
2892.171	50	100	34565.968	$9238^{\circ}_{9/2} - 43803_{7/2}$	2870.822	40	75	34823.007	$10572^{\circ}_{9/2} - 45395_{7/2}$
2891.815	150	100	34570.223	$9202^{\circ}_{7/2} - 43772_{5/2}$	2870.406	800r	300	34828.054	$1859_{3/2} - 36687^{\circ}_{5/2}$
2891.730	150	150	34571.239	$9238^{\circ}_{9/2} - 43809_{9/2}$	2870.285	8h	8	34829.522	$13468^{\circ}_{9/2} - 48298_{7/2}$
2891.249	300	300	34576.990	$22106_{5/2} - 56683^{\circ}_{7/2}$	2870.049	15	10	34832.386	$9720^{\circ}_{7/2} - 44552_{5/2}$
				$8378^{\circ}_{7/2} - 42955_{9/2}$	2869.916	100	200	34834.000	$10855_{7/2} - 45689^{\circ}_{7/2}$
2891.128	15	10	34578.438	$4490^{\circ}_{5/2} - 39068_{7/2}$	2869.528	2	3	34838.710	$12485^{\circ}_{7/2} - 47324_{5/2}$
2890.888	15	20	34581.308	$6244_{1/2} - 40825^{\circ}_{1/2}$	2868.679	40	100	34849.020	$8378^{\circ}_{7/2} - 43227_{5/2}$
2890.589	3		34584.885	$1859_{3/2} - 36444^{\circ}_{3/2}$	2868.416	5		34852.215	$12472^{\circ}_{5/2} - 47324_{3/2}$
2890.480	5b	10b	34586.189	$14790^{\circ}_{7/2} - 49377_{7/2}$	2867.920	5	10	34858.242	$9238^{\circ}_{9/2} - 44096_{9/2}$
2890.316	1		34588.151	$14101^{\circ}_{1/2} - 48689_{3/2}$	2867.120	5		34867.968	$8378^{\circ}_{7/2} - 43246_{7/2}$
2890.188	5	4	34589.683	$7828_{1/2} - 42418^{\circ}_{3/2}$	2867.067	10	5	34868.613	$1521_{5/2} - 36390^{\circ}_{3/2}$
2889.564	1		34597.152	$19248^{\circ}_{5/2} - 53845_{5/2}$	2867.029	5	5	34869.075	$14545^{\circ}_{5/2} - 49414_{3/2}$
2889.181	100r	25	34601.739	$9202^{\circ}_{7/2} - 43803_{7/2}$	2866.652	15	150	34873.660	$14484^{\circ}_{11/2} - 49357_{11/2}$
2888.904	5	5b	34605.056	$7331^{\circ}_{3/2} - 41936_{3/2}$	2866.407	25	20	34876.641	$4490^{\circ}_{5/2} - 39366_{5/2}$
2887.818	600	500	34618.069	$4146_{7/2} - 38764^{\circ}_{7/2}$	2865.242	15	20	34890.821	$7331^{\circ}_{5/2} - 42222_{7/2}$
2886.785	2	2	34630.456	$16033^{\circ}_{5/2} - 50663_{5/2}$	2864.980	2		34894.012	$9202^{\circ}_{7/2} - 44096_{9/2}$
2886.506	100	150	34633.803	$10855_{7/2} - 45489^{\circ}_{9/2}$	2864.657	50	200	34897.946	$17837^{\circ}_{7/2} - 52735_{3/2}$
2886.242	100	100	34636.971	$6691^{\circ}_{3/2} - 41328_{5/2}$					$17272^{\circ}_{9/2} - 52170_{11/2}$
2885.968	5	10	34640.260	$14484^{\circ}_{11/2} - 49124_{11/2}$	2863.069	1		34917.301	$24381_{7/2} - 59299^{\circ}_{5/2}$
2885.048	800	500	34651.305	$4113_{5/2} - 38764^{\circ}_{7/2}$	2862.732	1		34921.412	$19248^{\circ}_{5/2} - 54169_{7/2}$
2884.289	600	400	34660.423	$4490^{\circ}_{5/2} - 39150_{3/2}$	2862.646	3		34922.461	$8460_{3/2} - 43382^{\circ}_{5/2}$
2883.618	50b	20	34668.488	$9720^{\circ}_{7/2} - 44388_{5/2}$	2862.610	300r	20	34922.900	$1521_{5/2} - 36444^{\circ}_{3/2}$
2883.446	5	4	34670.556	$11725^{\circ}_{1/2} - 46395_{3/2}$	2862.527	8b	75	34923.912	$16906^{\circ}_{7/2} - 51830_{7/2}$
2883.184	2		34673.707	$13818^{\circ}_{7/2} - 48492_{5/2}$	2862.007	5		34930.257	$22014^{\circ}_{11/2} - 56945_{11/2}$
2882.959	2		34676.412	$12472^{\circ}_{5/2} - 47148_{3/2}$	2861.442	8b		34937.154	$10189^{\circ}_{11/2} - 45126_{9/2}$
2882.511	100	50	34681.802	$8605_{5/2} - 43287^{\circ}_{3/2}$	2861.415	300	300	34937.484	$10673^{\circ}_{5/2} - 45610_{5/2}$
2882.402	1		34683.113	$12488^{\circ}_{9/2} - 47171_{9/2}$	2861.331	100b	150b	34938.509	$9711_{7/2} - 44650^{\circ}_{7/2}$
2882.354	8	8	34683.691	$11116^{\circ}_{7/2} - 45800_{5/2}$	2861.271	15b	25b	34939.242	$9238^{\circ}_{9/2} - 44177_{11/2}$
2882.191	1		34685.652	$12485^{\circ}_{7/2} - 47171_{9/2}$	2859.691	1		34958.545	$16906^{\circ}_{7/2} - 51865_{5/2}$
2882.008	300s	300	34687.854	$11576^{\circ}_{3/2} - 46264_{3/2}$	2858.979	5	3	34967.251	$12902^{\circ}_{3/2} - 47869_{3/2}$
2881.137	100	150	34698.341	$6700^{\circ}_{9/2} - 41398_{9/2}$					$9585^{\circ}_{5/2} - 44552_{5/2}$
2880.803	1		34702.363	$16033^{\circ}_{5/2} - 50735_{3/2}$	2858.915	15	10	34968.034	$4490^{\circ}_{5/2} - 39458_{7/2}$
2880.313	1		34708.267	$21682^{\circ}_{7/2} - 56391_{5/2}$	2857.599	2	3	34984.137	$13468^{\circ}_{9/2} - 48453_{7/2}$
2879.958	2		34712.545	$9061_{3/2} - 43773^{\circ}_{7/2}$	2857.491	50	75	34985.459	$6691^{\circ}_{3/2} - 41676_{3/2}$
2879.531	40	75	34717.692	$8378^{\circ}_{7/2} - 43096_{3/2}$	2857.398	8	4	34986.597	$0_{3/2} - 34986^{\circ}_{3/2}$
2879.203	50b	20b	34721.647	$1859_{3/2} - 36581^{\circ}_{3/2}$	2857.262	2		34988.263	$6700^{\circ}_{9/2} - 41688_{7/2}$
2879.181	10b	10b	34721.912	$10673^{\circ}_{5/2} - 45395_{7/2}$	2856.300	2		35000.046	$17272^{\circ}_{9/2} - 52272_{7/2}$
2878.644	50b	75	34728.389	$15144^{\circ}_{3/2} - 49873_{3/2}$	2855.904	15b	100	35004.899	$11576^{\circ}_{3/2} - 46581_{3/2}$
2877.390	5		34743.523	$17121^{\circ}_{3/2} - 51865_{5/2}$	2855.867	10b	50b	35005.352	$7331^{\circ}_{5/2} - 42336_{5/2}$
2876.658	3		34752.364	$17983^{\circ}_{3/2} - 52735_{3/2}$	2854.918	10	100	35016.988	$15453^{\circ}_{7/2} - 50470_{9/2}$
2876.417	200b	150	34755.275	$6168^{\circ}_{7/2} - 40923_{5/2}$	2854.620	5	10	35020.643	$7331^{\circ}_{5/2} - 42352_{5/2}$
2875.641	25	200	34764.654	$20080^{\circ}_{7/2} - 54845_{9/2}$	2854.297	2		35024.606	$15710^{\circ}_{3/2} - 50735_{3/2}$

TABLE 3. *Classified lines of* Th II—Continued

Wavelength Å	Intensity		Wavenumber cm^{-1}	Classification	Wavelength Å	Intensity		Wavenumber cm^{-1}	Classification
	Lamp	Spark				Lamp	Spark		
2854.134	100	200	35026.606	$13818^{\circ}_{7/2} - 48844_{9/2}$	2832.314	1000r	400	35296.436	$4146_{7/2} - 39443^{\circ}_{9/2}$
2853.933	2		35029.073	$16906^{\circ}_{7/2} - 51935_{5/2}$	2832.012	10	25	35300.200	$10855_{7/2} - 46155^{\circ}_{5/2}$
2853.338	1		35036.377	$18973^{\circ}_{7/2} - 54010_{7/2}$	2831.206	15	100b	35310.249	$10379_{9/2} - 45689^{\circ}_{7/2}$
2852.799	1		35042.996	$14484^{\circ}_{11/2} - 49527_{13/2}$	2830.997	3		35312.855	$14101^{\circ}_{1/2} - 49414_{3/2}$
2852.501	15	150	35046.657	$14790^{\circ}_{7/2} - 49837_{9/2}$	2830.955	3		35313.380	$9585^{\circ}_{5/2} - 44898_{7/2}$
2851.443	200	150	35059.660	$1521_{5/2} - 36581^{\circ}_{3/2}$	2830.905	1		35314.003	$15710^{\circ}_{3/2} - 51024_{3/2}$
2851.260	600r	300	35061.910	$1521_{5/2} - 36583^{\circ}_{7/2}$	2830.683	5	8	35316.772	$6691^{\circ}_{3/2} - 42008_{1/2}$
2849.592	2	2	35082.433	$14275^{\circ}_{9/2} - 49357_{11/2}$	2830.441	200	150	35319.792	$6168^{\circ}_{7/2} - 41488_{7/2}$
2849.169	8		35087.641	$9720^{\circ}_{7/2} - 44807_{7/2}$	2829.932	25	100	35326.144	$11576^{\circ}_{3/2} - 46902_{5/2}$
2848.686	1		35093.590	$21297^{\circ}_{5/2} - 56391_{5/2}$	2829.645	3		35329.727	$16033^{\circ}_{5/2} - 51362_{5/2}$
2848.013	10b	75	35101.882	$17460^{\circ}_{5/2} - 52562_{7/2}$	2829.433	20	50	35332.374	$10572^{\circ}_{9/2} - 45904_{9/2}$
2847.890	2		35103.398	$21131^{\circ}_{3/2} - 56235_{3/2}$	2827.988	100	150	35350.427	$9202^{\circ}_{7/2} - 44552_{5/2}$
2847.354	150	200	35110.006	$10379_{9/2} - 45489^{\circ}_{9/2}$	2827.755	20	150	35353.339	$14484^{\circ}_{11/2} - 49837_{9/2}$
2847.231	5b		35111.523	$7001_{3/2} - 42112^{\circ}_{3/2}$	2827.280	10	75	35359.279	$11576^{\circ}_{3/2} - 46935_{3/2}$
2846.757	1		35117.369	$16564^{\circ}_{11/2} - 51681_{9/2}$	2826.855	500	200	35364.594	$8018_{3/2} - 43382^{\circ}_{5/2}$
2846.531	15	50	35120.157	$15349^{\circ}_{11/2} - 50470_{9/2}$	2825.941	15b	100	35376.032	$13468^{\circ}_{9/2} - 48844_{9/2}$
2845.966	3		35127.129	$10673^{\circ}_{5/2} - 45800_{5/2}$	2825.375	25	100l	35383.119	$12488^{\circ}_{9/2} - 47871_{7/2}$
2845.835	15b	75	35128.746	$16818_{7/2} - 51946^{\circ}_{5/2}$	2825.172	10	5	35385.661	$12485^{\circ}_{7/2} - 47871_{7/2}$
2845.186	15	50	35136.758	$11116^{\circ}_{7/2} - 46253_{9/2}$	2824.536	8	2	35393.628	$8378^{\circ}_{7/2} - 43772_{5/2}$
2843.553	8	2	35156.936	$0_{3/2} - 35156^{\circ}_{5/2}$	2824.365	1		35395.771	$21682^{\circ}_{7/2} - 57078_{9/2}$
2843.304	15b	75b	35160.015	$6168^{\circ}_{7/2} - 41328_{5/2}$	2824.232	8	10	35397.438	$12472^{\circ}_{3/2} - 47869_{3/2}$
2843.056	10	20	35163.081	$10572^{\circ}_{9/2} - 45735_{11/2}$	2824.091	4		35399.205	$12472^{\circ}_{5/2} - 47871_{7/2}$
2842.812	800	200	35166.099	$1521_{5/2} - 36687^{\circ}_{5/2}$	2823.553	50	100	35405.950	$9720^{\circ}_{7/2} - 45126_{9/2}$
2842.674	20	50	35167.806	$8605_{5/2} - 43773^{\circ}_{7/2}$	2823.132	25	75	35411.229	$15324^{\circ}_{1/2} - 50735_{3/2}$
2842.530	2		35169.588	$14790^{\circ}_{7/2} - 49960_{7/2}$	2822.832	15	40	35414.992	$14545^{\circ}_{5/2} - 49960_{7/2}$
2841.811	200	50	35178.485	$9720^{\circ}_{7/2} - 44898_{7/2}$	2822.741	2		35416.134	$20080^{\circ}_{7/2} - 55496_{9/2}$
2841.162	200	200	35186.521	$9202^{\circ}_{7/2} - 44388_{5/2}$	2822.688	25	150	35416.799	$7001_{3/2} - 42418^{\circ}_{5/2}$
2841.087	8	3	35187.450	$7331^{\circ}_{5/2} - 42518_{7/2}$	2822.559	20	150	35418.418	$12902^{\circ}_{3/2} - 48320_{5/2}$
2840.154	200	150	35199.008	$0_{3/2} - 35198^{\circ}_{1/2}$	2822.446	15	50	35419.835	$7331^{\circ}_{5/2} - 42751_{7/2}$
2839.605	20	100	35205.813	$13406^{\circ}_{13/2} - 48612_{13/2}$	2822.407	10	10b	35420.325	$11725^{\circ}_{1/2} - 47145_{1/2}$
2839.335	25	40	35209.161	$6700^{\circ}_{9/2} - 41909_{9/2}$	2822.359	20	25	35420.927	$9400_{3/2} - 44821^{\circ}_{5/2}$
2839.240	200	150	35210.339	$4490^{\circ}_{5/2} - 39700_{5/2}$	2822.275	2		35421.982	$20969^{\circ}_{7/2} - 56391_{5/2}$
2839.084	10	10	35212.273	$9238^{\circ}_{9/2} - 44450_{9/2}$	2822.181	15b	75	35423.161	$11725^{\circ}_{1/2} - 47148_{3/2}$
2838.593	8	5	35218.364	$7001_{3/2} - 42219^{\circ}_{5/2}$	2822.025	200	200	35425.119	$8378^{\circ}_{7/2} - 43803_{7/2}$
2838.255	10	15	35222.558	$9585^{\circ}_{5/2} - 44807_{7/2}$	2821.602	100b	200	35430.430	$8378^{\circ}_{7/2} - 43809_{9/2}$
2837.886	3		35227.138	$15242^{\circ}_{9/2} - 50470_{9/2}$	2820.589	2		35443.154	$19050^{\circ}_{3/2} - 54493_{5/2}$
2837.641	10b	5	35230.179	$6168^{\circ}_{7/2} - 41398_{9/2}$	2820.335	200	150	35446.346	$6700^{\circ}_{9/2} - 42146_{11/2}$
2837.295	1000r	500	35234.475	$6213_{9/2} - 41447^{\circ}_{11/2}$	2819.322	200	200	35459.081	$7828_{1/2} - 43287^{\circ}_{3/2}$
2837.201	8b	5	35235.642	$11116^{\circ}_{7/2} - 46352_{7/2}$	2818.875	3	2	35464.704	$11116^{\circ}_{7/2} - 46581_{5/2}$
2836.593	2		35243.194	$12488^{\circ}_{9/2} - 47731_{9/2}$	2818.505	5		35469.359	$9720^{\circ}_{7/2} - 45189_{5/2}$
2836.435	75b	20	35245.157	$6691^{\circ}_{3/2} - 41936_{3/2}$	2817.135	20	50	35486.607	$11116^{\circ}_{7/2} - 46603_{5/2}$
2836.205	25	15	35248.015	$9202^{\circ}_{7/2} - 44450_{9/2}$	2816.927	20	50	35489.228	$9238^{\circ}_{9/2} - 44727_{11/2}$
2836.047	500	300	35249.979	$4146_{7/2} - 39396^{\circ}_{7/2}$	2816.070	100	150	35500.027	$6700^{\circ}_{9/2} - 42200_{9/2}$
2835.305	2		35259.203	$21131^{\circ}_{5/2} - 56391_{5/2}$	2815.312	5	4	35509.585	$9711_{7/2} - 45221^{\circ}_{5/2}$
2834.776	25	40	35265.783	$9238^{\circ}_{9/2} - 44503_{7/2}$	2815.050	10	15	35512.890	$10855_{7/2} - 46368^{\circ}_{9/2}$
2834.530	50	75	35268.843	$11116^{\circ}_{7/2} - 46385_{7/2}$	2814.576	50	150	35518.870	$15144^{\circ}_{3/2} - 50663_{3/2}$
2834.482	150	100	35269.441	$8018_{3/2} - 43287^{\circ}_{3/2}$	2814.480	25b	75	35520.081	$6168^{\circ}_{7/2} - 41688_{7/2}$
2834.025	3	3	35275.128	$17460^{\circ}_{5/2} - 52735_{3/2}$	2814.473	2b		35520.170	$18973^{\circ}_{7/2} - 54493_{3/2}$
2833.532	15	150	35281.265	$15349^{\circ}_{11/2} - 50631_{11/2}$	2814.319	300	200	35522.114	$6700^{\circ}_{9/2} - 42222_{7/2}$
2833.334	200	100	35283.730	$8460_{3/2} - 43744^{\circ}_{1/2}$	2812.424	15b	100	35546.047	$10189^{\circ}_{11/2} - 45735_{11/2}$

TABLE 3. *Classified lines of* Th II—Continued

Wavelength Å	Intensity		Wavenumber cm^{-1}	Classification	Wavelength Å	Intensity		Wavenumber cm^{-1}	Classification
	Lamp	Spark				Lamp	Spark		
2812.187	2		35549.042	$20686^{\circ}_{5/2} - 56235_{3/2}$	2788.687	10	50	35848.596	$12472^{\circ}_{5/2} - 48320_{5/2}$
2811.744	8b		35554.643	$6691^{\circ}_{3/2} - 42246_{1/2}$	2788.077	10	15	35856.439	$1859_{3/2} - 37716^{\circ}_{1/2}$
2811.413	5	10	35558.829	$13818^{\circ}_{7/2} - 49377_{7/2}$	2787.666	5	50	35861.725	$14545^{\circ}_{5/2} - 50407_{7/2}$
2811.157	3	5	35562.067	$14275^{\circ}_{9/2} - 49837_{9/2}$	2787.131	50	75	35868.608	$6244_{1/2} - 42112^{\circ}_{3/2}$
2810.580	4	20	35569.367	$11576^{\circ}_{3/2} - 47145_{1/2}$	2786.915	10	150	35871.388	$13250_{5/2} - 49121^{\circ}_{7/2}$
2810.358	4		35572.177	$11576^{\circ}_{3/2} - 47148_{3/2}$	2786.684	8	75	35874.362	$15349^{\circ}_{11/2} - 51224_{9/2}$
2809.460	1		35583.547	$15324^{\circ}_{7/2} - 50907_{3/2}$	2786.239	4	50	35880.091	$15144^{\circ}_{5/2} - 51024_{3/2}$
2808.996	200b	200	35589.424	$9061_{5/2} - 44650^{\circ}_{7/2}$	2785.603	4	20b	35888.282	$9238^{\circ}_{9/2} - 45126_{9/2}$
2808.894	8		35590.716	$15144^{\circ}_{3/2} - 50735_{3/2}$	2785.544	5	15b	35889.042	$13468^{\circ}_{9/2} - 49357_{11/2}$
2808.864	25	20	35591.096	$10673^{\circ}_{5/2} - 46264_{3/2}$	2784.975	15	75	35896.375	$7331^{\circ}_{5/2} - 43227_{5/2}$
2807.827	200	200	35604.240	$9585^{\circ}_{5/2} - 45189_{5/2}$	2784.060	8	75	35908.172	$10673^{\circ}_{5/2} - 46581_{3/2}$
2807.715	100	100	35605.661	$9202^{\circ}_{7/2} - 44807_{7/2}$	2783.924	5	10	35909.926	$15453^{\circ}_{7/2} - 51362_{5/2}$
2807.048	10	50	35614.121	$17121^{\circ}_{3/2} - 52735_{3/2}$	2783.662	0	15	35913.306	$7331^{\circ}_{5/2} - 43244_{3/2}$
2806.879	10	25	35616.265	$14790^{\circ}_{7/2} - 50407_{7/2}$	2783.489	10b	75	35915.537	$7828_{1/2} - 43744^{\circ}_{1/2}$
2805.721	4		35630.964	$18214^{\circ}_{3/2} - 53845_{5/2}$	2783.053	50	75	35921.164	$4490^{\circ}_{5/2} - 40411_{7/2}$
2804.652	10	3	35644.544	$10572^{\circ}_{9/2} - 46216_{11/2}$	2782.824	0	20	35924.119	$9202^{\circ}_{7/2} - 45126_{9/2}$
2804.580	10	3	35645.459	$6691^{\circ}_{3/2} - 42336_{5/2}$	2782.364	4	15	35930.058	$10673^{\circ}_{5/2} - 46603_{5/2}$
2803.760	2		35655.883	$16906^{\circ}_{7/2} - 52562_{7/2}$	2781.353	2	8	35943.118	$15710^{\circ}_{3/2} - 51653_{1/2}$
2803.376	50b	50	35660.767	$9238^{\circ}_{9/2} - 44898_{7/2}$	2780.694	15b	75	35951.636	$13406^{\circ}_{13/2} - 49357_{11/2}$
2802.278	40	20	35674.739	$9720^{\circ}_{7/2} - 45395_{7/2}$	2780.410	3	75	35955.308	$20989^{\circ}_{9/2} - 56945_{11/2}$
2801.938	50	25	35679.068	$10673^{\circ}_{5/2} - 46352_{7/2}$	2779.671	2b	10b	35964.867	$12488^{\circ}_{9/2} - 48453_{7/2}$
				$14790^{\circ}_{7/2} - 50470_{9/2}$	2779.646	1	10b	35965.190	$15710^{\circ}_{3/2} - 51676_{3/2}$
2801.766	8		35681.258	$10572^{\circ}_{9/2} - 46253_{9/2}$	2779.476	2	10	35967.389	$12485^{\circ}_{7/2} - 48453_{7/2}$
2800.569	200	100	35696.508	$9202^{\circ}_{7/2} - 44898_{7/2}$	2778.704	10	75	35977.382	$9711_{7/2} - 45689^{\circ}_{7/2}$
2800.249	10	15	35700.587	$15324^{\circ}_{7/2} - 51024_{3/2}$	2778.426	1	5	35980.981	$12472^{\circ}_{5/2} - 48453_{7/2}$
2799.334	0	8	35712.256	$10673^{\circ}_{5/2} - 46385_{7/2}$	2778.401	1	5	35981.305	$15242^{\circ}_{9/2} - 51224_{9/2}$
2799.110	50	75	35715.114	$4146_{7/2} - 39861^{\circ}_{5/2}$	2778.055	5b	15	35985.786	$14484^{\circ}_{11/2} - 50470_{9/2}$
2798.921	3	10	35717.525	$8378^{\circ}_{7/2} - 44096_{9/2}$	2778.020	10	25	35986.240	$1859_{3/2} - 37846^{\circ}_{5/2}$
2798.866	2	10	35718.227	$13406^{\circ}_{13/2} - 49124_{11/2}$	2777.929	3	50	35987.419	$9202^{\circ}_{7/2} - 45189_{5/2}$
2798.661	50	50	35720.843	$9585^{\circ}_{5/2} - 45306_{3/2}$	2777.807	0	4	35988.999	$10379_{9/2} - 46368^{\circ}_{9/2}$
2798.499	5	15	35722.911	$10673^{\circ}_{5/2} - 46395_{3/2}$	2776.470	0	4	36006.328	$12485^{\circ}_{7/2} - 48492_{5/2}$
2798.263	20	100	35725.924	$8018_{3/2} - 43744^{\circ}_{1/2}$	2776.196	3	5	36009.882	$8378^{\circ}_{7/2} - 44388_{5/2}$
2797.736	200	150	35732.653	$4490^{\circ}_{5/2} - 40222_{3/2}$	2775.459	0	75	36019.443	$13818^{\circ}_{7/2} - 49837_{9/2}$
2797.020	50	150	35741.800	$1859_{3/2} - 37601^{\circ}_{3/2}$	2774.840	10	75	36027.478	$10189^{\circ}_{11/2} - 46216_{11/2}$
2796.509	20	25	35748.330	$4113_{5/2} - 39861^{\circ}_{5/2}$	2774.498	20	8	36031.919	$6168^{\circ}_{7/2} - 42200_{9/2}$
2795.528	5	25	35760.874	$9061_{5/2} - 44821^{\circ}_{5/2}$	2774.411	1	5	36033.048	$10673^{\circ}_{5/2} - 46706_{7/2}$
2795.195	10	25	35765.134	$7331^{\circ}_{5/2} - 43096_{5/2}$	2774.065	50	50	36037.54	$4146_{7/2} - 40184^{\circ}_{7/2}$
2794.716	0	3	35771.264	$15453^{\circ}_{7/2} - 51224_{9/2}$	2773.951	5	75	36039.024	$13250_{5/2} - 49289^{\circ}_{5/2}$
2794.255	25	100	35777.165	$9711_{7/2} - 45489^{\circ}_{9/2}$	2773.523	3	8	36044.585	$8605_{5/2} - 44650^{\circ}_{7/2}$
2794.012	4	50	35780.277	$10572^{\circ}_{9/2} - 46352_{7/2}$	2773.022	10	25	36051.096	$6700^{\circ}_{9/2} - 42751_{7/2}$
2793.567	4	15p	35785.976	$11116^{\circ}_{7/2} - 46902_{5/2}$	2772.808	1	4	36053.879	$6168^{\circ}_{7/2} - 42222_{7/2}$
2793.432	1	8	35787.705	$12902^{\circ}_{3/2} - 48689_{3/2}$	2772.741	2	8	36054.750	$13818^{\circ}_{7/2} - 49873_{5/2}$
2792.674	2	8	35797.418	$16033^{\circ}_{5/2} - 51830_{7/2}$					$11116^{\circ}_{7/2} - 47171_{9/2}$
2791.670	3	10	35810.292	$12488^{\circ}_{9/2} - 48298_{7/2}$	2772.010	50	25	36064.257	$10189^{\circ}_{11/2} - 46253_{9/2}$
2791.432	8b	75	35813.345	$10572^{\circ}_{9/2} - 46385_{7/2}$	2771.515	50b	100b	36070.698	$4113_{5/2} - 40184^{\circ}_{7/2}$
2791.007	50	75	35818.799	$6700^{\circ}_{9/2} - 42518_{7/2}$	2771.469	20b	100b	36071.297	$8378^{\circ}_{7/2} - 44450_{9/2}$
2790.868	3	10	35820.582	$9400_{5/2} - 45221^{\circ}_{5/2}$	2770.815	75	100	36079.810	$1521_{5/2} - 37601^{\circ}_{3/2}$
2790.420	5	50	35826.333	$12472^{\circ}_{5/2} - 48298_{7/2}$	2770.134	2	20	36088.680	$20989^{\circ}_{9/2} - 57078_{9/2}$
2789.981	1	4	35831.970	$16033^{\circ}_{5/2} - 51865_{5/2}$	2768.841	50	150	36105.531	$6213_{9/2} - 42319^{\circ}_{9/2}$
2789.729	0	5	35835.206	$12485^{\circ}_{7/2} - 48320_{5/2}$	2768.106	0	3	36115.118	$20120^{\circ}_{5/2} - 56235_{3/2}$

530-326 OL - 74 - 10

TABLE 3. *Classified lines of* Th II—Continued

Wavelength Å	Intensity		Wavenumber cm^{-1}	Classification	Wavelength Å	Intensity		Wavenumber cm^{-1}	Classification
	Lamp	Spark				Lamp	Spark		
2767.884	3	15	36118.014	$14545^{\circ}_{5/2} - 50663_{5/2}$	2738.816	15	20	36501.327	$4490^{\circ}_{5/2} - 40991_{3/2}$
2767.669	0	4l	36120.820	$13406^{\circ}_{13/2} - 49527_{13/2}$	2738.324	20	50	36507.885	$4146_{7/2} - 40654^{\circ}_{5/2}$
2767.357	4	25	36124.892	$8378^{\circ}_{7/2} - 44503_{7/2}$	2738.224	1	10	36509.218	$15144^{\circ}_{3/2} - 51653_{1/2}$
2766.637	3	5	36134.293	$10572^{\circ}_{9/2} - 46706_{7/2}$	2738.119	1	8	36510.618	$17983^{\circ}_{3/2} - 54493_{5/2}$
2765.124	50	150	36154.064	$4490^{\circ}_{5/2} - 40644_{3/2}$	2737.422	15	75	36519.914	$8378^{\circ}_{7/2} - 44898_{7/2}$
2764.640	20	150	36160.393	$9061_{5/2} - 45221^{\circ}_{5/2}$	2737.185	0	3	36523.076	$18973^{\circ}_{7/2} - 55496_{9/2}$
2764.180	2	5b	36166.410	$12902^{\circ}_{3/2} - 49068_{5/2}$	2736.710	2	25	36529.415	$16033^{\circ}_{3/2} - 52562_{7/2}$
2763.605	50b	100	36173.934	$6244_{1/2} - 42418^{\circ}_{3/2}$	2736.439	8	20	36533.032	$9720^{\circ}_{7/2} - 46253_{9/2}$
2762.835	3	15l	36184.016	$9720^{\circ}_{7/2} - 45904_{9/2}$	2736.177	4	5	36536.530	$6691^{\circ}_{3/2} - 43227_{5/2}$
2762.402	8	25	36189.687	$10189^{\circ}_{11/2} - 46378_{13/2}$	2735.837	20	500	36541.070	$4113_{5/2} - 40654^{\circ}_{5/2}$
2762.041	1	3	36194.417	$14275^{\circ}_{9/2} - 50470_{9/2}$	2735.197	1	10	36549.620	$17460^{\circ}_{5/2} - 54010_{7/2}$
2761.021	2	8	36207.787	$11116^{\circ}_{7/2} - 47324_{5/2}$	2735.060	4	15	36551.451	$12570_{7/2} - 49121^{\circ}_{7/2}$
2760.391	20	200	36216.051	$8605_{5/2} - 44821^{\circ}_{5/2}$	2734.907	3	4	36553.495	$6691^{\circ}_{3/2} - 43244_{3/2}$
2759.720	3	15	36224.856	$15710^{\circ}_{3/2} - 51935_{5/2}$	2734.405	50	75	36560.206	$4146_{7/2} - 40706^{\circ}_{7/2}$
2759.405	5	75	36228.991	$15453^{\circ}_{7/2} - 51681_{9/2}$	2733.529	3	15	36571.922	$14790^{\circ}_{7/2} - 51362_{5/2}$
2758.958	15	15	36234.860	$1521_{5/2} - 37756^{\circ}_{7/2}$	2733.205	15	25	36576.257	$1859_{3/2} - 38436^{\circ}_{3/2}$
2757.900	0	8	36248.760	$17272^{\circ}_{9/2} - 53520_{9/2}$	2732.808	50	50	36581.570	$0_{3/2} - 36581^{\circ}_{3/2}$
2757.382	8	15	36255.569	$6700^{\circ}_{9/2} - 42955_{9/2}$	2732.702	15	50	36582.989	$6168^{\circ}_{7/2} - 42751_{7/2}$
2756.855	2	8	36262.499	$10673^{\circ}_{3/2} - 46935_{3/2}$	2731.918	10	25	36593.487	$4113_{5/2} - 40706^{\circ}_{7/2}$
2755.955	4	50	36274.341	$16033^{\circ}_{5/2} - 52307_{3/2}$	2730.308	8b	150b	36615.064	$11116^{\circ}_{7/2} - 47731_{9/2}$
2755.561	0	3	36279.527	$18214^{\circ}_{3/2} - 54493_{5/2}$	2730.261	15b	150b	36615.694	$8605_{5/2} - 45221^{\circ}_{5/2}$
2755.051	4	15	36286.243	$7001_{3/2} - 43287^{\circ}_{3/2}$	2729.327	15	150	36628.224	$9061_{5/2} - 45689^{\circ}_{7/2}$
2754.890	2	10	36288.363	$9400_{5/2} - 45689^{\circ}_{7/2}$	2729.053	4	5	36631.901	$9720^{\circ}_{7/2} - 46352_{7/2}$
2754.801	1	10	36289.536	$10572^{\circ}_{9/2} - 46861_{11/2}$	2728.909	20	25	36633.834	$1859_{3/2} - 38493^{\circ}_{5/2}$
2754.520	2	5b	36293.238	$11576^{\circ}_{3/2} - 47869_{3/2}$	2728.701	0	10b	36636.626	$9061_{3/2} - 45697^{\circ}_{3/2}$
2754.252	4	15	36296.769	$9400_{5/2} - 45697^{\circ}_{3/2}$	2727.578	0	3	36651.709	$13818^{\circ}_{7/2} - 50470_{9/2}$
2753.092	5	50	36312.061	$12219_{3/2} - 48532^{\circ}_{1/2}$	2727.231	5	20	36656.373	$9711_{7/2} - 46368^{\circ}_{9/2}$
2752.166	75	100	36324.279	$1521_{5/2} - 37846^{\circ}_{5/2}$	2726.482	15	75	36666.442	$9238^{\circ}_{9/2} - 45904_{9/2}$
2751.754	2	50	36329.717	$15324^{\circ}_{1/2} - 51653_{1/2}$	2726.027	2	10	36672.562	$10189^{\circ}_{11/2} - 46861_{11/2}$
2751.572	4	3	36332.120	$15349^{\circ}_{11/2} - 51681_{9/2}$	2725.559	4	15	36678.858	$9585^{\circ}_{5/2} - 46264_{3/2}$
2750.538	1	4	36345.777	$12472^{\circ}_{5/2} - 48817_{3/2}$	2724.881	50	200	36687.984	$0_{3/2} - 36687^{\circ}_{5/2}$
2750.174	2	4	36350.587	$6168^{\circ}_{7/2} - 42518_{7/2}$	2723.821	0	10d	36702.261	$9202^{\circ}_{7/2} - 45904_{9/2}$
2749.713	8	100	36356.681	$12488^{\circ}_{9/2} - 48844_{9/2}$	2723.416	0	5	36707.719	$18214^{\circ}_{3/2} - 54922_{3/2}$
2749.531	50	100	36359.088	$4113_{5/2} - 40472^{\circ}_{3/2}$	2723.317	4	75	36709.053	$17460^{\circ}_{5/2} - 54169_{7/2}$
2749.355	25	25	36361.415	$8460_{3/2} - 44821^{\circ}_{5/2}$	2722.571	0	10	36719.111	$12570_{7/2} - 49289^{\circ}_{5/2}$
2748.805	5	50b	36368.690	$13468^{\circ}_{9/2} - 49837_{9/2}$	2722.468	3	10	36720.500	$15144^{\circ}_{3/2} - 51865_{5/2}$
2748.137	2	10	36377.530	$15453^{\circ}_{7/2} - 51830_{7/2}$	2722.380	25b	50b	36721.687	$1859_{3/2} - 38581^{\circ}_{5/2}$
2747.847	8	50	36381.369	$7001_{3/2} - 43382^{\circ}_{5/2}$					$10189^{\circ}_{11/2} - 46910_{13/2}$
2747.586	3	50	36384.825	$17460^{\circ}_{5/2} - 53845_{5/2}$	2722.313	5	50	36722.591	$14545^{\circ}_{5/2} - 51268_{7/2}$
2747.156	75	100	36390.520	$0_{3/2} - 36390^{\circ}_{3/2}$	2722.216	0	20b	36723.899	$17121^{\circ}_{3/2} - 53845_{5/2}$
2745.527	25	25	36412.110	$15453^{\circ}_{7/2} - 51865_{5/2}$	2721.691	20	200b	36730.982	$6213_{9/2} - 42944^{\circ}_{7/2}$
2744.247	3	4	36429.093	$8378^{\circ}_{7/2} - 44807_{7/2}$	2721.172	1	5	36737.988	$17272^{\circ}_{9/2} - 54010_{7/2}$
2743.499	1	5	36439.025	$15242^{\circ}_{9/2} - 51681_{9/2}$	2721.022	0	4	36740.013	$14484^{\circ}_{11/2} - 51224_{9/2}$
2743.155	3b	10	36443.594	$9711_{7/2} - 46155^{\circ}_{5/2}$	2720.822	0	15	36742.713	$7001_{3/2} - 43744^{\circ}_{1/2}$
2743.063	50	50	36444.816	$0_{3/2} - 36444^{\circ}_{3/2}$	2720.687	0	4	36744.536	$11576^{\circ}_{3/2} - 48320_{5/2}$
2740.712	1	4	36476.077	$7331^{\circ}_{5/2} - 43807_{3/2}$	2720.627	0	10	36745.347	$22642^{\circ}_{9/2} - 59387_{7/2}$
2740.469	3	50	36479.311	$14545^{\circ}_{5/2} - 51024_{3/2}$	2720.471	5	15	36747.454	$8378^{\circ}_{7/2} - 45126_{9/2}$
2740.218	1	15	36482.653	$15453^{\circ}_{7/2} - 51935_{5/2}$	2719.929	15	75	36754.776	$11116^{\circ}_{7/2} - 47871_{7/2}$
2739.545	0	50	36491.614	$13468^{\circ}_{9/2} - 49960_{7/2}$	2719.449	4	25	36761.263	$8460_{3/2} - 45221^{\circ}_{5/2}$
2739.133	2	4	36497.103	$9238^{\circ}_{9/2} - 45735_{11/2}$	2717.251	3	15	36790.998	$15144^{\circ}_{3/2} - 51935_{5/2}$

TABLE 3. *Classified lines of* Th II—Continued

Wavelength Å	Intensity		Wavenumber cm^{-1}	Classification	Wavelength Å	Intensity		Wavenumber cm^{-1}	Classification
	Lamp	Spark				Lamp	Spark		
2716.578	5	25	36800.112	$9585^{\circ}_{5/2} - 46385_{7/2}$	2690.311	25	20	37159.392	$10572^{\circ}_{9/2} - 47731_{9/2}$
2716.328	50	100	36803.499	$19880_{9/2} - 56683^{\circ}_{7/2}$	2690.102	1	15b	37162.279	$13468^{\circ}_{9/2} - 50631_{11/2}$
				$8018_{3/2} - 44821^{\circ}_{5/2}$	2690.064	3	15b	37162.804	$15144^{\circ}_{3/2} - 52307_{3/2}$
2715.156	0	10b	36819.384	$15453^{\circ}_{7/2} - 52272^{\circ}_{7/2}$	2689.371	2	5	37172.379	$7331^{\circ}_{5/2} - 44503_{7/2}$
2715.082	8	100b	36820.387	$15349^{\circ}_{11/2} - 52170_{11/2}$	2688.667	3	15	37182.112	$9720^{\circ}_{7/2} - 46902_{5/2}$
2713.768	0	25b	36838.215	$4490^{\circ}_{5/2} - 41328_{5/2}$	2688.582	2	3	37183.287	$9202^{\circ}_{7/2} - 46385_{7/2}$
2713.243	4	50	36845.342	$13818^{\circ}_{7/2} - 50663_{5/2}$	2688.337	8	15	37186.676	$4490^{\circ}_{5/2} - 41676_{3/2}$
2712.084	3	20	36861.087	$9720^{\circ}_{7/2} - 46581_{5/2}$	2687.903	3	20	37192.679	$22106_{5/2} - 59299^{\circ}_{5/2}$
2711.448	15b	75	36869.733	$12488^{\circ}_{9/2} - 49357_{11/2}$	2687.533	3b	8b	37197.800	$14484^{\circ}_{11/2} - 51681_{9/2}$
2711.130	0	5s	36874.057	$22513^{\circ}_{5/2} - 59387_{7/2}$	2687.500	5	10b	37198.257	$10673^{\circ}_{5/2} - 47871_{7/2}$
2710.474	5	50	36882.981	$9720^{\circ}_{7/2} - 46603_{5/2}$	2687.125	50b	100	37203.447	$8018_{3/2} - 45221^{\circ}_{5/2}$
2710.034	2	25	36888.969	$12488^{\circ}_{9/2} - 49377_{7/2}$	2685.586	3	15	37224.766	$13406^{\circ}_{13/2} - 50631_{11/2}$
2709.934	2	8	36890.331	$11116^{\circ}_{7/2} - 48006_{9/2}$	2685.024	0	8b	37232.557	$8605_{5/2} - 45838^{\circ}_{3/2}$
2709.843	3	25	36891.569	$12485^{\circ}_{7/2} - 49377_{7/2}$	2684.669	5	8	37237.480	$8460_{3/2} - 45697^{\circ}_{3/2}$
2709.407	2	25l	36897.505	$17272^{\circ}_{9/2} - 54169_{7/2}$	2684.288	50	100	37242.765	$1521_{5/2} - 38764^{\circ}_{7/2}$
2708.176	50	100	36914.276	$1521_{5/2} - 38436^{\circ}_{3/2}$	2682.018	0	5	37274.285	$6691^{\circ}_{3/2} - 43965_{1/2}$
2708.071	5	25b	36915.707	$11576^{\circ}_{3/2} - 48492_{5/2}$	2680.210	3	10	37299.428	$10572^{\circ}_{9/2} - 47871_{7/2}$
2707.525	8	10	36923.152	$14101^{\circ}_{1/2} - 51024_{3/2}$	2678.934	15	50	37317.193	$9585^{\circ}_{5/2} - 46902_{5/2}$
2706.408	2	25	36938.390	$13468^{\circ}_{9/2} - 50407_{7/2}$	2678.752	0	20	37319.728	$15242^{\circ}_{9/2} - 52562_{7/2}$
2704.489	3	50	36964.598	$11725^{\circ}_{1/2} - 48689_{3/2}$	2677.544	2	10	37336.564	$11116^{\circ}_{7/2} - 48453_{7/2}$
2703.957	75	200	36971.871	$1521_{5/2} - 38493^{\circ}_{5/2}$	2676.623	3	25	37349.411	$12488^{\circ}_{9/2} - 49837_{9/2}$
2703.189	3	15	36982.374	$10189^{\circ}_{11/2} - 47171_{9/2}$	2676.559	3	25	37350.304	$9585^{\circ}_{5/2} - 46935_{3/2}$
2702.922	5	25	36986.027	$9720^{\circ}_{7/2} - 46706_{7/2}$	2676.440	3	25s	37351.964	$12485^{\circ}_{7/2} - 49837_{9/2}$
2702.852	2	15	36986.985	$19248^{\circ}_{5/2} - 56235_{3/2}$	2675.670	5	50	37362.713	$9061_{5/2} - 46423^{\circ}_{3/2}$
2702.202	2	4b	36995.882	$9585^{\circ}_{5/2} - 46581_{5/2}$	2674.988	0	10d	37372.238	$17121^{\circ}_{3/2} - 54493_{5/2}$
2702.052	4	5	36997.935	$4490^{\circ}_{5/2} - 41488_{7/2}$	2674.580	0	5	37377.939	$8460_{3/2} - 45838^{\circ}_{3/2}$
2701.818	8	75	37001.139	$13468^{\circ}_{9/2} - 50470_{9/2}$	2673.281	2	4	37396.100	$6700^{\circ}_{9/2} - 44096_{9/2}$
2700.602	4	15	37017.799	$9585^{\circ}_{5/2} - 46603_{5/2}$	2672.945	50	40	37400.80	$9202^{\circ}_{7/2} - 46603_{5/2}$
2700.080	0	100	37024.955	$15710^{\circ}_{3/2} - 52735_{3/2}$	2672.171	4	5	37411.634	$15324^{\circ}_{1/2} - 52735_{3/2}$
2699.012	3	50	37039.605	$14790^{\circ}_{7/2} - 51830_{7/2}$	2671.469	4	50	37421.464	$8378^{\circ}_{7/2} - 45800_{5/2}$
2698.730	15b	75	37043.475	$6244_{1/2} - 43287^{\circ}_{3/2}$	2669.695	3	5	37446.329	$4490^{\circ}_{5/2} - 41936_{3/2}$
2698.169	5	15s	37051.177	$9202^{\circ}_{7/2} - 46253_{9/2}$	2669.447	3	25	37449.808	$13818^{\circ}_{7/2} - 51268_{7/2}$
2697.720	3	8	37057.343	$7331^{\circ}_{5/2} - 44388_{5/2}$	2667.544	8	15	37476.522	$7331^{\circ}_{5/2} - 44807_{7/2}$
2697.546	25	75	37059.733	$1521_{5/2} - 38581^{\circ}_{5/2}$	2667.504	2	4	37477.084	$6700^{\circ}_{9/2} - 44177_{11/2}$
2696.827	8	75	37069.613	$12219_{3/2} - 49289^{\circ}_{5/2}$	2667.193	0	5	37481.454	$14790^{\circ}_{7/2} - 52272_{7/2}$
2696.174	10	25	37078.591	$6168^{\circ}_{7/2} - 43246_{7/2}$	2666.412	2	5	37492.432	$11576^{\circ}_{3/2} - 49068_{5/2}$
2695.988	2	3	37081.149	$6691^{\circ}_{3/2} - 43772_{5/2}$	2665.884	5	50	37499.857	$6244_{1/2} - 43744^{\circ}_{1/2}$
2695.810	25	75	37083.597	$8605_{5/2} - 45689^{\circ}_{7/2}$	2664.051	5	15b	37525.657	$8378^{\circ}_{7/2} - 45904_{9/2}$
2695.553	50	150	37087.132	$10379_{9/2} - 47466^{\circ}_{11/2}$	2662.861	20	75	37542.426	$10189^{\circ}_{11/2} - 47731_{9/2}$
2695.203	50	100	37091.948	$8605_{5/2} - 45697^{\circ}_{3/2}$	2662.343	10	75	37549.730	$8605_{5/2} - 46155^{\circ}_{5/2}$
2695.017	8	50	37094.508	$9061_{3/2} - 46155^{\circ}_{5/2}$	2662.171	1	8	37552.156	$14101^{\circ}_{1/2} - 51653_{1/2}$
2694.341	5	15	37103.814	$6700^{\circ}_{9/2} - 43803_{7/2}$	2661.969	0	5	37555.005	$14275^{\circ}_{9/2} - 51830_{7/2}$
2693.959	30	30	37109.07	$6700^{\circ}_{9/2} - 43809_{9/2}$	2661.724	0	4	37558.462	$7331^{\circ}_{5/2} - 44889_{3/2}$
2693.628	2	100b	37113.635	$11576^{\circ}_{3/2} - 48689_{3/2}$	2661.386	15	75	37563.232	$9585^{\circ}_{5/2} - 47148_{3/2}$
2693.099	3	8	37120.925	$9585^{\circ}_{5/2} - 46706_{7/2}$	2661.090	1	25	37567.410	$7331^{\circ}_{5/2} - 44898_{7/2}$
2692.416	75	200	37130.341	$0_{3/2} - 37130^{\circ}_{1/2}$	2660.965	1	8	37569.174	$15349^{\circ}_{11/2} - 52918_{13/2}$
2691.513	0	8l	37142.798	$19248^{\circ}_{5/2} - 56391_{5/2}$	2660.680	0	4	37573.198	$17272^{\circ}_{9/2} - 54845_{9/2}$
2691.374	8b	15	37144.716	$14790^{\circ}_{7/2} - 51935_{5/2}$	2660.596	15	25	37574.384	$14101^{\circ}_{1/2} - 51676_{3/2}$
2691.172	10	75	37147.504	$9238^{\circ}_{9/2} - 46385_{7/2}$	2659.417	1	5	37591.041	$15144^{\circ}_{3/2} - 52735_{3/2}$
2690.994	8b	20	37149.961	$9202^{\circ}_{7/2} - 46352_{7/2}$	2658.664	25	75	37601.687	$0_{3/2} - 37601^{\circ}_{3/2}$

TABLE 3. *Classified lines of* Th II—Continued

Wavelength Å	Intensity		Wavenumber cm^{-1}	Classification	Wavelength Å	Intensity		Wavenumber cm^{-1}	Classification
	Lamp	Spark				Lamp	Spark		
2658.490	4	10b	37604.149	$9720^{\circ}_{7/2} - 47324_{5/2}$	2629.620	3	50	38016.971	$14545^{\circ}_{5/2} - 52562_{7/2}$
				$6168^{\circ}_{7/2} - 43772_{5/2}$	2629.365	0	3	38020.658	$18214^{\circ}_{3/2} - 56235_{3/2}$
2658.216	8	15	37608.024	$0_{3/2} - 37607^{\circ}_{1/2}$	2628.918	0	8	38027.122	$6700^{\circ}_{9/2} - 44727_{11/2}$
2656.262	4	8	37635.688	$6168^{\circ}_{7/2} - 43803_{7/2}$	2628.811	20	100	38028.670	$4490^{\circ}_{5/2} - 42518_{7/2}$
2655.887	3	20	37641.002	$6168^{\circ}_{7/2} - 43809_{9/2}$	2627.557	2	50	38046.818	$13818^{\circ}_{7/2} - 51865_{5/2}$
2655.408	0	10	37647.791	$10673^{\circ}_{5/2} - 48320_{5/2}$	2626.394	15	25	38063.665	$7331^{\circ}_{5/2} - 45395_{7/2}$
2653.163	2	25	37679.645	$16818_{7/2} - 54497^{\circ}_{7/2}$	2626.098	0	20	38067.955	$15453^{\circ}_{7/2} - 53520_{9/2}$
2652.065	15	50	37695.244	$8460_{3/2} - 46155^{\circ}_{3/2}$	2625.737	25	100	38073.188	$4146_{7/2} - 42219^{\circ}_{5/2}$
2651.907	4	3	37697.490	$6691^{\circ}_{3/2} - 44388_{5/2}$	2624.582	0	3b	38089.942	$21297^{\circ}_{5/2} - 59387_{7/2}$
2651.703	2	20	37700.390	$9202^{\circ}_{7/2} - 46902_{5/2}$	2624.033	2	3	38097.911	$6691^{\circ}_{3/2} - 44789_{1/2}$
2651.402	1	4	37704.670	$21682^{\circ}_{7/2} - 59387_{7/2}$	2623.448	25	100	38106.406	$4113_{3/2} - 42219^{\circ}_{5/2}$
2650.583	25	200	37716.319	$0_{3/2} - 37716^{\circ}_{1/2}$	2622.686	10	8	38117.477	$13818^{\circ}_{7/2} - 51935_{5/2}$
2649.866	15	100	37726.524	$10572^{\circ}_{9/2} - 48298_{7/2}$	2622.361	4	50	38122.201	$9202^{\circ}_{7/2} - 47324_{5/2}$
2649.736	1	5	37728.375	$11116^{\circ}_{7/2} - 48844_{9/2}$	2621.506	0	10	38134.633	$15710^{\circ}_{5/2} - 53845_{5/2}$
2649.477	10	25	37732.063	$4490^{\circ}_{5/2} - 42222_{7/2}$	2621.376	2	50	38136.524	$16033^{\circ}_{5/2} - 54169_{7/2}$
2648.994	1	8	37738.942	$9585^{\circ}_{5/2} - 47324_{5/2}$	2620.942	2	15	38142.839	$12488^{\circ}_{9/2} - 50631_{11/2}$
2648.210	3	20	37750.114	$6700^{\circ}_{9/2} - 44450_{9/2}$	2620.375	1	8	38151.092	$9720^{\circ}_{7/2} - 47871_{7/2}$
2647.844	0	4l	37755.332	$13468^{\circ}_{9/2} - 51224_{9/2}$	2619.008	10	75	38171.004	$15349^{\circ}_{11/2} - 53520_{9/2}$
2647.507	2	15b	37760.138	$11725^{\circ}_{1/2} - 49485_{1/2}$	2618.912	25b	100	38172.403	$4146_{7/2} - 42319^{\circ}_{9/2}$
2647.423	4	8	37761.335	$12902^{\circ}_{3/2} - 50663_{5/2}$	2618.625	0	3	38176.586	$18214^{\circ}_{3/2} - 56391_{3/2}$
2647.382	2	15	37761.920	$14545^{\circ}_{5/2} - 52307_{3/2}$	2617.114	20	15	38198.626	$6700^{\circ}_{9/2} - 44898_{7/2}$
2646.543	1	3	37773.891	$17722^{\circ}_{9/2} - 55496_{9/2}$	2616.850	10	15	38202.480	$8378^{\circ}_{7/2} - 46581_{5/2}$
2644.775	2	15	37799.141	$13468^{\circ}_{9/2} - 51268_{7/2}$	2616.631	1	10	38205.677	$14101^{\circ}_{1/2} - 52307_{3/2}$
2644.681	2	25	37800.484	$17121^{\circ}_{3/2} - 54922_{3/2}$	2615.641	2	5	38220.137	$7001_{3/2} - 45221^{\circ}_{5/2}$
2644.460	2	5	37803.643	$6700^{\circ}_{9/2} - 44503_{7/2}$	2615.345	3	50	38224.462	$17272^{\circ}_{9/2} - 55496_{9/2}$
2643.461	3	20	37817.929	$8605^{\circ}_{5/2} - 46423^{\circ}_{3/2}$					$8378^{\circ}_{7/2} - 46603_{5/2}$
2643.385	0	5	37819.016	$10673^{\circ}_{5/2} - 48492_{5/2}$	2612.875	3	25	38260.594	$11116^{\circ}_{7/2} - 49377_{7/2}$
2643.280	4	20	37820.518	$7001_{3/2} - 44821^{\circ}_{5/2}$	2612.688	2	10	38263.332	$12472^{\circ}_{5/2} - 50735_{3/2}$
2642.401	3	15	37833.098	$12902^{\circ}_{3/2} - 50735_{3/2}$	2612.465	0	10	38266.598	$10855_{7/2} - 49121^{\circ}_{7/2}$
2642.037	0	4	37838.311	$11576^{\circ}_{3/2} - 49414_{3/2}$	2612.031	0	4	38272.956	$10572^{\circ}_{9/2} - 48844_{9/2}$
2641.488	75	150	37846.174	$0_{3/2} - 37846^{\circ}_{5/2}$	2611.688	4	50	38277.982	$13250_{3/2} - 51528^{\circ}_{3/2}$
2640.424	2	5	37861.424	$6691^{\circ}_{3/2} - 44552_{5/2}$					$15242^{\circ}_{9/2} - 53520_{9/2}$
2640.391	5	10	37861.897	$4490^{\circ}_{5/2} - 42352_{5/2}$	2611.420	2	5	38281.910	$6168^{\circ}_{7/2} - 44450_{9/2}$
2640.269	10	25	37863.646	$13818^{\circ}_{7/2} - 51681_{9/2}$	2611.263	2	8	38284.212	$9585^{\circ}_{5/2} - 47869_{3/2}$
2639.879	4	50	37869.240	$7828_{1/2} - 45697^{\circ}_{3/2}$	2611.134	2b	10b	38286.103	$9585^{\circ}_{5/2} - 47871_{7/2}$
2639.503	25	50	37874.634	$1521_{5/2} - 39396^{\circ}_{7/2}$	2610.412	1	3	38296.692	$11576^{\circ}_{3/2} - 49873_{5/2}$
2639.053	1	5	37881.092	$10572^{\circ}_{9/2} - 48453_{7/2}$	2609.857	25	75	38304.835	$4113_{5/2} - 42418^{\circ}_{3/2}$
2637.098	0	8	37909.173	$11576^{\circ}_{3/2} - 49485_{1/2}$	2608.321	4	25	38327.391	$8378^{\circ}_{7/2} - 46706_{7/2}$
2635.414	3	10	37933.395	$9238^{\circ}_{9/2} - 47171_{9/2}$	2607.775	3	8	38335.415	$6168^{\circ}_{7/2} - 44503_{7/2}$
2635.290	3	15	37935.180	$12472^{\circ}_{5/2} - 50407_{7/2}$	2607.481	8	25	38339.738	$1521_{5/2} - 39861^{\circ}_{5/2}$
2635.043	0	5	37938.736	$16906^{\circ}_{7/2} - 54845_{9/2}$	2605.994	4	25	38361.613	$13468^{\circ}_{9/2} - 51830_{7/2}$
2634.108	2	20	37952.202	$11116^{\circ}_{7/2} - 49068_{5/2}$	2603.909	3	25	38392.328	$15453^{\circ}_{7/2} - 53845_{5/2}$
2633.327	10	50	37963.457	$8460_{3/2} - 46423^{\circ}_{3/2}$	2603.560	0	15	38397.474	$17837^{\circ}_{1/2} - 56235_{3/2}$
2632.925	2	10	37969.253	$9202^{\circ}_{7/2} - 47171_{9/2}$					$20989^{\circ}_{9/2} - 59387_{7/2}$
2632.641	2	15	37973.349	$8378^{\circ}_{7/2} - 46352_{7/2}$	2603.014	3	25b	38405.528	$8018_{3/2} - 46423^{\circ}_{3/2}$
2632.050	0	3	37981.875	$12488^{\circ}_{9/2} - 50470_{9/2}$	2602.154	0	4	38418.220	$20969^{\circ}_{7/2} - 59387_{7/2}$
2630.817	10	50	37999.675	$4113_{5/2} - 42112^{\circ}_{3/2}$	2601.820	3	10	38423.151	$10189^{\circ}_{11/2} - 48612_{13/2}$
2630.671	10	8	38001.784	$1859_{3/2} - 39861^{\circ}_{5/2}$	2601.630	2	3	38425.957	$6700^{\circ}_{9/2} - 45126_{9/2}$
2630.107	0	5	38009.932	$7828_{1/2} - 45838^{\circ}_{3/2}$	2601.045	2	5	38434.599	$14484^{\circ}_{11/2} - 52918_{13/2}$
2630.015	5	75	38011.262	$9720^{\circ}_{7/2} - 47731_{9/2}$	2600.935	8b	10	38436.225	$0_{3/2} - 38436^{\circ}_{3/2}$

TABLE 3. *Classified lines of* Th II—Continued

Wavelength Å	Intensity		Wavenumber cm^{-1}	Classification	Wavelength Å	Intensity		Wavenumber cm^{-1}	Classification
	Lamp	Spark				Lamp	Spark		
2600.880	25b	25	38437.037	$9238^{\circ}_{9/2} - 47675_{11/2}$	2552.923	0	3	39159.036	$11576^{\circ}_{3/2} - 50735_{3/2}$
2598.741	0	10	38468.673	$7331^{\circ}_{3/2} - 45800_{5/2}$	2552.281	0	8	39168.885	$10189^{\circ}_{11/2} - 49357_{11/2}$
2597.046	50b	150b	38493.778	$0_{3/2} - 38493^{\circ}_{5/2}$	2551.934	3	10	39174.211	$4113_{5/2} - 43287^{\circ}_{3/2}$
2595.036	8	20	38523.592	$8378^{\circ}_{7/2} - 46902_{5/2}$	2551.234	5	10	39184.96	$1521_{5/2} - 40706^{\circ}_{7/2}$
2594.662	2	20	38529.145	$9202^{\circ}_{7/2} - 47731_{9/2}$	2550.749	0	8	39192.409	$15305_{9/2} - 54497^{\circ}_{7/2}$
2592.786	0	15	38557.020	$15453^{\circ}_{7/2} - 54010_{7/2}$	2550.255	0	3	39200.000	$10673^{\circ}_{5/2} - 49873_{5/2}$
2591.370	2	5	38578.088	$9720^{\circ}_{7/2} - 48298_{7/2}$	2549.987	5	15	39204.120	$6700^{\circ}_{9/2} - 45904_{9/2}$
2590.229	4	20	38595.080	$7828_{1/2} - 46423^{\circ}_{3/2}$	2548.134	8l	50	39232.62	$9585^{\circ}_{5/2} - 48817_{3/2}$
2590.070	2	5	38597.449	$7828_{1/2} - 46426^{\circ}_{1/2}$	2547.898	15	75	39236.261	$4146_{7/2} - 43382^{\circ}_{5/2}$
2589.485	3	8	38606.169	$4490^{\circ}_{5/2} - 43096_{5/2}$	2547.016	0	3	39249.847	$7331^{\circ}_{3/2} - 46581_{5/2}$
2589.059	50	100	38612.520	$1859_{3/2} - 40472^{\circ}_{3/2}$	2546.953	0	8	39250.818	$9202^{\circ}_{7/2} - 48453_{7/2}$
2588.916	8	20	38614.653	$6691^{\circ}_{3/2} - 45306_{3/2}$	2545.744	8	25	39269.458	$4113_{5/2} - 43382^{\circ}_{5/2}$
2587.615	0	4	38634.067	$14101^{\circ}_{1/2} - 52735_{3/2}$	2545.339	8	50	39275.70	$6213_{9/2} - 45489^{\circ}_{9/2}$
2587.252	3	20	38639.486	$6168^{\circ}_{7/2} - 44807_{7/2}$	2544.364	0	8	39290.755	$11116^{\circ}_{7/2} - 50407_{7/2}$
2587.246	0	20	38639.576	$6168^{\circ}_{7/2} - 44807_{7/2}$	2543.217	0	8	39308.474	$12219_{3/2} - 51528^{\circ}_{3/2}$
2586.158	3	25b	38655.831	$10189^{\circ}_{11/2} - 48844_{9/2}$	2542.871	0	4l	39313.822	$4490^{\circ}_{5/2} - 43803_{7/2}$
2585.726	4	5	38662.289	$1521_{5/2} - 40184^{\circ}_{7/2}$	2542.642	4	25	39317.36	$4490^{\circ}_{5/2} - 43807_{3/2}$
2583.456	4	20	38696.258	$13250_{5/2} - 51946^{\circ}_{5/2}$	2540.865	0	3	39344.858	$12485^{\circ}_{7/2} - 51830_{7/2}$
				$7001_{3/2} - 45697^{\circ}_{3/2}$	2540.360	2	10b	39352.679	$8378^{\circ}_{7/2} - 47731_{9/2}$
2582.939	0	4b	38704.003	$10673^{\circ}_{5/2} - 49377_{7/2}$	2540.309	0	8b	39353.469	$11116^{\circ}_{7/2} - 50470_{9/2}$
2582.099	2	20	38716.593	$15453^{\circ}_{7/2} - 54169_{7/2}$	2538.931	10	20	39374.827	$7331^{\circ}_{5/2} - 46706_{7/2}$
2580.844	0	5	38735.419	$9585^{\circ}_{5/2} - 48320_{5/2}$	2538.832	0	5	39376.362	$12570_{7/2} - 51946^{\circ}_{5/2}$
2580.699	10	50	38737.595	$4490^{\circ}_{5/2} - 43227_{5/2}$	2538.680	0	3s	39378.719	$14790^{\circ}_{7/2} - 54169_{7/2}$
2580.354	5	50	38742.774	$10379_{9/2} - 49121^{\circ}_{7/2}$	2538.047	0	3	39388.540	$10572^{\circ}_{9/2} - 49960_{7/2}$
2580.264	0	15	38744.125	$13818^{\circ}_{7/2} - 52562_{7/2}$	2537.759	0	10l	39393.010	$12472^{\circ}_{5/2} - 51865_{5/2}$
2579.768	0	5	38751.574	$12902^{\circ}_{3/2} - 51653_{1/2}$	2535.873	4	20	39422.306	$7001_{3/2} - 46423^{\circ}_{3/2}$
2579.437	15	75b	38756.55	$4490^{\circ}_{5/2} - 43246_{7/2}$	2534.589	4	10	39442.275	$6168^{\circ}_{7/2} - 45610_{5/2}$
2578.958	2	25	38763.744	$13406^{\circ}_{13/2} - 52170_{11/2}$	2534.193	0	3	39448.438	$11576^{\circ}_{3/2} - 51024_{3/2}$
2578.619	0	10	38768.840	$9238^{\circ}_{9/2} - 48006_{9/2}$	2534.091	0	20	39450.026	$12485^{\circ}_{7/2} - 51935_{3/2}$
2578.238	0	4	38774.569	$17460^{\circ}_{5/2} - 56235_{3/2}$	2533.871	0	15	39453.451	$6244_{1/2} - 45697^{\circ}_{3/2}$
2576.910	10	50	38794.550	$1859_{3/2} - 40654^{\circ}_{5/2}$	2533.224	0	10	39463.527	$12472^{\circ}_{5/2} - 51935_{5/2}$
2576.688	25	75	38797.892	$4146_{7/2} - 42944^{\circ}_{7/2}$	2533.152	0	5	39464.648	$14545^{\circ}_{5/2} - 54010_{7/2}$
2576.322	0	75	38803.404	$13468^{\circ}_{9/2} - 52272_{7/2}$	2532.432	5	25	39475.86	$6213_{9/2} - 45689^{\circ}_{7/2}$
2576.209	0	8	38805.105	$10572^{\circ}_{9/2} - 49377_{7/2}$	2531.883	0	10	39484.427	$16906^{\circ}_{7/2} - 56391_{3/2}$
2574.485	15	5	38831.10	$4113_{5/2} - 42944^{\circ}_{7/2}$	2527.877	0	15	39546.995	$11116^{\circ}_{7/2} - 50663_{5/2}$
2573.631	0	10	38843.974	$11116^{\circ}_{7/2} - 49960_{7/2}$	2526.343	3	25	39571.007	$7331^{\circ}_{5/2} - 46902_{5/2}$
2570.653	0	50	38888.970	$16033^{\circ}_{5/2} - 54922_{3/2}$	2526.223	3b	15	39572.88	$6691^{\circ}_{3/2} - 46264_{3/2}$
2566.916	0	25	38945.583	$8378^{\circ}_{7/2} - 47324_{5/2}$	2525.925	0	25	39577.554	$9711_{7/2} - 49289^{\circ}_{5/2}$
2566.588	50	100	38950.559	$1521_{5/2} - 40472^{\circ}_{3/2}$	2524.229	2l	3	39604.144	$7331^{\circ}_{5/2} - 46935_{3/2}$
2565.593	75	100	38965.665	$1859_{3/2} - 40825^{\circ}_{1/2}$	2522.775	5	15	39626.969	$4146_{7/2} - 43773^{\circ}_{7/2}$
2562.675	0	8	39010.030	$11725^{\circ}_{1/2} - 50735_{3/2}$	2522.713	0	4	39627.942	$8378^{\circ}_{7/2} - 48006_{9/2}$
2561.938	0	75	39021.251	$6168^{\circ}_{7/2} - 45189_{5/2}$	2521.777	0	5	39642.650	$9202^{\circ}_{7/2} - 48844_{9/2}$
2561.149	0	25	39033.272	$12902^{\circ}_{3/2} - 51935_{5/2}$	2520.660	8	75	39660.216	$4113_{5/2} - 43773^{\circ}_{7/2}$
2560.934	2	75	39036.549	$14484^{\circ}_{11/2} - 53520_{9/2}$	2519.848	0	20	39672.995	$17272^{\circ}_{9/2} - 56945_{11/2}$
2559.793	0	10	39053.947	$7331^{\circ}_{3/2} - 46385_{7/2}$	2519.288	0	3	39681.813	$12488^{\circ}_{9/2} - 52170_{11/2}$
2558.328	0	10b	39076.310	$20310^{\circ}_{5/2} - 59387_{7/2}$	2519.070	0	15	39685.247	$6700^{\circ}_{9/2} - 46385_{7/2}$
2557.024	0	4	39096.236	$9202^{\circ}_{7/2} - 48298_{7/2}$	2516.430	0	50	39726.878	$12219_{3/2} - 51946^{\circ}_{5/2}$
2556.480	0	10	39104.555	$9585^{\circ}_{5/2} - 48689_{3/2}$	2515.997	0	3	39733.715	$15305_{9/2} - 55038^{\circ}_{9/2}$
2554.649	5	2	39132.58	$1521_{5/2} - 40654^{\circ}_{5/2}$	2515.853	0	5	39735.989	$6168^{\circ}_{7/2} - 45904_{9/2}$
2553.243	4	25	39154.128	$7001_{3/2} - 46155^{\circ}_{5/2}$	2511.414	0	8	39806.219	$17272^{\circ}_{9/2} - 57078_{9/2}$

TABLE 3. *Classified lines of* Th II—Continued

Wavelength Å	Intensity		Wavenumber cm^{-1}	Classification	Wavelength Å	Intensity		Wavenumber cm^{-1}	Classification
	Lamp	Spark				Lamp	Spark		
2511.159	5	10	39810.261	$4490^{\circ}_{5/2} - 44300_{3/2}$	2460.168	0	2	40635.335	$9202^{\circ}_{7/2} - 49837_{9/2}$
2509.969	3	20	39829.134	$9585^{\circ}_{5/2} - 49414_{3/2}$	2459.008	8	25	40654.503	$0_{3/2} - 40654^{\circ}_{5/2}$
2509.707	0	8	39833.291	$12902^{\circ}_{3/2} - 52735_{3/2}$	2458.015	0	5	40670.925	$9202^{\circ}_{7/2} - 49873_{5/2}$
2507.924	10	25l	39861.609	$0_{3/2} - 39861^{\circ}_{5/2}$	2457.746	2b	10	40675.376	$4146_{7/2} - 44821^{\circ}_{5/2}$
2505.611	8	25	39898.404	$4490^{\circ}_{3/2} - 44388_{5/2}$	2456.865	3	25	40689.961	$8378^{\circ}_{7/2} - 49068_{5/2}$
2504.279	10b	75	39919.62	$8378^{\circ}_{7/2} - 48298_{7/2}$	2456.380	5	10	40697.994	$1521_{5/2} - 42219^{\circ}_{5/2}$
2502.339	0	4	39950.570	$11725^{\circ}_{1/2} - 51676_{3/2}$	2456.290	4b	50	40699.485	$4490^{\circ}_{5/2} - 45189_{5/2}$
2499.696	0	5	39992.808	$7331^{\circ}_{5/2} - 47324_{5/2}$	2455.904	0	5	40705.882	$14790^{\circ}_{7/2} - 55496_{9/2}$
2498.873	8	75	40005.979	$6700^{\circ}_{9/2} - 46706_{7/2}$	2454.890	5	5	40722.694	$9238^{\circ}_{9/2} - 49960_{7/2}$
2498.405	8	20	40013.472	$4490^{\circ}_{5/2} - 44503_{7/2}$	2454.195	0	3	40734.225	$6168^{\circ}_{7/2} - 46902_{5/2}$
2496.522	2	10	40043.650	$15453^{\circ}_{7/2} - 55496_{9/2}$	2449.087	5	20	40819.178	$11116^{\circ}_{7/2} - 51935_{5/2}$
2496.014	1	5	40051.800	$13468^{\circ}_{9/2} - 53520_{9/2}$	2448.694	0	4	40825.729	$0_{3/2} - 40825^{\circ}_{1/2}$
2495.563	0	4	40059.038	$10572^{\circ}_{9/2} - 50631_{11/2}$	2444.463	10	25	40896.386	$15786_{5/2} - 56683^{\circ}_{7/2}$
2495.454	0	4	40060.787	$9061_{5/2} - 49121^{\circ}_{7/2}$					$1521_{5/2} - 42418^{\circ}_{5/2}$
2495.354	8	75	40062.39	$4490^{\circ}_{3/2} - 44552_{5/2}$	2443.953	10	15	40904.920	$4490^{\circ}_{5/2} - 45395_{7/2}$
2494.775	1	10	40071.690	$8460_{3/2} - 48532^{\circ}_{1/2}$	2437.536	0	75	41012.597	$14484^{\circ}_{11/2} - 55496_{9/2}$
2494.452	0	3	40076.878	$12485^{\circ}_{7/2} - 52562_{7/2}$	2436.353	0	5	41032.510	$12488^{\circ}_{9/2} - 53520_{9/2}$
2494.416	0	4	40077.457	$11576^{\circ}_{3/2} - 51653_{1/2}$	2432.847	8	50	41091.638	$10855_{7/2} - 51946^{\circ}_{5/2}$
2493.616	2	10	40090.313	$12472^{\circ}_{5/2} - 52562_{7/2}$	2431.140	8	8	41120.488	$4490^{\circ}_{5/2} - 45610_{5/2}$
2492.538	0	8	40107.651	$11116^{\circ}_{7/2} - 51224_{9/2}$	2429.041	0	8	41156.019	$6168^{\circ}_{7/2} - 47324_{5/2}$
2490.596	2	8	40138.921	$19248^{\circ}_{5/2} - 59387_{7/2}$	2426.927	0	10	41191.865	$10673^{\circ}_{5/2} - 51865_{5/2}$
2490.104	0	15	40146.852	$15349^{\circ}_{11/2} - 55496_{9/2}$	2423.665	0	75	41247.301	$13250_{5/2} - 54497^{\circ}_{7/2}$
2489.736	4	15	40152.785	$9720^{\circ}_{7/2} - 49873_{5/2}$	2422.457	2	3	41267.868	$9202^{\circ}_{7/2} - 50470_{9/2}$
2489.607	10	100	40154.866	$6213_{9/2} - 46368^{\circ}_{9/2}$	2422.246	3	8	41271.463	$8018_{3/2} - 49289^{\circ}_{5/2}$
2488.554	0	5	40171.856	$16906^{\circ}_{7/2} - 57078_{9/2}$	2419.979	0	5	41310.122	$4490^{\circ}_{5/2} - 45800_{5/2}$
2488.087	2	15	40179.395	$6244_{1/2} - 46423^{\circ}_{3/2}$	2418.074	5	10	41342.665	$4146_{7/2} - 45489^{\circ}_{9/2}$
2487.322	0	8	40191.752	$13818^{\circ}_{7/2} - 54010_{7/2}$	2413.407	25	50	41422.606	$1521_{3/2} - 42944^{\circ}_{7/2}$
2486.691	0	4	40201.950	$16033^{\circ}_{5/2} - 56235_{3/2}$	2412.043	0	4	41446.029	$11116^{\circ}_{7/2} - 52562_{7/2}$
2486.126	3	25	40211.085	$6691^{\circ}_{3/2} - 46902_{5/2}$	2411.291	0	25	41458.954	$8378^{\circ}_{7/2} - 49837_{9/2}$
2485.764	0	5	40216.941	$6168^{\circ}_{7/2} - 46385_{7/2}$	2411.143	0	4	41461.498	$9202^{\circ}_{7/2} - 50663_{5/2}$
2485.055	2	20	40228.42	$9061_{5/2} - 49289^{\circ}_{5/2}$	2407.574	5	8b	41522.956	$1859_{3/2} - 43382^{\circ}_{5/2}$
2484.330	0	4	40240.153	$9720^{\circ}_{7/2} - 49960_{7/2}$	2407.480	0	4b	41524.577	$12485^{\circ}_{7/2} - 54010_{7/2}$
2484.074	0	10	40244.300	$6691^{\circ}_{3/2} - 46935_{3/2}$	2407.137	10	10	41530.494	$7001_{3/2} - 48532^{\circ}_{1/2}$
2483.955	2	10	40246.228	$11116^{\circ}_{7/2} - 51362_{5/2}$	2406.704	0	10b	41537.965	$12472^{\circ}_{5/2} - 54010_{7/2}$
2483.489	0	4	40253.779	$15242^{\circ}_{9/2} - 55496_{9/2}$	2404.497	0	50	41576.088	$4113_{3/2} - 45689^{\circ}_{7/2}$
2482.892	0	5	40263.457	$12472^{\circ}_{5/2} - 52735_{3/2}$	2404.171	10	50	41581.72	$8378^{\circ}_{7/2} - 49960_{7/2}$
2481.813	2	5	40280.961	$10189^{\circ}_{11/2} - 50470_{9/2}$	2401.635	0	3	41625.630	$15453^{\circ}_{7/2} - 57078_{9/2}$
2481.405	2	25	40287.584	$9585^{\circ}_{5/2} - 49873_{5/2}$	2401.413	0	3	41629.478	$6691^{\circ}_{3/2} - 48320_{5/2}$
2479.557	0	8	40317.608	$4490^{\circ}_{5/2} - 44807_{7/2}$	2401.139	0	4	41634.228	$10673^{\circ}_{5/2} - 52307_{3/2}$
2477.087	0	15	40357.807	$16033^{\circ}_{5/2} - 56391_{5/2}$	2398.341	0	4	41682.796	$9585^{\circ}_{5/2} - 51268_{7/2}$
2476.971	8	25	40359.697	$1859_{3/2} - 42219^{\circ}_{5/2}$	2398.267	0	5	41684.083	$12485^{\circ}_{7/2} - 54169_{7/2}$
2476.898	0	25	40360.886	$14484^{\circ}_{11/2} - 54845_{9/2}$	2397.491	1	4	41697.573	$12472^{\circ}_{5/2} - 54169_{7/2}$
2471.005	1	5	40457.135	$6691^{\circ}_{3/2} - 47148_{3/2}$	2395.200	0	3	41737.454	$7331^{\circ}_{5/2} - 49068_{5/2}$
2470.148	0	15	40471.170	$6700^{\circ}_{9/2} - 47171_{9/2}$	2393.574	5	3	41765.805	$1521_{5/2} - 43287^{\circ}_{3/2}$
2468.151	5	100	40503.913	$4146_{7/2} - 44650^{\circ}_{7/2}$	2393.111	50	25	41773.88	$4490^{\circ}_{5/2} - 46264_{3/2}$
2467.416	2	15	40515.978	$8605_{3/2} - 49121^{\circ}_{7/2}$	2388.143	10	10	41860.779	$1521_{5/2} - 43382^{\circ}_{5/2}$
2466.904	0	5	40524.386	$15710^{\circ}_{3/2} - 56235_{3/2}$	2388.073	8	8	41862.006	$4490^{\circ}_{5/2} - 46352_{7/2}$
2466.128	10r	50	40537.14	$4113_{5/2} - 44650^{\circ}_{7/2}$	2386.179	0	3	41895.231	$4490^{\circ}_{5/2} - 46385_{7/2}$
2466.065	5	8	40538.172	$7331^{\circ}_{5/2} - 47869_{3/2}$	2384.358	5	20	41927.23	$12570_{7/2} - 54497^{\circ}_{7/2}$
2462.333	0	3	40599.609	$9238^{\circ}_{9/2} - 49837_{9/2}$	2379.751	0	4	42008.386	$12485^{\circ}_{7/2} - 54493_{5/2}$

TABLE 3. *Classified lines of* Th II—Continued

Wavelength Å	Intensity		Wavenumber cm^{-1}	Classification	Wavelength Å	Intensity		Wavenumber cm^{-1}	Classification
	Lamp	Spark				Lamp	Spark		
2377.830	25	100	42042.321	$4113_{5/2} - 46155^{\circ}_{5/2}$	2290.644	0	20	43642.388	$10855_{7/2} - 54497^{\circ}_{7/2}$
2375.076	15	25	42091.067	$4490^{\circ}_{3/2} - 46581_{3/2}$	2287.248	0	4	43707.181	$6700^{\circ}_{9/2} - 50407_{7/2}$
2373.991	1	4	42110.302	$9720^{\circ}_{7/2} - 51830_{7/2}$	2285.315	5	5	43744.147	$0_{3/2} - 43744^{\circ}_{1/2}$
2373.840	15	50	42112.981	$0_{3/2} - 42112^{\circ}_{3/2}$	2282.362	0	5	43800.739	$9720^{\circ}_{7/2} - 53520_{9/2}$
				$4490^{\circ}_{5/2} - 46603_{5/2}$	2281.965	4	20	43808.359	$4490^{\circ}_{5/2} - 48298_{7/2}$
2373.723	0	50	42115.057	$17272^{\circ}_{9/2} - 59387_{7/2}$	2280.425	20	50	43837.941	$1859_{3/2} - 45697^{\circ}_{3/2}$
2372.043	2	8	42144.882	$9720^{\circ}_{7/2} - 51865_{5/2}$	2277.538	0	3	43893.504	$8378^{\circ}_{7/2} - 52272_{7/2}$
2371.155	0	5	42160.664	$9202^{\circ}_{7/2} - 51362_{5/2}$	2276.922	0	5	43905.378	$12485^{\circ}_{7/2} - 56391_{5/2}$
2368.047	15	25	42215.994	$4490^{\circ}_{5/2} - 46706_{7/2}$	2275.594	0	3	43930.998	$6700^{\circ}_{9/2} - 50631_{11/2}$
2367.842	50	100	42219.649	$0_{3/2} - 42219^{\circ}_{5/2}$	2271.931	5	8	44001.821	$4490^{\circ}_{5/2} - 48492_{5/2}$
2367.725	0	3	42221.735	$4146_{7/2} - 46368^{\circ}_{9/2}$	2270.403	0	3	44031.431	$7331^{\circ}_{5/2} - 51362_{5/2}$
2366.991	10	100	42234.83	$9711_{7/2} - 51946^{\circ}_{5/2}$	2265.919	3	20b	44118.557	$10379_{9/2} - 54497^{\circ}_{7/2}$
2366.040	10	20	42251.801	$1521_{5/2} - 43773^{\circ}_{7/2}$	2263.408	5	15	44167.497	$1521_{5/2} - 45689^{\circ}_{7/2}$
2364.194	3	10	42284.789	$6168^{\circ}_{7/2} - 48453_{7/2}$	2261.759	0	4	44199.695	$4490^{\circ}_{5/2} - 48689_{3/2}$
				$8378^{\circ}_{7/2} - 50663_{5/2}$	2255.536	0	3	44321.630	$12570_{7/2} - 56892^{\circ}_{5/2}$
2364.025	0	25	42287.812	$6244_{1/2} - 48532^{\circ}_{1/2}$	2245.131	0	3	44527.018	$7001_{3/2} - 51528^{\circ}_{3/2}$
2362.759	3	5	42310.469	$4113_{5/2} - 46423^{\circ}_{3/2}$	2243.275	8	20	44563.855	$1859_{3/2} - 46423^{\circ}_{3/2}$
2362.021	0	4	42323.687	$6168^{\circ}_{7/2} - 48492_{5/2}$	2238.629	0	4	44656.333	$10189^{\circ}_{11/2} - 54845_{9/2}$
2360.533	0	3	42350.365	$9585^{\circ}_{5/2} - 51935_{5/2}$	2230.360	10	20	44821.879	$0_{3/2} - 44821^{\circ}_{5/2}$
2356.758	10	10	42418.20	$0_{3/2} - 42418^{\circ}_{3/2}$	2225.268	0	5	44924.433	$4490^{\circ}_{5/2} - 49414_{3/2}$
2355.242	15	20	42445.496	$4490^{\circ}_{5/2} - 46935_{3/2}$	2222.430	0	3	44981.795	$6700^{\circ}_{9/2} - 51681_{9/2}$
2355.003	0	4	42449.803	$12472^{\circ}_{5/2} - 54922_{3/2}$	2222.287	0	3	44984.689	$6691^{\circ}_{3/2} - 51676_{3/2}$
2354.030	8	25	42467.348	$9061_{5/2} - 51528^{\circ}_{3/2}$	2216.767	0	5	45096.695	$9400_{5/2} - 54497^{\circ}_{7/2}$
2349.686	0	4	42545.853	$9400_{5/2} - 51946^{\circ}_{5/2}$	2215.115	0	3	45130.324	$6700^{\circ}_{9/2} - 51830_{7/2}$
2349.344	0	3	42552.046	$9720^{\circ}_{7/2} - 52272_{7/2}$	2214.539	1	15	45142.061	$8378^{\circ}_{7/2} - 53520_{9/2}$
2343.494	0	10	42658.259	$4490^{\circ}_{5/2} - 47148_{3/2}$	2212.980	0	3	45173.859	$6691^{\circ}_{3/2} - 51865_{5/2}$
2343.242	1	5	42662.846	$9202^{\circ}_{7/2} - 51865_{5/2}$	2210.648	5	20	45221.508	$0_{3/2} - 45221^{\circ}_{5/2}$
2342.873	0	5	42669.565	$14275^{\circ}_{9/2} - 56945_{11/2}$	2207.592	0	5	45284.102	$6244_{1/2} - 51528^{\circ}_{3/2}$
2339.566	0	4	42729.873	$10189^{\circ}_{11/2} - 52918_{13/2}$	2206.445	0	5	45307.641	$10189^{\circ}_{11/2} - 55496_{9/2}$
2336.051	0	3	42794.163	$6691^{\circ}_{3/2} - 49485_{1/2}$	2200.186	2	10	45436.517	$9061_{5/2} - 54497^{\circ}_{7/2}$
2333.684	0	3	42837.564	$13248_{9/2} - 56086^{\circ}_{9/2}$	2198.736	1	10q	45466.478	$8378^{\circ}_{7/2} - 53845_{5/2}$
2333.258	3	10	42845.385	$8378^{\circ}_{7/2} - 51224_{9/2}$	2178.354	0	8	45891.845	$8605_{5/2} - 54497^{\circ}_{7/2}$
2330.868	4	25	42889.313	$8378^{\circ}_{7/2} - 51268_{7/2}$	2177.158	2	15	45917.053	$4490^{\circ}_{5/2} - 50407_{7/2}$
2329.057	0	10	42922.660	$8605_{5/2} - 51528^{\circ}_{3/2}$	2167.808	0	10	46115.076	$8378^{\circ}_{7/2} - 54493_{5/2}$
2326.920	50	50	42962.075	$1859_{3/2} - 44821^{\circ}_{5/2}$	2159.403	0	3	46294.549	$9202^{\circ}_{7/2} - 55496_{9/2}$
2325.729	0	8	42984.074	$8378^{\circ}_{7/2} - 51362_{5/2}$	2153.397	2	10	46423.655	$0_{3/2} - 46423^{\circ}_{3/2}$
2317.451	0	3	43137.602	$6700^{\circ}_{9/2} - 49837_{9/2}$	2151.412	0	10	46466.483	$8378^{\circ}_{7/2} - 54845_{9/2}$
2308.754	0	3	43300.085	$1521_{5/2} - 44821^{\circ}_{5/2}$	2148.266	0	5	46534.522	$4490^{\circ}_{5/2} - 51024_{3/2}$
2308.590	4	15	43303.161	$8378^{\circ}_{7/2} - 51681_{9/2}$	2141.930	0	4	46672.160	$1859_{3/2} - 48532^{\circ}_{1/2}$
2306.573	1	8	43341.025	$8605_{5/2} - 51946^{\circ}_{5/2}$	2132.770	2	15	46872.588	$4490^{\circ}_{5/2} - 51362_{5/2}$
2305.545	0	8	43360.348	$9202^{\circ}_{7/2} - 52562_{7/2}$	2118.875	0	3	47179.930	$9711_{7/2} - 56892^{\circ}_{5/2}$
2305.474	25	25	43361.683	$1859_{3/2} - 45221^{\circ}_{5/2}$	2118.604	0	3	47185.964	$4490^{\circ}_{5/2} - 51676_{3/2}$
2304.534	2	4	43379.368	$4490^{\circ}_{5/2} - 47869_{3/2}$	2111.708	0	10	47340.036	$4490^{\circ}_{5/2} - 51830_{7/2}$
2300.695	0	10	43451.746	$8378^{\circ}_{7/2} - 51830_{7/2}$	2110.148	0	4	47375.030	$4490^{\circ}_{5/2} - 51865_{5/2}$
2298.855	3	15	43486.521	$8460_{3/2} - 51946^{\circ}_{5/2}$	2092.794	0	3	47767.828	$1521_{5/2} - 49289^{\circ}_{5/2}$
2298.732	0	4	43488.848	$12902^{\circ}_{5/2} - 56391_{5/2}$	2091.383	0	4	47800.052	$4146_{7/2} - 51946^{\circ}_{5/2}$
2297.596	0	5	43510.348	$8018_{3/2} - 51528^{\circ}_{3/2}$	2090.632	0	15	47817.221	$4490^{\circ}_{5/2} - 52307_{3/2}$
2297.491	0	75	43512.337	$15786_{5/2} - 59299^{\circ}_{5/2}$	2089.920	0	15	47833.509	$4113_{5/2} - 51946^{\circ}_{5/2}$
2295.141	0	3	43556.885	$8378^{\circ}_{7/2} - 51935_{5/2}$	2088.053	0	2	47876.273	$9202^{\circ}_{7/2} - 57078_{9/2}$
2291.974	0	4	43617.066	$9061_{5/2} - 52678^{\circ}_{5/2}$	2079.541	0	5	48072.217	$4490^{\circ}_{5/2} - 52562_{7/2}$

TABLE 3. *Classified lines of* Th II—Continued

Wavelength Å	Intensity		Wavenumber cm^{-1}	Classification	Wavelength Å	Intensity		Wavenumber cm^{-1}	Classification
	Lamp	Spark				Lamp	Spark		
2072.081	0	3	48245.266	$4490^{\circ}_{5/2} - 52735_{3/2}$					
2059.848	0	8	48531.747	$4146_{7/2} - 52678^{\circ}_{5/2}$					
2028.185	0	3	49289.296	$0_{3/2} - 49289^{\circ}_{5/2}$					
1999.098	0	3	50006.353	$1521_{5/2} - 51528^{\circ}_{3/2}$					
1995.888	0	10	50086.766	$1859_{3/2} - 51946^{\circ}_{5/2}$					

JOURNAL OF RESEARCH of the National Bureau of Standards—A. Physics and Chemistry
Vol. 78A, No. 2, March–April 1974

Proposed Secondary Wavelength Standards and Line Classifications in Thorium Spectra Between 0.9 and 3 μm

A. Giacchetti,* J. Blaise, C. H. Corliss, and R. Zalubas**

Institute for Basic Standards, National Bureau of Standards, Washington, D.C. 20234

(December 19, 1973)

The spectrum of thorium as emitted by an electrodeless lamp has been recorded by Connes and collaborators by means of Fourier Transform Spectroscopy in the region 0.9 to 3 μm. Of the 3100 lines observed, about 1900 are classified as transitions in the energy level system of Th I and 412 in Th II. Since the average deviation between the observed and calculated wave numbers is less than 0.002 cm^{-1}, the observed wavelengths are suitable for use as standard wavelengths.

Key words: Classified lines of Th I and Th II; Fourier transform spectra of Th; infrared spectra of Th; spectra of Th; Th I and Th II; thorium spectra; wavelengths of Th.

1. Introduction

The spectra of Th I and Th II have been measured in the photographic range, 2000–12 000 Å, by Zalubas. Th I is being analysed by Zalubas [1968][1] and ThII by Zalubas and Corliss [1974]. Many thorium lines have also been interferometrically measured as suggested by Meggers [1957] and a list of 1556 secondary standard thorium wavelengths has been published by Giacchetti, Stanley, and Zalubas [1970].

Both Th I and Th II contain electron configurations of each parity that lie below 8000 cm^{-1} with respect to the ground level. For the precise determination of relative energy levels in such spectra it is useful to have accurate observations of infrared wavelengths. Furthermore, when the calculated secondary standard wavelengths for Th I were prepared by Giacchetti et al. [1970], the number of high-accuracy Th II lines was insufficient to obtain an extensive energy level array of high precision. Although there are other infrared observations of thorium lines, by Steers [1967] and by Bernage, Houdart, and Niay [1971], those in the present paper are more numerous and more accurate, since better spectroscopic means were available.

2. Observations

At the present time the most precise measurements of infrared wavelengths are carried out by means of the Fourier transformation of observations made with a variable spacing interferometer of a Michelson type as developed in recent years by Pierre and Janine Connes and their colleagues. Connes et al. [1970] have reported the observation of the spectrum from a thorium iodide electrodeless lamp in the region 0.9 to 3 μm. With the observation of 10^6 data points over a mirror displacement of one meter they attained a resolution of 0.02 cm^{-1}. The Fourier transformation of the data was traced on a plotter as a chart 80 m long. Portions of the spectrum are illustrated in the paper by Connes et al. [1970]. Inspection of the tracing in comparison with the computer printout of wave numbers permitted separation of the faintest real lines from the noise in the printout. An arbitrary logarithmic intensity scale of 0 to 9 was adopted with the strongest line at 8902 cm^{-1} set equal to 9 and the intensity numbers were read from the charts. No intensity standardization as a function of wavelength was attempted. The ghost intensities are about 1/1000 of the parent line but they are clearly asymmetrical and cannot be confused with real lines. They arise from periodic errors in the advance of the carriage of the moving mirror.

The reference wavelength was provided by a He-Xe laser line at 3.5 μm, sufficiently sharp to provide useful fringes over the whole range of travel of the moving carriage. The fringes provide control for the stepwise advancement of the carriage as well as the wavelength reference with respect to which the Th wave numbers are calculated from the results of the Fourier transformation.

The xenon reference wavelength is not accurately known and no correction for the dispersion of air was

*Argonne National Laboratory, Argonne, Ill. 60439. and Laboratorie Aimé Cotton, C.N.R.S., F–91405-Orsay, France. Present address: Dept. of Scientific Affairs, Organization of American States, Washington, D.C. 20006
**Laboratoire Aimé Cotton, C.N.R.S., F–91405–Orsay, France.

[1] Literature references are at the end of this paper.

made in the wave number calculations. In consequence we plotted (fig. 1) a correction curve with reference to internal standards of Th I lines whose wave numbers were calculated from the accurately known energy level values of Th I used by Giacchetti, Stanley and Zalubas [1970] in their calculation of the secondary-standard wavelengths below 1.2 μm. This converted the relative scale of wave numbers in air obtained from the Fourier transform calculation to an absolute scale of wave numbers in vacuum that is consistent with the secondary standards. The correction curve had the same amplitude and shape as a correction curve for the dispersion of air.

3. Classification of Lines

Analysis of Th I was begun by Schuurmans [1946] at Amsterdam and has been greatly extended by Zalubas [1968] at the National Bureau of Standards. The analysis of Th II was begun by McNally, Harrison, and Park [1942] at M.I.T. and independently by de Bruin, Schuurmans and Klinkenberg [1943, 1944] at Amsterdam and has been extended by Zalubas and Corliss [1974] and others. These analyses provide energy levels that classify most of the strong lines and many of the weaker lines emitted by electrodeless lamp discharges in thorium vapor.

To classify the Th I lines we searched our list for all possible transitions with $\Delta j = \pm 1, 0$. Many of the levels were known to three decimal places from Giacchetti, Stanley, and Zalubas [1970]; and most of the remainder were determined to three places with the aid of the present line list. Finally, 1907 lines were classified as Th I transitions by using all even levels below 33 100 cm^{-1}, all odd levels below 28 000 cm^{-1}, and a tolerance of ± 0.005 cm^{-1}. Levels above the given values were not used in order to reduce the number of mere chance coincidences of observed wave numbers with calculated level differences. Less than 5 percent of the lines classified as Th I differed from the calculated wave number by more than 0.003 cm^{-1}. The average value of O−C for Th I lines is 0.0016 cm^{-1}.

The levels of Zalubas and Corliss [1974] below 32 000 cm^{-1} were used to classify the Th II lines. The values of most of the levels were determined to three decimal places with the observed interferometric wave numbers. The lines were classified using a tolerance of ± 0.005 cm^{-1}. This procedure permitted classification of 412 lines of Th II, also with an average value of O−C of ± 0.0016 cm^{-1}. There remain 792 lines unclassified from the total of 3111 lines in the Fourier transform spectrum list.

4. Results and Their Relevance to Standard Wavelengths

The wavelengths in air, wave numbers in vacuum and intensities of 3111 infrared thorium lines are listed in table 1. For the classified lines the numerical values of the lower and upper energy levels with their J values are given, the decimal parts being omitted.

The average value of O−C given for Th II suggests that calculated standards for Th II would exceed the

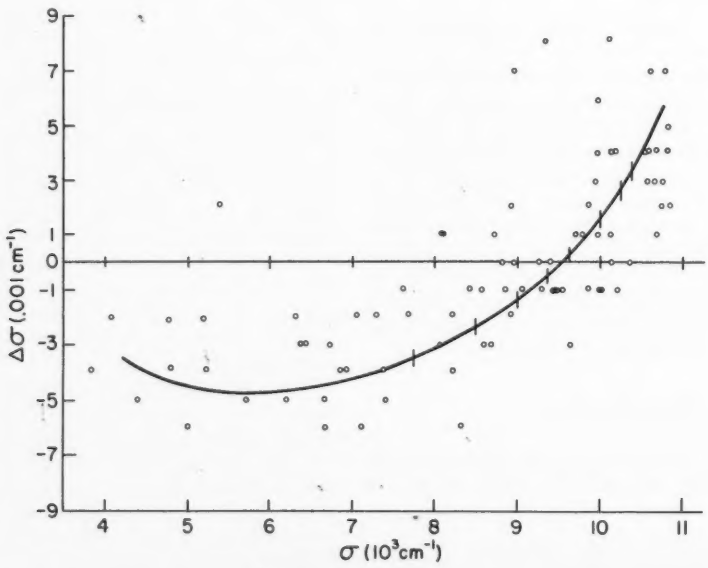

FIGURE 1. *Correction curve from relative wave numbers in air to absolute wave numbers in vacuum.*

accuracy criterion of 0.01 cm^{-1} suggested by Littlefield [1961] to Commission 14 of the I.A.U. for class B (secondary) standards. A report on this matter is now in preparation by Zalubas. Furthermore, the wavelengths in the present list themselves satisfy the criterion.

5. References

Bernage, P., Houdart, R., and Niay, P. [1971], Spectrochimica Acta **26B**, 261.

Connes. J., Delouis, H., Connes. P., Guelachvili. G., Maillard. J–P., and Michel. G. [1970], Nouv. Rev. d'Optique applique **1**, 3.

de Bruin, T. L., Schuurmans. P., and Klinkenberg, P. F. A. [1943]. Z. Phys. **121**, 667.

de Bruin, T. L., Klinkenberg, P. F. A., and Schuurmans. P. [1944], Z. Phys. **122**, 23.

Giacchetti. A., Stanley, R. W., and Zalubas. R. [1970]. J. Opt. Soc. Am. **69**, 474.

Littlefield. T. A. [1961]. Trans. I.A.U. **11B**, 211.

McNally, J. R., Harrison, G. R., and Park, H. B., [1942], J. Opt. Soc. Am. **32**, 334.

Meggers, W. F. [1957]. Trans. I.A.U. **9**, 225.

Schuurmans. P. [1946], Dissertation, Univ. Amsterdam (N.V. Noord-Hollandsche Uitgevers Maatschappij. Amsterdam).

Steers, E. B. M. [1967]. Spectrochimica Acta **23B**, 135.

Zalubas. R. [1968], J. Opt. Soc. Am. **58**, 1195.

Zalubas, R., and Corliss, C. H. [1974]. J. Res. Nat. Bur. Stand. (U.S.), **78A** (Phys. and Chem.) No. 2, p. 163.

(Paper 78A2–812)

TABLE 1. *Infrared spectral lines of thorium*

Wavelength Å	Wavenumber cm^{-1}	Intensity	Spectrum	Classification	Wavelength Å	Wavenumber cm^{-1}	Intensity	Spectrum	Classification
29662.822	3370.304	0	I	$9804_5 - 13175^{\circ}_4$	24007.982	4164.145	4	I	$6362_2 - 10526^{\circ}_3$
29068.481	3439.214	1	II	$10379_{4\frac{1}{2}} - 13818^{\circ}_{3\frac{1}{2}}$	23964.262	4171.742	3	II	$16818^{\circ}_{3\frac{1}{2}} - 20989^{\circ}_{4\frac{1}{2}}$
28574.421	3498.679	0	I	$12847_3 - 16346^{\circ}_4$	23940.033	4175.964	0	I	$24182^{\circ}_2 - 28358_3$
28477.471	3510.590	0			23907.149	4181.708	1	I	$17959_4 - 22141^{\circ}_3$
26734.663	3739.442	0	I	$7502_3 - 11241^{\circ}_3$	23865.994	4188.919	0	I	$22855^{\circ}_3 - 27044_3$
26377.115	3790.131	2	I	$10414^{\circ}_4 - 14204_5$	23850.490	4191.642	2	II	$8378^{\circ}_{3\frac{1}{2}} - 12570_{3\frac{1}{2}}$
25984.374	3847.417	1	I	$18549_2 - 22396^{\circ}_1$	23781.839	4203.742	4	I	$13297_4 - 17501^{\circ}_5$
25971.332	3849.349	0	I	$14204_5 - 18053^{\circ}_4$	23745.817	4210.119	1	II	$13250_{2\frac{1}{2}} - 17460^{\circ}_{2\frac{1}{2}}$
25913.673	3857.914	0	I	$23113^{\circ}_4 - 26971_4$	23742.146	4210.770	4	II	$6168^{\circ}_{3\frac{1}{2}} - 10379_{4\frac{1}{2}}$
25790.101	3876.399	1	I	$20522^{\circ}_2 - 24399_3$	23712.604	4216.016	0	I	$25336^{\circ}_6 - 29552_6$
25735.979	3884.551	1	I	$13962_1 - 17847^{\circ}_2$	23704.794	4217.405	1	I	$22163^{\circ}_4 - 26380_5$
25561.646	3911.044	1	I	$17166_5 - 21077^{\circ}_5$	23696.506	4218.880	1	II	$14349_{1\frac{1}{2}} - 18568^{\circ}_{1\frac{1}{2}}$
25401.710	3935.669	1	II	$10855_{3\frac{1}{2}} - 14790^{\circ}_{3\frac{1}{2}}$	23672.844	4223.097	1	I	$18809^{\circ}_4 - 23032_4$
25269.196	3956.308	1	I	$23015^{\circ}_5 - 26971_4$	23671.785	4223.286	1	I	$13175^{\circ}_4 - 17398_3$
25181.424	3970.098	1	II	$4490^{\circ}_{2\frac{1}{2}} - 8460_{1\frac{1}{2}}$	23663.487	4224.767	1	I	$14206^{\circ}_4 - 18431_3$
25111.575	3981.141	1	I	$22399^{\circ}_5 - 26380_5$	23621.480	4232.280	2	II	$4146_{3\frac{1}{2}} - 8378^{\circ}_{3\frac{1}{2}}$
25080.636	3986.052	2	I	$11877^{\circ}_1 - 15863_2$	23608.338	4234.636	0	I	$17411^{\circ}_3 - 21645_4$
25049.573	3990.995	2	I	$13175^{\circ}_4 - 17166_5$	23597.934	4236.503	1	II	$18118_{1\frac{1}{2}} - 22355^{\circ}_{1\frac{1}{2}}$
25032.462	3993.723	0	I	$25690^{\circ}_5 - 29684_5$	23588.463	4238.204	1	I	$18431_3 - 22669^{\circ}_3$
25000.730	3998.792	0			23551.636	4244.831	1	I	$15970_3 - 20214^{\circ}_3$
24997.523	3999.305	1	I	$13847_2 - 17847^{\circ}_2$	23514.732	4251.493	5	I	$11241^{\circ}_3 - 15493_4$
24973.732	4003.115	1	I	$26723^{\circ}_6 - 30726_7$	23504.277	4253.384	0		
24931.344	4009.921	1	I	$15493_4 - 19503^{\circ}_3$	23484.229	4257.015	1		
24926.551	4010.692	3	II	$9238^{\circ}_{4\frac{1}{2}} - 13248_{4\frac{1}{2}}$	23477.705	4258.198	0	I	$24421^{\circ}_3 - 28679_2$
24902.355	4014.589	1	I	$13945^{\circ}_3 - 17959_4$	23477.236	4258.283	1	II	$13468^{\circ}_{4\frac{1}{2}} - 17727_{5\frac{1}{2}}$
24887.997	4016.905	2	II	$14101^{\circ}_{1\frac{1}{2}} - 18118_{1\frac{1}{2}}$	23458.743	4261.640	0	II	$20120^{\circ}_{2\frac{1}{2}} - 24381_{3\frac{1}{2}}$
24810.069	4029.522	0			23437.525	4265.498	5	II	$4113_{2\frac{1}{2}} - 8378^{\circ}_{3\frac{1}{2}}$
24789.343	4032.891	1	I	$21890^{\circ}_3 - 25923_4$	23403.546	4271.691	0	I	$18930^{\circ}_3 - 23201_3$
24684.317	4050.050	0	I	$19227^{\circ}_6 - 23277_5$	23381.575	4275.705	0		
24516.271	4077.811	1	I	$23113^{\circ}_4 - 27191_5$	23372.954	4277.282	0	II	$20969^{\circ}_{3\frac{1}{2}} - 25246_{4\frac{1}{2}}$
24486.763	4082.725	0	I	$24259^{\circ}_4 - 28342_5$	23330.692	4285.030	2	I	$26645^{\circ}_5 - 30930_6$
24470.262	4085.478	0	I	$23481^{\circ}_1 - 27566_2$	23316.550	4287.629	1	II	$17727_{5\frac{1}{2}} - 22014^{\circ}_{5\frac{1}{2}}$
24439.138	4090.681	1			23314.380	4288.028	1	I	$22508^{\circ}_2 - 26796_3$
24428.586	4092.448	1	I	$22163^{\circ}_4 - 26255_4$	23297.038	4291.220	0	I	$24850^{\circ}_6 - 29141_5$
24420.077	4093.874	1	I	$22877^{\circ}_5 - 26971_4$	23270.076	4296.192	2	I	$11197^{\circ}_5 - 15493_4$
24352.698	4105.201	0	II	$10379_{4\frac{1}{2}} - 14484^{\circ}_{5\frac{1}{2}}$	23222.202	4305.049	1	II	$20158_{2\frac{1}{2}} - 24463^{\circ}_{2\frac{1}{2}}$
24345.717	4106.378	0	II	$9711_{3\frac{1}{2}} - 13818^{\circ}_{3\frac{1}{2}}$	23217.661	4305.891	1	I	$18549_2 - 22855^{\circ}_3$
24329.294	4109.150	0	I	$25575^{\circ}_4 - 29684_5$	23175.469	4313.730	3	I	$16554_6 - 20867^{\circ}_7$
24301.853	4113.790	1	I	$13297_4 - 17411^{\circ}_3$	23153.597	4317.805	4	I	$15736^{\circ}_1 - 20054_2$
24291.248	4115.586	3	II	$4490^{\circ}_{2\frac{1}{2}} - 8605_{2\frac{1}{2}}$	23127.608	4322.657	1	I	$13088_3 - 17411^{\circ}_3$
24262.390	4120.481	1	I	$18549_2 - 22669^{\circ}_3$	23121.211	4323.853	0	I	$25690^{\circ}_5 - 30014_4$
24216.068	4128.363	0	I	$21575_2 - 25703^{\circ}_2$	23085.081	4330.620	0	I	$14243^{\circ}_1 - 18574_1$
24214.789	4128.581	1			23075.703	4332.380	2	II	$12485^{\circ}_{3\frac{1}{2}} - 16818_{3\frac{1}{2}}$
24185.996	4133.496	0			23007.044	4345.309	1	I	$27948^{\circ}_4 - 32293_5$
24172.879	4135.739	2	I	$13088_3 - 17224^{\circ}_2$	23003.968	4345.890	2	II	$12472^{\circ}_{2\frac{1}{2}} - 16818_{3\frac{1}{2}}$
24171.733	4135.935	0	I	$11601_1 - 15736^{\circ}_1$	22978.346	4350.736	0	I	$17224^{\circ}_2 - 21575_2$
24138.665	4141.601	0	I	$24421^{\circ}_3 - 28562_4$	22964.759	4353.310	1	I	$21902^{\circ}_4 - 26255_4$
24136.264	4142.013	3	I	$20522^{\circ}_2 - 24664_3$	22959.448	4354.317	0		
24120.715	4144.683	1	I	$17501^{\circ}_5 - 21645_4$	22937.124	4358.555	2	II	$6213_{4\frac{1}{2}} - 10572^{\circ}_{4\frac{1}{2}}$
24060.000	4155.142	1	II	$6700^{\circ}_{4\frac{1}{2}} - 10855_{3\frac{1}{2}}$	22916.350	4362.506	0		

TABLE 1. *Infrared spectral lines of thorium*—Continued

Wavelength Å	Wavenumber cm^{-1}	Intensity	Spectrum	Classification	Wavelength Å	Wavenumber cm^{-1}	Intensity	Spectrum	Classification
22911.403	4363.448	0	II	$24982^{\circ}_{3\,1/2} - 29345_{2\,1/2}$	22103.641	4522.907	4	I	$16554_{6} - 21077^{\circ}_{5}$
22900.906	4365.448	2	I	$21890^{\circ}_{3} - 26255_{4}$	22098.511	4523.957	0	II	$15786_{2\,1/2} - 20310^{\circ}_{2\,1/2}$
22900.565	4365.513	0	I	$15166^{\circ}_{3} - 19532_{4}$	22082.481	4527.241	1	I	$25321^{\circ}_{3} - 29849_{4}$
22875.089	4370.375	0	I	$17224^{\circ}_{2} - 21594_{3}$	22073.514	4529.080	1	I	$19503^{\circ}_{3} - 24032_{4}$
22864.133	4372.469	2	I	$25180^{\circ}_{7} - 29552_{6}$	22029.034	4538.225	0	I	$21575_{2} - 26113^{\circ}_{2}$
22860.040	4373.252	0	I	$24561^{\circ}_{3} - 28934_{3}$	21990.719	4546.132	2	I	$15166^{\circ}_{3} - 19713_{3}$
22855.180	4374.182	2	I	$18614^{\circ}_{1} - 22988_{2}$	21987.769	4546.742	0	I	$19713_{3} - 24259^{\circ}_{4}$
22851.632	4374.861	3	I	$8800_{4} - 13175^{\circ}_{4}$				I	$26882^{\circ}_{0} - 31429_{1}$
22843.962	4376.330	1	I	$12847_{3} - 17224^{\circ}_{2}$	21986.275	4547.051	0	I	$21143_{5} - 25690^{\circ}_{5}$
22834.596	4378.125	2	I	$3865_{1} - 8243^{\circ}_{2}$	21978.488	4548.662	1		
22829.522	4379.098	2	I	$17959_{4} - 22338^{\circ}_{5}$	21973.106	4549.776	2		
22806.940	4383.434	0	I	$21539^{\circ}_{4} - 25923_{4}$	21959.399	4552.616	1	I	$15970_{3} - 20522^{\circ}_{2}$
22785.721	4387.516	1	I	$14226_{0} - 18614^{\circ}_{1}$	21952.080	4554.134	1	I	$17847^{\circ}_{2} - 22401_{1}$
22785.383	4387.581	1	II	$10855_{3\,1/2} - 15242^{\circ}_{4\,1/2}$	21944.958	4555.612	4	I	$3687_{2} - 8243^{\circ}_{2}$
22760.862	4392.308	0	I	$20522^{\circ}_{2} - 24915_{3}$	21925.759	4559.601	2	I	$15863_{2} - 20423^{\circ}_{1}$
22750.249	4394.357	1	I	$18699_{2} - 23093^{\circ}_{2}$	21907.002	4563.505	1	II	$10673^{\circ}_{2\,1/2} - 15236_{1\,1/2}$
22733.218	4397.649	0	II	$27526_{4\,1/2} - 31924^{\circ}_{5\,1/2}$	21906.445	4563.621	1	II	$9711_{3\,1/2} - 14275^{\circ}_{4\,1/2}$
22723.153	4399.597	0	I	$14032^{\circ}_{2} - 18431_{3}$	21883.548	4568.396	0	I	$18069^{\circ}_{3} - 22637_{3}$
22710.196	4402.107	3	I	$9804_{5} - 14206^{\circ}_{4}$	21871.813	4570.847	1	II	$4490^{\circ}_{2\,1/2} - 9061_{2\,1/2}$
22646.195	4414.548	3	I	$11802_{2} - 16217^{\circ}_{2}$	21862.515	4572.791	1	I	$23655^{\circ}_{4} - 28227_{4}$
22641.743	4415.416	0			21852.069	4574.977	2	II	$7001_{1\,1/2} - 11576^{\circ}_{1\,1/2}$
22631.728	4417.370	0	II	$9400^{\circ}_{2\,1/2} - 13818^{\circ}_{3\,1/2}$	21830.625	4579.471	1		
22616.700	4420.305	1	I	$13962_{1} - 18382^{\circ}_{0}$	21809.793	4583.845	0	I	$18053^{\circ}_{4} - 22637_{3}$
22614.383	4420.758	4	I	$6362_{2} - 10783^{\circ}_{2}$	21765.236	4593.229	0		
22582.257	4427.047	1	II	$15453^{\circ}_{3\,1/2} - 19880_{4\,1/2}$	21756.165	4595.144	1	I	$17073_{1} - 21668^{\circ}_{1}$
22571.571	4429.143	1	II	$19880_{4\,1/2} - 24309^{\circ}_{5\,1/2}$	21749.619	4596.527	1	I	$15970_{3} - 20566^{\circ}_{4}$
22544.420	4434.477	1	I	$25321^{\circ}_{3} - 29756_{4}$	21747.329	4597.011	1	I	$17501^{\circ}_{3} - 22098_{4}$
22537.763	4435.787	3	I	$15618^{\circ}_{3} - 20054_{2}$	21743.999	4597.715	5	II	$10855_{3\,1/2} - 15453^{\circ}_{3\,1/2}$
22518.913	4439.500	0	I	$17959_{4} - 22399^{\circ}_{5}$	21743.999	4597.715	5	I	$7280_{2} - 11877^{\circ}_{1}$
22513.933	4440.482	1	I	$24701^{\circ}_{5} - 29141_{5}$	21712.571	4604.370	4	I	$8243^{\circ}_{2} - 12847_{3}$
22506.128	4442.022	4	II	$8460_{1\,1/2} - 12902^{\circ}_{1\,1/2}$	21706.674	4605.621	1	I	$14204_{5} - 18809^{\circ}_{4}$
22496.819	4443.860	2	I	$19588^{\circ}_{5} - 24032_{4}$	21706.264	4605.708	1	I	$23752^{\circ}_{2} - 28358_{3}$
22467.732	4449.613	1	II	$15144^{\circ}_{1\,1/2} - 19594_{1\,1/2}$	21683.632	4610.515	0	I	$21143_{5} - 25753^{\circ}_{5}$
22446.273	4453.867	0	I	$21594_{3} - 26048^{\circ}_{4}$	21676.298	4612.075	0	I	$7502_{3} - 12114^{\circ}_{2}$
22445.678	4453.985	2	II	$8018_{1\,1/2} - 12472^{\circ}_{2\,1/2}$	21662.376	4615.039	0	II	$22642^{\circ}_{4\,1/2} - 27257_{3\,1/2}$
22439.688	4455.174	0	I	$15493_{4} - 19948^{\circ}_{4}$	21655.755	4616.450	2	I	$11601_{1} - 16217^{\circ}_{2}$
22437.386	4455.631	1	I	$14243^{\circ}_{1} - 18699_{2}$	21637.288	4620.390	2		
22412.467	4460.585	0			21628.998	4622.161	4	I	$11241^{\circ}_{3} - 15863_{2}$
22377.781	4467.499	1	I	$18809^{\circ}_{4} - 23277_{5}$	21605.654	4627.155	1	I	$24307^{\circ}_{2} - 28934_{3}$
22369.419	4469.169	1			21599.082	4628.563	1	I	$22637_{3} - 27266^{\circ}_{4}$
22350.905	4472.871	0	I	$23093^{\circ}_{2} - 27566_{2}$	21580.898	4632.463	0	I	$22338^{\circ}_{5} - 26971_{4}$
22344.755	4474.102	2	I	$11877^{\circ}_{1} - 16351_{0}$	21558.955	4637.178	2	II	$15242^{\circ}_{4\,1/2} - 19880_{4\,1/2}$
22343.861	4474.281	3	II	$13248_{4\,1/2} - 17722^{\circ}_{4\,1/2}$	21556.115	4637.789	0	I	$21252^{\circ}_{2} - 25890_{2}$
22323.993	4478.263	0	I	$21902^{\circ}_{4} - 26380_{5}$	21527.563	4643.940	0	I	$22877^{\circ}_{3} - 27521_{4}$
22318.327	4479.400	1	I	$19273_{2} - 23752^{\circ}_{2}$	21519.111	4645.764	0	I	$23916^{\circ}_{4} - 28562_{4}$
22283.623	4486.376	0	I	$13945^{\circ}_{3} - 18431_{3}$	21472.877	4655.767	1	I	$25355^{\circ}_{4} - 30011_{3}$
22264.353	4490.259	6	II	$0_{1\,1/2} - 4490^{\circ}_{2\,1/2}$	21442.806	4662.296	1	I	$18431_{3} - 23093^{\circ}_{2}$
22215.926	4500.047	1	I	$18549_{2} - 23049^{\circ}_{1}$	21424.751	4666.225	0	I	$22855^{\circ}_{3} - 27521_{4}$
22135.320	4516.434	0			21418.725	4667.538	0	I	$14032^{\circ}_{2} - 18699_{2}$
22115.259	4520.531	0	I	$23752^{\circ}_{2} - 28273_{2}$	21415.242	4668.297	2	I	$19713_{3} - 24381^{\circ}_{2}$

530-326 OL - 74 - 11

TABLE 1. *Infrared spectral lines of thorium*—Continued

Wavelength Å	Wavenumber cm^{-1}	Intensity	Spectrum	Classification
21408.148	4669.844	0		
21406.777	4670.143	1	I	$19532_4 - 24202^\circ_4$
21387.561	4674.339	1	II	$24757^\circ_{3\frac{1}{2}} - 29431_{3\frac{1}{2}}$
21375.118	4677.060	3	I	$9804_5 - 14481^\circ_6$
21358.737	4680.647	1		
21353.185	4681.864	3	I	$18431_3 - 23113^\circ_4$
21329.914	4686.972	1	II	$6168^\circ_{3\frac{1}{2}} - 10855_{3\frac{1}{2}}$
21328.149	4687.360	0	I	$23655^\circ_4 - 28342_5$
21319.166	4689.335	1	I	$22877^\circ_1 - 27566_2$
21280.628	4697.827	1		
21264.265	4701.442	0	II	$14349_{\frac{1}{2}} - 19050^\circ_{1\frac{1}{2}}$
21262.841	4701.757	1	II	$12570_{3\frac{1}{2}} - 17272^\circ_{4\frac{1}{2}}$
21260.824	4702.203	0	I	$24850^\circ_6 - 29552_6$
21256.077	4703.253	0	I	$23655^\circ_4 - 28358_3$
21250.077	4704.581	0	I	$25306^\circ_2 - 30011_3$
21247.182	4705.222	0	I	$22338^\circ_3 - 27044_3$
21239.694	4706.881	1	I	$23521^\circ_3 - 28227_4$
21205.593	4714.450	0		
21203.367	4714.945	0	I	$20054_2 - 24769^\circ_5$
21199.298	4715.850	0		
21198.664	4715.991	0	I	$21539^\circ_4 - 26255_4$
21173.002	4721.707	1	I	$15493_4 - 20214^\circ_5$
21162.697	4724.006	5	II	$7001_{1\frac{1}{2}} - 11725^\circ_{1\frac{1}{2}}$
21148.510	4727.175	3	I	$23306^\circ_6 - 28034_5$
21143.170	4728.369	4	I	$11241^\circ_2 - 15970_3$
21132.654	4730.722	2	I	$19039^\circ_2 - 23769_1$
21123.018	4732.880	0	II	$13250_{2\frac{1}{2}} - 17983^\circ_{2\frac{1}{2}}$
21121.474	4733.226	1	II	$10572^\circ_{4\frac{1}{2}} - 15305_{4\frac{1}{2}}$
21117.677	4734.077	0	I	$21143_5 - 25877^\circ_4$
21108.367	4736.165	1	I	$17166_5 - 21902^\circ_4$
21095.446	4739.066	0	I	$15493_4 - 20232^\circ_4$
			I	$21645_4 - 26384^\circ_4$
21046.638	4750.056	0	II	$23187^\circ_{5\frac{1}{2}} - 27937_{5\frac{1}{2}}$
21019.525	4756.183	2	I	$13297_4 - 18053^\circ_5$
21014.864	4757.238	2	II	$9061_{2\frac{1}{2}} - 13818^\circ_{3\frac{1}{2}}$
21011.808	4757.930	2	I	$21165^\circ_3 - 25923_4$
21009.229	4758.514	1	I	$13088_3 - 17847^\circ_2$
20981.790	4764.737	0	I	$17398_3 - 22163^\circ_4$
20973.743	4766.565	1	I	$13847_2 - 18614^\circ_1$
20965.562	4768.425	1	I	$21594_3 - 26363^\circ_2$
20951.480	4771.630	1	I	$13297_4 - 18069^\circ_5$
20941.487	4773.907	0		
20936.496	4775.045	1		
20935.448	4775.284	0		
20934.926	4775.403	0	II	$15305_{4\frac{1}{2}} - 20080^\circ_{5\frac{1}{2}}$
20920.513	4778.693	1	I	$26363^\circ_2 - 31141_3$
20895.196	4784.483	0		
20893.881	4784.784	0	I	$13175^\circ_1 - 17959_4$
20879.577	4788.062	1	I	$21575_2 - 26363^\circ_2$
20869.452	4790.385	4	I	$17847^\circ_2 - 22637_3$
20863.115	4791.840	0	I	$23481^\circ_5 - 28273_5$
20862.579	4791.963	2	I	$22399^\circ_5 - 27191_5$
20833.885	4798.563	1	I	$25753^\circ_5 - 30552_4$
20792.737	4808.059	1	I	$14465^\circ_2 - 19273_2$
20735.100	4821.424	0	I	$18699_2 - 23521^\circ_3$
20730.370	4822.524	0		
20717.817	4825.446	0	I	$20054_2 - 24880^\circ_1$
20716.744	4825.696	2	I	$22669^\circ_5 - 27495_4$
20715.963	4825.878	0	I	$25306^\circ_2 - 30132_2$
20702.372	4829.046	0	I	$15493_4 - 20322^\circ_5$
20692.063	4831.452	6	II	$1859_{1\frac{1}{2}} - 6691^\circ_{1\frac{1}{2}}$
20682.889	4833.595	4	II	$9711_{3\frac{1}{2}} - 14545^\circ_{2\frac{1}{2}}$
20681.631	4833.889	0	I	$24850^\circ_6 - 29684_5$
20680.125	4834.241	4	I	$7280_2 - 12114^\circ_2$
20674.386	4835.583	1		
20661.764	4838.537	1	I	$20566^\circ_4 - 25405_4$
20651.478	4840.947	0	I	$21539^\circ_4 - 26380_5$
20649.114	4841.501	1	II	$22685^\circ_{3\frac{1}{2}} - 27526_{4\frac{1}{2}}$
20634.364	4844.962	6	I	$8243^\circ_2 - 13088_3$
20618.818	4848.615	0	I	$19713_3 - 24561^\circ_3$
20610.588	4850.551	1	I	$17398_3 - 22248^\circ_2$
20609.747	4850.749	1	II	$17983^\circ_{2\frac{1}{2}} - 22834_{3\frac{1}{2}}$
20605.987	4851.634	2	I	$22669^\circ_5 - 27521_4$
20584.349	4856.734	0	I	$24561^\circ_3 - 29418_2$
20575.702	4858.775	0		
20575.042	4858.931	0	I	$21252^\circ_2 - 26111_1$
20562.003	4862.012	0	I	$16783^\circ_1 - 21645_4$
20561.348	4862.167	2	I	$21645_4 - 26508^\circ_5$
20554.521	4863.782	3	II	$10379_{4\frac{1}{2}} - 15242^\circ_{4\frac{1}{2}}$
20550.363	4864.766	1		
20541.715	4866.814	1	I	$24274^\circ_5 - 29141_5$
20528.880	4869.857	4	II	$8378^\circ_{3\frac{1}{2}} - 13248_{4\frac{1}{2}}$
20521.311	4871.653	2	II	$8378^\circ_{3\frac{1}{2}} - 13250_{2\frac{1}{2}}$
20513.976	4873.395	0	I	$15863_2 - 20737^\circ_1$
20489.032	4879.328	1	I	$6362_2 - 11241^\circ_3$
20478.858	4881.752	1	I	$24259^\circ_4 - 29141_5$
20468.653	4884.186	4	II	$8018_{1\frac{1}{2}} - 12902^\circ_{1\frac{1}{2}}$
20468.318	4884.266	0		
20453.217	4887.872	0	I	$15166^\circ_3 - 20054_2$
20450.627	4888.491	1	II	$7331^\circ_{2\frac{1}{2}} - 12219_{1\frac{1}{2}}$
20450.008	4888.639	1	I	$19532_4 - 24421^\circ_3$
20443.773	4890.130	2	II	$12570_{3\frac{1}{2}} - 17460^\circ_{2\frac{1}{2}}$
20430.283	4893.359	0	II	$18118_{1\frac{1}{2}} - 23012^\circ_{1\frac{1}{2}}$
20428.437	4893.801	1	I	$21902^\circ_4 - 26796_3$
20421.761	4895.401	3	I	$17959_4 - 22855^\circ_3$
20419.379	4895.972	0	I	$19503^\circ_3 - 24399_3$
20395.738	4901.647	3	II	$12219_{1\frac{1}{2}} - 17121^\circ_{1\frac{1}{2}}$
20392.064	4902.530	0	I	$26363^\circ_2 - 31265_3$
20391.719	4902.613	0	I	$22141^\circ_3 - 27044_3$
20389.710	4903.096	4	II	$6213_{4\frac{1}{2}} - 11116^\circ_{3\frac{1}{2}}$

TABLE 1. *Infrared spectral lines of thorium*—Continued

Wavelength Å	Wavenumber cm^{-1}	Intensity	Spectrum	Classification	Wavelength Å	Wavenumber cm^{-1}	Intensity	Spectrum	Classification
20381.309	4905.117	3	I	$21143_5 - 26048^c_4$	19768.543	5057.161	0		
20377.894	4905.939	1	I	$21890^c_3 - 26796_3$	19765.178	5058.022	3	I	$21738^c_2 - 26796_3$
20374.476	4906.762	1	I	$18574_1 - 23481^c_1$	19764.361	5058.231	0	I	$15863_2 - 20922^c_2$
20358.092	4910.711	0	II	$4490^c_{2\frac{1}{2}} - 9400_{2\frac{1}{2}}$	19762.115	5058.806	0	I	$22508^c_2 - 27566_2$
20321.907	4919.455	0	I	$18069^c_3 - 22988_2$	19758.662	5059.690	1		
20317.777	4920.455	4	I	$23113^c_4 - 28034_5$	19757.006	5060.114	0	I	$18930^c_3 - 23990_2$
20292.710	4926.533	0			19741.428	5064.107	5	I	$8111_4 - 13175^c_4$
20264.464	4933.400	0			19736.666	5065.329	0	I	$24769^c_3 - 29835_3$
20263.141	4933.722	0	I	$26995^c_3 - 31929_3$	19733.467	5066.150	1	I	$26363^c_2 - 31429_1$
20234.945	4940.597	0	I	$17398_3 - 22338^c_3$	19721.637	5069.189	0	I	$21902^c_4 - 26971_4$
20205.662	4947.757	0	I	$25703^c_2 - 30651_3$	19719.303	5069.789	1	II	$25414^c_{3\frac{1}{2}} - 30484_{3\frac{1}{2}}$
20191.383	4951.256	3	I	$19039^c_2 - 23990_2$	19717.004	5070.380	0		
20183.242	4953.253	0	I	$27087^c_1 - 32041_2$	19705.256	5073.403	0	I	$15493_4 - 20566^c_4$
20165.057	4957.720	3			19703.648	5073.817	1	II	$7828_{1\frac{1}{2}} - 12902^c_{1\frac{1}{2}}$
20158.039	4959.446	2	I	$12114^c_2 - 17073_1$	19703.283	5073.911	1	II	$10379_{4\frac{1}{2}} - 15453^c_{3\frac{1}{2}}$
20139.866	4963.921	1	II	$13250_{2\frac{1}{2}} - 18214^c_{1\frac{1}{2}}$	19701.761	5074.303	0	II	$15236_{1\frac{1}{2}} - 20310^c_{1\frac{1}{2}}$
			I	$18069^c_3 - 23032_4$	19696.195	5075.737	1	I	$23603^c_2 - 28679_2$
20128.687	4966.678	3	I	$10526^c_3 - 15493_4$	19692.738	5076.628	1	I	$13962_1 - 19039^c_2$
20122.241	4968.269	0	I	$20922^c_2 - 25890_2$	19692.319	5076.736	0		
20118.722	4969.138	1			19683.409	5079.034	5	II	$9711_{3\frac{1}{2}} - 14790^c_{3\frac{1}{2}}$
20108.593	4971.641	2	I	$18549_2 - 23521^c_3$	19683.215	5079.084	4	I	$10414^c_4 - 15493_4$
20082.971	4977.984	1			19676.823	5080.734	1	I	$10783^c_2 - 15863_2$
20077.401	4979.365	2	I	$18053^c_4 - 23032_4$	19674.535	5081.325	3	I	$21890^c_3 - 26971_4$
20061.498	4983.312	0			19669.905	5082.521	2	I	$13847_2 - 18930^c_3$
20047.945	4986.681	2	I	$24769^c_3 - 29756_4$	19668.461	5082.894	4	I	$20322^c_3 - 25405_4$
20026.106	4992.119	2			19645.360	5088.871	1		
19998.121	4999.105	1	I	$12847_3 - 17847^c_2$	19644.523	5089.088	4	II	$14790^c_{3\frac{1}{2}} - 19880_{4\frac{1}{2}}$
19984.221	5002.582	0	II	$26770^c_{5\frac{1}{2}} - 31773_{4\frac{1}{2}}$	19643.457	5089.364	1	I	$18431_3 - 23521^c_3$
19935.599	5014.783	0	I	$27948^c_4 - 32963_5$	19639.120	5090.488	1	I	$21165^c_3 - 26255_4$
19922.803	5018.004	1	I	$23916^c_4 - 28934_5$	19626.624	5093.729	0		
19919.437	5018.852	0	I	$23015^c_5 - 28034_5$	19626.212	5093.836	1		
19908.520	5021.604	0	I	$18011^c_3 - 23032_4$	19622.548	5094.787	0	I	$22248^c_2 - 27343_3$
19902.706	5023.071	4	I	$14204_5 - 19227^c_6$	19617.154	5096.188	2	I	$22399^c_5 - 27495_4$
19890.383	5026.183	2			19595.083	5101.928	3	I	$18930^c_3 - 24032_4$
19885.078	5027.524	0			19593.390	5102.369	0	II	$19880_{4\frac{1}{2}} - 24982^c_{3\frac{1}{2}}$
19882.301	5028.226	2	I	$22163^c_4 - 27191_5$	19586.250	5104.229	0	I	$22508^c_2 - 27612_3$
19862.586	5033.217	0	I	$24981^c_3 - 30014_4$	19571.602	5108.049	2	I	$19273_2 - 24381^c_2$
19857.666	5034.464	2	I	$19273_2 - 24307^c_2$	19561.688	5110.638	2	I	$24307^c_2 - 29418_2$
19852.906	5035.671	2	I	$23306^c_6 - 28342_5$	19540.414	5116.202	1	II	$10189^c_{3\frac{1}{2}} - 15305_{4\frac{1}{2}}$
19850.778	5036.211	1	I	$25336^c_6 - 30372_6$	19535.499	5117.489	0	II	$22139^c_{4\frac{1}{2}} - 27257_{3\frac{1}{2}}$
19848.224	5036.859	0						I	$26878^c_3 - 31995_4$
19847.455	5037.054	0	I	$24381^c_2 - 29418_2$	19528.833	5119.236	0		
19844.520	5037.799	0	II	$25414^c_{5\frac{1}{2}} - 30452_{4\frac{1}{2}}$	19519.076	5121.795	0	I	$27674^c_2 - 32796_3$
19840.952	5038.705	1			19505.411	5125.383	0	I	$22855^c_3 - 27980_3$
19829.520	5041.610	1	I	$23521^c_3 - 28562_4$	19503.105	5125.989	1	II	$23697^c_{3\frac{1}{2}} - 28823_{2\frac{1}{2}}$
19797.857	5049.673	0	I	$23481^c_1 - 28531_2$	19476.782	5132.917	1	I	$18069^c_3 - 23201_3$
19786.004	5052.698	5	I	$7795^c_4 - 12847_3$	19474.463	5133.528	2		
19784.595	5053.058	1	I	$18699_2 - 23752^c_2$	19473.652	5133.742	1		
19774.295	5055.690	6	II	$4146_{3\frac{1}{2}} - 9202^c_{3\frac{1}{2}}$	19449.859	5140.022	0		
19770.799	5056.584	1	I	$24084^c_6 - 29141_5$	19444.483	5141.443	1	I	$17847^c_2 - 22988_2$

TABLE 1. *Infrared spectral lines of thorium*—Continued

Wavelength Å	Wavenumber cm^{-1}	Intensity	Spectrum	Classification	Wavelength Å	Wavenumber cm^{-1}	Intensity	Spectrum	Classification
19432.597	5144.588	3	II	$9400_{2½}-14545^{0}_{2½}$	19082.536	5238.963	3	II	$12488^{0}_{2½}-17727_{3½}$
19430.829	5145.056	2	I	$8800_{4}-13945^{0}_{3}$	19080.012	5239.656	1	I	$24182^{0}_{2}-29422_{1}$
19420.664	5147.749	1	I	$19516^{0}_{2}-24664_{3}$	19078.887	5239.965	1	I	$25690^{0}_{5}-30930_{6}$
19418.336	5148.366	1	I	$18053^{0}_{4}-23201_{3}$	19076.390	5240.651	0	II	$12219_{1½}-17460^{0}_{2½}$
19402.768	5152.497	2	II	$12570_{2½}-17722^{0}_{2½}$	19074.406	5241.196	3	I	$14032^{0}_{2}-19273_{2}$
19400.479	5153.105	3	I	$20737^{0}_{1}-25890_{2}$	19073.289	5241.503	2	I	$21143_{5}-26384^{0}_{4}$
19396.794	5154.084	2	I	$21890^{0}_{3}-27044_{3}$	19050.366	5247.810	0	I	$14465^{0}_{2}-19713_{3}$
19391.319	5155.539	1	I	$18614^{0}_{1}-23769_{1}$	19042.039	5250.105	0		
19388.002	5156.421	1	I	$22877^{0}_{5}-28034_{5}$	19035.208	5251.989	0	I	$20054_{2}-25306^{0}_{2}$
19353.457	5165.625	0	II	$20080^{0}_{3½}-25246_{4½}$	19033.646	5252.420	1	I	$24880^{0}_{1}-30132_{2}$
19345.173	5167.837	0	I	$22098_{4}-27266^{0}_{4}$	19018.615	5256.571	2	I	$13175^{0}_{4}-18431_{3}$
19342.209	5168.629	2	I	$19532_{4}-24701^{0}_{5}$	18984.562	5266.000	0	I	$18011^{0}_{5}-23277_{5}$
19338.976	5169.493	7	II	$1521_{2½}-6691^{0}_{1½}$	18964.790	5271.490	1	I	$17398_{3}-22669^{0}_{3}$
19336.983	5170.026	0	I	$22396^{0}_{1}-27566_{2}$	18961.873	5272.301	1	II	$25607^{0}_{2½}-30879_{3½}$
19321.626	5174.135	0	I	$26363^{0}_{2}-31537_{3}$	18958.367	5273.276	1	I	$22338^{0}_{5}-27612_{3}$
19320.977	5174.309	1			18957.939	5273.395	0	I	$24561^{0}_{3}-29835_{3}$
19317.885	5175.137	3	I	$17073_{1}-22248^{0}_{2}$	18942.594	5277.667	0	I	$26651^{0}_{2}-31929_{3}$
19307.868	5177.822	2	II	$10855_{3½}-16033^{0}_{3½}$	18942.109	5277.802	1	I	$24274^{0}_{5}-29552_{6}$
19291.493	5182.217	1	I	$23752^{0}_{2}-28934_{3}$	18938.047	5278.934	1	I	$23603^{0}_{2}-28882_{2}$
19290.328	5182.530	0	I	$22338^{0}_{3}-27521_{4}$	18931.513	5280.756	1		
19273.916	5186.943	2	I	$10783^{0}_{2}-15970_{3}$	18925.238	5282.507	0	I	$15970_{3}-21252^{0}_{2}$
19268.474	5188.408	0			18919.776	5284.032	2	I	$12114^{0}_{2}-17398_{3}$
19264.749	5189.411	1	I	$20922^{0}_{2}-26111_{1}$	18911.609	5286.314	0		
19261.710	5190.230	0	I	$20214^{0}_{3}-25405_{4}$	18907.334	5287.509	2	I	$24561^{0}_{3}-29849_{4}$
19261.001	5190.421	0	I	$23655^{0}_{4}-28845_{4}$	18905.486	5288.026	1		
19257.450	5191.378	0	I	$13847_{2}-19039^{0}_{2}$	18904.263	5288.368	0	I	$19273_{2}-24561^{0}_{3}$
19256.382	5191.666	1	I	$18549_{2}-23741^{0}_{1}$	18893.288	5291.440	0	I	$27260^{0}_{5}-32551_{3}$
19244.968	5194.745	0	I	$24561^{0}_{3}-29756_{4}$	18892.767	5291.586	0		
19244.035	5194.997	1	I	$15970_{3}-21165^{0}_{3}$	18886.685	5293.290	6	I	$7795^{0}_{4}-13088_{3}$
19241.246	5195.750	0	I	$21594_{3}-26790^{0}_{4}$	18885.747	5293.553	0		
19240.420	5195.973	0	I	$11877^{0}_{1}-17073_{1}$	18885.154	5293.719	1	I	$24838^{0}_{1}-30132_{2}$
19204.660	5205.648	1	I	$12847_{3}-18053^{0}_{4}$	18884.038	5294.032	0		
19190.670	5209.443	2	I	$27084^{0}_{6}-32293_{5}$	18880.700	5294.968	0	II	$22642^{0}_{4½}-27937_{5½}$
19188.567	5210.014	0			18872.185	5297.357	1		
19188.114	5210.137	0			18865.586	5299.210	3	I	$16346^{0}_{4}-21645_{4}$
19179.419	5212.499	3	II	$8605_{2½}-13818^{0}_{3½}$	18858.490	5301.204	1	I	$15863_{2}-21165^{0}_{3}$
19178.389	5212.779	2	I	$23015^{0}_{3}-28227_{4}$	18856.508	5301.761	0		
19165.340	5216.328	1	II	$12902^{0}_{1½}-18118_{1½}$	18850.731	5303.386	2	I	$21077^{0}_{5}-26380_{5}$
19162.549	5217.088	1	I	$26048^{0}_{4}-31265_{3}$	18840.854	5306.166	0	I	$21738^{0}_{2}-27044_{3}$
19158.359	5218.229	0			18824.439	5310.793	0	I	$22669^{0}_{3}-27980_{3}$
19151.815	5220.012	4	I	$5563_{1}-10783^{0}_{2}$	18811.879	5314.339	7	I	$16783^{0}_{4}-22098_{4}$
19147.846	5221.094	3	I	$12847_{3}-18069^{0}_{3}$	18802.414	5317.014	3	I	$16351_{0}-21668^{0}_{1}$
19145.601	5221.706	7	II	$4490^{0}_{2½}-9711_{3½}$	18799.282	5317.900	0	I	$22248^{0}_{2}-27566_{2}$
19143.281	5222.339	1	I	$18809^{0}_{4}-24032_{4}$	18788.340	5320.997	0	I	$18431_{3}-23752^{0}_{2}$
19138.077	5223.759	1	I	$18053^{0}_{4}-23277_{5}$	18781.224	5323.013	1	I	$17073_{1}-22396^{0}_{1}$
			I	$23049^{0}_{5}-28273_{5}$	18772.446	5325.502	3	I	$14206^{0}_{4}-19532_{4}$
19113.116	5230.581	2	I	$25321^{0}_{3}-30552_{4}$	18763.740	5327.973	0	I	$13945^{0}_{3}-19273_{2}$
19108.517	5231.840	0			18737.838	5335.338	0	I	$24421^{0}_{3}-29756_{4}$
19091.898	5236.394	0	I	$23609^{0}_{2}-28845_{4}$	18730.785	5337.347	2	I	$10526^{0}_{3}-15863_{2}$
19088.610	5237.296	3	I	$19532_{4}-24769^{0}_{5}$	18689.399	5349.166	0	I	$16554_{6}-21903^{0}_{7}$

TABLE 1. *Infrared spectral lines of thorium* – Continued

Wavelength Å	Wavenumber cm^{-1}	Intensity	Spectrum	Classification	Wavelength Å	Wavenumber cm^{-1}	Intensity	Spectrum	Classification
18685.648	5350.240	0	I	$26645^{\circ}_{5} - 31995_{4}$	18228.371	5484.456	4	II	$9061_{2\frac{1}{2}} - 14545^{\circ}_{2\frac{1}{2}}$
18685.274	5350.347	1	I	$22877^{\circ}_{5} - 28227_{4}$	18225.855	5485.213	1	I	$18431_{3} - 23916^{\circ}_{4}$
18682.627	5351.105	0			18221.955	5486.387	1	I	$23655^{\circ}_{4} - 29141_{5}$
18664.162	5356.399	2	I	$20566^{\circ}_{4} - 25923_{4}$	18209.323	5490.193	0	I	$27061^{\circ}_{2} - 32551_{3}$
18663.748	5356.518	0			18192.490	5495.273	0		
18657.231	5358.389	2	I	$22163^{\circ}_{4} - 27521_{4}$	18174.187	5500.807	0		
18651.748	5359.964	0	I	$19039^{\circ}_{2} - 24399_{3}$	18173.926	5500.886	1	I	$26036^{\circ}_{3} - 31537_{3}$
18625.408	5367.544	0	I	$26645^{\circ}_{5} - 32012_{4}$	18170.303	5501.983	1	I	$21143_{5} - 26645^{\circ}_{5}$
18624.701	5367.748	0	II	$14790^{\circ}_{3\frac{1}{2}} - 20158_{2\frac{1}{2}}$	18169.715	5502.161	1	I	$7795^{\circ}_{4} - 13297_{4}$
18595.874	5376.069	3	I	$18614^{\circ}_{1} - 23990_{2}$	18166.638	5503.093	1	I	$22855^{\circ}_{3} - 28358_{3}$
18568.136	5384.100	1			18161.579	5504.626	2	I	$21539^{\circ}_{4} - 27044_{3}$
18557.981	5387.046	3	I	$18382^{\circ}_{0} - 23769_{1}$	18156.664	5506.116	0	I	$14206^{\circ}_{4} - 19713_{3}$
18557.117	5387.297	1			18141.007	5510.868	0		
18547.718	5390.027	3	II	$9400_{2\frac{1}{2}} - 14790^{\circ}_{3\frac{1}{2}}$	18135.791	5512.453	1	I	$13297_{4} - 18809^{\circ}_{4}$
18546.830	5390.285	1	I	$25336^{\circ}_{6} - 30726_{7}$	18125.969	5515.440	5	I	$6362_{2} - 11877^{\circ}_{1}$
18531.218	5394.826	1			18119.136	5517.520	1		
18520.188	5398.039	0	I	$19516^{\circ}_{2} - 24915_{3}$	18112.220	5519.627	1		
18509.757	5401.081	1	I	$23481^{\circ}_{1} - 28882_{2}$	18111.639	5519.804	0		
18490.644	5406.664	4	I	$8800_{4} - 14206^{\circ}_{4}$	18103.118	5522.402	2	I	$24850^{\circ}_{6} - 30372_{6}$
18469.362	5412.894	1	II	$12570_{3\frac{1}{2}} - 17983^{\circ}_{2\frac{1}{2}}$	18087.083	5527.298	2	I	$24307^{\circ}_{2} - 29835_{3}$
18468.454	5413.160	3	I	$17224^{\circ}_{2} - 22637_{3}$	18082.856	5528.590	4	II	$6691^{\circ}_{1\frac{1}{2}} - 12219_{1\frac{1}{2}}$
18452.242	5417.916	0	I	$22855^{\circ}_{5} - 28273_{2}$	18075.163	5530.943	1	II	$9711_{3\frac{1}{2}} - 15242^{\circ}_{4\frac{1}{2}}$
18440.493	5421.368	4	I	$11802_{2} - 17224^{\circ}_{2}$	18072.340	5531.807	4	I	$17501^{\circ}_{5} - 23032_{4}$
18427.858	5425.085	0	I	$27674^{\circ}_{2} - 33099_{3}$	18070.540	5532.358	1	I	$23609^{\circ}_{5} - 29141_{5}$
18402.093	5432.681	0			18060.792	5535.344	1		
18396.840	5434.232	0	I	$17073_{1} - 22508^{\circ}_{2}$	18049.109	5538.927	0		
18381.291	5438.829	3	II	$4146_{3\frac{1}{2}} - 9585^{\circ}_{2\frac{1}{2}}$	18034.646	5543.369	0		
18380.568	5439.043	0			18029.644	5544.907	2		
18353.121	5447.177	0			18025.092	5546.307	2		
18348.035	5448.687	1	I	$19532_{4} - 24981^{\circ}_{3}$	18023.692	5546.738	1	I	$25180^{\circ}_{7} - 30726_{7}$
18339.435	5451.242	0	I	$25306^{\circ}_{2} - 30758_{2}$	18007.579	5551.701	2	I	$11802_{2} - 17354^{\circ}_{1}$
18335.284	5452.476	2	I	$4961_{4} - 10414^{\circ}_{4}$	18000.660	5553.835	1	I	$24202^{\circ}_{4} - 29756_{4}$
18334.595	5452.681	0	I	$24561^{\circ}_{3} - 30014_{4}$	17993.769	5555.962	3	I	$10414^{\circ}_{4} - 15970_{3}$
18331.495	5453.603	1	I	$21890^{\circ}_{3} - 27343_{3}$	17991.742	5556.588	0	I	$26645^{\circ}_{5} - 32202_{5}$
18331.136	5453.710	0	I	$24381^{\circ}_{2} - 29835_{3}$	17987.035	5558.042	1	I	$22669^{\circ}_{3} - 28227_{4}$
18320.410	5456.903	0	I	$17398_{3} - 22855^{\circ}_{3}$	17976.979	5561.151	4	I	$17959_{4} - 23521^{\circ}_{3}$
18301.976	5462.399	1	I	$26995^{\circ}_{3} - 32458_{4}$	17969.554	5563.449	0	I	$24981^{\circ}_{3} - 30544_{2}$
18293.755	5464.854	1	II	$21297^{\circ}_{2\frac{1}{2}} - 26762_{1\frac{1}{2}}$	17964.920	5564.884	6	I	$4961_{4} - 10526^{\circ}_{3}$
18293.550	5464.915	1	I	$22877^{\circ}_{5} - 28342_{5}$	17962.477	5565.641	0	I	$19273_{2} - 24838^{\circ}_{1}$
18286.901	5466.902	1	I	$20423^{\circ}_{1} - 25890_{2}$	17960.037	5566.397	0	I	$26363^{\circ}_{2} - 31929_{3}$
18281.471	5468.526	1	I	$24182^{\circ}_{2} - 29650_{2}$	17955.860	5567.692	2	I	$20543^{\circ}_{6} - 26111_{1}$
18280.488	5468.820	0	I	$18930^{\circ}_{3} - 24399_{3}$	17945.777	5570.820	3		
18278.904	5469.294	0			17938.774	5572.995	0		
18274.319	5470.666	0	I	$22141^{\circ}_{3} - 27612_{3}$	17936.434	5573.722	7	II	$4146_{3\frac{1}{2}} - 9720^{\circ}_{3\frac{1}{2}}$
18271.367	5471.550	5	II	$1859_{1\frac{1}{2}} - 7331^{\circ}_{2\frac{1}{2}}$	17900.307	5584.971	4	II	$9720^{\circ}_{3\frac{1}{2}} - 15305_{4\frac{1}{2}}$
18269.704	5472.048	3	II	$4113_{2\frac{1}{2}} - 9585^{\circ}_{2\frac{1}{2}}$	17893.451	5587.111	0	I	$13945^{\circ}_{3} - 19532_{4}$
18247.402	5478.736	0			17890.207	5588.124	0		
18239.409	5481.137	5	II	$6244_{1\frac{1}{2}} - 11725^{\circ}_{1\frac{1}{2}}$	17887.982	5588.819	3	I	$20522^{\circ}_{2} - 26111_{1}$
18236.594	5481.983	1			17886.677	5589.227	2	I	$18809^{\circ}_{4} - 24399_{3}$
18233.507	5482.911	0			17886.181	5589.382	0	I	$24259^{\circ}_{4} - 29849_{4}$

TABLE 1. *Infrared spectral lines of thorium*—Continued

Wavelength Å	Wavenumber cm^{-1}	Intensity	Spectrum	Classification	Wavelength Å	Wavenumber cm^{-1}	Intensity	Spectrum	Classification
17883.051	5590.360	2	I	$14226_0 - 19817^0_1$	17620.591	5673.629	0		
17877.768	5592.012	0			17614.900	5675.462	1	I	$20214^0_3 - 25890_2$
17873.738	5593.273	2	I	$24421^0_3 - 30014_4$	17614.015	5675.747	1	I	$22855^0_3 - 28531_2$
17873.620	5593.310	1	I	$21902^0_4 - 27495_4$	17597.889	5680.948	1	I	$14032^0_2 - 19713_3$
17872.284	5593.728	1	I	$19713_3 - 25306^0_2$	17595.542	5681.706	1	I	$18699_2 - 24381^0_2$
17854.649	5599.253	2	I	$24084^0_6 - 29684_5$	17584.517	5685.268	7	I	$9804_3 - 15490^0_5$
17849.848	5600.759	1	I	$20322^0_5 - 25923_4$	17578.779	5687.124	1		
17838.977	5604.172	1	I	$8243^0_2 - 13847_2$	17575.945	5688.041	1	I	$20423^0_1 - 26111_1$
17837.933	5604.500	1	II	$14275^0_{4\frac{1}{2}} - 19880_{4\frac{1}{2}}$	17573.115	5688.957	3	I	$20566^0_4 - 26255_4$
17834.907	5605.451	1	I	$21890^0_3 - 27495_4$	17568.106	5690.579	0		
17830.167	5606.941	5	II	$4113_{2\frac{1}{2}} - 9720^0_{3\frac{1}{2}}$	17553.728	5695.240	1	I	$17959_4 - 23655^0_4$
17827.385	5607.816	1	I	$18574_1 - 24182^0_2$	17552.671	5695.583	4	I	$17398_3 - 23093^0_3$
17826.416	5608.121	0	I	$18699_2 - 24307^0_2$	17551.531	5695.953	1	I	$25575^0_4 - 31271_5$
17825.875	5608.291	5	I	$11802_2 - 17411^0_3$	17549.205	5696.708	0	I	$26096^0_3 - 31793_4$
17823.987	5608.885	1	I	$19713_3 - 25321^0_3$	17547.178	5697.366	0	I	$27266^0_4 - 32963_5$
17795.604	5617.831	3	II	$12219_{1\frac{1}{2}} - 17837^0_{1\frac{1}{2}}$	17535.679	5701.102	1		
17788.214	5620.165	2	I	$21645_4 - 27266^0_4$	17535.396	5701.194	0	II	$23730^0_{4\frac{1}{2}} - 29431_{3\frac{1}{2}}$
17783.170	5621.759	4	I	$17411^0_3 - 23032_4$	17534.504	5701.484	5	II	$11116^0_{3\frac{1}{2}} - 16818_{3\frac{1}{2}}$
17778.391	5623.270	1	I	$11601_1 - 17224^0_2$	17528.629	5703.395	0		
17763.368	5628.026	0	I	$26384^0_4 - 32012_4$	17521.738	5705.638	2	I	$24838^0_1 - 30544_2$
17757.108	5630.010	2	I	$24381^0_2 - 30011_3$	17516.448	5707.361	0	I	$22855^0_3 - 28562_4$
17753.195	5631.251	0			17508.350	5710.001	2	I	$21902^0_4 - 27612_3$
17752.753	5631.391	1	I	$21890^0_5 - 27521_4$	17507.525	5710.270	0	II	$25246_{4\frac{1}{2}} - 30956^0_{4\frac{1}{2}}$
17744.898	5633.884	5	I	$17354^0_1 - 22988_2$	17503.828	5711.476	1	I	$17166_5 - 22877^0_5$
17742.618	5634.608	0	I	$22399^0_5 - 28034_5$	17492.573	5715.151	2	I	$17398_3 - 23113^0_4$
17721.115	5641.445	4	II	$8460_{1\frac{1}{2}} - 14101^0_{1\frac{1}{2}}$	17492.364	5715.219	0		
17720.358	5641.686	2	I	$22338^0_3 - 27980_3$	17490.072	5715.968	0		
17717.673	5642.541	0	I	$19713_3 - 25355^0_4$	17481.041	5718.921	7	I	$8243^0_2 - 13962_1$
17705.162	5646.528	3	II	$12472^0_{2\frac{1}{2}} - 18118_{1\frac{1}{2}}$	17473.699	5721.324	2	I	$13088_3 - 18809^0_4$
17703.673	5647.003	3	I	$21143_5 - 26790^0_4$	17468.689	5722.965	1		
17699.808	5648.236	0	II	$23697^0_{3\frac{1}{2}} - 29345_{2\frac{1}{2}}$	17462.260	5725.072	3	II	$13248_{4\frac{1}{2}} - 18973^0_{3\frac{1}{2}}$
17696.443	5649.310	2			17461.866	5725.201	0		
17689.714	5651.459	0			17456.286	5727.031	0	II	$19880_{4\frac{1}{2}} - 25607^0_{4\frac{1}{2}}$
17688.744	5651.769	2	I	$21539^0_4 - 27191_5$	17455.753	5727.206	0	II	$24757^0_{4\frac{1}{2}} - 30484_{3\frac{1}{2}}$
17683.810	5653.346	3	I	$15490^0_5 - 21143_5$	17447.564	5729.894	3	II	$9061_{2\frac{1}{2}} - 14790^0_{3\frac{1}{2}}$
17683.237	5653.529	0	I	$22877^0_1 - 28531_2$	17441.114	5732.013	0	I	$23113^0_4 - 28845_4$
17677.815	5655.263	0			17437.704	5733.134	1	I	$18574_1 - 24307^0_2$
17677.481	5655.370	3	I	$13847_2 - 19503^0_3$	17413.587	5741.074	2	II	$9711_{3\frac{1}{2}} - 15453^0_{3\frac{1}{2}}$
17670.229	5657.691	1	I	$24850^0_6 - 30508_5$	17405.417	5743.769	3	II	$9400_{2\frac{1}{2}} - 15144^0_{1\frac{1}{2}}$
17669.614	5657.888	3	I	$25306^0_2 - 30964_3$	17404.332	5744.127	4	I	$14204_5 - 19948^0_4$
17663.853	5659.733	0	I	$25877^0_4 - 31537_5$	17401.230	5745.151	1	I	$26048^0_4 - 31793_4$
17658.896	5661.322	0	I	$26113^0_4 - 31774_5$	17388.612	5749.320	0	I	$25877^0_4 - 31626_5$
17649.490	5664.339	2	I	$24880^0_1 - 30544_2$	17385.370	5750.392	4	I	$25180^0_7 - 30930_6$
17645.848	5665.508	0			17381.909	5751.537	7	I	$16346^0_4 - 22098_4$
17634.332	5669.208	4	I	$13847_2 - 19516^0_2$	17380.610	5751.967	5	I	$6362_2 - 12114^0_2$
17633.725	5669.403	0	I	$23752^0_2 - 29422_1$	17375.665	5753.604	1	I	$11601_1 - 17354^0_1$
17629.891	5670.636	0			17372.868	5754.530	1	I	$20054_2 - 25809^0_1$
17627.118	5671.528	0	I	$21645_4 - 27317^0_3$	17346.089	5763.414	1	II	$12219_{1\frac{1}{2}} - 17983^0_{2\frac{1}{2}}$
17626.046	5671.873	3	I	$15493_4 - 21165^0_5$	17334.404	5767.299	1	I	$23916^0_4 - 29684_5$
17623.094	5672.823	6	I	$7502_3 - 13175^0_4$	17333.121	5767.726	1	I	$13945^0_3 - 19713_3$

TABLE 1. *Infrared spectral lines of thorium*—Continued

Wavelength Å	Wavenumber cm^{-1}	Intensity	Spectrum	Classification	Wavelength Å	Wavenumber cm^{-1}	Intensity	Spectrum	Classification
17323.648	5770.880	0	I	$18431_3 - 24202^{\circ}_4$	17103.520	5845.153	1	I	$16554_6 - 22399^{\circ}_5$
17323.507	5770.927	0			17088.335	5850.347	2	I	$22508^{\circ}_2 - 28358_3$
17311.753	5774.845	1	I	$24769^{\circ}_6 - 30544_8$	17085.097	5851.456	0	I	$24701^{\circ}_5 - 30552_4$
17307.662	5776.210	7	I	$17501^{\circ}_5 - 23277_5$	17083.605	5851.967	0		
17304.463	5777.278	0			17078.798	5853.614	3	I	$16783^{\circ}_4 - 22637_3$
17295.913	5780.134	0			17075.750	5854.659	3	I	$13962_1 - 19817^{\circ}_1$
17294.865	5780.484	0			17069.452	5856.819	1		
17290.627	5781.901	1	I	$14204_5 - 19986^{\circ}_6$	17054.299	5862.023	0	I	$18699_2 - 24561^{\circ}_3$
17277.735	5786.215	0	I	$25355^{\circ}_4 - 31141_3$	17030.220	5870.311	3	II	$6700^{\circ}_{4\frac{1}{2}} - 12570_{3\frac{1}{2}}$
17271.005	5788.470	0	I	$23093^{\circ}_2 - 28882_2$	17028.599	5870.870	1	I	$22163^{\circ}_4 - 28034_5$
17267.932	5789.500	3	I	$19532_4 - 25321^{\circ}_3$	17026.334	5871.651	1	I	$18549_2 - 24421^{\circ}_3$
17264.172	5790.761	3	I	$17411^{\circ}_3 - 23201_3$	17020.168	5873.778	1		
17261.632	5791.613	0	I	$21252^{\circ}_2 - 27044_3$	17019.670	5873.950	0	I	$20922^{\circ}_2 - 26796_3$
17244.366	5797.412	1	II	$22139^{\circ}_{4\frac{1}{2}} - 27937_{5\frac{1}{2}}$	17018.885	5874.221	2	I	$21738^{\circ}_2 - 27612_3$
17235.699	5800.327	1	II	$13250_{2\frac{1}{2}} - 19050^{\circ}_{1\frac{1}{2}}$	17014.224	5875.830	1		
17229.251	5802.498	0	II	$20686^{\circ}_{2\frac{1}{2}} - 26488_{2\frac{1}{2}}$	17014.114	5875.868	1	I	$19039^{\circ}_2 - 24915_3$
17227.152	5803.205	0	I	$25442^{\circ}_3 - 31245_2$	17013.556	5876.061	0	I	$18431_3 - 24307^{\circ}_2$
17225.670	5803.704	3	I	$17073_1 - 22877^{\circ}_1$	17012.360	5876.474	0	I	$24850^{\circ}_6 - 30726_7$
17221.632	5805.065	1	I	$15863_2 - 21668^{\circ}_1$	17008.982	5877.641	0		
17217.782	5806.363	2	I	$21165^{\circ}_3 - 26971_4$	17008.562	5877.786	2	I	$24880^{\circ}_1 - 30758_2$
17216.726	5806.719	0	I	$18574_1 - 24381^{\circ}_2$	17008.100	5877.946	0		
17208.215	5809.591	8	II	$1521_{2\frac{1}{2}} - 7331^{\circ}_{2\frac{1}{2}}$	17005.290	5878.917	2	I	$27084^{\circ}_3 - 32963_5$
17198.807	5812.769	0	I	$26645^{\circ}_5 - 32458_4$	17004.697	5879.122	3	I	$21165^{\circ}_3 - 27044_3$
17195.420	5813.914	0	I	$20566^{\circ}_4 - 26380_5$	16997.972	5881.448	0	I	$24769^{\circ}_3 - 30651_3$
17192.605	5814.866	1	I	$23603^{\circ}_2 - 29418_2$	16992.702	5883.272	0		
17186.894	5816.798	2	I	$19588^{\circ}_5 - 25405_4$	16989.777	5884.285	1	I	$25442^{\circ}_3 - 31326_4$
17182.265	5818.365	0			16976.362	5888.935	0	I	$22338^{\circ}_3 - 28227_4$
17173.440	5821.355	0	I	$23113^{\circ}_4 - 28934_3$	16964.222	5893.149	0	I	$26036^{\circ}_3 - 31929_3$
17168.126	5823.157	0	I	$19532_4 - 25355^{\circ}_4$	16960.892	5894.306	1	I	$21077^{\circ}_5 - 26971_4$
17165.765	5823.958	2	I	$22855^{\circ}_3 - 28679_2$	16958.427	5895.163	1		
17163.009	5824.893	1	I	$24307^{\circ}_2 - 30132_2$	16956.701	5895.763	2	II	$15786_{2\frac{1}{2}} - 21682^{\circ}_{3\frac{1}{2}}$
17155.413	5827.472	1	II	$23518^{\circ}_{3\frac{1}{2}} - 29345_{2\frac{1}{2}}$	16954.783	5896.430	0		
17153.591	5828.091	2	I	$18431_3 - 24259^{\circ}_4$	16952.178	5897.336	0	I	$23521^{\circ}_3 - 29418_2$
17152.876	5828.334	1			16949.485	5898.273	0	I	$23752^{\circ}_2 - 29650_2$
17152.288	5828.534	1	I	$22399^{\circ}_5 - 28227_4$	16947.451	5898.981	0		
17151.508	5828.799	1	I	$21738^{\circ}_2 - 27566_2$	16945.150	5899.782	0	I	$26651^{\circ}_2 - 32551_3$
17151.178	5828.911	0	I	$24182^{\circ}_2 - 30011_3$	16941.790	5900.952	0	II	$7001_{1\frac{1}{2}} - 12902^{\circ}_{1\frac{1}{2}}$
17146.766	5830.411	0	I	$23015^{\circ}_5 - 28845_4$	16938.730	5902.018	3	I	$19503^{\circ}_3 - 25405_4$
17143.105	5831.656	2			16918.744	5908.990	0	I	$26384^{\circ}_4 - 32293_5$
17135.330	5834.302	4	I	$8111_4 - 13945^{\circ}_3$	16915.692	5910.056	0	I	$25355^{\circ}_4 - 31265_3$
17134.167	5834.698	4	I	$23306^{\circ}_6 - 29141_5$	16915.097	5910.264	1	I	$19532_4 - 25442^{\circ}_3$
17133.189	5835.031	1	I	$25306^{\circ}_2 - 31141_3$	16912.370	5911.217	1	II	$21682^{\circ}_{3\frac{1}{2}} - 27593_{2\frac{1}{2}}$
17124.268	5838.071	1	I	$15736^{\circ}_1 - 21575_2$	16911.655	5911.467	0		
17121.318	5839.077	3	I	$22141^{\circ}_3 - 27980_3$	16906.064	5913.422	0	II	$23518^{\circ}_{3\frac{1}{2}} - 29431_{3\frac{1}{2}}$
17120.840	5839.240	0	I	$27260^{\circ}_3 - 33099_3$	16900.345	5915.423	1	I	$25355^{\circ}_4 - 31271_5$
17120.083	5839.498	1	I	$23916^{\circ}_4 - 29756_4$	16890.066	5919.023	5	II	$7331^{\circ}_{2\frac{1}{2}} - 13250_{2\frac{1}{2}}$
17113.767	5841.653	1			16887.173	5920.037	1	I	$15970_3 - 21890^{\circ}_3$
17113.542	5841.730	2	I	$13088_3 - 18930^{\circ}_3$	16883.454	5921.341	0	I	$18069^{\circ}_3 - 23990_2$
17111.210	5842.526	0			16879.312	5922.794	2	I	$17847^{\circ}_2 - 23769_1$
17105.103	5844.612	1			16875.970	5923.967	0	I	$25321^{\circ}_3 - 31245_2$

TABLE 1. *Infrared spectral lines of thorium*—Continued

Wavelength Å	Wavenumber cm^{-1}	Intensity	Spectrum	Classification	Wavelength Å	Wavenumber cm^{-1}	Intensity	Spectrum	Classification
16852.625	5932.173	2	I	$15970_3 - 21902^0_4$	16588.332	6026.687	0		
16849.382	5933.315	0	I	$20322^0_5 - 26255_4$	16587.815	6026.875	3	I	$15618^0_3 - 21645_4$
16846.815	5934.219	0	I	$22338^0_3 - 28273_2$	16587.044	6027.155	0	I	$22855^0_3 - 28882_2$
16846.017	5934.500	0	I	$25336^0_4 - 31271_5$	16578.581	6030.232	1		
16840.767	5936.350	0	I	$25690^0_5 - 31626_5$	16578.017	6030.437	0		
16832.896	5939.126	0	I	$25306^0_2 - 31245_2$	16569.667	6033.476	0	I	$19273_2 - 25306^0_2$
16827.445	5941.050	0			16540.424	6044.143	5	I	$11802_2 - 17847^0_2$
16823.435	5942.466	1			16538.399	6044.883	3	I	$16351_0 - 22396^0_1$
16820.947	5943.345	1	I	$23609^0_5 - 29552_6$	16534.332	6046.370	2	I	$15493_4 - 21539^0_4$
16818.657	5944.154	0			16531.417	6047.436	1	I	$23603^0_2 - 29650_2$
16811.787	5946.583	0	I	$26790^0_4 - 32737_5$	16522.232	6050.798	0		
16806.361	5948.503	1			16521.658	6051.008	1	I	$24838^0_1 - 30889_1$
16804.426	5949.188	0			16520.919	6051.279	3	II	$10855_{3/2} - 16906^0_{3/2}$
16801.531	5950.213	0	I	$24182^0_2 - 30132_2$	16518.765	6052.068	3	II	$9400_{2/2} - 15453^0_{3/2}$
16800.478	5950.586	1	I	$13088_3 - 19039^0_2$	16503.791	6057.559	4	I	$18614^0_1 - 24671_2$
16797.452	5951.658	1			16501.244	6058.494	0	I	$20054_2 - 26113^0_2$
16785.229	5955.992	2	I	$21539^0_4 - 27495_4$	16495.017	6060.781	0	II	$15236_{1/2} - 21297^0_{2/2}$
16785.046	5956.057	2	I	$15618^0_3 - 21575_2$	16492.394	6061.745	2	II	$13818^0_{3/2} - 19880_{4/2}$
16782.389	5957.000	1	I	$17959_4 - 23916^0_4$	16477.433	6067.249	2	II	$9238^0_{4/2} - 15305_{4/2}$
16771.639	5960.818	1			16461.254	6073.212	1	I	$19817^0_1 - 25890_2$
16768.550	5961.916	6	I	$12847_3 - 18809^0_4$	16453.368	6076.123	0	II	$20686^0_{2/2} - 26762_{1/2}$
16761.533	5964.412	0	I	$26048^0_4 - 32012_4$	16452.932	6076.284	0	I	$21594_3 - 27670^0_3$
16750.771	5968.244	0			16447.180	6078.409	0	I	$21902^0_4 - 27980_3$
16748.433	5969.077	5	I	$11197^0_5 - 17166_5$	16443.836	6079.645	0		
16747.499	5969.410	2	I	$13847_2 - 19817^0_1$	16436.507	6082.356	2		
16746.683	5969.701	1			16436.339	6082.418	3		
16741.938	5971.393	0	I	$25355^0_4 - 31326_4$	16433.049	6083.636	2	II	$9061_{2/2} - 15144^0_{1/2}$
16730.028	5975.644	3	I	$17073_1 - 23049^0_1$	16428.820	6085.202	2	II	$8460_{1/2} - 14545^0_{2/2}$
16725.712	5977.186	0			16420.336	6088.346	0		
16724.318	5977.684	1	I	$17224^0_2 - 23201_3$	16414.399	6090.548	1	I	$21890^0_3 - 27980_3$
16720.218	5979.150	0	I	$24307^0_2 - 30286_1$	16412.823	6091.133	3	I	$21252^0_2 - 27343_3$
16718.081	5979.914	1			16403.906	6094.444	0	I	$23916^0_4 - 30011_3$
16712.444	5981.931	3	I	$21539^0_4 - 27521_4$	16394.343	6097.999	1	I	$24274^0_5 - 30372_6$
16707.945	5983.542	0	I	$24981^0_3 - 30964_3$	16390.870	6099.291	0	I	$21575_2 - 27674^0_2$
16704.639	5984.726	3	I	$18930^0_3 - 24915_3$	16380.898	6103.004	6	II	$9202^0_{3/2} - 15305_{4/2}$
16694.697	5988.290	0	I	$24769^0_3 - 30758_2$	16377.984	6104.090	0		
16691.676	5989.374	1	I	$18431_3 - 24421^0_3$	16375.188	6105.132	1	I	$18809^0_4 - 24915_3$
16688.906	5990.368	1	I	$19713_3 - 25703^0_2$	16367.427	6108.027	1		
16687.560	5990.851	0	I	$24561^0_5 - 30552_4$	16363.631	6109.444	2	I	$22248^0_2 - 28358_2$
16686.678	5991.168	1	I	$26790^0_4 - 32781_4$	16349.247	6114.819	1		
16634.036	6010.128	0			16343.137	6117.105	0		
16630.351	6011.460	0			16340.749	6117.999	2	I	$14204_5 - 20322^0_5$
16624.607	6013.537	2	I	$18614^0_1 - 24627_1$	16329.816	6122.095	2	I	$20922^0_2 - 27044_3$
16612.968	6017.750	0			16326.067	6123.501	2	I	$24421^0_3 - 30544_2$
16606.290	6020.170	1	I	$17073_1 - 23093^0_2$	16316.903	6126.940	0		
16604.436	6020.842	1	I	$18011^0_3 - 24032_4$	16310.703	6129.269	3	I	$20867^0_7 - 26997_6$
16599.350	6022.687	3	I	$14032^0_2 - 20054_2$	16308.851	6129.965	2	I	$18431_3 - 24561^0_3$
16594.999	6024.266	0	I	$22248^0_2 - 28273_2$	16308.606	6130.057	2		
16592.118	6025.312	2			16305.893	6131.077	0		
16589.555	6026.243	1	I	$15863_2 - 21890^0_3$	16304.920	6131.443	0	I	$24421^0_3 - 30552_4$

TABLE 1. *Infrared spectral lines of thorium*—Continued

Wavelength Å	Wavenumber cm^{-1}	Intensity	Spectrum	Classification	Wavelength Å	Wavenumber cm^{-1}	Intensity	Spectrum	Classification
16304.149	6131.733	3	I	$21902^{\circ}_{4} - 28034_{5}$	16006.680	6245.685	0	I	$23306^{\circ}_{6} - 29552_{6}$
16297.533	6134.222	0	I	$22396^{\circ}_{1} - 28531_{2}$	16005.763	6246.043	4	I	$11601_{1} - 17847^{\circ}_{2}$
16284.058	6139.298	1	I	$18699_{2} - 24838^{\circ}_{1}$	15997.841	6249.136	2	I	$16783^{\circ}_{4} - 23032_{4}$
16280.282	6140.722	3	I	$17166_{5} - 2\,3306^{\circ}_{6}$	15981.974	6255.340	0		
16273.373	6143.329	0	I	$17847^{\circ}_{2} - 2\,.990_{2}$	15978.393	6256.742	2	I	$17398_{3} - 23655^{\circ}_{4}$
16270.823	6144.292	0	I	$26651^{\circ}_{2} - 3\,.796_{3}$	15973.502	6258.658	1	I	$23752^{\circ}_{2} - 30011_{3}$
16269.133	6144.930	3	II	$10673^{\circ}_{2\frac{1}{2}\frac{3}{2}} - 1\,6818_{3\frac{1}{2}\frac{3}{2}}$	15972.593	6259.014	0	I	$25753^{\circ}_{5} - 32012_{4}$
16263.051	6147.228	1	I	$23609^{\circ}_{5} - 29756_{4}$	15963.355	6262.636	0		
16250.275	6152.061	1			15960.024	6263.943	2	I	$22877^{\circ}_{5} - 29141_{5}$
16240.450	6155.783	2	I	$15490^{\circ}_{5} - 21645_{4}$	15954.449	6266.132	4	I	$11802_{2} - 18069^{\circ}_{3}$
16238.115	6156.668	3	I	$11241^{\circ}_{3} - 17398_{3}$	15951.379	6267.338	0	II	$20989^{\circ}_{4\frac{1}{2}\frac{3}{2}} - 27257_{3\frac{1}{2}\frac{3}{2}}$
16234.453	6158.057	0	I	$19532_{4} - 25690^{\circ}_{5}$	15944.136	6270.185	0		
16224.530	6161.823	0			15941.439	6271.246	0	I	$25355^{\circ}_{4} - 31626_{5}$
16220.740	6163.263	3	I	$22399^{\circ}_{5} - 28562_{4}$	15939.011	6272.201	1	II	$6213_{4\frac{1}{2}\frac{3}{2}} - 12485^{\circ}_{3\frac{1}{2}\frac{3}{2}}$
16217.564	6164.470	0	I	$19713_{3} - 25877^{\circ}_{4}$	15936.374	6273.239	4	II	$7828_{1\frac{1}{2}\frac{3}{2}} - 14101^{\circ}_{1\frac{1}{2}\frac{3}{2}}$
16212.890	6166.247	1			15936.069	6273.359	3	I	$20522^{\circ}_{2} - 26796_{3}$
16211.744	6166.683	0	I	$26384^{\circ}_{4} - 32551_{3}$	15932.409	6274.800	6	II	$6213_{4\frac{1}{2}\frac{3}{2}} - 12488^{\circ}_{4\frac{1}{2}\frac{3}{2}}$
16204.728	6169.353	0			15927.216	6276.846	0	II	$24982^{\circ}_{3\frac{1}{2}\frac{3}{2}} - 31259_{2\frac{1}{2}\frac{3}{2}}$
16204.604	6169.400	1	I	$19273_{2} - 25442^{\circ}_{3}$	15925.011	6277.715	1	I	$15863_{2} - 22141^{\circ}_{3}$
16195.248	6172.964	1	I	$26790^{\circ}_{4} - 32963_{5}$	15924.829	6277.787	0	I	$24274^{\circ}_{5} - 30552_{4}$
16188.147	6175.672	0	I	$22669^{\circ}_{3} - 28845_{4}$	15922.130	6278.851	4	I	$15970_{3} - 22248^{\circ}_{2}$
16182.835	6177.699	0	II	$20310^{\circ}_{2\frac{1}{2}\frac{3}{2}} - 26488_{2\frac{1}{2}\frac{3}{2}}$	15920.010	6279.687	0		
16180.368	6178.641	0	I	$21165^{\circ}_{5} - 27343_{3}$	15919.042	6280.069	1	I	$4961_{4} - 11241^{\circ}_{3}$
16178.472	6179.365	2	I	$22163^{\circ}_{4} - 28342_{5}$	15915.448	6281.487	1	I	$18699_{2} - 24981^{\circ}_{3}$
16172.466	6181.660	1	I	$25355^{\circ}_{4} - 31537_{3}$	15913.906	6282.096	0	I	$22248^{\circ}_{2} - 28531_{2}$
16163.327	6185.155	3	II	$8605_{2\frac{1}{2}\frac{3}{2}} - 14790^{\circ}_{3\frac{1}{2}\frac{3}{2}}$	15899.553	6287.767	3	I	$24084^{\circ}_{6} - 30372_{6}$
16147.600	6191.179	3	I	$12847_{3} - 19039^{\circ}_{2}$	15898.637	6288.129	1	II	$20969^{\circ}_{3\frac{1}{2}\frac{3}{2}} - 27257_{3\frac{1}{2}\frac{3}{2}}$
16145.326	6192.051	1	I	$22338^{\circ}_{3} - 28531_{2}$	15895.139	6289.513	1	I	$18549_{2} - 24838^{\circ}_{1}$
16142.758	6193.036	2	I	$15970_{3} - 22163^{\circ}_{4}$	15893.090	6290.324	1	I	$25336^{\circ}_{6} - 31626_{5}$
16140.194	6194.020	0	I	$23655^{\circ}_{4} - 29849_{4}$	15891.854	6290.813	3	I	$16346^{\circ}_{4} - 22637_{3}$
16137.810	6194.935	0	I	$24769^{\circ}_{3} - 30964_{3}$	15891.564	6290.928	4	I	$13297_{4} - 19588^{\circ}_{5}$
16125.805	6199.547	0	I	$25575^{\circ}_{4} - 31774_{3}$	15887.023	6292.726	1	I	$24259^{\circ}_{4} - 30552_{4}$
16120.565	6201.562	0			15880.810	6295.188	1		
16109.798	6205.707	5	I	$13297_{4} - 19503^{\circ}_{3}$	15877.380	6296.548	0	II	$21297^{\circ}_{2\frac{1}{2}\frac{3}{2}} - 27593_{2\frac{1}{2}\frac{3}{2}}$
16100.958	6209.114	0	I	$23752^{\circ}_{2} - 29961_{1}$	15871.650	6298.821	0		
16084.899	6215.313	0	I	$25321^{\circ}_{3} - 31537_{3}$	15868.987	6299.878	2	I	$17959_{4} - 24259^{\circ}_{4}$
16081.086	6216.787	1	I	$22141^{\circ}_{3} - 28358_{3}$	15861.758	6302.749	1	I	$21645_{4} - 27948^{\circ}_{4}$
16072.590	6220.073	3			15854.989	6305.440	1	I	$24202^{\circ}_{4} - 30508_{5}$
16071.988	6220.306	1	I	$18549_{2} - 24769^{\circ}_{3}$	15853.227	6306.141	0		
16070.913	6220.722	0	I	$23741^{\circ}_{1} - 29961_{1}$	15851.771	6306.720	0		
16068.852	6221.520	1	I	$19532_{4} - 25753^{\circ}_{5}$	15847.733	6308.327	3	I	$20054_{2} - 26363^{\circ}_{2}$
16056.201	6226.422	0	I	$22877^{\circ}_{5} - 29104_{4}$	15843.848	6309.874	0	II	$9400_{2\frac{1}{2}\frac{3}{2}} - 15710^{\circ}_{1\frac{1}{2}\frac{3}{2}}$
16048.543	6229.393	1	I	$24701^{\circ}_{5} - 30930_{6}$	15835.343	6313.263	1		
16047.145	6229.936	0			15833.507	6313.995	0	I	$23521^{\circ}_{3} - 29835_{3}$
16045.762	6230.473	0	I	$25306^{\circ}_{2} - 31537_{3}$	15832.882	6314.244	0	I	$21252^{\circ}_{2} - 27566_{2}$
16042.116	6231.889	0			15831.752	6314.695	7	I	$5563_{1} - 11877^{\circ}_{1}$
16038.518	6233.287	3	I	$24274^{\circ}_{5} - 30508_{5}$	15825.176	6317.319	2	I	$12114^{\circ}_{2} - 18431_{3}$
16033.162	6235.369	2	I	$4961_{4} - 11197^{\circ}_{3}$	15815.492	6321.187	6	II	$9711_{3\frac{1}{2}\frac{3}{2}} - 16033^{\circ}_{2\frac{1}{2}\frac{3}{2}}$
16014.426	6242.664	2	I	$17959_{4} - 24202^{\circ}_{4}$	15810.170	6323.315	1	I	$19713_{3} - 26036^{\circ}_{3}$
16008.311	6245.049	3	I	$18382^{\circ}_{0} - 24627_{1}$	15807.445	6324.405	0	I	$23093^{\circ}_{2} - 29418_{2}$

TABLE 1. *Infrared spectral lines of thorium*—Continued

Wavelength Å	Wavenumber cm^{-1}	Intensity	Spectrum	Classification
15804.308	6325.660	1	I	$21902^{\circ}_{4} - 28227_{4}$
15794.600	6329.548	0		
15793.353	6330.048	0	I	$18069^{\circ}_{5} - 24399_{3}$
15792.250	6330.490	0	I	$21165^{\circ}_{5} - 27495_{4}$
15791.447	6330.812	1	I	$18549_{2} - 24880^{\circ}_{1}$
15788.721	6331.905	0	I	$25442^{\circ}_{5} - 31774_{3}$
15781.849	6334.662	1	I	$19588^{\circ}_{5} - 25923_{4}$
15767.555	6340.405	3	II	$13818^{\circ}_{3/2} - 20158_{2 1/2}$
15754.904	6345.496	1	I	$18053^{\circ}_{4} - 24399_{3}$
15747.955	6348.296	1	II	$12219_{1 1/2} - 18568^{\circ}_{1/2}$
15745.306	6349.364	0		
15743.881	6349.939	2	I	$24202^{\circ}_{4} - 30552_{4}$
15733.987	6353.932	0	I	$21594_{3} - 27948^{\circ}_{4}$
15732.702	6354.451	0	I	$25575^{\circ}_{4} - 31929_{3}$
15728.365	6356.203	0	I	$23655^{\circ}_{4} - 30011_{3}$
15727.808	6356.428	0	I	$21165^{\circ}_{5} - 27521_{4}$
15720.977	6359.190	1	I	$23655^{\circ}_{5} - 30014_{4}$
15719.798	6359.667	1	I	$21252^{\circ}_{2} - 27612_{3}$
15716.044	6361.186	1		
15713.149	6362.358	4	I	$14204_{3} - 20566^{\circ}_{4}$
15706.454	6365.070	2	II	$4490^{\circ}_{2 1/2} - 10855_{3 1/2}$
15703.035	6366.456	0		
15702.559	6366.649	1	I	$8800_{4} - 15166^{\circ}_{5}$
15701.306	6367.157	3	I	$13847_{2} - 20214^{\circ}_{5}$
15698.032	6368.485	0	II	$20120^{\circ}_{2 1/2} - 26488_{2 1/2}$
15697.541	6368.684	0		
15697.019	6368.896	1	I	$15970_{3} - 22338^{\circ}_{5}$
15696.943	6368.927	1	I	$23049^{\circ}_{1} - 29418_{2}$
15690.237	6371.649	1		
15676.166	6377.368	3	I	$23306^{\circ}_{5} - 29684_{5}$
15671.451	6379.287	0		
15662.128	6383.084	0	I	$21890^{\circ}_{3} - 28273_{2}$
15647.283	6389.140	1		
15641.777	6391.389	0	I	$24259^{\circ}_{4} - 30651_{3}$
15641.596	6391.463	1		
15641.344	6391.566	3	I	$23741^{\circ}_{1} - 30132_{2}$
15640.438	6391.936	5	II	$9061_{2 1/2} - 15453^{\circ}_{3 1/2}$
15637.160	6393.276	3	II	$11725^{\circ}_{1/2} - 18118_{1 1/2}$
15634.482	6394.371	2	I	$19986^{\circ}_{6} - 26380_{5}$
15631.483	6395.598	1	II	$15710^{\circ}_{1 1/2} - 22106_{2 1/2}$
15628.272	6396.912	3	I	$15493_{4} - 21890^{\circ}_{3}$
15624.606	6398.413	1	II	$17983^{\circ}_{2 1/2} - 24381_{3 1/2}$
15621.888	6399.526	0	I	$22163^{\circ}_{4} - 28562_{4}$
15620.165	6400.232	2	I	$19713_{3} - 26113^{\circ}_{2}$
15616.447	6401.756	1	I	$21165^{\circ}_{3} - 27566_{2}$
15615.505	6402.142	1	II	$6168^{\circ}_{3 1/2} - 12570_{3 1/2}$
15613.859	6402.817	0		
15612.710	6403.288	0	II	$12570_{3 1/2} - 18973^{\circ}_{3 1/2}$
15608.939	6404.835	2	I	$20566^{\circ}_{4} - 26971_{4}$
15608.145	6405.161	1	I	$23609^{\circ}_{5} - 30014_{4}$
15602.299	6407.561	0	I	$17073_{1} - 23481^{\circ}_{1}$
15598.808	6408.995	4	I	$7795^{\circ}_{4} - 14204_{3}$
15598.676	6409.049	4	I	$15493_{4} - 21902^{\circ}_{4}$
15597.528	6409.521	0		
15593.649	6411.115	1	II	$13468^{\circ}_{4 1/2} - 19880_{4 1/2}$
15585.229	6414.579	3	I	$13088_{3} - 19503^{\circ}_{3}$
15583.635	6415.235	2	I	$17354^{\circ}_{1} - 23769_{1}$
15576.584	6418.139	6	I	$16783^{\circ}_{4} - 23201_{3}$
15575.870	6418.433	1	I	$21077^{\circ}_{5} - 27495_{4}$
15574.463	6419.013	1	I	$25355^{\circ}_{5} - 31774_{3}$
15572.352	6419.883	2	I	$19503^{\circ}_{3} - 25923_{4}$
15572.117	6419.980	4	I	$16217^{\circ}_{2} - 22637_{3}$
15569.510	6421.055	3	I	$22141^{\circ}_{3} - 28562_{4}$
15568.155	6421.614	0	I	$20922^{\circ}_{2} - 27343_{3}$
15565.585	6422.674	0	I	$26645^{\circ}_{3} - 33068_{3}$
15559.575	6425.155	2		
15558.814	6425.469	2	II	$4146_{3 1/2} - 10572^{\circ}_{4 1/2}$
15553.233	6427.775	2	I	$15166^{\circ}_{3} - 21594_{3}$
15551.679	6428.417	4	I	$13088_{3} - 19516^{\circ}_{2}$
15547.561	6430.120	1	I	$19273_{2} - 25703^{\circ}_{2}$
15542.668	6432.144	2	I	$19948^{\circ}_{4} - 26380_{5}$
15537.904	6434.116	0	I	$22669^{\circ}_{5} - 29104_{4}$
15523.156	6440.229	1	I	$21902^{\circ}_{4} - 28342_{5}$
15516.436	6443.018	6	I	$7502_{3} - 13945^{\circ}_{3}$
15513.174	6444.373	1	I	$21077^{\circ}_{5} - 27521_{4}$
15508.866	6446.163	1	I	$22399^{\circ}_{5} - 28845_{4}$
15505.455	6447.581	0	I	$26651^{\circ}_{2} - 33099_{3}$
15503.005	6448.600	0	I	$24202^{\circ}_{4} - 30651_{3}$
15499.015	6450.260	1	I	$24307^{\circ}_{2} - 30758_{2}$
15485.384	6455.938	0		
15479.404	6458.432	1		
15475.060	6460.245	1	I	$12114^{\circ}_{2} - 18574_{1}$
15473.472	6460.908	1	I	$16554_{6} - 23015^{\circ}_{5}$
15473.326	6460.969	1	I	$13962_{1} - 20423^{\circ}_{1}$
15472.864	6461.162	3	I	$17959_{4} - 24421^{\circ}_{3}$
15467.501	6463.402	1		
15461.432	6465.939	0		
15456.917	6467.828	1	I	$25306^{\circ}_{2} - 31774_{3}$
15455.882	6468.261	0	I	$21890^{\circ}_{3} - 28358_{3}$
15454.759	6468.731	0	I	$24182^{\circ}_{2} - 30651_{3}$
15447.452	6471.791	1		
15440.113	6474.867	4	I	$18930^{\circ}_{3} - 25405_{4}$
15439.546	6475.105	2	I	$15863_{2} - 22338^{\circ}_{5}$
15429.783	6479.202	7	I	$15618^{\circ}_{3} - 22098_{4}$
15425.673	6480.928	2	II	$22106_{2 1/2} - 28587^{\circ}_{2 1/2}$
15400.599	6491.480	0		
15395.715	6493.539	2	I	$16783^{\circ}_{4} - 23277_{5}$
15392.243	6495.004	0		
15390.079	6495.917	0	I	$24769^{\circ}_{5} - 31265_{3}$
15373.158	6503.067	0	I	$26048^{\circ}_{4} - 32551_{3}$

TABLE 1. *Infrared spectral lines of thorium*—Continued

Wavelength Å	Wavenumber cm^{-1}	Intensity	Spectrum	Classification	Wavelength Å	Wavenumber cm^{-1}	Intensity	Spectrum	Classification
15372.295	6503.432	0			15158.232	6595.273	1	I	$18809^{e}_{4} - 25405_{4}$
15364.893	6506.565	1	I	$22338^{e}_{3} - 28845_{4}$	15157.340	6595.661	0	I	$18069^{e}_{3} - 24664_{3}$
15355.694	6510.463	5	I	$14226_{0} - 20737^{e}_{1}$	15156.775	6595.907	1	I	$22338^{e}_{3} - 28934_{3}$
15342.358	6516.122	1	I	$19532_{4} - 26048^{e}_{4}$	15143.355	6601.752	2	I	$17959_{4} - 24561^{e}_{3}$
15336.766	6518.498	0	I	$17398_{3} - 23916^{e}_{4}$	15137.607	6604.259	0	I	$21668^{e}_{1} - 28273_{2}$
15320.133	6525.575	0	I	$16351_{0} - 22877^{e}_{1}$	15135.223	6605.299	0	II	$10855_{3/2} - 17460^{e}_{2 1/2}$
15317.814	6526.563	3	II	$4146_{3 1/2} - 10673^{e}_{2 1/2}$	15128.735	6608.132	1		
15315.929	6527.366	5	II	$8018_{1 1/2} - 14545^{e}_{2 1/2}$	15112.474	6615.242	2	I	$10783^{e}_{2} - 17398_{3}$
15315.660	6527.481	2	II	$10379_{4 1/2} - 16906^{e}_{3 1/2}$	15100.835	6620.341	2	I	$21738^{e}_{2} - 28358_{3}$
15309.803	6529.978	0			15099.336	6620.998	4	I	$17411^{e}_{3} - 24032_{4}$
15307.300	6531.046	6	I	$17501^{e}_{5} - 24032_{4}$	15096.026	6622.450	2		
15299.948	6534.184	2			15095.376	6622.735	1	I	$25306^{e}_{2} - 31929_{3}$
15297.656	6535.163	0	I	$21738^{e}_{2} - 28273_{2}$	15090.817	6624.736	2	I	$20566^{e}_{4} - 27191_{5}$
15296.303	6535.741	0			15084.090	6627.690	1		
15295.651	6536.020	0	I	$19273_{2} - 25809^{e}_{1}$	15077.746	6630.479	0		
15293.025	6537.142	0	II	$20989^{e}_{4 1/2} - 27526_{4 1/2}$	15073.742	6632.240	0		
15292.511	6537.362	1	I	$23015^{e}_{5} - 29552_{6}$	15065.723	6635.770	1	I	$17354^{e}_{1} - 23990_{2}$
15291.203	6537.921	2	I	$13175^{e}_{4} - 19713_{3}$	15060.159	6638.222	1		
15288.921	6538.897	4	II	$8605_{2 1/2} - 15144^{e}_{1 1/2}$	15059.608	6638.729	0		
15285.339	6540.429	1			15051.950	6641.842	2	I	$24084^{e}_{6} - 30726_{7}$
15284.311	6540.869	0	I	$22877^{e}_{1} - 29418_{2}$	15049.671	6642.848	2	I	$23113^{e}_{4} - 29756_{4}$
15282.038	6541.842	2	I	$9804_{5} - 16346^{e}_{4}$	15045.413	6644.728	3	I	$20922^{e}_{2} - 27566_{2}$
15280.959	6542.304	2	II	$11576^{e}_{1 1/2} - 18118_{1 1/2}$	15037.137	6648.385	0	I	$15493_{4} - 22141^{e}_{3}$
15278.264	6543.458	1	I	$22338^{e}_{3} - 28882_{2}$	15035.312	6649.192	0	I	$20322^{e}_{5} - 26971_{4}$
15273.332	6545.571	2	I	$17224^{e}_{2} - 23769_{1}$	15034.068	6649.742	3	II	$9061_{2 1/2} - 15710^{e}_{1 1/2}$
15266.440	6548.526	4	II	$6700^{e}_{4 1/2} - 13248_{4 1/2}$	15033.345	6650.062	0		
15265.258	6549.033	0	I	$24880^{e}_{1} - 31429_{1}$	15031.317	6650.959	1	I	$13297_{4} - 19948^{e}_{4}$
15264.344	6549.425	2	I	$18431_{3} - 24981^{e}_{3}$	15021.804	6655.171	3	I	$12847_{3} - 19503^{e}_{3}$
15260.157	6551.222	2	I	$5563_{1} - 12114^{e}_{2}$	15017.893	6656.904	0	I	$24307^{e}_{2} - 30964_{3}$
15246.115	6557.256	1	I	$24769^{e}_{3} - 31326_{4}$	15015.230	6658.085	2	II	$6244_{1/2} - 12902^{e}_{1 1/2}$
15242.228	6558.928	0			15013.595	6658.810	0	II	$17722^{e}_{4 1/2} - 24381_{3 1/2}$
15241.775	6559.123	1	II	$6691^{e}_{1 1/2} - 13250_{2 1/2}$	15010.031	6660.391	3	I	$21902^{e}_{4} - 28562_{4}$
15240.242	6559.783	7	II	$4113_{2 1/2} - 10673^{e}_{2 1/2}$	15009.909	6660.445	2	II	$22685^{e}_{3 1/2} - 29345_{2 1/2}$
15239.289	6560.193	4	I	$13962_{1} - 20522^{e}_{2}$	15007.406	6661.556	0	I	$14481^{e}_{6} - 21143_{5}$
15230.042	6564.176	2			14994.654	6667.221	3	I	$19588^{e}_{5} - 26255_{4}$
15226.150	6565.854	0			14994.569	6667.259	2	I	$17073_{1} - 23741^{e}_{1}$
15218.677	6569.078	1			14990.632	6669.010	1	I	$12847_{3} - 19516^{e}_{2}$
15218.580	6569.120	0			14988.603	6669.913	4	I	$15493_{4} - 22163^{e}_{4}$
15215.038	6570.649	0	I	$23113^{e}_{4} - 29684_{5}$	14984.882	6671.569	4	I	$11877^{e}_{1} - 18549_{2}$
15214.240	6570.994	1	II	$20686^{e}_{2 1/2} - 27257_{3 1/2}$	14982.726	6672.529	1	I	$21890^{e}_{5} - 28562_{4}$
15212.582	6571.710	0			14980.034	6673.728	0	I	$25321^{e}_{3} - 31995_{4}$
15203.638	6575.576	0	I	$24182^{e}_{2} - 30758_{2}$	14977.689	6674.773	0		
15195.303	6579.183	0	I	$17411^{e}_{3} - 23990_{2}$	14977.332	6674.932	3	I	$22877^{e}_{5} - 29552_{6}$
15190.777	6581.143	3	I	$20214^{e}_{3} - 26796_{3}$	14976.848	6675.148	0		
15190.369	6581.320	2	I	$13962_{1} - 20543^{e}_{0}$	14970.942	6677.781	1		
15188.855	6581.976	5	II	$17727_{5 1/2} - 24309^{e}_{5 1/2}$	14970.770	6677.858	1		
15180.335	6585.670	0			14969.772	6678.303	1	II	$25246_{4 1/2} - 31924^{e}_{5 1/2}$
15171.406	6589.546	1			14968.497	6678.872	2	I	$17073_{1} - 23752^{e}_{2}$
15168.869	6590.648	0			14960.529	6682.429	0	I	$22163^{e}_{4} - 28845_{4}$
15167.182	6591.381	0	I	$26508^{e}_{3} - 33099_{3}$	14956.476	6684.240	2	I	$24561^{e}_{3} - 31245_{2}$

TABLE 1. *Infrared spectral lines of thorium*—Continued

Wavelength Å	Wavenumber cm^{-1}	Intensity	Spectrum	Classification	Wavelength Å	Wavenumber cm^{-1}	Intensity	Spectrum	Classification
14955.641	6684.613	1	I	$26096^{\circ}_{3} - 32781_{4}$	14740.403	6782.221	0	I	$24182^{\circ}_{2} - 30964_{3}$
14951.792	6686.334	1	I	$16346^{\circ}_{4} - 23032_{4}$	14739.988	6782.412	0		
14947.310	6688.339	2	I	$21539^{\circ}_{4} - 28227_{4}$	14736.470	6784.031	0	I	$17398_{3} - 24182^{\circ}_{2}$
14947.021	6688.468	1	I	$26048^{\circ}_{4} - 32737_{5}$	14719.449	6791.876	1	I	$23752^{\circ}_{2} - 30544_{2}$
14943.987	6689.826	6	I	$8800_{4} - 15490^{\circ}_{5}$	14718.799	6792.176	5	I	$19588^{\circ}_{5} - 26380_{5}$
14940.492	6691.391	7	II	$0_{11/2} - 6691^{\circ}_{13/2}$	14716.370	6793.297	2	I	$22141^{\circ}_{3} - 28934_{3}$
14939.197	6691.971	1	II	$12902^{\circ}_{13/2} - 19594_{9/2}$	14714.650	6794.091	1		
14929.051	6696.519	3			14711.400	6795.592	1		
14928.485	6696.773	4	I	$11877^{\circ}_{1} - 18574_{1}$	14710.285	6796.107	1		
14925.498	6698.113	1			14702.750	6799.590	0		
14921.758	6699.792	0	I	$15970_{3} - 22669^{\circ}_{3}$	14699.723	6800.990	2	II	$16033^{\circ}_{21/2} - 22834_{31/2}$
14920.495	6700.359	3	II	$16818_{31/2} - 23518^{\circ}_{31/2}$	14695.579	6802.908	3	I	$21539^{\circ}_{4} - 28342_{5}$
14911.028	6704.613	2	I	$22399^{\circ}_{5} - 29104_{4}$	14690.666	6805.183	0	I	$21143_{5} - 27948^{\circ}_{4}$
14910.459	6704.869	2			14689.932	6805.523	0	I	$23481^{\circ}_{1} - 30286_{1}$
14899.905	6709.618	2	II	$15305_{41/2} - 22014^{\circ}_{31/2}$	14688.909	6805.997	0	I	$15863_{2} - 22669^{\circ}_{3}$
14889.079	6714.497	0			14687.576	6806.615	0	I	$22877^{\circ}_{3} - 29684_{5}$
14880.943	6718.168	0	I	$11241^{\circ}_{3} - 17959_{4}$	14680.667	6809.818	0	I	$17959_{4} - 24769^{\circ}_{3}$
14875.259	6720.735	1	I	$24421^{\circ}_{3} - 31141_{3}$	14677.249	6811.404	5	I	$11802_{2} - 18614^{\circ}_{1}$
14873.575	6721.496	1	I	$23113^{\circ}_{4} - 29835_{3}$	14672.400	6813.655	0	II	$18568^{\circ}_{9/2} - 25381_{11/2}$
14866.776	6724.570	0			14665.680	6816.777	0		
14850.034	6732.151	0	I	$18574_{1} - 25306^{\circ}_{2}$	14661.334	6818.798	0	I	$21539^{\circ}_{4} - 28358_{3}$
14842.404	6735.612	0	I	$23113^{\circ}_{4} - 29849_{4}$	14654.914	6821.785	7	I	$11877^{\circ}_{1} - 18699_{2}$
14830.215	6741.148	3	I	$17959_{4} - 24701^{\circ}_{3}$	14651.482	6823.383	3	I	$20054_{2} - 26878^{\circ}_{3}$
14830.001	6741.245	1	I	$23015^{\circ}_{5} - 29756_{4}$	14644.393	6826.686	1	I	$18699_{2} - 25526^{\circ}_{1}$
14809.031	6750.791	2	I	$17166_{3} - 23916^{\circ}_{4}$	14638.811	6829.289	0	I	$20214^{\circ}_{3} - 27044_{3}$
14806.456	6751.965	5	I	$7280_{2} - 14032^{\circ}_{2}$	14638.217	6829.566	1	I	$20737^{\circ}_{1} - 27566_{2}$
14805.415	6752.440	3	I	$19503^{\circ}_{3} - 26255_{4}$	14633.086	6831.961	3	II	$13248_{41/2} - 20080^{\circ}_{31/2}$
14805.099	6752.584	1	I	$16554_{6} - 23306^{\circ}_{6}$	14628.703	6834.008	2	I	$23015^{\circ}_{5} - 29849_{4}$
14804.483	6752.865	0			14627.874	6834.395	4	II	$15305_{41/2} - 22139^{\circ}_{41/2}$
14797.874	6755.881	2			14624.891	6835.789	1		
14797.624	6755.995	0			14618.976	6838.555	7	I	$3687_{2} - 10526^{\circ}_{3}$
14796.452	6756.530	0	I	$20214^{\circ}_{3} - 26971_{4}$	14615.924	6839.983	1	I	$19273_{2} - 26113^{\circ}_{2}$
14795.403	6757.009	0			14609.166	6843.147	0		
14789.356	6759.772	1	I	$26036^{\circ}_{5} - 32796_{3}$	14604.155	6845.495	2	I	$24084^{\circ}_{6} - 30930_{6}$
14784.758	6761.874	1	I	$13962_{1} - 20724^{\circ}_{0}$	14603.558	6845.775	3	I	$15493_{4} - 22338^{\circ}_{3}$
14781.114	6763.541	0	I	$23609^{\circ}_{5} - 30372_{6}$	14603.174	6845.955	0	I	$18069^{\circ}_{3} - 24915_{3}$
14780.863	6763.656	0			14599.499	6847.678	1	I	$19948^{\circ}_{4} - 26796_{3}$
14777.907	6765.009	1	I	$22338^{\circ}_{3} - 29104_{4}$	14591.907	6851.241	1	I	$19039^{\circ}_{2} - 25890_{2}$
14777.230	6765.319	1	I	$24561^{\circ}_{3} - 31326_{4}$	14582.663	6855.584	1		
14772.419	6767.522	0	I	$24769^{\circ}_{3} - 31537_{3}$	14579.735	6856.961	6	II	$1521_{21/2} - 8378^{\circ}_{31/2}$
14772.031	6767.700	3	I	$25690^{\circ}_{5} - 32458_{4}$	14573.635	6859.831	2	I	$13088_{3} - 19948^{\circ}_{4}$
14769.918	6768.668	0			14570.349	6861.378	3	I	$17398_{3} - 24259^{\circ}_{4}$
14769.355	6768.926	1			14565.023	6863.887	0	II	$8460_{11/2} - 15324^{\circ}_{9/2}$
14764.746	6771.039	2	I	$16217^{\circ}_{2} - 22988_{2}$	14563.856	6864.437	0		
14757.373	6774.422	0			14563.603	6864.556	0	I	$24381^{\circ}_{2} - 31245_{2}$
14756.630	6774.763	3	I	$13962_{1} - 20737^{\circ}_{1}$	14561.641	6865.481	1		
14751.515	6777.112	0	I	$20566^{\circ}_{4} - 27343_{3}$	14560.886	6865.837	0		
14747.581	6778.920	0			14557.004	6867.668	4	II	$10855_{31/2} - 17722^{\circ}_{41/2}$
14741.842	6781.559	0			14553.980	6869.095	1	I	$20322^{\circ}_{5} - 27191_{5}$
14741.329	6781.795	5	I	$11601_{1} - 18382^{\circ}_{0}$	14551.849	6870.101	0		

TABLE 1. *Infrared spectral lines of thorium*—Continued

Wavelength Å	Wavenumber cm^{-1}	Intensity	Spectrum	Classification	Wavelength Å	Wavenumber cm^{-1}	Intensity	Spectrum	Classification
14548.134	6871.855	2	I	$10526^{\circ}_{3} - 17398_{3}$	14343.260	6970.010	6	II	$4146_{3\frac{1}{2}} - 11116^{\circ}_{3\frac{1}{2}}$
14545.954	6872.885	2	I	$14204_{5} - 21077^{\circ}_{5}$	14340.036	6971.577	0	I	$22877^{\circ}_{5} - 29849_{4}$
14541.314	6875.078	1	I	$18431_{3} - 25306^{\circ}_{2}$	14339.066	6972.049	2	II	$9061_{2\frac{1}{2}} - 16033^{\circ}_{2\frac{1}{2}}$
14533.419	6878.813	4	I	$22877^{\circ}_{5} - 29756_{4}$	14326.032	6978.392	1	I	$22163^{\circ}_{4} - 29141_{5}$
14519.935	6885.201	2	I	$15970_{3} - 22855^{\circ}_{3}$	14324.702	6979.040	0	I	$9804_{5} - 16783^{\circ}_{4}$
14510.851	6889.511	0	I	$13847_{2} - 20737^{\circ}_{1}$	14323.255	6979.745	1	I	$22855^{\circ}_{3} - 29835_{3}$
14508.948	6890.415	1	II	$19880_{4\frac{1}{2}} - 26770^{\circ}_{3\frac{1}{2}}$	14322.367	6980.178	1		
14503.235	6893.129	6	II	$10379_{4\frac{1}{2}} - 17272^{\circ}_{4\frac{1}{2}}$	14313.992	6984.262	4	I	$10414^{\circ}_{4} - 17398_{3}$
14502.932	6893.273	1	I	$18549_{2} - 25442^{\circ}_{3}$	14306.560	6987.890	2	I	$17411^{\circ}_{3} - 24399_{3}$
14501.117	6894.136	0			14297.496	6992.320	0	I	$21890^{\circ}_{5} - 28882_{2}$
14500.307	6894.521	1			14296.656	6992.731	2	I	$18930^{\circ}_{5} - 25923_{4}$
14493.424	6897.795	2	I	$23113^{\circ}_{4} - 30011_{3}$	14294.346	6993.861	0	I	$22855^{\circ}_{3} - 29849_{4}$
14491.248	6898.831	1	I	$23609^{\circ}_{5} - 30508_{5}$	14289.338	6996.312	1		
14487.168	6900.774	0			14287.043	6997.436	0		
14482.670	6902.917	0			14283.487	6999.178	1	I	$23015^{\circ}_{5} - 30014_{4}$
14476.391	6905.911	0	I	$24421^{\circ}_{3} - 31326_{4}$	14281.708	7000.050	0		
14475.836	6906.176	4	I	$15493_{4} - 22399^{\circ}_{5}$	14275.223	7003.230	0	II	$4113_{3\frac{1}{2}} - 11116^{\circ}_{3\frac{1}{2}}$
14472.395	6907.818	1	II	$20686^{\circ}_{2\frac{1}{2}} - 27593_{2\frac{1}{2}}$	14271.876	7004.872	1	I	$24769^{\circ}_{5} - 31774_{3}$
14469.188	6909.349	2	I	$17398_{3} - 24307^{\circ}_{2}$	14270.962	7005.321	1	I	$23752^{\circ}_{2} - 30758_{2}$
14467.109	6910.342	0	I	$22508^{\circ}_{2} - 29418_{2}$	14266.229	7007.645	1		
14462.402	6912.591	0	II	$16818_{3\frac{1}{2}} - 23730^{\circ}_{4\frac{1}{2}}$	14262.156	7009.646	0		
14461.502	6913.021	0			14259.243	7011.078	5	I	$19986^{\circ}_{6} - 26997_{6}$
14452.427	6917.362	0	I	$23093^{\circ}_{2} - 30011_{3}$	14254.713	7013.306	5	I	$11601_{1} - 18614^{\circ}_{1}$
14452.147	6917.496	2	I	$13297_{4} - 20214^{\circ}_{3}$	14254.065	7013.625	0	I	$15863_{3} - 22877^{\circ}_{3}$
14451.758	6917.682	4	I	$3865_{1} - 10783^{\circ}_{2}$	14253.783	7013.764	1	I	$19273_{2} - 26287^{\circ}_{1}$
14449.799	6918.620	1	I	$25877^{\circ}_{4} - 32796_{3}$	14249.904	7015.673	0		
14449.350	6918.835	2	I	$17166_{5} - 24084^{\circ}_{6}$	14247.867	7016.676	0		
14441.112	6922.782	0			14244.211	7018.477	2	I	$15618^{\circ}_{5} - 22637_{3}$
14438.799	6923.891	3	I	$18431_{3} - 25355^{\circ}_{4}$	14239.881	7020.611	1	I	$21252^{\circ}_{2} - 28273_{2}$
14433.541	6926.413	1	II	$8378^{\circ}_{3\frac{1}{2}} - 15305_{4\frac{1}{2}}$	14238.660	7021.213	2	I	$17959_{4} - 24981^{\circ}_{3}$
14424.537	6930.737	7	I	$16346^{\circ}_{4} - 23277_{5}$	14237.955	7021.561	1	I	$22396^{\circ}_{1} - 29418_{2}$
14423.392	6931.287	2	I	$15166^{\circ}_{3} - 22098_{4}$	14235.729	7022.659	2	I	$17398_{3} - 24421^{\circ}_{3}$
14412.536	6936.508	4	I	$14206^{\circ}_{4} - 21143_{5}$	14234.902	7023.067	2	I	$19948^{\circ}_{4} - 26971_{4}$
14407.785	6938.795	1	I	$19713_{3} - 26651^{\circ}_{2}$				I	$21539^{\circ}_{2} - 28562_{4}$
14403.474	6940.872	1	I	$22163^{\circ}_{4} - 29104_{4}$	14233.051	7023.980	0	I	$24769^{\circ}_{3} - 31793_{4}$
14403.132	6941.037	0	I	$23603^{\circ}_{2} - 30544_{2}$	14231.327	7024.831	4	I	$13297_{4} - 20322^{\circ}_{5}$
14398.454	6943.292	2	I	$21902^{\circ}_{4} - 28845_{4}$	14230.620	7025.180	0	I	$20566^{\circ}_{3} - 27591_{5}$
14393.566	6945.650	0			14230.460	7025.259	0	I	$22396^{\circ}_{1} - 29422_{1}$
14382.181	6951.148	1			14224.305	7028.299	0		
14374.424	6954.899	2	I	$20566^{\circ}_{4} - 27521_{4}$	14220.096	7030.379	1		
14373.329	6955.429	1	I	$21890^{\circ}_{5} - 28845_{4}$	14217.138	7031.842	1	I	$24981^{\circ}_{5} - 32012_{4}$
14370.393	6956.850	0	I	$21077^{\circ}_{5} - 28034_{5}$	14214.389	7033.202	0	I	$20054_{2} - 27087^{\circ}_{1}$
14368.039	6957.990	0			14209.924	7035.412	1		
14367.834	6958.089	0			14202.775	7038.953	0		
14364.711	6959.602	2	I	$13962_{1} - 20922^{\circ}_{2}$	14192.323	7044.137	4	I	$20522^{\circ}_{2} - 27566_{2}$
14363.687	6960.098	2	I	$18930^{\circ}_{3} - 25890_{2}$	14191.050	7044.769	2	I	$21890^{\circ}_{5} - 28934_{3}$
14360.388	6961.697	0	II	$15144^{\circ}_{1\frac{1}{2}} - 22106_{2\frac{1}{2}}$	14189.283	7045.646	0	I	$20566^{\circ}_{4} - 27612_{3}$
14358.938	6962.400	2	I	$22141^{\circ}_{3} - 29104_{4}$	14188.681	7045.945	0		
14357.839	6962.933	3	I	$7502_{3} - 14465^{\circ}_{3}$	14187.489	7046.537	2	I	$25690^{\circ}_{5} - 32737_{5}$
14355.909	6963.869	0	I	$7280_{2} - 14243^{\circ}_{1}$	14170.625	7054.923	0	I	$16554_{6} - 23609^{\circ}_{5}$

TABLE 1. *Infrared spectral lines of thorium*—Continued

Wavelength Å	Wavenumber cm^{-1}	Intensity	Spectrum	Classification	Wavelength Å	Wavenumber cm^{-1}	Intensity	Spectrum	Classification
14168.671	7055.896	7	I	$8111_4 - 15166^{\circ}_3$	13904.491	7189.955	6	I	$11241^{\circ}_3 - 18431_3$
14160.194	7060.120	1	I	$24981^{\circ}_3 - 32041_2$	13898.031	7193.297	1	I	$21165^{\circ}_3 - 28358_3$
14159.556	7060.438	0	II	$13250_{2\frac{1}{2}} - 20310^{\circ}_{2\frac{1}{2}}$	13895.433	7194.642	3	II	$9711_{3\frac{1}{2}} - 16906^{\circ}_{3\frac{1}{2}}$
14154.750	7062.835	0	I	$21165^{\circ}_3 - 28227_4$	13891.459	7196.700	0		
14148.646	7065.882	2	I	$23306^{\circ}_6 - 30372_6$	13886.527	7199.256	4	I	$20322^{\circ}_5 - 27521_4$
14113.635	7083.410	0			13882.834	7201.171	1	I	$23306^{\circ}_6 - 30508_5$
14107.467	7086.507	1	I	$22669^{\circ}_5 - 29756_4$	13872.468	7206.552	0	I	$25575^{\circ}_4 - 32781_4$
14101.396	7089.558	3	I	$20522^{\circ}_2 - 27612_3$	13862.050	7211.968	0	I	$23752^{\circ}_2 - 30964_3$
14100.879	7089.818	2	I	$19273_2 - 26363^{\circ}_2$	13861.889	7212.052	0		
14095.249	7092.650	1	I	$24701^{\circ}_3 - 31793_4$	13859.106	7213.500	1	I	$21668^{\circ}_1 - 28882_2$
14090.246	7095.168	7	I	$3687_2 - 10783^{\circ}_2$	13844.566	7221.076	0	I	$25575^{\circ}_4 - 32796_3$
14083.851	7098.390	0			13836.909	7225.072	0	II	$15786_{2\frac{1}{2}} - 23012^{\circ}_{1\frac{1}{2}}$
14079.818	7100.423	5	I	$12847_3 - 19948^{\circ}_4$	13828.453	7229.490	1	I	$24307^{\circ}_2 - 31537_3$
14073.329	7103.697	2			13828.057	7229.697	1		
14070.742	7105.003	5	II	$8605_{2\frac{1}{2}} - 15710^{\circ}_{1\frac{1}{2}}$	13827.979	7229.738	1		
14070.200	7105.277	3			13822.377	7232.668	0	II	$9585^{\circ}_{2\frac{1}{2}} - 16818_{3\frac{1}{2}}$
14063.614	7108.604	2	I	$17166_5 - 24274^{\circ}_5$	13818.508	7234.693	1	I	$18574_1 - 25809^{\circ}_1$
14061.486	7109.680	0	I	$18699_2 - 25809^{\circ}_1$	13815.598	7236.217	1	I	$11802_2 - 19039^{\circ}_2$
14061.215	7109.817	1	I	$14465^{\circ}_3 - 21575_2$	13814.181	7236.959	0	I	$23521^{\circ}_3 - 30758_2$
14054.652	7113.137	1	I	$18809^{\circ}_4 - 25923_4$	13813.983	7237.063	0		
14054.140	7113.396	2			13813.265	7237.439	0	I	$23049^{\circ}_1 - 30286_1$
14053.546	7113.697	1			13811.481	7238.374	4	II	$20288^{\circ}_{3\frac{1}{2}} - 27526_{4\frac{1}{2}}$
14052.066	7114.446	0			13809.796	7239.257	1	I	$21902^{\circ}_4 - 29141_5$
14043.929	7118.568	1	II	$15236_{1\frac{1}{2}} - 22355^{\circ}_{1\frac{1}{2}}$	13799.139	7244.848	0	I	$25306^{\circ}_2 - 32551_3$
14038.143	7121.502	0	I	$24307^{\circ}_2 - 31429_1$	13795.378	7246.823	1	I	$24182^{\circ}_2 - 31429_1$
14032.419	7124.407	1	I	$24202^{\circ}_4 - 31326_4$	13792.422	7248.376	5	I	$16783^{\circ}_4 - 24032_4$
14030.586	7125.338	0			13788.405	7250.488	1	II	$8460_{1\frac{1}{2}} - 15710^{\circ}_{1\frac{1}{2}}$
14028.560	7126.367	4	I	$13088_3 - 20214^{\circ}_3$	13787.653	7250.883	1		
14028.205	7126.547	3	II	$8018_{1\frac{1}{2}} - 15144^{\circ}_{1\frac{1}{2}}$	13786.380	7251.553	1	I	$15736^{\circ}_1 - 22988_2$
14027.270	7127.022	0			13779.592	7255.125	1	I	$22877^{\circ}_1 - 30132_2$
14026.605	7127.360	5	I	$11802_2 - 18930^{\circ}_3$	13778.916	7255.481	6	II	$6213_{4\frac{1}{2}} - 13468^{\circ}_{4\frac{1}{2}}$
14025.216	7128.066	2	II	$10855_{3\frac{1}{2}} - 17983^{\circ}_{3\frac{1}{2}}$	13777.235	7256.366	1	II	$12902^{\circ}_{1\frac{1}{2}} - 20158_{2\frac{1}{2}}$
14022.503	7129.445	0			13774.118	7258.008	1	I	$19532_4 - 26790^{\circ}_4$
14008.158	7136.746	0	I	$22877^{\circ}_5 - 30014_4$	13760.203	7265.348	2	I	$21077^{\circ}_5 - 28342_5$
14007.683	7136.988	1	II	$20120^{\circ}_{3\frac{1}{2}} - 27257_{3\frac{1}{2}}$	13757.224	7266.921	0		
14007.173	7137.248	0	I	$23752^{\circ}_2 - 30889_1$	13756.558	7267.273	2		
13995.011	7143.450	0	I	$15970_3 - 23113^{\circ}_4$	13752.928	7269.191	2	I	$13297_4 - 20566^{\circ}_4$
13993.145	7144.403	1	I	$21738^{\circ}_2 - 28882_2$	13752.277	7269.535	0	I	$20322^{\circ}_5 - 27591_5$
13976.090	7153.121	2	I	$22399^{\circ}_5 - 29552_6$	13748.535	7271.514	0	I	$24769^{\circ}_3 - 32041_2$
13975.932	7153.202	4	I	$19227^{\circ}_6 - 26380_5$	13748.149	7271.718	2	I	$18431_3 - 25703^{\circ}_2$
13974.383	7153.995	1	I	$18549_2 - 25703^{\circ}_2$	13746.311	7272.690	0		
13972.014	7155.208	1	II	$10572^{\circ}_{4\frac{1}{2}} - 17727_{5\frac{1}{2}}$	13745.894	7272.911	0	I	$25690^{\circ}_5 - 32963_5$
13970.381	7156.044	2	I	$22855^{\circ}_3 - 30011_3$	13739.956	7276.054	5	I	$18614^{\circ}_1 - 25890_2$
13964.777	7158.916	2	I	$12114^{\circ}_2 - 19273_2$	13738.583	7276.781	3	I	$22141^{\circ}_3 - 29418_2$
13957.824	7162.482	0			13735.446	7278.443	2	I	$21252^{\circ}_2 - 28531_2$
13950.984	7165.994	0			13734.218	7279.094	2	I	$19516^{\circ}_2 - 26796_3$
13936.736	7173.320	5	I	$20322^{\circ}_5 - 27495_4$	13731.271	7280.656	2	I	$20214^{\circ}_3 - 27495_4$
13930.234	7176.668	3	I	$15493_4 - 22669^{\circ}_5$	13729.372	7281.663	2		
13928.452	7177.586	1			13728.599	7282.073	0		
13927.042	7178.313	0			13727.340	7282.741	1	I	$19713_3 - 26995^{\circ}_3$

TABLE 1. *Infrared spectral lines of thorium*—Continued

Wavelength Å	Wavenumber cm^{-1}	Intensity	Spectrum	Classification	Wavelength Å	Wavenumber cm^{-1}	Intensity	Spectrum	Classification
13723.460	7284.800	0	I	$22399^{\circ}_{5} - 29684_{5}$	13540.748	7383.097	3	I	$19588^{\circ}_{5} - 26971_{4}$
13719.712	7286.790	2			13538.429	7384.362	2	I	$15493_{4} - 22877^{\circ}_{5}$
13709.552	7292.190	1	II	$22139^{\circ}_{4\frac{1}{2}} - 29431_{3\frac{1}{2}}$	13532.204	7387.759	2	I	$14206^{\circ}_{4} - 21594_{3}$
13699.211	7297.695	3	II	$23187^{\circ}_{6\frac{1}{2}} - 30484_{5\frac{1}{2}}$	13529.689	7389.132	1	I	$16351_{0} - 23741^{\circ}_{1}$
13680.790	7307.521	0	I	$17073_{1} - 24381^{\circ}_{2}$	13524.811	7391.797	1	II	$12488^{\circ}_{4\frac{1}{2}} - 19880_{4\frac{1}{2}}$
13680.494	7307.679	1	I	$11241^{\circ}_{3} - 18549_{2}$	13520.057	7394.396	1	II	$12485^{\circ}_{3\frac{1}{2}} - 19880_{4\frac{1}{2}}$
13677.064	7309.512	2	I	$23655^{\circ}_{4} - 30964_{3}$	13518.143	7395.443	6	I	$11877^{\circ}_{1} - 19273_{2}$
13672.580	7311.909	0	I	$24701^{\circ}_{5} - 32012_{4}$	13517.712	7395.679	2	I	$17959_{4} - 25355^{\circ}_{4}$
13672.490	7311.957	0	I	$22338^{\circ}_{3} - 29650_{2}$	13514.671	7397.343	1	I	$20214^{\circ}_{3} - 27612_{3}$
13668.402	7314.144	0	I	$25753^{\circ}_{5} - 33068_{6}$	13508.886	7400.511	0	I	$25336^{\circ}_{6} - 32737_{5}$
13665.979	7315.441	0	II	$14790^{\circ}_{3\frac{1}{2}} - 22106_{2\frac{1}{2}}$	13503.654	7403.378	0		
13664.755	7316.096	1			13501.001	7404.833	4	I	$13847_{2} - 21252^{\circ}_{2}$
13664.604	7316.177	3	II	$7828_{1\frac{1}{2}} - 15144^{\circ}_{1\frac{1}{2}}$	13498.256	7406.339	0		
13662.574	7317.264	2	I	$17354^{\circ}_{1} - 24671_{2}$	13494.985	7408.134	0	II	$8378^{\circ}_{3\frac{1}{2}} - 15786_{2\frac{1}{2}}$
13662.466	7317.322	1	I	$13847_{2} - 21165^{\circ}_{3}$	13493.439	7408.983	4		
13654.606	7321.534	0	II	$18118_{1\frac{1}{2}} - 25440^{\circ}_{2\frac{1}{2}}$	13491.454	7410.073	1	I	$23916^{\circ}_{4} - 31326_{4}$
13647.606	7325.289	5	I	$18930^{\circ}_{5} - 26255_{4}$	13487.329	7412.339	0		
13636.063	7331.490	5	II	$0_{1\frac{1}{2}} - 7331^{\circ}_{2\frac{1}{2}}$	13484.963	7413.640	1	I	$18699_{2} - 26113^{\circ}_{2}$
13630.233	7334.626	2			13484.304	7414.002	3	I	$15618^{\circ}_{3} - 23032_{4}$
13628.932	7335.326	1	I	$14204_{5} - 21539^{\circ}_{4}$	13483.659	7414.357	3		
13626.318	7336.733	1			13478.127	7417.400	0	I	$22338^{\circ}_{3} - 29756_{4}$
13626.116	7336.842	4	II	$15305_{4\frac{1}{2}} - 22642^{\circ}_{4\frac{1}{2}}$	13468.267	7422.830	0		
13618.580	7340.902	0			13465.671	7424.261	0	I	$24202^{\circ}_{4} - 31626_{5}$
13612.012	7344.444	0	I	$22669^{\circ}_{3} - 30014_{4}$	13461.947	7426.315	0		
13609.614	7345.738	2	I	$19532_{4} - 26878^{\circ}_{3}$	13460.761	7426.969	1		
13603.594	7348.989	1			13460.143	7427.310	3	II	$8605_{2\frac{1}{2}} - 16033^{\circ}_{2\frac{1}{2}}$
13602.938	7349.343	0			13449.197	7433.355	4	I	$10526^{\circ}_{3} - 17959_{4}$
13599.702	7351.092	3	I	$20922^{\circ}_{2} - 28273_{2}$	13448.036	7433.997	1	I	$24561^{\circ}_{3} - 31995_{4}$
13598.599	7351.688	3	I	$24850^{\circ}_{6} - 32202_{5}$	13447.755	7434.152	4	I	$13088_{3} - 20522^{\circ}_{2}$
13598.305	7351.847	1			13447.160	7434.481	0		
13598.167	7351.922	2	I	$20214^{\circ}_{3} - 27566_{2}$	13445.057	7435.644	0	II	$13250_{2\frac{1}{2}} - 20686^{\circ}_{2\frac{1}{2}}$
13597.830	7352.104	1	I	$24274^{\circ}_{5} - 31626_{5}$	13443.925	7436.270	4	I	$20922^{\circ}_{2} - 28358_{3}$
13595.363	7353.438	0	I	$25442^{\circ}_{3} - 32796_{3}$	13440.583	7438.119	4	I	$11601_{1} - 19039^{\circ}_{2}$
13592.829	7354.809	0	I	$24182^{\circ}_{2} - 31537_{3}$	13439.085	7438.948	1	I	$14206^{\circ}_{4} - 21645_{4}$
13589.496	7356.613	0			13436.414	7440.427	0	I	$17224^{\circ}_{2} - 24664_{3}$
13588.783	7356.999	4	I	$22399^{\circ}_{5} - 29756_{4}$	13433.332	7442.134	3	I	$14226_{0} - 21668^{\circ}_{1}$
13587.748	7357.559	0	I	$23015^{\circ}_{5} - 30372_{6}$	13429.635	7444.183	1		
13584.089	7359.541	0			13427.136	7445.568	3	II	$10673^{\circ}_{3\frac{1}{2}} - 18118_{1\frac{1}{2}}$
13582.026	7360.659	0	II	$22513^{\circ}_{2\frac{1}{2}} - 29873_{3\frac{1}{2}}$	13426.907	7445.695	3	I	$18809^{\circ}_{4} - 26255_{4}$
13579.485	7362.036	2			13426.686	7445.818	2	I	$18431_{3} - 25877^{\circ}_{4}$
13579.410	7362.077	4	I	$15493_{4} - 22855^{\circ}_{3}$	13425.849	7446.282	0	II	$20080^{\circ}_{3\frac{1}{2}} - 27526_{4\frac{1}{2}}$
13579.201	7362.190	0			13423.480	7447.596	2	I	$17224^{\circ}_{2} - 24671_{2}$
13572.266	7365.952	0	I	$21165^{\circ}_{3} - 28531_{2}$	13421.280	7448.817	0		
13570.411	7366.959	3	I	$12847_{3} - 20214^{\circ}_{3}$	13419.576	7449.763	4	I	$22399^{\circ}_{5} - 29849_{4}$
13565.665	7369.536	7	I	$15618^{\circ}_{3} - 22988_{2}$	13418.102	7450.581	0	I	$23093^{\circ}_{2} - 30544_{2}$
13562.388	7371.317	2	I	$17398_{3} - 24769^{\circ}_{3}$	13404.943	7457.895	4	I	$11241^{\circ}_{3} - 18699_{2}$
13553.046	7376.398	0			13400.553	7460.338	0		
13551.673	7377.145	0			13395.691	7463.046	4	II	$4113_{2\frac{1}{2}} - 11576^{\circ}_{1\frac{1}{2}}$
13549.102	7378.545	2	I	$19273_{2} - 26651^{\circ}_{2}$	13395.136	7463.355	1	I	$19532_{4} - 26995^{\circ}_{3}$
13544.406	7381.103	1	II	$15453^{\circ}_{3\frac{1}{2}} - 22834_{3\frac{1}{2}}$	13391.987	7465.110	0		

TABLE 1. *Infrared spectral lines of thorium*—Continued

Wavelength Å	Wavenumber cm^{-1}	Intensity	Spectrum	Classification	Wavelength Å	Wavenumber cm^{-1}	Intensity	Spectrum	Classification
13387.914	7467.381	0	I	$20566^{\circ}_{4} - 28034_{5}$	13247.730	7546.399	4	I	$8800_{4} - 16346^{\circ}_{4}$
13386.236	7468.317	2	I	$19503^{\circ}_{3} - 26971_{4}$	13246.336	7547.193	0	I	$19948^{\circ}_{4} - 27495_{4}$
13382.214	7470.562	4	I	$15166^{\circ}_{2} - 22637_{3}$	13245.664	7547.576	2	I	$18549_{2} - 26096^{\circ}_{3}$
13376.396	7473.811	0	II	$20120^{\circ}_{3\frac{1}{2}} - 27593_{2\frac{1}{2}}$	13241.997	7549.666	0	II	$12570_{3\frac{1}{2}} - 20120^{\circ}_{2\frac{1}{2}}$
13373.859	7475.229	3			13239.744	7550.951	4	I	$15970_{3} - 23521^{\circ}_{3}$
13370.573	7477.066	1	I	$24981^{\circ}_{3} - 32458_{4}$	13236.164	7552.993	3	I	$19713_{3} - 27266^{\circ}_{4}$
13370.190	7477.280	2	II	$19880_{4\frac{1}{2}} - 27357^{\circ}_{4\frac{1}{2}}$	13234.852	7553.742	2	I	$3687_{2} - 11241^{\circ}_{3}$
13368.792	7478.062	6	I	$13088_{3} - 20566^{\circ}_{4}$	13230.970	7555.958	0		
13367.083	7479.018	1			13223.385	7560.292	3	II	$9711_{3\frac{1}{2}} - 17272^{\circ}_{4\frac{1}{2}}$
13360.349	7482.788	0	I	$17959_{4} - 25442^{\circ}_{3}$	13222.361	7560.878	0	II	$14545^{\circ}_{2\frac{1}{2}} - 22106_{2\frac{1}{2}}$
13355.490	7485.510	0	I	$21077^{\circ}_{5} - 28562_{4}$	13219.366	7562.591	0	I	$14032^{\circ}_{2} - 21594_{3}$
13353.446	7486.656	0	I	$23655^{\circ}_{4} - 31141_{3}$	13217.149	7563.859	0	I	$18549_{2} - 26113^{\circ}_{2}$
13352.939	7486.940	0	I	$18549_{2} - 26036^{\circ}_{3}$	13216.178	7564.415	1	I	$21539^{\circ}_{4} - 29104_{4}$
13350.017	7488.579	1			13215.207	7564.971	0	I	$22396^{\circ}_{1} - 29961_{1}$
13348.625	7489.360	1	I	$25306^{\circ}_{2} - 32796_{3}$	13205.290	7570.652	6	I	$18809^{\circ}_{4} - 26380_{5}$
13342.411	7492.848	1	I	$23015^{\circ}_{5} - 30508_{5}$	13202.889	7572.029	1	I	$24202^{\circ}_{4} - 31774_{3}$
13336.712	7496.050	3	I	$22338^{\circ}_{5} - 29835_{3}$	13200.969	7573.130	1	I	$19948^{\circ}_{4} - 27521_{4}$
13334.671	7497.197	1	I	$18614^{\circ}_{1} - 26111_{1}$	13199.517	7573.963	0		
13322.946	7503.795	0	I	$17411^{\circ}_{3} - 24915_{3}$	13198.322	7574.649	0		
13319.676	7505.637	1	II	$9400_{3\frac{1}{2}} - 16906^{\circ}_{3\frac{1}{2}}$	13188.919	7580.049	2	II	$9238^{\circ}_{4\frac{1}{2}} - 16818_{3\frac{1}{2}}$
13315.518	7507.981	1	I	$8111_{4} - 15618^{\circ}_{3}$	13185.440	7582.049	0		
13314.704	7508.440	1	I	$24421^{\circ}_{3} - 31929_{3}$	13184.286	7582.713	2	I	$17398_{3} - 24981^{\circ}_{3}$
13311.623	7510.178	2	II	$12570_{3\frac{1}{2}} - 20080^{\circ}_{3\frac{1}{2}}$	13183.941	7582.911	3	I	$6362_{2} - 13945^{\circ}_{3}$
13310.052	7511.064	1	II	$20120^{\circ}_{2\frac{1}{2}} - 27631_{1\frac{1}{2}}$	13183.783	7583.002	3	I	$15618^{\circ}_{3} - 23201_{3}$
13306.095	7513.298	2	II	$20080^{\circ}_{3\frac{1}{2}} - 27593_{2\frac{1}{2}}$	13179.568	7585.427	0		
13304.846	7514.003	2	II	$19248^{\circ}_{2\frac{1}{2}} - 26762_{1\frac{1}{2}}$	13179.277	7585.595	0	II	$15786_{2\frac{1}{2}} - 23372^{\circ}_{1\frac{1}{2}}$
13303.409	7514.815	1	I	$24259^{\circ}_{4} - 31774_{3}$	13176.103	7587.422	2	I	$18699_{2} - 26287^{\circ}_{1}$
13296.036	7518.982	1	I	$24274^{\circ}_{5} - 31793_{4}$	13171.565	7590.036	0		
13292.355	7521.064	0	I	$22163^{\circ}_{4} - 29684_{5}$	13169.665	7591.131	0	I	$24202^{\circ}_{4} - 31793_{4}$
13290.823	7521.931	1	I	$15493_{4} - 23015^{\circ}_{5}$	13168.345	7591.892	0	I	$24421^{\circ}_{3} - 32012_{4}$
13289.735	7522.547	0			13167.879	7592.161	0	I	$24182^{\circ}_{2} - 31774_{3}$
13288.387	7523.310	1	II	$17722^{\circ}_{4\frac{1}{2}} - 25246_{4\frac{1}{2}}$	13156.601	7598.669	1	I	$12114^{\circ}_{2} - 19713_{3}$
13286.526	7524.364	0	I	$25575^{\circ}_{4} - 33099_{3}$	13150.947	7601.936	1	I	$21539^{\circ}_{4} - 29141_{5}$
13283.226	7526.233	1	II	$21297^{\circ}_{2\frac{1}{2}} - 28823_{2\frac{1}{2}}$	13146.765	7604.354	1	I	$19713_{3} - 27317^{\circ}_{3}$
13281.453	7527.238	4	I	$19516^{\circ}_{2} - 27044_{3}$	13146.229	7604.664	1	I	$18431_{3} - 26036^{\circ}_{3}$
13279.662	7528.253	0	I	$21890^{\circ}_{3} - 29418_{2}$	13145.904	7604.852	7	II	$6213_{4\frac{1}{2}} - 13818^{\circ}_{3\frac{1}{2}}$
13278.433	7528.950	0			13144.547	7605.637	1	I	$19986^{\circ}_{6} - 27591_{5}$
13275.351	7530.698	5	I	$16554_{6} - 24084^{\circ}_{6}$	13142.940	7606.567	2		
13271.329	7532.980	0			13136.162	7610.492	0	I	$23655^{\circ}_{4} - 31265_{3}$
13269.677	7533.918	1	I	$24259^{\circ}_{4} - 31793_{4}$	13130.308	7613.885	1	II	$22106_{2\frac{1}{2}} - 29720^{\circ}_{1\frac{1}{2}}$
13268.368	7534.661	0			13128.501	7614.933	2	I	$22399^{\circ}_{5} - 30014_{4}$
13267.880	7534.938	2	I	$17166_{3} - 24701^{\circ}_{3}$	13127.923	7615.268	5	I	$16783^{\circ}_{4} - 24399_{3}$
13263.633	7537.351	2	I	$23015^{\circ}_{5} - 30552_{4}$	13126.998	7615.805	1	II	$9202^{\circ}_{3\frac{1}{2}} - 16818_{3\frac{1}{2}}$
13262.164	7538.186	2	II	$10189^{\circ}_{5\frac{1}{2}} - 17727_{5\frac{1}{2}}$	13126.337	7616.188	0	I	$20054_{2} - 27670^{\circ}_{5}$
13261.338	7538.655	0	I	$18574_{1} - 26113^{\circ}_{2}$	13124.108	7617.482	1	I	$15863_{2} - 23481^{\circ}_{1}$
13257.081	7541.076	3	I	$19503^{\circ}_{3} - 27044_{3}$	13120.544	7619.551	1	I	$20054_{2} - 27674^{\circ}_{2}$
13253.863	7542.907	5	I	$15490^{\circ}_{5} - 23032_{4}$	13119.476	7620.171	1	I	$24421^{\circ}_{3} - 32041_{2}$
13251.713	7544.131	2	II	$7001_{1\frac{1}{2}} - 14545^{\circ}_{2\frac{1}{2}}$	13116.755	7621.752	1	I	$24307^{\circ}_{2} - 31929_{3}$
13250.406	7544.875	1	I	$2869_{2} - 10414^{\circ}_{4}$	13115.845	7622.281	0		
13248.848	7545.762	2	I	$10414^{\circ}_{4} - 17959_{4}$	13111.862	7624.596	0	I	$22508^{\circ}_{2} - 30132_{2}$

TABLE 1. *Infrared spectral lines of thorium*—Continued

Wavelength Å	Wavenumber cm^{-1}	Intensity	Spectrum	Classification	Wavelength Å	Wavenumber cm^{-1}	Intensity	Spectrum	Classification
13107.912	7626.894	1	I	$25336^{\circ}_{6} - 32963_{5}$	12949.037	7720.470	1	I	$16554_{6} - 24274^{\circ}_{5}$
13103.036	7629.732	0	I	$13945^{\circ}_{3} - 21575_{2}$	12948.255	7720.936	0	I	$24274^{\circ}_{5} - 31995_{4}$
13102.832	7629.851	1	I	$21252^{\circ}_{2} - 28882_{2}$	12940.934	7725.304	2		
13101.858	7630.418	1	I	$22877^{\circ}_{5} - 30508_{5}$	12940.654	7725.471	7	II	$1859_{1/2} - 9585^{\circ}_{3/2}$
13101.123	7630.846	2			12939.572	7726.117	1		
13092.193	7636.051	1			12938.933	7726.499	2	I	$8243^{\circ}_{2} - 15970_{3}$
13079.586	7643.411	1	I	$19948^{\circ}_{4} - 27591_{5}$	12936.840	7727.749	1	I	$19532_{4} - 27260^{\circ}_{3}$
13070.834	7648.529	6	I	$10783^{\circ}_{2} - 18431_{3}$	12935.233	7728.709	3	I	$18382^{\circ}_{0} - 26111_{1}$
13069.399	7649.369	3	I	$13945^{\circ}_{3} - 21594_{3}$	12934.697	7729.029	0		
13063.724	7652.692	0			12933.760	7729.589	1	I	$20054_{2} - 27784^{\circ}_{2}$
13062.628	7653.334	1			12933.539	7729.721	5	II	$4490^{\circ}_{3/2} - 12219_{1/2}$
13058.026	7656.031	0			12932.107	7730.577	2	I	$17959_{4} - 25690^{\circ}_{5}$
13056.097	7657.162	2	I	$15863_{2} - 23521^{\circ}_{3}$	12930.664	7731.440	1	II	$15786_{3/2} - 23518^{\circ}_{3/2}$
13055.889	7657.284	6	I	$2869_{3} - 10526^{\circ}_{3}$	12930.425	7731.583	1	I	$25336^{\circ}_{6} - 33068_{6}$
13049.034	7661.307	2	I	$20566^{\circ}_{4} - 28227_{4}$	12925.892	7734.294	3		
13048.139	7661.832	1	I	$23609^{\circ}_{5} - 31271_{5}$	12925.197	7734.710	1	I	$19713_{3} - 27447^{\circ}_{2}$
13045.340	7663.476	1	I	$18699_{2} - 26363^{\circ}_{2}$	12924.885	7734.897	0		
13044.181	7664.157	1			12923.256	7735.872	0	I	$24259^{\circ}_{4} - 31995_{4}$
13043.407	7664.612	4	I	$7502_{3} - 15166^{\circ}_{3}$	12921.032	7737.203	3		
13042.243	7665.296	0			12920.304	7737.639	0	I	$18549_{2} - 26287^{\circ}_{1}$
13034.773	7669.689	2	I	$6362_{2} - 14032^{\circ}_{2}$	12919.299	7738.241	3	I	$24274^{\circ}_{5} - 32012_{4}$
13031.133	7671.831	3	I	$23655^{\circ}_{4} - 31326_{4}$	12916.981	7739.630	4	I	$15863_{2} - 23603^{\circ}_{2}$
13030.257	7672.347	0	I	$22338^{\circ}_{3} - 30011_{3}$	12911.946	7742.648	1		
13029.053	7673.056	0	II	$12485^{\circ}_{3/2} - 20158_{2/2}$	12901.919	7748.665	2	II	$9711_{3/2} - 17460^{\circ}_{3/2}$
13026.187	7674.744	6	I	$12847_{3} - 20522^{\circ}_{2}$	12900.246	7749.670	2	I	$19817^{\circ}_{1} - 27566_{2}$
13023.092	7676.568	1	I	$23752^{\circ}_{2} - 31429_{1}$	12898.865	7750.500	4	I	$20522^{\circ}_{2} - 28273_{2}$
13016.640	7680.373	5	II	$1521_{2/2} - 9202^{\circ}_{3/2}$	12888.182	7756.924	2	I	$19039^{\circ}_{2} - 26796_{3}$
13013.722	7682.095	1			12881.709	7760.822	0	I	$21890^{\circ}_{5} - 29650_{2}$
13010.439	7684.034	1	I	$21738^{\circ}_{2} - 29422_{1}$	12880.819	7761.358	0		
13010.154	7684.202	3	I	$17166_{5} - 24850^{\circ}_{6}$	12874.595	7765.110	1	I	$17073_{1} - 24838^{\circ}_{1}$
13008.873	7684.959	0			12873.533	7765.751	1	I	$20214^{\circ}_{3} - 27980_{3}$
13008.742	7685.036	0	I	$15970_{3} - 23655^{\circ}_{4}$	12872.702	7766.252	3	I	$10783^{\circ}_{2} - 18549_{2}$
13007.832	7685.574	5	I	$16346^{\circ}_{4} - 24032_{4}$	12866.644	7769.909	7	I	$19227^{\circ}_{6} - 26997_{6}$
13006.151	7686.567	2	II	$12472^{\circ}_{2/2} - 20158_{2/2}$	12861.651	7772.925	4	I	$16217^{\circ}_{2} - 23990_{2}$
13004.273	7687.677	4			12854.102	7777.490	1	I	$25321^{\circ}_{5} - 33099_{3}$
12994.532	7693.440	3	I	$22141^{\circ}_{3} - 29835_{3}$	12846.823	7781.897	1	I	$24769^{\circ}_{3} - 32551_{3}$
12990.876	7695.605	0			12845.690	7782.583	1	I	$15970_{3} - 23752^{\circ}_{2}$
12989.585	7696.370	1	I	$9804_{5} - 17501^{\circ}_{5}$	12841.750	7784.971	2	I	$19532_{4} - 27317^{\circ}_{3}$
12988.177	7697.204	1	I	$22855^{\circ}_{5} - 30552_{4}$	12837.894	7787.309	2	I	$15490^{\circ}_{5} - 23277_{5}$
12986.920	7697.949	4	I	$7795^{\circ}_{4} - 15493_{4}$	12836.536	7788.133	1	I	$19273_{2} - 27061^{\circ}_{2}$
12983.105	7700.211	0	I	$11802_{2} - 19503^{\circ}_{3}$	12834.733	7789.227	2		
12982.529	7700.553	1	I	$13945^{\circ}_{3} - 21645_{4}$	12831.063	7791.455	0	I	$10783^{\circ}_{2} - 18574_{1}$
12974.600	7705.259	0			12830.547	7791.768	3	I	$20566^{\circ}_{4} - 28358_{3}$
12970.735	7707.555	2	I	$22141^{\circ}_{3} - 29849_{4}$	12828.909	7792.763	0		
12966.746	7709.926	0	I	$23916^{\circ}_{4} - 31626_{5}$	12828.379	7793.085	1	I	$24202^{\circ}_{4} - 31995_{4}$
12964.195	7711.443	2	II	$19050^{\circ}_{1/2} - 26762_{1/2}$	12827.456	7793.646	0	I	$22338^{\circ}_{3} - 30132_{2}$
12963.697	7711.739	2	I	$20322^{\circ}_{5} - 28034_{5}$	12826.806	7794.041	3	I	$17959_{4} - 25753^{\circ}_{5}$
12961.197	7713.227	1			12799.956	7810.390	2	I	$24202^{\circ}_{4} - 32012_{4}$
12959.819	7714.047	7	I	$11802_{2} - 19516^{\circ}_{2}$	12798.586	7811.226	0		
12952.082	7718.655	5	I	$12847_{3} - 20566^{\circ}_{4}$	12796.262	7812.645	0		

530-326 OL - 74 - 12

TABLE 1. *Infrared spectral lines of thorium*—Continued

Wavelength Å	Wavenumber cm^{-1}	Intensity	Spectrum	Classification	Wavelength Å	Wavenumber cm^{-1}	Intensity	Spectrum	Classification
12782.294	7821.182	1	I	$13847_2 - 21668^\circ_1$	12604.640	7931.416	2	I	$18431_3 - 26363^\circ_2$
12782.059	7821.326	2	I	$18069^\circ_3 - 25890_2$	12591.895	7939.444	1	II	$16818_{3\frac{1}{2}} - 24757^\circ_{4\frac{1}{2}}$
12781.578	7821.620	4	I	$15166^\circ_3 - 22988_2$	12590.688	7940.205	0		
12776.786	7824.554	1			12587.889	7941.971	4	I	$20737^\circ_1 - 28679_2$
12773.189	7826.757	1	I	$19516^\circ_2 - 27343_3$	12583.229	7944.912	1	I	$21890^\circ_3 - 29835_3$
12762.096	7833.560	6	I	$13088_3 - 20922^\circ_2$	12582.855	7945.148	1		
12760.142	7834.760	0			12580.239	7946.800	1	I	$15970_3 - 23916^\circ_4$
12756.360	7837.083	1			12580.100	7946.888	1	I	$21902^\circ_4 - 29849_4$
12752.448	7839.487	0			12571.690	7952.204	2	I	$18699_2 - 26651^\circ_2$
12750.649	7840.593	0	I	$19503^\circ_3 - 27343_3$	12568.412	7954.278	2		
12743.510	7844.985	2			12563.833	7957.177	0	I	$17398_3 - 25355^\circ_4$
12742.669	7845.503	1	II	$9061_{2\frac{1}{2}} - 16906^\circ_{3\frac{1}{2}}$	12562.651	7957.926	2	I	$19713_3 - 27670^\circ_3$
12738.275	7848.209	0	I	$22163^\circ_4 - 30011_3$	12561.555	7958.620	3	I	$18549_2 - 26508^\circ_3$
12733.582	7851.102	3	I	$23113^\circ_4 - 30964_3$	12561.165	7958.867	1	I	$14204_5 - 22163^\circ_4$
12722.917	7857.683	2			12558.855	7960.331	1	I	$20922^\circ_2 - 28882_2$
12720.812	7858.983	1			12553.032	7964.024	5	I	$19227^\circ_6 - 27191_5$
12710.230	7865.526	1			12552.801	7964.170	4	I	$23306^\circ_6 - 31271_5$
12709.820	7865.780	4	I	$18930^\circ_3 - 26796_3$	12540.971	7971.683	2	I	$23655^\circ_4 - 31626_5$
12709.330	7866.083	5	I	$15166^\circ_3 - 23032_4$	12527.232	7980.426	2		
12703.962	7869.407	0	I	$18053^\circ_4 - 25923_4$	12522.256	7983.597	1	I	$8800_4 - 16783^\circ_4$
12703.428	7869.738	1	I	$22141^\circ_3 - 30011_3$	12519.264	7985.505	0		
12691.421	7877.183	4	I	$15863_2 - 23741^\circ_1$	12518.195	7986.187	3	I	$18809^\circ_4 - 26796_3$
12690.790	7877.575	0			12512.531	7989.802	0		
12690.055	7878.031	2			12510.096	7991.357	1		
12687.216	7879.794	0			12508.396	7992.443	2	I	$19503^\circ_3 - 27495_4$
12685.466	7880.881	1	I	$16783^\circ_4 - 24664_3$	12507.967	7992.717	0		
12684.798	7881.296	3			12502.990	7995.899	0		
12684.317	7881.595	0	I	$6362_2 - 14243^\circ_1$	12502.774	7996.037	2	I	$20566^\circ_4 - 28562_4$
12683.507	7882.098	1	I	$23655^\circ_4 - 31537_3$	12499.696	7998.006	2		
12683.213	7882.281	4	II	$7828_{1\frac{1}{2}} - 15710^\circ_{1\frac{1}{2}}$	12488.669	8005.068	1	I	$19039^\circ_2 - 27044_3$
12682.679	7882.613	0	I	$22669^\circ_3 - 30552_4$	12479.376	8011.029	1	II	$9711_{3\frac{1}{2}} - 17722^\circ_{4\frac{1}{2}}$
12680.944	7883.691	1	I	$22248^\circ_2 - 30132_2$	12477.297	8012.364	7	I	$3865_1 - 11877^\circ_1$
12673.959	7888.036	2	I	$25180^\circ_7 - 33068_6$	12476.305	8013.001	3	I	$20214^\circ_3 - 28227_4$
12670.936	7889.918	2			12474.364	8014.248	2	I	$11802_2 - 19817^\circ_1$
12670.355	7890.280	1	I	$13847_2 - 21738^\circ_2$	12473.069	8015.080	0		
12668.767	7891.269	2	I	$14206^\circ_4 - 22098_4$	12471.346	8016.187	1	I	$23521^\circ_5 - 31537_3$
12649.241	7903.450	1			12470.867	8016.495	0		
12648.388	7903.983	1	I	$17501^\circ_5 - 25405_4$	12469.228	8017.549	4	I	$10414^\circ_4 - 18431_3$
12646.536	7905.141	8	I	$10526^\circ_3 - 18431_3$	12468.606	8017.949	1	II	$11576^\circ_{1\frac{1}{2}} - 19594_{1\frac{1}{2}}$
12645.697	7905.665	4	I	$20322^\circ_5 - 28227_4$	12466.651	8019.206	0	I	$24274^\circ_5 - 32293_5$
12642.339	7907.765	3			12465.206	8020.136	1		
12641.383	7908.363	3	I	$17398_3 - 25306^\circ_2$	12465.053	8020.234	3	I	$20322^\circ_5 - 28342_5$
12636.142	7911.643	5	I	$18011^\circ_5 - 25923_4$	12460.967	8022.864	4	I	$10526^\circ_3 - 18549_2$
12633.943	7913.020	0			12458.068	8024.731	1	II	$19912^\circ_{2\frac{1}{2}} - 27937_{3\frac{1}{2}}$
12632.545	7913.896	3	I	$2869_3 - 10783^\circ_2$	12455.465	8026.408	0	I	$24769^\circ_3 - 32796_3$
12629.269	7915.949	0	I	$11601_1 - 19516^\circ_2$	12454.517	8027.019	2		
12617.523	7923.318	1			12453.262	8027.828	3	I	$15493_4 - 23521^\circ_3$
12617.200	7923.521	1	I	$17398_3 - 25321^\circ_3$	12447.488	8031.552	5	I	$11241^\circ_3 - 19273_2$
12611.214	7927.282	0	I	$24274^\circ_5 - 32202_5$	12446.347	8032.288	1	I	$19948^\circ_4 - 27980_3$
12610.394	7927.797	2			12445.393	8032.904	3	I	$15736^\circ_1 - 23769_1$

TABLE 1. *Infrared spectral lines of thorium*—Continued

Wavelength Å	Wavenumber cm^{-1}	Intensity	Spectrum	Classification	Wavelength Å	Wavenumber cm^{-1}	Intensity	Spectrum	Classification
12442.013	8035.086	5	I	$15166^{\circ}_{3} - 23201_{3}$	12325.069	8111.325	0		
12440.650	8035.966	2	I	$24701^{\circ}_{5} - 32737_{5}$	12323.962	8112.054	0	I	$21902^{\circ}_{4} - 30014_{4}$
12440.364	8036.151	1			12322.400	8113.082	1	I	$24850^{\circ}_{6} - 32963_{5}$
12437.583	8037.948	0	I	$22248^{\circ}_{2} - 30286_{1}$	12321.120	8113.925	3	I	$18930^{\circ}_{3} - 27044_{3}$
12433.627	8040.505	1			12318.487	8115.659	1	II	$12570_{3\frac{1}{2}} - 20686^{\circ}_{2\frac{1}{2}}$
12430.756	8042.362	1	I	$13847_{2} - 21890^{\circ}_{3}$	12318.050	8115.947	3	I	$15493_{4} - 23609^{\circ}_{5}$
12430.591	8042.469	1			12316.913	8116.696	2	I	$7502_{3} - 15618^{\circ}_{5}$
12429.285	8043.314	1	I	$17847^{\circ}_{2} - 25890_{2}$	12316.372	8117.053	1	I	$24084^{\circ}_{6} - 32202_{5}$
12424.510	8046.405	0			12314.487	8118.295	0		
12423.210	8047.247	0			12312.736	8119.450	2	I	$23655^{\circ}_{4} - 31774_{3}$
12422.300	8047.837	4	I	$19986^{\circ}_{6} - 28034_{5}$	12310.069	8121.209	3	I	$21890^{\circ}_{3} - 30011_{3}$
12421.310	8048.478	1	II	$21297^{\circ}_{2\frac{1}{2}} - 29345_{2\frac{1}{2}}$	12303.742	8125.385	1		
12419.161	8049.871	2	I	$19516^{\circ}_{2} - 27566_{2}$	12295.924	8130.551	0	I	$24421^{\circ}_{3} - 32551_{3}$
12417.933	8050.667	0			12294.985	8131.172	1	I	$16783^{\circ}_{4} - 24915_{3}$
12415.160	8052.465	5	I	$16346^{\circ}_{4} - 24399_{3}$	12292.964	8132.509	0		
12414.206	8053.084	1			12285.424	8137.500	1	II	$20686^{\circ}_{2\frac{1}{2}} - 28823_{2\frac{1}{2}}$
12406.195	8058.284	1	I	$20214^{\circ}_{3} - 28273_{2}$	12283.851	8138.542	1	I	$19532_{4} - 27670^{\circ}_{3}$
12402.749	8060.523	1	II	$9061_{2\frac{1}{2}} - 17121^{\circ}_{1\frac{1}{2}}$	12277.781	8142.566	0		
12400.331	8062.095	3	II	$6213_{4\frac{1}{2}} - 14275^{\circ}_{4\frac{1}{2}}$	12276.652	8143.315	1	II	$7001_{1\frac{1}{2}} - 15144^{\circ}_{1\frac{1}{2}}$
12398.153	8063.511	2	II	$1521_{2\frac{1}{2}} - 9585^{\circ}_{2\frac{1}{2}}$	12276.430	8143.462	0	I	$20214^{\circ}_{3} - 28358_{3}$
12397.849	8063.709	4	I	$19503^{\circ}_{3} - 27566_{2}$	12273.859	8145.168	2	I	$20737^{\circ}_{1} - 28882_{2}$
12396.828	8064.373	0	I	$21077^{\circ}_{5} - 29141_{5}$	12271.398	8146.801	2	I	$16554_{6} - 24701^{\circ}_{5}$
12384.580	8072.348	2			12263.449	8152.082	1	I	$23113^{\circ}_{4} - 31265_{3}$
12381.813	8074.152	3	I	$12847_{3} - 20922^{\circ}_{2}$	12262.250	8152.879	1	I	$13945^{\circ}_{3} - 22098_{4}$
12379.808	8075.460	0			12261.910	8153.105	2	I	$22399^{\circ}_{5} - 30552_{4}$
12378.451	8076.345	1	I	$18431_{3} - 26508^{\circ}_{3}$	12256.743	8156.542	2	I	$20522^{\circ}_{2} - 28679_{2}$
12378.290	8076.450	2	I	$17959_{4} - 26036^{\circ}_{3}$	12251.360	8160.126	0	II	$22834_{3\frac{1}{2}} - 30994^{\circ}_{3\frac{1}{2}}$
12377.115	8077.217	0	I	$18574_{1} - 26651^{\circ}_{2}$	12249.188	8161.573	4	I	$18809^{\circ}_{4} - 26971_{4}$
12372.881	8079.981	0			12246.140	8163.604	0		
12372.484	8080.240	4	II	$4490^{\circ}_{2\frac{1}{2}} - 12570_{3\frac{1}{2}}$	12245.483	8164.042	3	I	$13088_{3} - 21252^{\circ}_{2}$
12372.007	8080.552	2	I	$24701^{\circ}_{5} - 32781_{4}$	12244.970	8164.384	3	II	$16818_{3\frac{1}{2}} - 24982^{\circ}_{3\frac{1}{2}}$
12364.267	8085.610	1	I	$19948^{\circ}_{4} - 28034_{3}$	12244.077	8164.980	1		
12362.538	8086.741	0			12242.874	8165.782	0	I	$21252^{\circ}_{2} - 29418_{2}$
12361.433	8087.464	0			12237.332	8169.480	1	I	$21252^{\circ}_{2} - 29422_{1}$
12359.625	8088.647	2	I	$17959_{4} - 26048^{\circ}_{4}$	12236.549	8170.003	2	I	$14226_{0} - 22396^{\circ}_{1}$
12356.076	8090.970	2	II	$12219_{1\frac{1}{2}} - 20310^{\circ}_{2\frac{1}{2}}$	12234.949	8171.071	1	I	$23603^{\circ}_{2} - 31774_{3}$
12355.491	8091.353	0	I	$24202^{\circ}_{4} - 32293_{5}$	12233.199	8172.240	5	I	$14465^{\circ}_{2} - 22637_{3}$
12351.988	8093.648	3			12231.942	8173.080	8	I	$10526^{\circ}_{3} - 18699_{2}$
12349.478	8095.293	2	I	$19516^{\circ}_{2} - 27612_{3}$	12229.332	8174.824	1	I	$7795^{\circ}_{4} - 15970_{3}$
12348.314	8096.056	0	I	$23916^{\circ}_{4} - 32012_{4}$	12228.284	8175.525	1		
12348.094	8096.200	0			12226.604	8176.648	1	I	$17398_{3} - 25575^{\circ}_{4}$
12346.884	8096.994	0	I	$21738^{\circ}_{2} - 29835_{3}$	12226.177	8176.934	4	I	$11877^{\circ}_{1} - 20054_{2}$
12344.348	8098.657	0			12223.788	8178.532	2	I	$18699_{2} - 26878^{\circ}_{3}$
12341.497	8100.528	0			12219.156	8181.632	0	I	$16217^{\circ}_{2} - 24399_{3}$
12338.612	8102.422	0	I	$18549_{2} - 26651^{\circ}_{2}$	12216.424	8183.462	1	I	$24274^{\circ}_{5} - 32458_{4}$
12337.998	8102.825	7	I	$6362_{2} - 14465^{\circ}_{2}$	12211.865	8186.517	2	I	$18069^{\circ}_{3} - 26255_{4}$
12330.800	8107.555	1	I	$20423^{\circ}_{1} - 28531_{2}$	12206.894	8189.851	7	I	$3687_{2} - 11877^{\circ}_{1}$
12329.207	8108.603	2	I	$22399^{\circ}_{5} - 30508_{5}$	12202.844	8192.569	1		
12328.492	8109.073	1	I	$21902^{\circ}_{4} - 30011_{3}$	12200.702	8194.007	1	II	$18568^{\circ}_{1\frac{1}{2}} - 26762_{1\frac{1}{2}}$
12328.408	8109.128	0	I	$19503^{\circ}_{3} - 27612_{3}$	12194.157	8198.405	8	II	$1521_{2\frac{1}{2}} - 9720^{\circ}_{3\frac{1}{2}}$

TABLE 1. *Infrared spectral lines of thorium*—Continued

Wavelength Å	Wavenumber cm^{-1}	Intensity	Spectrum	Classification	Wavelength Å	Wavenumber cm^{-1}	Intensity	Spectrum	Classification
12188.866	8201.964	1	I	$18053^{\circ}_{4} - 26255_{4}$	12055.291	8292.843	0	I	$21668^{\circ}_{1} - 29961_{1}$
12188.576	8202.159	0			12051.267	8295.612	1	I	$22248^{\circ}_{2} - 30544_{2}$
12182.019	8206.574	3	I	$9804_{5} - 18011^{\circ}_{5}$	12050.486	8296.150	0	I	$18699_{2} - 26995^{\circ}_{3}$
12178.456	8208.975	2	I	$24084^{\circ}_{6} - 32293_{5}$	12043.786	8300.765	1	II	$8605_{3/2} - 16906^{\circ}_{3/2}$
12178.009	8209.276	0			12042.947	8301.343	0		
12177.607	8209.547	2			12038.242	8304.588	1	I	$19039^{\circ}_{2} - 27343_{3}$
12171.815	8213.454	4	I	$4961_{4} - 13175^{\circ}_{4}$	12037.639	8305.004	4	I	$17398_{3} - 25703^{\circ}_{3}$
12171.754	8213.495	2			12020.095	8317.125	1	I	$12847_{3} - 21165^{\circ}_{3}$
12171.023	8213.988	0			12018.718	8318.078	7	I	$16346^{\circ}_{4} - 24664_{3}$
12170.869	8214.092	0			12018.054	8318.538	4	I	$15863_{2} - 24182^{\circ}_{2}$
12167.821	8216.150	3	I	$11601_{1} - 19817^{\circ}_{1}$	12015.950	8319.994	4	I	$23306^{\circ}_{6} - 31626_{5}$
12166.851	8216.805	0	I	$21539^{\circ}_{4} - 29756_{4}$	12015.478	8320.321	1	I	$19532_{4} - 27852^{\circ}_{5}$
12162.431	8219.791	3			12011.883	8322.811	0	II	$7001_{1/2} - 15324^{\circ}_{1/2}$
12161.908	8220.144	0	I	$18431_{3} - 26651^{\circ}_{2}$	12007.854	8325.604	5	II	$4146_{3/2} - 12472^{\circ}_{3/2}$
12149.443	8228.578	2			12007.313	8325.979	0	I	$23603^{\circ}_{2} - 31929_{3}$
12146.324	8230.691	2			12005.953	8326.922	1	I	$18053^{\circ}_{4} - 26380_{5}$
12143.705	8232.466	0	I	$15970_{3} - 24202^{\circ}_{4}$	12004.504	8327.927	1		
12140.955	8234.331	3	I	$18809^{\circ}_{3} - 27044_{3}$	11999.611	8331.323	0		
12140.751	8234.469	1	I	$24561^{\circ}_{5} - 32796_{3}$	11986.392	8340.511	0	I	$23655^{\circ}_{4} - 31995_{4}$
12139.017	8235.645	1	I	$8111_{4} - 16346^{\circ}_{4}$	11984.664	8341.714	8	II	$4146_{3/2} - 12488^{\circ}_{3/2}$
12136.565	8237.309	1	II	$22642^{\circ}_{3/2} - 30879_{3/2}$	11980.135	8344.867	1	I	$22163^{\circ}_{4} - 30508_{5}$
12132.020	8240.395	3	I	$20322^{\circ}_{5} - 28562_{4}$	11979.873	8345.050	2	II	$15786_{3/2} - 24132^{\circ}_{1/2}$
12129.427	8242.157	5	I	$13297_{4} - 21539^{\circ}_{4}$	11976.025	8347.731	1	I	$20214^{\circ}_{5} - 28562_{4}$
12128.913	8242.506	1	I	$21890^{\circ}_{5} - 30132_{2}$	11974.695	8348.658	1	II	$16033^{\circ}_{3/2} - 24381_{3/2}$
12127.302	8243.601	8	I	$0_{2} - 8243^{\circ}_{2}$	11974.134	8349.049	1	I	$24202^{\circ}_{4} - 32551_{3}$
12126.918	8243.862	1	I	$24307^{\circ}_{2} - 32551_{3}$	11961.578	8357.813	1	I	$23655^{\circ}_{4} - 32012_{4}$
12126.419	8244.201	5	I	$18011^{\circ}_{5} - 26255_{4}$	11960.136	8358.821	3	II	$4113_{3/2} - 12472^{\circ}_{3/2}$
12124.024	8245.830	0			11956.759	8361.182	0	I	$22396^{\circ}_{1} - 30758_{2}$
12119.644	8248.810	3	I	$9804_{5} - 18053^{\circ}_{4}$	11955.885	8361.793	0	I	$18699_{2} - 27061^{\circ}_{2}$
12117.950	8249.963	0	I	$22508^{\circ}_{2} - 30758_{2}$	11952.411	8364.223	0		
12113.062	8253.292	0	I	$21165^{\circ}_{3} - 29418_{2}$	11952.063	8364.467	4	I	$19227^{\circ}_{6} - 27591_{5}$
12109.655	8255.614	0	I	$24202^{\circ}_{4} - 32458_{4}$	11946.618	8368.279	1	I	$20566^{\circ}_{4} - 28934_{3}$
12109.434	8255.765	3	I	$20423^{\circ}_{1} - 28679_{2}$	11945.362	8369.159	6	I	$18011^{\circ}_{5} - 26380_{5}$
12109.313	8255.847	1	I	$23015^{\circ}_{5} - 31271_{5}$	11942.130	8371.424	5	I	$15618^{\circ}_{3} - 23990_{2}$
12102.779	8260.304	1	II	$17121^{\circ}_{1/2} - 25381_{1/2}$	11940.834	8372.333	2	II	$4113_{3/2} - 12485^{\circ}_{3/2}$
12099.785	8262.348	2	I	$24701^{\circ}_{5} - 32963_{5}$	11940.638	8372.470	7	I	$2869_{3} - 11241^{\circ}_{3}$
12093.304	8266.776	1			11934.349	8376.882	1	II	$20969^{\circ}_{3/2} - 29345_{3/2}$
12087.362	8270.840	2	II	$6213_{4/2} - 14484^{\circ}_{3/2}$	11927.809	8381.475	0	I	$18809^{\circ}_{4} - 27191_{5}$
12086.503	8271.428	3	II	$9711_{3/2} - 17983^{\circ}_{3/2}$	11925.197	8383.311	1		
12086.289	8271.574	0			11919.113	8387.590	0		
12083.777	8273.294	0	I	$21738^{\circ}_{2} - 30011_{3}$	11916.586	8389.369	3	I	$22163^{\circ}_{4} - 30552_{4}$
12082.221	8274.359	2	I	$23655^{\circ}_{4} - 31929_{3}$	11911.501	8392.950	4		
12075.537	8278.939	1	I	$20566^{\circ}_{4} - 28845_{4}$	11910.840	8393.416	0	I	$22877^{\circ}_{5} - 31271_{5}$
12074.667	8279.536	2	I	$19948^{\circ}_{4} - 28227_{4}$	11910.542	8393.626	0		
12066.559	8285.099	0	I	$23916^{\circ}_{4} - 32202_{5}$	11909.862	8394.105	1	I	$19948^{\circ}_{4} - 28342_{5}$
12061.506	8288.570	2			11904.795	8397.678	2	I	$19273_{2} - 27670^{\circ}_{3}$
12060.198	8289.469	2			11903.594	8398.525	0		
12059.895	8289.677	0	I	$15970_{3} - 24259^{\circ}_{4}$	11899.837	8401.177	4	I	$13847_{2} - 22248^{\circ}_{2}$
12058.422	8290.690	0	I	$11241^{\circ}_{3} - 19532_{4}$	11894.942	8404.634	3	I	$12847_{3} - 21252^{\circ}_{2}$
12055.394	8292.772	0			11888.825	8408.958	1		

TABLE 1. *Infrared spectral lines of thorium*—Continued

Wavelength Å	Wavenumber cm^{-1}	Intensity	Spectrum	Classification	Wavelength Å	Wavenumber cm^{-1}	Intensity	Spectrum	Classification
11887.357	8409.997	1	I	$19948^{\circ}_{4} - 28358_{3}$	11777.121	8488.716	0		
11886.085	8410.897	2	I	$22141^{\circ}_{3} - 30552_{4}$	11776.403	8489.233	5	II	$9238^{\circ}_{4\frac{1}{2}} - 17727_{5\frac{1}{2}}$
11884.530	8411.997	5	I	$11802_{2} - 20214^{\circ}_{3}$	11775.163	8490.127	4	I	$10783^{\circ}_{2} - 19273_{2}$
11882.776	8413.239	2	I	$15618^{\circ}_{3} - 24032_{4}$	11773.211	8491.535	0		
11879.545	8415.527	0			11772.698	8491.905	1	I	$23521^{\circ}_{3} - 32012_{4}$
11878.611	8416.189	2	I	$19532_{4} - 27948^{\circ}_{4}$	11761.537	8499.963	1	I	$20922^{\circ}_{2} - 29422_{1}$
11874.629	8419.011	2	I	$22338^{\circ}_{3} - 30758_{2}$	11757.273	8503.046	1		
11874.199	8419.316	3	II	$12570_{3\frac{1}{2}} - 20989^{\circ}_{4\frac{1}{2}}$	11746.350	8510.953	0		
11873.851	8419.563	2	I	$13175^{\circ}_{4} - 21594_{3}$	11746.174	8511.080	1	I	$19273_{2} - 27784^{\circ}_{2}$
11870.629	8421.848	1	I	$17501^{\circ}_{5} - 25923_{4}$	11739.687	8515.783	2	II	$8605_{2\frac{1}{2}} - 17121^{\circ}_{1\frac{1}{2}}$
11868.373	8423.449	3			11737.416	8517.431	1		
11868.045	8423.682	0	I	$15493_{4} - 23916^{\circ}_{4}$	11736.880	8517.820	0		
11867.085	8424.363	1			11729.339	8523.296	1	I	$14465^{\circ}_{2} - 22988_{2}$
11865.636	8425.392	4	II	$15305_{4\frac{1}{2}} - 23730^{\circ}_{4\frac{1}{2}}$				I	$20322^{\circ}_{5} - 28845_{4}$
11864.247	8426.378	7	I	$3687_{2} - 12114^{\circ}_{2}$	11729.109	8523.463	0		
11862.597	8427.550	1			11724.039	8527.149	0		
11862.198	8427.834	1			11723.279	8527.702	2	I	$19039^{\circ}_{2} - 27566_{2}$
11858.382	8430.546	4	I	$14206^{\circ}_{4} - 22637_{3}$	11722.487	8528.278	1	I	$16351_{0} - 24880^{\circ}_{1}$
11853.098	8434.304	1	I	$13962_{1} - 22396^{\circ}_{1}$	11720.628	8529.631	3		
11848.313	8437.710	1	I	$23603^{\circ}_{2} - 32041_{2}$	11715.587	8533.301	1	II	$9585^{\circ}_{2\frac{1}{2}} - 18118_{1\frac{1}{2}}$
11846.202	8439.214	2	II	$8378^{\circ}_{3\frac{1}{2}} - 16818_{3\frac{1}{2}}$	11713.893	8534.535	2		
11842.232	8442.043	0			11712.220	8535.754	3	I	$17354^{\circ}_{1} - 25890_{2}$
11840.529	8443.257	0	I	$23093^{\circ}_{2} - 31537_{3}$	11712.007	8535.909	1		
11839.689	8443.856	1	I	$15863_{2} - 24307^{\circ}_{2}$	11709.471	8537.758	0	I	$24561^{\circ}_{3} - 33099_{3}$
11837.186	8445.642	2	I	$19588^{\circ}_{5} - 28034_{5}$	11704.645	8541.278	1	I	$23916^{\circ}_{4} - 32458_{4}$
11836.168	8446.368	0	I	$18549_{2} - 26995^{\circ}_{3}$	11703.457	8542.145	7	I	$15490^{\circ}_{5} - 24032_{4}$
11834.938	8447.246	1	I	$16217^{\circ}_{2} - 24664_{3}$	11698.831	8545.523	3	I	$13962_{1} - 22508^{\circ}_{2}$
11831.941	8449.386	0	I	$22877^{\circ}_{5} - 31326_{4}$	11695.652	8547.846	0	II	$18214^{\circ}_{1\frac{1}{2}} - 26762_{1\frac{1}{2}}$
11829.730	8450.965	4	I	$15970_{3} - 24421^{\circ}_{3}$	11695.263	8548.130	2	I	$17959_{4} - 26508^{\circ}_{3}$
11829.640	8451.029	5	I	$13088_{3} - 21539^{\circ}_{4}$	11694.285	8548.845	3	I	$21738^{\circ}_{2} - 30286_{1}$
11827.583	8452.499	4	I	$17073_{1} - 25526^{\circ}_{1}$	11694.000	8549.053	2	I	$13847_{2} - 22396^{\circ}_{1}$
11824.901	8454.416	1	I	$16217^{\circ}_{2} - 24671_{2}$	11690.334	8551.734	0	I	$22877^{\circ}_{1} - 31429_{1}$
11822.640	8456.033	4	I	$19817^{\circ}_{1} - 28273_{2}$	11682.909	8557.169	1	I	$15863_{2} - 24421^{\circ}_{3}$
11821.839	8456.606	1	I	$22508^{\circ}_{2} - 30964_{3}$	11680.650	8558.824	1		
11821.500	8456.848	0	I	$7280_{2} - 15736^{\circ}_{1}$	11678.305	8560.543	1	I	$18699_{2} - 27260^{\circ}_{3}$
11819.155	8458.526	0			11675.696	8562.456	0		
11818.546	8458.962	1	I	$20423^{\circ}_{1} - 28882_{2}$	11673.465	8564.092	1	I	$18431_{3} - 26995^{\circ}_{3}$
11811.926	8463.703	2	I	$19516^{\circ}_{2} - 27980_{3}$	11671.783	8565.326	1		
11811.172	8464.243	0			11667.638	8568.369	5	I	$16346^{\circ}_{4} - 24915_{3}$
11811.055	8464.327	0	I	$20214^{\circ}_{3} - 28679_{2}$	11666.014	8569.562	1		
11808.476	8466.176	0	II	$12219_{1\frac{1}{2}} - 20686^{\circ}_{2\frac{1}{2}}$	11662.923	8571.833	2		
11804.617	8468.943	6	I	$5563_{1} - 14032^{\circ}_{2}$	11661.167	8573.124	3	I	$19039^{\circ}_{2} - 27612_{3}$
11804.116	8469.303	3	I	$21903^{\circ}_{7} - 30372_{6}$	11658.782	8574.878	2		
11802.102	8470.748	1	I	$13175^{\circ}_{4} - 21645_{4}$	11657.259	8575.998	1	I	$22669^{\circ}_{3} - 31245_{2}$
11801.327	8471.304	0	I	$11241^{\circ}_{3} - 19713_{3}$	11655.207	8577.508	1	II	$6213_{4\frac{1}{2}} - 14790^{\circ}_{3\frac{1}{2}}$
11793.069	8477.236	1	I	$24259^{\circ}_{4} - 32737_{5}$	11653.134	8579.034	1	I	$24202^{\circ}_{4} - 32781_{4}$
11792.645	8477.541	1	I	$19503^{\circ}_{3} - 27980_{3}$	11648.639	8582.344	1	II	$11576^{\circ}_{1\frac{1}{2}} - 20158_{2\frac{1}{2}}$
11790.463	8479.110	0			11648.509	8582.440	1	I	$21252^{\circ}_{2} - 29835_{3}$
11790.382	8479.168	1	I	$17411^{\circ}_{3} - 25890_{2}$	11641.195	8587.832	1	I	$17166_{5} - 25753^{\circ}_{5}$
11779.528	8486.981	2	I	$16351_{0} - 24838^{\circ}_{1}$	11636.590	8591.231	2	I	$18930^{\circ}_{3} - 27521_{4}$

TABLE 1. *Infrared spectral lines of thorium*—Continued

Wavelength Å	Wavenumber cm^{-1}	Intensity	Spectrum	Classification
11636.496	8591.300	1	I	$21165^{\circ}_{3} - 29756_{4}$
11636.155	8591.552	3	I	$15970_{3} - 24561^{\circ}_{5}$
11634.601	8592.699	4	I	$13297_{4} - 21890^{\circ}_{3}$
11632.343	8594.367	2		
11631.948	8594.659	3	II	$10379_{4\frac{1}{2}} - 18973^{\circ}_{3\frac{1}{2}}$
11630.479	8595.745	0	I	$22669^{\circ}_{3} - 31265_{3}$
11629.776	8596.264	1		
11627.313	8598.085	0		
11621.783	8602.177	2		
11621.209	8602.602	0		
11618.190	8604.837	3	I	$13297_{4} - 21902^{\circ}_{4}$
11617.462	8605.376	5	I	$14032^{\circ}_{2} - 22637_{3}$
11615.211	8607.044	1	I	$21077^{\circ}_{5} - 29684_{5}$
11613.318	8608.447	3		
11609.914	8610.971	2	I	$8800_{4} - 17411^{\circ}_{5}$
11606.246	8613.692	1	I	$24182^{\circ}_{2} - 32796_{3}$
11605.473	8614.266	3	I	$19948^{\circ}_{4} - 28562_{4}$
11602.596	8616.402	0	I	$22141^{\circ}_{3} - 30758_{2}$
11600.761	8617.765	0	I	$18699_{2} - 27317^{\circ}_{3}$
11600.523	8617.942	0	I	$21668^{\circ}_{1} - 30286_{1}$
11597.002	8620.558	1	I	$11802_{2} - 20423^{\circ}_{1}$
11595.985	8621.314	6	I	$16783^{\circ}_{3} - 25405_{4}$
11594.834	8622.170	0	II	$16818_{3\frac{1}{2}} - 25440^{\circ}_{2\frac{1}{2}}$
11589.953	8625.801	4	I	$16554_{6} - 25180^{\circ}_{7}$
11588.544	8626.850	2		
11584.866	8629.589	0	I	$17073_{1} - 25703^{\circ}_{2}$
11584.675	8629.731	1	I	$18431_{3} - 27061^{\circ}_{2}$
11583.465	8630.633	0	I	$20214^{\circ}_{3} - 28845_{4}$
11582.709	8631.196	1		
11581.313	8632.236	1		
11579.846	8633.330	2		
11578.263	8634.510	2		
11577.991	8634.713	1	I	$23916^{\circ}_{4} - 32551_{3}$
11575.518	8636.558	4	I	$18930^{\circ}_{3} - 27566_{2}$
11573.652	8637.950	1	I	$17398_{3} - 26036^{\circ}_{3}$
11571.485	8639.568	5	I	$19588^{\circ}_{5} - 28227_{4}$
11565.916	8643.728	0		
11563.750	8645.347	0		
11558.214	8649.488	3	I	$13088_{3} - 21738^{\circ}_{2}$
11557.337	8650.144	3	I	$17398_{3} - 26048^{\circ}_{4}$
11557.225	8650.228	0	I	$21902^{\circ}_{4} - 30552_{4}$
11554.767	8652.068	0	I	$24084^{\circ}_{6} - 32737_{5}$
11551.616	8654.428	0	I	$21890^{\circ}_{3} - 30544_{2}$
11543.905	8660.209	2		
11543.824	8660.270	2	I	$13847_{2} - 22508^{\circ}_{2}$
11543.157	8660.770	0		
11542.494	8661.268	3	II	$8460_{1\frac{1}{2}} - 17121^{\circ}_{1\frac{1}{2}}$
11541.028	8662.368	0	I	$21890^{\circ}_{5} - 30552_{4}$
11536.071	8666.090	2	I	$17224^{\circ}_{2} - 25890_{2}$
11530.938	8669.948	3	I	$21165^{\circ}_{3} - 29835_{3}$
11526.904	8672.982	5		
11526.460	8673.316	4	I	$14204_{5} - 22877^{\circ}_{5}$
11525.422	8674.097	1		
11521.827	8676.804	2	II	$15786_{2\frac{1}{2}} - 24463^{\circ}_{2\frac{1}{2}}$
11517.393	8680.144	1	I	$23113^{\circ}_{4} - 31793_{4}$
11516.800	8680.591	0		
11516.456	8680.850	5	I	$5563_{1} - 14243^{\circ}_{1}$
11516.297	8680.970	1		
11515.375	8681.665	0	II	$16564^{\circ}_{5\frac{1}{2}} - 25246_{4\frac{1}{2}}$
11514.959	8681.979	4	I	$18930^{\circ}_{5} - 27612_{3}$
11512.800	8683.607	0		
11512.063	8684.163	3	I	$5563_{1} - 14247^{\circ}_{0}$
11511.566	8684.538	6	I	$20867^{\circ}_{7} - 29552_{6}$
11511.286	8684.749	1	I	$23609^{\circ}_{5} - 32293_{5}$
11510.028	8685.698	3	I	$18809^{\circ}_{4} - 27495_{4}$
11506.079	8688.679	1	I	$24274^{\circ}_{5} - 32963_{5}$
11502.185	8691.621	3	I	$12847_{3} - 21539^{\circ}_{4}$
11501.478	8692.155	4	I	$13945^{\circ}_{5} - 22637_{3}$
11494.068	8697.759	2	I	$15863_{2} - 24561^{\circ}_{3}$
11489.885	8700.925	5	I	$8800_{4} - 17501^{\circ}_{5}$
11483.227	8705.970	0		
11481.957	8706.933	0		
11478.781	8709.342	1	I	$15493_{4} - 24202^{\circ}_{2}$
11478.678	8709.420	2	II	$7001_{1\frac{1}{2}} - 15710^{\circ}_{1\frac{1}{2}}$
11476.910	8710.762	0	I	$18549_{2} - 27260^{\circ}_{3}$
11476.074	8711.396	1	I	$17166_{5} - 25877^{\circ}_{4}$
11475.757	8711.637	3	I	$18809^{\circ}_{4} - 27521_{4}$
11472.823	8713.865	2	I	$19817^{\circ}_{1} - 28531_{2}$
11471.073	8715.194	0	I	$7502_{3} - 16217^{\circ}_{2}$
11468.598	8717.075	3		
11465.039	8719.781	5	I	$11802_{2} - 20522^{\circ}_{2}$
11464.786	8719.973	2	I	$20214^{\circ}_{3} - 28934_{3}$
11458.461	8724.787	1	I	$19503^{\circ}_{3} - 28227_{4}$
11456.776	8726.070	0		
11455.648	8726.929	1	II	$12570_{3\frac{1}{2}} - 21297^{\circ}_{2\frac{1}{2}}$
11455.545	8727.008	1	I	$18069^{\circ}_{3} - 26796_{3}$
11454.332	8727.932	0		
11448.044	8732.726	0		
11444.419	8735.492	2	I	$17073_{1} - 25809^{\circ}_{1}$
11442.751	8736.765	1	I	$14465^{\circ}_{2} - 23201_{3}$
11441.097	8738.028	0		
11436.956	8741.192	0		
11432.844	8744.336	2		
11432.593	8744.528	4	I	$14243^{\circ}_{1} - 22988_{2}$
11429.704	8746.738	6	I	$10526^{\circ}_{3} - 19273_{2}$
11427.901	8748.118	1	I	$18699_{2} - 27447^{\circ}_{2}$
11426.433	8749.242	0	I	$22877^{\circ}_{5} - 31626_{5}$
11423.611	8751.403	1		
11420.044	8754.137	1	I	$19588^{\circ}_{5} - 28342_{5}$
11419.693	8754.406	1	I	$17501^{\circ}_{5} - 26255_{4}$

TABLE 1. *Infrared spectral lines of thorium*—Continued

Wavelength Å	Wavenumber cm^{-1}	Intensity	Spectrum	Classification	Wavelength Å	Wavenumber cm^{-1}	Intensity	Spectrum	Classification
11417.309	8756.234	3	I	$19516^{\circ}_{2} - 28273_{2}$	11306.901	8841.735	0		
11416.708	8756.695	0			11303.787	8844.171	5	I	$13297_{4} - 22141^{\circ}_{3}$
11415.542	8757.589	1	I	$22508^{\circ}_{2} - 31265_{3}$	11303.544	8844.361	4	I	$7502_{3} - 16346^{\circ}_{4}$
11412.071	8760.253	2	II	$4490^{\circ}_{2\frac{1}{2}} - 13250_{2\frac{1}{2}}$				I	$17411^{\circ}_{3} - 26255_{4}$
11411.321	8760.829	1	I	$24202^{\circ}_{4} - 32963_{5}$	11301.136	8846.246	1	I	$21165^{\circ}_{3} - 30011_{3}$
11408.167	8763.251	0			11300.160	8847.010	0		
11406.101	8764.838	0			11297.608	8849.008	1	I	$23609^{\circ}_{5} - 32458_{4}$
11403.120	8767.129	0			11297.490	8849.101	0		
11402.009	8767.984	0	I	$18549_{2} - 27317^{\circ}_{3}$	11296.103	8850.187	0		
11398.870	8770.398	0			11292.744	8852.820	0		
11397.100	8771.760	0			11292.585	8852.944	0		
11387.846	8778.888	1	II	$17983^{\circ}_{2\frac{1}{2}} - 26762_{1\frac{1}{2}}$	11290.238	8854.785	0	II	$8605_{2\frac{1}{2}} - 17460^{\circ}_{2\frac{1}{2}}$
11386.235	8780.130	5	I	$15618^{\circ}_{3} - 24399_{3}$	11289.645	8855.250	2	I	$19503^{\circ}_{3} - 28358_{3}$
11384.471	8781.491	3	I	$15493_{4} - 24274^{\circ}_{5}$	11288.321	8856.288	0		
11383.920	8781.916	3	I	$18809^{\circ}_{4} - 27591_{5}$	11285.357	8858.614	2		
11383.489	8782.248	0			11277.612	8864.698	0	I	$23916^{\circ}_{4} - 32781_{4}$
11374.713	8789.024	6	II	$4113_{2\frac{1}{2}} - 12902^{\circ}_{1\frac{1}{2}}$	11276.818	8865.322	4	I	$15166^{\circ}_{3} - 24032_{4}$
11371.299	8791.663	1	I	$24307^{\circ}_{2} - 33099_{3}$	11276.338	8865.700	2	I	$13297_{4} - 22163^{\circ}_{3}$
11369.091	8793.370	2	I	$24274^{\circ}_{5} - 33068_{6}$	11273.574	8867.873	4	I	$21890^{\circ}_{3} - 30758_{2}$
11366.315	8795.518	2	I	$14481^{\circ}_{6} - 23277_{5}$	11264.063	8875.361	0		
11361.606	8799.163	0			11262.936	8876.249	2		
11360.181	8800.267	0			11260.143	8878.451	1	I	$24084^{\circ}_{6} - 32963_{5}$
11358.564	8801.520	1	I	$22163^{\circ}_{4} - 30964_{3}$	11258.986	8879.363	4	I	$17501^{\circ}_{5} - 26380_{5}$
11358.499	8801.570	3	I	$13088_{3} - 21890^{\circ}_{3}$	11258.130	8880.038	3	I	$21252^{\circ}_{2} - 30132_{2}$
11357.450	8802.383	0	I	$18809^{\circ}_{4} - 27612_{3}$	11255.513	8882.103	0	I	$23113^{\circ}_{4} - 31995_{4}$
11356.910	8802.802	0	I	$22338^{\circ}_{3} - 31141_{3}$	11255.092	8882.435	3	I	$17166_{5} - 26048^{\circ}_{4}$
11356.608	8803.036	1	I	$23655^{\circ}_{4} - 32458_{4}$	11252.925	8884.146	1		
11354.715	8804.503	8	I	$6362_{2} - 15166^{\circ}_{3}$	11249.018	8887.231	0	I	$17224^{\circ}_{2} - 26111_{1}$
11352.128	8806.510	2	I	$21738^{\circ}_{2} - 30544_{2}$	11246.685	8889.075	1	I	$20214^{\circ}_{3} - 29104_{4}$
11351.924	8806.668	6	I	$19227^{\circ}_{6} - 28034_{5}$	11245.412	8890.081	2	I	$12847_{3} - 21738^{\circ}_{2}$
11350.081	8808.098	1			11244.356	8890.916	1		
11346.494	8810.883	1	I	$14204_{5} - 23015^{\circ}_{5}$	11244.310	8890.952	2	II	$13248_{4\frac{1}{2}} - 22139^{\circ}_{4\frac{1}{2}}$
11344.334	8812.560	1			11238.982	8895.167	2	I	$23306^{\circ}_{6} - 32202_{5}$
11343.709	8813.046	4	I	$11241^{\circ}_{3} - 20054_{2}$	11238.344	8895.672	0	I	$20522^{\circ}_{2} - 29418_{2}$
11343.167	8813.467	0			11236.858	8896.849	1	I	$24202^{\circ}_{4} - 33099_{3}$
11342.857	8813.708	3	I	$13088_{3} - 21902^{\circ}_{4}$	11233.671	8899.373	2	I	$20522^{\circ}_{2} - 29422_{1}$
11338.588	8817.026	0			11232.320	8900.443	2	II	$6244_{1\frac{1}{2}} - 15144^{\circ}_{1\frac{1}{2}}$
11335.713	8819.262	0	I	$20322^{\circ}_{5} - 29141_{5}$	11230.255	8902.080	9	I	$5563_{1} - 14465^{\circ}_{2}$
11332.045	8822.117	4	I	$13847_{2} - 22669^{\circ}_{3}$	11225.532	8905.825	3	I	$15863_{2} - 24769^{\circ}_{3}$
11331.384	8822.632	1	I	$14226_{0} - 23049^{\circ}_{1}$	11221.176	8909.282	1	I	$14204_{5} - 23113^{\circ}_{4}$
11330.428	8823.376	5			11215.651	8913.671	2	I	$20737^{\circ}_{1} - 29650_{2}$
11327.681	8825.516	0			11212.583	8916.110	1	I	$22877^{\circ}_{5} - 31793_{4}$
11326.973	8826.067	3	I	$14206^{\circ}_{4} - 23032_{4}$	11211.484	8916.984	0	I	$24182^{\circ}_{2} - 33099_{3}$
11326.400	8826.514	1			11208.602	8919.277	1		
11323.876	8828.481	0	I	$18431_{3} - 27260^{\circ}_{3}$	11205.579	8921.683	4	I	$11601_{1} - 20522^{\circ}_{2}$
11322.408	8829.626	1			11204.818	8922.289	2	II	$9061_{2\frac{1}{2}} - 17983^{\circ}_{2\frac{1}{2}}$
11321.659	8830.210	2	I	$8243^{\circ}_{2} - 17073_{1}$	11203.831	8923.075	1	I	$13175^{\circ}_{4} - 22098_{4}$
11321.249	8830.530	2	I	$17959_{4} - 26790^{\circ}_{4}$	11202.078	8924.471	1	II	$17837^{\circ}_{1\frac{1}{2}} - 26762_{1\frac{1}{2}}$
11311.417	8838.205	1			11195.293	8929.880	1	I	$10783^{\circ}_{2} - 19713_{3}$
11307.314	8841.412	3	I	$19516^{\circ}_{2} - 28358_{3}$	11190.716	8933.532	3		

TABLE 1. *Infrared spectral lines of thorium*—Continued

Wavelength Å	Wavenumber cm^{-1}	Intensity	Spectrum	Classification	Wavelength Å	Wavenumber cm^{-1}	Intensity	Spectrum	Classification
11189.689	8934.352	2	I	$11802_2 - 20737_1^\circ$	11043.146	9052.911	3	I	$15618_3^\circ - 24671_2$
11186.716	8936.727	0	II	$20158_{2\frac{1}{2}} - 29095_{2\frac{1}{2}}^\circ$	11042.986	9053.042	2	I	$13088_3 - 22141_3^\circ$
11185.925	8937.359	5	I	$7280_2 - 16217_2^\circ$	11038.296	9056.889	2		
11184.628	8938.395	0	I	$22855_3^\circ - 31793_4$	11036.319	9058.511	4	I	$16346_4^\circ - 25405_4$
11182.846	8939.819	2			11035.091	9059.519	0	I	$19503_3^\circ - 28562_4$
11179.105	8942.811	3	I	$11601_1 - 20543_0^\circ$	11031.608	9062.380	1	I	$21902_4^\circ - 30964_3$
11171.377	8948.997	1	I	$17847_2^\circ - 26796_3$	11031.091	9062.804	0		
11165.579	8953.644	1			11028.089	9065.271	1	I	$19817_1^\circ - 28882_2$
11162.099	8956.436	3	I	$14032_2^\circ - 22988_2$	11026.975	9066.187	1		
11159.387	8958.612	1			11023.604	9068.960	1		
11157.560	8960.079	1	I	$18011_5^\circ - 26971_4$	11021.768	9070.470	3	I	$14206_4^\circ - 23277_5$
11155.405	8961.810	0			11021.045	9071.065	0		
11151.802	8964.706	0	I	$17398_3 - 26363_2^\circ$	11017.161	9074.263	0		
11148.272	8967.544	0	I	$21165_3^\circ - 30132_2$	11016.787	9074.571	4	I	$13088_3 - 22163_4^\circ$
11148.078	8967.700	0			11016.018	9075.205	1		
11147.197	8968.409	0	I	$21539_4^\circ - 30508_5$	11013.293	9077.450	1		
11139.881	8974.299	3	I	$19588_5^\circ - 28562_4$	11010.266	9079.946	1	II	$6244_{1/2} - 15324_{1/2}^\circ$
11139.415	8974.674	0			11001.800	9086.933	3	I	$13962_1 - 23049_1^\circ$
11138.971	8975.032	1	I	$15863_2 - 24838_1^\circ$	11000.900	9087.676	1	I	$13945_3^\circ - 23032_4$
11138.821	8975.153	4	I	$18069_3^\circ - 27044_3$	10999.236	9089.051	0	I	$21668_1^\circ - 30758_2$
11134.469	8978.661	1	I	$22163_4^\circ - 31141_3$	10990.207	9096.518	2		
11128.287	8983.649	5	I	$4961_4 - 13945_3^\circ$	10986.695	9099.426	0		
11126.995	8984.692	1			10983.633	9101.963	5	I	$13297_4 - 22399_5^\circ$
11125.541	8985.866	4	I	$18011_5^\circ - 26997_6$	10983.207	9102.316	2		
11124.745	8986.509	2	I	$19948_3^\circ - 28934_3$	10982.982	9102.502	3	I	$22163_4^\circ - 31265_3$
11124.026	8987.090	3	I	$23306_6^\circ - 32293_5$	10982.910	9102.562	4	I	$14204_5 - 23306_6^\circ$
11114.372	8994.896	0	I	$20423_1^\circ - 29418_2$	10982.260	9103.101	0		
11114.157	8995.070	3	I	$14206_4^\circ - 23201_3$	10981.861	9103.431	1	II	$8018_{1\frac{1}{2}} - 17121_{1\frac{1}{2}}^\circ$
11107.735	9000.271	0	II	$8460_{1\frac{1}{2}} - 17460_{2\frac{1}{2}}^\circ$	10976.518	9107.863	0	I	$22163_4^\circ - 31271_5$
11106.476	9001.291	0			10974.389	9109.630	1	I	$17398_3 - 26508_3^\circ$
11101.804	9005.079	5	I	$9804_5 - 18809_4^\circ$	10965.252	9117.220	1	I	$15863_2 - 24981_3^\circ$
11098.788	9007.526	2	I	$13847_2 - 22855_3^\circ$	10964.829	9117.572	1	I	$20566_4^\circ - 29684_5$
11094.494	9011.012	2	I	$15970_3 - 24981_3^\circ$	10963.975	9118.282	1	I	$10414_4^\circ - 19532_4$
11092.159	9012.909	1	I	$21539_4^\circ - 30552_4$	10962.885	9119.189	5	I	$11802_2 - 20922_2^\circ$
11090.735	9014.066	3	I	$19516_2^\circ - 28531_2$	10956.004	9124.916	1	I	$18549_2 - 27674_2^\circ$
11087.646	9016.578	1			10955.633	9125.225	1		
11074.809	9027.029	5			10954.915	9125.823	0		
11073.735	9027.904	3	I	$19503_3^\circ - 28531_2$	10948.154	9131.459	4	I	$13962_1 - 23093_2^\circ$
11071.877	9029.419	1	II	$6213_{4\frac{1}{2}} - 15242_{4\frac{1}{2}}^\circ$	10946.696	9132.675	1		
11071.478	9029.745	1	I	$13847_2 - 22877_1^\circ$	10942.432	9136.234	3	I	$16554_6 - 25690_5^\circ$
11069.049	9031.726	3	II	$7001_{1\frac{1}{2}} - 16033_{2\frac{1}{2}}^\circ$	10942.244	9136.391	8	II	$6213_{4\frac{1}{2}} - 15349_{3\frac{1}{2}}^\circ$
11065.025	9035.011	0			10941.617	9136.914	4	II	$6168_{3\frac{1}{2}}^\circ - 15305_{4\frac{1}{2}}$
11062.840	9036.795	1			10938.909	9139.176	1	I	$16783_4^\circ - 25923_4$
11060.720	9038.527	0			10934.177	9143.131	0		
11057.009	9041.561	4	I	$13297_4 - 22338_3^\circ$	10933.859	9143.397	1		
11054.989	9043.213	4	I	$13945_3^\circ - 22988_2$	10927.204	9148.966	1		
11054.133	9043.913	1			10924.483	9151.245	4	II	$1521_{2\frac{1}{2}} - 10673_{2\frac{1}{2}}^\circ$
11051.898	9045.742	7	I	$15618_3^\circ - 24664_3$	10923.725	9151.880	2	I	$21738_2^\circ - 30889_1$
11050.978	9046.495	1	I	$23916_4^\circ - 32963_3$	10915.734	9158.579	0		
11046.224	9050.389	4	I	$18930_3^\circ - 27980_3$	10913.581	9160.386	3	I	$13088_3 - 22248_2^\circ$

TABLE 1. *Infrared spectral lines of thorium*—Continued

Wavelength Å	Wavenumber cm^{-1}	Intensity	Spectrum	Classification	Wavelength Å	Wavenumber cm^{-1}	Intensity	Spectrum	Classification
10911.329	9162.277	2	I	$19516^{\circ}_{2} - 28679_{2}$	10759.049	9291.956	1	I	$21252^{\circ}_{2} - 30544_{2}$
10907.689	9165.334	1			10757.771	9293.060	0	II	$7828_{1/2} - 17121^{\circ}_{1/2}$
10901.193	9170.796	4	I	$18809^{\circ}_{4} - 27980_{3}$	10754.878	9295.560	0	I	$21077^{\circ}_{5} - 30372_{6}$
10894.875	9176.114	1	I	$19503^{\circ}_{3} - 28679_{2}$	10754.328	9296.035	4	I	$15618^{\circ}_{3} - 24915_{3}$
10892.630	9178.005	0	II	$15236_{1/2} - 24414^{\circ}_{1/2}$	10752.475	9297.637	2	I	$18930^{\circ}_{3} - 28227_{4}$
10890.287	9179.980	4	I	$18011^{\circ}_{5} - 27191_{5}$	10751.857	9298.172	1		
10887.285	9182.511	0	I	$23916^{\circ}_{4} - 33099_{3}$	10749.481	9300.227	2		
10883.902	9185.365	1	I	$22141^{\circ}_{3} - 31326_{4}$	10749.434	9300.268	3	I	$17959_{4} - 27260^{\circ}_{3}$
10883.233	9185.930	0	I	$22855^{\circ}_{3} - 32041_{2}$	10744.370	9304.651	2	I	$14465^{\circ}_{2} - 23769_{1}$
10882.569	9186.490	1	I	$10526^{\circ}_{3} - 19713_{3}$	10741.809	9306.869	2		
10882.153	9186.842	0	I	$23015^{\circ}_{5} - 32202_{5}$	10741.603	9307.048	0		
10869.967	9197.141	4	I	$17847^{\circ}_{2} - 27044_{3}$	10740.457	9308.041	1	II	$10572^{\circ}_{3/2} - 19880_{4 1/2}$
10866.949	9199.695	1	I	$16554_{6} - 25753^{\circ}_{5}$	10732.245	9315.163	5	I	$12847_{3} - 22163^{\circ}_{4}$
10865.480	9200.939	0			10726.926	9319.782	8	I	$2558_{0} - 11877^{\circ}_{1}$
10864.601	9201.683	2	I	$13847_{2} - 23049^{\circ}_{1}$	10725.418	9321.092	6	I	$11601_{1} - 20922^{\circ}_{2}$
10862.508	9203.456	4	I	$20214^{\circ}_{2} - 29418_{2}$	10723.921	9322.394	7	II	$4146_{3/2} - 13468^{\circ}_{1/2}$
10861.797	9204.059	1	II	$12902^{\circ}_{1/2} - 22106_{2 1/2}$	10720.051	9325.759	0	I	$22669^{\circ}_{5} - 31995_{4}$
10857.355	9207.824	1	I	$15493_{4} - 24701^{\circ}_{5}$	10715.361	9329.841	2		
10853.458	9211.130	3	I	$8800_{4} - 18011^{\circ}_{5}$	10707.531	9336.663	1	I	$15970_{3} - 25306^{\circ}_{5}$
10845.004	9218.311	1			10700.359	9342.921	1	I	$18930^{\circ}_{5} - 28273_{2}$
10844.405	9218.820	4	I	$17166_{5} - 26384^{\circ}_{4}$	10700.194	9343.065	0	I	$22669^{\circ}_{3} - 32012_{4}$
10843.465	9219.619	1			10690.175	9351.822	1	I	$15970_{3} - 25321^{\circ}_{3}$
10837.713	9224.512	0	I	$20737^{\circ}_{1} - 29961_{1}$	10678.631	9361.931	1	I	$20322^{\circ}_{5} - 29684_{5}$
10835.309	9226.559	2	II	$20288^{\circ}_{3/2} - 29515_{4 1/2}$	10678.369	9362.161	3	I	$11802_{2} - 21165^{\circ}_{3}$
10834.611	9227.153	2	II	$15236_{1/2} - 24463^{\circ}_{2 1/2}$	10668.486	9370.834	2	I	$7795^{\circ}_{4} - 17166_{5}$
10834.179	9227.521	3			10666.640	9372.456	0	I	$13297_{4} - 22669^{\circ}_{5}$
10832.716	9228.767	0			10665.735	9373.251	0		
10826.499	9234.067	0	I	$19039^{\circ}_{2} - 28273_{2}$	10664.767	9374.102	0	I	$22163^{\circ}_{4} - 31537_{3}$
10826.144	9234.370	0			10664.234	9374.570	5	I	$6362_{2} - 15736^{\circ}_{1}$
10820.075	9239.549	5	II	$6213_{4 1/2} - 15453^{\circ}_{3 1/2}$	10663.178	9375.499	1	I	$21890^{\circ}_{5} - 31265_{3}$
10819.530	9240.015	1			10660.847	9377.549	3	II	$8605_{2 1/2} - 17983^{\circ}_{2 1/2}$
10813.573	9245.105	4	I	$2869_{3} - 12114^{\circ}_{2}$	10658.585	9379.539	1	II	$18214^{\circ}_{1/2} - 27593_{2 1/2}$
10813.395	9245.257	6	I	$4961_{4} - 14206^{\circ}_{4}$	10656.144	9381.687	0		
10812.281	9246.209	5	I	$13847_{2} - 23093^{\circ}_{2}$	10654.499	9383.136	1		
10807.344	9250.433	3	I	$13080_{3} - 22338^{\circ}_{3}$	10651.842	9385.476	0	I	$15970_{3} - 25355^{\circ}_{4}$
10804.527	9252.845	2			10649.651	9387.407	1	I	$21165^{\circ}_{3} - 30552_{4}$
10803.918	9253.367	4	I	$8800_{4} - 18053^{\circ}_{4}$	10646.516	9390.171	2	I	$8111_{4} - 17501^{\circ}_{5}$
10802.535	9254.551	1	I	$14226_{0} - 23481^{\circ}_{1}$	10644.118	9392.287	0		
10800.157	9256.589	4	I	$6362_{2} - 15618^{\circ}_{3}$	10642.859	9393.398	1	II	$13248_{4 1/2} - 22642^{\circ}_{4 1/2}$
10800.053	9256.678	5	I	$13945^{\circ}_{3} - 23201_{3}$	10640.329	9395.631	1	I	$22141^{\circ}_{3} - 31537_{3}$
10794.056	9261.821	3	II	$9711_{3 1/2} - 18973^{\circ}_{3 1/2}$	10629.842	9404.901	2	I	$14204_{5} - 23609^{\circ}_{5}$
10790.541	9264.838	0	II	$10855_{3 1/2} - 20120^{\circ}_{2 1/2}$	10624.881	9409.292	1		
10788.554	9266.544	1	I	$22508^{\circ}_{2} - 31774_{3}$	10624.279	9409.825	1		
10786.371	9268.420	3	I	$20566^{\circ}_{4} - 29835_{3}$	10623.608	9410.420	1		
10785.912	9268.814	4	I	$8800_{4} - 18069^{\circ}_{5}$	10622.548	9411.359	2		
10779.100	9274.672	2	I	$18069^{\circ}_{3} - 27343_{3}$	10615.008	9418.044	4	I	$18809^{\circ}_{4} - 28227_{4}$
10778.635	9275.072	1	I	$23521^{\circ}_{3} - 32796_{3}$	10613.388	9419.481	4	I	$13088_{3} - 22508^{\circ}_{3}$
10776.984	9276.493	4	I	$15493_{4} - 24769^{\circ}_{5}$	10609.955	9422.529	1	I	$9804_{5} - 19227^{\circ}_{6}$
10774.344	9278.766	1	I	$23015^{\circ}_{5} - 32293_{5}$	10608.458	9423.859	0		
10772.436	9280.409	2			10607.807	9424.437	0		

TABLE 1. *Infrared spectral lines of thorium*—Continued

Wavelength Å	Wavenumber cm^{-1}	Intensity	Spectrum	Classification	Wavelength Å	Wavenumber cm^{-1}	Intensity	Spectrum	Classification
10607.108	9425.058	1	I	$21539^{\circ}_{4} - 30964_{5}$	10509.543	9512.555	1		
10605.464	9426.519	4	I	$18069^{\circ}_{5} - 27495_{4}$	10503.182	9518.316	1		
10601.345	9430.182	2	I	$23306^{\circ}_{6} - 32737_{5}$	10502.592	9518.851	4	I	$13962_{1} - 23481^{\circ}_{1}$
10600.597	9430.847	1	I	$21077^{\circ}_{5} - 30508_{5}$	10498.496	9522.565	5	I	$14247^{\circ}_{0} - 23769_{1}$
10596.909	9434.129	1	I	$20322^{\circ}_{5} - 29756_{4}$	10495.610	9525.183	1	I	$14465^{\circ}_{2} - 23990_{2}$
10595.992	9434.946	0	II	$13250_{21/2} - 22685^{\circ}_{21/2}$	10494.843	9525.879	6	I	$14243^{\circ}_{1} - 23769_{1}$
10595.264	9435.594	1	I	$22338^{\circ}_{5} - 31774_{5}$	10492.255	9528.229	6	I	$10526^{\circ}_{5} - 20054_{2}$
10594.780	9436.025	1	I	$20214^{\circ}_{5} - 29650_{2}$	10487.427	9532.615	1	I	$18809^{\circ}_{4} - 28342_{5}$
10592.495	9438.061	0	I	$23113^{\circ}_{4} - 32551_{3}$	10483.360	9536.313	4		
10591.350	9439.081	2	I	$20522^{\circ}_{2} - 29961_{1}$	10481.173	9538.303	0	I	$20423^{\circ}_{1} - 29961_{1}$
10589.207	9440.991	0			10479.584	9539.749	1		
10587.588	9442.435	1	II	$8018_{11/2} - 17460^{\circ}_{21/2}$	10478.801	9540.462	1		
10587.100	9442.870	3	I	$15863_{2} - 25306^{\circ}_{2}$	10477.700	9541.465	1	I	$20214^{\circ}_{5} - 29756_{4}$
10586.930	9443.022	1	I	$23015^{\circ}_{5} - 32458_{4}$	10477.082	9542.028	2		
10585.524	9444.276	0	I	$23655^{\circ}_{4} - 33099_{5}$	10469.974	9548.506	1	I	$18809^{\circ}_{4} - 28358_{3}$
10585.028	9444.718	2	I	$20566^{\circ}_{4} - 30011_{3}$	10467.587	9550.683	0		
10583.191	9446.358	0			10466.685	9551.506	3		
10581.711	9447.679	1	I	$13962_{1} - 23410^{\circ}_{0}$	10459.723	9557.864	4	I	$13297_{4} - 22855^{\circ}_{3}$
10580.518	9448.744	0			10452.445	9564.519	0		
10579.481	9449.670	1	I	$11802_{2} - 21252^{\circ}_{2}$	10450.448	9566.346	3	I	$19986^{\circ}_{6} - 29552_{6}$
10578.136	9450.872	1	I	$14204_{5} - 23655^{\circ}_{4}$	10448.996	9567.676	0		
10576.600	9452.244	1	II	$15305_{41/2} - 24757^{\circ}_{21/2}$	10439.505	9576.374	3	I	$16346^{\circ}_{4} - 25923_{4}$
10576.362	9452.457	2	I	$18069^{\circ}_{3} - 27521_{4}$	10436.870	9578.792	2	I	$15863_{2} - 25442^{\circ}_{3}$
10572.824	9455.620	1	II	$10855_{21/2} - 20310^{\circ}_{21/2}$	10435.094	9580.422	3	I	$18011^{\circ}_{5} - 27591_{5}$
10570.129	9458.031	0	I	$15863_{2} - 25321^{\circ}_{3}$	10434.890	9580.609	2		
10569.146	9458.911	0	I	$23609^{\circ}_{5} - 33068_{6}$	10434.109	9581.326	1	I	$13088_{3} - 22669^{\circ}_{3}$
10567.177	9460.673	1	I	$12114^{\circ}_{2} - 21575_{2}$	10429.665	9585.409	6	II	$0_{11/2} - 9585^{\circ}_{21/2}$
10565.306	9462.349	6	I	$13175^{\circ}_{4} - 22637_{3}$	10424.885	9589.804	0		
10563.181	9464.252	1			10424.126	9590.502	1	I	$22338^{\circ}_{3} - 31929_{3}$
10560.617	9466.550	1	II	$6244_{1/2} - 15710^{\circ}_{11/2}$	10423.795	9590.807	2	II	$14790^{\circ}_{31/2} - 24381_{31/2}$
10559.107	9467.904	0	I	$18053^{\circ}_{4} - 27521_{4}$	10421.511	9592.909	0	I	$21165^{\circ}_{3} - 30758_{2}$
10556.454	9470.283	7	I	$17501^{\circ}_{5} - 26971_{4}$	10419.574	9594.692	7	II	$1521_{21/2} - 11116^{\circ}_{31/2}$
10554.837	9471.734	4	I	$16783^{\circ}_{4} - 26255_{4}$	10417.881	9596.251	1	I	$22399^{\circ}_{5} - 31995_{4}$
10553.890	9472.584	1	I	$15970_{3} - 25442^{\circ}_{3}$	10417.087	9596.983	1		
10545.902	9479.759	1	I	$17398_{3} - 26878^{\circ}_{3}$	10412.996	9600.753	4	I	$18930^{\circ}_{3} - 28531_{2}$
10545.290	9480.309	2	I	$12114^{\circ}_{2} - 21594_{3}$	10412.507	9601.204	0	I	$19817^{\circ}_{1} - 29418_{2}$
10543.947	9481.517	0			10410.424	9603.125	2	I	$7795^{\circ}_{4} - 17398_{3}$
10542.787	9482.560	1			10408.497	9604.903	1	I	$19817^{\circ}_{1} - 29422_{1}$
10540.958	9484.205	5	I	$18011^{\circ}_{5} - 27495_{4}$	10404.502	9608.591	3		
10540.219	9484.870	2			10403.056	9609.927	1	I	$20522^{\circ}_{2} - 30132_{2}$
10539.400	9485.607	1	II	$10673^{\circ}_{21/2} - 20158_{21/2}$	10402.349	9610.580	1	II	$17983^{\circ}_{21/2} - 27593_{21/2}$
10538.316	9486.583	2	II	$7331^{\circ}_{21/2} - 16818_{31/2}$	10401.401	9611.456	1	I	$22163^{\circ}_{4} - 31774_{3}$
10536.866	9487.888	2	I	$15493_{4} - 24981^{\circ}_{3}$	10392.041	9620.113	0	I	$20214^{\circ}_{3} - 29835_{3}$
10533.385	9491.024	3	I	$12847_{3} - 22338^{\circ}_{3}$	10391.352	9620.750	0	II	$12485^{\circ}_{31/2} - 22106_{21/2}$
10532.567	9491.761	2			10387.498	9624.320	1	I	$17166_{5} - 26790^{\circ}_{4}$
10527.789	9496.069	5	I	$17501^{\circ}_{5} - 26997_{6}$	10386.273	9625.455	0		
10527.134	9496.660	1	I	$17847^{\circ}_{2} - 27343_{3}$	10378.821	9632.366	1	I	$18930^{\circ}_{5} - 28562_{4}$
10525.841	9497.826	4			10378.146	9632.993	1	I	$17411^{\circ}_{3} - 27044_{3}$
10518.190	9504.735	2	I	$20867^{\circ}_{7} - 30372_{6}$	10377.490	9633.601	2	I	$13847_{2} - 23481^{\circ}_{1}$
10512.209	9510.143	5	I	$18011^{\circ}_{5} - 27521_{4}$	10376.812	9634.231	0	I	$20214^{\circ}_{3} - 29849_{4}$

TABLE 1. *Infrared spectral lines of thorium* – Continued

Wavelength Å	Wavenumber cm^{-1}	Intensity	Spectrum	Classification
10376.020	9634.966	1	I	$21902^{\circ}_{4} - 31537_{3}$
10373.462	9637.342	0	II	$15236_{1/2} - 24873^{\circ}_{3/2}$
10369.528	9640.998	4	I	$13962_{1} - 23603^{\circ}_{2}$
10362.966	9647.103	1	I	$21890^{\circ}_{3} - 31537_{3}$
10359.998	9649.867	3	II	$9400_{2/2} - 19050^{\circ}_{1/2}$
10358.167	9651.573	3	I	$11601_{1} - 21252^{\circ}_{2}$
10357.832	9651.885	0		
10357.615	9652.087	0	I	$22141^{\circ}_{3} - 31793_{4}$
10356.372	9653.246	2	II	$15786_{2/2} - 25440^{\circ}_{2/2}$
10355.806	9653.773	1		
10350.334	9658.877	1	I	$18614^{\circ}_{1} - 28273_{2}$
10349.051	9660.074	5	I	$12847_{3} - 22508^{\circ}_{2}$
10346.944	9662.041	0		
10346.540	9662.419	3	I	$15863_{2} - 25526^{\circ}_{1}$
10345.899	9663.017	0	I	$17398_{3} - 27061^{\circ}_{2}$
10344.287	9664.523	1		
10335.840	9672.422	1		
10334.926	9673.277	3	I	$13847_{2} - 23521^{\circ}_{3}$
10327.838	9679.916	0		
10326.442	9681.224	0		
10317.951	9689.191	1		
10317.364	9689.743	1		
10316.894	9690.184	4	I	$17501^{\circ}_{5} - 27191_{5}$
10316.006	9691.018	1	II	$10189^{\circ}_{3/2} - 19880_{4/2}$
10314.894	9692.063	2	I	$20322^{\circ}_{5} - 30014_{4}$
10309.821	9696.832	0		
10308.549	9698.028	5	I	$19986^{\circ}_{6} - 29684_{5}$
10307.509	9699.007	1		
10304.810	9701.547	2	II	$10379_{4/2} - 20080^{\circ}_{3/2}$
10304.082	9702.233	2	I	$22338^{\circ}_{3} - 32041_{2}$
10301.391	9704.767	1		
10301.161	9704.984	6	II	$4113_{2/2} - 13818^{\circ}_{3/2}$
10299.876	9706.195	1		
10298.388	9707.597	1		
10294.714	9711.062	0	I	$17959_{4} - 27670^{\circ}_{3}$
10293.052	9712.630	4	I	$14204_{5} - 23916^{\circ}_{4}$
10288.987	9716.467	4	II	$1859_{1/2} - 11576^{\circ}_{1/2}$
10285.485	9719.775	0	I	$17847^{\circ}_{2} - 27566_{2}$
10283.118	9722.012	4	I	$7502_{3} - 17224^{\circ}_{2}$
10278.860	9726.040	1	I	$21539^{\circ}_{4} - 31265_{3}$
10278.350	9726.522	1		
10278.263	9726.605	0		
10276.804	9727.985	1		
10275.694	9729.036	0	I	$20922^{\circ}_{2} - 30651_{3}$
10272.063	9732.475	2		
10271.191	9733.302	2	I	$15970_{3} - 25703^{\circ}_{2}$
10268.554	9735.801	1	I	$19948^{\circ}_{4} - 29684_{5}$
10260 162	9743.764	0		
10257.374	9746.413	5	I	$14243^{\circ}_{1} - 23990_{2}$
10255.580	9748.118	2	I	$15166^{\circ}_{3} - 24915_{3}$
10250.684	9752.773	4	I	$18809^{\circ}_{4} - 28562_{4}$
10249.314	9754.077	1		
10247.561	9755.746	4	I	$13847_{2} - 23603^{\circ}_{2}$
10247.419	9755.881	1		
10244.986	9758.198	1	II	$22014^{\circ}_{3/2} - 31773_{4/2}$
10241.779	9761.253	2	I	$22306^{\circ}_{6} - 33068_{6}$
10241.463	9761.555	2	II	$13250_{2/2} - 23012^{\circ}_{1/2}$
10236.031	9766.735	4	I	$13088_{3} - 22855^{\circ}_{3}$
10229.541	9772.931	1		
10223.662	9778.551	3	I	$13962_{1} - 23741^{\circ}_{1}$
10220.712	9781.373	2		
10219.382	9782.646	2	II	$14349_{1/2} - 24132^{\circ}_{1/2}$
10218.434	9783.554	5	I	$9804_{5} - 19588^{\circ}_{5}$
10214.957	9786.884	0		
10214.676	9787.153	1		
10214.442	9787.377	1	I	$21539^{\circ}_{4} - 31326_{4}$
10213.806	9787.987	0		
10211.538	9790.161	2	I	$13962_{1} - 23752^{\circ}_{2}$
10208.285	9793.281	0	II	$20080^{\circ}_{3/2} - 29873_{3/2}$
10205.020	9796.414	1	I	$20214^{\circ}_{3} - 30011_{3}$
10203.228	9798.134	0		
10202.133	9799.186	1	I	$21738^{\circ}_{5} - 31537_{3}$
10197.163	9803.962	0	II	$17722^{\circ}_{3/2} - 27526_{4/2}$
10194.906	9806.132	1		
10193.720	9807.273	0	I	$20737^{\circ}_{1} - 30544_{2}$
10192.965	9808.000	0	I	$19948^{\circ}_{4} - 29756_{4}$
10188.418	9812.377	3		
10184.539	9816.114	2	I	$13297_{4} - 23113^{\circ}_{4}$
10180.909	9819.614	0	II	$8018_{1/2} - 17837^{\circ}_{1/2}$
10180.596	9819.916	2	I	$17224^{\circ}_{2} - 27044_{3}$
10179.844	9820.641	0		
10178.522	9821.917	5	I	$12847_{3} - 22669^{\circ}_{3}$
10177.086	9823.303	1		
10175.012	9825.305	4	I	$14206^{\circ}_{4} - 24032_{4}$
10169.296	9830.828	2	II	$10855_{3/2} - 20686^{\circ}_{1/2}$
10160.324	9839.509	0	I	$15863_{2} - 25703^{\circ}_{2}$
10156.406	9843.305	0	I	$19039^{\circ}_{2} - 28882_{2}$
10145.521	9853.865	0		
10144.266	9855.084	4	I	$6362_{2} - 16217^{\circ}_{2}$
10141.399	9857.870	6	I	$13175^{\circ}_{4} - 23032_{4}$
10140.434	9858.808	4	I	$20867^{\circ}_{7} - 30726_{7}$
10137.390	9861.769	2	I	$17398_{3} - 27260^{\circ}_{3}$
10136.787	9862.355	0	I	$15493_{4} - 25355^{\circ}_{4}$
10133.559	9865.497	7	II	$1859_{1/2} - 11725^{\circ}_{1/2}$
10131.371	9867.628	2	I	$17398_{3} - 27266^{\circ}_{4}$
10127.552	9871.349	0	I	$22141^{\circ}_{3} - 32012_{4}$
10126.557	9872.318	1	I	$21902^{\circ}_{4} - 31774_{3}$
10123.103	9875.687	0		
10120.661	9878.070	1		
10118.774	9879.912	1		

TABLE 1. *Infrared spectral lines of thorium* — Continued

Wavelength Å	Wavenumber cm^{-1}	Intensity	Spectrum	Classification	Wavelength Å	Wavenumber cm^{-1}	Intensity	Spectrum	Classification
10118.187	9880.485	1			9998.963	9998.296	2	I	$14204_5 - 24202^\circ_4$
10117.993	9880.675	2	I	$14204_5 - 24084^\circ_8$	9998.513	9998.746	2		
10114.788	9883.805	1			9993.866	10003.395	2	II	$15242^\circ_{4\frac{1}{2}} - 25246_{4\frac{1}{2}}$
10113.985	9884.590	0			9993.364	10003.898	0		
10111.877	9886.651	1	I	$19948^\circ_4 - 29835_3$	9992.656	10004.607	3	I	$18930^\circ_5 - 28934_3$
10107.000	9891.421	0	I	$21902^\circ_4 - 31793_4$	9991.846	10005.418	0	I	$13088_3 - 23093^\circ_2$
10105.549	9892.842	0	I	$17959_4 - 27852^\circ_5$	9989.939	10007.327	2	I	$12847_3 - 22855^\circ_3$
10105.080	9893.301	2	I	$13847_2 - 23741^\circ_1$	9988.024	10009.246	2	II	$7828_{1\frac{1}{2}} - 17837^\circ_{1\frac{1}{2}}$
10104.307	9894.058	1	I	$16217^\circ_2 - 26111_1$	9987.636	10009.635	6	I	$8800_4 - 18809^\circ_4$
10103.176	9895.165	0			9985.052	10012.225	5	I	$16783^\circ_4 - 26796_3$
10102.579	9895.750	2	I	$19039^\circ_2 - 28934_3$	9974.693	10022.623	3	I	$18011^\circ_5 - 28034_5$
10098.624	9899.625	1	I	$22141^\circ_3 - 32041_2$	9973.365	10023.958	0		
10097.463	9900.764	1	I	$19948^\circ_4 - 29849_4$	9973.092	10024.232	1		
10092.535	9905.598	0			9970.467	10026.872	4	I	$13175^\circ_4 - 23201_3$
10091.483	9906.631	2			9963.495	10033.888	3	I	$16346^\circ_4 - 26380_5$
10089.136	9908.935	7	I	$7502_3 - 17411^\circ_3$	9958.059	10039.365	1	I	$21890^\circ_5 - 31929_3$
			I	$16346^\circ_4 - 26255_4$	9957.528	10039.900	1		
10086.406	9911.617	2	I	$18069^\circ_3 - 27980_3$	9957.181	10040.250	0		
10085.323	9912.681	1	II	$9061_{2\frac{1}{2}} - 18973^\circ_{3\frac{1}{2}}$	9956.844	10040.590	1		
10083.788	9914.190	5	I	$19227^\circ_6 - 29141_5$	9955.781	10041.662	1		
10082.880	9915.083	4	I	$15490^\circ_5 - 25405_4$	9952.375	10045.099	3	I	$13945^\circ_5 - 23990_2$
10082.719	9915.242	1	I	$19503^\circ_5 - 29418_2$	9948.171	10049.344	1	I	$17398_3 - 27447^\circ_2$
10081.227	9916.709	1	I	$18614^\circ_1 - 28531_2$	9947.082	10050.444	1	I	$20322^\circ_5 - 30372_6$
10079.542	9918.367	2			9943.061	10054.508	6	II	$1521_{2\frac{1}{2}} - 11576^\circ_{1\frac{1}{2}}$
10079.413	9918.494	0			9939.967	10057.638	1		
10078.906	9918.993	1	I	$17398_3 - 27317^\circ_3$	9938.839	10058.779	1	I	$22399^\circ_5 - 32458_4$
10065.187	9932.512	1	I	$17411^\circ_3 - 27343_3$	9935.203	10062.461	2	I	$20867^\circ_7 - 30930_6$
10058.937	9938.684	1			9934.723	10062.947	1	I	$19948^\circ_4 - 30011_3$
10056.214	9941.375	2	I	$20566^\circ_4 - 30508_5$	9932.777	10064.918	0	I	$18614^\circ_1 - 28679_2$
10055.842	9941.743	2			9930.047	10067.685	2		
10054.960	9942.615	1	I	$8111_4 - 18053^\circ_4$	9929.814	10067.922	3	I	$11601_1 - 21668^\circ_1$
10054.189	9943.377	0			9927.326	10070.445	2	I	$14204_5 - 24274^\circ_5$
10053.375	9944.182	0	I	$7280_2 - 17224^\circ_2$	9926.172	10071.616	0	II	$12570_{2\frac{1}{2}} - 22642^\circ_{4\frac{1}{2}}$
10051.735	9945.805	1			9923.310	10074.520	1		
10048.041	9949.461	3	I	$15493_4 - 25442^\circ_3$	9919.448	10078.443	0	I	$15970_3 - 26048^\circ_4$
10045.996	9951.486	0	II	$15236_{1\frac{1}{2}} - 25188^\circ_{1\frac{1}{2}}$	9916.122	10081.823	1	I	$15493_4 - 25575^\circ_4$
10045.316	9952.160	2	I	$18930^\circ_5 - 28882_2$	9913.628	10084.360	1	I	$17411^\circ_3 - 27495_4$
10044.021	9953.443	0			9912.205	10085.807	2	I	$22877^\circ_5 - 32963_5$
10041.807	9955.638	0			9911.116	10086.915	4	I	$13945^\circ_5 - 24032_4$
10039.364	9958.060	7	I	$8111_4 - 18069^\circ_3$	9910.837	10087.199	2	I	$11802_2 - 21890^\circ_5$
10039.101	9958.321	2	I	$14032^\circ_5 - 23990_2$	9907.464	10090.634	1	I	$17501^\circ_5 - 27591_5$
10037.115	9960.292	1			9906.948	10091.159	1	I	$16554_6 - 26645^\circ_5$
10036.377	9961.024	0			9904.771	10093.377	1	I	$21902^\circ_4 - 31995_4$
10033.226	9964.152	2	I	$19588^\circ_5 - 29552_6$	9902.362	10095.833	4	I	$19588^\circ_5 - 29684_5$
10032.967	9964.410	1			9898.356	10099.918	2	I	$17166_5 - 27266^\circ_4$
10032.174	9965.197	1	II	$8018_{1\frac{1}{2}} - 17983^\circ_{2\frac{1}{2}}$	9896.050	10102.272	3	I	$13175^\circ_4 - 23277_5$
10029.545	9967.809	1	I	$20922^\circ_5 - 30889_1$	9892.286	10106.116	0		
10011.398	9985.877	3	I	$20566^\circ_4 - 30552_4$	9892.187	10106.217	0	II	$14275^\circ_{4\frac{1}{2}} - 24381_{3\frac{1}{2}}$
9999.614	9997.645	0	I	$21539^\circ_4 - 31537_3$	9890.522	10107.918	1	II	$8460_{1\frac{1}{2}} - 18568^\circ_{1\frac{1}{2}}$
9999.430	9997.829	1			9888.819	10109.659	0	II	$15305_{4\frac{1}{2}} - 25414^\circ_{3\frac{1}{2}}$

TABLE 1. *Infrared spectral lines of thorium*—Continued

Wavelength Å	Wavenumber cm^{-1}	Intensity	Spectrum	Classification	Wavelength Å	Wavenumber cm^{-1}	Intensity	Spectrum	Classification
9880.782	10117.882	2	II	$6700^{\circ}_{3\frac{1}{2}} - 16818_{3\frac{1}{2}}$	9736.216	10268.115	1	I	$18614^{\circ}_{1} - 28882_{2}$
9878.520	10120.199	2	II	$7001_{1\frac{1}{2}} - 17121^{\circ}_{1\frac{1}{2}}$	9734.696	10269.718	1	II	$13248_{4\frac{1}{2}} - 23518^{\circ}_{3\frac{1}{2}}$
9876.688	10122.076	0	II	$13250_{2\frac{1}{2}} - 23372^{\circ}_{1\frac{1}{2}}$	9718.665	10286.658	0		
9874.790	10124.022	0			9718.489	10286.844	2		
9873.821	10125.015	3	I	$18809^{\circ}_{4} - 28934_{3}$	9716.146	10289.325	2	I	$18069^{\circ}_{3} - 28358_{3}$
9872.635	10126.231	1	I	$22669^{\circ}_{3} - 32796_{3}$	9702.272	10304.038	3	I	$15618^{\circ}_{3} - 25923_{4}$
9872.185	10126.693	0			9701.580	10304.773	1	I	$18053^{\circ}_{4} - 28358_{3}$
9871.998	10126.885	2	I	$15970_{3} - 26096^{\circ}_{3}$	9700.564	10305.852	7	I	$2869_{3} - 13175^{\circ}_{4}$
9869.929	10129.008	0	II	$4146_{3\frac{1}{2}} - 14275^{\circ}_{4\frac{1}{2}}$	9695.033	10311.732	2	I	$13297_{4} - 23609^{\circ}_{5}$
9868.922	10130.041	2	I	$8800_{4} - 18930^{\circ}_{3}$	9684.806	10322.621	1		
9867.890	10131.101	2	I	$7280_{3} - 17411^{\circ}_{3}$	9679.111	10328.695	0		
9865.451	10133.605	1	I	$17847^{\circ}_{2} - 27980_{3}$	9678.235	10329.629	0	I	$20214^{\circ}_{5} - 30544_{2}$
9864.226	10134.864	3			9676.940	10331.012	0	I	$8243^{\circ}_{2} - 18574_{1}$
9864.094	10135.000	1			9676.840	10331.118	3	I	$18011^{\circ}_{3} - 28342_{3}$
9863.866	10135.234	1	II	$12219_{1\frac{1}{2}} - 22355^{\circ}_{1\frac{1}{2}}$	9676.107	10331.901	2	I	$19503^{\circ}_{3} - 29835_{3}$
9862.127	10137.021	0	I	$11601_{1} - 21738^{\circ}_{2}$	9674.790	10333.308	2	I	$11241^{\circ}_{3} - 21575_{2}$
9855.745	10143.585	3	I	$9804_{5} - 19948^{\circ}_{4}$	9670.794	10337.577	1		
9845.690	10153.944	2			9666.379	10342.299	0		
9840.923	10158.863	1	I	$18069^{\circ}_{3} - 28227_{4}$	9664.700	10344.096	6	I	$3687_{2} - 14032^{\circ}_{2}$
9838.008	10161.873	1	I	$21165^{\circ}_{3} - 31326_{4}$	9663.647	10345.223	1	I	$13962_{1} - 24307^{\circ}_{2}$
9837.258	10162.648	0	I	$14465^{\circ}_{2} - 24627_{1}$	9663.062	10345.849	0	II	$12488^{\circ}_{1\frac{1}{2}} - 22834_{3\frac{1}{2}}$
9834.008	10166.006	3			9656.439	10352.945	1	I	$11241^{\circ}_{3} - 21594_{3}$
9833.424	10166.610	8	I	$3865_{1} - 14032^{\circ}_{2}$	9652.004	10357.702	0	I	$13297_{4} - 23655^{\circ}_{4}$
9831.676	10168.418	2			9643.649	10366.676	0		
9826.452	10173.823	7	I	$5563_{1} - 15736^{\circ}_{1}$	9643.322	10367.027	1	I	$14032^{\circ}_{2} - 24399_{3}$
9819.178	10181.360	1	I	$9804_{5} - 19986^{\circ}_{5}$	9643.147	10367.215	0	I	$20522^{\circ}_{2} - 30889_{1}$
9814.962	10185.733	1	I	$20322^{\circ}_{5} - 30508_{5}$	9642.471	10367.942	4	II	$8605_{3\frac{1}{2}} - 18973^{\circ}_{3\frac{1}{2}}$
9813.153	10187.611	0	I	$16783^{\circ}_{4} - 26971_{4}$	9636.906	10373.929	1	I	$17073_{1} - 27447^{\circ}_{2}$
9812.698	10188.083	7	I	$8243^{\circ}_{2} - 18431_{3}$	9632.647	10378.516	6	I	$3865_{1} - 14243^{\circ}_{1}$
9801.710	10199.505	0	I	$14465^{\circ}_{2} - 24664_{3}$	9630.745	10380.565	1	I	$14247^{\circ}_{0} - 24627_{1}$
9800.586	10200.674	0			9629.572	10381.830	6	I	$3865_{1} - 14247^{\circ}_{0}$
9800.366	10200.903	1			9629.231	10382.198	0	I	$22399^{\circ}_{5} - 32781_{4}$
9797.252	10204.145	1	I	$18069^{\circ}_{3} - 28273_{2}$	9627.672	10383.879	1	I	$14243^{\circ}_{1} - 24627_{1}$
9796.200	10205.241	5	I	$4961_{4} - 15166^{\circ}_{3}$	9627.058	10384.541	0		
9795.646	10205.819	0			9625.740	10385.963	1		
9789.508	10212.218	2	I	$17354^{\circ}_{1} - 27566_{2}$	9625.204	10386.541	3	I	$19986^{\circ}_{6} - 30372_{6}$
9785.356	10216.551	0	I	$18011^{\circ}_{5} - 28227_{4}$	9623.414	10388.473	0	I	$22163^{\circ}_{4} - 32551_{3}$
9782.141	10219.908	0	I	$13962_{1} - 24182^{\circ}_{2}$	9619.222	10393.001	1	I	$15970_{3} - 26363^{\circ}_{2}$
9781.891	10220.170	2			9613.689	10398.982	5	II	$4146_{3\frac{1}{2}} - 14545^{\circ}_{2\frac{1}{2}}$
9779.461	10222.709	1			9608.933	10404.129	1	I	$11241^{\circ}_{3} - 21645_{4}$
9778.427	10223.790	0			9608.494	10404.605	2		
9769.538	10233.092	2	I	$15863_{2} - 26096^{\circ}_{3}$	9607.535	10405.643	0		
9764.606	10238.261	0	I	$15166^{\circ}_{3} - 25405_{4}$	9605.809	10407.513	0	I	$16783^{\circ}_{4} - 27191_{5}$
9757.222	10246.009	1	I	$12847_{3} - 23093^{\circ}_{2}$	9595.395	10418.808	4	I	$13962_{1} - 24381^{\circ}_{2}$
9757.159	10246.075	0			9593.115	10421.284	0		
9754.019	10249.374	1	I	$15863_{2} - 26113^{\circ}_{2}$	9590.348	10424.291	1		
9753.597	10249.817	2	I	$21077^{\circ}_{5} - 31326_{4}$	9588.809	10425.964	0	I	$19588^{\circ}_{5} - 30014_{4}$
9746.464	10257.318	7	I	$3687_{2} - 13945^{\circ}_{3}$	9587.027	10427.902	1	I	$14243^{\circ}_{1} - 24671_{2}$
9743.565	10260.370	4	I	$16783^{\circ}_{4} - 27044_{3}$	9583.076	10432.201	3	II	$4113_{3\frac{1}{2}} - 14545^{\circ}_{2\frac{1}{2}}$
9738.624	10265.576	1	I	$12847_{3} - 23113^{\circ}_{4}$	9582.816	10432.484	4	I	$13088_{3} - 23521^{\circ}_{3}$

TABLE 1. *Infrared spectral lines of thorium*—Continued

Wavelength Å	Wavenumber cm^{-1}	Intensity	Spectrum	Classification
9577.344	10438.445	3	II	$9720^{\circ}_{3\frac{1}{2}} - 20158_{2\frac{1}{2}}$
9571.505	10444.813	1	I	$19516^{\circ}_{2} - 29961_{1}$
9570.405	10446.013	1	I	$11802_{2} - 22248^{\circ}_{2}$
9567.826	10448.829	2	I	$11197^{\circ}_{3} - 21645_{4}$
9567.283	10449.422	1	I	$16346^{\circ}_{4} - 26796_{3}$
9565.567	10451.297	1		
9563.778	10453.251	0		
9563.709	10453.327	1		
9563.307	10453.767	1		
9563.177	10453.909	0		
9561.736	10455.484	1		
9561.245	10456.021	5	I	$8243^{\circ}_{2} - 18699_{2}$
9559.932	10457.457	0		
9553.984	10463.967	1		
9548.028	10470.495	1		
9536.411	10483.250	1		
9521.958	10499.162	1		
9514.025	10507.916	0		
9510.950	10511.313	0	I	$17847^{\circ}_{2} - 28358_{3}$
9507.656	10514.955	2	I	$13088_{3} - 23603^{\circ}_{2}$
9505.395	10517.456	5	I	$9804_{5} - 20322^{\circ}_{5}$
9501.443	10521.831	0	I	$19986^{\circ}_{6} - 30508_{5}$
9500.302	10523.095	2	I	$12114^{\circ}_{2} - 22637_{3}$
9500.053	10523.370	0		
9498.244	10525.375	0		
9497.191	10526.541	7	I	$0_{2} - 10526^{\circ}_{3}$
9495.500	10528.416	7	I	$4961_{4} - 15490^{\circ}_{5}$
9494.041	10530.034	1	II	$11576^{\circ}_{1\frac{1}{2}} - 22106_{2\frac{1}{2}}$
9486.929	10537.928	3	I	$15970_{3} - 26508^{\circ}_{3}$
9483.850	10541.349	0	II	$18973^{\circ}_{3\frac{1}{2}} - 29515_{4\frac{1}{2}}$
9482.290	10543.084	1		
9482.271	10543.105	1		
9474.882	10551.327	7	I	$7502_{3} - 18053^{\circ}_{4}$
9470.684	10556.003	6	I	$3687_{2} - 14243^{\circ}_{1}$
9467.200	10559.888	5	I	$16783^{\circ}_{4} - 27343_{3}$
9462.907	10564.679	1		
9461.905	10565.798	0		
9461.208	10566.576	3	I	$13088_{3} - 23655^{\circ}_{4}$
9461.031	10566.774	6	I	$7502_{3} - 18069^{\circ}_{3}$
9460.871	10566.952	2	I	$7280_{2} - 17847^{\circ}_{2}$
9458.783	10569.285	0		
9458.629	10569.457	0	I	$17411^{\circ}_{3} - 27980_{3}$
9456.023	10572.370	0	II	$19912^{\circ}_{6\frac{1}{2}} - 30484_{5\frac{1}{2}}$
9455.205	10573.284	2	I	$13847_{2} - 24421^{\circ}_{3}$
9452.674	10576.116	1		
9450.464	10578.589	1	I	$16217^{\circ}_{2} - 26796_{3}$
9448.890	10580.351	0		
9446.992	10582.477	0		
9439.854	10590.479	0	II	$8460_{1\frac{1}{2}} - 19050^{\circ}_{1\frac{1}{2}}$
9436.815	10593.889	2	I	$11802_{2} - 22396^{\circ}_{1}$
9432.589	10598.635	0		
9432.280	10598.983	3	II	$9711_{3\frac{1}{2}} - 20310^{\circ}_{2\frac{1}{2}}$
9431.600	10599.747	5	I	$3865_{1} - 14465^{\circ}_{2}$
9430.921	10600.510	0	I	$17073_{1} - 27674^{\circ}_{2}$
9423.850	10608.464	0		
9422.317	10610.190	0	I	$18069^{\circ}_{3} - 28679_{2}$
9420.621	10612.100	2	I	$14226_{0} - 24838^{\circ}_{1}$
9420.493	10612.244	2	II	$1859_{1\frac{1}{2}} - 12472^{\circ}_{2\frac{1}{2}}$
9417.463	10615.659	0	I	$19516^{\circ}_{2} - 30132_{2}$
9414.090	10619.462	2	I	$13297_{4} - 23916^{\circ}_{4}$
9413.682	10619.922	1		
9413.135	10620.540	1		
9409.353	10624.808	4	I	$16346^{\circ}_{4} - 26971_{4}$
9406.896	10627.583	1		
9405.282	10629.407	1		
9399.091	10636.408	7	I	$7795^{\circ}_{4} - 18431_{3}$
9396.673	10639.145	0		
9394.096	10642.064	0	II	$9238^{\circ}_{4\frac{1}{2}} - 19880_{4\frac{1}{2}}$
9393.770	10642.433	1		
9392.268	10644.135	0	I	$15863_{2} - 26508^{\circ}_{3}$
9392.016	10644.421	1	II	$4146_{3\frac{1}{2}} - 14790^{\circ}_{3\frac{1}{2}}$
9390.723	10645.886	0		
9390.588	10646.040	2	I	$14204_{5} - 24850^{\circ}_{6}$
9388.933	10647.916	4	I	$11601_{1} - 22248^{\circ}_{2}$
9384.103	10653.397	0	I	$14226_{0} - 24880^{\circ}_{1}$
9383.275	10654.337	5	I	$5563_{1} - 16217^{\circ}_{2}$
9380.642	10657.327	0	I	$4961_{4} - 15618^{\circ}_{3}$
9379.736	10658.357	1		
9374.051	10664.821	0	II	$17272^{\circ}_{4\frac{1}{2}} - 27937_{5\frac{1}{2}}$
9366.797	10673.079	0	I	$12847_{3} - 23521^{\circ}_{3}$
9366.743	10673.141	0	II	$0_{1\frac{1}{2}} - 10673^{\circ}_{2\frac{1}{2}}$
9362.794	10677.643	0	II	$4113_{2\frac{1}{2}} - 14790^{\circ}_{3\frac{1}{2}}$
9362.640	10677.819	1	II	$9202^{\circ}_{3\frac{1}{2}} - 19880_{4\frac{1}{2}}$
9360.989	10679.702	2	II	$9400_{3\frac{1}{2}} - 20080^{\circ}_{3\frac{1}{2}}$
9357.253	10683.966	0	I	$17847^{\circ}_{2} - 28531_{2}$
9357.055	10684.192	0		
9355.995	10685.402	0		
9349.246	10693.116	1	II	$6213_{4\frac{1}{2}} - 16906^{\circ}_{5\frac{1}{2}}$
9344.207	10698.882	1	I	$8111_{4} - 18809^{\circ}_{4}$
9344.096	10699.009	1	I	$20566^{\circ}_{4} - 31265_{3}$
9340.708	10702.890	4	I	$8800_{4} - 19503^{\circ}_{5}$
9336.161	10708.102	1	I	$14206^{\circ}_{4} - 24915_{3}$
9327.252	10718.330	0		
9320.071	10726.589	0	I	$13945^{\circ}_{5} - 24671_{2}$
9317.727	10729.287	3	I	$10414^{\circ}_{4} - 21143_{5}$
9310.448	10737.675	2	I	$16783^{\circ}_{4} - 27521_{4}$
9307.899	10740.616	4	I	$19986^{\circ}_{6} - 30726_{7}$
9300.018	10749.718	1	I	$20214^{\circ}_{5} - 30964_{3}$
9294.976	10755.549	1	I	$12847_{3} - 23603^{\circ}_{2}$
9294.782	10755.773	2		

TABLE 1. *Infrared spectral lines of thorium* – Continued

Wavelength Å	Wavenumber cm^{-1}	Intensity	Spectrum	Classification	Wavelength Å	Wavenumber cm^{-1}	Intensity	Spectrum	Classification
9289.564	10761.815	5	I	$9804_5 - 20566^{\circ}_4$	9266.208	10788.941	6	I	$7280_2 - 18069^{\circ}_3$
9287.583	10764.110	0			9263.682	10791.882	0	I	$10783^{\circ}_2 - 21575_2$
9277.170	10776.192	0			9260.327	10795.792	2	I	$11601_1 - 22396^{\circ}_1$
9276.273	10777.234	5	I	$3687_2 - 14465^{\circ}_2$	9252.860	10804.504	0		
9272.832	10781.234	0			9250.579	10807.168	0	I	$12847_3 - 23655^{\circ}_4$
9271.181	10783.153	1	I	$0_2 - 10783^{\circ}_2$	9248.125	10810.036	1		
9270.155	10784.347	2	I	$19588^{\circ}_5 - 30372_6$	9245.257	10813.389	1	I	$18069^{\circ}_3 - 28882_2$
9267.686	10787.220	2	II	$7331^{\circ}_{21/2} - 18118_{11/2}$	9243.767	10815.133	1		
9267.082	10787.923	3			9239.328	10820.329	1	I	$15970_3 - 26790^{\circ}_4$
9266.920	10788.111	4	I	$8800_4 - 19588^{\circ}_5$					

JOURNAL OF RESEARCH of the National Bureau of Standards—A. Physics and Chemistry
Vol. 78A, No. 2, March-April 1974

Publications of the National Bureau of Standards*

Citations with Selected Abstracts

J. Res. Nat. Bur. Stand. (U.S.), **78A** *(Phys. and Chem.)*, No. 1, (Jan.-Feb. 1974), SD Catalog No. C13.22/sec.A:78/1.

Thermophysical measurements on iron above 1500 K using a transient (subsecond) technique, A. Cezairliyan and J. L. McClure.

Measurement of melting point, normal spectral emittance (at melting point) and electrical resistivity (near melting point) of some refractory alloys, A. Cezairliyan.

Comparative density measurements for solid specimens weighing a few milligrams, A. D. Franklin and J. R. Donaldson.

A density scale based on solid objects, H. A. Bowman, R. M. Schoonover, and C. L. Carroll.

Geometrical considerations in the measurement of the volume of an approximate sphere, D. P. Johnson.

Note on diffusion of vapor into flowing gas, D. P. Johnson.

Theoretical analysis of miscibility gaps in the alkali-borates, P. B. Macedo and J. H. Simmons.

J. Res. Nat. Bur. Stand. (U.S.), **78B** *(Math. Sci.)*, Nos. 1 and 2, SD Catalog No. C13.22/sec.B:78/1&2.

A class of positive stable matrices, D. Carlson.

The Smith normal form of a partitioned matrix, M. Newman.

A Lyapunov theorem for angular cones, C. R. Johnson.

Second, third, and fourth order *D*-stability, C. R. Johnson.

Comparison of some FORTRAN programs for matrix inversion, K. E. Fitzgerald.

On characters of subgroups, R. Merris.

Integer arithmetic determination of polynomial real roots, G. W. Reitwiesner.

Monogr. 132. **A compilation and evaluation of mechanical, thermal, and electrical properties of selected polymers,** R. E. Schramm, A. F. Clark, and R. P. Reed, Nat. Bur. Stand. (U.S.), Monogr. 132, 848 pages (Sept. 1973) $10.25, SD Catalog No. C13.44:132.

Key words: Compilation; electrical properties; mechanical properties; plastics; polymers; thermal properties.

This compilation abstracts original experimental data on the mechanical, thermal, and electrical properties of six commercially available polymers. After an extensive review of the open literature, all available data were collected together in graphical and tabular form along with material characterization, experimental method, and reference to the original publication. The data are also summarized and a brief description of each polymer is included.

Monogr. 136. **Graphical recoupling of angular momenta,** D. R. Lehman and J. S. O'Connell, Nat. Bur. Stand. (U.S.), Monogr. 136, 18 pages (Oct. 1973) 50 cents, SD Catalog No. C13.44:136.

Key words: Angular momentum; diagrams; graphs; quantum theory; recoupling; transformation theory.

A diagrammatic method for solving angular momentum recoupling problems is presented. It is shown that a few graphical elements with a set of rules for their use lead to the solution of many types of recoupling problems in an intuitive and systematic way. Several examples are given together with exercise to develop the reader's facility with the method.

Monogr. 137. **Applications of waveguide and circuit theory to the development of accurate microwave measurement methods and standards,** R. W. Beatty, Nat. Bur. Stand. (U.S.), Monogr. 137, 322 pages (Aug. 1973) $5.20, SD Catalog No. C13.44:137.

Key words: Attenuation definitions; attenuation measurement; barretter mount efficiency; coaxial connectors; impedance measurement; microwave network theory; mismatch errors; phase shift-measurement; power measurement; reflectometers; waveguide joints; waveguide theory.

The basic theory and analytical methods used in the development of accurate microwave measurement methods and standards are presented.

Developments at the U.S. National Bureau of Standards during 1948-1968 are described in which the above theory and analytical methods were applied.

These developments were in the fields of power, impedance, attenuation and phase shift, and led to the establishment of National Standards and calibration methods at frequencies from about 300 MHz to 30 GHz.

SP260-32. **Standard reference materials: Standard quartz cuvettes for high accuracy spectrophotometry,** R. Mavrodineanu and J. W. Lazar, Nat. Bur. Stand. (U.S.), Spec. Publ. 260-32, 27 pages (Dec. 1973) 55 cents, SD Catalog No. C13.10:260-32.

Key words: Cuvette, spectrophotometry; lightpath; pathlength; quartz, cuvette; radiation pathlength.

Accurate knowledge of lightpath and parallelism of cuvettes used in spectrophotometry is one of the indispensable parameters which must be determined when accurate transmittance measurements of liquid materials is considered. A description is given of the design and techniques developed at NBS for the production of quartz cuvettes having a nominal radiation pathlength of 10 mm $\pm$ 0.03 mm and a parallelism certified both with an uncertainty of $\pm$ 0.0005 mm. The method and instrumentation used to determine these parameters is also described in the paper.

SP300. Volume 10. **Precision measurement and calibration.** Selected NBS papers on image optics, C. S. McCamy, Editor, Nat. Bur. Stand. (U.S.), Spec. Publ. 300, Vol. 10, 953 pages (Nov. 1972) $11.10, SD Catalog No. C13.10:300, Vol. 10.

Key words: Camera calibration; image evaluation; image optics; image stability; interferometry; lens testing; light filters; light sources; photography.

This volume is one of an extended series which brings together the previously published papers, monographs, abstracts, and bibliographies by NBS authors dealing with precision measurement of specific

530-326 OL - 74 - 13

physical quantities and the calibration of the related metrology equipment. The contents have been selected as being useful to the standards laboratories of the United States in tracing to NBS standards the accuracies of measurement needed for research work, factory production, or field evaluation.

Volume 10 deals with image optics, including photography. It contains 57 reprints assembled in 4 sections: (1) Refractometry and Optical Homogeneity; (2) Interferometry in Image Optics; (3) Optical Image Evaluation; (4) Photography. Each section is introduced by an interpretive foreword, including in some instances, pertinent references.

SP305. Supplement 4. **Publications of the National Bureau of Standards 1972 catalog. A compilation of abstracts and key word and author indexes,** B. L. Oberholtzer, Nat. Bur. Stand. (U.S.), Spec. Publ. 305 Suppl. 4, 449 pages (July 1973) $3.75, SD Catalog No. C13.10:305 Suppl. 4.

Key words: Abstracts, NBS publications; key words; publications.

This supplement to Special Publication 305 Supplements 1, 2, and 3 of the National Bureau of Standards lists the publications of the Bureau issued between January 1, 1972 and December 31, 1972. It includes an abstract of each publication (plus some earlier papers omitted from Special Publication 305 Supplement 3), key-word and author indexes; and general information and instructions about NBS publications.

Miscellaneous Publication 240 (covering the period July 1, 1957 through June 30, 1960) and its supplement (covering the period July 1, 1960 through June 30, 1966), Special Publication 305 (covering the period July 1966 through December 1967) and Special Publication 305 Supplement 1 (covering the period 1968-1969), Special Publication 305 Supplement 2 (covering the period 1970), and Special Publication 305 Supplement 3 (covering the period 1971) remain in effect. Two earlier lists, Circular 460 (Publications of the National Bureau of Standards, 1901 to June 1947) and its supplement (Supplementary List of Publications of the National Bureau of Standards, July 1, 1947 to June 30, 1957) are also still in effect.

SP320. Supplement 2. **Bibliography on atomic transition probabilities July 1971 through June 1973,** J. R. Fuhr and W. L. Wiese, Nat. Bur. Stand. (U.S.), Spec. Publ. 320 Suppl. 2, 63 pages (Nov. 1973) 95 cents, SD Catalog No. C13.10:320.

Key words: Allowed; atomic; discrete; forbidden; transition probability.

This is the second supplement to the NBS Special Publication 320, "Bibliography on Atomic Transition Probabilities," and it covers the most recent literature on the subject from July 1971 through June 1973. The papers are arranged according to elements and stages of ionization, and the method employed and classification of transitions are indicated for each reference. Only articles on discrete transitions, both allowed and forbidden, are listed. Papers containing data for many elements within isoelectronic sequences are collected separately in front of the list in order to keep this bibliography to a reasonable size. Also included is a selected list of new papers dealing with the subject of atomic transition probabilities from a general point of view.

SP381. **Bibliography of ion-molecule reaction rate data (January 1950-October 1971),** G. A. Sinnott, Nat. Bur. Stand. (U.S.), Spec. Publ. 381, 73 pages (Oct. 1973) $1.00, SD Catalog No. C13.10:381.

Key words: Atoms; bibliography; cross-sections; ions; molecules; rate coefficients; reactions.

A bibliography is presented of papers in the open literature that contain original experimental data on ion-molecule reaction rates or cross sections. Positive and negative ion-molecule and ion-ion reactions are included but not electron impact processes. For papers to be included, the reactants must have been identified and data for kinetic energies below 10 electron volts must have been presented.

SP387. **Laser induced damage in optical materials: 1973.** Proceedings of a symposium sponsored by Office of Naval Research, The American Society for Testing and Materials and by the National Bureau of Standards, Boulder, Colo. May 15-16, 1973, A. J. Glass and A. H. Guenther, Editors, Nat. Bur. Stand. (U.S.), Spec. Publ. 387, 285 pages (Dec. 1973) $2.65, SD Catalog No. C13.10:387.

Key words: IR windows and mirrors; laser damage; laser materials; self-focusing; thin films.

The Fifth ASTM-ONR-NBS Symposium on Laser Induced Damage in Optical Materials was held at the National Bureau of Standards in Boulder, Colo. on May 15 and 16 of this year. These Symposia are held as part of the activities of Subcommittee II on Lasers and Laser Materials, of the ASTM. Subcommittee II is charged with the responsibilities of formulating standards and test procedures for laser materials, components, and devices. The chairman of Subcommittee II is Haynes Lee, of Owens-Illinois, Inc. Co-chairmen for the Damage Symposia are Dr. Arthur H. Guenther, Scientific Director, Technology Division of the Air Force Weapons Laboratory, and Dr. Alexander J. Glass, Head, Basic Studies, Y Division, Lawrence Livermore Laboratory.

Approximately 135 attendees at the Symposium heard 25 papers on topics relating to laser induced damage in crystalline and nonlinear optical materials, at dielectric surfaces, and in thin film coatings as well as discussions of damage problems in the infrared region due both to cw and pulsed irradiation. In addition, several reports on the theoretical analysis of laser-materials interaction, relative to the damage process were given, along with tabulations of fundamental materials properties of importance in evaluation of optical material response to high power laser radiation. Several papers presented by title only are included within the proceedings for completeness.

The proceedings of these Symposia represent the major sources of information in the field of laser induced damage in optical materials. The Symposia themselves, along with the periodic meetings of Subcommittee II, provide a unique forum for the exchange of information regarding laser materials specifications among the manufacturers and users of laser devices, components, and systems. The Symposia also serve as a mechanism of information gathering to enable the Subcommittee to write informed and realistic specifications.

SP389. **Some references on metric information with charts on all you need to know about metric and metric conversion factors,** W. R. Tilley, Editor, Nat. Bur. Stand. (U.S.), Spec. Publ. 389, 8 pages (Dec. 1973) 25 cents, SD Catalog No. C13.10:389.

Key words: Metric charts; metric information sources; metric publications.

A bibliography of metric publications issued by NBS along with a list of organizations that market metric publications, lists, and films for educators. Also includes two metric charts "All you need to know about metric" and "Metric conversion factors."

NSRDS-NBS45. **Radiation chemistry of nitrous oxide gas. Primary processes, elementary reactions, and yields,** G. R. A. Johnson, Nat. Stand. Ref. Data Ser., Nat. Bur. Stand. (U.S.), 45, 27 pages (Dec. 1973) 60 cents, SD Catalog No. C13.48:45.

Key words: Chemical kinetics; data compilation; dosimetry; G; gas; nitrous oxide; radiation chemistry; rates; review.

Data on the radiation yields from nitrous oxide gas, and the effects of variables, including dose-rate, total dose, pressure, temperature, applied fields and scavengers are reviewed and tabulated. The use of N_2O as a gas-phase, chemical dosimeter is discussed. Primary

processes in irradiated N_2O are discussed and elementary reactions, relevant to the system, are listed.

PS56-73. **Structural glued laminated timber,** *(ANS A190. 1-1973),* K. G. Newell, Jr., Technical Standards Coordinator, Nat. Bur. Stand. (U.S.), Prod. Stand. 56-73, 12 pages (Oct. 1973) 45 cents, SD Catalog No. C13.20/2:56-73.

Key words: Glued laminated timber; laminated timber; structural glued laminated timber; timber, structural glued laminated.

This Voluntary Product Standard covers requirements for the dimensions, grade combinations, lumber for laminating, appearance grades, adhesive, and laminating of structural glued laminated timber as well as inspection and test procedures, marking, and the certification by a qualified inspection and testing agency. Definitions of the trade terms used are given, and guides for ordering and information on inspection practices are provided in the appendices.

TN392. (Revised September 1973). **Thermodynamic properties of compressed gaseous and liquid fluorine,** R. Prydz and G. C. Straty, Nat. Bur. Stand. (U.S.), Tech. Note 392, 197 pages (Sept. 1974) $1.50, SD Catalog No. C13.46:392 (Rev. 1973).

Key words: Density; enthalpy; entropy; fixed points (PVT); fluorine; Joule-Thomson; latent heat; melting curve; PVT measurements; saturation densities; specific heats; vapor pressure; velocity of sound; virial coefficients.

An apparatus has been constructed and used successfully to measure vapor pressure and PVT data of fluorine from the triple point to 300 K at pressures to about 24 MN/m^2. Material problems caused by the toxic and corrosive nature of fluorine were solved. A network of isotherm and isochore polynomials and a truncated virial equation were used to represent all PVT data. These equations represent the data with an average standard deviation of about 0.02 percent in density, the corresponding accuracy being estimated at 0.1 percent. Equations for the saturated liquid and vapor densities, the vapor pressure curve, the melting line, and the ideal gas properties are also presented. Comparisons are given to published values of the second virial coefficients, vapor pressures, and saturation densities. Additional comparisons are also made to measured specific heats and latent heats of vaporization. New values are reported for the triple point and critical point parameters together with the temperature and saturation densities at the normal boiling point. Finally, extensive tables of thermodynamic properties of fluorine are given which include pressure, temperature, density, isotherm and isochore derivatives, internal energy, enthalpy, entropy, specific heats at constant pressure and volume and velocity of sound. Some erroneous values for the internal energy and enthalpy of the compressed liquid below 135 K, published previously, have been corrected in this revision.

TN641. **Survey of the properties of the hydrogen isotopes below their critical temperatures,** H. M. Roder, G. E. Childs, R. D. McCarty, and P. E. Angerhofer, Nat. Bur. Stand. (U.S.), Tech. Note 641, 122 pages (Oct. 1973) $1.25, SD Catalog No. C13.46:641.

Key words: Compilation; density; deuterium; electrical properties; enthalpy; entropy; fixed points; hydrogen; mechanical properties; optical properties; specific heat; thermophysical properties; transport properties; tritium; vapor pressure.

The survey covers PVT, thermodynamic, thermal, transport, electrical radiative and mechanical properties. All isotopic as well as ortho-para modifications of hydrogen have been included. Temperatures are limited to those below the respective critical points, in general below 40 K. The pressure range is not restricted, that is solid, liquid, and gas phases are covered. However, with the exception of hydrogen, very little data exists at pressures other than saturation. The literature surveyed includes all references available to the Cryogenic Data Center up to June of 1972, and for several subjects, through March of 1973. The total number of documents considered was nearly 1500 of which about 10 percent contain pertinent information and are referenced in this report. The various properties are presented in the form of tables of graphs; if extensive tables have been published elsewhere, the reader is referred to the original sources.

TN642. **Summary of WR15 flange evaluation at 60 GHz,** B. C. Yates and G. J. Counas, Nat. Bur. Stand. (U.S.), Tech. Note 642, 32 pages (Oct. 1973) 40 cents, SD Catalog No. C13.46:642.

Key words: Attenuation; flange measurements; reflection coefficients; VSWR.

The measurement results of flange loss and reflection coefficient magnitude at 60 GHz (WR15 waveguide) of various flange configurations are presented. Included are the effects of alignment pins, surface finish, metallic contact surface, contact area, and flange bolt torque.

TN644. **Application of a non-ideal sliding short to two-port loss measurement,** M. P. Weidman and G. F. Engen, Nat. Bur. Stand. (U.S.), Tech. Note 644, 40 pages (Oct. 1973) 50 cents, SD Catalog No. C13.46:644.

Key words: Efficiency; loss; reflectometer; sliding short; two-port.

A detailed, applications-oriented, description of a method for measuring two-port losses is given. The technique involved uses a non-ideal sliding short circuit and a tuned four-arm reflectometer. Most, if not all, of the components used in this technique can be put together using commercially available items. It is the intent of this discussion to provide enough detail and explanation so that a technician with some working knowledge of microwave measurements can set up and make loss measurements.

The reference made to two-ports implies a broad range of devices from a simple flange or connector to waveguide coaxial adaptors and even more elaborate configurations with a definable input and output connection.

TN645. **Time and frequency broadcast experiments from the ATS-3 satellite,** D. W. Hanson and W. F. Hamilton, Nat. Bur. Stand. (U.S.), Tech. Note 645, 115 pages (Nov. 1973) $1.00, SD Catalog No. C13.46:645.

Key words: Dissemination; frequency; satellites; synchronization; time.

An experiment designed to reveal the advantages and special problems associated with the broadcasting of time and frequency information from geostationary satellites is discussed. Included are discussions concerning satellite motion, time delay variation, doppler shift due to the motion, and calculation of delay. Receiver or ground station equipment requirements, time recovery techniques, timing resolution and accuracy, and special advantages of satellite broadcasts for time and frequency dissemination are also discussed. Specially equipped sites in North and South America gathered data from the experimental satellite broadcast which in turn were used to determine the potential accuracy of satellite dissemination, the results of which are presented. Delay computation aids for the user were designed to provide a simple and inexpensive means of computing free space delays between the master clock and the user via a geostationary satellite. The aids, delay overlays on an earth map and a circular slide rule, are discussed with examples. Qualitative discussions of the signals and broadcast format are given. Final comments are made concerning the results of the experiment and how they might reflect upon a final system design for a permanent service using one or more geostationary satellites.

TN740. **SETAB: An edit insert program for automatic typesetting of spectroscopic and other computerized tables,** R. C. Thompson and J. Hilsenrath, Nat. Bur. Stand. (U.S.),

Tech. Note 740, 30 pages (Dec. 1973) 55 cents, SD Catalog No. C13.46:740.

Key words: Automatic typesetting; computer-assisted typesetting; edit insertion program; FORTRAN program; phototypesetting of spectroscopic tables; typesetting of tables.

SETAB is a FORTRAN program which accepts a card deck or FORTRAN records on magnetic tape and inserts the appropriate flags and shift symbols required by many programs associated with phototypesetting devices. The program is specialized to the particular application, the phototypesetter and typography programs, and to the desired typefaces by means of parameter cards supplied at run time. Examples are shown of spectroscopic tables typeset on the Linofilm phototypesetter at the Government Printing Office using the Autoset Typography Program. The program has also been used for tables of other types of data. The program can handle any records which can be read by a FORTRAN "READ" statement under "A" format control. The original record can be divided into as many as 40 fields and these fields can be combined in any order with any of 26 strings in front of or between the pieces. The program will, on a signal, replace a field by another field or by a combination of fields and strings. The output lines are blocked and paged via the insertion of the required strings between blocks and pages.

TN794. **NBS corridor fire tests: Energy and radiation models,** F. C. W. Fung, R. Suchomel, and P. L. Oglesby, Nat. Bur. Stand. (U.S.), Tech. Note 794, 127 pages (Oct. 1973) $1.40, SD Catalog No. C13.46:794.

Key words: Ceiling radiation; corridor fires; critical energy input; flame spread, calculation, and observations; floor covering evaluations; heat balances; heat transfer mechanisms; models, energy balance, radiation, and scaling.

The NBS corridor fire program is a continuing program to investigate the growth and spread of fire and smoke through a corridor when fire is initiated in an adjoining room. Due to recent fires involving floor coverings [1], and controversies over current floor covering flammability test methods, floor coverings have received special attention during the first phase of the corridor fire program. Results of the NBS program on corridor fires are presented under the unifying concepts of energy and radiation models. The major findings are: (1) One type of carpet fire hazard has been identified as the rapid flame spread over pile surface; (2) The dominant mechanism that causes this flame spread is energy transfer from ceiling radiation. This is substantiated by measurements and calculations; (3) Carpet evaluation by critical cumulative energy input into the corridor has been found to be feasible and informative in terms of heat transfer mechanisms; (4) Finally, a radiant panel test appears to be a promising approach to simulate the corridor environment for second generation flooring tests.

TN798. **Collaborative research program between NBS and Indian Scientific Institutions. Special foreign currency program 1973 status,** H. S. Peiser, M. B. McNeil, and D. M. Bluebond, Editors, Nat. Bur. Stand. (U.S.), Tech. Note 798, 139 pages (Nov. 1973) $1.50, SD Catalog No. C13.46:798.

Key words: Binational research cooperation; international scientific cooperation; India science and technology; physical science research administration; research planning; scientific research abstracts; Special Foreign Currency.

An overview is given of grants awarded by the National Bureau of Standards under the Special Foreign Currency Program in India, authorized by Public Law 480 and its amendments. Each grant is identified by title, principal investigator, institution in India, NBS monitor charged with working in close technical touch with the project in India, and the monitor's organizational unit within NBS. The relevant work is then described briefly under the three headings "Summary Description of Project Goals," "Results and Implications to Date," and "List of Publications that Resulted from the Project." To demonstrate the wide use of such grants over the entire Program Structure of NBS, the grant descriptions are ordered by the elements of that Program Structure. Editorial comment on the significance and purpose of the NBS/SFCP grant program is confined to a Foreword and Introduction. The editors judge this grant program to have had a high benefit to cost ratio from the viewpoint of NBS.

TN799. **User procedures standardization for network access,** A. J. Neumann, Nat. Bur. Stand. (U.S.), Tech. Note 799, 43 pages (Oct. 1973) 70 cents, SD Catalog No. C13.46:799.

Key words: Network access procedures; networking; standardization; user protocols.

User access procedures to information systems have become of crucial importance with the advent of computer networks, which have opened new types of resources to a broad spectrum of users. This report surveys user access protocols of six representative systems. Functional access requirements are outlined, and implementation of access procedures is analyzed by means of a common methodology.

Qualitative assessment of standardization possibilities identify standardization candidates such as: system and user signals, on-line user entries, system requests, and network wide categories of message content.

TN802. **Network user information support,** A. J. Neumann, Nat. Bur. Stand. (U.S.), Tech. Note 802, 27 pages (Dec. 1973) 60 cents, SD Catalog No. C13.46:802.

Key words: Computers; consultation; documentation; information support; networks; on-line support; user needs; user support.

With increasing interest in the development of computer networks and the proliferation of remote entry capability from user terminals, user support takes on new dimensions. Some user characteristics are outlined as they affect user support. User support requirements are identified for training, terminal operation, and general information to aid in network operations. Support capabilities include on-line aids, information available on request, and tutorial information available at the terminal. User support also includes pertinent documentation and human consultation. Areas of future research are identified as: interactive language design, tutorial design, integration of hard-copy and on-line capabilities, and further development of user feedback capability.

TN806. **Methods of measurement for semiconductor materials, process control, and devices. Quarterly report, April 1 to June 30, 1973,** W. M. Bullis, Editor, Nat. Bur. Stand. (U.S.), Tech. Note 806, 77 pages (Nov. 1973) $1.00, SD Catalog No. C13.46:806.

Key words: Beam leads; carrier lifetime; delay time; die attachment; electrical properties; electronics; epitaxial silicon; generation centers; gold-doped silicon; methods of measurement; microelectronics; microwave diodes; mobility; pull test; recombination centers; resistivity; resistivity standards; scanning electron microscopy; semiconductor devices; semiconductor materials; semiconductor process control; silicon; S-parameters; spreading resistance; thermal resistance; thermally stimulated properties; trapping centers; wire bonds.

This quarterly progress report, twentieth of a series, describes NBS activities directed toward the development of methods of measurement for semiconductor materials, process control, and devices. Significant accomplishments during this reporting period include (1) completion of an initial identification of the more important problems in process control for integrated circuit fabrication and assembly as a basis for and expanded effort to be conducted in cooperation with ARPA, (2) completion of preparations for making silicon bulk re-

sistivity wafer standards available to the industry, and (3) undertaking of new work to establish the relationship between carrier mobility and impurity density in silicon and to investigate test patterns for use in process control and evaluation. Because of the general applicability of the first of these, a summary of the findings is presented in a separate appendix. Work is continuing on measurement of resistivity of semiconductor crystals; characterization of generation-recombination-trapping centers, including gold, in silicon; evaluation of wire bonds and die attachment; study of scanning electron microscopy for wafer inspection and test; measurement of thermal properties of semiconductor devices; determination of S-parameters and delay time in junction devices; and characterization of noise and conversion loss of microwave detector diodes. Supplementary data concerning staff, standards committee activities, technical services, and publications are also included as appendices. This is the last report in this form; future reports in this series will appear under the title, Semiconductor Measurement Technology.

TN807. **Building performance in the 1972 Managua earthquake,** R. N. Wright and S. Kramer, Nat. Bur. Stand. (U.S.), Tech. Note 807, 155 pages (Nov. 1973) $1.60, SD Catalog No. C13.36:807.

Key words: Building codes; buildings; earthquakes; hazards; natural disasters; structures.

Following the Managua, Nicaragua, earthquake of Dec. 23, 1972, a team of engineers representing the U.S. Department of Commerce's National Bureau of Standards (NBS) and the National Academy of Engineering (NAE) performed field investigations in Managua, Nicaragua, from Dec. 26, 1972, to Jan. 4, 1973. The objectives were to assist the Nicaraguan government in surveying major buildings to determine whether each was suitable for emergency use, repairable, or appropriate for clearance. The team also viewed the patterns of successful performance and damage to identify needs for improvements in building practices for mitigation of earthquake hazards and opportunities for more detailed investigations which could provide information for future improvements in practices. In general, the damages cannot be attributed to unusual intensities of ground shaking or severity of surface faulting. Most damages appeared to result from deficiencies in building practices; deficiencies which had been exhibited many times before in previous earthquakes, deficiencies which would be avoided by implementation of up-to-date provisions for earthquake resistant design and construction. However, Managua did not employ a building code with seismic design requirements appropriate to its earthquake risk, and furthermore, did not have a building regulatory system capable of effective implementation of its building code provisions. This report documents the observations of damages by the NBS/NAE team and points out relationships to inadequacies in the building practices employed. Most of these inadequacies have been well known; however, the Managuan experience may serve as an incentive to improvement of building practices in many other areas which are subject to substantial earthquake risks and have not consistently accounted for these risks in their building codes and building regulatory system.

TN808. **Potential systems for lead hazard elimination: Evaluations and recommendations for use,** D. Waksman, J. B. Ferguson, M. Godette, and T. Reichard, Nat. Bur. Stand. (U.S.), Tech. Note 808, 192 pages (Dec. 1973) $1.95, SD Catalog No. C13.46:808.

Key words: Abrasion; adhesion; colorfastness; covering; materials; flash point; flame spread; impact resistance; lead paint poisoning; materials; performance; properties; scratch resistance; smoke generation; toxic combustion products; toxicity; washability; water vapor permeance.

The National Bureau of Standards is providing technical support to the Department of Housing and Urban Development which is required by Public Law 91-695 (the Lead Paint Poisoning Prevention Act) to carry out a research program to evaluate and make recommendations regarding technology for the removal of the lead based paint hazard from the Nation's housing.

Potential hazard elimination methods have been identified by means of a survey of available technology. This report describes testing and evaluation methodologies used to determine (1) the suitability for use of a series of removal and lead barrier systems, (2) the results of this evaluation, and (3) recommendations concerning the use of said systems.

Paint removal systems were evaluated in terms of the hazards that they present in the course of their use. Both the flammability and the toxicity of the solvents found in removers were considered. Covering systems were evaluated for their suitability for use as barrier layers over lead bearing paints in housing. The effectiveness of covering systems in protecting children from leaded paint, their fire hazard properties and functional properties which are related to their serviceability were considered in making this evaluation. The properties of the systems were assessed in terms of minimum acceptable performance levels and recommendations are given for their use in a field evaluation program.

TN810. **Fire incidents involving sleepwear worn by children ages 6-12,** J. A. Slater, Nat. Bur. Stand. (U.S.), Tech. Note 810, 23 pages (Dec. 1973) 50 cents, SD Catalog No. C13.46:810.

Key words: Accidents; burns; children; clothing fires; deaths; FFACTS; fire; flammable fabrics; injury; sleepwear; standards; statistics.

Sleepwear was the first fabric item ignited more frequently than any other item in over 1,900 fire incidents reported to the National Bureau of Standards Flammable Fabrics Accident Case and Testing System (FFACTS). Information acquired since promulgation of the current sleepwear flammability standard protecting children of ages 0-5 indicates a problem of comparable magnitude exists for children of ages 6-12. Of 316 incidents involving non-contaminated sleepwear that was first to ignite, about one-fourth involved children 0-5 years old and one-fourth involved children 6-12 years old. For the 6-12 group, sleepwear ignited first more often than all other garment items combined. Females outnumbered males 4-to-1 in the 6-12 group, due mostly to the involvement of nightgowns and kitchen ranges, the most common ignition source for this age group. Five of the 6-12 year old children died and 52 of 74 victims were hospitalized. Almost all of the first-to-ignite sleepwear in this group was cotton. Data from Shriners Burns Institute and the National Burn Information Exchange provide further evidence of the involvement of children ages 6-12 in garment fires. It is recommended that a new standard be issued covering sleepwear sizes 7 through 14 to effectively protect 6-12 year old children.

This column lists all outside publications by the NBS staff, as soon after issurance as practical. For completeness, earlier references not previously reported may be included from time to time.

Abrams, M. D., Hudson, J. A., Meissner, P., Pyke, T. N., Jr., Rosenthal, R. M., Ulmer, F. H., **Use of computer networks in support of interactive graphics for computer-aided design and engineering,** *NBSIR 73-217,* 47 pages (June 30, 1972). (Available as COM 74-10470 from the National Technical Information Service, Springfield, Va. 22151.)

Key words: Computer-aided design; computer networks; interactive graphics, performance measurement; remote computer utilization.

This report covers work performed between 1 July 1971 and 30 June 1972 as part of a long-term study of interactive computer-aided techniques. The primary emphasis during this period has been on investigating the feasibility of using computer networks in support of interactive graphics for computer-aided design and engineering. Alternative means for providing remote computer service have been studied. An experimental configuration has been devised taking ad-

vantage of the fact that there is located at the National Bureau of Standards a node of the ARPA Computer Network. Arrangements were made via this configuration for users at the Electronics Command to utilize a structural design program, NASTRAN, at a remote computer site. Emphasis has been placed on the evaluation of performance of interactive design techniques using displays supported by local and remote computers in a hierarchical arrangement. A variety of problems are identified which must be considered in order to support interactive graphics via a computer network; these are compounded where the network itself is in an evolving state of development. The report includes an outline of a synchronous communication protocol which was developed for use between ECOM and NBS.

Abrams, M. D., **Remote computing: The administrative side,** *Comput. Decisions*, pp. 42-46 (Oct. 1973).

Key words: Administration; batch; computing; documentation; remote; service; users.

The administration and management of remote computing services are discussed with the objective of making both users and administrators aware of the potential problems. Likely difficulties are anticipated and coupled with discussions of assistance, operation, documentation and other features which make it more possible to utilize the technical services. The response to technical questions is covered in terms of written, on-line, and direct contact assistance. A question and answer organization is employed.

Andrews, J. R., **Random sampling oscilloscope time base,** *NBSIR 73-309*, 86 pages (June 1973). (Available as COM 73-11981 from the National Technical Information Service, Springfield, Va. 22151.)

Key words: Mercury switch; oscilloscope; picosecond; pulse; random sampling; risetime; sampling; time base; transition time.

With the advent of new miniaturized mercury (Hg) switches with reputed transition times of the order of 10 picoseconds, interest has been rekindled in their use in high speed pulse measurements. Since there is no pre-trigger signal available from a Hg switch, normal sequential sampling techniques are not usable to measure the fast Hg switch transition time. For this reason a new random sampling time base unit was designed to perform these measurements at the low repetition rate of Hg switches (< 100 Hz). The time base may be used with commercial sampling oscilloscope systems through suitable interconnection terminals or possible interface equipment. It features three selectable time windows of 1 μs, 100 ns, and 10 ns. Using its time magnifier, the fastest sweep rate is 10 ps/cm. A variable trigger lead time control is provided. The trigger sensitivity is 10 mV. The long term timing stability of the time base is excellent with less than 15 ps/h drift.

Baker, M. A., **Observing porcelain enamels with a scanning electron microscope,** *Proc. Porcelain Enamel Institute Technical Forum, The Ohio State University, Columbus, Ohio, Oct. 6-8, 1971*, **33**, 84-90 (Porcelain Enamel Institute, Inc., Washington, D.C., 1971).

Key words: Corrosion; pinhole-type defects; porcelain enamel; scanning electron microscope; weathering tests; non-dispersive x-ray spectrometer.

Porcelain enamel surfaces and enamel-metal interfaces have been observed with a scanning electron microscope. The increased depth of field and the extended range of magnifications of the scanning electron microscope were utilized in studies of the enamel-metal interface and of weathering test specimens that corroded after relatively short periods of exposure. The nondispersive x-ray spectrometer accessory for the scanning electron microscope was used to determine the elements present in the enamel surface and to obtain qualitative distributions of these elements.

Baker, M. A., **Weathering tests of porcelain enamels on steel and aluminum,** *Proc. Porcelain Enamel Institute Technical Forum, The University of Illinois, Urbana, Ill., Oct. 11-13, 1972*, **34**, 186-198 (Porcelain Enamel Institute, Inc., Washington, D.C., 1972).

Key words: Accelerated tests; acid resistance; aluminum; color; gloss; porcelain enamel; steel; weather resistance.

The Porcelain Enamel Institute and the National Bureau of Standards have been conducting weathering tests of porcelain enamels since 1939. The four tests now in progress contain matte and glossy porcelain enamels on both steel and aluminum. When the data obtained from these weathering tests were compared with accelerated test data on laboratory specimens, an excellent correlation was found. It was also found that the enamels in all four tests changed gloss and color in practically the same manner.

Ballantyne, J. P., Yakowitz, H., Nixon, W. C., **Simultaneous x-ray microanalysis and resistance measurement of electron beam induced direct metallic deposition,** (Proc. 6th Int. Conf. on X-Ray Optics and Microanalysis, Osaka, Japan, Sept. 1971), Paper in *Proceedings of the Sixth International Conference on X-Ray Optics and Microanalysis*, G. Shinoda, K. Kohra and T. Ichinokawa, Eds., pp. 219-227 (University of Tokyo Press, Tokyo, Japan, 1972).

Key words: Deposited thin film; electron beam metal deposition; scanning electron microscopy; x-ray microanalysis.

The decomposition of thin film AgCl, vapor deposited onto an oxidized silicon substrate, was caused by electron bombardment in a scanning electron microscope operating at a pressure of 10^{-8} torr. This decomposition was monitored by nondispersive x-ray analysis techniques. At the same time, the resistance of the film was also recorded.

The curves of chlorine concentration and resistance as a function of exposure are very similar in shape. The chlorine content of the film reaches a level that does not alter with increasing exposure. At this point, film resistance is about 1000 Ω and remains essentially constant with increasing exposure. The residual chlorine can be removed by chemical treatment after which the resistance values drop to less than 50Ω.

The quantitation of the x-ray results must await new correction procedures presently under study. However, a simple correction procedure has been employed in order to illustrate important trends in the direct metallic deposition process.

Ballard, L. D., Edelman, S., Epstein, W. S., Smith, E. R., **A suggestion for determining g by a two interferometer technique,** *SPIE J.* **9**, No. 5, 166-168 (June/July 1971).

Key words: Acceleration; counter; filter; g; gravity; interferometer; laser.

A method for determining the acceleration due to gravity is suggested. Two falling interferometer reflectors illuminated by a laser are used. The falling reflectors are separated by a ΔT and thus have a constant velocity differential, this generates a frequency linearly proportional to acceleration ($g = kf = \Delta V/\Delta T$).

Thus, the metrology of measuring g is simplified by having g linearly proportional to frequency.

Barber, W. C., Hayward, E., Sazama, J., **Nuclear scattering of plane-polarized photons,** (Proc. Int. Conf. on Nuclear Structure Studies using Electron Scattering and Photoreaction, Sendai, Japan, Sept. 12-15, 1972), Paper in *Nuclear Structure Studies Using Electron Scattering and Photoreaction*, Supplement to *Research Report of Laboratory of Nuclear Science*, K. Shoda and H. Ui, Eds., **5**, 313-317 (Tohoku University, Tomizawa, Sendai, Japan, 1972).

Key words: Dynamic collective model; giant resonance; photon scattering; polarized photons.

A beam of plane-polarized, monochromatic photons has been produced by the resonance fluorescence of the well-known 1^+ state in ^{12}C. These have been scattered a second time from targets of cadmium, tin, tantalum, gold, and bismuth. A measurement of the number of photons scattered along and perpendicular to the polarization vector in the incident 15.1 MeV beam allows a determination of the relative contribution of incoherent and coherent scattering to the total scattering cross section. These results can be compared to the predictions of the dynamic collective model.

Barnes, J. D., **Inelastic neutron scattering study of the "rotator" phase transition in *n*-nonadecane,** *J. Phys. Chem.* **58,** No. 12, 5193-5201 (June 15, 1973).

Key words: Molecular dynamics; *n*-alkanes; *n*-nonadecane; neutron scattering; paraffin; rotator phase.

A simple kinematic model for rotational jump diffusion of a normal alkane about its long axis (circular random walk model) is developed. Inelastic neutron scattering data obtained on the Fermi chopper time-of-flight instrument at the National Bureau of Standards reactor using an incident neutron wavelength of 2.47 Å ($\Delta\lambda/\lambda \simeq 3.8$ %) are compared with the predictions of the model. Data taken below the temperature of the "rotator" phase transition in *n*-nonadecane (295 °K) show no quasielastic scattering due to diffusive motions. Data taken in *n*-nonadecane in its disordered solid phase show quasielastic scattering consistent with the circular random walk model. Estimates for values of the model parameters of 3.5 psec. for τ_1 and $N \geq 8$ are obtained.

Barton, J. A., Jr., Burns, C. L., Chandler, H. H., Bowen, R. L., **An experimental radiopaque composite material,** *J. Dent. Res.* **52,** No. 4, 731-739 (1973).

Key words: Barium glass; dental composites; dental reinforcements; physical properties; resins; silica; x-ray opacity.

Physical properties of a composite material, developed for use as a temporary posterior restorative material, have been investigated. The material is based on isomeric phthalate esters of 2-hydroxyethyl methacrylate and reinforcing fillers consisting of particles of vitreous silica and an x-ray-opaque glass. Properties investigated include hardening time, tensile and compressive strengths, indentation and recovery, hardness, water sorption, solubility, polymerization shrinkage, optical and x-ray opacity, color stability and thermal expansion. All properties were studied using 3 different powder-liquid rations: 1.10, 1.35 and 1.45 Gm of powder to 0.4 ml of monomer, under wet and dry storage conditions. The powder-liquid ratio had little effect on compressive strength; e.g., 1.45 ratios, respectively. The tensile strength of the 1.10 ratio specimens was lower than those of the 1.35 and 1.45 ratio specimens (at six hours, 25.5 as compared to 30.4 MN/m^2). Water sorption at one week was 0.2 to 0.3 mg/cm^2.

Becker, D. A., LaFleur, P. D., **Neutron activation analysis: Application to trace element analysis in biological and environmental materials,** *Proc. 5th Annual Conf. on Trace Substances in Environmental Health, University of Missouri, Columbia, Mo., 1971,* pp. 447-453 (1972).

Key words: Biological samples; biological standards; chemical separations; environmental samples; neutron activation analysis (NAA); nondestructive; reagent blanks; trace element analysis.

Neutron activation analysis (NAA) has been found useful for trace element analysis of biological and environmental samples. The favorable characteristics of this technique include high sensitivity, wide applicability, great specificity, and reduced contamination and reagent blank problems. The utilization of this technique for the analysis of several elements (Mn, Na, Cu, Zn, U) in the recently certified NBS Biological Standard Reference Material: Orchard Leaves, is described. Techniques used include both nondestructive analysis and destructive analysis using radiochemical separations. In addition, the analytical results obtained by NAA on the Orchard Leaves, is compared to that obtained by other analytical techniques.

Bellet, J., Lafferty, W. J., Steenbeckeliers, G., **Microwave spectra of $D_2{}^{17}O$ and $D_2{}^{18}O$,** *J. Mol. Spectrosc.* **47,** No. 3, 388-402 (Sept. 1973).

Key words: Centrifugal distortion constants; $D_2{}^{17}O$; $D_2{}^{18}O$; quadrupole coupling constants; rotational constants; rotational spectra.

Forty lines of the microwave spectra of $D_2{}^{17}O$ and $D_2{}^{18}O$ have been measured in the region from 8 to 400 GHz and analyzed according to Watson's centrifugal distortion theory. Comparison of the results obtained for $D_2{}^{16}O$, $D_2{}^{17}O$, and $D_2{}^{18}O$ demonstrates their internal consistency. The transferability of the parameters according to the isotopic substitution rules is evidence for the validity of the model chosen for the study of the ground state of heavy water.

The effective rotational constants deduced from the observed spectra are very close to the values calculated using Oka's second order theory. The values obtained in MHz are:

$$A = 456766.9, B = 218041.0, C = 144701.5 \ (D_2{}^{17}O);$$

$$A = 451891.9, B = 218045.2, C = 144201.7 \ (D_2{}^{18}O).$$

The hyperfine structure of the $D_2{}^{17}O$ lines has been analyzed using as a reference the corresponding quadrupole coupling tensor of $HD^{17}O$ with the appropriate rotation. The values of χ_{gg} in MHz used for the analysis are:

$$\chi_{xx} = -1.2104, \chi_{yy} = 10.1068, \chi_{zz} = -8.8964.$$

Benzinger, M., Benzinger, T. H., **Tympanic clinical temperature,** (Proc. 5th Symp. on Temperature, Its Measurement and Control in Science and Industry, Washington, D.C., June 21-24, 1971), Paper in *Temperature, Its Measurement and Control in Science and Industry,* H. H. Plumb, Editor-in-Chief, **4,** Part 3, 2089-2102 (Instrument Society of America, Pittsburgh, Pa., 1972).

Key words: Anesthesiology; brain temperature; carotid artery; clinical medicine; cold stress (diver); disposable thermometry; esophageal thermometer; fever; fulminant hyperpyrexia; heart temperature; hypothalamus heat stress; hypothermia; obstetrics; ovulation-detection; open heart surgery; pediatric surgery; pyrogens; sweating; temperature, central body; thermocouple disconnect; thermoelectric thermometry; thermometer; vasodilation; warm sensitive neurons.

Tympanic thermometry, first introduced in physiology where it was instrumental in finding the mechanisms of human temperature regulation, has passed the test of application to clinical medicine. In the clinical situations thus far tested, which included anesthesia of various types, hypothermia for surgery, extreme heat and cold stress, extracorporeal circulation for open heart procedure and one case of terminal cooling toward exitum after stroke, tympanic and esophageal patterns were found identical for practical purposes. Rectal tracings deviated grossly from the significant central patterns which monitor the temperature of the heart, the brain and the centers of thermoregulation. These central patterns can now be conveniently obtained, by way of the tympanic approach, with clean disposable probes on awake patients, and without embarrassment, discomfort or airway interference, in hospitals or at home. For hospital use, instruments are commercially available. For home use, small and inexpensive readout instruments have yet to be developed.

Benzinger, T. H., **A new concept in thermodynamics and its implication in molecular biology and pharmacology,** Chapter 14 in *Methods in Pharmacology* **2,** Part 2, 481-488 (Appleton-Century Crofts, New York, N.Y., 1972).

Key words: Characteristic function (Planck); chemical bonding energy; double helix; heat integrals; molecular biology; thermal free energy; thermodynamics.

An extended statement of chemical equilibrium of the integral $\int_0^T (\Delta Cp/T)\,dT (= T\Delta S_T°)$ and $\Delta H_T°$ – the classical terms of the equation $-RTlnK = \Delta H_T° - T\Delta S_T°$. The integral $\int_0^T \Delta CpdT$ is not negligible for macromolecules and particularly biopolymers, and its direct experimental determination at all temperatures down to 0 K is therefore indispensable for thermodynamic understanding of the objects of molecular biology.

Blomquist, D. S., **An experimental investigation of foam windscreens,** (Proc. 1973 International Noise Control Engineering Conference, Copenhagen, Denmark, Aug. 22-24, 1973), Paper in *Inter-Noise 73 Proceedings,* O. J. Pedersen, Ed., pp. 589-593 (Inter-Noise 73, Technical University, Lyngby, Denmark, 1973).

Key words: Acoustic attenuation; foam windscreens; wind-generated noise.

The amount of reduction in wind-generated noise and the amount of acoustic attenuation of the signal as a function of frequency for four different pore sizes and various diameters of open-cell polyurethane foam windscreens is presented.

Blomquist, D. S., Leasure, W. A., Jr., **An hourly noise exposure meter,** (Proc. 1973 International Noise Control Engineering Conference, Copenhagen, Denmark, Aug. 22-24, 1973), Paper in *Inter-Noise 73 Proceedings,* O. J. Pedersen, Ed., pp. 67-69 (Inter-Noise 73, Technical University, Lyngby, Denmark, 1973).

Key words: Acoustics (sound); environmental acoustics; instrumentation; noise exposure.

An instrument has been designed which provides information regarding the average noise exposure over each hour rather than simply a singly measure of noise exposure over an 8-hour work period. The theory of operation and examples of practical measurements utilizing this device will be discussed in the verbal presentation.

Boone, T. H., Ray, T. R., Street, W. G., **Pilot demonstration of lead based paint hazard elimination methods,** *NBSIR 73-242,* 38 pages (June 1973). (Available as PB 224654 from the National Technical Information Service, Springfield, Va. 22151.)

Key words: Cost analysis; hazard elimination; housing; lead based paint; materials; surface preparation; surface refinishing.

This report describes the elimination of the hazard of lead bearing paints in a one bedroom apartment using materials and procedures that are undergoing laboratory and field evaluation by the National Bureau of Standards (NBS). Paint removal was used to eliminate the hazard from some surfaces and two nonhazardous membrane type coverings were installed as barrier materials over the residual leaded paint on other surfaces. The preparation and refinishing of the interior surfaces are described and work rates and cost data are presented.

This pilot demonstration is the first of a series of studies that will be used to determine the merits of various lead based paint hazard elimination methods when applied to actual housing conditions.

Final recommendations for further use of materials and systems, described in this report, are not presented due to the preliminary nature of this work. The completion of the projected series of demonstrations and the long term evaluation of the in-use performance of the materials and systems will be required before final recommendations can be made.

Bowen, B. E., Cram, S. P., Leitner, J. E., Wade, R. L., **High precision sampling for chromatographic separations,** *Anal. Chem.* **45,** No. 13, 2185-2191 (Nov. 1973).

Key words: Computer-based data acquisition; gas chromatography.

The precision of several chromatographic sampling valves of original design is shown to approach 0.05 percent for unretained solutes. Hybrid-fluidic, high pressure, and commercial valves have been characterized by measuring the precision of their column input profiles and statistical moments. A computer-based data acquisition and control system was developed for use with high precision algorithms.

Bowen, R. L., Argentar, H., **A method for determining the optimum peroxide-to-amine ratio for self-curing resins,** *J. Appl. Polym. Sci.* **17,** 2213-2222 (1973).

Key words: Accelerators; amines; dental materials; initiators; peroxides; polymerization.

The rate of polymerization of a methacrylate monomer was influenced by the molar ratio of benzoyl peroxide to an aromatic tertiary amine accelerator when the product of the concentrations of these was kept constant. The maximum rate, measured as the minimum gel time, occurred in monomer solutions containing about 1.5 moles of peroxide per mole of amine.

Bowen, R. L., Chandler, H. H., **Metal-filled resin composites,** *J. Dental Res.* **52,** No. 3, 522-532 (May-June 1973).

Key words: Aluminum; composites; coupling agents gold; mercaptan; methacrylates; polymers; resin; silane; tantalum; zirconium.

Certain physical properties of metal-filled resin composite materials can be improved if properly selected and applied coupling agents are used in treating the surfaces of the metal particles.

Brauer, G. M., Termini, D. J., **Grafting of acrylates and vinyl chains onto collagen with ceric initiator,** *J. Appl. Polym. Sci.* **17,** 2557-2568 (1973).

Key words: Acrylate copolymers; ceric ion initiated; grafting collagen; graft polymerization; modification of collagenous surfaces.

To determine the scope of the grafting reaction, over 30 monomers were grafted to steer hide collagen and collagen films using ceric ammonium nitrate as initiator. High yields of apparent graft polymer were obtained with most acrylate and methacrylate esters. Yields were not changed greatly by employing the higher homologues. Moreover, monomers containing such diverse substituents as hydroxy, cyano, chloro, trifluoroethyl, or glycidyl groups may be grafted onto collagen. The presence of these functional groups in the products provides potential reaction centers to further modify the collagenous surface. Presence of vinyl polymer was confirmed by IR spectra. The large number of monomers of varying polarity which were found to undergo apparent grafting makes it possible to vary widely the surface properties of collagen. It was shown that certain monomers impart water and oil repellency to collagenous surfaces, whereas others increased the hydrophilicity or oleophilicity of the substrate. Thus, by proper selection of monomers, the desired degree of hydrophilic to hydrophobic or oleophilic to oleophobic balance of the collagen surface to suit specific applications can be obtained.

Brenner, F. C., Kondo, A., Cohen, G. B., **Research for a uniform quality grading system for tires V. Effect of environment on tread wear rate,** *Rubber Chem. Technol.* **44,** No. 4, 952-959 (Sept. 1971).

Key words: Automobile tires; environmental effects; test method; tread wear.

This paper is a continuation of work reported in *Rubber Chem. Tech.* **44,** (1971). The results of an additional tread wear test are re-

ported. This and the earlier data are analyzed to determine environmental effects on rate of tread wear.

For all types of commercial passenger car tires our test results support the thesis that the rate of wear on the tire is independent of the extent of wear. Our results also indicated that the rate of tread wear is greater on wet pavements than on dry. An explanation for this phenomenon is discussed.

Broadhurst, M. G., **Fluctuation-barrier model for rotational relaxation,** (Proc. Conf. Electrical Insulation and Dielectric Phenomena, Buck Hill Falls, Pa., Oct. 20-22, 1969), Chapter in *1969 Annual Report of the Conference Electrical Insulation and Dielectric Phenomena,* pp. 48-54 (National Research Council, National Academy of Sciences, Washington, D.C., 1970).

Key words: Elastic barrier; lattice; molecular rotation; relaxation; temperature dependence.

A model is presented where the barrier to molecular rotation in solids is taken to be the work to elastically expand the lattice around the molecule. This barrier is shown to increase with pressure and decrease with temperature. The model calculations are compared to data on long chain paraffin-like solids for the dielectrically active relaxation involving rotation of the entire molecule around its chain axis (analogous to the α relaxation in polymers). The model accurately predicts the temperature dependence of the relaxation time (the activation entropy in the Eyring Theory), and the Eyring activation energy (the activation energy does not equal the elastic barrier height). The predicted pressure dependence of the relaxation time is in error by a factor of 2 indicating the need for further refinement of the model. This paper reports the current status of this problem.

Broadhurst, M. G., Malmberg, C. G., Mopsik, F. I., Harris, W. P., **Piezo- and pyroelectricity in polymer electrets,** (Proc. Conf. on Electrets, Charge Storage and Transport in Dielectrics, Miami Beach, Fla., Oct. 8-13, 1972), Paper in *Electrets, Charge Storage and Transport in Dielectrics,* M. M. Perlman, Ed., pp. 492-504 (The Electrochemical Society, Inc., Princeton, N.J., 1973). (Available as AD 758730 from the National Technical Information Service, Springfield, Va. 22151).

Key words: Electret; piezoelectric; polymer electret; poly(vinyl chloride); pyroelectric.

A model for a polymer electret, based on an elastically isotropic solid with orientationally frozen molecular dipoles, was developed and tested experimentally. This electret is shown to be both piezoelectric and pyroelectric. The polarization is shown to change with mechanically and thermally induced strains in the polarization direction. The currents generated by the electret will be proportional to the strain rate and, for thin contact electrodes and uniform strains, unaffected by the presence of real charges. Poly(vinyl chloride) films were poled at 80 °C, just above their glass transition temperature. The pressure- and temperature-induced short-circuit currents in the polarization direction equalled 0.15 (pA/cm²)/(bar/min) and 2.2 (pA/cm²)/(K/min) respectively for a specimen poled at 320 kV/cm. These currents were 1) reversible and proportional to the rate of temperature or pressure change, 2) proportional to poling voltage up to 320 kV/cm, 3) in the direction corresponding to increasing polarization with increasing pressure and decreasing temperature, 4) stable with time without special storage conditions, 5) about 1.6 times as great for temperature induced strains as for equivalent pressure induced strains and 6) about 2-4 times as great in magnitude as expected from dielectric constant measurements. The apparent polarization from temperature measurements for the 320 kV/cm specimen was about 1.7 μC/cm², or about 1/3 the value expected for maximum alignment of dipoles. In the same specimen the pyroelectric coefficient was found to be $p_3 = -0.39$ nC/cm² K and, assuming elastic isotropy, the piezoelectric strain coefficients were found to be $d_{31} = d_{32} = d_{33} = -0.89$ pC/N.

Broadhurst, M. G., Mopsik, F. I., **Vibrational frequency spectrum for polymers,** *J. Chem. Phys.* **55,** No. 8, 3708-3711 (Oct. 15, 1971).

Key words: Frequency spectrum; linear chains; *n*-alkanes; polyethylene; polymer.

A method is given for calculating the vibrational frequency spectrum of a model linear polymer. The model is a chain of N masses having bending and stretching force constants. Each mass is quasiharmonically coupled to a Debye lattice which has a cutoff frequency ω_L. Each of the $3N$ free chain eigenfrequencies ω_j becomes a band with a low frequency cutoff $\omega_{jmin}^2 = \omega_j^2$, a high frequency cutoff $\omega_{jmax}^2 = \omega_j^2 + \omega_L^2$, and a pseudo-$n$-dimensional Debye distribution $g_j(\omega) = n\omega^{n-1}/(\omega_{jmax}^n - \omega_{jmin}^n)$ for $\omega_{jmin} < \omega < \omega_{jmax}$. The total frequency distribution agrees closely with the results by Genensky and Newell for the Stockmayer and Hecht lattice using their force constants and compares reasonably well with results of GF matrix calculations for polyethylene.

Bur, A. J., **Dielectric properties of fluorine-containing polymers,** Chapter 15 in *Fluoropolymers,* L. A. Wall, Ed., **25,** 475-505 (John Wiley-Interscience, New York, N.Y., 1972).

Key words: Dielectric constant; dielectric loss; fluoropolymer; relaxation phenomena; review.

The dielectric properties of polytetrafluorethylene, polychorotrifluoroethylene, polyvinylidene fluoride, and fluorinated ethylene propylene copolymer are reviewed. Relaxation phenomena as a function of temperature and crystallinity is emphasized. Molecular interpretations of the data are discussed. The effects of humidity changes on the dielectric properties of polytetrafluoroethylene and fluorinated ethylene-propylene copolymer show that these polymers are insensitive to humidity changes. Eighty references are cited.

Burnett, E. F. P., Somes, N. F., Leyendecker, E. V., **Residential buildings and gas-related explosions,** *NBSIR 73-208,* 31 pages (June 1973). (Available as COM 74–10127 from the National Technical Information Service, Springfield, Va. 22151.)

Key words: Building; explosion; frequency; gas; gas industry; progressive collapse; risk; statistics; structure.

The findings of an analysis of available statistics concerning the frequency of gas-related explosions in residential buildings are presented. The study was confined to incidents involving piped gas systems as they affect residential and commercial buildings. Though due regard has to be taken of the limitations inherent in the available statistics, it is concluded that in the USA the probability of occurrence of an explosion capable of causing significant structural damage could be 2.2 per million housing units per year.

Bussey, H. E., **Wavelength of a slotted rectangular line containing two dielectrics,** *NBSIR 73-326,* 17 pages (July 1973). (Available as COM 73-11465-AS from the National Technical Information Service, Springfield, Va. 22151.)

Key words: Capacitance; dielectric measurement; slab line; slotted line.

The titled electromagnetic wave property is obtained approximately for a rectangular slab line with two dielectrics. The perturbing dielectric is a thin sheet set on the center conductor and slotted to permit travel of the probe when the line is used as a slotted line. The purpose is to measure an unknown dielectric filling most of the line, but perturbed by the thin sheet.

Candela, G. A., Kahn, A. H., Negas, T., **Magnetic susceptibility of $Co^{4+}(d^5)$ in octahedral and tetrahedral environments,** *J. Solid State Chem.* **7,** No. 4, 360-369 (1973).

Key words: Co^{4+} compounds; crystal fields; magnetic susceptibility; theory of magnetic susceptibility.

Measurements of magnetic susceptibility on compounds containing stoichiometric Co^{4+} are reported. The compound Ba_2CoO_4 has the $Co^{4+}(d^5)$ ion at a tetrahedral site and displays a susceptibility of the expected magnitude for $S=5/2$. The compounds $Ba_3Co_2CO_9$ and $BaCoO_3$ have the Co^{4+} at an octahedral site and show a susceptibility expected for low spin, $S=1/2$. For the low spin case significant deviations from Kotani's calculated susceptibility were observed. Improvement of the theory was made through incorporation of the effects of distortion from perfect octahedral symmetry and the inclusion of higher electronic configurations above t_2^5 in the $^2T_2$ ground state. A case of low spin Ni in octahedral environment is also reported.

Carpenter, B. S., Samuel, D., Wasserman, I., **Quantitative applications of ^{17}O tracer,** *Radiat. Eff. Short Commun.* **19,** 59 (1973).

Key words: Alpha tracks; alumina; cellulose acetate; citric acid; image analyzing system; nuclear track technique; oxygen tracer; thermal neutrons.

We describe the use of alpha tracks from the $^{17}O(n, \alpha)^{14}C$ as a means of oxygen determination and distribution in biological material. A determination of oxygen in alumina and citric acid using enriched tracer was made.

Chertok, B. T., Sheffield, C., Lightbody, J. W., Jr., Penner, S., Blum, D., **Low-q^2 electron scattering from the 15.109-MeV state of ^{12}C and the conserved-vector-current test,** *Phys. Rev. C* **8,** No. 1, 23-36 (July 1973).

Key words: Electron scattering; extrapolation, Γ_γ; low q^2; 1^+ state; 15.11 MeV.

High-precision electron scattering measurements from the 15.109-MeV 1^+ state in ^{12}C are made at $\theta=75$ and $110°$ with $35 \leq E \leq 55$ MeV. From the measurements B ($M1$) is extrapolated to the photon point and the radiative width is determined, $\Gamma_\gamma = 37.0 \pm 1.1$ eV. The corresponding weak magnetism results for β decay and μ capture are given.

Chesler, S. N., Cram, S. P., **Iterative curve fitting of chromatographic peaks,** *Anal. Chem.* **45,** No. 8, 1354-1359 (July 1973).

Key words: Chromatography; curve fittings; moment analysis.

Iterative curve fitting of an eight parameter function to chromatographic peak profiles by nonlinear residual least squares is reported. Gaussian, exponential, and hyperbolic tangent functions are convoluted and iteratively fit to any experimental chromatographic peak shape and integrated to give total statistical moments with errors as small as 1 percent, even for the higher order moments. Exponential and band broadening operators are deconvolved for measurement of physicochemical and analytical studies. The models and calculations may be extended to the resolution of overlapping peaks and complex elution profiles for the measurement of the rate of on-column chemical reactions.

Chignell, C. F., Benzinger, T. H., **Heatburst microcalorimetry,** Chapter 14 in *Methods in Pharmacology* **2,** Part 1, 465-489 (Appleton-Century Crofts, New York, N.Y., 1972).

Key words: Adenosinetriphosphate-thermodynamics; chemical bond energy; coiled helix thermopiles; drug receptor complexing; entropy; enzyme detection+analysis; equilibrium; free energy; free entropy concept; heat of reaction; heatburst principle; hydrogen bonding; immunoreaction calorimetry; microcalorimetry; molecular biology; pharmacology; protein calorimetry; polynucleotide calorimetry; purity assay; reaction coupling; thermodynamics; warfarin.

In this chapter the heatburst principle will be briefly discussed followed by a description of the construction and operation of the heatburst microcalorimeter. In the next section, it will be shown how heat can not only be used as an indicator for chemical or biochemical change but can also be used to derive thermodynamic data for the system under study. In a third section, some further possible applications of heatburst microcalorimetry to current problems in molecular biology and pharmacology will be suggested. In a separate section, following this article, the classical determination of the laws of chemical equilibrium and the driving energies of chemical change will be re-examined, and a new determination, more suited to the objects of molecular biology and pharmacology, will be derived.

Christ, B. W., **Effects of misalignment on the pre-macroyield region of the uniaxial stress-strain curve,** *Met. Trans.* **4,** 1961-1965 (Aug. 1973).

Key words: Bending; capacitance strain gage; tensile; Ti-6Al-4V; uniaxial loading; 4340 steel.

Some bending usually occurs in uniaxial testing systems due to small unavoidable misalignment. The resulting elastic strain gradient can lead to significant differences between axial strain and extreme surface bending strains, especially at small strains. A three-point microstrain measurement around a cylindrical sample permits evaluation of the extreme strains and of the precision of alignment. A three-point, parallel-plate capacitance strain gage having a linear output with displacement was designed to evaluate bending of tensile samples in the microstrain range. The resolution of the gage was 3 parts in 10,000 at plate separations of 0.010 in. Varying misalignment resulted in extreme elastic bending strains at the sample surface of the order of tens to hundreds of micro-in. per in. larger than the axial strain. Analysis of the mechanics of bending in uniaxial loading demonstrated that: 1) the average applied stress divided by the average elastic strain always gives a unique number, Young's modulus, and 2) the average microplastic strain is not uniquely related to the average applied stress, but rather depends upon precision of alignment. The influence of bending on the determination of the average stress at which microplastic flow initiates is discussed, and a method for making meaningful comparisons of plastic microstrain data generated with significant misalignment is suggested.

Clifton, J. R., Beeghly, H. F., Mathey, R. G., **Interim Report No. 7. Chemical resistance and physical durability testing of coating materials,** *NBSIR 73-295,* 22 pages (Aug. 1973). (Available as COM 74-10471 from the National Technical Information Service, Springfield, Va. 22151.)

Key words: Bridge decks; corrosion; creep testing; epoxy coatings; polyvinylchloride coatings; steel reinforcing bars.

The possibilities of protecting steel reinforcing bars embedded in concrete of bridge decks from corrosion by using organic barrier-type coatings are being investigated in this project. This corrosion is accelerated by the chloride ions of the two most commonly applied deicing materials, sodium chloride and calcium chloride.

In this report, physiochemical studies performed on coatings and coated bars are discussed, including: immersion studies of coatings in corrosive solutions; impact and embedded in concrete.

Cohen, E. R., Taylor, B. N., **A reevaluation of the fundamental physical constants,** (Proc. 4th Int. Conference on Atomic Masses and Fundamental Constants, Teddington, England, Sept. 3-7, 1971), Paper in *Atomic Masses and Fundamental Constants,* J. H. Sanders and A. H. Wapstra, Eds., Part 13, 543-563 (Plenum Publishing Co., New York, N.Y., 1972).

Key words: Data analysis; fundamental constants; least-squares adjustments.

This paper is a progress report on our current efforts to revise and update the comprehensive review of the fundamental physical constants by Taylor, Parker, and Langenberg (1), including their set of best or recommended values. That such an updating is necessary just two years after their review appeared is due to the extraordinary amount of new experimental and theoretical work which has since been completed. Here, we very briefly summarize the experimental

and theoretical evidence, with emphasis on the new results which have become available within the last two years, and discuss various treatments of the data. However, no new set of recommended constants is given since such a set will necessarily require the inclusion of the new data which has become available at this Conference.

Collier, R. S., Ellerbruch, D., Cruz, J. E., Stokes, R. W., Luft, P. E., Peterson, R. G., Hiester, A. E., **Mass quantity gauging by rf mode analysis,** *NBSIR 73-318*, 196 pages (June 1973). (Available as N73-27390 from the National Technical Information Service, Springfield, Va. 22151.)

Key words: Gauging; hydrogen; nitrogen; radio frequency; total mass.

This is a summary report of work done to date on NASA (Johnson Space Center) purchase order T-1738B concerning Radio Frequency (RF) Mass Quantity Gauging. Experimental apparatus has been designed and tested which measures the resonant frequencies of a tank in the "time domain." These frequencies correspond to the total mass of fluid within the tank. Experimental results are discussed for nitrogen and hydrogen in normal gravity both in the supercritical state and also in the two phase (liquid-gas) region. Theoretical discussions for more general cases are given.

Collins, R. C., Haller, W., **Protein-sodium dodecyl sulfate complexes: Determination of molecular weight, size and shape by controlled pore glass chromatography,** *Anal. Biochem.* **54,** 47-53 (1973).

Key words: Chromatography; controlled pore glass; molecular size; porous glass chromatography; protein; protein-sodium dodecyl sulfate complexes; sodium dodecyl sulfate-complexes.

The peak position vs log molecular weight curves of protein-SDS complexes chromatographed on controlled pore glass of narrow pore size distribution is linear over a molecular weight range of 17,000-385,000. A glass with a pore size of approximately 500 Å allows the inclusion of all complexes in this range. Peak position curves on glasses with broad pore distributions show decreased resolution and deviate from linearity at low elution coefficients.

Exclusion size analysis of the elution coefficients of individual complexes from different columns with pore diameters ranging from 197 to 650 Å gives from 120 to 423 Å as their longest dimension. Assuming constant hydration and SDS-to-protein ration, the found dimension suggests the shape of a football, rather than a sphere or rigid rod.

Comeford, J. J., Birky, M., **A method for the measurement of smoke and HCl evolution from poly(vinyl chloride),** *Fire Technol.* **8,** No. 2, 85-90 (May 1972).

Key words: HCl: He-Ne laser; poly(vinyl chloride); pyrolysis; smoke; thermal decomposition.

As poly(vinyl chloride) becomes more popular as a building material and electrical insulation, it becomes more important to life safety to determine its smoke and hydrogen chloride evolution characteristics during pyrolysis. The authors have devised a method of measuring the two simultaneously.

Coriell, S. R., Sekerka, R. F., **Morphological stability near a grain boundary groove in a solid-liquid interface during solidification of a binary alloy,** *J. Cryst. Growth* **19,** 285-293 (1973).

Key words: Alloy; grain boundary; morphology; solidification; stability.

In order to further explore the influence of grain boundaries on the phenomenon of morphological stability, we have extended our previous treatment for a pure substance to a binary alloy. For unidirectional solidification at constant velocity, the shape, $y = W(x,t)$, of a nearly planar interface, intersected perpendicularly by a grain boundary, is calculated. The stability-instability criterion is identical to that for an interface without a grain boundary. If the interface is unstable, the main influence of the grain boundary is to provide an initial perturbation and the time evolution of the interface shape can be treated by approximate analytical methods. For times sufficiently large that initial transients have decayed but sufficiently small that linear theory is applicable, $W(x,t)$ is proportional to $\exp(t/\tau)\cos(\omega_0\chi)\exp(-x^2/4\mathscr{D}t)$, where ω_0, τ, and $\mathscr{D}$ are constants that depend on experimental conditions. After initial transients have decayed, a stable interface attains a time-independent shape. For this case, $W(\chi,t\leftarrow\infty)$ is evaluated numerically; it is found that $W(\chi,t\leftarrow\infty)$ can be an oscillatory function of χ. The size of the oscillations and the depth of the grain boundary groove increase as the stability-instability demarcation is approached, giving the specious appearance of premature instability.

Coriell, S. R., Sekerka, R. F., **Morphological stability near a grain boundary groove in a solid-liquid interface during solidification of a pure substance,** *J. Cryst. Growth* **19,** 90-104 (1972).

Key words: Crystal growth; grain boundary; morphological stability; solidification.

In order to explore the influence of a specific type of defect on the phenomenon of morphological instability, we have calculated the time-dependent shape of a nearly planar interface, intersected perpendicularly by a grain boundary, during solidification of a pure substance at constant velocity. The calculational methods and principal assumptions are similar to those employed in previous theories of morphological stability except that the slope of the interface is maintained at a finite and constant value, s, in the immediate vicinity of the grain boundary groove. The position of the solid-liquid interface is described by the equation $y = W(\chi,t)$ where t is the time and $W(\chi, 0)\rightarrow 0$ as $|\chi|\rightarrow\infty$ (all quantities are assumed independent of z). Whereas the stability-instability criterion is found to be identical to that for an interface without a grain boundary, the boundary is found to be an effective initial perturbation. Under conditions for instability the depth of the grain boundary groove increases exponentially with time and an oscillatory instability propagates laterally from the boundary. Under conditions for stability, the interface eventually attains a time-independent shape given by $W(\chi,t\rightarrow\infty)=(-s/a)\exp(-a\chi)$, where $a^2=(\mathscr{G}_S+\mathscr{G}_L)/2T_M\Gamma$, $\mathscr{G}_S$ and $\mathscr{G}_L$ are conductivity-weighted temperature gradients in solid and liquid, respectively, T_M is the melting temperature and Γ is a capillary constant. For conditions corresponding to the demarcation between stability and instability, a mode of thermal grooving, similar to that previously described by Mullins, is found. A meaningful criterion for instability is shown to be the exponential growth of perturbations while, conversely, stability entails their exponential decay; phenomena such as the algebraic increase of amplitude characteristic of thermal grooving are shown to be manifestations of constraints. Finally, the situation where the interface shape is allowed to depend on z is shown to be describable by a superposition of $W(\chi,t)$ with a function $W_0(\chi,z,t)$ that corresponds to the conventional case where the grain boundary is absent.

Creitz, E. C., **Extinction of fires by halogenated compounds—a suggested mechanism,** *Fire Technol.* **8,** No. 2, 131-141 (May 1972).

Key words: Extinguishment; flame inhibition; inhibition mechanisms.

It is suggested that halogenated compounds extinguish diffusion flames by promoting recombination of reactive oxygen atoms to form less reactive molecular oxygen. Oxygen atoms are important in the branching steps of the hydrogen-oxygen chain reaction. For a fuel containing carbon, CO is an intermediate product which appears in the region in which inhibition takes place. Inhibition of its oxidation

appears to take place because of the paucity of hydroxyl radicals which are a product of the hydrogen-oxygen chain reaction. The mechanism is suggested in an attempt to rationalize a number of apparently disparate observations reported in the literature of both normal and inhibited flames. Data in support of the suggested mechanism are discussed.

Creitz, E. C., **Gas chromatographic determination of composition profiles of stable species around a propane diffusion flame,** *J. Chromatogr. Sci.* **10,** 168-173 (Mar. 1972).

Key words: Flame gases; flame inhibition; gas analysis; gas chromatographic techniques.

An analytical method was developed for determining, quantitatively, with a GC, the gases present around a 2.4 cm high propane diffusion flame burning in air. The method gives quantitative results on samples having some constituents which may not be eluted from the column. Outside the yellow mantle the only fuel species found were carbon, hydrogen and carbon monoxide. The oxygen concentration dropped to zero at a distance of 0.57 mm from the yellow mantle indicating that pyrolysis of the fuel was essentially without O_2. The absence of other fuel species implicates the hydrogen-oxygen chain reaction as having a part in the mechanism of inhibition. When CF_3Br was added to the air, its decomposition was complete at a distance of 2.56 mm from the yellow mantle. The decomposition appeared to be chemical rather than thermal.

Creswell, R. A., Lafferty, W. J., **Microwave spectrum, dipole moment, and conformation of 3,6-dioxabicyclo[3.1.0]hexane,** *J. Mol. Spectrosc.* **46,** No. 3, 371-380 (June 1973).

Key words: Boat conformation; dipole moment; microwave spectrum; ring conformation; rotational constants; 3,6-Dioxabicyclo[3.1.0]hexane.

The microwave spectrum of 3,6-dioxabicyclo[3.1.0]hexane has been obtained. The rotational lines of one ring conformation only have been observed and assigned. Ground state rotational constants are $A_0 = 6287.302 \pm 0.011$ MHa, $B_0 = 4683.546 \pm 0.008$ MHz, and $C_0 = 3358.517 \pm 0.089$ MHz. The dipole moment components obtained from Stark effect measurements are $\mu_a = 0.276 \pm 0.010$ D and $\mu_c = 2.47 \pm 0.04$ giving $\mu = 2.485 \pm 0.040$ for the dipole moment of the molecule. The rotational constants and dipole moment components obtained experimentally can be satisfactorily explained only if the boat form is the most stable ring conformation.

Currie, L. A., **On the use of small calculators having stacked registers,** *Anal. Lett.* **6,** No. 9, 847-864 (1973).

Key words: Instruction list; iteration; memory register; operational stack; pop-up; Polish notation; push-down; radioactivity and isotopic calculations; recursion; statistical calculations.

The incorporation of an operational stack considerably enhances the potential of the small calculator. Full use of the stack permits calculations involving a stored constant or two or more intermediate results, but it requires careful planning and execution. Regardless of whether the calculator is "programmable," an explicit instruction list, preferably written down, may contribute greatly to the rapidity and accuracy of such calculations. The "pop-up" feature of the stack is of particular interest, for it can be utilized to increase the permanent storage capacity. A comparison between conventional (memory) storage and stack storage is given, and examples are presented for the application of a calculator having a 4-register stack (plus 1-memory register) to problems involving 2 parameters and/or summations, iterative solution of a transcendental equation, and recursion.

Currie, L. A., **The limit of precision in nuclear and analytical chemistry,** *Nucl. Instrum. Methods* **100,** 387-395 (1972).

Key words: Counting precision; excess variability; limiting precision; photonuclear chemistry; Poisson statistics; single and multiple parameter nuclear analyses; statistical weights; 14 MeV neutron activation.

The precision associated with an experiment in nuclear chemistry or activation analysis is commonly estimated by means of Poisson counting statistics. Such an estimate, as well as the conclusion that the precision may be indefinitely improved by increasing the number of counts obtained, is necessarily wrong when additional sources of random error are operating. Knowledge of the additional, non-Poisson component of random error is required for reliable estimates of parameters and their standard errors, to detect model errors, to plan counting experiments efficiently, and to establish the limit of precision when the Poisson counting error becomes negligible. For these purposes, an iterative computation program—XESS—has been developed to take into account the additional variance and unequal statistical weights. The significance and detectability of excess variance is illustrated with data from studies of photonuclear reactions and activation analysis.

Danielson, S. L., Howe, D. A., **Use of the television vertical interval to broadcast time for everyone and program captions for the deaf,** *Commun. Soc.* **11,** No. 5, 3-6 (Nov. 1973).

Key words: Digital code; integrated circuit chip; program captioning; television; time and frequency dissemination; TvTime.

This paper describes the events leading to the development of the NBS TvTime System for both time and frequency dissemination and program captioning for the deaf. It explains how the system works, its advantages over other systems, and its cost. Finally, it discusses the possible implications of such a system for future communication applications. The text is written in laymen's language to suit the publication.

Davis, G. T., Eby, R. K., **Glass transition of polyethylene: Volume relaxation,** *J. Appl. Phys.* **44,** No. 10, 4274-4281 (Oct. 1973).

Key words: Dilatometer; isothermal volume change; polyethylene; specific volume; superposition; thermal expansion; volume relaxation, WLF.

Data are presented to show that when linear polyethylene is quenched from room temperature to temperatures below 273 K, it exhibits a volume decrease for times long compared with that required to establish temperature equilibrium. The time, temperature, and density dependence of this decrease is shown to be consistent with a relaxation occurring in the amorphous portion (lamella boundary layers) of the samples. The data can be superposed and the shift factors follow the WLF formalism. Analysis by this method yields a T_g of 231 ± 9 K but the uncertainties preclude any correlation with specific volume over the range 1.01 – 1.05 $cm^3\ g^{-1}$. The data indicate the absence of any comparably strong time dependence of the volume near 150 K. This method of detecting a glass transition in partially crystalline polymers is relatively freer of subjective judgment than most.

Dellepiane, G., Gussoni, M., Hougen, J. T., **Hamiltonian, symmetry group, and vibrational coordinates for the nonrigid molecule $CXY_2 - C \equiv C - CXY_2$,** *J. Mol. Spectrosc.* **47,** No. 3, 515-530 (Sept. 1973).

Key words: Double-valued presentation; free internal rotation; Hamiltonian energy operator; non-rigid molecules; permutation-inversion group; vibrational coordinates.

A vibration-torsion-rotation Hamiltonian is derived for a molecule of the type $CXY_2 - C \equiv C - CXY_2$ exhibiting nearly free internal rotation. The Hamiltonian obtained preserves many of the features of the ordinary Wilson-Howard vibration-rotation Hamiltonian and is based qualitatively on the idea of a slowly varying torsional reference configuration from which the atoms make rapid vibrational displacements. The appropriate molecular symmetry group for this molecule

is found to be a double group of the simple Longuet-Higgins permutation-inversion symmetry group. The indeterminacy of symmetry species (single-valued vs double-valued) for coordinates used to describe the small amplitude vibrations is illustrated and clarified using a simple model for the skeletal bending vibrations.

Dewitt, D. P., Richmond, J. C., **Theory and measurement of the thermal radiation properties of metals,** Chapter 1 in *Measurement of Physical Properties: Some Special Properties*, E. Passaglia, Ed., **VI,** Part 1, 1-90 (Interscience Publ., New York, N.Y., 1972).

Key words: Absorptance; electromagnetic theory; emittance; measurement techniques; metals; reflectance; surface effects; thermal radiation properties.

This is a general review of the thermal radiation properties of metals, and includes (1) description and definition of the properties, and a discussion of their interrelationships, (2) a brief review of the physical laws relating to blackbody radiation, (3) discussion of the theory of the interaction of electromagnetic waves with electrical conductors, (4) the effect of surface condition—profile and surface films— on thermal radiation properties of metals, and (5) a review of methods of measuring thermal radiation properties of metals.

Dibeler, V. H., Walker, J. A., McCulloh, K. E., **Observations on hot bands in the molecular and dissociative photoionization of acetylene and the heat of formation of the ethynyl ion,** *J. Chem. Phys.* **59,** No. 5, 2264-2268 (Sept. 1, 1973).

Key words: Ethynyl ion; heat of formation; ionization threshold; mass spectrometry; vacuum ultraviolet.

Photoion yield curves in the vicinity of threshold are obtained for the molecular and the ethynyl ions of acetylene and acetylene-d_2 at ion source temperatures of 360, 298, and 130 K. Weak ionization below the adiabatic threshold for $C_2H_2^+$ and $C_2D_2^+$ is ascribed to the ionization of molecules excited by one quantum of the bending vibrations, ν_4 and ν_5. Consideration of selection rules suggests a change in symmetry from the linear ground state molecule to a bent ground state ion. The 0 K curves for C_2H^+ and C_2D^+ are estimated from the observed 130 K data. Satisfactory agreement is obtained when the 298 K data are compared with a curve calculated from the 0 K curve by convolution with vibrational and rotational distributions. The 0 K thresholds corrected for kinetic energy are used to calculate $\Delta Hf°_0(C_2H^+) = 17.47 \pm 0.01$ eV (402.8 ± 0.2 kcal mol^{-1}) and $\Delta Hf°_0(C_2D^+) = 17.43 \pm 0.02$ eV (402.0 ± 0.5 kcal mol^{-1}). The ionization energy of the ethynyl radical is estimated to be 11.96 ± 0.05 eV.

Diller, D. E., Sarkes, L. A., **Properties data for LNG,** *Amer. Gas Ass. Mon.* **55,** No. 9, 27-28 (Sept. 1973).

Key words: Calculation methods; densities; ethane; liquefied natural gas mixtures; methane; pure components; propane; properties data.

The need for new physical and thermodynamic properties data for liquefied natural gas mixtures at low temperatures is discussed. A plan is given for calculating properties data for liquid mixtures at temperatures well below the critical temperature. The National Bureau of Standards Cryogenics Division's program to provide accurate input data for calculating properties data for LNG is described.

Ederer, D. L., **Cross-section profiles of resonances in the photoionization continuum of krypton and xenon (600-400 Å),** *Phys. Rev. A* **4,** No. 6, 2263-2270 (Dec. 1971).

Key words: Autoionization; configuration interaction; inner shell excitation; photoionization cross section; resonance profiles; uv absorption spectroscopy.

The cross-section profiles in krypton and xenon have been measured for one- and two-electron excitations of the type $ns^2np^6(^1S_0) \rightarrow nsnp^6(^2S_{1/2})mp$ or $ns^2np^6(^1S_0) \rightarrow ns^2np^4(^3P, {}^1D, {}^1S)\, mlm'l'$. These cross sections were assumed to have the form

$$\sigma(E) = C(E) + \sum_i \frac{(E-E_i)(\Gamma_i/2)a_i + (\Gamma_i/2)^2 b_i}{(E-E_i)^2 + (\Gamma_i/2)^2},$$

where the adjustable parameters $C(E)$, b_i, a_i, E_i, and Γ_i were determined by a least-squares unfolding process which separated the smearing effect of the monochromator slit from the true optical density. Parameter values and cross-section curves are given for 12 krypton resonances and 11 xenon resonances.

Ederer, D. L., Lucatorto, T., Madden, R. P., **Resonances in the photoionization continuum of lithium I (55 to 70 eV),** *J. Phys.* **32,** Supplement to No. 10, C4-85—C4-87 (Oct. 1971).

Key words: Absorption; heat pipe; K-edge; lithium; resonances; spectrum.

Resonances in the photoionization continuum of lithium have been observed by absorption spectroscopy in the region of 55 to 70 eV. These resonances are associated with configurations of the type (1 s 2 snl) and (1 snln'l') and lie more than 50 eV above the ionization potential; the lowest lying most prominent of these can be idenitified with configurations of the type (1 s 2 snp) ^{2}P. A multiconfiguration calculation for the first five members of the series (performed by A. Weiss) has yielded values for the energies which agree with experimental results to within 2 eV.

The design of the lithium vapor absorption furnace was based on the heat-pipe principle. Argon, which has very little structure in the region from 55 to 70 eV, was used as a buffer gas and was contained inside the furnace by thin film aluminum windows. The light source was the 180 MeV NBS synchrotron.

Ely, J. F., Hanley, H. J. M., Straty, G. C., **Analysis of the pressure virials and Clausius-Mossotti function for polyatomic gases,** *J. Chem. Phys.* **59,** No. 2, 842-848 (July 15, 1973).

Key words: Clausius-Mossotti function; dielectric virial coefficients; m-6-8 potential; polarizability; polyatomic gases; pressure second virial coefficients; quadrupole moment; statistical mechanics.

Statistical mechanical equations for the second pressure virial coefficient and the second and third dielectric virial coefficients for quadrupolar molecules are evaluated using the *m*-6-8 potential function. The results are compared with experimental data for nitrogen and fluorine. An approximate value for the quadrupole moment of fluorine is estimated. Agreement between theory and experiment is generally good.

Etz, E. S., Robinson, R. A., Bates, R. G., **Dissociation constant of protonated tris(hydroxymethyl)aminomethane in N-methylpropionamide and related thermodynamic quantities from 10 to 55 °C,** *J. Solution Chem.* **2,** No. 4, 405-415 (1973).

Key words: Acidic dissociation; dissociation constant; emf measurements; ionization processes; N-methylpropionamide; solvation; tris(hydroxymethyl)aminomethane.

The dissociation constant of protonated tris(hydroxymethyl)aminomethane (tris · H^+) in the solvent *N*-methylpropionamide (*NMP*) has been determined at intervals of 5 °C from 10 to 55 °C by measurement of the emf of cells without liquid junction using hydrogen and silver-silver chloride electrodes. At 25 °C, pK_a was found to be 8.831, as compared with 8.075 in water. The standard changes in Gibbs energy, enthalpy, and entropy for the dissociation process have been evaluated from the dissociation constant and its change with temperature. By comparison with similar data for the dissociation of tris · H^+ in water, thermodynamic functions for the transfer from water to *NMP* have been derived. The dissociation process is isoelectric, and the solvent dielectric constant is high ($\epsilon =$

176 at 25 °C). Consequently, electrostatic charging effects are expected to be minimal, and the change in dissociation constant depends primarily on solute-solvent interactions. The results, combined with transfer energies for *HCl*, tris, and tris · *HCl* from emf and solubility measurements, demonstrate that the decreased acidic strength of tris · H^+ in *NMP* is attributable in large part to the fact that *NMP* is less effective than water in stabilizing tris and its salts.

Evans, A. G., **Strength degradation by projectile impacts,** *J. Amer. Ceram. Soc.* **56,** No. 8, 405-409 (Aug. 1973).

Key words: Ceramics; fracture; impact; projectiles.

The impacting of ceramic components by small projectiles can lead to strength degradation caused by the formation of Hertzian cracks. The conditions which produce degradation are analyzed in terms of the momentum and elastic properties of the projectile. A critical momentum must be exceeded before strength loss can occur, and the critical condition depends on the surface condition of the ceramic. Comparison of the analytical predictions with data for SiC confirms the reliability of the analysis.

Falge, R. L., Jr., Swartzendruber, L. J., **Influence of clustering on the paramagnetic behavior of a Cu-Ni alloy,** *Phys. Lett.* **44A,** No. 4, 285-286 (June 18, 1973).

Key words: Clustering; critical phenomena; Cu-Ni alloy; heat treatment; magnetism; susceptibility.

The equation usually reserved for the critical behavior of a ferromagnet just above T_c also describes the susceptibility of $Cu_{0.47}Ni_{0.53}$ over a very large temperature range. The parameters, which vary with heat treatment suggest lamellar clustering.

Fatiadi, A. J., **Facile coupling of sterically hindered 2,6-dialkylphenols with periodic acid,** *Synthesis Commun. No. 6,* 357-358 (June 1973).

Key words: Coupling; dialkylphenols; dimethylformamide; hindered; oxidation; periodic acid.

A procedure has been developed by which sterically hindered phenols can produce coupling products (diphenoquinones) in 60 to 94 percent yield when treated with periodic acid in an aqueous N,N-dimethylformamide.

Fatiadi, A. J., **Mechanism of formation of tris(phenylhydrazones) on treatment of cyclohexane-1,3-diones with phenylhydrazine,** *Chem. Ind.*, pp. 38-40 (Jan. 6, 1973).

Key words: Cyclohexane-1,3-dione; formation; free-radical; ionic; mechanism; phenylhydrazine.

The e.s.r. studies show that the formation of the 2-oxo-1,3-bis(phenylhydrazones) and tris(phenylhydrazones) from cyclohexane-1,3-diones, and of bis(phenylhydrazones) from cyclohexane-1,2-diones, following treatment with phenylhydrazine in polar solvents most likely proceeds by a concerted process, involving both ionic and free-radical pathways.

Feldman, A., Horowitz, D., Waxler, R. M., **Laser damage in materials,** *NBSIR 73-268,* 44 pages (Aug. 1973). (Available as AD 768-303 from the National Technical Information Service, Springfield, Va. 22151.)

Key words: Absorption coefficient; calcite; damage threshold; deuterated potassium dihydrogen phosphate; electrostriction; electrostrictive self-focusing; inclusion damage; Kerr effect; laser damage; lithium niobate; nonlinear index of refraction; potassium dihydrogen phosphate; self-focusing; thermal self-focusing; thoria:yttrium oxide ceramic; yttrium aluminum garnet.

Neodymium:glass laser induced damage is observed in lithium niobate ($LiNbO_3$), calcite ($CaCO_3$), potassium dihydrogen phosphate (KDP), and deuterated potassium dihydrogen phosphate (KD*P). The damage at the lowest power levels is caused by inclusions. At higher power levels, filamentary damage, which is indicative of self-focusing, is observed in $LiNbO_3$. An analysis of self-focusing data in yttrium aluminum garnet shows that the Kerr effect is the dominant self-focusing mechanism, with some contribution from the thermal effect. Bulk and surface damage thresholds in neodymium-doped thoria:yttrium oxide ceramic are obtained relative to bulk damage thresholds in several optical materials. For solid materials relationships are obtained between the stress-optic coefficients and the electrostrictive coefficients under different geometric boundary conditions.

Fickett, F. R., **Magnetoresistivity of copper and aluminum at cryogenic temperatures,** *(Proc. 4th Int. Conf. on Magnet Technology, Brookhaven National Laboratory, Upton, N.Y., Sept. 19-22, 1972),* pp. 539-541 (Atomic Energy Commission, Washington, D.C., 1972).

Key words: Aluminum; copper; electrical properties; magnetoresistance.

Results of recent measurements of the magnetoresistance of polycrystalline wires of aluminum and copper are presented. The measurements were made in the temperature range 4 K to 35 K and in magnetic fields to 100 kOe. The aluminum wires ranged in purity from RRR = 1000 – 30 000 and the copper wires from RRR = 200 – 7000. RRR = R(273 K)/R(4 K).

Field, R. W., Tilford, S. G., Howard, R. A., Simmons, J. D., **Fine structure and perturbation analysis of the $a^3\Pi$ state of CO,** *J. Mol. Spectrosc.* **44,** No. 2, 347-382 (Nov. 1972).

Key words: $a^3\Pi$ state; CO; electronic spectra; rotational analysis; vibrational analysis.

The Cameron absorption bands of CO ($v' = 1 - 8$; $v'' = 0$) have been photographed at high resolution. The analysis of these bands along with a reanalysis of the $a^3\Pi$, $v = 0$ level and an analysis of the perturbations of the $a^3\Pi$ state by levels of the $a'^3\Sigma^+$, $e^3\Sigma^+$, $d^3\Delta_i$ and $I^1\Sigma^-$ states will be presented. Deperturbed molecular constants for the $a^3\Pi$ state and accurate perturbation parameters for the interactions of $a^3\Pi$ with nearby states have been determined by a last-squares matrix diagonalization technique. The input data included: (i) earlier measurements from triplet-triplet emission transitions, (ii) the new measurements of the Cameron bands, (iii) rf measurements of $a^3\Pi$ lambda doubling transitions, and (iv) measurements of absorption to the neighboring perturbing states.

Field, R. W., Wicke, B. G., Simmons, J. D., Tilford, S. G., **Analysis of perturbations in the $a^3\Pi$ and $A^1\Pi$ states of CO,** *J. Mol. Spectrosc.* **44,** No. 2, 383-399 (Nov. 1972).

Key words: $a^3\Pi$, $A^1\Pi$ states; CO; configuration interaction; electronic perturbation parameters; matrix element; perturbation analysis.

The results of an analysis of perturbation of the CO $a^3\Pi$ and $A^1\Pi$ states of the...$(\pi 2p)^4(\sigma^2 p)(\pi^* 2p)$ electronic configuration by states of the ...$(\pi 2p)^3(\sigma 2p)^2(\pi^* 2p)$ configuration provide evidence for the following conclusions: (i) For perturbations between vibronic levels of a given pair of electronic states, the perturbation matrix element is the product of a vibrational factor and a constant electronic factor. (ii) Simple single configuration arguments successfully predict that all the electronic factors for the perturbations between levels of each pair of states can be related to two constants which are joint properties of the two electronic configurations $\sigma\pi^n$ and $\pi^3\pi^n$.

Finkel, P. W., Miller, T. R., **A proficiency test assessment of clinical laboratory capability in the United States,** *NBSIR 73-163,* 147 pages (May 1973). (Available as COM-73-11190/8 from the National Technical Information Service, Springfield, Va. 22151.)

Key words: Accuracy; clinical chemistry; hematology; medical usefulness; microbiology; proficiency testing.

The proficiency of a representative sample of physician, hospital and independent laboratories was assessed with respect to their ability to analyse clinical chemistry and hematology samples and to identify microbiological organisms. For the assessment of clinical chemistry and hematology proficiency, the laboratories were grouped, and determinations of group accuracy and group precision were made. Further analyses were performed to determine relative accuracy and precision of the techniques presently applied by these groups. There was no significant difference at the 95 percent confidence level in the accuracy achieved by the various laboratory groups involved in clinical chemistry and hematology analysis. In clinical chemistry, the Medicare-Certified Independent Laboratories, CDC Tested Laboratories and JCAH-Members generally proved more precise than Physician's Office and Medicare-Certified Hospital Laboratories. However, none of the laboratory groups were sufficiently accurate to permit the monitoring over time of variation in an individual patient's constituent concentrations. It would appear that poor selection of techniques was an important contributor to this low performance level. In hematology the Physician's Office Laboratories proved to be the least precise of the groups. There was no noticeable difference in precision between participants in the CDC proficiency testing program and nonparticipants. With respect to microbiology, 76 percent of the identifications by laboratories participating in the CDC testing program were incorrect, while 19.4 percent of all other identifications were incorrect.

Finkel, P. W., Miller, T. R., **A proficiency test assessment of clinical laboratory capability in the United States: Appendix Volume,** *NBSIR 73-163*, Appendix, 48 pages (May 1973). (Available as COM-73-11193/2 from the National Technical Information Service, Springfield, Va. 22151.)

Key words: Accuracy; clinical chemistry; hematology; medical usefulness; microbiology; proficiency testing.

Appendices of NBS Report 73-163 which was abstracted as follows: The proficiency of a selected sample of physician, hospital and independent laboratories was assessed with respect to their ability to analyze clinical chemistry and hematology samples and to identify microbiological organisms. For the assessment of clinical chemistry and hematology proficiency, the laboratories were grouped and determinations of group accuracy and group precision were made. Further analyses were performed to determine relative accuracy and precision of the techniques presently applied by these groups. There was no significant difference at the 95 percent confidence level in the accuracy achieved by the various laboratory groups involved in clinical chemistry and hematology analysis. In clinical chemistry, the Medicare-Certified Independent Laboratories, CDC Tested Laboratories and JCAH-Members generally proved more precise than Physicians' Office and Medicare-Certified Hospital Laboratories. However, none of the laboratory groups were sufficiently accurate to permit the monitoring over time of variation in an individual patient's constituent concentrations. It would appear that poor selection of techniques was an important contributor to this low performance level. In hematology the Physicians' Office Laboratories proved to be the least precise of the groups. There was no noticeable difference in precision between participants in the CDC proficiency testing program and non-participants. With respect to microbiology, 7.6 percent of the identifications by laboratories participating in the CDC testing program were incorrect, while 19.4 percent of all other identifications were incorrect.

Finnegan, T. F., Witt, T. J., Field, B. F., Toots, J., **Measurements of $2e/h$ via the AC Josephson effect,** (Proc. 4th Int. Conf. on Atomic Masses and Fundamental Constants, Teddington, England, Sept. 6-10, 1971), Paper in *Atomic Masses and Fundamental Constants* **4,** J. H. Sanders and A. H. Wapstra, Eds., pp. 403-410 (Plenum Press, New York, N.Y., 1972).

Key words: Josephson junction; standard cell; voltage comparison.

Recent sub-part-per-million determinations of $2e/h$ have been reported by several groups. The accuracies of these determinations have been limited to a large extent by uncertainties in the local voltage standard (i.e., standard cells). The present state of agreement between the various $2e/h$ determinations will be reviewed by using the results of the triennial international volt comparisons at BIPM, as well as the results of direct volt comparisons between NBS and other national laboratories, to relate the various national as-maintained units of voltage.

Progress on the NBS project to maintain a unit of emf via a Josephson junction device will also be reported. The results of a series of $2e/h$ measurements made at the site of the NBS reference group of standard cells will be presented. The implications of these measurements on the stability of the NBS reference group of standard cells, and on the fundamental physical constants (i.e., the fine structure constant) will be discussed.

Flynn, J. H., **Instrumental limitations upon the measurement of temperature and rate of energy production by differential scanning calorimetry,** (Proc. 3d Int. Conf. on Thermal Analysis, Davos, Switzerland, Aug. 23-28, 1971), Paper in *Thermal Analysis*, H. G. Wiedemann, Ed. **1,** 127-138 (Birkhäuser Verlag, Basel, Switzerland, 1972).

Key words: Cooling curve temperature calibration; differential scanning calorimetry; evaluation of thermal apparatus; temperature calibration; thermal analysis.

Instrumental time constants for rate of energy production response, temperature-programming response and temperature-averaging network response, time constants for a wide variety of conditions for interfacial conductivity between the sample and the calorimeter cup, and for the thermal conductivity of the sample are catalogued for the differential scanning calorimeter. Assessment of the effects of these factors upon the net rate of power production sensitivity and the temperature calibration results in the establishment of limits of precision in the measurement of temperature, specific heat and heats and rates of enthalpy change during chemical and physical transformations. The vulnerability of these calibrations to instrumental readjustment and variation in experimental techniques is also quantitatively evaluated.

Frederikse, H. P. R., Hosler, W. R., **Electrical conductivity of coal slag,** *J. Amer. Ceram. Soc.* **56,** No. 8, 418-419 (Aug. 1973).

Key words: Electrical conductivity; slag; transfer.

The electrical conductivity of natural and synthetic slags (containing 14 to 36 wt% Fe) was measured from 1200 to 1700 K at O_2 pressures from 1 to 2×10^{-6} atm. The conductivity is relatively high ($\approx 10^{-2}\ \Omega^{-1}\ cm^{-1}$ at 1700 K) and stems from the transfer of electrons between Fe^{2+} and Fe^{3+} ions. Anomalies in the conductivity around 1600 K are the result of devitrification of the glass samples.

Freeman, D. H., Kuehner, E. C., **Laser detection of small particles in liquids,** *Annals N.Y. Acad. Sci.* **158,** Article 3, 731-740 (June 20, 1969).

Key words: Air pollution; laser; light scattering; liquid pollution; particulate matter; water pollution.

A 0.3 milliwatt He-Ne laser is used with a photomultiplier to survey the light scattered by particulate matter suspended in small (7 ml) samples of liquids. Estimates of weight compositions are inferred by calibration against reference solutions of suspended polystyrene latex. A small size dependence is observed in the particle size range of 0.1 to 2.0 microns. The method is useful in the range of one part per million (PPM) to one part per billion (PPB). Results are reproducible with relative errors of approximately twenty percent.

Samples of solid chemical reagents dissolved in distilled water have been examined. The results show variable contamination levels up to 1 ppm. A sample of NBS pond water indicated 1 ppm. The ef-

fect of ultra filtration is easily demonstrated. As a side benefit, the scattered laser beam is easily inspected in liquids to show gross presence or absence of suspended matter.

Fribush, S. L., Bowser, D., Chapman, R., **Estimates of vehicular collisions with multistory residential buildings,** *NBSIR 73-175*, 72 pages (Apr. 1973). (Available as COM 74–10395 from the National Technical Information Service, Springfield, Va. 22151.)

Key words: Collisions of vehicles with buildings; multistory buildings; progressive collapse of buildings; residential buildings; vehicular impact.

Through analysis of data from Oklahoma and Illinois along with national statistics, estimates are made of the number of vehicular collisions with buildings on an annual, nationwide basis. The best estimate is on the order of tens of thousands. However, since the impetus for the study was on multistory buildings and the likelihood of their being subject to progressive collapse the calculations have been refined to apply to substantial damage to multistory residential buildings. In 1970, such accidents were only on the order of 40, hence the probability of a given building being so affected in a single year is approximately one in 10,000. Some discussion is provided on improvement for data collection for the future.

Fried, C., Ramsburg, R., Butler, S., **A survey of the sanitary conditions of migrant labor camps,** *NBSIR 73-248*, 81 pages (Aug. 1973). (Available as COM 74–10474 from the National Technical Information Service, Springfield, Va. 22151.)

Key words: Health standards; migrant labor camps; questionnaire construction; regulations; survey design.

The Community Health Service (CHS) of the Department of Health, Education, and Welfare has been assigned the responsibility of providing health care services to migrant farmworkers. Since poor sanitation can be a major factor in the health of migrants, CHS requested NBS' Technical Analysis Division (TAD) to perform a field survey of the current state of the sanitary conditions of migrant housing.

A survey form was developed by TAD as an aid in evaluating migrant housing. The form was derived from the checklist procedure employed by sanitarians to determine whether migrant housing meets state and local housing regulations.

Field visits were made to migrant labor camps in five different regions of the United States. These regions were selected because they contained a large number of camps open at the time of the visits. Within each region, camps were selected on a modified random basis.

A description of the findings of the survey is provided in both tabular and narrative form. A discussion of the limitations in the procedures used in conducting the survey is also included, and changes are suggested which could be incorporated into future surveys.

Fuller, E. G., **Photonuclear Physics 1973. Where we are and how we got there,** (Proc. Int. Conf. on Photonuclear Reactions and Applications, Pacific Grove, Calif., Mar. 26-30, 1973), Paper in *International Conference on Photonuclear Reactions and Applications*, B. L. Berman, Ed., pp. 1201-1224 (Ernest O. Lawrence Livermore Laboratory, University of California, Livermore, Calif., 1973). (Available as CONF-730301 from the National Technical Information Service, Springfield, Va. 22151).

Key words: Data; experimental facilities; history; photonuclear reactions; research programs; survey.

A brief history is presented of the study of photonuclear reactions from the time of the first measurements in 1934 through the most recent measurements in 1972 and early 1973. Trends are indicated both for the specific types of measurements carried out, as well as for the geographic areas of the world active in the field. A review is given of the data obtained since 1955 as a function of element and isotope and the areas where data are missing are pointed out. Finally, the results of a survey made in early 1973 are given. This survey covered the existing experimental facilities, as well as the research programs directed toward the study of the interaction of electromagnetic radiation with nuclei.

Fung, F. C. W., **Evaluation of a pressurized stairwell smoke control system for a 12 story apartment building,** *NBSIR 73-277*, 53 pages (June 1973). (Available as PB 225–278 from the National Technical Information Service, Springfield, Va. 22151.)

Key words: Analysis; basic correlation formulas; computer calculations; high-rise building fire; operation BREAKTHROUGH; pressurized stairwell; quantitative experiment; smoke control; smoke simulation.

An NBS study to evaluate the effectiveness of a pressurized stairwell smoke control system in a high rise apartment building is summarized and discussed in the light of experimental results, analysis, and computer prediction. A quantitative experimental technique of smoke simulation and smoke movement measurement is described, supplemented by basic physical laws necessary for correlation with small fires, and illustrated by the results of an actual field experiment. Experiments were conducted in a 12 story apartment building constructed on the Operation BREAKTHROUGH prototype site in St. Louis, Missouri. The experimental results are then further extended to a wider range of ambient weather conditions by way of computer prediction calculations. General conclusions and relevant recommendations as a result of the study are also presented.

Furukawa, G. T., Reilly, M. L., **Application of precise heat-capacity data to the analysis of the temperature intervals of the international practical temperature scale of 1968 in the region of 90 K,** (Proc. 5th Symp. on Temperature, Its Measurement and Control in Science and Industry, Washington, D.C., June 21-24, 1971), Paper in *Temperature, Its Measurement and Control in Science and Industry*, H. H. Plumb, Editor-in-Chief, **4,** Part 1A, 27-36 (Instrument Society of America, Pittsburgh, Pa., 1972).

Key words: Heat capacity; specific heat; temperature intervals; temperature scale.

Precise heat-capacity data were employed to analyze the temperature intervals or smoothness of the International Practical Temperature Scale of 1968 (IPTS-68) between 15 and 380 K, particularly in the region of 90 K, as it is maintained at the National Bureau of Standards. Results show that there are no local irregularities in the temperature scale within the precision (±0.02 percent) of the heat-capacity data between 40 and 380 K. Below 40 to 15 K the uniformity of the temperature scale is less certain because of the lower precision of the heat-capacity data in the temperature range.

Gadzuk, J. W., Plummer, E. W., **Field emission energy distribution (FEED),** *Rev. Mod. Phys.* **45,** No. 3, 487-548 (July 1973).

Key words: Chemisorption; electronic properties of metals; field emission; surface physics.

The technique of measuring the energy distribution of electrons which have been field emitted from a cold cathode is considered. The general historical and introductory theory is presented. A survey of the experimental techniques and existing energy analyzers is given. Specific studies on clean metal surfaces in which work functions, band structure effects, surface states, thermal effects, and many-body effects have been studied are reviewed from both the experimental and theoretical points of view. Field emission energy distributions have been particularly valuable in studies of atoms chemisorbed on surfaces. Several theories of enhanced resonance tunneling due to chemisorbed atoms are discussed. Specific systems studied experimentally are reviewed. Inelastic adsorbate enhanced tunneling is also treated.

Giarrantano, P. J., Hess, R. C., Jones, M. C., **Forced convection heat transfer to subcritical Helium I,** *NBSIR 73-322*, 43 pages (May 1973). (Available as COM 73-11464-AS from the National Technical Information Service, Springfield, Va. 22151.)

Key words: Centrifugal pump; critical heat flux; film boiling; forced convection; heat transfer; helium; nucleate boiling; subcritical; supercritical.

Preliminary results of an experimental investigation of heat transfer to liquid helium under forced flow conditions are reported for a 0.213 cm i.d. × 10 cm long test section subject to the following range of operating conditions:

System pressures 1.1 – 2.1 atm

Mass velocities 4 – 64 g/s-cm²

Heat fluxes 0.04 – 0.53 W/cm²

Inlet subcooling 0.03 – 0.10 K

The effect of the above system parameters on the heat transfer and critical heat flux is discussed; a comparison of forced convection boiling with other modes of heat transfer (pool boiling and supercritical) and the performance of a centrifugal pump used for circulating the liquid helium are also included in the report.

Gilman, F. J., Kugler, M., Meshkow, S., **Pionic transitions as tests of the connection between current and constituent quarks,** *Phys. Lett.* **45B,** No. 5, 481-486 (Aug. 20, 1973).

Key words: Baryon decays; constituent quarks; current quarks; pionic transitions; su(3); $su(6)_w$.

A proposed connection between current and constituent quarks is discussed and tested through comparison with the magnitudes and signs of amplitudes for pionic transitions between hadrons.

Greenspan, M., **Transducer measurements: Use of the current probe,** *J. Acoust. Soc. Amer. Tech. Notes and Res. Briefs* **53,** No. 4, 1186-1187 (Apr. 1973).

Key words: Current probe; impedance measurements; piezoelectric transducer measurements; transducer measurements; ultrasonic instruments.

It has been found that various measurements commonly made on piezoelectric transducers are simplified by use of the current probe, a commercially available instrument. Examples are impedance, ultrasonic interferometry, and power.

Greifer, B., Taylor, J. K., **Survey of various approaches to the chemical analysis of enviromentally important materials,** *NBSIR 73-209*, 237 pages (July 1973). (Available as COM 74–10469 from the National Technical Information Service, Springfield, Va. 22151.)

Key words: Air pollution; atomic absorption; electron microprobe; emission spectroscopy; environmental analysis; industrial effluents; ion-selective electrodes; nuclear activation analysis; particulate analysis; polarography; spark source mass spectrometry; spectrophotometry; trace elements; water pollution; x-ray fluorescence.

Various approaches to the chemical analysis of heavy industry process materials and effluents for trace element constituents that might contribute to environmental pollution are summarized.

The capabilities and costs of nuclear methods, spark source mass spectrometry, x-ray fluorescence and electron microprobe spectrometry, atomic absorption spectrometry, absorption spectrophotometry, atomic emission spectroscopy, voltammetry (polarography) and potentiometry (ion-selective electrodes) for determining traces (less than 100 parts per million) of mercury, beryllium, cadmium, arsenic, vanadium, manganese, nickel, antimony, chromium, zinc, copper, lead, selenium, boron, fluorine, lithium, silver, tin, iron, strontium, sodium, potassium, calcium, silicon, magnesium, uranium, and thorium in such matrices as fly ash, coal, oil, ores, minerals, metals, alloys, organometallics, incinerator particulates, slurry streams, and feeds to and from sedimentation processes have been assessed.

The report includes a critically selected bibliography of the current literature.

Haar, L., **The ideal gas-calorimetric thermometer,** *Science* **176,** 1293-1296 (June 23, 1972).

Key words: Ammonia; calorimetry; flow calorimeter; heat capacity; ideal-gas; temperature; thermodynamic temperature; thermometer.

A new thermometer is suggested for probing the difference between the thermodynamic temperature scale and a practical scale, say the International Practical Temperature Scale–1968. The method is based on the fact that the fractional difference of the heat capacity as measured on two scales is very nearly equal to the temperature derivative of the difference in hotness between the scales. Now, the heat capacity on the thermodynamic scale is by definition that of the ideal gas calculated from the molecular structure using statistical mechanics. This we compare with the analogous quantity measured calorimetrically and extrapolated to the ideal gas limit. The feasibility of the method is illustrated using very accurate data for gaseous ammonia.

Hallowell, P. L., Bertozzi, W., Heisenberg, J., Kowalski, S., Maruyama, X., Sargent, C. P., Turchinetz, W., Williamson, C. F., Fivozinsky, S. P., Lightbody, J. W., Jr., Penner, S., **Electron scattering from ^{19}F and ^{40}Ca,** *Phys. Rev. C* **7,** No. 4, 1396-1409 (Apr. 1973).

Key words: Electron scattering; inelastic; ^{19}F; ^{40}Ca; transition strengths.

Electron scattering form factors were measured for the low-lying levels of ^{19}F and ^{40}Ca for momentum transfers between 0.55 and 1.00 fm^{-1}. Elastic scattering from ^{19}F yields an rms charge radius of 2.885 ± 0.015 fm. Transition strengths and transition radii are obtained for the lowest $5/2^+$, $5/2^-$, and $3/2^+$ states in ^{19}F. A deformed rotational model gives a very good fit to the form factors for the positive-parity levels with ground-state deformation parameters of $\beta_2 = 0.41$ and $\beta_4 = 0.17$. The form factors for excitation of the 3^- and 2^+ states in ^{40}Ca are analyzed by phase-shift analysis, and transition strengths and transition radii are also obtained for these levels.

Hampson, R. F., Garvin, D., Herron, J. T., Huie, R. E., Kurylo, M. J., Laufer, A. H., Okabe, H., Scheer, M. D., Tsang, W., **Chemical kinetics data survey VI: Photochemical and rate data for twelve gas phase reactions of interest for atmospheric chemistry,** *NBSIR 73-207*, 127 pages (Aug. 1973). (Available as AD 769266 from the National Technical Information Service, Springfield, Va. 22151.)

Key words: Atmospheric chemistry; chemical kinetics; data evaluation; gas phase reaction; optical absorption cross section; photochemistry; quantum yield; rate constants.

Photochemical and rate data have been evaluated for twelve gas phase reactions of interest for the chemistry of the stratosphere. The results are presented in data sheets, one for each reaction. For each reaction the data are summarized. A preferred value is given for the rate constant or the primary quantum yield and photoabsorption cross section.

Hartman, A. W., Rosberry, F. W., Simpson, J. A., **A non-contacting length comparator with 10 nanometer precision,** *Opt. Eng.* **12,** No. 3, 95-101 (May/June 1973).

Key words: Dimensional metrology; displacement measurement; microscope; non-contact sensing; optical surface probe; surface detection.

530-326 OL - 74 - 14

A non-contacting length comparator utilizing two specially designed photo-electric microscopes has been constructed. Performance tests of this comparator, using lapped and polished steel surfaces demonstrate a resolution of ~ 1 nanometer, a precision of ~ 10 nanometers, and a linear range in excess of 50 micrometers.

Hastie, J. W., **Mass spectrometric analysis of 1 atm flames: Apparatus and the CH_4-O_2 system,** *Combust. Flame* **21,** 187-194 (1973).

Key words: CH_3; flames; H; mass spectrometry; OH; radicals.

A mass spectrometric system is described for the measurement of reactive intermediates in 1 atm flames. The system has been tested on $CH_4 - O_2$ and $CH_4 - O_2 - N_2$ flames and provides for the first time a complete analysis of such flames for species in excess of 10^{-5} mole fraction concentration.

Hjortenberg, P. E., McLaughlin, W. L., **Use of radiochromic dye systems for dosimetry,** (Proc. Regional Conf. on Radiation Protection, Jerusalem, Israel, Mar. 1973), Paper in *Radiation Protection*, Y. Feige and T. S. Schlesinger, Eds., **1,** 122-140 (Israel Atomic Energy Commission, Yavne, Israel, 1973).

Key words: Accelerator; blood irradiators; dosimetry; electron beams; gamma rays; radiochromic dyes; x-rays.

Radiochromic dye systems have been developed at the U.S. National Bureau of Standards and have been further investigated at the Accelerator Department, The Danish Atomic Energy Commission Research Establishment Riso. Measurable absorbed doses range from 10^2 to 10^6 rads, depending on the particular system. Some characteristic properties are as follows: long shelf life, dose rate independence, low atomic number constituents (C, H, N, O), small temperature dependence, sensitivity to ultraviolet light, linear dose response, rather insensitive to organic impurities. In this paper a liquid system with a useful dose range of 10^2-10^5 rads is described. Results demonstrate its capabilities for calibration of radiation fields including isotope irradiators and electron accelerators. Intercomparisons were made with Fricke- and thermoluminescence dosimetry.

Hord, J., **Cavitation in liquid cryogens. III—Ogives,** *NASA CR-2242,* 235 pages (National Aeronautics and Space Administration, Washington, D.C., May 1973).

Key words: Cavitation; cryogenics; hydrofoil; nucleation; ogives; pumps; venturi.

This document constitutes the third of four volumes to be issued on the results of continuing cavitation studies. Experimental results for three, scaled, quarter-caliber ogives are given. Both desinent and developed cavity data, using liquid hydrogen and liquid nitrogen, are reported here. The desinent data do not exhibit a consistent ogive size effect, but the developed cavity data were consistently influenced by ogive size—B-factor increases with increasing ogive diameter. The developed cavity data indicated that stable thermodynamic equilibrium exists throughout the vaporous cavities. These data were correlated using the extended theory derived in Volume II of this report series. The new correlating parameter, MTWO, improves data correlation for the ogives, hydrofoil, and venturi and appears attractive for future predictive applications. The cavitation coefficient, $K_{c,min}$, and equipment size effects are shown to vary with specific equipment-fluid combinations. A method of estimating $K_{c,min}$ from knowledge of the noncavitating pressure coefficient is suggested.

Hougen, J. T., **Tabulation of hyperfine splittings in rotational F_1 and F_2 levels of the ground vibrational state of $^{12}CH_4$, for $J \leq 20$,** *J. Mol. Spectrosc.* **46,** No. 3, 490-501 (June 1973).

Key words: Computer tabulation; ground vibrational state; hyperfine splittings; methane; quantum mechanical Hamiltonian; rotational levels.

To a good approximation, hyperfine splittings for F_1 and F_2 rotational levels of the ground vibrational state of $^{12}CH_4$ depend linearly on three hyperfine interaction parameters. Coefficients in these linear expressions have been computed in a relatively simple manner and tabulated for levels with $1 \leq J \leq 20$. The hyperfine pattern for the $J = 7$ $F_2^{(2)}$ level computed from these expressions using values for the three hyperfine interaction parameters reported recently by Yi, Ozier and Ramsey [1] agrees well with the pattern obtained from new He-Ne laser measurements of Hall and Bordé [2] on the $P(7)F_2^{(2)}$ line of the ν_3 band of methane.

Hummer, D. G., Kunasz, C. V., Kunasz, P. B., **Numerical evaluation of the formal solution of radiative transfer problems in spherical geometries,** *Comput. Phys. Commun.* **6,** 38-57 (1973).

Key words: Early-type stars; model atmospheres; radiative transfer; spectral line formation; spherical geometry.

If the source function and opacity are specified numerically on a grid of radius and frequency points in a spherically symmetric atmosphere, the program described here calculates the formal solution of the radiative transfer equation, that is, the intensity of radiation on the corresponding grid, and evaluates the first three angular moments of the radiation field. Extensive use of cubic splines in the analysis has made possible an extremely rapid and compact procedure for this calculation. This program has been used extensively in the solution for line formation problems in spherically symmetric atmospheres.

Issen, L. A., **Report of fire tests on flexible connectors in HVAC systems,** *NBSIR 73-267,* 67 Pages (July 1973). (Available as COM 73-11955 from the National Technical Information Service, Springfield, Va. 22151.)

Key words: Aluminum; ductwork; fabric; fiberglass; fire tests; high rise buildings; HVAC systems; steel; terminal units.

The contemporary high rise building with its control air conditioning system and high content of synthetic materials presents a higher hazard than those erected prior to 1950. The ability of the duct work to resist fire breaking into it and spreading through the duct system is an important factor affecting the integrity of the building. Since they penetrate fire barriers, the flexible connectors between the main ducts and the terminal units are important elements in maintaining the desired fire resistance. Flexible connectors made of four different materials (aluminum, galvanized steel, felted fiberglass and woven fiberglass fabric) and two attachment techniques were subjected to fire tests in accordance with ASTM E119. The results show that the materials of the connectors must withstand the fire exposure, the connectors must remain tightly attached to the main duct, and the penetrations through the fire barrier must be suitably blocked in order to prevent fire from breaking into the duct system. The tests also showed that rubber and plastic materials in the terminal units can produce significant amounts of irritating smoke.

Judd, D. B., Eastman, A. A., **Prediction of target visibility from the colors of target and surround,** *Illum. Eng.* **66,** No. 4, 256-266 (Apr. 1971).

Key words: Color; contrast; detection; tritanopia; visibility; vision.

The target visibilities of each of 266 combinations of target and surround colors have been measured by means of the Eastman contrast-threshold visibility meter. The targets and surrounds were Munsell papers, and the targets were of such size and distance from the observer (AAE) that they subtended 10 minutes of arc. Analysis of these data shows that a modification of the 1964 CIE uniform color space applied to the fluxes leaving target and surround accounts for two-thirds of the observed variation in visibility among the 266 combinations. This modification for 10-minute targets consists of neglecting the violet-greenyellow component of the color differences entirely

and of counting the red-green component less than one-tenth that proper for 60-minute targets. By taking into account the fact that the lens system of the human eye, because of chromatic aberration, causes some of the flux leaving the surround to fall on the retinal image of the target, this modified color space has been shown to account for four-fifths of the observed variations in visibility.

Kartaschoff, P., Jarvis, S., Jr., **Notes on infrared absorption experiments in a methane molecular beam,** *NBSIR 73-312*, 32 pages (May 1973). (Available as COM 73-11893/7AS from the National Technical Information Service, Springfield, Va. 22151.)

Key words: Frequency standard; methane resonance; molecular beam; Ramsey resonance; saturated absorption; stabilized laser; transition probability.

The problem of calculating the transition probability of methane molecules in a molecular beam interacting with an infrared (3.39 μ) radiation beam is discussed. Contrary to the usual microwave molecular beam experiments, first-order Doppler frequency shifts cannot be neglected. This makes the solution of the wave-equations more difficult. Weak field approximations to the transition probability have been calculated. Single optical beam experiments analogous to the Rabi-type interaction result in a Doppler-broadened absorption line with an estimated half-power width of a few MHz. For separated multiple field experiments analogous to the Ramsey-type interaction, no observable response is predicted, the expected sharp resonance pattern being smeared out by the random Doppler shifts due to the spread of the molecular beam trajectories. Further investigations are required in order to predict the resonance line shapes for strong fields, i.e., saturated absorption.

Kaufman, V., Sugar, J., **One-electron spectrum of singly ionized ytterbium (Yb II),** *J. Opt. Soc. Amer.* **63,** No. 9, 1168-1172 (Sept. 1973).

Key words: Energy levels; spectrum; ytterbium.

The spectrum produced by the hollow-cathode discharge was measured from 2107 to 1377 Å. With these new data and the previously published observations of Yb II at longer wavelengths, new $4f^{14}nl$ series terms were found, including 1 0s, $7p$, $7-11d$, $5-14f$, and $5-6g$. A value of 98 269(50) cm^{-1} was deduced for the ionization energy.

Kidnay, A. J., Hiza, M. J., Miller, R. C., **Liquid-vapour equilibria research on systems of interest in cryogenics—A survey,** *Cryogenics* **13,** No. 10, 575-599 (Oct. 1973).

Key words: Annotated bibliography; binary systems; cryogenic fluid mixtures; liquid-vapour equilibria; multicomponent systems; survey.

This survey provides a convenient summary of available data on liquid-vapour equilibria for systems of interest in cryogenics. An annotated bibliography of 392 references has been compiled, current to January 1973. These references have been scanned individually with few exceptions, and cross-indexed by system with notation of extent of data and other significant features. The systems included are those made up of the possible combinations of H_2(D_2, HD), N_2, O_2, F_2, CO, H_2S, He(He^3), Ne, Ar, Kr, Xe, and the saturated and unsaturated hydrocarbon through the C_4s.

Klein, W., **Perturbation solution of the Kirkwood-Salsburg equation,** *J. Math. Phys.* **14,** No. 8, 1049-1059 (Aug. 1973).

Key words: Asymptotic behavior at large cluster separations; Banach space; Kirkwood-Salsburg equation; perturbation expansion; product property; strip operator approximation.

A formal series solution to the Kirkwood-Salsburg equation and its radius of convergence are derived. This solution leads naturally to the establishment of an approximate hierarchy of equations for the distribution functions which needs no closure. The asymptotic behavior of the solutions to this approximate hierarchy is studied as well as the behavior of the derivatives of the pair function with respect to the interparticle distance.

Krauss, M., Julienne, P. S., **Dissociative recombination of $e+CH^+$ ($X^1\Sigma^+$),** *Astrophys. J.*, **183,** L139-L141 (Aug. 1, 1973).

Key words: CH, CH^+; dielectronic recombination; electron-ion recombination; energy curve; Rydberg excited state; valence excited state.

The ratio of the dissociative recombination rate for $e+CH^+$ to the dielectronic recombination rate is calculated to be of the order of 10^3. These rates place a serious constraint on homogeneous gas-phase production of interstellar CH^+ and CH from ground-state atoms.

Kruger, J., Ambrose, J. R., **The role of passive film growth kinetics and properties in stress corrosion and crevice corrosion susceptibility,** *NBSIR 73-244*, 75 pages (July 1973). (Available as AD 767326 from the National Technical Information Service, Springfield, Va. 22151.)

Key words: Chloride; crevice corrosion; dissolved oxygen; ellipsometry; nitrates; pH; repassivation kinetics; stainless steel; stress corrosion cracking; titanium alloys.

Repassivation kinetics of an AISI 304 stainless steel have been determined in 1.0N NaCl solutions using the triboellipsometry technique which permits measurement of film growth and total reaction rates following removal of the surface film by abrasion. Although deoxygenation of the solution resulted in little change in either film growth kinetics or the ratio of total change to film thickness (R_p), changing the solution pH affected both the mechanism and rate of film growth which resulted in increased rates of metal dissolution in acidic (pH3) and basic (pH11) solutions.

The triboellipsometry technique was also used to determine repassivation kinetics and stress corrosion cracking (SCC) susceptibility for Ti-8Al-1Mo-1V alloy. Repassivation transient behavior in a 1.0N NaCl solution, where cracks have been found to propagate, was compared to that in a 1.0N $NaNO_3$ solution where SCC susceptibility has never been detected. Susceptibility was found to be related to film growth kinetics in the two solutions.

The early stages of crevice corrosion of AISI 304 stainless steel in 1.0N NaCl solution have been detected using the ellipsometer to measure changes in optical properties occurring within the crevice between a polished metal surface and a glass plate. Changes in the ellipsometer parameters Δ and ψ begin almost immediately upon creation of the crevice and can be interpreted as resulting from a build-up of soluble species within the crevice solution, followed by an overall thinning of the protective film and general corrosion attack.

LaFleur, P. D., Thompson, B. A., **Gamma-ray spectroscopy,** Paper in the *Encyclopedia of Chemistry, Third Edition*, C. Hampel and G. G. Hawley, Eds., pp. 1032-1033 (Van Nostrand Reinhold Co., New York, N.Y., 1973).

Key words: Activation analysis; gamma-ray spectroscopy; Ge(Li) detectors; group separations; instrumentation.

This article has been prepared for the third edition of the Encyclopedia of Chemistry. It is a revision of an article which appeared in the previous edition, published by Reinhold Publishing Company in 1966.

Leasure, W. A., Jr., Bender, E. K., **Tire-road interaction noise,** (Proc. 1973 International Noise Control Engineering Conference, Copenhagen, Denmark, Aug. 22-24, 1973), Paper in *Inter-Noise 73 Proceedings*, O. J. Pedersen, Ed., pp. 421-425 (Inter-Noise 73, Technical University, Lyngby, Denmark, 1973).

Key words: Acoustics; noise (sound); tire noise; transportation noise.

The important parameters influencing tire noise are discussed and the basic mechanisms of tire-noise generation are briefly described from a theoretical viewpoint. Areas for future research are identified—based on gaps in the existing data base and a rather primitive level of understanding of tire noise-generating mechanisms.

Levine, J., Stebbins, R. T., **Ultrasensitive laser interferometers and their application to problems of geophysical interest,** *Phil. Trans. Roy. Soc. London A* **274,** 279-284 (1973).

Key words: Earth tides; interferometer; normal modes; strainmeter.

A 30 m laser strainmeter is currently being operated in an unworked gold mine near Boulder, Colorado. The strainmeter consists of an evacuated Fabry-Perot interferometer illuminated by a 3.39 μm He-Ne laser. A second 3.39 μm laser is stabilized by means of saturated absorption in methane and its wavelength serves as the reference length for the system. We shall describe the instrument in some detail and present the latest results in our investigation of the Earth tides and the Earth normal modes.

Levine, J., Stebbins, R., **Upper limit on the gravitational flux reaching the earth from the Crab pulsar,** *Phys. Rev. D* **5,** No. 7, 1465-1468 (Apr. 1, 1972).

Key words: Crab pulsar; gravitational waves; laser strainmeter; precision interferometry.

A 30-m laser interferometer has been used in a search for gravitational radiation from the Crab pulsar. The minimum detectable signal would be produced by an incident gravitational flux of 10^9 ergs/sec cm^2 and we find no effect at this level.

Livingston, R. C., Rothschild, W. G., Rush, J. J., **Molecular reorientation in plastic crystals: Infrared and Raman band shape analysis of neopentane,** *J. Chem. Phys.* **59,** No. 5, 2498-2508 (Sept. 1, 1973).

Key words: Band shape analysis; diffusion models; infrared; jump diffusion; molecular reorientation; neopentane; phase transition; plastic crystal; Raman; and rotational diffusion.

An infrared and Raman band shape analysis of the broadened 924 cm^{-1} fundamental for neopentane in its liquid and plastic crystal phases is presented. Correlation functions and times for molecular reorientation derived from both the infrared and Raman data show the liquidlike behavior of the plastic phase of neopentane, with the molecules rotating "freely" through $\sim 10°$ (175 K) to $\sim 30°$ (300 K) around an inertial axis with the corresponding reduced intermolecular torques ($< L^2 >^{1/2}/kT$) decreasing from 8.2 to 3.8. Furthermore, the linewidth and correlation time results show no indication of a change in rotational behavior in passing through the plastic crystal-liquid phase transition. Theoretical fits of our experimental infrared and Raman correlation function with Gordon's M and J diffusion models, as extended by McClung for spherical molecules, show that the experimental results lie between the functions predicted by these two models. The time between rotational "collisions" (angular momentum correlation time) varies continuously from 0.4×10^{-12} sec for the room-temperature liquid to 0.2×10^{-12} sec at the lowest temperature in the plastic phase. Activation energies for molecular reorientation of 4.1 and 3.6 kJ/mol are obtained, respectively, from the experimental half-widths and from the angular momentum correlation times, in good agreement with previous NMR and neutron scattering results. The results prove that neopentane melts in two stages: near 140 K, the rotational degrees of freedom of the (rigid) molecule are liberated, whereas near 253 K the translational degrees of freedom are liberated without observable change of the characteristics of the rotational motion.

Llewellyn, L. G., Peiser, C., **NEPA and the environmental movement: a brief history,** *NBSIR 73-218,* 40 pages (July 1973). (Available from the National Technical Information Service, Springfield, Va. 22151.)

Key words: Environment; environmental impact statement; environmental movement; National Environmental Policy Act (NEPA); politics and the environment.

This paper traces some of the critical events leading up to the National Environmental Policy Act (NEPA) of 1969. The opening section spotlights the rapid growth of an environmental ethic in this country, the impact of some highly visible ecological disasters, and the subsequent pressure for environmental reform exerted by opinion leaders and the mass media. The Federal Government's response to perceived changes in public priorities is the focal point of the second section. The activities of Congress and the Nixon Administration are charted in a two-year chronology spanning the 1968 and the 1970 elections, a key period in the development of environmental policy. The final section provides a critique of NEPA with special attention devoted to the controversial requirement for environmental impact statements. The paper concludes with a brief discussion of some of the challenges facing the environmental movement today.

Lovejoy, R. W., Olson, W. B., **Ground state rotational constants for $^{28}SiH_3D$,** *J. Chem. Phys. Letters to Editor* **57,** No. 5, 2224-2225 (Sept. 1, 1972).

Key words: Infrared spectrum; monodeuterosilane; perturbation allowed transitions; rotational constants; stretching vibrations.

The infrared spectrum of the ν_1 and ν_4 stretching vibrations of SiH_3D have been recorded with high resolution. The ground state rotational constants have been determined with much greater precision than has previously been reported. Observed perturbation allowed transitions have also made possible the determination of A_0-$B_0 5D_0^K$.

Lyndon, R., McDonough, T., Newman, M., **On products of powers in groups,** *Proc. Amer. Math. Soc.* **40,** No. 2, 419-420 (Oct. 1973).

Key words: Free groups; powers.

In this note we show that a product of Nth powers in a group cannot in general be expressed as a product of fewer Nth powers. This extends a result of Lyndon and Newman.

Mabie, C. P., **Petrographic study of the refractory performance of high-fusing dental alloy investments: II. Silica-bonded investments,** *J. Dent. Res.* **52,** No. 4, 758-773 (1973).

Key words: Alloy; casting; chromium; investment; mold.

Petrographic study of the refractory performance of silica-bonded investments revealed that recrystallized silica bonds consisting of tridymite and cristobalite are formed during burnout. The major reaction product created during casting is eskolaite. Liquefaction and sintering in the investment at and near its interface with the casting plugs pores and may lower permeability.

Maki, A. G., **Infrared spectra of CS_2: Measurement of "hot" bands associated with the 2325 cm^{-1} and 2962 cm^{-1} bands,** *J. Mol. Spectrosc.* **47,** No. 2, 217-225 (Aug. 1973).

Key words: Absorption spectra; carbon disulfide; energy levels; high resolution; infrared; molecular spectra.

The $12^01 - 00^00$ and $02^01 - 00^00$ transitions of CS_2 have been measured with a resolution of 0.025 cm^{-1}. The following "hot" bands associated with these transitions were also measured $13^11 - 01^10$, $22^01 - 10^00$, $14^01 - 02^00$, $14^21 - 02^20$, $03^11 - 01^10$, $12^01 - 10^00$, $04^01 - 02^00$, $04^21 - 02^20$, $13^11 - 11^10$, and $22^01 - 20^00$. Improved rotational constants are given for the ground state and the first bending state. A consistent set of band constants is given for all the above vibrational transitions.

Maki, A. G., Johnson, D. R., **Microwave spectra of carbonyl sulfide: Measurements of ground state and vibrationally excited $^{16}O^{13}C^{32}S$, $^{18}O^{12}C^{32}S$, and other isotopic species,** *J. Mol. Spectrosc.* **47,** No. 2, 226-233 (Aug. 1973).

Key words: Bond distances; carbonyl sulfide; microwave spectra; molecular parameters; rotational transitions; spectra.

Microwave measurements have been made on isotopically enriched samples of ^{13}C-carbonyl sulfide and ^{18}O-carbonyl sulfide. Centrifugal distortion constants and l-type doubling constants have been determined for these isotopically substituted molecules. Rotational constants have been measured for all vibrational states below 2150 cm^{-1} and B_e values have been determined. The equilibrium bond distances calculated from different pairs of isotopes are compared and a substitution equilibrium structure is given. Some new measurements are also reported for the isotopic species $^{18}O^{13}C^{32}S$, $^{18}O^{13}C^{34}S$, $^{18}O^{12}C^{34}S$, and $^{16}O^{13}C^{34}S$.

Mandel, J., **Structure analysis in two-way tables of measurement data,** *Proc. 39th Session of the International Statistical Institute, Vienna, Austria, Aug. 20-30, 1973,* **2,** 697-705 (International Statistical Institute, Vienna, Austria, 1973).

Key words: Analysis of variance; interaction; principal components; structure; two-way tables.

A general procedure is presented for the elucidation of the structure of a two-way table. The method is based on a partitioning of the row by column interaction into a sum of multiplicative terms. To this partitioning corresponds a breakdown of the sum of squares of interaction and of the corresponding degrees of freedom in the analysis of variance table.

By studying the interrelationships of the parameters occurring in the model, the internal structure of the data can generally be ascertained. An illustrative example taken from an actual study is discussed.

Martin, W. C., Sugar, J., **Classifications of the resonance lines of europium** III, *Astrophys. J.* **184,** 671-674

Key words: Atomic ions; atomic spectra; classified lines; energy levels; europium; ionization energy; stellar spectra.

A first analysis of Eu III by Russell *et al.* in 1941 yielded classifications of seven lines (2350-2523 Å) as transitions from the $4f^7\ {}^8S^0_{7/2}$ ground level to upper levels identified only as belonging to the $4f^6\ 5d$ configuration. We have diagonalized a truncated energy matrix for $4f^6(^7F)5d$, using parameter values appropriate for Eu III. Comparison of the results with available data for the lines allows identifications of the seven experimental upper levels. These show that the seven lines include the three lines of the basic $4f^7\ {}^8S^0 - 4f^6(^7F)5d\ {}^8P$ multiplet, the strongest resonance lines of Eu III, and account for most of the oscillator strength of the $4f^7\ {}^8S^0 - 4f^6\ 5d$ group.

Masters, L. W., Wolfe, W. C., Rossiter, W. J., Jr., Shaver, J. R., **State of the art on durability testing of building components and materials,** *NBSIR 73-132,* 128 pages (Mar. 1973). (Available as PB222300 from the National Technical Information Service, Springfield, Va. 22151.)

Key words: Accelerated aging; aging of buildings; building components; climate; criteria; deterioration; durability; materials: mechanisms; nondestructive testing; testing.

This report is a summary of the present knowledge pertaining to durability predictions for building components and materials which are subjected to the effects of outdoor exposure. The various chapters of the report include discussions of the nature of aging, the measurement of properties to predict durability, nondestructive evaluation techniques, outdoor exposure techniques, accelerated aging techniques, techniques for applying testing data to durability predictions and difficulties which arise in predicting durability. Conclusions and recommendations are also included.

An appendix, which summarizes ASTM Standards for durability testing of building components and materials, is included.

McNeil, M. B., **Report to AID on an NBS/AID workshop on standardization and measurement services in industrializing economics,** *NBSIR 73-275,* 64 pages (May 4-18, 1973). (Available as COM 74-10126 from the National Technical Information Service, Springfield, Va. 22151.)

Key words: AID; assistance; economics; foreign relations; industrializing nations; LDC's; measurement services; standardization.

On May 4-18, 1973, a Workshop was held at the National Bureau of Standards (Gaithersburg), under the sponsorship of AID, whose object was to give standards officials of industrializing nations insight into the standards and measurement systems in the United States and the role of the National Bureau of Standards, so that these officials might consider what parts of the U.S. system might usefully be adapted to conditions in their home countries. The report contains copies of speeches and presentations by representatives of both the U.S. and the industrializing nations, in addition to a general agenda of talks, presentations, and tours of laboratories both of NBS and of other organizations.

Meinke, W. W., **Is radiochemistry the ultimate in trace analysis?,** *Pure Appl. Chem.* **34,** 93-104 (1973).

Key words: Accuracy error limits; activation analysis; atomic absorption; instrument biases; isotope-dilution; method biases; nuclear track technique; practical samples; radiochemistry; trace analysis techniques.

Proponents of widely-used analysis methods such as atomic absorption, spark source mass spectrometry, polarography, activation analysis, etc. often give the impression that their methods alone can solve a large fraction of the problems of trace analysis. In addition, from time to time new, specialized trace methods are reported and sometimes find use in solving special analytical problems. However, the trace analyst deceives himself and, worse yet, gives false impressions to others unless he is able to understand the biases of his methods and instruments in relation to other possible methods and instruments,—and in addition express these biases quantitatively as accuracy error limits. Our experience at NBS in certifying trace element Standard Reference Materials in matrices as diverse as glass, orchard leaves, gold, zinc, beef liver, tuna fish and coal has given us an insight into the optimum contributions which can be made of these methods. The advantages and disadvantages of activation analysis as well as of several other types of radiochemical methods will be discussed in relation to other trace analysis techniques, based on our NBS experience in practical trace analysis. It is concluded that activation analysis ranks high among the methods for trace analysis of real samples.

Mielenz, K. D., Eckerle, K. L., Madden, R. P., Reader, J., **New reference spectrophotometer,** *Appl. Opt.* **12,** No. 7, 1630-1641 (July 1973).

Key words: Beam geometry; high accuracy; optical design; spectrophotometer; systematic errors; transmittance.

A new single beam spectrophotometer is described in which transmittance is measured by placing samples normal to a parallel beam of light. Collimation and focusing of the main beam are achieved by means of off-axis parabolic mirrors. The wavelength at which the transmittance is to be measured is selected by a plane grating monochromator having off-axis parabolic mirrors and circular holes as entrance and exit apertures. The instrument has an inherent *accuracy* estimated to be 0.0001 transmittance unit. Its *precision* is characterized by a repeatability of 0.00004 transmittance units for neutral-density filters with transmittances between 10 and 30 percent. The design philosophy used to achieve these results is presented. A discussion of some systematic errors commonly

neglected in routine spectrophotometric measurements is given. Systematic errors such as detector nonlinearity and stray radiant energy are measured.

Miller, G. K., Goodman, K. M., **The Shirley Highway Express-Bus-on Freeway demonstration project—first year results,** *DOT/UMTA* **2,** 120 pages (Urban Mass Transportation Administration, Department of Transportation, Washington, D.C., Nov. 1972). (Available as PB 214333 from the National Technical Information Service, Springfield, Va. 22151).

Key words: Bus fringe parking; bus priority lanes; bus priority lanes in District of Columbia; bus transit operation; exclusive bus lanes; express-bus-on-freeway technology; Shirley Highway Corridor in Northern Virginia; urban mass transit demonstration project.

The purpose of the Shirley Highway Express-Bus-On exclusive freeway lane demonstration project is to determine the effectiveness of this technology in easing urban traffic congestion and improving the urban environment. This project, jointly sponsored by the Urban Mass Transportation Administration and the Federal Highway Administration, Department of Transportation, is comprised of three elements—exclusive bus lanes, new feature buses, and park-ride lots coordinated with the express bus service.

The objectives of this demonstration project are: (1) Determine the magnitude of the modal shift (auto-to-bus) in the Shirley Highway Corridor and develop an effective planning tool that may be used to transfer the knowledge gained from the Bus-on-Freeway experiment to other geographic areas; (2) Promote economic viability of transit operation; (3) Reduce traffic congestion during peak periods; (4) Increase people-moving efficiency of Shirley Highway; (5) Reduce vehicle-related air pollution; (6) Reduce travel times for motorists and transit users; (7) Improve reliability of transit service; (8) Increase perceived value of transit; and (9) Improve mobility of young, old, physically handicapped, and low income travelers.

The Technical Analysis Division, National Bureau of Standards is evaluating the demonstration project by monitoring performance in terms of attaining the project objectives, and by determining the contributions of project features to increases in the percentage of commuter trips by bus.

This report presents the results of the evaluation at the end of the first eighteen month period (June 1972) of this multi-year demonstration project.

Miller, G., **The Shirley Highway Express-Bus-on Freeway demonstration project—Project description,** *Report DOT/UMTA* **1,** 87 pages (Urban Mass Transportation Administration, Department of Transportation, Washington, D.C., Aug. 1971). (Available as PB 218983 from the National Technical Information Service, Springfield, Va. 22151).

Key words: Bus fringe parking; bus priority lanes, bus priority lanes in District of Columbia; bus transit operation; exclusive bus lanes, express-bus-on freeway technology; Shirley Highway Corridor in Northern Virginia; Urban Mass Transit Demonstration Project.

This report describes the three major demonstration project elements: (1) the busway, including the exclusive lane on Shirley Highway and the bus priority lanes in the District; (2) the bus transit operation, involving new buses (with special features) on new routes and schedules; and (3) the residential fringe parking, with shopping centers and new lots providing free parking for bus riders. The existing roadway and bus operations are documented and the improvements planned for 1971-72 are presented. The Shirley Highway Corridor where the bus and auto commuters live is described, as is the major employment destination areas. Data are also presented on bus and auto travel volumes for 1970-1971, before the busway was completed and the new buses placed into operation.

Milligan, D. E., Jacox, M. E., Guillory, W. A., **Infrared spectrum on the NO_2^- ion isolated in an argon matrix,** *J. Chem. Phys.* **52,** No. 8, 3864-3868 (Apr. 15, 1970).

Key words: Alkali metal reactions; electron attachment; infrared spectrum; matrix isolation; NO_2^-; photodetachment; photoionization.

The molecular ion NO_2^- has been stabilized in an argon matrix in sufficient concentration for detection of its antisymmetric stretching fundamental, ν_3, at 1244 cm^{-1} by electron bombardment or photoionization of matrix-isolated NO_2 and by the interaction of an alkali-metal atomic beam with NO_2 in an argon matrix. In contrast to the position of this fundamental in an inert, nonionic environment, a value of approximately 1275 cm^{-1} is characteristic of the crystalline material. Isotopic data are consistent with a 115° valence angle for NO_2^-, independent of environment. Irradiation of the sample with light of wavelength near 3150 Å leads to the destruction of the NO_2^- absorption in the studies of the electron bombardment and photoionization of NO_2, but not in the experiments in which the alkali metal atoms provide a reservoir of photoelectrons.

Milligan, D. E., Jacox, M. E., **Infrared and ultraviolet spectroscopic studies of a number of small free radicals and molecular ions in a matrix environment,** (Proc. Symp. on Spectroscopic Methods in Cryochemistry and of the Chemistry of High Temperature Species, Minneapolis, Minn., Apr. 1969), Paper in *Advances in High Temperature Chemistry*, Leroy Eyring, Ed. **4,** 1-42 (Academic Press, Inc., New York, N.Y., 1971).

Key words: Free radicals; infrared spectrum; matrix isolation; molecular ions; photolysis; ultraviolet spectrum.

The development of the matrix isolation technique is summarized, and the principles which have been found to be important for the *in situ* photoproduction of free radicals trapped in inert solid matrices in sufficient concentration for direct infrared and ultraviolet spectroscopic observation are considered. A survey of the small free radical species heretofore studied using these techniques is given. Examples of the successful application of the technique are drawn from recent studies of the vacuum-ultraviolet photolysis of matrix-isolated methane and silane and of their chloro- and fluoro-derivatives. Results of experiments designed to permit the trapping in inert, nonionic matrices of negatively charged molecular ions are presented.

Molino, J. A., **Pure-tone equal-loudness contours for standard tones of different frequencies,** *Perception Psychophysics* **14,** No. 1, 1-4 (1973).

Key words: Loudness; noise; psychoacoustics; psychophysics.

Six Ss made judgments of equal loudness by adjusting the intensity of comparison tones of 10 different frequencies. The comparison tones were presented diotically alternately with standard tones. Each standard tone remained fixed at one frequency (125, 1,000, or 8,000 Hz) and one intensity (10, 20, 40, or 70 dB sensation level) while collecting the data for any single equal-loudness contour. In this manner, families of equal-loudness contours were generated for each of the three standard frequencies. The contours for the 1,000-Hz standard were compared with those in the literature. The families of contours for the 125- and 8,000-Hz standards, determined by the same algorithm, differed in the spacing of the contours from the 1,000-Hz standard family as well as from each other. Implications for the reflexive, symmetric, and transitive properties of the equal-loudness relation are discussed.

Mopsik, F. I., Broadhurst, M. G., **Grüneisen constants of polymers,** *J. Appl. Phys.* **44,** No. 10, 4261-4264 (Oct. 1973).

Key words: Bulk modulus; Grüneisen constant; infrared; lattice vibrations; polyethylene; polymers.

One result of recent interest in Grüneisen constants, $\gamma = -d \ln \nu / d \ln V$, of polymers is a considerable spread of reported γ's for solids like polyethylene. From elasticity data (bulk modulus or sound velocities for example) one finds $\gamma \approx 6$ for linear polymer solids. Values of γ from thermal data are much lower than 6 because the relationship usually employed, $\gamma = \alpha BV/C_v$, is not valid for polyatomic solids. Measurements of the shifts in lattice frequencies with volume strains are the most direct way of measuring γ. However, the results for pressure-induced strains differ from those for temperature-induced strains, and both differ from the results from elasticity data. In this paper we consider vibrations in a simple anharmonic well and show how the apparent shifts in vibrational frequency with pressure and temperature can be derived from changes in force constants.

Morris, J. C., Walker, J. H., **Electron-neutral transport cross section of mercury,** *J. Appl. Phys.* **44,** No. 10, 4558-4561 (Oct. 1973).

Key words: Arc mercury; conductivity; cross section; electrical conductivity of mercury; electron-neutral; electron-neutral transport cross section of mercury; mercury arc.

The electron-neutral transport cross section and the electrical conductivity of Hg have been determined using a constricted dc Hg arc. This arc has a novel configuration which permits the precise measurement of the pressure, the voltage gradient, the temperature profile, and the total current. For the temperature range 5000-6500 K, the electron-neutral transport cross section was found to be 1×10^{-14} cm^2 with a precision of ± 6 percent and an absolute accuracy of ± 20 percent. A description of the apparatus and technique is presented as well as a comparison with other existing data.

Morrissey, B. W., Powell, C. J., **Interpolation of refractive index data,** *Appl. Opt.* **12,** No. 7, 1588-1591 (July 1973).

Key words: Cubic-spline interpolation; cyclohexane; interpolation; polystyrene; refractive index; sapphire.

A comparison of the interpolation of index of refraction data for Czochralski sapphire, cyclohexane, and polystyrene dissolved in cyclohexane using a three-term Sellmeier equation, the Lorentz-Lorenz equation with six terms, third and fifth order polynomials, and a cubic-spline technique indicates that the cubic spline method is extremely valuable for simple interpolation. Not only were the magnitudes of the rms and average absolute residuals the smallest, but the fits showed no systematic errors.

Mosburg, E. R., Jr., **A study of the CW 28-μm water-vapor laser,** *IEEE J. Quantum Electron.* **QE-9,** No. 8, 843-851 (Aug. 1973).

Key words: Infrared laser; vibrational excitation; water vapor discharge; water vapor laser.

The low signal gain of a CW water-vapor laser at 28 μm was measured as a function of the discharge current and pressure. Together with the measurement of other quantities such as the axial electric field and the concentration of OH, a partial interpretation of the mechanisms involved in pumping the 28-μm transition was possible.

Thermal equilibrium between the ν_0, $2\nu_2$, and n_3 vibrational levels will result in a large absorption at the elevated gas temperatures observed (800-1000 K). The strong dependence of gain on the electron temperature strongly suggests that the vibrational excitation proceeds through electron-impact excitation. Only the electron-impact excitation of H_2O is quantitatively capable of overcoming the large thermally induced absorption. Although vibrational-excitation transfer from H_2 to H_2O seems insufficient, by itself, to overcome this absorption, it may provide appreciable additional gain. Pumping of the 28-μm line through electron-ion recombination and by reactions involving OH can be ruled out.

Mulholland, G. W., **Line of symmetry for the classical equation of state,** *J. Chem. Phys.* **59,** No. 5, pp. 2738-2741 (Sept. 1, 1973).

Key words: Classical equation of state; coexistence curve; critical phenomena; diameter of coexistence curve; line of symmetry; liquid-vapor phase transition.

The existence and properties of the Widom-Stillinger line of symmetry are examined for the "classical" equation of state, that is, an equation of state in which the chemical potential is expressed as a power series in density and temperature. In doing this, the chemical potential is shown to be an analytic function of temperature in the two phase region. This analyticity has been anticipated for a number of years.

Mullen, L. O., **High and ultra-high vacuum by pumping with cryocooled surfaces,** (Proc. American Institute of Chemical Engineers, Symp. Series on Cryogenic Pumping, Denver, Colo., 1971), Paper in *Vacuum Technology at Low Temperatures,* **125,** No. 68, 24-30 (1972).

Key words: Cryopumping; cryosorption; gettering; vacuum pump; vapor pressures.

This presentation reviews the principles of pumping with cryogenically-cooled surfaces to produce high and ultra-high vacuum. The theory of cryopumping and entrapment by cryopumping, as well as some advantages and limitations are discussed.

Myers, V. W., **Klein-Gordon equation for a charged particle interacting with an electromagnetic wave,** *J. Franklin Inst. Brief Commun.* **295,** No. 6, 497-499 (June 1973).

Key words: Expectation values; Klein-Gordon equation; plane electromagnetic wave.

A solution of the two-component Klein-Gordon equation is obtained from a solution of the corresponding one-component equation for the example of a charged particle interacting with a plane electromagnetic wave. Expectation values for momentum components and the total energy of the particle are calculated.

Negas, T., Roth, R. S., Parker, H. S., Brower, W. S., **Crystal chemistry of lithium in octahedrally coordinated structures. I. Synthesis of $Ba_8(Me_6Li_2)O_{24}$(Me = Nb or Ta) and $Ba_{10}(W_6Li_4)O_{30}$. II. The tetragonal bronze phase in the system BaO-Nb_2O_5-Li_2O,** *J. Solid State Chem.* **8,** No. 1, 1-13 (1973).

Key words: $Ba_8Nb_6Li_2O_{24}$; BaO-Nb_2O_5-Li_2O systems; $Ba_8Ta_6Li_2O_{24}$; $Ba_{10}W_6Li_4O_{30}$; close-packed oxides; crystal growth; tetragonal bronzes.

The preparation, single crystal growth, and crystallographic properties of a close-packed, eight-layer, hexagonal ($a = 5.803$ Å, $c = 19.076$ Å) modification having the stoichiometry $Ba_8Nb_6Li_2O_{24}$ and of a close-packed, ten-layer, hexagonal ($a = 5.760$ Å, $c = 23.742$ Å) phase with $Ba_{10}W_6Li_4O_{30}$ stoichiometry are discussed. The isostructural $Ba_8Ta_6Li_4O_{24}$ form of the eight-layer phase was also prepared ($a = 5.802$ Å, $c = 19.085$ Å). Proposed crystal structures involve the pairing of lithium and metal (Nb, Ta, or W) octahedra to yield face-sharing units. The relationship of this phenomenon to other known close-packed phases containing Li is demonstrated. An investigation of the $Ba_8Nb_6Li_2O_{24} - Ba_{10}W_6Li_4O_{30}$ system is reported.

A tetragonal bronze phase homogeneity region was delimited at 1200 °C in the $BaO - Nb_2O_5 - Li_2O$ system. A new orthorhombic phase ($a = 10.197$ Å, $b = 14.882$ Å, $c = 7.942$ Å) was prepared with the stoichiometry $Ba_4Li_2Nb_{10}O_{30}$.

Nelson, J. D., Blair, W., Brinckman, F. E., Colwell, R. R., Iverson, W. P., **Biodegradation of phenylmercuric acetate by mercury-resistant bacteria,** *Appl. Microbiol.* **26,** No. 3, 321-326 (Sept. 1973).

Key words: Atomic absorption; biodegradation; mercury-resistant bacteria; mercury transformations; phenylmercuric acetate, Pseudomonas.

Selected cultures of mercury-resistant bacteria degrade the fungicide-slimicide phenylmercuric acetate. By means of a closed system incorporating a flameless atomic absorption spectrophotometer and a vapor phase chromatograph, it was demonstrated that elemental mercury vapor and benzene were products of phenylmercuric acetate degradation.

Newbury, D. E., Yakowitz, H., Myklebust, R. L., **Monte Carlo calculations of magnetic contrast from cubic materials in the scanning electron microscope,** *Appl. Phys. Lett.* **23,** No. 8, 488-490 (Oct. 15, 1973).

Key words: Contrast mechanism; electron backscattering energy filtering; iron; magnetic domains; Monte Carlo methods; scanning electron microscopy; transformer steel.

Monte Carlo calculations confirm that contrast observed in the scanning electron microscope from magnetic domains in materials of cubic anisotropy is due to the alteration of electron trajectories within the specimen. Results are presented for the effects of electron accelerating potential, specimen tilt, and rotation. The contrast arises mainly from the high-energy portion of the back-scattered electron distribution.

Newell, A. C., Baird, R. C., Wacker, P. F., **Accurate measurement of antenna gain and polarization at reduced distances by an extrapolation technique,** *IEEE Trans. Antennas Propagat.* **AP-21,** No. 4, 418-431 (July 1973).

Key words: Antenna gain; antenna polarization; extrapolation technique; 3-antenna technique.

A new technique is described for determining power gain and polarization of antennas at reduced range distances. It is based on a generalized three-antenna approach which, for the first time, permits absolute gain and polarization measurements to be performed without quantitative *a priori* knowledge of the antennas. The required data are obtained by an extrapolation technique which includes provisions for rigorously evaluating and correcting for errors due to proximity and multipath interference effects. The theoretical basis provides a convenient and powerful approach for describing and solving antenna measurement problems, and the experimental method employed illustrates the utility of this approach. Examples of measurements are included which exhibit errors in gain as small as ± 0.11 dB (3σ).

O'Connell, J. S., **Electromagnetic sum rules,** (Proc. Int. Conf. on Photonuclear Reactions and Applications, Pacific Grove, Calif., Mar. 26-30, 1973), Paper in *International Conference on Photonuclear Reactions and Applications,* B. L. Berman, Ed., pp. 71-94 (Ernest O. Lawrence Livermore Laboratory, University of California, Livermore, Calif., 1973). (Available as CONF-730301 from the National Technical Information Service, Springfield, Va. 22151).

Key words: Effective interaction; electron scattering; nucleon-nucleon correlations; photoabsorption; photon scattering; sum rules.

A survey of total and partial nuclear cross section sum rules for photoabsorption and electron scattering is presented. The sums are derived from closure or the dispersion relation and are compared with available data and discussed in the context of the single particle shell model. A few of the rules are model-independent or relate observables, but most are influenced either by the form of the effective two-nucleon interaction or by nucleon-nucleon correlations in the nuclear ground state. The relation of electron scattering sums in the low momentum transfer region to photo sums is emphasized. A new sum rule for elastic photon scattering is given.

O'Connell, J. S., **Neutrino disintegration of the deuteron,** (Proc. Int. Conf. on Few Particle Problems in the Nuclear Interaction, Los Angeles, Calif., Aug. 28-Sept. 1, 1972). Paper in *Few Particle Problems in the Nuclear Interaction,* I. Slaus, S. A. Moszkowski, R. P. Haddock, and W. T. H. van Oers, Eds., pp. 906-909 (North Holland Publishing Co., Amsterdam, The Netherlands, 1972).

Key words: Carbon; deuteron; interaction neutrino; neutron.

The cross section for the reaction $D(\nu_e,e^-)2p$ averaged over the neutrino spectrum expected from the beam stops of high-intensity proton accelerators is given. Calculations were carried out using a multipole expression for the neutrino-nucleus interaction and the effective-range theory for the electromagnetic breakup of the deuteron.

Ogburn, F., Johnson, C. E., **Banded structure of electroless nickel,** *Plating Technical Brief,* pp. 1043-1044 (Oct. 1973).

Key words: Electroless nickel; electroless plating; nickel phosphorus.

The cross section of an electroless nickel deposit was scanned for phosphorus with an electron probe. The variations in phosphorus content corresponded inversely with the degree of etching with the usual nitric-acetic acid etchant, which develops the striations characteristic of electroless nickel deposits.

Ogburn, F., Johnson, C. E., **Effects of electroless nickel process variables on quality requirements,** *NBSIR 73-240,* 34 pages (June 1973). (Available from the National Technical Information Service, Springfield, Va. 22151.)

Key words: Chemical nickel; coatings; electroless nickel; metal coatings; nickel; nickel-phosphorus.

Deposition rate, phosphorus content, hardness, appearance, and metal distribution are reported for deposits from two acid, hypophosphite type electroless nickel baths, one proprietary and one non-proprietary. The baths were operated under a variety of conditions with variations of composition. Extensive data is given on the relation of deposit hardness to phosphorus content and to heat treatment at 100, 200, and 400 °C.

Okabe, H., Dibeler, V. H., **Photon impact studies of C_2HCN and CH_3CN in the vacuum ultraviolet; heats of formation of C_2H and CH_3CN,** *J. Chem. Phys.* **59,** No. 5, 2430-2435 (Sept. 1, 1973).

Key words: Acetonitrile; cyanoacetylene; C_2H; heat of formation; photodissociation; photoionization; vacuum ultraviolet.

A photodissociation process to produce CN $B^2\Sigma$ from C_2HCN and CH_3CN has been studied as a function of incident wavelength. Threshold photon energies required for the production of CN $B^2\Sigma$ from C_2HCN and CH_3CN are 9.41 ± 0.04 and 8.52 ± 0.03 eV, respectively, from which $D_0(C_2H - CN) \leq 6.21 \pm 0.04$ eV and $D_0(CH_3 - CN) \leq 5.32 \pm 0.03$ eV are obtained. The photoionization yield curves have been measured for the C_2HCN^+ and C_2H^+ ions. Threshold photon energies obtained for the production of CN $B^2\Sigma$, C_2HCN^+, and C_2H^+ from C_2HCN lead to the following thermochemical values; I.P.$(C_2HCN) = 11.64 \pm 0.01$ eV, I.P.$(C_2H) = 11.96 \pm 0.05$ eV, $\Delta Hf_0°$ $(C_2HCN) \geq 85 \pm 1$ kcal mol^{-1} (355 ± 4 kJ mol^{-1}). $\Delta Hf_0°$ $(C_2H) = 127 \pm 1$ kcal mol^{-1} (531 ± 4 kJ mol^{-1}) and D_0 $(C_2H - H) = 5.38 \pm 0.05$ eV. $\Delta Hf_0°$ (C_2H) obtained is in good agreement with the recent value obtained directly from a study of the high temperature reactions of graphite with hydrocarbons. $\Delta Hf_0°$ $(CH_2CN) \geq 14 \pm 1$ kcal mol^{-1} (59 ± 4 kJ mol^{-1}) derived from D_0 $(CH_3 - CN)$ agrees within the stated error limit with the value obtained recently by bomb calorimetry. The fluorescence efficiency vs incident wavelength curves for C_2HCN and CH_3CN show several peaks corresponding to Rydberg states indicating that the process is predissociative. The absorption coefficient of C_2HCN has been measured in the vacuum ultraviolet. The photoionization yield curve for C_2HCN^+ shows at least two Rydberg series converging to vibrationally excited C_2HCN^+ ions.

Olf, H. G., Fanconi, B., **Low frequency Raman-active lattice vibrations of *n*-paraffins,** *J. Chem. Phys.* **59,** No. 1, 534-544 (July 1, 1973).

Key words: *n*-paraffins; polyethylene phonon dispersion curves; Raman spectroscopy-lattice vibrations.

Raman spectra in the frequency range 5 – 200 cm^{-1} have been measured for a series of crystalline *n*-paraffins from *n*-C_5H_{12} to *n*-$C_{68}H_{54}$ and also *n*-$C_{32}H_{66}$, *n*-$C_{35}H_{72}$, and *n*-$C_{36}H_{74}$. It is found that the spectral data may be grouped consonant with crystal structures exhibited by *n*-paraffins. The data are used to map out portions of the transverse acoustical phonon dispersion curves of the orthorhombic polyethylenelike lattice and of one triclinic crystalline form. A band whose frequency is independent of chain length is observed for the orthorhombic *n*-paraffins and is assigned to the B_{3g} rotatory lattice mode of polyethylene.

Olson, W. B., **A precision photoelectric azimuthal polarimeter,** *Opt. Eng.* **12,** No. 3, 102-105 (May/June 1973).

Key words: Instrument; polarimeter; polarimetry quartz; signal-to-noise ratio; throughput.

A high precision photoelectric azimuthal polarimeter has been designed and constructed. The instrument is designed to determine the angle of rotation with an accuracy (3σ) of better than 1 part in 10^4. The instrument is of a relatively compact design and quite simple in construction.

Ordman, E. T., **Convergence and abstract spaces in functional analysis,** *J. Undergraduate Math.* **1,** No. 2, 79-96 (Sept. 1969); **2,** No. 1, 25-36 (Mar. 1970).

Key words: Convergence; filter; function space; limit space; linear topological space; net; topological space.

This paper is an expository survey of the theory of limit spaces, discussing and contrasting approaches by way of nets and filters and considering a number of the extant ways of axiomatizing such a structure. Applications are given to a number of common notions of convergence of functions and to the topology of function spaces linear topological spaces.

Ott, W. R., Fieffe-Prevost, P., Wiese, W. L., **VUV radiometry with hydrogen arcs. 1: Principle of the method and comparisons with blackbody calibrations from 1650 Å to 3600 Å,** *Appl. Opt.* **12,** No. 7, 1618-1629 (July 1973).

Key words: Continuum emission coefficient; hydrogen arc; radiometry; vacuum ultraviolet.

A method is described that utilizes the continuum emission from a wall-stabilized arc discharge as a radiometric standard in the vuv. Ultimately, this standard will cover the wavelength range from 500 Å to 3600 Å. Results of a first experiment comparing this method to two other calibration methods in the region above 1650 Å are presented. A calibrated tungsten strip lamp is used between 2500 Å and 3600 Å; the method of blackbody limited lines is applied at two wavelengths in the vuv. The hydrogen arc method depends upon the fact that the continuum emission coefficient for a hydrogen plasma at typical arc temperatures of about 14,000 K is calculable to within a few percent since the essential spectroscopic constants, continuum absorption coefficients, and transition probabilities are exactly known. The accuracy of the method depends primarily on the capability of spatially resolving in an end-on measurement the nearly homogeneous plasma layers near the axis of the cylindrically symmetric arc column.

Ott, W. R., Wiese, W. L., **Far ultraviolet spectral radiance calibrations at NBS,** *Opt. Eng.* **12,** No. 3, 86-94 (May/June 1973).

Key words: Calibrations; deuterium lamp; far ultraviolet; hydrogen; Krefft-Rössler lamp; spectral radiance; transfer standards; wall-stabilized arc.

The range of NBS radiometric calibration services has been extended into the far ultraviolet region of the spectrum where a dc high power hydrogen wall-stabilized arc is used as a primary standard of spectral radiance. A capability in the range 130 nm to 360 nm (overlapping conventional tungsten strip lamp radiometry) is presently available with estimated uncertainties between 5 and 10 percent depending upon wavelength. The status of radiometric source standards in the far ultraviolet is briefly reviewed and the hydrogen arc and NBS calibration facility are described in detail. The use of commercially available mercury Krefft-Rössler lamps and deuterium arc lamps as transfer or secondary standards is discussed and the spectra of these lamps calibrated with the hydrogen arc standard are presented.

Paabo, M., **Analytical methods for the detection of toxic elements in dry paint matrices—a literature survey,** *NBSIR 73-251,* 49 pages (July 1973). (Available as PB 224688 from the National Technical Information Service, Springfield, Va. 22151.)

Key words: Analytical methods; antimony; arsenic; cadmium; lead; mercury; review; selenium; toxic elements in paints.

This report is a summary description of the chemical procedures currently available for the analysis of selected toxic elements in dried paint. The elements included in this report are lead, mercury, cadmium, antimony, arsenic, and selenium. The literature search upon which this report is based was directed primarily toward references pertaining to the analysis of dried paint. A bibliography of 57 references to wet chemical analysis, colorimetry, atomic absorption spectroscopy, electrochemistry, neutron activation analysis, and x-ray emission analysis is presented.

Page, C. H., **Logarithmic quantities and units,** *Proc. IEEE Letters* **61,** No. 10, 1516-1517 (Oct. 1973).

Key words: Decibel; logarithm.

Recent letters on *decibel* are commented upon, and standardization proposed by the International Electrotechnical Commission (IEC) is mentioned.

Parrish, W. R., Hiza, M. J., **Calculated liquid phase thermodynamic properties and liquid-vapor equilibria for fluorine-oxygen (FLOX) mixtures,** *NBSIR 73-338,* 30 pages (Sept. 1973). (Available as COM73-11660 from the National Technical Information Service, Springfield, Va. 22151.)

Key words:; Calculated thermophysical properties; compressed liquid phase, fluorine-oxygen mixtures, hard-sphere model; liquid-vapor equilibria.

Liquid phase thermodynamic properties and liquid-vapor equilibria of fluorine-oxygen mixtures, for which no experimental data exist, have been calculated. The results are based on excess properties predicted from the Snider-Herrington equations, with an adjusted combining rule, and the corresponding data for the pure fluids. Mixtures considered are 0.6, 0.7, 0.8, 0.88, and 0.9 weight fraction of fluorine from 55 to 90 K up to 70×10^5 Pa. In the compressed liquid, molar volumes, enthalpy, entropy, and constant pressure specific heat were determined. Along the saturation boundary, coexistent vapor compositions and solution vapor pressures were determined as well. Corresponding properties of pure fluorine from experimental data have also been included. Results are tabulated in both British and S.I. units.

Pella, P. A., DeVoe, J. R., **Internal standardization in Mössbauer spectrometry,** *Appl. Spectrosc.* **25,** No. 4, 472-474 (July/Aug. 1971).

Key words: Beta-tin; internal standardization; Mössbauer spectroscopy.

The concept of internal standardization is applied in quantitative analytical studies using the Mössbauer spectrometric technique. The

ratio of the absorption intensity of SnO_2 (analyte absorber) to that of β—Sn (internal standard absorber) is measured using $BaSn^{119m}O_3$ as the source. The results demonstrate that the systematic error which arises because of differences in the chemical composition between the analyte samples and standards can be eliminated by using an internal standard.

Penn, D. R., **The concept of the surface molecule in chemisorption,** *Surface Sci.* **39,** 333-340 (1973).

Key words: Density of states at the adsorbate; energy levels; S state adsorbate; surface molecule; tight binding calculation; W substrate.

Under certain circumstances the binding of an adsorbate to a metal surface may be thought of as the formation of a surface molecule composed of the adsorbate and the metal. This point of view is reasonable if the metal density of states at the adsorbate resembles that of an atom, i.e., exhibits a small number of well defined peaks as a function of energy. The width of these peaks must be small compared to the metal band width. Within the context of a simple tight binding model for the metal we find that for an S state adsorbate on W there are certain adsorbate positions for which the surface molecule concept should be valid.

Petersen, F. R., McDonald, D. G., Cupp, J. D., Danielson, B. L., **Rotational constants for $^{12}C^{16}O_2$ from beats between Lamb-dip-stabilized lasers,** *Phys. Rev. Lett.* **31,** No. 9, 573-576 (Aug. 27, 1973).

Key words: Accurate rotational constants; carbon dioxide ($^{12}C^{16}O_2$); Josephson junction; Lamb-dip-stabilized lasers.

New experimental measurements of the frequency separations of 30 pairs of $^{12}C^{16}O_2$ laser lines in the 10.4-μm band and 26 pairs in the 9.4-μm band have been made with Lamb-dip-stabilized lasers. The use of a Josephson junction as the frequency-mixing element simplified the measurements. Uncertainties in existing rotational constants for the laser vibrational levels were reduced 20 to 30 times and an additional rotational constant H_v was determined for the first time.

Phelan, R. J., Jr., Cook, A. R., **Electrically calibrated pyroelectric optical-radiation detector,** *Appl. Opt.* **12,** No. 10, 2494-2500 (Oct. 1973).

Key words: Calibration; detector; infrared; pyroelectric; radiometers; ultraviolet.

An electrically calibrated optical detector has been developed using a pyroelectric response of the plastic, polyvinylfluoride. An in-depth look at the modulation frequency response was performed to substantiate the equivalence of the optical and electrical inputs, indicate the optimum structure and allow for a clearer understanding of the device limitations. The experimental results of the dynamic range, linearity, uniformity, and detectivity confirm the device's utility.

Piganiol, M. P., Balke, S., Branscomb, L. M., Hamada, S., Hookway, H. T., Tell, B. V., **Ad Hoc Group on Scientific and Technical Information OECD, INFORMATION for a changing society, some policy considerations,** *Organisation for Economic Co-operation and Development*, 46 pages (OECD Publications, Paris, France, 1971).

Key words: Information packages; information policy; information systems; information users; OECD; technical information.

Early in 1969 the Secretary General of OECD established an Ad Hoc Group on Scientific and Technical Information, requesting the Group to "explore the nature, magnitude, and implications of the needs for scientific and technical information and data in science, the economy and society, and how these needs may be met through changes in the structures, technologies and policies, and management concepts." The Ad Hoc Group reached 13 conclusions and recommendations dealing with the scope of action of OECD, the usefulness and applicability of scientific and technological information systems, quality control of content and procedure of information systems, education for information system needs, and international cooperation. The report describes the observations and arguments leading to the conclusions and recommendations.

Powell, C. J., **Semiautomated data-recording and control system for an electron energy analyzer,** *Rev. Sci. Instrum.* **44,** No. 8, 1031-1033 (Aug. 1973).

Key words: Auger-electron spectra; characteristic electron energy-loss spectra; digital data-recording and control system; electron energy analyzer; liquid aluminum; tungsten.

A description is given of a digital data-recording and control system that has been used with a high resolution low energy electron scattering apparatus for the measurement of characteristic electron energy-loss spectra and Auger-electron spectra of solids (at room and elevated temperatures) and liquids. This system is based on a multichannel analyzer and has the following features: (a) Specimens can be prepared many times with data accumulated in arbitrarily short times after preparation (prior to specimen contamination), and final spectra of high precision can be obtained by summation of individual runs; (b) the voltage sweep applied to the electron energy analyzer can be calibrated dynamically; and (c) data can be accumulated and the target heated by electron bombardment in a cyclic manner with variable accumulation and heating periods. Characteristic loss spectra of tungsten at 800 °C and of liquid aluminum are presented as examples of operation of the system.

Prince, E., Donnay, G., Martin, R. F., **Neutron diffraction refinement of an ordered orthoclase structure,** *Amer. Mineral.* **58,** 500-507 (1973).

Key words: Aluminum silicate; feldspar; neutron refinement; orthoclase, silicate minerals; silicon aluminum ordering.

The crystal structure of a pegmatitic monoclinic potassium feldspar, $(K_{0.86}Na_{0.10}\square_{0.04})(Si_{3.00}Al_{1.00})[O_{7.96}(OH)_{0.04}]$, from the Himalaya mine in the Mesa Grande pegmatite district, Calif., has been refined with 3-dimensional neutron-diffraction data to an unweighted R value of 0.031 for 721 symmetry-independent observed reflections. Atomic coordinates differ by no more than 3 estimated standard deviations from those of Spencer B adularia, yet the specimen does not have the adularia morphology, and no diffuse reflections with $(h+k)$ odd have been observed. Direct refinement of the tetrahedral cation distribution shows that the Al content of the $T(2)$ sites is not significantly different from zero (actually -0.016 with an e.s.d. of 0.029); in other words the Al-Si ordering in the tetrahedral sites is essentially complete. The mean Si-O distance in the $T(2)$ sites is 1.616 Å, appreciably greater than the values predicted by various regression lines relating bond distance to aluminum content. This indicates that the observed mean $T_1(m)$-O, $T_2(O)$-O, and $T_2(m)$-O bond lengths reported for low albite and maximum microcline are consistent with full Si occupancy. This ordered orthoclase occurs in gem pockets in a microcline-bearing pegmatite. The association suggests stable growth of ordered orthoclase above the field of stability of microcline and metastable persistence to lower temperatures. Perhaps because of more rapid crystal growth, the bulk of the pegmatitic K-feldspar ordered to common orthoclase, then transformed to maximum microcline.

Quindry, T. L., Flynn, D. R., **On a simplified field measurement of noise reduction between spaces,** (Proc. 1973 International Noise Control Engineering Conference, Copenhagen, Denmark, Aug. 22-24, 1973), Paper in *Inter-Noise 73 Proceedings*, O. J. Pedersen, Ed., pp. 199-207 (Inter-Noise 73, Technical University, Lyngby, Denmark, 1973).

Key words: Absorption coefficient; acoustics; airborne sound insulation index; frequency; noise reduction; transmission loss.

This paper investigates the relationships between ratings based on the 1/3-octave band data and more easily obtained ratings of isolation based on A-weighted or C-weighted sound level data. The effects of the source room sound power spectrum, source and receive room absorptions and other parameters on the correlation obtained are discussed.

Reader, J., Epstein, G., **Zeeman effect and revised analysis of singly ionized rubidium (Rb II)**, *J. Opt. Soc. Amer.* **63, No. 9, 1153-1167 (Sept. 1973).**

Key words: Rubidium; spectra; ultraviolet; wavelengths; Zeeman effect.

The spectrum of Rb II has been observed in a sliding-spark discharge with the NBS 10.7-m normal-incidence vacuum spectrograph and in an electrodeless discharge with the NBS 10.7-m Eagle spectrograph in air. The Zeeman effect was observed from 2200 to 5200 Å with an electrodeless lamp in a magnetic field of 31 000 G. The analysis has confirmed all ten of the previously known levels of the $4p^5 5p$ configuration. The $4p^5 4d$, $4p^5 5s$, $4p^5 5d$, and $4p^5 6s$ configurations have been considerably revised and extended. Almost all levels of these configurations are now known, as well as those of $4p^5 6d$, $4p^5 7s$, and $4p^5 4f$, which were newly located. All configurations have been theoretically interpreted, with configuration interaction included. The energy parameters determined from a least-squares fit to the observed level values are compared with Hartree-Fock calculations. The ionization energy as derived from the $4p^5 ns$ series, $n = 5, 6, 7$, is 220 070 ± 25 cm^{-1} (27.285 ± 0.003 eV).

Roberts, J. R., Andersen, T., Sørensen, G., **Determination of atomic lifetimes and absolute oscillator strengths for neutral and ionized titanium,** *Nucl. Instrum. Methods* **110,** 119-125 (1973).

Key words: Absolute transition probabilities; arc; beam foil; experimental; lifetimes; titanium.

Measurements of atomic lifetimes by the beam-foil technique and branching ratios by use of a gas-flow stabilized arc have led to an experimental determination of absolute oscillator strengths of Ti II. Some lifetimes of Ti I, Ti III and Ti IV are also presented.

Robertson, A. F., **Tests indicate venting increases smoke from some polymerics,** *Fire Eng.* **126,** No. 9, 97-98 (Sept. 1973).

Key words: Buildings; cellulosics; fires; polymers; smoke; venting.

The problem of voluminous smoke production during burning of plastic or polymeric materials is considered. Experimental data on smoke density resulting from both smouldering and flaming pyrolysis of cellulosic and polymeric sheet and foam materials are presented and compared. It is concluded that in general, although exceptions occur for specific materials, cellulosics produce much less smoke than polymerics under flaming exposure. The smoke production under smouldering exposure is roughly comparable for the two classes of materials. However, the polymeric materials show a marked increase of smoke production for flaming vs. smouldering while the converse is true for cellulosics. It is suggested that the fire fighting ventilation tactics developed and used for fires involving cellulosic materials may aggravate rather than ameliorate the problem of fighting fires involving polymeric materials.

Rowe, J. M., Livingston, R. C., Rush, J. J., **Neutron quasielastic scattering study of SH^- reorientation in the cubic phases of cesium and rubidium hydrosulfide,** *J. Chem. Phys.* **58,** No. 12, 5469-5473 (June 15, 1973).

Key words: Alkali hydrosulfides; hydrosulfide ion; ion reorientation; neutron scattering; phase transition; quasielastic scattering.

The orientational disorder of the hydrosulfide ions in CsSH (CsCl phase) and RbSH (NaCl phase) has been investigated by quasielastic neutron scattering with high energy resolution ($\Delta E_{1/2max} = 0.25$ meV). The experimental results provide a clear demonstration of the theoretically predicted separation of the quasielastic neutron peaks for rotating groups or molecules into unbroadened and broadened components which reflect, respectively, the geometric and time behavior of the rotation. Jump reorientation of the ions between equilibrium directions is established as the dominant mechanism creating the rotational disorder in the hydrosulfides, and both small-step rotational diffusion and quasifree rotation are clearly ruled out. Average residence times between reorientation jumps are derived from comparisons of the experimental results with theoretical calculations based on jump reorientation models, but it is not possible to determine the equilibrium orientation of the SH^- ions. Mean-square vibrational amplitudes for the hydrogen atoms are also obtained from the observed integrated intensities of the elastic peaks. The present results are compared in detail with previous lower-resolution neutron results on NaSH and CsSH. It is concluded that in most cases measurements using single crystals will be necessary to establish the details of orientation disorder in solids.

Rush, J. J., de Graaf, L. A., Livingston, R. C., **Neutron scattering investigation of the rotational dynamics and phase transitions in sodium and cesium hydrosulfides,** *J. Chem. Phys.* **58,** No. 8, 3439-3448 (Apr. 15, 1973).

Key words: Cesium hydrosulfide; hydrosulfides; ion reorientation; libration; neutron scattering; phase transition; quasielastic; residence time; sodium hydrosulfide.

The rotational motions of the hydrosulfide ions in the trigonal and fcc phases of NaSH and in the pseudo-bcc (CsCl) phase of CsSH have been studied by quasielastic and inelastic neutron scattering. NaSH and CsSH are members of a broad group of compounds $M^+(XY^-)$ which have cubic symmetry in the solid phase just below the melting point and a lower symmetry in lower temperature crystal phases. The measured inelastic neutron spectra above and below the trigonal to cubic phase transition in NaSH show that SH^- ion "librations" about equilibrium orientations persist in passing through the transition. The maximum of the broad librational bands for both NaSH and CsSH occurs near 400 cm^{-1}. A temperature and momentum-transfer (Q) dependent broadening is observed, however, in the quasielastic peaks in the cubic phases of the hydrosulfides, which indicates a rapid reorientation of the SH^- ions. The experimental quasielastic scattering results are compared with theoretical calculations of quasielastic scattering behavior based on the assumption of instantaneous reorientational jumps between a limited number of quasiequilibrium orientations. The widths of the measured quasielastic peaks plotted vs Q show an oscillatory behavior as predicted by the theoretical calculations. An isotropic reorientation model is ruled out, and the differences in the rotational disorder in NaSH and CsSH are discussed. Relaxation times (τ) for the SH^- motions are derived from the theoretical analysis. The τ values for fcc NaSH vary from 0.4 t0 0.15 psec between 103 and 212 °C, while the values for pseudo-bcc CsSH vary from 2.0 to 0.75 psec between 23 and 140 °C.

Saks, T. H., Yates, R. F., Goodman, K. M., **The Shirley Highway Express-Bus-on-Freeway demonstration project-users' reactions to innovative bus features,** *NBSIR 73-265,* 53 pages (June 1973). (Available as COM 73-11453 from the National Technical Information Service, Springfield, Va. 22151).

Key words: Attitudinal survey; bus-on-freeway; exclusive bus lanes; importance assessments; interior bus features; mass transit technology; satisfaction assessments; transit service features.

The Shirley Highway Express Bus-on-Freeway Project demonstrates the application of a new mass transit technology. The elements tested in this demonstration project include: an exclusive bus

lane in the median of a freeway and bus priority lanes in the downtown distribution area; fringe parking facilities which are coordinated with the bus service; new-look/new-feature buses; and extension of service to additional residential areas in an overall systems approach to the improvement of mass transit. As part of the evaluation of this demonstration project, a survey of commuters on board these buses was undertaken in order to obtain users attitudes concerning the special interior bus features as well as transit service features.

The results obtained from this study should be of interest to persons considering how to allocate expenditures for new bus vehicles and transit service improvements.

Bus commuters perceptions of the relative importance of various bus interior features (i.e., carpeting, special lighting, etc.) and transit service features (i.e., reliable schedules, assurance of a seat, etc.) are analyzed in this report, along with their relative satisfaction assessments of the special bus interior features. Analyses were conducted to determine if marginal improvements in interior comfort and aesthetic features proved significantly more appealing to bus commuters. The relative impact of various project marketing and promotional techniques is also presented.

Sanchez, I. C., Colson, J. P., Eby, R. K., **Theory and observations of polymer crystal thickening,** *J. Appl. Phys.* **44,** No. 10, 4332-4339 (Oct. 1973).

Key words: Annealing; comonomer inclusion; copolymers; lamella thickness; theoretical and experimental; thickening; unit cell.

The thickening of polymer crystals during isothermal annealing is usually observed to be an irreversible process. Phenomenological laws that govern such processes take the form of simple proportionalities—flux being proportional to force. For polymer crystals, a thermodynamic force capable of driving the thickening phenomenon arises from the unequal free energies of the fold and lateral surfaces. By analogy with other irreversible phenomena, the rate of crystal thickening is taken to be proportional to the derivative of the surface free energy with respect to crystal thickness. After certain assumptions, integration yields an equation in which three parameters characterize the system: an initial thickness l_0, an equilibrium thickness l^*, and a relaxation time τ which is a function of the "undercooling." The theory provides a basis for considering the effects of parameters such as time, temperature, thermal history, pressure, and liquids on the thickening rate. In particular, the theory adequately describes the time and temperature dependence of crystal thickening in random copolymers of tetrafluorethylene and hexafluoropropylene which exhibit thickening behavior completely analogous to that of homopolymers. During thickening, the unit cell dimensions of *these quenched-crystallized copolymers* decrease in a manner that is consistent with the concept of complete comonomer inclusion upon crystallization.

Santoro, A., Mighell, A. D., **Coincidence-site lattices,** *Acta Crystallogr.* **A29,** Part 2, 169-175 (Mar. 1973).

Key words: Crystal aggregates; crystals; grain boundaries; lattices; sublattices; superlattices.

Coincidence-site lattices are characterized mathematically, in the general case, by a method that can be applied to a pair of original lattices of any symmetry, either metrically identical or metrically different, does not involve inspection and is readily adaptable to computer calculations. The procedure is illustrated by several numerical examples. The proposed characterization of coincidence-site lattices is based on the theory of derivative lattices and makes extensive use of the concepts of superlattice and sublattice. Appended is a simple procedure for determining the transformation matrices needed to generate superlattices and sublattices of any multiplicity.

Santoro, A., Mighell, A. D., **Properties of crystal lattices: The derivative lattices and their determination,** *Acta Crystallogr.* **A28,** Part 3, 284-287 (May 1972).

Key words: Crystallography; lattices; sub-lattices; super-lattices.

Derivative lattices are classified as super, sub and composite, on the basis of the properties of the transformation matrices relating them to the lattice from which they are derived. A method for obtaining the transformation matrices generating these lattices is given. The method has been applied to derivation of the unique super and sublattices in a few important cases.

Seltzer, S. M., Berger, M. J., Rosenberg, T. J., **Auroral bremsstrahlung at balloon altitudes,** *NASA Spec. Publ. 3081,* 25 pages (National Aeronautics and Space Administration, Washington, D.C., 1973).

Key words: Atmosphere; auroral electrons; balloon experiment; bremsstrahlung; energy spectrum; transport calculation.

Data from a Monte Carlo calculation of the transport of electrons and secondary bremsstrahlung are presented in tabular and graphical form. These data describe bremsstrahlung flux spectra at various atmospheric depths between 3.0g/cm² and 15.0 g/cm² caused by a wide-area uniform precipitation into the atmosphere of electrons with energies between 30 and 2000 keV. The angular distribution of the incident electrons has been assumed to be isotropic over the downward hemisphere. A basic set of results is given for incident monoenergetic electron beams, which can be used to treat incident electron beams with any spectrum of interest. A comprehensive set of results, in the form of differential and integral bremsstrahlung flux spectra, has been obtained for the case of electron beams with exponential energy spectra, for e-folding energies between 5 and 200 keV.

Shives, T. R., Willard, W. A., **MFPG detection, diagnosis, and prognosis,** *NBSIR 73-252,* 266 pages (Sept. 1973). (Available as AD 772-082 from the National Technical Information Service, Springfield, Va. 22151.)

Key words: Condition monitoring; failure detection; failure diagnosis; failure prevention; failure prognosis; diagnostic systems.

These proceedings consist of a group of sixteen submitted papers and discussions from the 18th meeting of the Mechanical Failures Prevention Group which was held at the National Bureau of Standards on November 8-10, 1972. Failure detection, diagnosis, and prognosis represent the central theme of the proceedings. Bearing condition monitoring, diagnostic systems technology and applications, and new approaches in sensing and processing are discussed.

Shirley, J. H., **Semiclassical theory of saturated absorption in gases,** *Phys. Rev. A* **8,** No. 1, 347-368 (July 1973).

Key words: Gas laser theory; lamb-dip; saturated absorption.

A three-dimensional theory for the resonant interaction of electromagnetic waves with a gas of two-level atoms is formulated in terms of macroscopic variables. The theory is utilized to find the steady-state attenuation of a plane wave in the presence of another plane wave running in the opposite direction with different amplitude. Contributions are included from the reflection of the oppositely running wave by an induced standing-wave inhomogeneity in the population inversion of the medium. The resulting attenuation and reflection coefficients are expressed as velocity integrals of continued fractions. Correspondence is made with existing gas-laser theories, yielding the formulation of a high-intensity ring-laser theory. Analytic approximations for the coefficients are presented for the Doppler-limit cases of both waves weak, one wave weak, and negligible reflection (rate-equation approximation). More-general cases have been calculated numerically. The attenuation coefficients exhibit a Lamb-dip feature. The relative depth of the dip increases rapidly with power at low saturation levels, slowly at high saturation, and is greater in the attenuation of the weaker wave. The width of the dip is nonlinearly power broadened. The shape of the dip is very nearly

Lorentzian, except for one special case at high power in which the line splits. The propagation equations for the two waves are integrated over long absorption paths. A large resulting attenuation increases the relative size of the dip while decreasing the power broadening.

Simmons, J. D., Keller, R. A., **Interferometric effects on the output of organic dye lasers,** *Appl. Opt.* **12,** No. 9, 2033 (Sept. 1973).

Key words: Dye laser continua; high resolution; interferometric effects; optical components; organic dye lasers; wedged optical surfaces.

This note illustrates the necessity of using wedged optical components in organic dye laser systems to avoid interferometric effects.

Siu, M. C. I., **Equations for thermal transpiration,** *J. Vac. Sci. Technol.* **10,** No. 2, 368-372 (Mar./Apr. 1973).

Key words: Anomalous Knudsen limit; diffuse scattering; irreversible thermodynamics; specular scattering; thermal transpiration.

A formalism for analytically obtaining an expression for the thermal transpiration pressure ratio R is presented. An experimental parameter σ, which is associated with the type of molecule-solid surface collisions, is introduced. A completely diffuse scattering and a completely specular scattering from a solid surface correspond to $\sigma = 0$ and $\sigma = 1$, respectively. A known distribution function is used to derive a practical formula for R in the case of long tubes and very low pressures. Quantitative results obtained from this formula indicate that deviations from completely diffuse scattering of molecules from solid surfaces give rise to an anomalous Knudsen limit.

Smith, M. W., Martin, G. A., Wiese, W. L., **Systematic trends and atomic oscillator strengths,** *Nucl. Instrum. Methods* **110,** 219-226 (1973).

Key words: Atomic oscillator strengths; homologous atoms; isoelectronic sequences; regularities; spectral series; systematic trends.

A number of newly established or significantly improved systematic trends of atomic oscillator strengths in isoelectronic sequences and spectral series are presented. For most of these trends, beam-foil experiments have played a prominent role in supplying critically needed points. Of particular interest are the changes in several transitions of the Be and C sequences brought about by improved beam-foil results and more refined theoretical calculations. Also of significance are newly detected trends in the Li and Al isoelectronic sequences. An example will be given where the analysis of the f-value dependence along a sequence, coupled with an understanding of the changes in the energy level structure, points out areas where future beam-foil experiments would be desirable in clearing up discrepancies. The n^{*3} dependence of oscillator strengths for perturbed series will be illustrated with another interesting example.

Son, B. C., **Fire endurance tests of unprotected wood-floor constructions for single-family residences,** *NBSIR 73-263,* 65 pages (July 1973). (Available as PB225-284 from the National Technical Information Service, Springfield, Va. 22151.)

Key words: Fire endurance; fire test; flame through; full scale; housing; operation BREAKTHROUGH; single family residence; small scale; thermal resistance; wood floor; wood joist.

Fire endurance tests were performed on two full-scale and twelve small scale wood floor constructions. The fire endurance ratings on unfinished wood joist and plywood subfloor constructions varied from 10 to 13 minutes and were mainly determined by the time to "flame through." In small-scale tests, the addition of carpeting with a hair pad delayed the time of "flame through" approximately 8 minutes. Time to "flame through" may be estimated from the thermal resistance of the construction, and may be modified by the effects of applied load or construction details such as gaps, joints, and penetrations.

Son, B. C., Fang, J. B., **Fire spread on exterior walls due to flames emerging from a window in close proximity to a reentrant wall corner,** *NBSIR 73-266,* 35 pages (Apr. 1973). (Available as PB225-286 from the National Technical Information Service, Springfield, Va. 22151.)

Key words: Exterior wall; fire spread; fire test; ignition; operation BREAKTHROUGH; reentrant corner.

As a part of the research program concerning the recommended criteria for fire safety in Operation BREAKTHROUGH, two full scale fire tests were performed on a mockup of a reentrant corner, i.e., the interior corner formed at the intersection of the exterior walls of adjacent buildings, such as townhouses and garden apartments.

In each test, two wall specimens representing exterior walls were erected perpendicular to a wall containing a window opening into a fire room. One wall was located 1 foot east and the other one 5 feet west of the edges of the window. The objective of the reentrant corner fire test was to study the potential ignition and spread of fire from the room to an adjacent exterior combustible wall.

In the first test, charring on the east wall, but no surface ignition was observed during the test. The peak temperature measured did not exceed 350 °C (660 °F). In the second test, surface ignition occurred on the east wall 9 minutes after the wood crib, representing the combustible contents of the room, was ignited. No significant changes were observed on the west wall during either test.

The instantaneous heat flux incident on the east wall just prior to ignition and the total heat energy absorbed were estimated to be on the order of 1.0 W/cm² and 175 Joules/cm² respectively.

Sparks, L. L., Powell, R. L., **Calibration of capsule platinum resistance thermometers at the triple point of water,** (Proc. 5th Symp. on Temperature, Its Measurement and Control in Science and Industry, Washington, D.C., June 21-24, 1971), Paper in *Temperature, Its Measurement and Control in Science and Industry,* H. H. Plumb, Editor-in-Chief, **4,** Part 2, 1415-1421 (Instrument Society of America, Pittsburgh, Pa., 1972).

Key words: Resistance thermometers; temperature measuring instruments; triple point; water.

Temperature determinations by means of a platinum resistance thermometer, both above and below the triple point temperature of water, depend upon an accurate value for the resistance at the triple point, 0.01 °C. A good general methodology for making such a determination was described by H. F. Stimson at the 1955 Temperature Symposium. However, several aspects of the method must be refined or modified for accurate measurements on capsule thermometers. After a series of development tests, we were able to isolate and correct for several types of systematic experimental errors that were significant, but not immediately obvious. Some of the effects that must be carefully controlled in order to guarantee high precision are (1) thermal resistance between the thermometer and the freezing interface; (2) thermal conductance down to the thermometer from the ambient environment; (3) high-resistance electrical leakage between leads in the heat exchange fluid; and (4) freezing conditions in the triple point cell itself. Using the procedures developed during the test program, we have been able to obtain reproducibilities and statistical imprecisions of about 10 $\mu\Omega$ or 100 μK.

Spurgeon, J. C., **Response characteristics of a portable x-ray fluorescence lead detector: Detection of lead in paint,** *NBSIR 73-231,* 37 pages (June 1973). (Available as PB 224645 from the National Technical Information Service, Springfield, Va. 22151.)

Key words: Lead paint detection; portable x-ray fluorescence lead detector; portable x-ray fluorescence lead calibration standards.

The objective of this investigation was to obtain an indication of the validity of the field data resulting from the use of portable x-ray fluorescence lead detectors by local lead paint detection programs. This report is intended to provide guidance in the use of portable x-ray fluroescence lead detectors by housing and/or health authorities who are responsible for the collection and interpretation of field data as part of lead paint control programs.

The response characteristics of such an instrument to conditions that are related to those encountered in the field have been investigated and the results are presented in this report. The effects of calibration standards, state of charge, paint overlayers, substrate, and distance on instrument response are discussed, in addition to the limit of detection and precision. The accomplishment of these tasks required the development of panel-type lead calibration standard. These standards encompass the concentration range from 0.1 mg/cm² to 9.0 mg/cm².

Stabler, T. M., **National program of metrology for Ecuador,** *NBSIR 73-157*, 33 pages (Apr. 1973). (Available as COM 74–10394 from the National Technical Information Service, Springfield, Va. 22151.)

Key words: Calibration and testing; Ecuadorian Institute of Standardization (INEN); field inspections; mass, length, and volume standards; metrology laboratory; model law and regulations; technical education; U.S. AID.

At the request of the Ecuadorian Institute of Standardization (INEN) the U.S. AID made arrangements for a weights and measures advisor to assist in the development of a program for scientific and legal metrology, including the design of a metrology laboratory, inspection system, a training program, and other essential features. A four week survey by an NBS representative has resulted in recommendations for a metrology laboratory, physical standards, an Ecuadorian weights and measures law, regulations, and control program.

Considered also were the Ecuadorian National Standards of mass, length, and volume; precision balances, and other laboratory instruments. A program of technical education was recommended for an INEN engineer (Program Administrator) and for other members of the INEN laboratory staff.

Stephenson, J. C., **Vibrational energy transfer in NO,** *J. Chem. Phys.* **59,** No. 3, 1523-1527 (Aug. 1, 1973).

Key words: Infrared lasers; laser pumping of molecules; nitric oxide; vibrational energy transfer.

Laser-excited vibrational fluorescence measurements have been used to obtain rate constants at room temperature for vibrational relaxation of the $V=1$ state of NO in collisions with He, Ar, H_2, CO, NO, N_2, and CO_2. Pulses from a CO_2 laser, frequency doubled in a tellurium crystal, provided the excitation source. The rate for the $V-V$ exchange $NO(1)+NO(1)\rightarrow NO(0)+NO(2)$ was obtained.

Stillman, R. B., **The concept of weak substitution in theorem-proving,** *J. Ass. Comput. Mach.* **20,** No. 4, 648-667 (Oct. 1973).

Key words: Associative processing; first-order predicate calculus; resolution; subsumption; theorem-proving; unification.

Many of the centrally important predicates which occur within theorem-proving programs involve, in their computation, a subcalculation aimed at determining whether or not a substitution exists satisfying certain constraints. Some of the principal difficulties in achieving efficient theorem-proving programs are traceable to the amount of computation required by this "substitution-existence analysis." In this investigation, the concept of "weak substitution" is introduced and its utility and applicability in the subsumption and unification computations are examined. The main motivation for considering weak substitutions is this: the existence of a *weak* substitution having certain properties is relatively easy to detect, whereas the existence of a substitution proper having the same properties is not. Furthermore, the absence of such a weak substitution is a sufficient condition for the absence of the substitution proper. Using the concept of weak substitution, a particularly efficient implementation of the subsumption and unification computations on an associative processor is presented.

Straty, G. C., Younglove, B. A., **Some sound velocity measurements on liquid fluorine,** *J. Chem. Phys.* **58,** No. 5, 2191-2192 (Mar. 1, 1973).

Key words: Compressed liquid; fluorine; saturated liquid; sound velocity.

Some sound velocity measurements on liquid fluorine at 110 K and 130 K at pressures to 21 MN/m² are reported. Data were acquired prior to a destructive reaction in the cell which prevented further measurements.

Sugar, J., Reader, J., **Ionization energies of doubly and triply ionized rare earths,** *J. Chem. Phys.* **59,** No. 4, 2083-2089 (Aug. 15, 1973).

Key words: Cerium; dysprosium; erbium; europium; gadolinium; hafnium; holmium; ionization energy; lanthanum; lutetium; neodymium; praseodymium; promethium; samarium; terbium; thulium; ytterbium.

Values for the ionization energies of the doubly and triply ionized rare earth atoms have been derived from interpolated spectroscopic properties of the $4f^N ns$ series, and from interpolated energy intervals relating the first series member, $4f^N 6s$, to the ground state. The results in eV are

La III	19.1774(6)	
Ce	20.198(3)	IV 36.758(5)
Pr	21.624(3)	38.98(2)
Nd	22.14(30)	40.41(20)
Pm	22.32(36)	41.09(32)
Sm	23.43(30)	41.37(38)
Eu	24.70(32)	42.65(32)
Gd	20.63(10)	44.01(35)
Tb III	21.91(10)	IV 39.79(20)
Dy	22.79(30)	41.47(20)
Ho	22.84(10)	42.48(32)
Er	22.74(10)	42.65(21)
Tm	23.68(10)	42.69(20)
Yb	25.03(2)	43.74(20)
Lu	20.9596(10)	45.19(2)
Hf		33.33(2)

The values for the doubly ionized atoms agree to within ~ 1 percent with those deduced from thermodynamic measurements on lanthanide oxides. A value for the ionization energy of Gd II of 12.09(8) eV was determined by using new spectroscopic data for Gd II Gd III.

Trechsel, H. R., **Swiss building and housing research activities,** *NBSIR 73-288*, 63 pages (Aug. 1973). (Available as COM73-11861 from the National Technical Information Service, Springfield, Va. 22151.)

Key words: Building research; buildings; cooperation; housing; international; Switzerland.

Following up earlier contacts of CBT management with representatives of Swiss building research organizations, the author visited Switzerland in the Fall of 1972 for two weeks.

This report discusses the results of meetings with representatives of the Swiss Federal Commission for Housing Research (FKW), major educational and research establishments, architects, contractors, builders, and local building officials. Topics covered in the

discussions included building economics, modular coordination, pre-evaluation of performance of housing projects, pre-evaluation of research projects, building design, land use and planning, transportation, and building laws, codes, and standards.

It appears that cooperative programs in any or all of these areas could be profitable to NBS, and to the corresponding Swiss organizations.

Treu, S., **Characterization and testing of interactive graphics for computer-aided design and engineering,** *NBSIR 73-289*, 36 pages (June 30, 1973). (Available as COM 74–10475 from the National Technical Information Service, Springfield, Va. 22151.)

Key words: Characteristics; computer-aided design; interactive graphics; man-machine interaction; performance measurement.

This report presents material developed as part of a long-term "Interactive Computer-Aided Techniques Study." The report outlines the stages of development in the utilization of interactive graphics as a tool for Computer-Aided Design and Engineering (CAD/E). A series of characteristics are presented which are of significance to the designers and users of such systems and a series of questions of evaluative interest posed. These questions are intended to delineate the extent to which a system under examination achieves its stated design objectives. The characteristics are grouped in accordance with the nature and complexity of the experiments which would need to be conducted to establish values for them. The report suggests selected characteristics of particular interest and suggests the design of experiments for examining them in detail. The report makes specific reference to the MEDEA design terminal concept under development within the Graphical Systems and Technology Branch of ECOM.

Verdier, P. H., **Fluctuations in autocorrelation functions in diffusing systems,** Chapter in *Stochastic Processes in Chemical Physics*, K. E. Shuler, Ed., **15,** 137-148 (John Wiley & Sons, Inc., New York, N.Y. 1969).

Key words: Autocorrelation; correlation; diffusion; fluctuations; relaxation; time correlation.

The relative rates of relaxation of the autocorrelation function and the fluctuations in its sampled values are derived for several simple diffusing systems. It is found that in general, the autocorrelation function and its fluctuations relax at rates which are different, but of the same order of magnitude. In the cases studied, the ratio of the relaxation time for the fluctuations to that for the autocorrelation function varies from about 1/2 to about 1 1/6.

Waterstrat, R. M., Manuszewski, R. C., **The chromium-iridium constitution diagram,** *J. Less-Common Metals* **32,** 79-89 (1973).

Key words: Chromium alloys; constitution diagram; equilibrium diagram; iridium alloys; phase diagram.

The Cr-Ir alloy system has been investigated over the entire composition range by metallography, x-ray diffraction and electron microprobe studies. There are two intermediate phases in this system. The β phase possesses a Cr_3Si ($A15$)-type crystal structure and is stable from about 73 to 82 at.% Cr. The ϵ phase has a hexagonal close-packed crystal structure and is stable between 30 and 68 at.% Cr. The face-centered cubic iridium terminal solid solution can dissolve about 28 at.% Cr. Atomic ordering occurs within this solid solution, beginning at about 16 at.% Cr and forming a Cu_3Au type structure up to the limit of solid solubility. Iridium is soluble in the body-centered cubic chromium terminal solid solution to the extent of about 12 at.% Ir at 1680 °C but the solubility decreases at lower temperatures. Two peritectic reactions were observed at 1750 ± 10 °C and at 2200 ± 50 °C. A eutectic reaction is indicated at 1680 ± 10 °C.

Waterstrat, R. M., **The chromium-platinum constitution diagram,** *Met. Trans.* **4,** 1585-1592 (June 1973).

Key words: Alloys; chromium; constitution diagram; equilibrium diagram; phase diagram; platinum.

The system Cr-Pt has been investigated over the entire composition range by metallography, x-ray diffraction, and electron microprobe studies. There is only one intermediate phase and it has a Cr_3Si(A15)-type crystal structure. The fcc platinum terminal solid solution extends to 71 at.pct Cr at 1530 °C and forms a congruent melting maximum at about 1790 °C. Atomic ordering within this solid solution range begins at about 17 at.pct Cr and there is a continuous change from the Cu_3Au-type structure to the CuAu-type structure with increasing chromium content. Two eutectic reactions at 1530 ± 10 °C and 1500 ± 10 °C were indicated and there is evidence of a syntectic reaction at 1580 ± 10 °C. Platinum is soluble in the bcc chromium terminal solid solution up to about 10 at.pct Pt at 1500 °C but the solubility decreases rapidly at lower temperatures.

Wiederhorn, S. M., **Environmental stress corrosion cracking of glass,** (Proc. Int. Conf. on Corrosion Fatigue, Chemistry, Mechanics and Microstructure, University of Connecticut, Storrs, Conn., June 14-18, 1971), Paper in *Corrosion Fatigue*, **NACE-2,** 731-742 (National Association of Corrosion Engineers, Houston, Texas, 1972).

Key words: Cracked propagation of glass; glass; glass fibers; hardness of glass; static fatigue of glass; strength of glass; stress corrosion cracking of glass; structure of glass.

A review is presented on the effect of environment on the strength of glass. The structure of glass and its strength in the absence of environment are discussed briefly. Experimental results on environmental cracking of glass are presented. Finally, theroretical treatments are given and discussed with respect to available experimental data.

Woolley, M. L., **Bibliography of the electromagnetics division June 30, 1972 to June 30, 1973,** *NBSIR 73-320*, 22 pages (June 1973). (Available as COM73–11971 from the National Technical Information Service, Springfield, Va. 22151.)

Key words: Antenna parameters; attenuation; current; electromagnetic measurements; field strength; impedance; waveguide theory.

This bibliography lists the publications of the NBS Electromagnetics Division between June 30, 1972 and June 30, 1973.

Wyly, R. S., Rorrer, D. E., **Field test of hydraulic performance of a single-stack drainage system at the operation BREAKTHROUGH prototype site in King County, Washington,** *NBSIR 73-161*, 66 pages (May 1973). (Available as PB225–310 from the National Technical Information Service, Springfield, Va. 22151.)

Key words: Crossflow; field testing, plumbing; performance criteria, plumbing; performance, functional; single-stack drainage; siphonage, induced; siphonage, self; test loads, hydraulic; trap-seal reduction detector; trap-seal retention.

A procedure for measuring the hydraulic performance of drain-waste-vent (DWV) systems in the field is described, and the results obtained with this procedure in a field demonstration of the hydraulic performance of a single-stack DWV system are presented.

Among the most important criteria for hydraulic performance of drain-waste-vent systems are the following: (1) Trap-seal retention in idle fixtures; (2) Ability of the system to resist the rejection of suds, sewage, or foul gases due to hydrostatic or pneumatic pressures in the DWV system; (3) Absence of cross flow between fixtures; (4) Absence of self-siphonage in the individual fixture traps.

Considering the needs for minimization of maintenance in service and for the continuation of venting during cold weather, the following additional criteria can be identified: (5) Ability to maintain adequate

hydraulic performance over a long period of service without excessive maintenance of branch piping; (6) Adequacy of performance under climatic conditions conducive to frost closure of vent terminals.

The procedures for selection and application of hydraulic loads, based on state-of-the-art guidelines, are described as applied to the soil and waste stacks evaluated for conformance to criteria (1) through (4) above.

The results show adequate performance in relation to criteria (1) through (4), with a single example of non-conformance on criterion (3), subject to the limiting condition that some uncertainty exists as to the degree of leak resistance of the DWV systems made available for the tests.

Recommendations are offered concerning further work that could provide information to confirm estimated conformance to criteria (5) and (6).

Yates, J. T., Jr., Madey, T. E., Dresser, M. J., **Adsorption and decomposition of formaldehyde on tungsten (100) and (111) crystal planes,** *J. Catal.* **30,** No. 2, 260-275 (Aug. 1973).

Key words: Carbon dioxide; catalytic; chemisorption; decomposition; formaldehyde; methane; tungsten.

The chemisorption of formaldehyde at ~ 100 K has been investigated on two single crystal planes of tungsten, W(100) and W(111). At low H_2CO coverages, only H_2 and CO are observed as thermal desorption products. At higher H_2CO coverages both CH_4 and CO_2 are observed as additional desorption products. Work function and flash desorption measurements indicate that the dissociative adsorption of H_2CO into H(ads) and CO(ads) is accompanied at higher surface coverages by the formation of other surface complexes.

A detailed comparison of W(100) with W(111) indicates that crystallographic differences play a minor role in the surface catalyzed decomposition of H_2CO by tungsten.

**Publications with prices and SD Catalog numbers may be purchased directly from the Superintendent of Documents, U.S. Government Printing Office, Washington, D.C. 20402 (foreign: one-fourth additional). Microfiche copies are available from the National Technical Information Service (NTIS), Springfield, Va. 22151. Reprints from outside journals and the NBS Journal of Research may often be obtained directly from the authors.*

UNITED STATES
GOVERNMENT PRINTING OFFICE
PUBLIC DOCUMENTS DEPARTMENT
WASHINGTON, D.C. 20402

OFFICIAL BUSINESS
PENALTY FOR PRIVATE USE, $300

U.S. DEPARTMENT OF COMMERCE
POSTAGE AND FEES PAID
COM-375

JOURNAL OF RESEARCH of the National B
A. Physics and Chemistry

Mar.–Apr. 1974

SJRA UNIVE300UA R 1
UNIVERSITY MICROFILMS INC
ATTN SERIALS SECTION
300 NORTH ZEEB RD
ANN ARBOR MI 48106

Page

The formation of curved polymer crystals: Polyoxymethylene. F. Khoury and J. D. Barnes. 95

Solid-phase behavior of several long-chain *n*-paraffins, esters, and a ketone. Peter K. Sullivan. 129

Simultaneous measurements of heat capacity, electrical resistivity, and hemispherical total emittance by a pulse heating technique: Vanadium, 1500 to 2100 K. A. Cezairliyan, F. Righini, and J. L. McClure. 143

The shape of idealized grain boundaries. S. R. Coriell. 149

Reactions of fluorocarbon ions in C_2F_6. Implications for the radiolysis. L. W. Sieck, R. Gorden, Jr., and P. Ausloos. 151

A simple technique for the generation of dilute mixtures of pollutant gases. W. Tsang. 157

Energy levels and classified lines in the second spectrum of thorium (Th II). Romuald Zalubas and Charles H. Corliss. 163

Proposed secondary wavelength standards and line classifications in thorium spectra between 0.9 and 3 μm. A. Giacchetti, J. Blaise, C. H. Corliss, and R. Zalubas. 247

Publications of the National Bureau of Standards. 283

Library of Congress Catalog Card Number: 62-37059

For sale by the Superintendent of Documents, U.S. Government Printing Office, Washington, D.C. 20402. (Order by SD Catalog No. C 13.22/sec.A:78/2). Single copy price varies. Subscription price: $17.00 a year; $4.25 additional for foreign mailing.

UNITED STATES GOVERNMENT PRINTING OFFICE, WASHINGTON : 1974